MODELLING, CONTROL AND DESIGN OF FLEXIBLE AC TRANSMISSION SYSTEMS (FACTS), CUSTOM POWER DEVICES AND VARIABLE SPEED DRIVES FOR TRANSMISSION AND DISTRIBUTION ARCHITECTURES

A thesis submitted to

The Department of Electronic and Electrical Engineering

University of Strathclyde

for the degree of

Doctor of Philosophy

by

NIKOLAOS P. ATHANASIADIS

SEPTEMBER 1999

DECLARATION

Nikolaos Athanasiadis

September 1999

CONTENTS

ABSTRACT

The main tasks of power electronics in power transmission and distribution systems is to process and control the flow of electric energy by supplying voltages and currents in a form that is suitable for user loads. In recent years, the field of power electronics has experienced a large growth. Electric utilities expected that by the year 2000 over half of the electrical load may be supplied through power electronic systems. In order to take advantage of this highly developed technology a number of detailed modelling procedures and simulation facilities are needed.

The work in this thesis is concentrated on modelling, control and design of various power electronic based models for use within transmission and distribution systems. The overall objective is to provide effective methods and tools for assessing the impact of the latest technology based on power electronic devices in the reinforcement of power system networks.

The thesis clarifies modelling and control of various variable speed drive models , such as the six-step, PWM and vector control and gives a detailed account of the systematic derivation of equations that are necessary for the dynamic and transient analysis of a multi-machine multi-node power system with associated adjustable speed drives.

Simulation of Flexible AC Transmission Systems (FACTS) models has also been developed for a number of devices including: the SVC (Static Var Compensator), the STATCON (Static Condenser) and the UPFC (Unified Power Flow Controller). The methodologies for development of the models are described and a number of case studies are included in order to give a broad overview of the applications and to prove the usefulness of the results.

The last part of the thesis includes simulation, control and design of Custom Power Devices for use within distribution system architectures. It starts with a complete control system strategy for the modelling of a solid-state switch and continues with the modelling of a Dynamic Voltage Restorer model, using an innovative control system.

The creation of the power electronics models library provides several opportunities for future developments, which are discussed in the concluding sections of the thesis.

ACKNOWLEDGEMENTS

The work presented in this thesis was carried out under the supervisions of Professors J.McDonald and J.R.Smith, Professors of the Rolls-Royce University Technology Centre of Electrical Power Engineering and the Machines and Power Electronics Group, respectively, at Strathclyde university. The author wishes to express his gratitude to both professors for their interest, enthusiasm and guidance.

I extend my gratitude to the Rolls-Royce Industrial Power Group and Scottish Power for funding this research. I would like to thank Dr. G.Taylor and Dr. J.Hill from the Rolls-Royce Industrial Power Group, for their contributions and help during the conduct of this project.

Thanks are also due to the staff of the Centre for Electrical Power Engineering (CEPE), Mr. Grant, Dr F.P. Flynn , Dr R.D Slater ,Dr Campbell Booth and Dr G.Burt for their invaluable discussions, suggestions and technical assistance.

Finally, special thanks are due to my parents Pavlos and Maria and my brother Stathis, for their unfailing patience, encouragement and understanding, and without their support the work would have been impossible.

LIST OF PRINCIPAL SYMBOLS

The principal symbols used in this thesis are defined in the list below. Sometimes a symbol may serve more than one purpose. Symbols which do not appear in the list will be defined in the text as they are introduced.

A	System state matrix
B	System control matrix
d, q	Direct and quadrature axes of a synchronous machine
f	frequency
G	Rotational matrix
H	Inertia constant
i, I	Current
K	Gain of transfer function
L	Inductance
M	Mutual inductance
P	Active power
p	Differential operator
p.f.	Power factor
R	Resistance
t	time
T	torque or transfer function time constant
V	Voltage
x	Vector of system states
θ	Angular rotor displacement
λ	Flux linkage or eigenvalue
ψ	Flux linkage
ω_b	Base angular velocity
ω_r	Rotor speed
ω_s	Synchronous speed

FACTS	Flexible AC transmission systems
SVC	Static Var Compensator
HVDC	High voltage direct current
GTO	Gate turn off thyristor
IGBT	Insulated Gate Bipolar Transistor
STATCON	Static Condenser
TCSC	Thyristor Controlled Series Capacitor
UPFC	Unified Power Flow Controller
EMTP	Electromagnetic Transients Simulation Program
σ	conduction angle
TCR	Thyristor Controlled reactor
α	firing angle
B	susceptance
SPWM	Sinusoidal Pulse Width Modulation
m	modulation ratio
TACS	Transient Analysis of Controlled Systems
DVR	Dynamic Voltage Restorer
D-STATCON	Distribution Static Condenser
SCR	Silicon Controlled Rectifier
SSB	Solid State Breaker
CLIS	Current limiting Interrupting switch
SSTS	Solid State Transfer Switch

CHAPTER 1

INTRODUCTION

1.1 Overview

In this thesis, it will be demonstrated that there is a significant requirement for modelling, simulation and control of power electronic based devices, such as variable speed drives, Flexible AC transmission systems (FACTS) and Custom Power developed within transmission and distribution systems. This requirement exists as a result of the following factors:

- The use of electrical variable speed drives makes an important contribution to the efficient operation of processes in several branches of industry. Developments in the areas of control and power electronics and, to an increasing degree, the advance of automation have steadily extended the applications of variable speed drives. The properties of these drives have been continuously improved, so that today the highest demands on speed regulation, accuracy, flexibility and availability are fulfilled [1,2]. In the last few years, novel techniques (such as the regular symmetric sampling PWM and the regular asymmetric sampling PWM) have been developed as a result of the advances in microprocessor technology [3,4].

- Flexible AC Transmission Systems (FACTS) is a technology that was introduced a few years ago and embodies the application of power electronics in order to enhance the controllability and capacity of electric utility transmission systems [5-9]. By using reliable, high-speed power electronics based controllers, this offers significant opportunities to improve the operational efficiency of power systems.
- The term Custom Power describes the value-added power that electric utilities and other service providers will be able to offer their customers in the future [10,11]. The improved level of reliability of this power, in terms of reduced interruptions and less variation, will stem from an integrated solution to present problems, of which a prominent feature will be the application of power electronic controllers to utility distribution systems and/or at the supply end of many industrial and commercial customers.

The thesis, by way of introduction, will describe various power electronics based models, control strategies and design and modelling methods for applications of these devices to transmission and distribution systems.

The main body of the thesis will concentrate on the description of a number of novel modelling methods which have been developed as a result of this research. Following on from these descriptions, various case studies will be presented in order to test and validate the proposed techniques through an analysis of the results from dynamic simulations.

Finally, a review of the thesis and an overview of future work will be presented.

1.2 Modelled devices

Despite their different structures, requirements and applications in power systems, variable speed drives, Flexible AC transmission systems and Custom Power devices, have a common characteristic, in that they owe their individual operating principles and applications to the exchange of power with the system that they are connected.

This interaction (from AC to DC, DC to AC or AC to AC) is possible due to the introduction and advances of semiconductor technology.

Although there is a lot of research work currently undertaken in the field of power electronics technology, there are many aspects of the topic that require further research attention. Many variations of power electronics-based plant components are already available and various modelling methodologies have been developed with further proposals appearing regularly. In this thesis the variable speed drives, FACTS controllers and Custom Power devices which have been identified as likely to improve the performance of AC systems are the following:

- Six step inverter
- Natural sampling PWM inverter
- Regular symmetric sampling PWM inverter
- Regular asymmetric sampling PWM inverter
- Vector controlled inverter
- Static Var Compensator (SVC)
- Static Condenser (STATCON)
- Unified Power Flow Controller (UPFC)
- Solid State Switch
- Dynamic Voltage Restorer (DVR)

In order to determine the effectiveness of this new generation of power system devices on a network-wide basis, it will become necessary to upgrade most of the analysis tools on which power engineers rely in order to plan and to operate their systems. Some of the tools which require immediate attention are:

- Transient stability
- Electromagnetic Transients
- Harmonic analysis
- Power flows

This research is related to modelling and analysis of the new generation of power electronics-based plant components presently emerging as a result of the advances in the semiconductor and microprocessor technology, in order to provide engineers with simulation and analytical tools, for planning, operation, etc.

1.3 Previous related work

Modern software systems now offer engineers several opportunities for improved design, validation and general understanding of power electronics based components and schemes. Furthermore, such platforms introduce the capability of providing detailed models of the dynamic behaviour of power electronic based devices.

The research reported in this thesis was undertaken in collaboration with Rolls Royce and Scottish Power and its remit was to develop a suite of power electronic based models, such as variable speed drives, a library of Flexible AC transmission systems (FACTS) and Custom Power devices, to investigate new methodologies and modelling techniques and to realise the potential benefits of utilising such detailed models.

The potential for modelling variable speed drives, FACTS and Custom Power devices became apparent as soon as computers became available on the market (for variable speed drives) and as soon as the technology was apparent (for FACTS and Custom Power). There are several publications concerning the dynamic modelling of these power electronic based devices.

Leonard [12], Murphy and Turnbull [1] presented control functions of the six step inverter and analogue implemented PWM techniques. Bowes [2,13] first introduced the software implemented control techniques such as regular PWM symmetric sampling and regular PWM asymmetric sampling. He presented [13] the basic equations and the fundamentals of the microprocessor based methods. Similar techniques were presented by Zubek [14] and Brod [15]. Adams [16] proposed

another software implemented method, the harmonic elimination PWM. In this paper the basic principles of this control method were reported.

The principles of the vector control method were analysed by Vas [17] and Blaschke [18], while the advantages of this technique compared to the PWM methods were reported by Acarnley and Finch [19]. Ho [20] and Sathikumar [21] presented dynamic simulation results based on the direct vector control method. The importance of the rotor resistance in the vector control method was reported by Matsuo [22] and Atkinson [23].

Modelling and extended simulation results of electric power systems were reported by Smith [24] and Say [25].

The harmonic interaction always provided a challenge for power system planners and engineers. Reeve and Subba [26] investigated the harmonic interaction between AC and DC systems, while Magnusson [27] proposed harmonic filters for harmonic elimination.

Papers in the FACTS area span the last decade. These publications describe modelling methods for the control of Static Var Compensators (SVCs), Static Condensers (STATCONs), Unified Power Flow Controllers (UPFCs) etc. The improvement of power system performance by inserting FACTS controllers as an alternative to traditional methods was presented by Besanger [28,29] and Gillis [30].

The use of Static Var compensators to increase power transfer capacity and to improve system damping has long been recognised and several schemes have been implemented using both Thyristor Control Reactor-Fixed Capacitor (TCR-FC) and Thyristor Control Reactor-Thyristor Switched Capacitor (TCR-TSC) models. Gole and Sood [31] describe the design and operation of an 167 MVA lead/100 lag TSC-TCR (2 stages of 83MVA capacitance) in a 500MW back to back HVDC system. Similar analysis was also reported by Vasconcelos and Ramos [32].

SVC control strategies for damping power system oscillations were reported by Hammad [33]. Analysis of a grid control system using d-q-z transformation for static compensator systems were investigated by Gole, Sood and Mootoosamy [34]. For a more detailed description of related work in modelling methods for the SVC refer to chapter 7.

Several modelling techniques have been presented over the last few years for power flow controllers such as the Static Condenser (STATCON) and the Unified Power Flow Controller (UPFC). Gyugyi and Eldis [35,36,37,38] presented the basic principles of the Unified Power Flow Controller, while Schauder and Mehta [39,40,41] described the fundamentals of the Static Condenser. Ooi and Galiana [42] presented a solid state PWM shifter model and basically introduced the PWM method as a very promising method for the control of power flow controllers. Martinez, Capolino and Gole [43,44,45] presented very useful power electronic models using the Electromagnetic Transients Program (in terms of providing useful guidelines for modelling power electronic based devices). Nelson and Hill [46] investigated the transient stability of power system networks with FACTS controllers.

Since Custom Power is a technology that only recently emerged there are only a limited number of publications in this field. The majority of the papers deals with measurements and technical characteristics of the devices, rather than with modelling methods. Smith and Mehta [47] presented the application requirements and control strategies of a solid state breaker, while Woodley and Malkin [48] developed and demonstrated a similar model based on GTO (Gate Turn-off Thyristor) technology. The advantages of Custom Power technology over conventional methods have been reported by Taylor [49,50], Douglas [51], Hingorani [52] and Osborne [53,54].

The use of a device known as the Dynamic Voltage Restorer (DVR), which is used to maintain a constant voltage at the load terminals during disturbances in the transmission or the distribution system, has also been reported in the literature over the last 3-4 years. Taylor described the operating principles of the Dynamic Voltage

Restorer together with other Custom Power solutions [49]. Osborne, Kitchin and Ryan reported the benefits of the use of DVRs compared to other Custom Power solutions[53,54]. Mohaparta, Zayegh, Kalam and Coulter analysed the use of the DVR in a system with other energy storage devices [55]. For a more detailed description of work relating to the DVR refer to chapter 10.

This thesis presents new methodologies and control techniques in order to provide an integrated modelling approach for power electronic based devices, including a number of different control techniques for variable speed drives, a library of FACTS controllers and modelling of Custom Power devices. This complete modelling approach provides a useful framework for establishing the behaviour of novel power system architectures including the modelled devices under various system scenarios (both normal and abnormal).

1.4 Motivation and research justification

In broad terms, the task of power electronics is to process and control the flow of electric energy by supplying voltages and currents in a form that is optimally suited for user loads [56]. In recent years, the field of power electronics has experienced a large growth due to the confluence of several factors. Revolutionary advances in semiconductor technology have made it possible to significantly improve the voltage and current handling capabilities and the switching speeds of power semiconductor devices. At the same time, the market of power electronics has significantly expanded. Electric utilities expect that by the year 2000 over 50% of the electrical load may be supplied though power electronic systems [57].

The use of power electronics in power systems was initially for High Voltage Direct Current (HVDC) interconnections [58-68]. The work in this thesis deals with modern power electronic systems, which consist of power electronic converters using solid state semiconductor devices. Accordingly, three research areas are of interest: variable speed drives, FACTS and Custom Power devices.

1.4.1 Variable speed drives

In many modern adjustable-speed drives the demand is for precise and continuous control of speed and torque, good transient performance and high efficiency [16,69]. In the past, dc motors have satisfied some of these requirements, and have been extensively used in many industrial applications [1]. However, its mechanical commutators are often undesirable because of the regular maintenance required. These problems can be overcome by the application of ac motors, which are brushless and have a relatively robust rotor construction, high reliability and are economic.

In recent years, the R&D work carried out in the field of adjustable-speed drives has been concentrated mainly in two directions [3,17,70]. The first is concerned with the use of microprocessors and power transistors using PWM techniques [3,70], while the second is concerned with the application of field orientation methods [17]. The work in this thesis presents various innovative microprocessor based modelling techniques, such as the regular symmetric PWM sampling and the regular asymmetric PWM sampling as alternatives to the traditional natural sampling PWM and the six step. The benefits of the software implemented methods compared to the traditional methods, are also reported.

In this thesis an indirect vector control method is demonstrated and applied to control a variable speed drive. The mathematical model and the advantages over the PWM methods are also presented. However, the complexity of the vector control techniques (complicated control structure and complex co-ordinate transformation) make the PWM methods the standard control techniques for applications of variable speed drives within power system networks. In the succeeding chapters the PWM technique will be used for the control of variable speed drives when they are connected to power systems.

The power systems of today, by and large, are mechanically controlled. Several processing and analytical functions are software-based; however, when control signals resulting from these functions are sent to the power circuits, the control

devices are mechanical and there is little high-speed control. Power system planners, operators and engineers have learned to live with this limitation by using a variety of ingenious techniques to make the system work effectively, but at a price of allowing significant inefficiencies and greater operating margins. However, these problems can now be effectively solved with the advent of new technologies such as FACTS and Custom Power [71,72,73].

1.4.2 FACTS

The main aims of the FACTS technology can be summarised in the following [71]:

1) To increase power transfer capacity and utilisation of existing transmission lines
2) To introduce more controllability and flexibility in power systems operation in such a way as to enhance steady-state and transient stability
3) To overcome the technical limitations and high costs associated with existing thyristor controlled devices.

In order to assist power system engineers in assessing the effects of FACTS devices on power system performance, it has become necessary to upgrade existing power systems software, or in some cases to develop a new generation of software. Before meaningful results can be obtained from application studies, realistic mathematical models for the transmission system and FACTS controllers needed to be realised, coded and extensively verified.

From the operational point of view, FACTS technology is concerned with the ability to control, in an adaptive fashion, the path of the power flows throughout the network and to improve the voltage stability. At present, high speed control is almost non-existent. In this context, simulation programs should offer a very useful tool for system planners and operators to evaluate the technical and economical benefits of a wide range of alternative solutions offered by FACTS technology.

In many instances, existing software which has been in use for many years has been shown to be inflexible. Hence modification is achieved with great difficulty and

expense. This has provided the motivation for developing new, well designed and efficient software where both established and emerging components can be modelled along side each other with minimum effort and without the compromises often imposed when inflexible existing software is modified.

Bearing this in mind, the efforts in this research are concentrated on building a library of dynamic models of FACTS devices using the Electromagnetic Transients Simulation Program (EMTP). Innovative control techniques and modelling methodologies have been selected to verify FACTS models, such as the Static Var Compensator (SVC), the Static Condenser (STATCON) and the Unified Power Flow Controller (UPFC) and to prove the virtues of developing a new generation of software suitable for the analysis of large scale networks.

1.4.3 Custom Power

Custom Power is a technology driven product and service solution which embraces a family of devices which will provide power quality functions at distribution voltages [49,52]. It has been made possible by the now widespread availability of cost effective high power solid state switches such as GTO'S (Gate Turn-Off Thyristors) and IGBT's (Insulated Gate Bipolar Transistors). The first uses for Custom Power devices are likely to be within applications where power quality is a known ongoing problem and where rectifying that problem by conventional means (e.g. installation of new feeder, primary equipment replacement etc.) is likely to be costly, and not guaranteed to solve the problem. By analysing the problem via an application study, it should be possible to determine a Custom Power solution which provides a viable economic alternative. A further advantage of Custom Power devices is that using the technology can also defer the need for line reinforcement. The main Custom Power devices now appearing at distribution systems are the solid state switch and the Dynamic Voltage Restorer (DVR).

Due to the fact that the Custom Power technology is a very new technology that has only emerged in the last 3-4 years, there are not sufficient tools to assist power

system engineers and operators to assess the effect of Custom Power devices on a distribution system's performance. For this reason, it has become necessary to build up a suite of distribution system software and modelling techniques. Using these tools, power system planners can evaluate the technical and economical benefits of this latest technology and develop a wide range of distribution system solutions to the problems now facing the power industry.

The efforts in the research reported in this thesis are concentrated on developing a generic control methodology for a solid state switch and the modelling, control and design of a DVR model using an innovative simulation technique. It is believed that the methods developed in this thesis will contribute to the incorporation and application of this key technology within power systems architectures and will lead power system designers to new distribution system configurations.

All of the aspects described above contribute to the motivation and justification for extensive research on the creation of dynamic models of power electronic based equipment and the integration of different modelling paradigms as reported in this thesis.

A list of associated publications by the author, which have been produced throughout the course of the research reported in this thesis, is included later in this chapter.

1.5 Objectives

In order to explore the wide area of applications, the objectives of this work were defined at the outset:

a) To develop the following models of variable speed drives suitable for inclusion in power system studies:

- Six step, open and closed loop voltage fed inverter drive
- Natural sampling, open and closed loop voltage fed inverter drive
- Regular symmetric sampling, open and closed loop voltage fed inverter drive
- Regular asymmetric sampling, open and closed loop voltage fed inverter drive

- Indirect vector controlled voltage fed inverter drive

b) To verify the ability of the variable speed drives to carry out their intended functions in electric power networks:

- To develop digital computer programs based on the latest control techniques suitable for the analysis of the dynamic performance of variable speed drives
- To develop equations and guidelines to model power system components in electric networks
- To develop a general algorithm for modelling and simulation of multi-machine power systems with interconnected AC/DC converter stations/variable speed drives
- To investigate the effect of harmonic penetration caused by the AC/DC converter stations/variable speed drives in electric power systems
- To provide filter circuit configurations for absorption of the unwanted harmonics caused by the AC/DC converter stations/variable speed drives

c) To create a library of dynamic models of FACTS devices for use within transmission systems based on the :

- Static Var Compensator (SVC)
- Static Condenser (STATCON)
- Unified Power Flow Controller (UPFC)

d) To verify the ability of the FACTS devices to carry out their intended functions in electric power networks:

- To develop a control system for modelling and simulation of a Static Var Compensator (SVC)
- To investigate the effect of the SVC on the dynamic and transient stability of a power system

- To provide filter circuit configurations for absorption of the unwanted harmonics that the SVC generates in power systems
- To develop open loop control systems for modelling and simulation of a Static Condenser (STATCON) and a Unified Power Flow Controller (UPFC)
- To investigate the effect of the STATCON and the UPFC on real and reactive power flows in transmission systems

e) To create dynamic models of Custom Power devices for use within distribution systems such as the :

- Solid State Switch
- Dynamic Voltage Restorer (DVR)

f) To develop computer simulation programs and control strategies for application of Custom Power devices in distribution systems:

- To propose a control strategy for modelling and design of a solid state switch
- To develop a novel simulation program for modelling of a Dynamic Voltage Restorer (DVR)
- To design a DVR and its associated filters, using results taken from the dynamic simulations

1.6 Novelty of the reported research

In terms of the novelty of the research reported in this thesis, the following contributions are identifiable:

- The development of computer simulation programs based on the control systems presented in this thesis for the six step and the PWM techniques (such as the natural sampling and the symmetric/asymmetric sampling) along with an

investigation on the dynamic behaviour of the six step and the PWM inverters under various operating conditions.

- The development of a computer program for the closed-loop vector control method coded in the Fortran language and a report on the behaviour of indirect vector control machines under various operating conditions, such as free acceleration to rated speed, step load applied on the shaft of the motor, fast speed reversal and operation in the field weakening region.
- The development of a new generalised approach to power system modelling, which incorporates modelling of AC systems with DC converter stations/variable speed drives.
- The creation of a computer code for the interconnected AC/DC power system and variable speed drives coded in the Fortran language and an investigation on the influence of harmonic pollution to power systems using DC converter stations. Results from the dynamic simulations carried out in this thesis are presented for a number of operating conditions. Where appropriate, analytical equations and explanations are given which will ensure acceptable system conditions.
- An efficient and realistic method to model the Static Var Compensator (SVC), using comprehensive control and firing systems has been developed, along with guidelines for designing the harmonic filters. The SVC was considered to be a continuously variable-shunt susceptance which was adjusted in order to achieve a specified voltage magnitude.
- Comparison of the control and firing methods proposed in this chapter with other control methods and firing systems (such as the Phase Locked Loop) method. The validation of the techniques that were presented in this thesis demonstrates that the proposed SVC controller gives a very good representation of a practical system. The results that were presented using the proposed firing method prove the effectiveness of the technique that was used in this thesis, show that is insensitive to voltage waveform distortion and capable of establishing accurate firing timing in a timescale similar to using the Phase Locked Loop method; consequently it can be used as an alternative to the PLL method for the control of Static Var Compensator models. Moreover, by using the firing technique presented in this

thesis the problem caused by using the PLL method which is that the dynamics of the PLL require a very small time step which demands a high CPU time, can be avoided.

- The problems encountered in the process of building power flow controllers such as the Static Condenser (STATCON) and the Unified Power Flow Controller (UPFC) and the way of handling them using the Electromagnetic Transients Program (EMTP) were discussed and useful guidelines were given for applications of such power electronic based devices by power system engineers using the EMTP.
- The development of a generic control strategy for control and design for a number of devices based on the solid state switch.
- The creation of an innovative closed-loop control system for the Dynamic Voltage Restorer. The control mechanism consists of individual voltage and power controllers for the control of the DVR using the Sinusoidal Pulse Width Modulation technique (SPWM). The effectiveness of the proposed control system was tested under various operating conditions and results taken from the dynamic simulations were validated using actual test results from DVR installations.
- The development of a computer code using the Electromagnetic Transients Simulation Program (EMTP) based on the control system described in this chapter can be used for the effective design of the DVR and its associated controls and filters.

1.7 Benefits of the reported research to the academic community and to the power system industry

The contributions of this research work are mainly concerned with benefits to both the academic community as well as to power system planners and engineers.

From an academic point of view, is it believed that the modelling methods and techniques presented and demonstrated in this thesis, will help researchers in the field of power electronics to:

- gain a better understanding of new modelling tools and methodologies for a wide range of power electronic based devices (variable speed drives, FACTS, Custom Power devices)
- gain a better knowledge for the control of these devices in power systems, since there is insufficient research related in this area, due to the fact that this technology is based on the semiconductor technology that has been introduced relatively recently
- use some of the modelling techniques as the basis for the simulation and control of other power electronic devices (e.g. use the method for the DVR as the basis for modelling the Distribution STATCON)
- propose and evaluate various power system configurations from the results of the dynamic simulations carried out in this research project.

From an industrial perspective, is it believed that the proposed computer simulation programs will help power system engineers and planners to obtain a better understanding of :

- a complete system solution incorporating power system and power electronics components
- how the power electronic devices (variable speed drives, FACTS, Custom Power devices) :

⇒work

⇒can be controlled

⇒can be incorporated in power system architectures

⇒can be designed with significant economic impact

⇒can be tested in a more optimal fashion though the availability of well-defined and validated mechanisms.

1.8 Thesis outline

The structure of the thesis is summarised below:

The work described in chapters 2 to 5 in this thesis is concerned with the modelling and development of various variable speed drive models for use within interconnected power systems.

- Chapter 2 presents the modelling and simulation of six-step and various PWM variable speed drives, including open and closed loop speed control of six-step, natural sampling PWM, symmetric sampling PWM and asymmetric sampling PWM adjustable speed drives. Harmonic analysis showing the benefits of the PWM technique over the six step method is also included.
- Chapter 3 describes the development and modelling of vector controlled variable speed drives with emphasis on the use of indirect vector controlled adjustable speed drives.
- The purpose of chapter 4 is to develop various 3-phase mathematical models of the main components of a modern power system such as synchronous machines, induction machines, three phase transformers and filters for use as a basis of the subsequent simulation activities. In addition, the chapter covers some essential and common models of automatic voltage regulators, prime movers and also represents the mathematical model of an AC/DC converter station.
- Chapter 5 presents a modelling technique and simulation results of multi-machine power systems with AC/DC converter stations and PWM variable speed drives. The proposed method is tested under different system scenarios. The interaction between the AC and DC systems is also analysed in detail using filters for harmonic elimination. Harmonic analysis showing the improvement of harmonic content due to the use of filters is also included.

The work described in chapters 6 to 8 includes the main application of FACTS devices and modelling, simulation and design of various FACTS controllers, such as

the SVC (Static Var Compensator), the STATCON (Static Condenser) and the UPFC (Unified Power Flow Controller).

- Chapter 6 reviews current and future potential FACTS applications in power transmission systems, describes the circuitry of the main FACTS devices and describes the basic control functions of power flow controllers.
- Chapter 7 deals with the development of a Static Var Compensator (SVC) model for use in transmission system networks. This includes a detailed description of the main power circuit, the measurement, control and firing systems of the SVC and the proposed modelling technique. Simulation results are presented for a number of different case studies under steady state and transient conditions. Comparison and validation of the control and firing methods proposed in this thesis with other control methods and firing techniques (such as the Phase Locked Loop) method are also presented.
- Chapter 8 presents modelling and simulation work with respect to power flow controllers and especially to Static Condenser (STATCON) and to Unified Power Flow Controller (UPFC) devices. In this chapter, the main types and the operating principles of voltage source inverter models for power flow controller studies are analysed and a description of the techniques for simulation of these devices using the Electromagnetic Transient Program (EMTP) is presented. Simulation results of open-loop STATCON and UPFC models using simple power system networks are also illustrated.

The work described in chapters 9 and 10 is concerned with the development of dynamic models of Custom Power devices for use within distribution systems.

- In chapter 9, the three predominant Custom Power devices, the Dynamic Voltage Restorer (DVR), the Distribution Static Condenser (D-STATCON) and the solid state switch are presented, including a description of the design specifications and application requirements. A control strategy is also illustrated for applications of devices based on the solid state switch in distribution systems.

- Chapter 10 describes modelling, simulation and design of a Dynamic Voltage Restorer (DVR) model for use in distribution systems. The operating principles and the application of the DVR are reported and different case studies are investigated for open and closed loop control systems. Validation of the proposed modelling method is performed by comparing results from the dynamic simulations carried out in this thesis with actual test results from DVR installations. The importance of the novel modelling technique used for the closed-loop control system to power system planners and engineers is very significant, since Custom Power technology is novel in nature and there is insufficient knowledge of both the impact of such devices on the electrical system and of how these Custom Power devices can be used most effectively in distribution systems.

- Finally, in chapter 11, conclusions are drawn from the research and suggestions for further work are proposed.

1.9 Associated publications

The following publications have arisen from the research detailed in this thesis:

1. Athanasiadis N, McDonald J.R, Burt G.M, Booth C, "Dynamic FACTS modelling: "Methodology and validation using the voltage stability problem", 33rd Universities Power Engineering Conference (UPEC), pp 234-237, Edinburgh, UK, September 1998.
2. Athanasiadis N, McDonald J.R, Booth C, "Modelling and simulation of FACTS devices using the electromagnetic transients program (EMTP)", European EMTP Users Group (EEUG), pp 1-15, Prague, Czech Republic, November 1998.
3. Athanasiadis N, McDonald J.R, Booth C, " Modelling and control of FACTS and Custom Power devices using the electromagnetic transients program (EMTP)", paper prepared for submission to IEE/IEEE.

4. Athanasiadis N, McDonald J.R, Grant D, Booth C, " Modelling, control and design of a Dynamic Voltage Restorer model (DVR) for distribution system architectures", paper prepared for submission to IEE/IEEE.
5. Athanasiadis N, Ault G, Edwards F, McDonald J.R, " Power system models for new distribution imperatives", paper prepared for submission to IEE/IEEE.
6. Athanasiadis N, McDonald J.R, Simpson R, Booth C, "Dynamic modelling, control and economic consideration of the Unified Power Flow Controller (UPFC) and the Dynamic Voltage Restorer (DVR) for transmission and distribution systems", paper prepared for submission to IEE/IEEE.
7. Athanasiadis N, Smith J.R, Grant D, "Simulation and harmonic analysis of a large AC/DC power system with adjustable speed drives using a new generalised modelling approach", paper prepared for submission to IEE/IEEE.
8. Athanasiadis N, Smith J.R, Grant D, "Dynamic response of an AC/DC system with variable speed drives using an integrated modelling technique", paper prepared for submission to IEE/IEEE.
9. Athanasiadis N, Smith J.R, McDonald J.R, Grant D, "Integrated power electronics modelling and control: voltage sag ride-though for AC variable speed drives with Dynamic Voltage Restorers", paper prepared for submission to IEE/IEEE.

1.10 References

1. Murphy, J.M.D. and Turnbull, F.G. ,"Power electronic control of a.c. motors," Pergamon Press plc., England, 1988.
2. Bowes, S.R and Mount, M.J : "Microprocessor control of PWM inverters", IEE Proceedings B, 1981, pp 293-305.
3. Grant,T.L.,Bardon T.H ,"Control strategies for P.W.M drives", IEEE Transactions 1980, IA-16, pp 211-215.
4. Zubek, J., Abbondanti, A and Nordby C.J "Pulse-width modulated inverter motor drives with improved modulation", IEEE Transactions 1975, IA-11,pp 695-703.
5. D.T. McGillis, M. Toussaint, F.Galliana, G.Joos, R.Marceau, D.Atanackovic, J.Cheng, "An investigation into the realities of FACTS devices", AC and DC Power Transmission, No.423, 1996, pp 252-257.
6. . IEE: Flexible AC Transmission Systems (FACTS) - "The Key to Increased Utilisation of Power Systems", IEE Colloquium Digest, January, 1994, London. No .087, p.10/1p.
7. Thanawala, H.L., "Voltage Control and Stability and Improved Quality of Electricity Supply", Symposium of Power Engineering Innovations and Environment, Nov. 1992, Hong Kong.
8. Lavsey, E., Weaver, T. IEEE-CIGRE Working Groups Joint Document: "FACTS Overview", IEEE Publication April, 1995, pp 95-TP-108.
9. Le Du A. Toutini, "Which FACTS Equipment for Which Need? ",CIGRE Winfield, 1992, France Paper 14/37/38-08.
10. Hingorani N, "Introducing custom power", IEEE Spectrum, June 1995, pp 41-48.
11. Douglas J, "Custom power :Optimising distribution services", EPRI Journal, June 1996, pp 1-6.
12. Leonard W., "Control of Electrical Machines", Springer-Verlag, 1985.
13. Bowes, S.R and Bird B.M, "Novel approach to the analysis and synthesis of modulation processes in power convertors", Proceedings IEE 1978, 125 pp 507-513.

14. Zubek, J., Abbondanti, A and Nordby C.J "Pulse-width modulated inverter motor drives with improved modulation", IEEE Transactions 1975, IA-11,pp 695-703.
15. Brod, D.M and Novotny, D.W. "Current control of VSI-PWM inverters," IEEE Transactions on Industry Applications, vol. IA-21, May/June 1985, pp 562-570.
16. Adams, R.D. and Fox R.S., "Several modulation techniques for the P.W.M inverter", IEEE Transactions, IA-8, 1978, pp 636-643.
17. Peter, V.A.S. "Vector control of a.c machines," Oxford University Press, New York, 1990.
18. Blaschke F., "The principle of field orientation as applied to the new transvector closed-loop control system for rotating-field machines", Siemens Review XXXIX, No. 5, 1972, pp.217-220.
19. Acarnley P.P., Finch J.W., Atkinson D.J., "Field-orientation in AC Drives: State-Of-Art and future prospects", IEE 3rd Int. Conf. On Electrical Machines and Drives, London, Nov.1987, pp 285-289.
20. Ho E.Y.Y., Sen P.C., "Decoupling control of induction motor drives", IEEE Transactions. Ind. Electronics, Vol.35, No.2, 1988, pp253-262.
21. Sathikumar S., Vithayathil J., "Digital simulation of field-oriented control of induction motor", IEEE Trans. Ind. Electronics, Vol.IE-31, No.2, 1984, pp 141-148.
22. Matsuo T., and Lipo T.A., "A rotor parameter identification scheme for vector-controlled induction motor drives", IEEE Trans. on Industry Applications, vol. IA-21, May/June 1985, pp 624-632.
23. Atkinson, D. J., Acarrney, P.P. and Finch, J.W. "Application of estimation techniques in vector-controlled induction motor drives", IEE Fourth International Conference on Power Electronics and Variable-speed drives, 1989, pp 358-363.
24. Smith J.R. and Chen Meng-Jen, Three-Phase Electrical Machine Systems-computer simulation, Research Studies Press Ltd, 1993.
25. Say M.G. "Alternating Current Machines", Longman Scientific & Technical 1983.

26. Reeve J, and Subba Rao, T. "Dynamic Analysis of Harmonic Interaction between AC and DC Power Systems", IEEE Transactions on PAS, Vol. PAS-93, No.2, March/April 1974, pp 640-646.

27. Magnusson P, "Resistively Bridged Harmonic Filter for Power Converters", IEEE Transactions on Power Apparatus and systems, Vol PAS-87, June 1968, pp 1481-1484.

28. Y. Besanger, J.C. Passelergue, N. Hadjsaid, R.Feuillet, "Improvement of power system performance by inserting FACTS devices", AC and DC Power Transmission, No 423, 1996, pp263-267.

29. Y.Besanger, J.C.Passelergue, N.Hadjsaid, "Improvement of Power System Performance by inserting FACTS devices", AC and DC Power Transmission, IEE 1996, pp 263-267.

30. D.T. McGillis, M. Toussaint, F.Galliana, G.Joos, R.Marceau, D.Atanackovic, J.Cheng, "An investigation into the realities of FACTS devices", AC and DC Power Transmission, No.423, 1996, pp 252-257.

31. A.M.Gole, V.K.Sood,"A Static Compensator model for use with Electromagnetic Transients Simulation Programs", IEEE Transactions,Vol.5,No.3,July 1990, pp 1398-1407.

32. A.N Vasconcelos, A.J.P. Ramos ,J.S Monteiro ,M.Lima, H.Silva ,L.R.Lin, "Detailed Modelling of an actual Static Var Compensator for Electromagnetic Transient Studies", Transactions on Power Systems ,Vol.7,No.1,February 1992, pp 11-17.

33. A.E. Hammad, "Analysis of Power System Stability enhancement by Static Var Compensators", IEEE Transactions on Power Systems ,Vol.1 ,November 1996, pp 222-227.

34. A.M.Gole, V.K.Sood, L.Mootoosamy, "Validation and analysis of a Grid Control System using d-q-z Transformation for Static Compensator Systems", Canadian Conference on Electrical and Computer Engineering, September 1989,pp 745-748.

35. L.Gyugyi, C.D.Schauder, S.L. Williams, T.R. Rietman, D.R. Torgerson, A. Eldis, "The Unified Power Flow Controller: A New Approach To Power Transmission

Control", IEEE Transactions on Power Delivery, Vol 10, No.2 , April 1995, pp 1085-1097.

36. L.Gyugyi, "Dynamic Compensation of AC Transmission Lines by Solid-State Synchronous Voltage Sources", IEEE Transactions on Power Delivery, Vol 9, No.2 April 1994, pp 904-911.
37. L.Gyugyi, "Unified power flow control concept for flexible AC transmission systems", IEE Proceedings Vol.139, No 4, July 1992, pp 323-331.
38. Gyugyi, L., "Unified Power-flow Control Concept for Flexible AC Transmission Systems", IEE Proceedings, Vol. 139. No. 4, July, 1992, pp 323-331.
39. C.Schauder, H.Mehta, "Vector analysis and control of advanced static VAR compensators", IEE Proceedings, Vol.140, No.4 July 1993, pp 299-306.
40. C.Schauder, M.Gernhardt, E.Stacey, T.W.Cease, A.Edris, "Development of a ±100MVAR Static Condenser for Voltage Control of Transmission Systems", IEEE Transactions on Power Delivery, Vol 10, No.3, July 1995, pp 1487-1493.
41. Schauder, C. "Vector Analysis and Control of Advanced Static VAR Compensators" IEE Proceedings,Part C, Vol. 140, No. 4, July 1993, pp.299-306.
42. B.Ooi, S.Z.Dai, F.Galiana, "A Solid-State PWM Phase-Shifter", IEEE Transactions on Power Delivery, Vol 8, No.2, 1993, pp 573-579.
43. Martinez J.A and Capolino G.A "Simulation of power electronics using the EMTP. Part I: Power converters. A survey", UPEC'94, September 14-16, 1994, Galway.
44. Martinez J.A and Capolino G.A "Simulation of power electronics using the EMTP. Part II: Electrical drives. A survey", UPEC'94, September 14-16, 1994, Galway.
45. Gole A.M., Keri A, Nwankpa C, "Guidelines for modelling power electronics in electric power engineering applications", , IEEE Transactions on Power Delivery, January 1997, pp 505-513.
46. R.J.Nelson, J.Bian, D.G.Ramey, T.Lemak, T.R.Rietman, J.Hill, "Transient Stability with FACTS Controllers", AC and DC Power Transmission,IEE 1996,pp 269-274.

47. Smith R.K., Slade P.G., Sarkozi M., Stacey E.J., Bonk J.J., Mehta H., "Solid state distribution current limiter and circuit breaker: application requirements and control strategies", IEEE Transactions on Power Delivery, Vol 8, No.3, July 1993, pp 1155-1164.

48. Woodley N, Sarkozi M, Lopez F, Tahiliani V, Malkin P, "Solid-state 13-Kv distribution class circuit breaker: planning, development and demonstration", IEE Conference Publication 1994, pp 163-167.

49. Taylor G "Power quality hardware solutions for distribution systems: Custom power", IEE Colloquium (Digest), pp 11/1-11/7.

50. Taylor G.A, Burden A.B. "Wide area power quality-decision processes and options for sensitive users", CIRED, 1997, pp 2.30.1-2.30.5.

51. Douglas J, "Custom power :Optimising distribution services", EPRI Journal, June 1996, pp 1-6.

52. Hingorani N, "Introducing custom power", IEEE Spectrum, June 1995, pp 41-48.

53. Osborne MM, Kitchin RH, Ryan HM, "Emergence of custom power technology in distribution systems", Proceedings of the Universities Power Engineering Conference, 1995, Vol 2, pp 777-780.

54. Osborne M, Kitchin R, Ryan H, "Custom power technology in distribution systems: an overview", IEE Symposium, pp 10/1-10/10.

55. Mohapatra GR, Zayegh A, Kalam A, Coulter RJ, "Energy sources, energy storage and power electronic devices", Proceedings of the Universities Power Engineering Conference 1996, Vol 1 ,pp 155-158.

56. Mohan N, Underland T, Robbins W, "Power electronics : Converters,Applications and Design", John Wiley and Sons, Inc, 1995.

57. Dugan R, McGranaghan M, Wayne H, 'Electrical Power Systems Quality', McGraw-Hill, 1995.

58. Taleb M, Ortmeyer T.H., "Examination of the current injection technique", IEEE Transactions on Power Delivery, Vol 7, January 1992, pp 442-448.

59. Emanuel A, Yang M, "On the harmonic compensation in nonsinusoidal systems", IEEE Transactions on Power Delivery, Vol 8, January 1993, pp 393-399.

60. Mohan N, Rastogi M, Naik R, "Analysis of a new power electronics interface with approximately sinusoidal 3-phase utility currents and a regulated dc output", IEEE Transactions on Power Delivery, April 1993, pp 540-546.
61. Grotzbach M, Frankkenberg W, "Injected currents of controlled AC/DC converters for harmonic analysis in industrial power plants", IEEE Transaction on Power Delivery, Vol 8, April 1993, pp 511-517.
62. Woodford D, "Secondary arc effects in AC/DC hybrid transmission", IEEE Transactions on Power Delivery, 1992, pp 704-711.
63. Carpinelli G., Gagliardi F., Russo M., Sturchio A., "Steady state mathematical models of battery storage plants with line-commutated converters", IEEE Transactions on Power Delivery, Vol. 8, No.2, April 1993, pp 494-501.
64. Hingorani N.G., Hay J.L, Crosbie R.E., "Dynamic simulation of h.v.d.c transmission systems on digital computers", Proceedings of IEE, , May 1966, pp 793-805.
65. Htsui J.S.C., Shepherd W., "Method of digital computation of thyristor switching circuits", Proceedings of IEE, August 1971, pp 743-748.
66. Rumph E., Ranade S., "Comparison of suitable control systems for HVDC stations connected to weak ac systems. Part II. Operational behaviour of the HVDC transmission", IEEE Transactions on Power Delivery, , May 1971, pp 555-564.
67. Hingorani N, Burbery F., "Simulation of AC system impedances in HVDC system studies", IEEE Transactions on Power Apparatus and Systems, , May 1970, pp 819-826.
68. Rumph E., Ranade S., "Comparison of suitable control systems for HVDC stations connected to weak ac systems. Part I. New control systems" Transactions on Power Delivery, , May 1971, pp 549-555.
69. Mohan N, Underland T, Robbins W ,"Power electronics: Converters, Applications and Design", John Wiley and Sons 1995.
70. Bose, B.K. "Adjustable Speed AC Drives-A Technology Status Review," Proceedings IEEE, Vol. 70, Feb. 1982, pp 116-135.

71. Y. Besanger, J.C. Passelergue, N. Hadjsaid, R.Feuillet, "Improvement of power system performance by inserting FACTS devices", AC and DC Power Transmission, No 423, 1996, pp263-267.

72. D.T. McGillis, M. Toussaint, F.Galliana, G.Joos, R.Marceau, D.Atanackovic, J.Cheng, "An investigation into the realities of FACTS devices", AC and DC Power Transmission, No.423, 1996, pp 252-257.

73. J.A Martinez, "Simulation of a microprocessor controlled SVC",21th European EMTP Meeting, June 5-7 ,1992,Crete (Greece).

CHAPTER 2

MODELLING OF ADJUSTABLE - SPEED A.C DRIVES

2.1 Introduction

The dispute between direct current (D.C.) motors and alternating current (A.C.) motors has been a popular topic for many years[1].

The separately excited d.c. motor has been used mainly for applications where there was a requirement of fast response with high performance. However , d.c. motors have certain disadvantages, which are due to the existence of the commutator and the brushes. That is, they require regular maintenance; Maintenance causes difficulty when interruptions cannot be tolerated.

AC motors such as the cage-rotor induction motor are brushless and have a robust rotor construction which permits reliable maintenance-free operation at high speed. The simple rotor construction also results in a lower cost motor and a higher power/weight ratio. Unfortunately, the induction motors are inflexible in speed when operated on a standard constant-frequency ac supply. The induction motors run slightly below synchronous speed, which is determined by the supply frequency and the number of poles for which the stator is wound. Efficient wide-range speed control of synchronous-type motors or cage-rotor induction motor is only possible when an

adjustable-frequency ac supply is available. Consequently, in this chapter attention is largely concentrated on the adjustable frequency method of obtaining adjustable-speed ac induction motor drive systems.

2.2 Application Consideration for Adjustable-Speed AC drives

The problem in selecting an adjustable-speed drive for a particular application is to choose the system that can most economically provide the required range of speed or torque or position control with the desired accuracy and fast response. The ac commutator motor has been used in the past, because it can be supplied directly from the ac utility supply, but for a reversible drive with continuous speed control over a very wide range, the dc motor has been the most popular solution. The separately excited dc motor can be rapidly and efficiently controlled by variation of the armature voltage and field current. In recent years, the dc supply has been obtained from the ac utility network by mean of static converters, which permit controlled rectification of the alternating voltage, so that an adjustable direct voltage is provided for the armature. Precise speed control is achieved by the adoption of closed-loop feedback methods[2].

However, the dc motor is not the ideal solution to the problem of adjustable-speed motor operation. The elaborate construction increases the cost of the dc motor and reduces its power/weight ratio. The total armature voltage is limited to a maximum of about 1500 V. The magnitude of the armature current and its rate of change are also restricted by commutation difficulties.

The cage-rotor, or squirrel-cage, induction motor, on the other hand, has a rotor circuit consisting of a short-circuited winding that can be often be made from a single casting. The cage rotor has a low inertia and can operate at high temperature and high speed for prolonged periods without maintenance. In addition, the cost of the cage-rotor induction motor is about one-tenth that of a dc motor of the same speed and power rating. The power/weight ratio of the squirrel-cage motor is about twice that of the dc machine, and induction motors are manufactured in much higher power ratings because the stator current is not limited by commutation and the stator voltage can be

15 kV or more. It is obvious, therefore, why numerous attempts have been made to obtain economic and efficient speed control of the cage-rotor induction motor.

The provision of an adjustable-frequency supply by static frequency converter is often expensive. Consequently, the high cost of the frequency conversion equipment may offset the savings resulting from the replacement of the dc motor by the lower cost cage-rotor machine. However, the static frequency converter provides an adjustable-speed drive with high accuracy and reliability, and with an initial capital cost that is frequently justified by the improved performance and lower running costs.

The adjustable-frequency speed drive is particularly attractive in multimotor systems when large numbers of small ac motors are supplied simultaneously with the same frequency and voltage. In such applications, the cost of the frequency converter is justified by the significant reduction in machine costs due to the large number of motors involved. If these motors are required to run at closely co-ordinated speeds, the adjustable-frequency system is highly advantageous because modern static frequency converters can deliver an output frequency of extremely high precision and long-term stability.

Because the static frequency converter includes much specialised electronic circuitry, its maintenance might appear to present some difficulty. However, the techniques of modular construction with removable units permit a faulty circuit unit to be readily located and replaced. The repair of the faulty module can then be carried out by the maintenance staff under specific conditions.

The use of microprocessors can increase the reliability of the electronic control circuitry. Power semiconductor transient voltage and current ratings are limiting and must be carefully observed during the design procedure.

When first developed, the cost of the power semiconductor devices was prohibitive, but costs fell steadily as production grew. AC speed control systems using static frequency converters are now highly competitive with more traditional methods. The proof of this competitiveness lies in the widespread application of such equipment and in the wide range of units, from a few kVA to several tens of thousands of kVA in single unit, now available from various manufacturers. In future years, as circuit development continues and power semiconductor and microprocessor control costs

fall, there is no doubt that the use of static frequency converters will continue to grow in importance.

2.3 Inverter operation

An approximation of an induction motor equivalent circuit is illustrated in the figure 2.1,

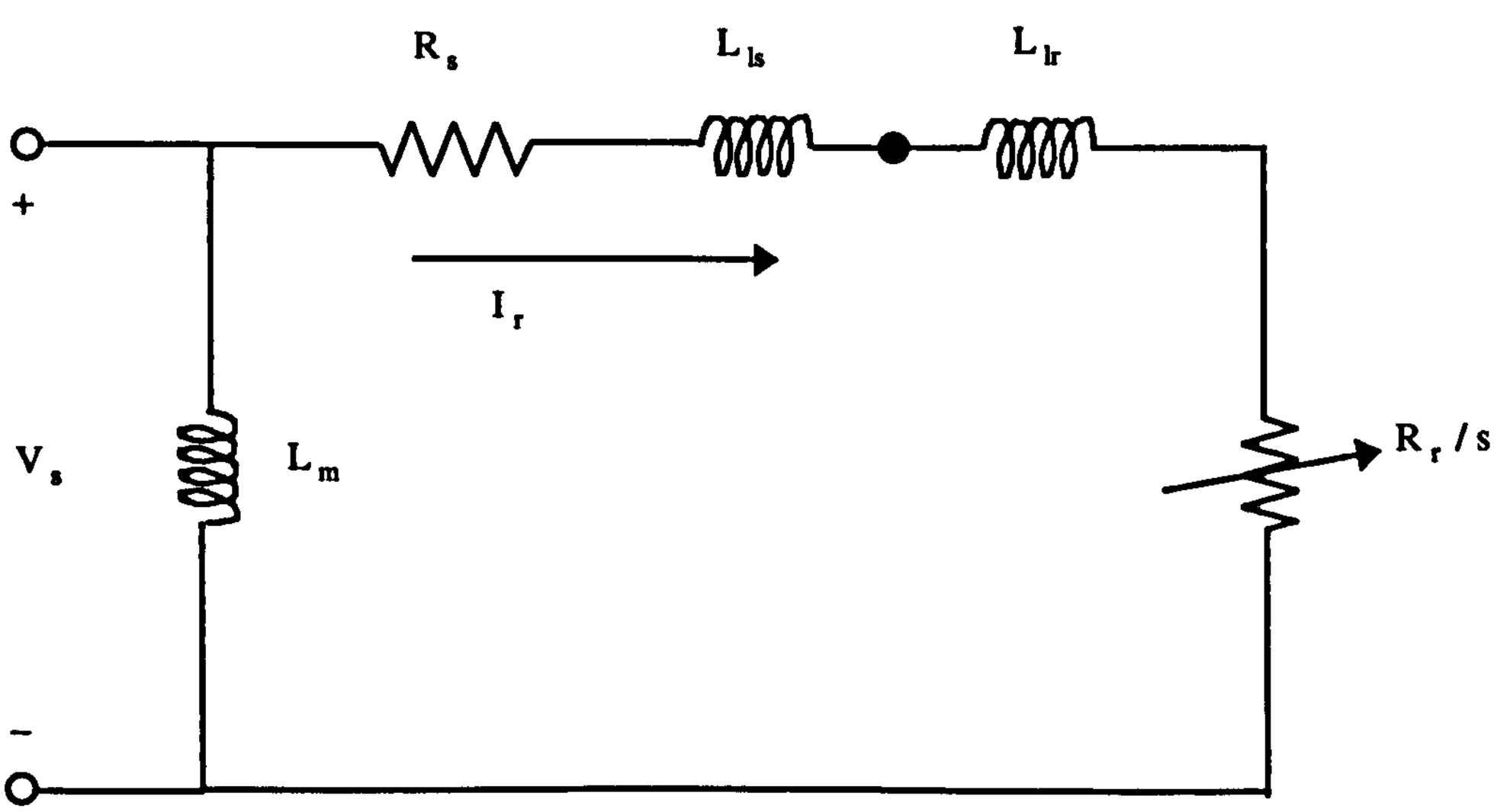

Figure 2.1 Approximate equivalent circuit of an induction motor

where, V_s is the stator voltage, L_m is the magnetising inductance, R_s is the stator resistance, L_{ls} is the stator leakage inductance, L_{lr} is the rotor leakage inductance, R_r is the rotor resistance and s is the slip of the motor ,with all the rotor parameters referred to the stator. For this system the equation for the developed torque will be given by [1]:

$$T_e = 3\left(\frac{P}{2}\right)\left(\frac{V_s}{\omega_e}\right)^2 \frac{\omega_{sl} R_r}{R_r^{\,2} + \omega_{sl}^{\,2} L_{lr}^{\,2}} \qquad (2.1)$$

where P is the number of poles, ω_e is the supply frequency and ω_{sl} is the slip frequency of the motor. If the stator frequency is increased beyond the rated value,

the air gap flux and the stator current will decrease according to the following equations,

$$\psi_m = \frac{V_s}{\omega_e} \tag{2.2}$$

$$I_r = \frac{sV_s}{\sqrt{R_r^2 + \omega_{sl}^2 L_{lr}^2}} \tag{2.3}$$

$$I_s = I_r + I_m \tag{2.4}$$

where ψ_m is the air gap flux and I_r is the rotor current (referred to the stator), I_m is the magnetising current and I_s is the stator current. Because of the reduction of the air gap flux and the stator current the maximum developed torque will also decrease. The maximum developed torque as a function of slip can be given from equation (2.5)

$$T_{em} = 3\left(\frac{P}{2}\right)\left(\frac{V_s}{\omega_e}\right)^2 \frac{\omega_{slm} R_r}{R_r^2 + \omega_{slm}^2 L_{lr}^2} \tag{2.5}$$

where $\omega_{slm} = R_r / L_{lr}$ is the slip frequency at maximum torque.

If an attempt is made to decrease the supply frequency at rated voltage, the air gap flux will saturate, causing excessive stator current. Therefore the region below the base frequency ω_b should be accompanied by the corresponding reduction of stator voltage so as to maintain constant air gap flux.

In order to produce constant torque, the controller must maintain a constant flux and consequently a constant V/Hz output. As the frequency decreases, the maximum torque available and the breakdown torque decreases. This is caused by the stator resistance voltage drop which becomes significant at lower frequencies where low

voltage would be applied. This reduction in maximum torque at low frequencies can be overcome by introducing an offset or voltage boost at low frequencies. This voltage would be adjusted to offset the resistance voltage drop of the stator winding. The resulting V/Hz characteristic is shown in figure 2.2. Once the offset is adjusted, the motor will develop constant torque over the speed range. Up to this point, only constant torque operation has been discussed. However, the V/Hz curve, can be adjusted to provide constant horsepower operation above synchronous speed.

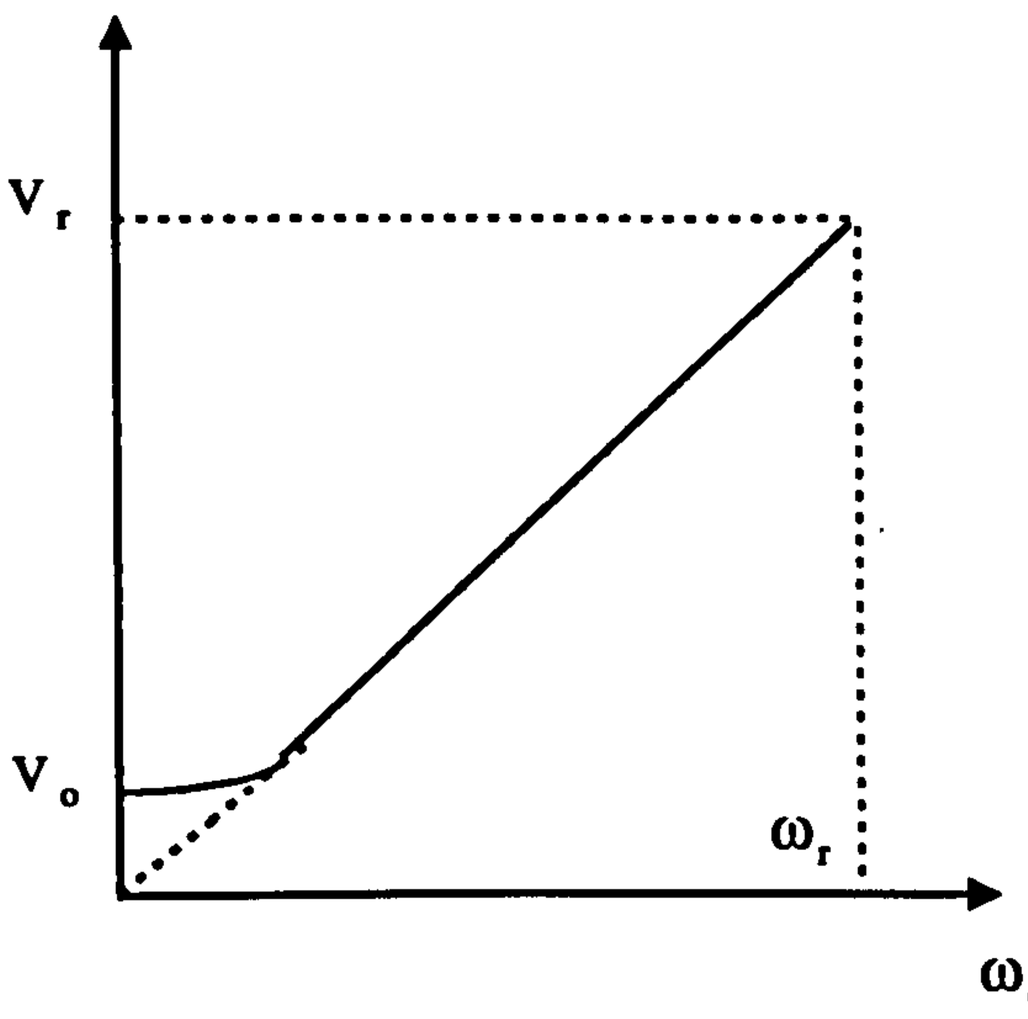

Figure 2.2 Volts/Hertz with offset voltage

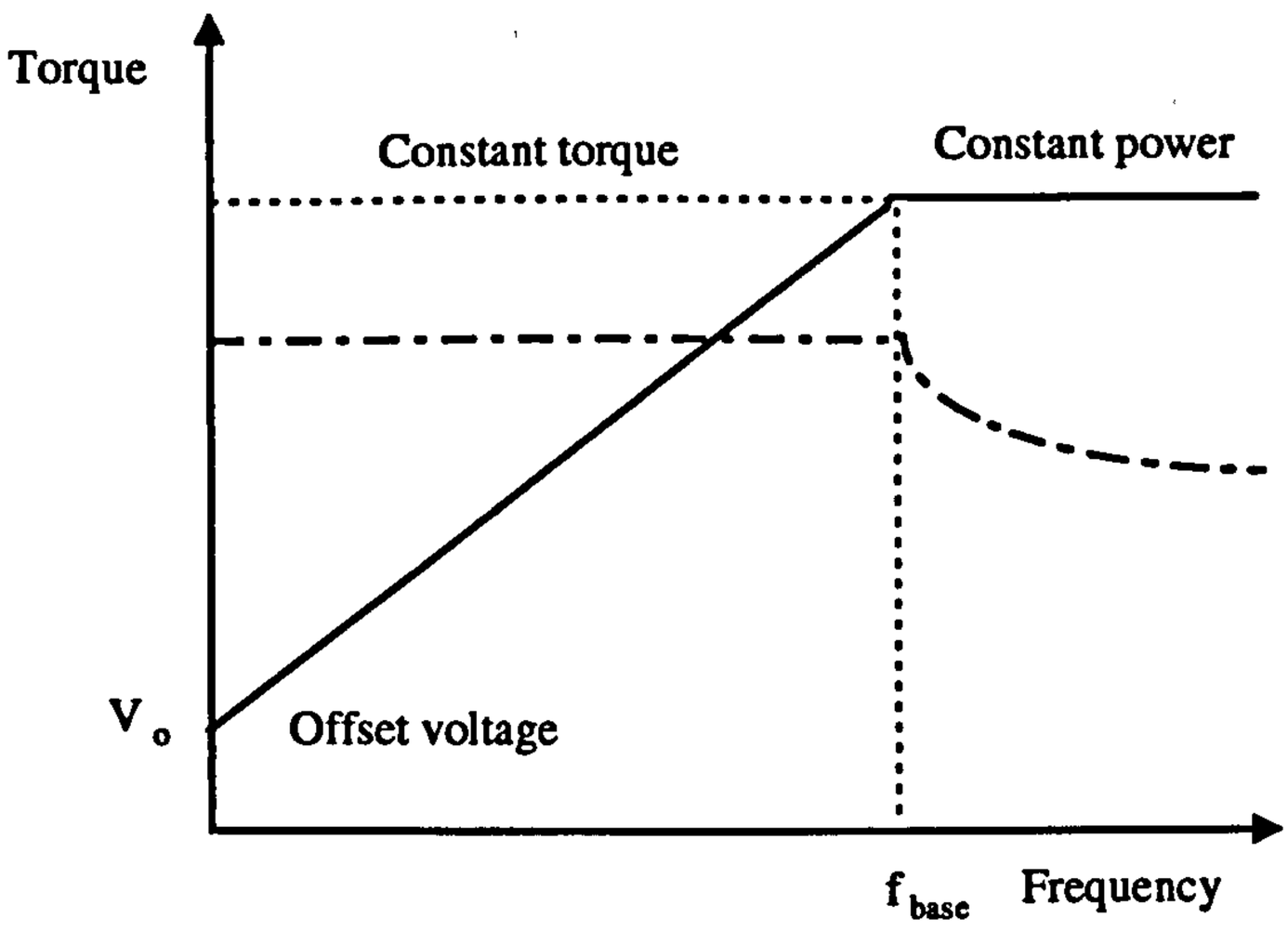

Figure 2.3 Voltage-frequency relation of an ac machine

Figure 2.3 shows the resulting speed-torque curve of an induction motor and the associated controller V/Hz output. Above base speed the magnitude of the motor flux decreases and therefore so does the rotor torque[1].

The most common way of producing a variable voltage, variable frequency supply is to use an inverter circuit. In an inverter circuit, the main incoming AC supply is first rectified to DC. The DC voltage will contain ripple which is filtered by using an R-L-C filter which helps to ensure a nearly constant D.C. input voltage. The resulting ' clean ' DC is then inverted using an inverter. The anti-parallel diodes across the inverter ensure that any inductive load current is diverted away from the switching devices when they are off. These diodes are also used for regeneration feeding power back into the D.C. line.

There are two main ways of producing a variable voltage output. The first solution is to use a controlled rectifier at the incoming end of the inverter. This produces a variable voltage DC bus level. The inverter then inverts the DC voltage level to AC using six-step inversion. The circuit required to achieve this is shown below.

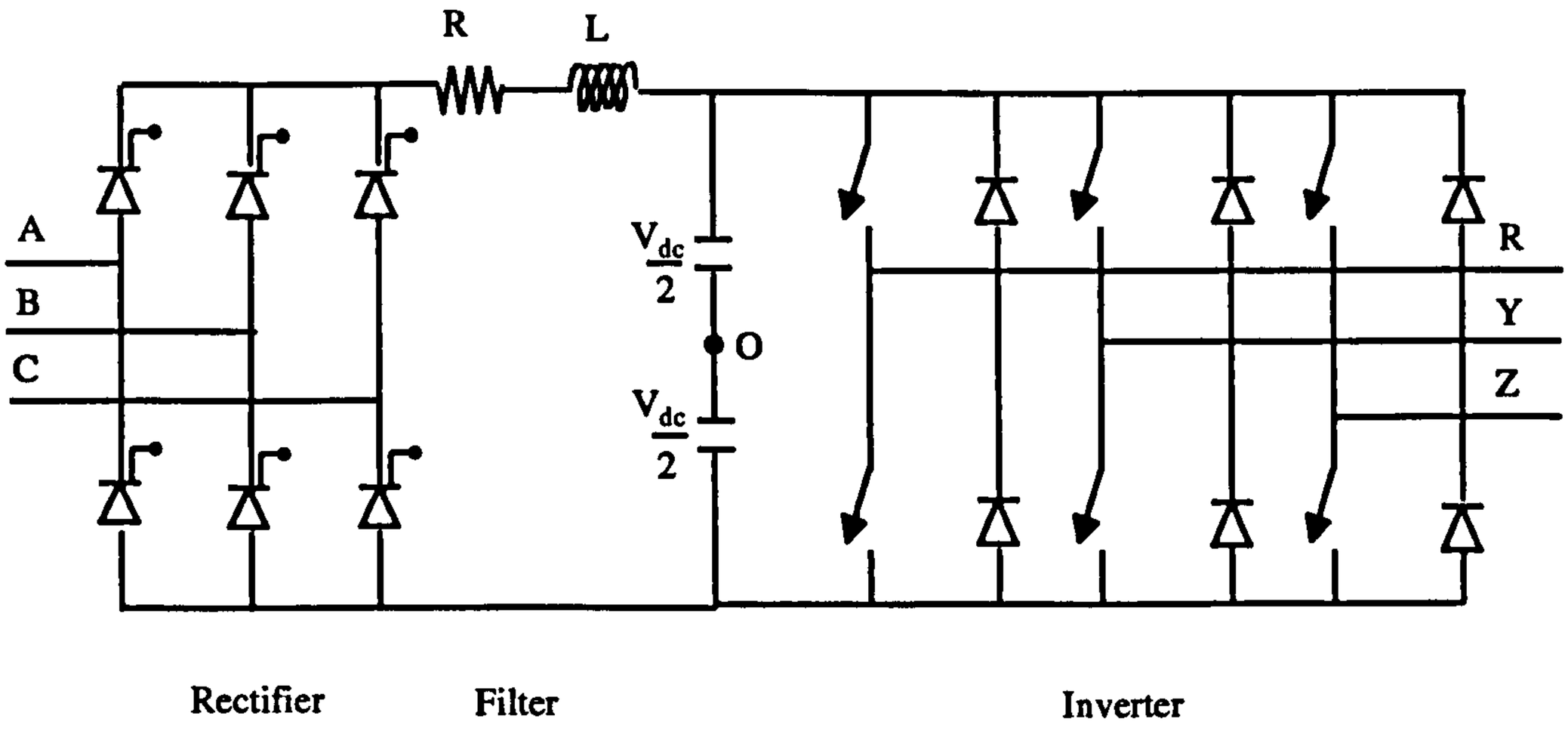

Figure 2.4 Six-step voltage source inverter

The principles of six-step inversion are discussed later. The second way to achieve the variable voltage output of the inverter is to have a constant voltage DC bus level and use PWM strategy to achieve the variable voltage output. The circuit required to implement this inversion strategy is shown below.

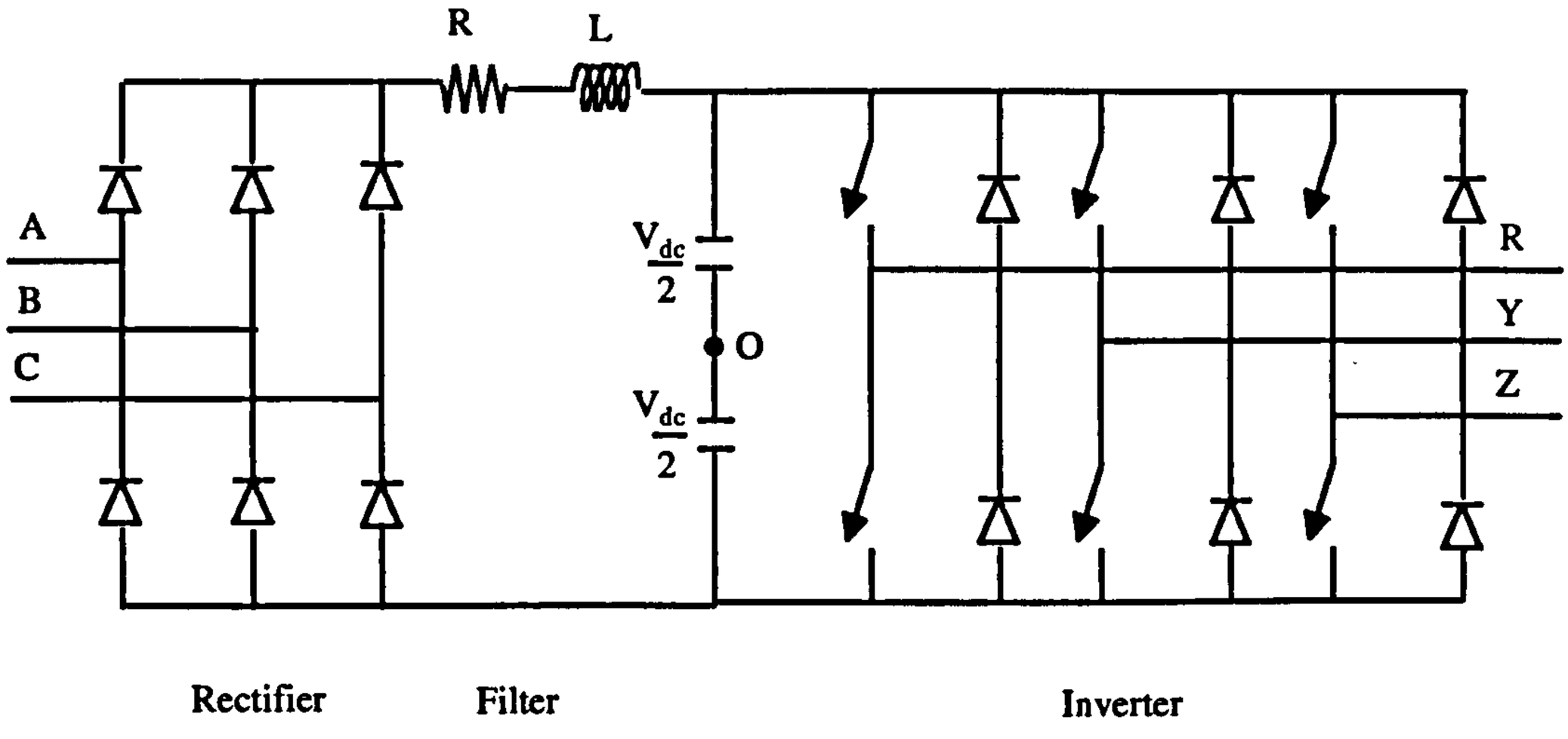

Figure 2.5 PWM voltage source inverter

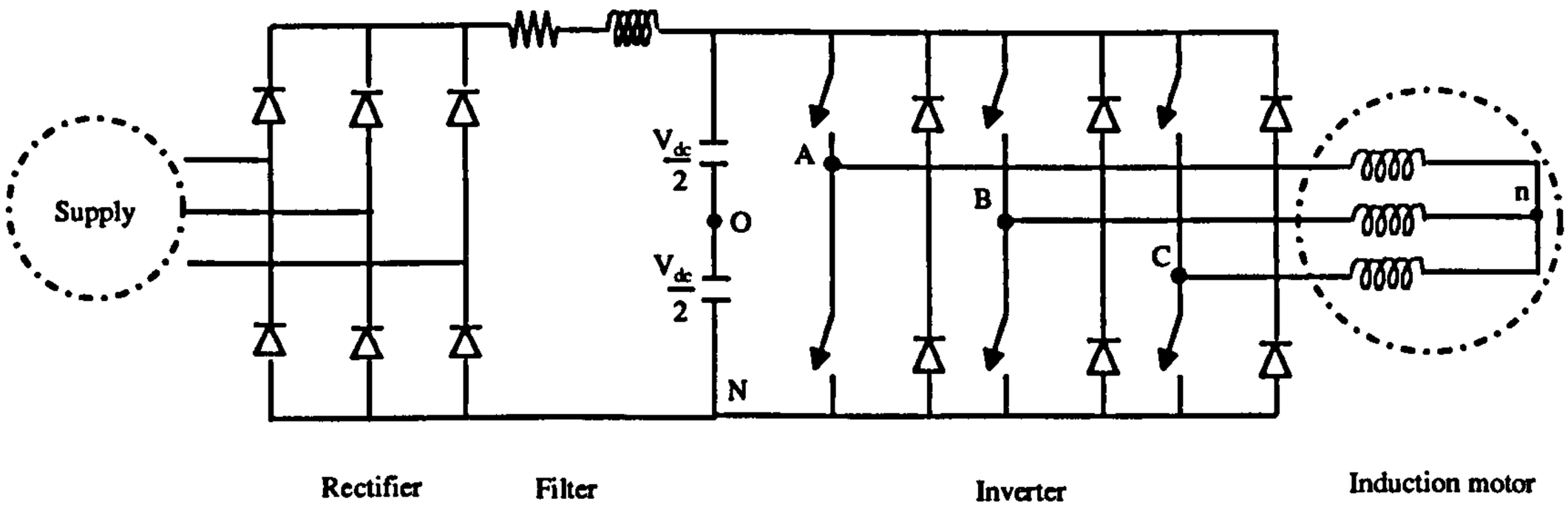

Figure 2.6 PWM inverter connected to an induction motor

There are many PWM inverter strategies currently employed to control inverters. To clarify the current situation, there are three distinct approaches. The first and most commonly used is the method which uses analogue techniques - natural sampling. The second strategy is a software implemented technique - regular sampling, and the third method uses the so-called optimised PWM switching strategy.

The way in which the PWM technique is performed depends on the application of the inverter. The higher switching frequency of the inverter the more precisely desired output can be developed. The use of microprocessors plays an important role in the flexibility of the PWM generation.

2.3.1 Six-Step Voltage-fed Inverter

The three-phase six-step, or quasi-square-wave, inverter is a voltage-source inverter that has been widely used in commercial adjustable-speed ac motor drives. As shown in figure 2.4 the inverter consists of three half-bridge units where the upper and lower thyristors (GTO's) of each unit are switched on and off alternately for 180° intervals. Recent advances in the semiconductor technology include the use of controllable switches (such as GTO's, MOSFETs, BJTs) which have the ability to be turned on and off by control signals applied to the control terminal of the devices.

The three half-bridges are phase-shifted by 120° and the dc supply voltage is assumed centre-tapped for convenience of waveform synthesis. The inverter output voltage wave shapes are determined by the circuit configuration and switching pattern and are not affected by the load condition. These waveforms are rich in harmonics, but the current waves are somewhat smoother, due to the filtering effect of the load. The bypass diodes of the inverter permit reverse current flow during regeneration.

The phase voltages with respect to the centre tap can be described by Fourier series as follows[3]:

$$V_{AO} = \frac{2}{\pi} V_{dc}\left(\sin \omega t + \frac{1}{3}\sin 3\omega t + \frac{1}{5}\sin 5\omega t + \ldots\ldots\ldots\right) \quad (2.6)$$

$$V_{BO} = \frac{2}{\pi} V_{dc}\left(\sin(\omega t - 2\pi/3) + \frac{1}{3}\sin 3(\omega t - 2\pi/3) + \frac{1}{5}\sin 5(\omega t - 2\pi/3) + \ldots\ldots\ldots\right) \quad (2.7)$$

$$V_{CO} = \frac{2}{\pi} V_{dc}\left(\sin(\omega t + 2\pi/3) + \frac{1}{3}\sin 3(\omega t + 2\pi/3) + \frac{1}{5}\sin 5(\omega t + 2\pi/3) + \ldots\ldots\ldots\right) \quad (2.8)$$

The line voltages can therefore be constructed as

$$V_{AB} = V_{AO} - V_{BO}$$
$$V_{BC} = V_{BO} - V_{CO} \qquad (2.9)$$
$$V_{CA} = V_{CO} - V_{AO}$$

The line voltage waves have a characteristic six-stepped wave shape with the presence of odd harmonics $6n \pm 1$, where n is any positive integer. The fundamental and harmonic voltages are balanced and mutually shifted by 120°. This type of inverter is defined as a square or stepped-wave inverter because of the characteristic wave shapes.

The complete Fourier series expression for the line voltage is

$$V_{AB} = \frac{2\sqrt{3}}{\pi} V_{dc}\left(\sin(\omega t + \pi/6) - \frac{1}{5}\sin 5(\omega t + \pi/6) - \frac{1}{7}\sin 7(\omega t + \pi/6) + \ldots\ldots\ldots\ldots\right) \quad (2.10)$$

$$V_{BC} = \frac{2\sqrt{3}}{\pi} V_{dc}\left(\sin(\omega t - \pi/2) - \frac{1}{5}\sin 5(\omega t + \pi/2) - \frac{1}{7}\sin 7(\omega t + \pi/2) + \ldots\ldots\ldots\ldots\right) \quad (2.11)$$

$$V_{CA} = \frac{2\sqrt{3}}{\pi} V_{dc}\left(\sin(\omega t + 5\pi/6) - \frac{1}{5}\sin 5(\omega t + 5\pi/6) - \frac{1}{7}\sin 7(\omega t + 5\pi/6) + \ldots\ldots\ldots\right) \quad (2.12)$$

For the wye-connected load with isolated neutral as shown in figure 2.6, it is possible to express the inverter phase output voltages (with respect to the load neutral n), in terms of the inverter output voltages with respect to the negative dc bus N:

$$V_{AO} = V_{An} + V_{nN}$$
$$V_{BO} = V_{Bn} + V_{nN} \qquad (2.13)$$
$$V_{CO} = V_{Cn} + V_{nN}$$

Since for balanced three-phase supply $V_{An} + V_{Bn} + V_{Cn} = 0$, adding the equations above we get

$$V_{nO} = \frac{1}{3}\left(V_{AO} + V_{BO} + V_{CO}\right) \tag{2.14}$$

Therefore , substituting (2.14) at (2.13) yields

$$V_{An} = V_{AO} - V_{nO} = \frac{1}{3}\left(2V_{AO} - V_{BO} - V_{CO}\right)$$

$$V_{Bn} = V_{BO} - V_{nO} = \frac{1}{3}\left(2V_{BO} - V_{AO} - V_{CO}\right) \tag{2.15}$$

$$V_{Cn} = V_{CO} - V_{nO} = \frac{1}{3}\left(2V_{CO} - V_{AO} - V_{BO}\right)$$

These voltage waveforms are valid for any balanced three-phase load or ac motor.

Figure 2.8 illustrates the voltage waveforms for the three phase six-step inverter.

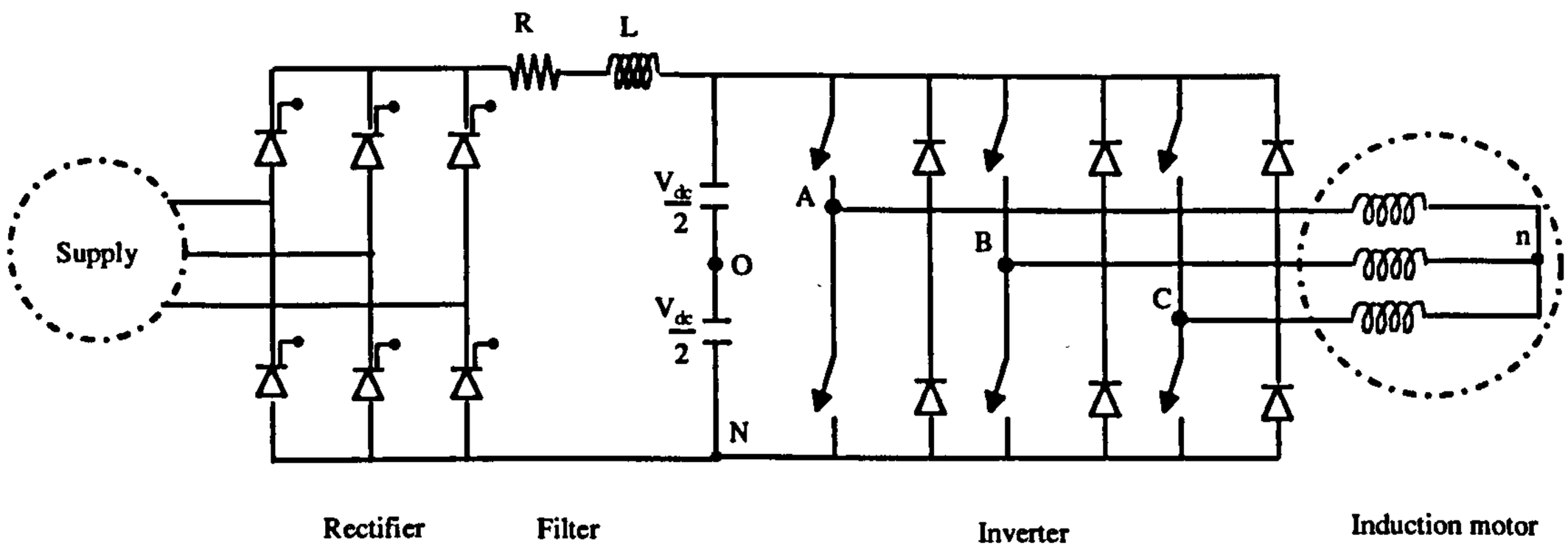

Figure 2.7. Six-step inverter connected to an induction motor

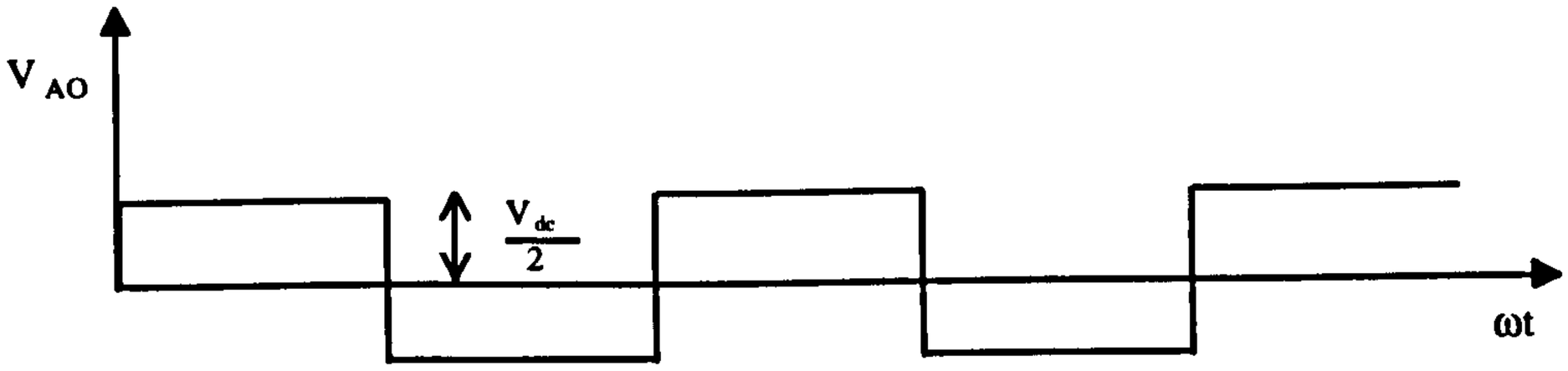

(a)

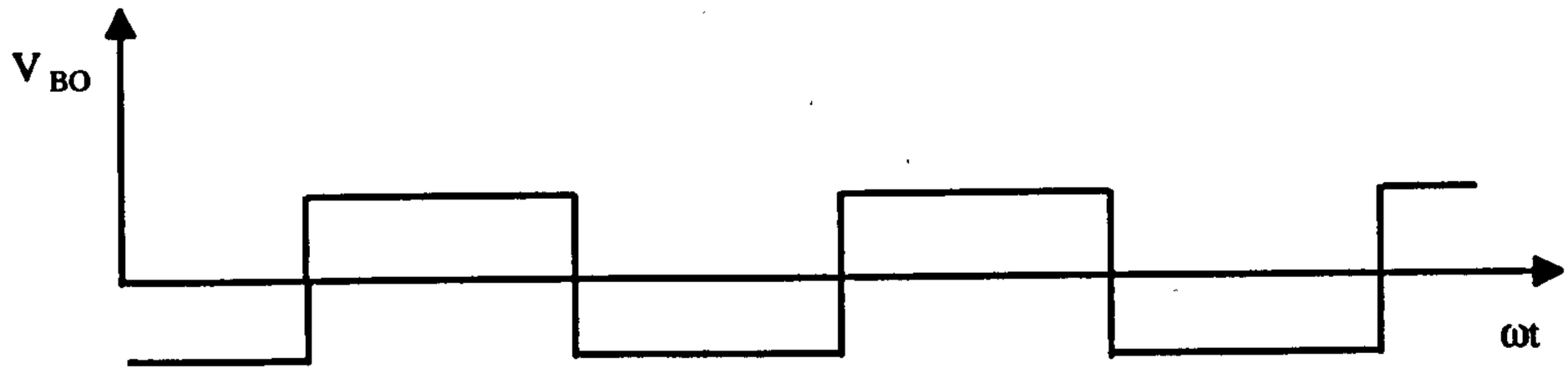

(b)

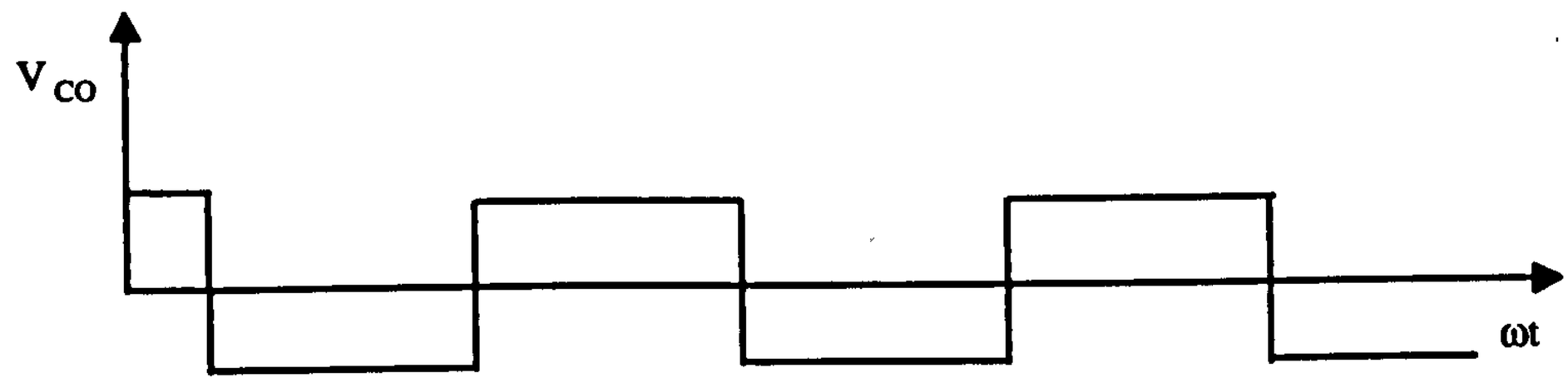

(c)

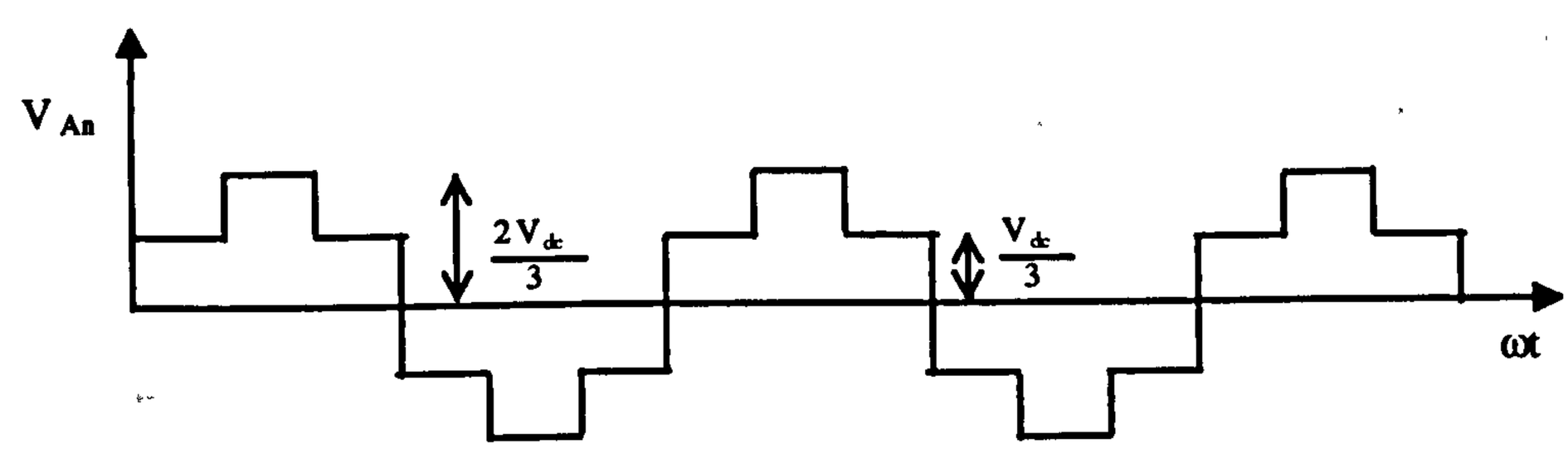

(d)

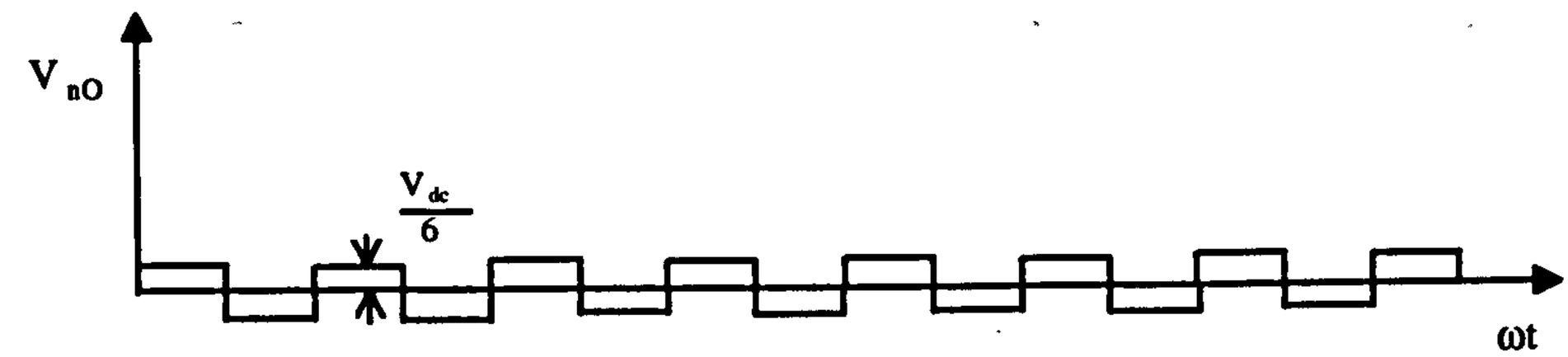

(e)

Figure 2.8 Voltage waveforms for a three-phase six-step inverter,(a),(b),(c) pole voltages,(d) phase voltage,(e) voltage between neutral and dc midpoint

2.3.2 PWM Inverters

It is generally recognised that PWM inverters offer a number of advantages over rival convertor techniques[4-14]. These advantages are usually gained at the expense of more complex control and power circuit configurations. Developments of PWM inverter systems should eliminate many of the practical limitations which have been experienced in the past, and allow the full potential and versatility of PWM control techniques to be realised.

An analytical approach to investigate a wide range of PWM systems, uses the digital computer to model the PWM process, employing software simulation techniques. The computer model can then be used as the basis for computer investigations of a wide range of operating modes, using both time and frequency domain analysis techniques. It is possible, by surveying the literature over the last decade[4], to trace the historical development of PWM inverter control techniques and relate these developments to the changes in technology. To clarify the current situation, it is helpful to recognise three distinct approaches currently in vogue to formulate the PWM strategy. The first, and the one which has been most widely used because of its ease of implementation using analogue techniques, is based on "natural sampling"[5,6]. Another switching strategy[3], referred to as "regular sampling", has been proposed which is considered to have a number of advantages when implemented using digital or microprocessor techniques. The third approach uses the so-called "optimal" PWM switching strategies which are based on the minimisation of certain performance criteria[7]; for example, elimination or minimisation of particular harmonics, or the minimisation of harmonic current distortion, peak current, torque ripple, etc.

a) Natural sampling

Most analogue implemented PWM inverter control schemes employ natural sampling techniques. A practical implementation, showing the general figures of this mode of

sampling, is illustrated in figure 2.9. From this figure, it can be seen that a triangular carrier wave (sampling signal) is compared directly with a sinusoidal modulating wave to determine the switching instants, and therefore the resultant pulse widths.

It is important to note that, because the switching edge of the width-modulated pulse is determined by the instantaneous intersection of the two waves, the resultant pulse width is proportional to the amplitude of the modulating wave at the instant that switching occurs. This has two important consequences: the first is that the centres of the pulses in the resultant PWM are not uniformly spaced and secondly it is not possible to define the widths of the pulses using analytic expressions.

The second point above means that it is not feasible to calculate the width of the modulating pulses using a software routine in a real time situation. Indeed, the switching points can only be obtained by solving the following transcendental equation using a numerical method based on successive iterations such as the Newton-Raphson method.

$$t_P = \frac{T}{2}\left(1+\frac{M}{2}\sin(\omega_m t_1 + \sin\omega_m t_2)\right) \qquad (2.16)$$

where t_P is the pulse length, T is the period of the carrier signal, M is the modulation index, t_1 and t_2 are the present and next switching points. The solution of the above equation using the Newton-Raphson method will have the form

$$x_{i+1} = x_i - \frac{f(x_i)}{f'(x_i)} \qquad (2.17)$$

where x_{i+1} is the switching angle at the next point, x_i is the switching angle at the present point, and $f(x_i)$ is a function that includes both the modulating and the carrier signal.

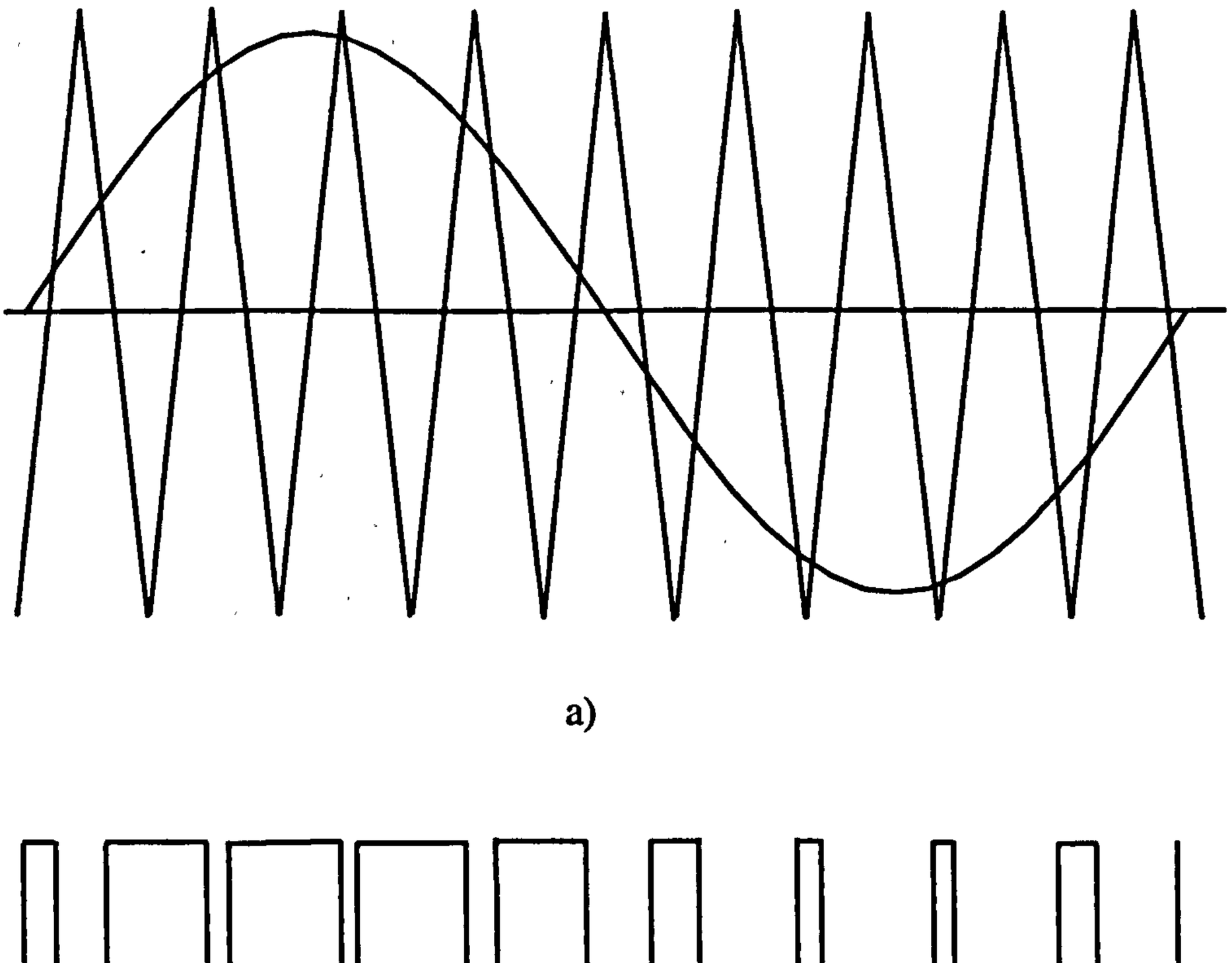

a)

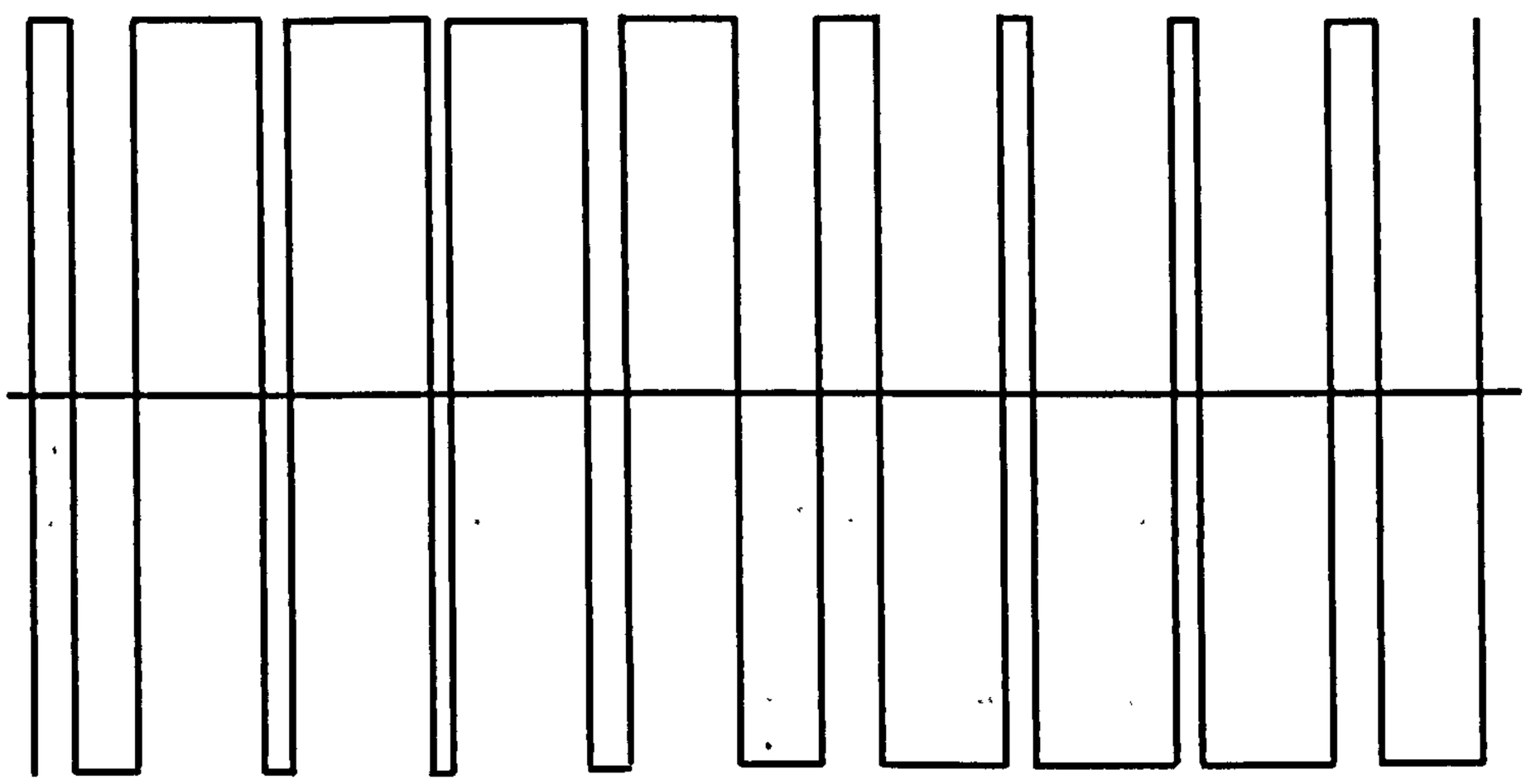

b)

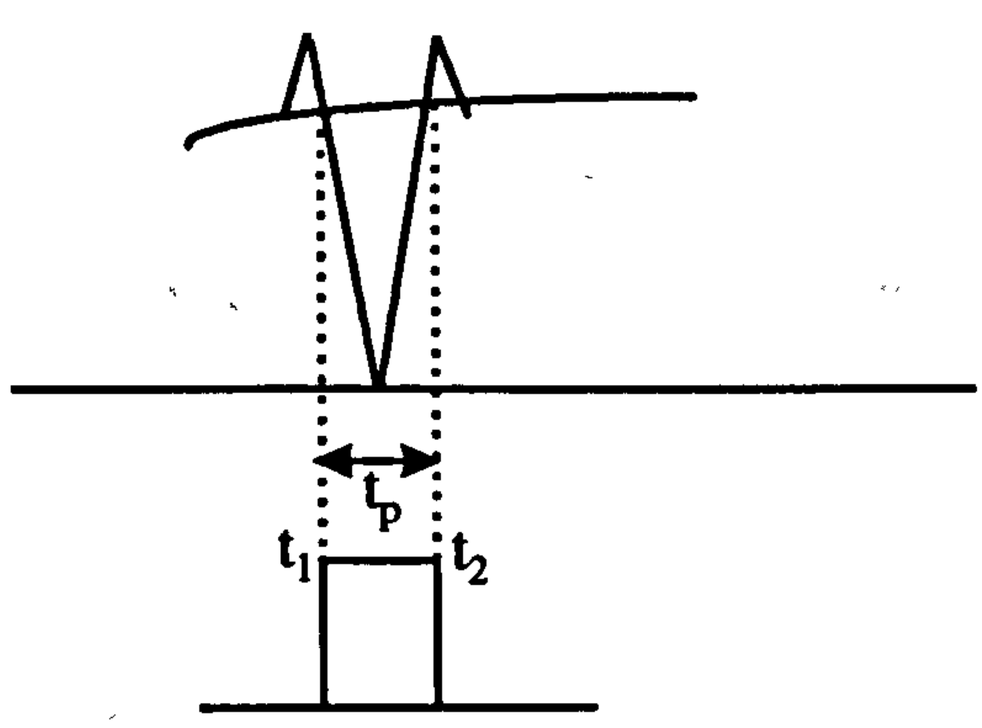

(c)

Figure 2.9 Waveforms for the natural sampling PWM

The only way to realise natural sampling PWM using a microprocessor is to calculate the switching angles on a computer and store them in ROM for call up by a control microprocessor. The waveform of the figure 2.9(b) is the typical of the inverter line to the DC link centre-tap voltage, and includes the carrier frequency harmonics. If the carrier frequency is a multiple of 3 of the modulating frequency, these harmonics will cancel out in the lines. A common carrier can be used for all the three phases. The output voltage waveform contains a fundamental component of which the frequency and the amplitude can be varied by varying the frequency and voltage, respectively of the modulating wave. A Fourier analysis of the output wave will have the following form:

$$V(t) = m\frac{V_d}{2}\sin(\omega_s t + \varphi) + \text{Bessel function harmonic terms} \qquad (2.18)$$

where m is the modulation index, ω_s is the fundamental frequency and φ is the phase shift of the output depending on the position of the modulating wave.

There are many features common to all PWM techniques which must be taken into consideration for a real inverter system. For brevity, these will only be mentioned for natural sampling PWM.

1. Minimum pulse width and pulse elimination. In practise, it is necessary to ensure that the minimum delay time for switching devices in the inverter power circuit is maintained to safequard the inverter commutating ability and to prevent short circuits on the DC link. At modulation depths close to unity, and when overmodulation is used, pulses appear in the PWM voltage waveform with widths below a certain value. The process of eliminating these short pulses is sometimes referred as pulse-dropping, and the width of the pulses which are dropped depends on the particular inverter power circuit used and the type of power electronic devices. For reliable inverter operation, it is therefore essential that any theoretical PWM control strategy should take due account of this requirement. The most common way to implement pulse dropping is to hold the pulse to be eliminated at its minimum width and then suddenly drop it. This has the effect of producing a non-linear voltage/frequency characteristic and also increasing the magnitude of the lower odd

harmonics. The main advantage of this method is its simplicity and its ability to be implemented in an analogue system.

2. Carrier frequency ratio changing. The generation of subharmonics in the inverter output can be avoided if the carrier frequency is varied so that it is always an integer multiple of the modulating frequency, i.e. the modulating and the carrier frequency are said to be synchronous. The output contains harmonics that are only integer multiples of the fundamental frequency. Therefore, the synchronous PWM method is capable of producing a waveform in which the unwanted components are at a frequency much higher than that of the fundamental. Changes in carrier ratio are designed so that the inverter switching frequency lies between predetermined upper and lower limits: The upper limit avoids excessive inverter switching losses, and the lower limit maintains good waveform quality without excessive current ripple. A large number of gear changes are necessary when operation is required down to very low output frequencies, but waveform quality is excellent.

In an AC variable-speed drive, the required frequency range is commonly 10:1 and is often greater. It is not usually practical to allow the carrier frequency to vary so widely. For high carrier ratios, however, waveform quality is unaffected by the adoption of a free-running strategy in which carrier and reference waveform are unsynchronised. With the carrier frequency remain constant, as the reference frequency increases, the carrier ratio falls and the unsynchronised waveforms produce low-frequency subharmonic beat components in the inverter output voltage. As a result the PWM waveform may vary slightly from cycle to cycle. For large carrier ratios, these beat-frequency subharmonics are negligible, but when the carrier ratio is less than nine, the beating effect can cause intolerable low-frequency pulsations in motor current, torque, and speed. Consequently, as the output frequency is increased and the carrier ratio falls below nine, the PWM inverter must transition to a synchronised mode of operation. Practical systems have an asynchronous carrier for modulation indexes of 0-0.9 followed by a synchronous above 0.9. Above 0.9 the ratio is usually 9 or 12 i.e an integer multiple of 3.

3. Lockout and associated losses and degradation of waveform. In order to prevent

short-circuit of the DC link, it is necessary to have a lockout period between the turning off of one device in a power leg and the turning on of the other device. This lets the device which has turned off regain its blocking state before the other device is turned on. This has an obvious effect on the resulting output since the switching times are not those required to achieve the desired output voltage. This causes a decrease in fundamental output voltage and the introduction of a pulse of the magnitude of the DC link voltage pulsating at carrier frequency and having a time span equal to that of the lockout time. This produces an energy loss proportional to the lockout time. Attempts have been made to lessen the effect of lockout by altering the modulation index and decreasing the lockout time to a minimum. However this problem will always exist since infinitely fast switching devices can not be manufactured.

4. Overmodulation. To utilise fully the voltage capabilities of the PWM inverter, it is usually necessary, in variable speed drives, to change from sinusoidal PWM operation into quasi-square-wave at some specified output frequency-usually base speed. One approach is to overmodulate the PWM waveform. As the modulation index approaches unity, adjacent pulses progressively merge (using pulse elimination strategies) redusing the effective PWM pulse number, until the quasi-square condition is reached. This effect gives a peak sinusoidal output voltage of $2/3\ V_{dc}$.

In summary, natural sampling is a simple analogue method for producing a PWM inverter output. However, control of the voltage-frequency characteristic is difficult around modulation indexes of 0.9-1 where pulse dropping occurs unless complex algorithms are used which defeats natural samplings main-benefit- its simplicity.

b) Regular symmetric sampled PWM

Regular sampling PWM control is a software implemented approximation to sinusoidal PWM control. Figure 2.10 illustrates the waveforms for the regular symmetric sampled PWM. In this mode of control, the amplitude of the modulating signal α (figure 2.10(a))at the sample instant t_1 is stored by a sample-and hold circuit(operated at the carrier frequency), and is maintained at a constant level during the intersample period t_1 and t_2 until the next sample is taken. This produces a sample-hold, or amplitude-modulated, version of the modulating signal b . Comparison of this signal with the carrier signal c (figure 2.10(b)) defines the points of intersection used to determined the switching instants of the width-modulated pulses. As a result of this process, the modulating wave has a constant amplitude while each sample is being taken, and so the widths of the pulses are proportional to the amplitude of the modulating wave at uniformly spaced sampling times[3].

It is an important characteristic of regular sampling that the sampling positions and sampled values can be defined unambiguously, such that the pulses produced are predictable both in width and position. This was not the case with natural sampling as discussed earlier in this report.

Because of this ability to define precisely the pulse configuration, it is now possible to derive a simple trigonometric function to calculate the pulse widths. With reference to figure 2.10 (c) the width of a pulse may be defined in terms of the sampled value of the modulating wave taken at time t_1. Thus

$$t_p = \frac{T}{2}\left(1 + M\sin(\omega_m t_1)\right) \qquad (2.19)$$

The first term of this equation refers to the unmodulated carrier frequency pulse width, and the second term corresponds to the sinusoidal modulation required at time t_1 . This equation can be used to calculate the pulse widths directly. It is therefore possible to calculate pulse widths using microprocessor software based algorithms.

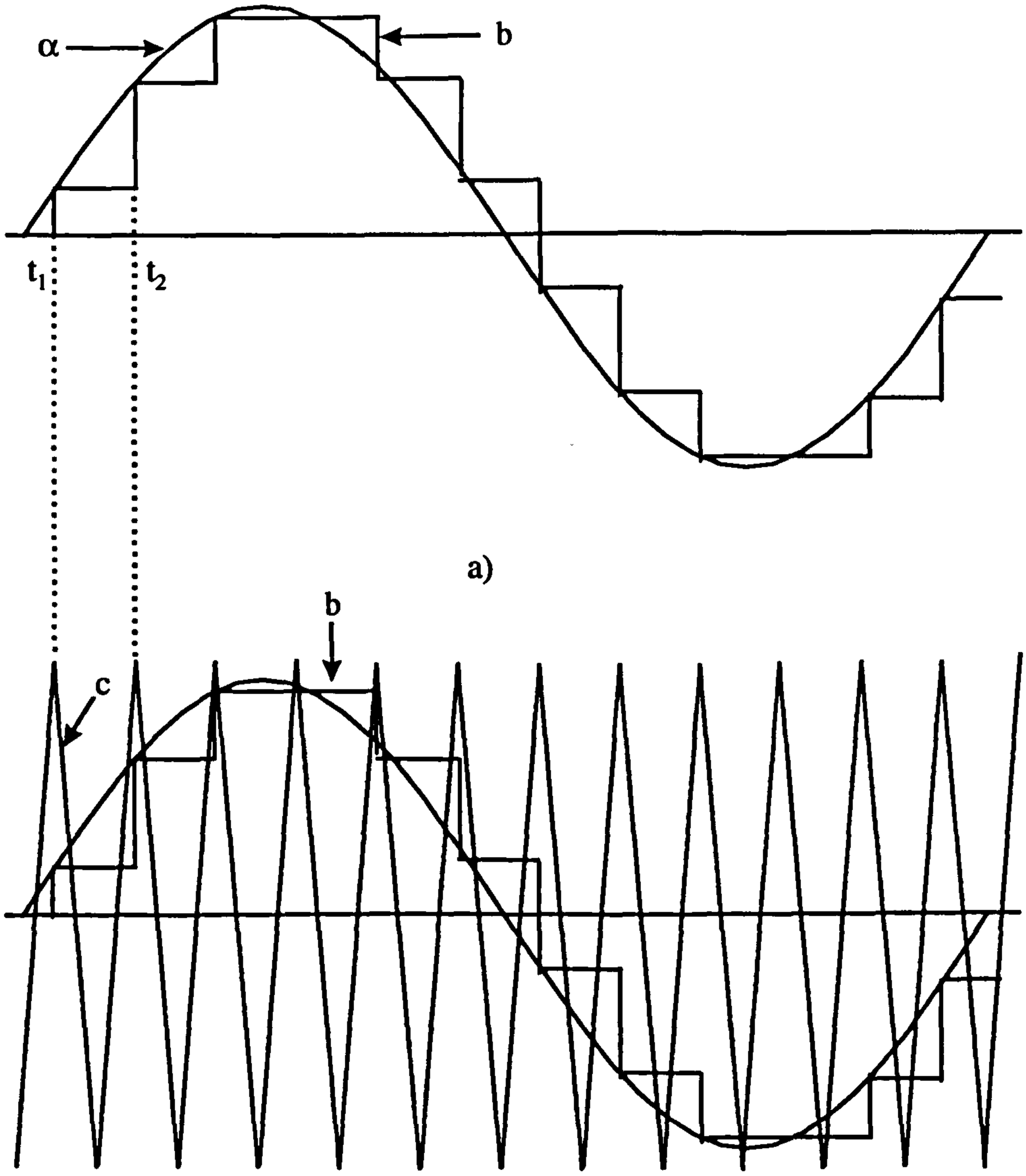

(c) Figure 2.10 Waveforms for the symmetric sampling PWM

c) Regular asymmetric sampled PWM

The type of modulation described before was one where the samples of the sine wave were taken only once per carrier cycle (at positive carrier signal peaks). If the samples are taken twice per carrier cycle (at both positive and negative carrier signal peaks), this produces a better approximation to the modulating sine wave. This is termed asymmetric regular sampling and is shown on figure 2.11. With reference to this figure the leading and the trailing edges of each pulse are determined, using two different samples of the modulating wave, taken at time instants t_1 and t_3 respectively. The width of the resulting pulse may be defined in terms of these sampling times as below,

$$t_p = \frac{T}{2}\left(1+\frac{M}{2}\left(\sin(\omega_m t_1)+\sin(\omega_m t_3)\right)\right) \qquad (2.20)$$

More information about the modulating wave is contained in the asymmetric modulated PWM waveform, its harmonic spectrum is superior to that produced using symmetric modulation. It should be noted however that the number of calculations required to generate asymmetric PWM is double that required for symmetric PWM. This can significant extend the computation time required if a microprocessor software based calculation is used to generate the PWM control waveform, and therefore reduces the maximum inverter output frequency.

In summary, regular sampling techniques give real time control capability with two degrees of accuracy- symmetric sampling and asymmetric sampling. Voltage boost can be achieved and pulse elimination strategies can be implemented by use of software elimination algorithms.

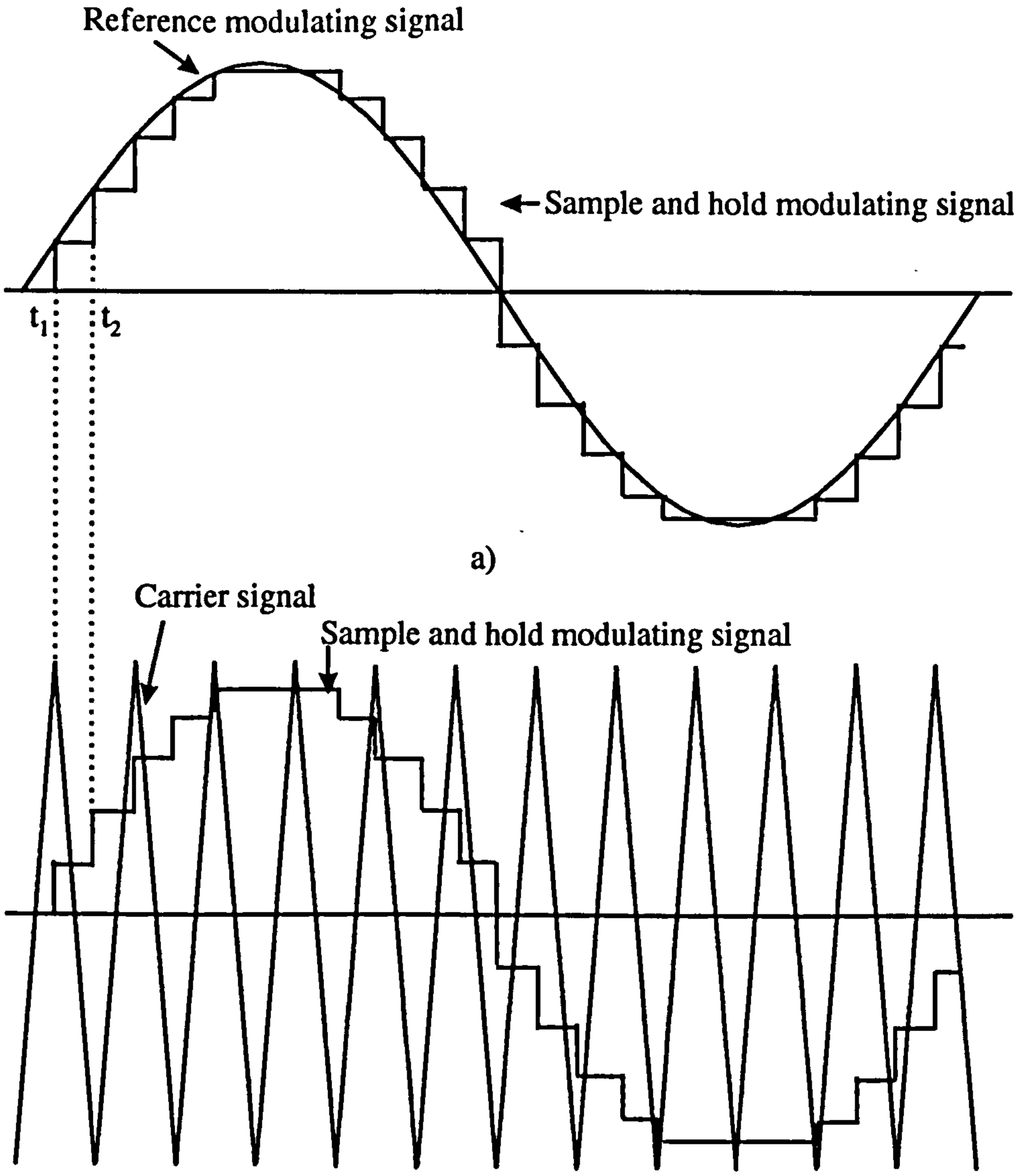

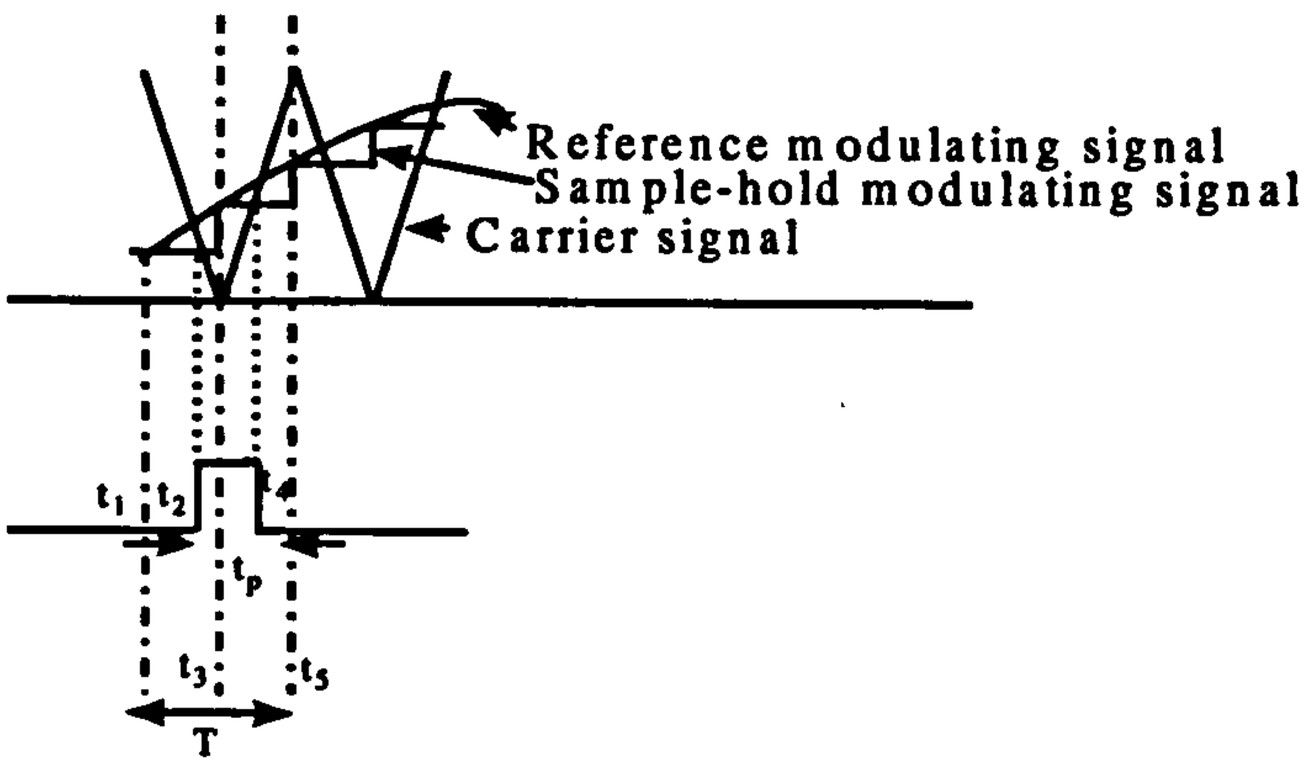

(c) Figure 2.11 Waveforms for the asymmetric sampling PWM

d) Selective Harmonic Elimination

Optimal PWM strategies enhance a specific characteristic of the inverter output or the motor performance by altering both the amount of switching angles per cycle and the value of switching angles themselves. In order to implement such strategies, the switching angles require to be calculated using a mainframe computer and stored in ROM in the inverter control circuit. Selective Harmonic Elimination is one of these methods.

It is assumed that the wave produced by selective harmonic elimination is periodic with quarter cycle symmetry, and half cycle antisymmetry as shown on figure 2.12 Fourier analysis on this figure gives the following equation for the magnitude of the voltage harmonics

$$V_n = \frac{2V_{dc}}{n\pi}\left(1+2\sum_{k=1}^{k}(-1)^k \cos(n\alpha_k)\right) \qquad (2.21)$$

This whole equation can be solved for all values of alpha for any set of zero harmonics using an iterative method such as the Newton-Raphson method already outlined in the natural sampling section. Since the waveform has both quarter cycle symmetry and half cycle antisymmetry, no even harmonics exist in the Fourier analysis. Only odd harmonics exist in the waveform. Multiples of the third harmonics are of no interest since these cancel in a three phase balanced isolated system. The harmonics left of interest are of the 5^{th},7^{th},11^{th} and 13^{th} orders. These produce the 6^{th} and 12^{th} order pulsating torques which are detrimental to machine performance. Thus eliminating these harmonics would eliminate the torques which are detrimental to low speed operation. The results of the iteration show that n+1 switching angles per quarter cycle are needed to eliminate n harmonics.

The main drawback of this method compared to the other PWM techniques that already been discussed is that the complete elimination of certain harmonics results in a marked increase in the magnitude of the lowest uneliminated harmonics. This method will not be used for modelling purposes in the analysis that will follow.

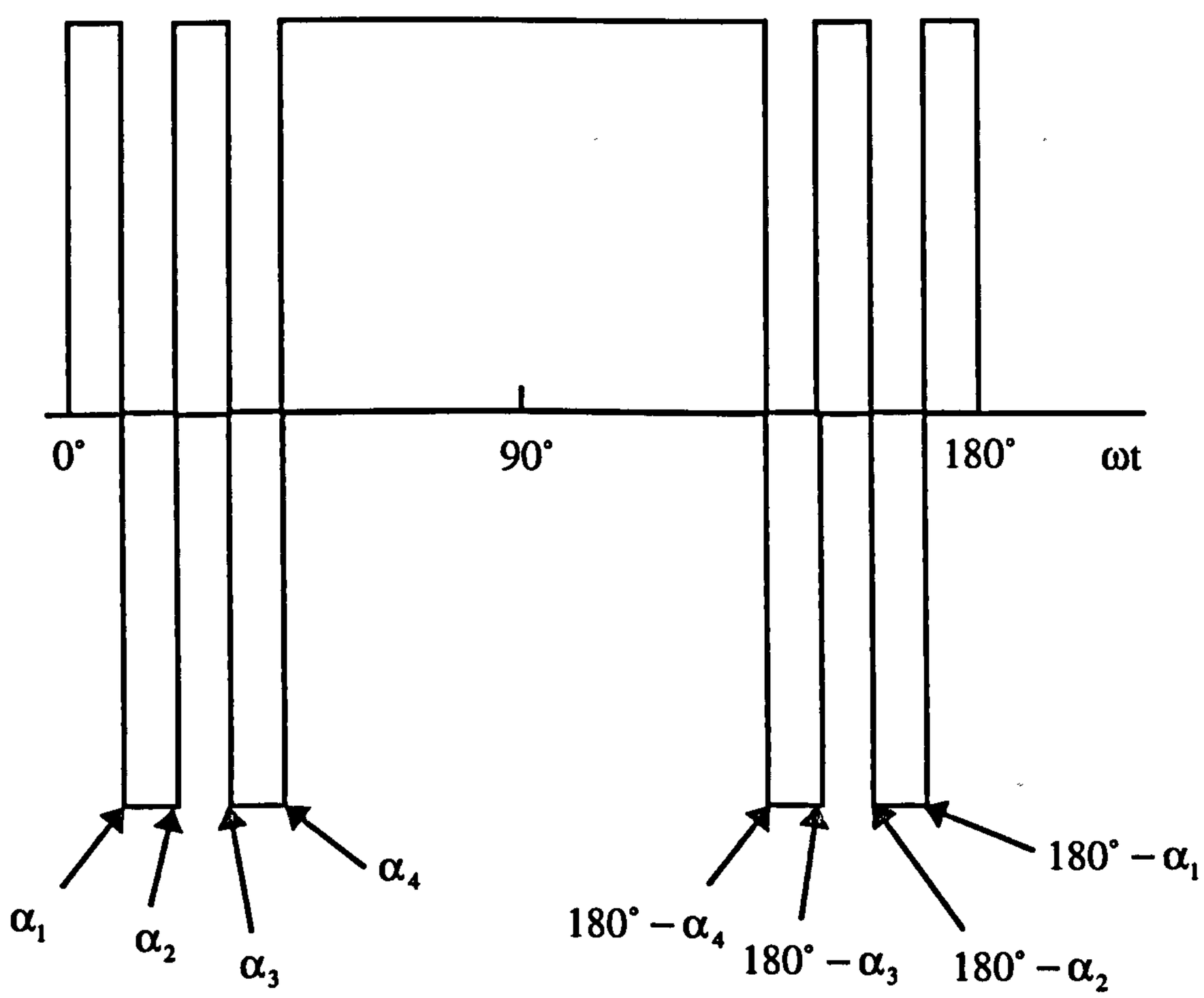

Figure 2.12 Voltage wave in harmonic elimination method

2.4 Electromagnetic braking

In adjustable-speed ac drives, the machines may be subjected to electrical braking for reduction of speed. In electrical braking, the motor is operated in the generating mode and the kinetic energy stored in the system inertia is converted to electrical energy. During braking, the voltage polarity across the dc-capacitor remains the same as in the motoring mode. Therefore, the direction of the dc bus current to the inverter gets reversed. Since the current direction through the diode rectifier bridge normally used in PWM drives cannot reverse, some mechanism must be implemented to handle this energy during braking; otherwise the dc-voltage can reach destructive levels.
One way to accomplish this goal is to switch on a resistor in parallel with the dc-bus capacitor as is shown in figure 2.13, if the capacitor exceeds a present level, in order to dissipate the braking energy.

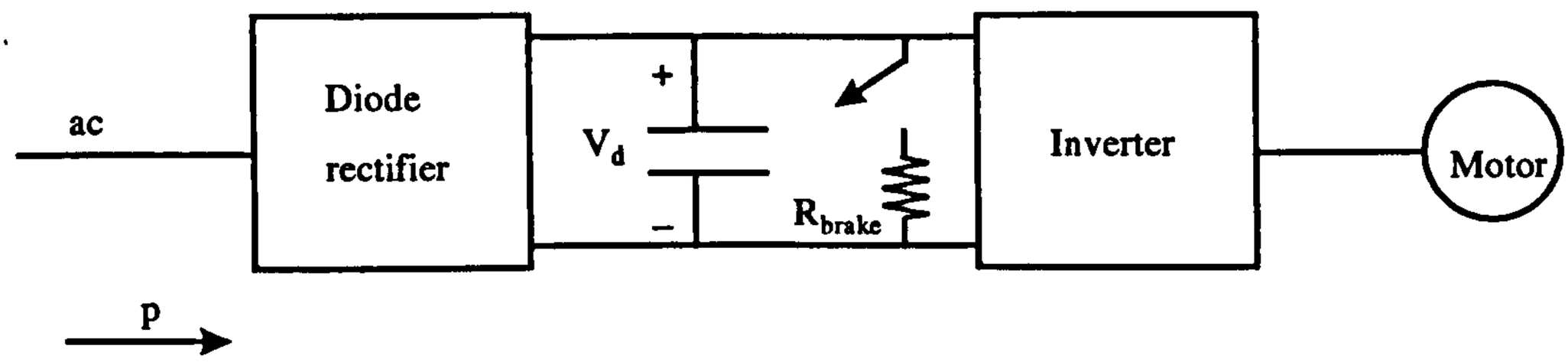

Figure 2.13 Dissipative braking

An energy-efficient technique is to use a four-quadrant converter at the front end in place of the diode bridge rectifier. This would allow the energy recovered from the motor-load inertia to be fed back to the utility supply, as shown in figure 2.14, since the current through the four-quadrant converter used for interfacing with the utility source can reverse in direction. This is called regenerative braking since the recovery energy is not wasted. The decision to employ regenerative braking over dissipative braking depends on the additional equipment cost versus the savings on energy recovered.

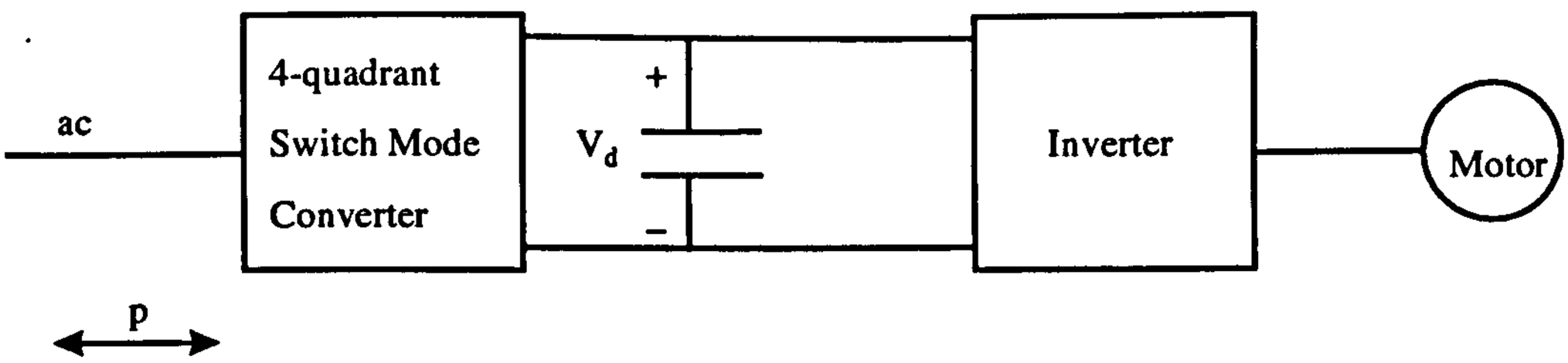

Figure 2.14 Regenerative braking

2.5 Control of variable-speed induction motor drives

The control of ac machines is considerably more complex than that of dc machines. The complexity arises because of the variable-frequency power supply, and complex dynamics of the ac machine. The induction machines can have various methods of control, and the particular method to be adopted depends on the nature of the application. Scalar control techniques relate to magnitude control of a variable, and the command and feedback signals are dc quantities which are proportional to the respective variables.

2.5.1 Implementation of PI controller

The control loop may contain a PI controller that is usually given in the form of Laplace transfer function. For software implementation, it is necessary to convert them into the time domain in the form of differential equations.
The proportional plus integral controller (PI) can be expressed

$$\frac{Y(s)}{X(s)} = K_p + \frac{K_i}{s} \tag{2.22}$$

If the sampling time T_s is small, a derivative can be represented in finite difference form, and therefore the equation (2.22) can be written as

$$\frac{Y(N+1)-Y(N)}{T_s} = K_i X(N+1) + K_p\left(\frac{X(N+1)-X(N)}{T_s}\right) \tag{2.23}$$

where N and N+1 are the consecutive sampling instants. Equation (2.23) can be written as

$$Y(N+1)-Y(N) = K_i T_s X(N) + K_p X(N+1) - K_p X(N)$$

or

$$Y(N+1) = Y(N) + K_p X(N+1) + (K_i T_s - K_p)X(N) \tag{2.24}$$

2.5.2 Control of the Square-wave inverter drive

In these inverters, the input dc voltage is controlled in order to control the magnitude of the output ac voltage, and therefore the inverter has to control only the frequency of the output voltage. Control of the output voltage can be achieved by varying the firing angle of a phase controlled rectifier[8,10].

A static frequency converter can independently control the motor voltage V_s and frequency ω_e, but a programmed voltage/frequency characteristic reduces the number of command variable to one, allowing simple volts/hertz control. Figure 2.15 shows a block diagram of an open loop variable-speed drive with terminal volts/hertz control. The offset linear voltage/frequency characteristic is implemented. The voltage command, V_s^* is also determined from the set speed signal as shown. For the system in figure 2.16 assuming a continuously flowing current through the rectifier, and for simplicity ignoring the line side inductances, the output voltage at the capacitor terminals is given by

$$V_d = 1.35 V_{LL} \cos\alpha \tag{2.25}$$

where V_{LL} is the line to line rms voltage. The equation for the motor line-line voltage for a given V_d is

$$V_{LL1}^{motor} = 0.78 V_d \tag{2.26}$$

From the above equations

$$V_{LL1}^{motor} = 1.05 V_{LL} \cos\alpha \cong V_{LL} \cos\alpha \tag{2.27}$$

Assuming the ratio V_s/f to be constant then

$$\frac{\omega_s}{\omega_{s,rated}} \cong \frac{V_{LL1}}{V_{LL}} \cong \cos\alpha \tag{2.28}$$

From the above equation the firing angle can be calculated and so the output voltage at the capacitor terminals can be varied.

The above technique is perfectly satisfactory for single or multiple ac machine drives where high dynamic performance is not required.

Open-loop speed control has the disadvantage that the rotor slip increases and the ac machine slows down slightly when load torque is applied. Open-loop speed control has a poor dynamic performance, and a closed-loop system with tachometer feedback is preferred. Improved speed regulation can be achieved when the motor's natural droop in speed with load is compensated by means of a slip compensation technique. Motor speed is then adjusted to the commanded value, giving improved speed regulation and reduced speed sensitivity to shaft load fluctuations.

The closed-loop speed control is shown in figure 2.16. The error of the speed control loop generates the slip command ω_{sl}^* through a proportional-integral(PI) controller and limiter. The slip is added with the speed signal to generate the frequency command. The frequency command also generates the voltage command through a

volts/hertz function generator which incorporates the low-frequency stator drop compensation. From the voltage command the firing angles of the controlled rectifier can be obtained, as in the open-loop case.

2.5.3 Control of PWM inverter drives

In these inverters, the input dc voltage is essentially constant in magnitude, where a diode rectifier is used to rectify the line voltage. Therefore the inverter must control both the magnitude and the frequency of the ac output voltages[8,11].

The model developed for natural sampling PWM control with no speed feedback is shown in figure 2.17. The set speed from the potentiometer is used as a synchronous speed reference. This is fed to two simple calculations which calculate the frequency corresponding to the synchronous speed demanded and the voltage to maintain a constant V/f ratio (or to boost the ratio at low speeds). The frequency signal dictates the frequency of the modulating signal and the voltage signal dictates the amplitude of the modulating signal. The resultant modulating wave is then compared with a triangular carrier with the error generated being used to drive a saturated comparator. This provides a high for the upper power semiconductor device to be turned on and a low for the lower to be turned on.

The inherent problem associated with this method of control is that the machine will never reach the speed demanded by the operator. Natural sampling PWM with speed feedback is a much better performer than its counterpart without speed feedback. The block diagram is shown in figure 2.18. As in the six-step case, the set speed for the motor is compared with the motor actual speed and the error is fed into a PI controller. The output of the controller is the slip speed required. Since torque is proportional to slip speed, the torque generated by the motor can be limited by limiting the output of the PI controller. The slip speed demand is then added to the actual speed to produce a synchronous speed demand. This is converted to drive signals for the power semiconductors in the same way as shown for natural sampling without speed feedback.

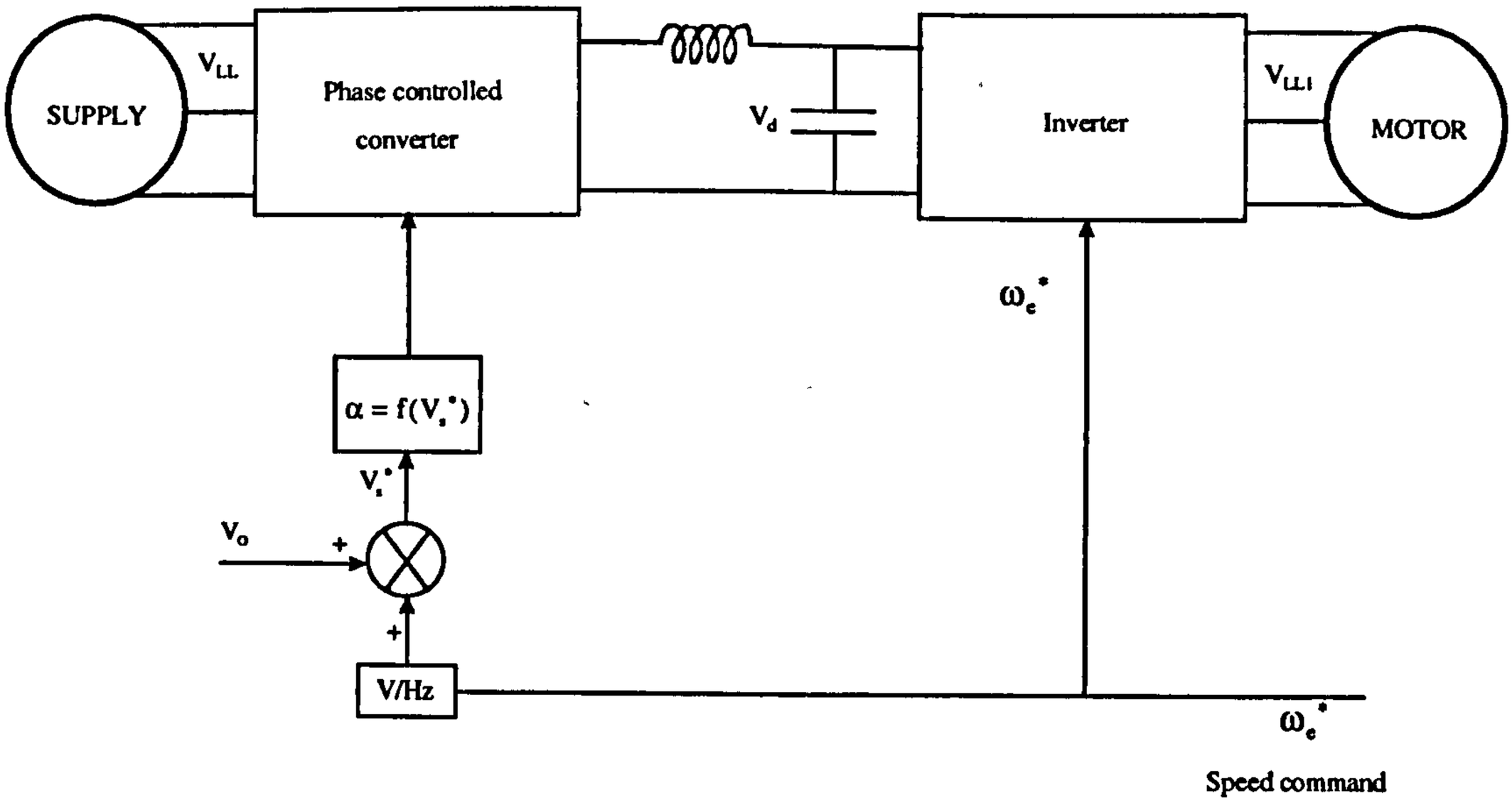

Figure 2.15 Open-loop volts/hertz control

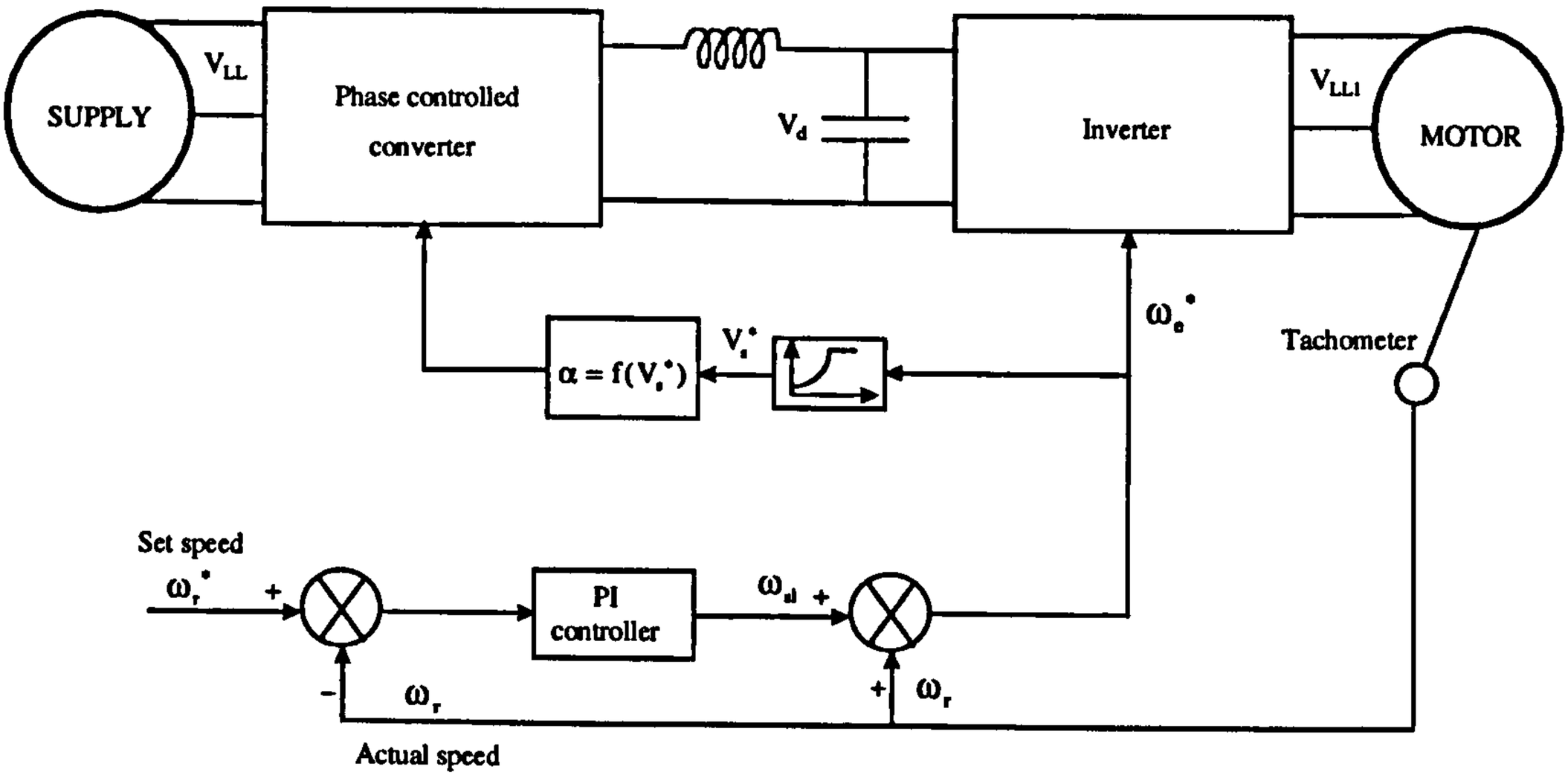

Figure 2.16 Closed-loop volts/hertz speed control with slip regulation

With a step-up speed command, the machine accelerates freely with a slip limit that corresponds to maximum torque and then settles down to slip value at steady state as dictated by the load torque. If the command speed is reduced the slip becomes negative and the motor goes into the dynamic or regenerative braking mode.

A similar control method is followed for the main digital or microprocessor techniques such as symmetric sampling PWM and asymmetric sampling PWM. The only difference is that a sample and hold circuit is added in the control system. For the symmetrical sampled PWM control a reference modulating wave is sampled at the positive peaks of a triangular carrier signal, while for the asymmetrical sampled PWM control the modulating signal is sampled at both positive and negative peaks of a triangular carrier signal. The resultant sampled signal's intersection with the carrier wave defines the switching moments for one leg of the inverter. The switching patterns for the remaining two legs of the inverter are defined in the same way with the reference modulating signals displaced by a further 120° in each case. The open and closed-loop control systems for either the symmetric or the asymmetric sampling PWM techniques (depending on the function of the sampled and hold circuit) are illustrated in the figures 2.19 and 2.20.

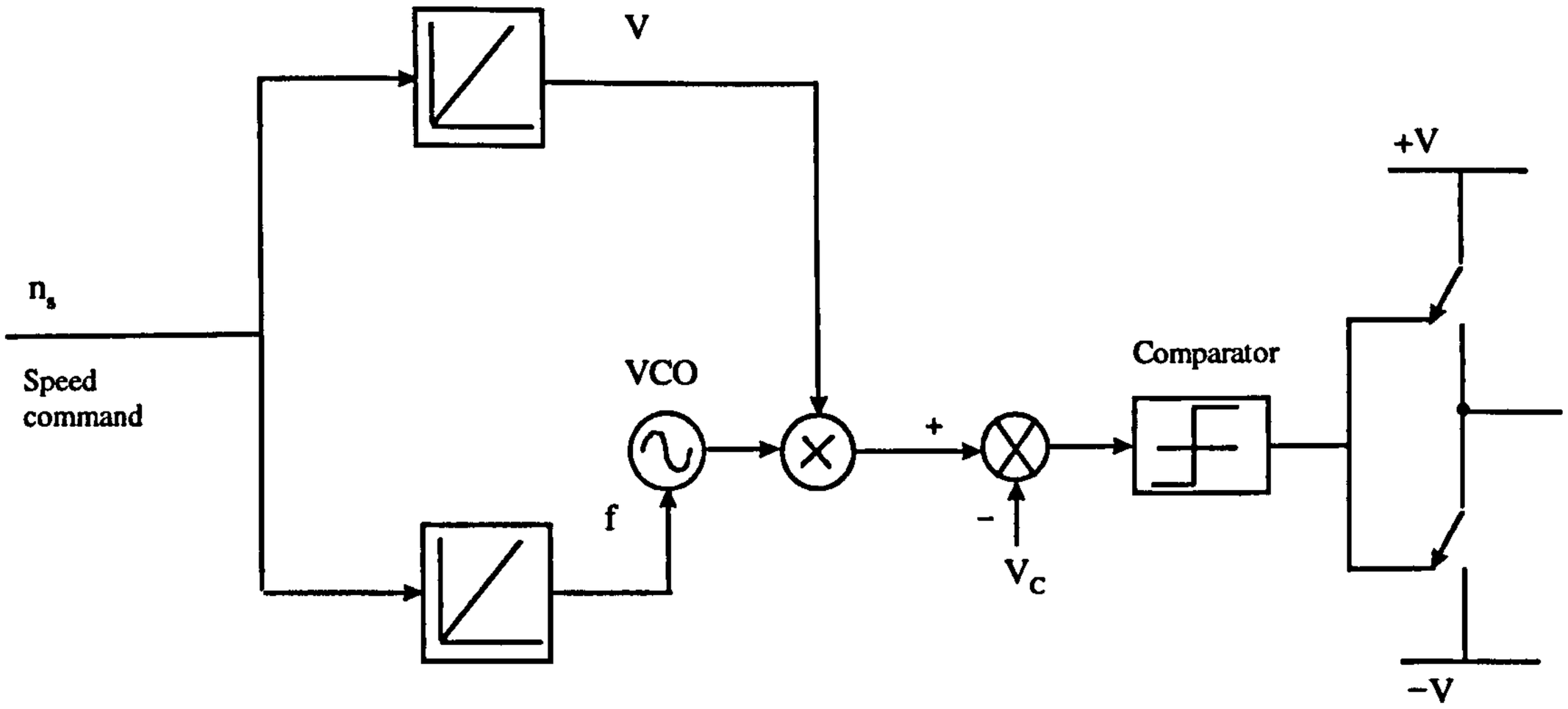

Figure 2.17 Open-loop control system using natural sampling PWM

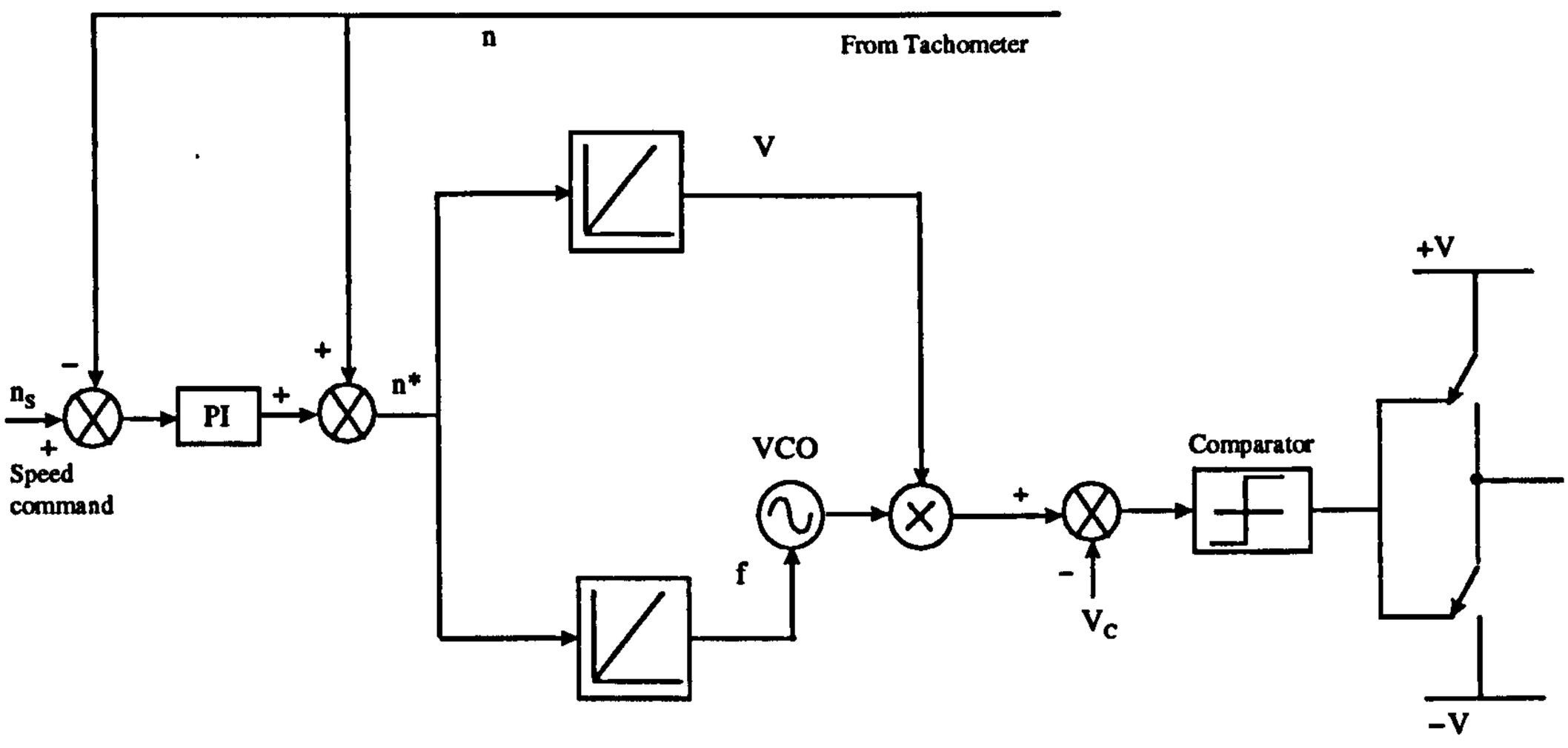

Figure 2.18 Closed-loop control system using natural sampling PWM

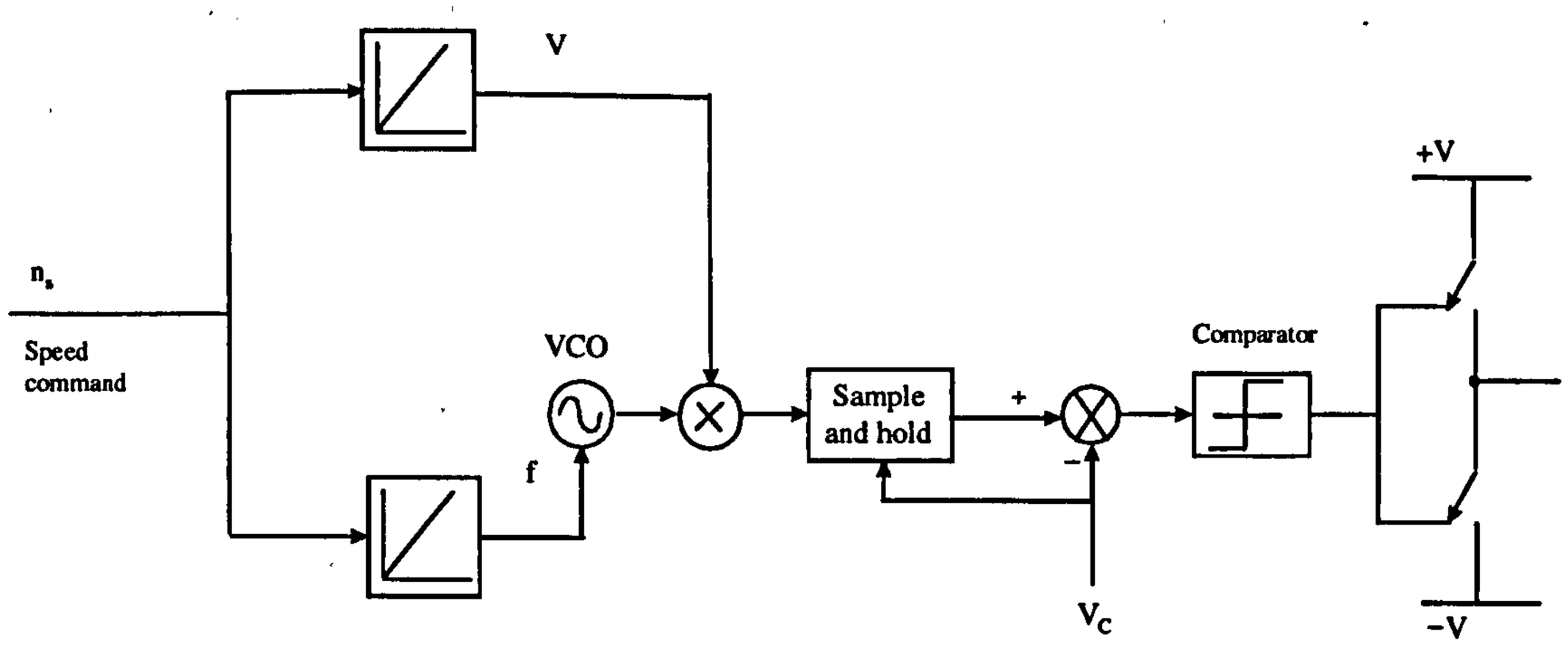

Figure 2.19 Open-loop control system using symmetric/asymmetric sampling PWM

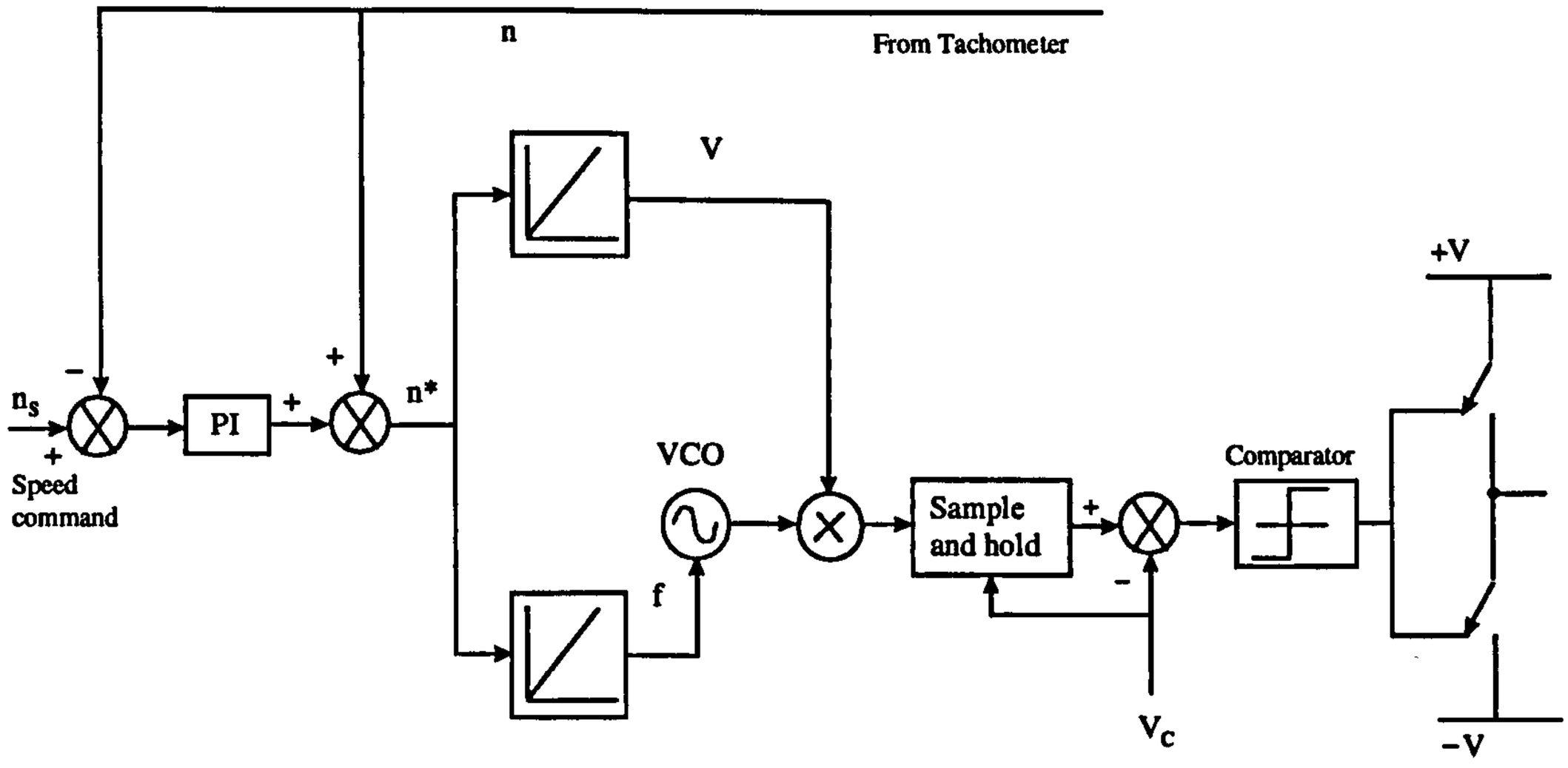

Figure 2.20 Closed-loop control system using symmetric/asymmetric sampling PWM

2.6 Simulation and harmonic analysis of six step and PWM inverter control of the induction motor

The simulation models can be separated into two distinct sections: the inverter model and the induction motor model. For the induction motor model the following assumptions are made to simplify the analysis[15,16]:

1. The air gap of the machine is uniform.
2. Saturation, hysteresis and eddy current effects are neglected.
3. A current in any winding sets up an mmf wave which is sinusoidally distributed in space around the air-gap.

Taking into account these three assumptions, the voltage equations in machine variables may expressed as

$$
\begin{aligned}
V_{as} &= r_s i_{as} + p\lambda_{as} \\
V_{bs} &= r_s i_{bs} + p\lambda_{bs} \\
V_{cs} &= r_s i_{cs} + p\lambda_{cs} \\
V_{ar} &= r_s i_{ar} + p\lambda_{ar} \\
V_{br} &= r_s i_{br} + p\lambda_{br} \\
V_{cr} &= r_s i_{cr} + p\lambda_{cr}
\end{aligned}
\tag{2.29}
$$

In the above equations the s subscript denotes variables and parameters associated with the stator circuits and the r subscript denotes variables and parameters associated with the rotor circuits. Both r_s and r_r are diagonal matrices each with equal nonzero elements and λ is the flux linkage vector. The current-derivative vector p[i] is obtained by solving (2.29) with $[\lambda] = [L][i]$.

The per unit air-gap electromagnetic torque equation of the induction motor in terms of stator quantities can be expressed as:

$$T_e = \frac{2}{3\sqrt{3}}\omega_s(\lambda_{as}(i_{bs} - i_{cs}) + \lambda_{bs}(i_{cs} - i_{as}) + \lambda_{cs}(i_{as} - i_{bs})) \quad (2.30)$$

where ω_s is the synchronous speed in electrical radians/second.

The mechanical equation of the motion can be expressed as:

$$p\omega_r = \frac{(T_e - T_{LOAD})}{2H} \quad (2.31)$$

where T_{LOAD} is the load torque and H is the inertia constant for the motor and load.

Also the rotor displacement angle is given by the following equation:

$$p\theta_r = \omega_r. \quad (2.32)$$

The inverter model is split into two parts, the modelling of the switching pattern generated by the inverter and the representation of the D.C. link filter.

The switching patterns are defined according to the switching strategies outlined in previous sections.

The equations governing the filter's behaviour are expressed below in state space form. The rectifier current is given by:

$$p[i_r] = \frac{V_R - V_{DC} - i_r R_F}{L_F} \quad (2.33)$$

where i_r is the rectifier current, V_R is the voltage at the rectifier terminals, V_{DC} is the DC voltage at the capacitor, R_F is the resistance at the D.C filter and L_F is the inductance at the D.C filter.

The equation of the D.C voltage at the capacitor terminals is given by:

$$pV_{DC} = (i_r - i_{inv})C_F \quad (2.34)$$

where i_{inv} is the inverter current and C_F is the capacitance of the D.C filter.

Open and closed-loop speed control systems for the induction motor driven by a six-step or a PWM inverter were considered for simulation purposes. The block diagram for a six-step inverter drive connected to an induction motor was given in Fig.2.7 and for a PWM inverter controlled induction motor drive in Fig 2.6. The system parameters used in the simulation are given in appendix 1. The dynamic equations described previously for the induction motor and inverter models were solved by the Runge-Kutta method. The PWM controlled inverter drives will be also used in succeeding chapters in a three phase modelling environment. A flowchart in Fig 2.21 presents the simulation steps of the six-step or the PWM inverter controlled induction motor drives. All the models were coded in the Fortran language.

For the systems illustrated in Figs 2.16, 2.18 and 2.20 the proportional and the integral gains of the PI controller were $G_P = 5$ and $G_I = 2$. The values of the gains were chosen as optimal values derived from previous simulation runs. The simulation step was 0.1msec for the six-step inverter drive and 0.01msec for the PWM inverter drive cases.

Figures 2.22 (a)-(f) show simulation results of phase currents, speed, frequency and torque during an acceleration to the rated speed of an unloaded motor using six-step inverter control with the closed loop control system illustrated in Figure 2.16. The induction motor reaches the desired speed of 1.0 pu at steady state. It should be addressed that both six-step and PWM inverter drives cannot give accurate speed control down to zero speed, but have a finite frequency at which they can operate. Most manufactures give a bottom working frequency of between 4-8% of the rated speed. This bottom frequency can be noticed from the waveform of the stator frequency (e).

The same conditions as in the previous no-load case were repeated in Fig 2.23 but with the motor loaded (load torque proportional to the motor speed). The drive system successfully achieved the demanded set speed (1.0 pu) and torque (1.0 pu). In waveform (e) the frequency is above the rated because of the slip regulation.

Figures 2.24(a)-(f) illustrate the last case of the six-step inverter controlled induction motor drive where the demanded speed in the control system of Fig. 2.16 was set to 0.8 pu with the motor loaded (load proportional to the motor speed). The phase

currents are less than in the previous case due to the smaller stator voltages that apply to the motor terminals. The stator frequency is again greater than 0.8 pu because of the slip regulation loop of the closed-loop system in Fig 2.16.

PWM inverter control using natural sampling with the closed-loop speed control of Fig(2.18) is simulated in Figs 2.25 (a)-(f) with the induction motor unloaded. The results shown that the drive successfully achieved the demanded speed and torque.

The same conditions as before were repeated in Figs 2.26 (a)-(f) with the motor loaded (load torque proportional to the motor speed). In Fig 2.26(e) the stator frequency is above the rated because of the slip regulation loop. A similar model but using the open-loop system of figure 2.17 is illustrated in Figs 2.27 (a)-(f). The control can be seen to be poorer compared with the previous case , with a motor speed less than the rated at steady state conditions.

The same conditions with system conditions similar to figure 2.26 but using the software implemented approximations of natural sampling, the symmetric and the asymmetric regular sampling were repeated in Figs 2.28 (a)-(f) and 2.29 (a)-(f). The control systems for these cases studies were given in Fig 2.20. The results of these simulations show that the microprocessor based control methods can be used very efficiently to control induction motor drives. The differences on the waveforms are because of the different switching instants of the semiconductor devices.

Figs 2.30 (a)-(f) illustrate the response of the PWM inverter controlled induction motor drive where the demanded speed in the control system of Fig 2.18 was 1.0 pu with the motor fully loaded for a small period after it had reached steady state conditions. When the load is applied to the motor shaft there is an increase in the frequency (e), because of the additional slip. However, the speed despite the load change gets back to its pre-load conditions (d), because of the correct operation of the closed-loop speed control system.

Figs 2.31 (a)-(f) show simulation results of the last example of the PWM inverter drive where the demanded speed in the control system of Fig. 2.18 was set to 0.8 pu with the motor loaded (load proportional to the motor speed). For these results the stator frequency is greater than 0.8 pu because of the slip regulation loop of the

closed-loop system in Fig 2.18 and currents are less than in figure 2.26 due to the smaller stator voltages that are applied to the motor terminals.

From the above results it was observed that there are a number of different strategies to control a variable speed drive. Six-step inversion is a relatively simple method, but rich in harmonics. PWM techniques have a number of advantages but require more complex control and power circuit configurations. With the increase in the number of microprocessors, software implemented methods can be used to eliminate the problems that were existed in the past. In order to quantify the distortion in the current waveforms (and so the harmonic content) in figure 2.32 a quantity called the total harmonic distortion THD is defined as [8]:

$$\%\mathrm{THD} = 100 \times \frac{\left(\sum_{h=2}^{\infty} I_h^{\,2}\right)^{1/2}}{I_1} \qquad (2.35)$$

where I_1 is the fundamental frequency rms value of the current and I_h is the rms magnitude at the harmonic of order h. In order to compare the harmonic content produced by the above methods harmonic analysis was carried out using the results from the simulations in figures 2.24 and 2.31. The results refer to the dynamic performance of the variable speed drive with the load proportional to the motor speed for 0.8 pu speed demand using closed-loop speed control. In figure 2.32 the steady state stator currents are illustrated using the six step and the natural sampling PWM method. Harmonic analysis was carried out using the above waveforms and the results are presented in tables 1 and 2 showing the dominant harmonics for each method. For the six step method the harmonic analysis produced the results showing in table 1:

ORDER OF HARMONICS	CONTENT %
1	100% of fundamental
5	20.9% of fundamental
7	10.8% of fundamental
11	4.20% of fundamental
13	3.00% of fundamental
17	1.70% of fundamental
19	1.40% of fundamental
THD %	24.30 %

Table 1 Harmonic analysis for the six step inverter

For the PWM method (natural sampling) the harmonic analysis produced the following results:

ORDER OF HARMONICS	CONTENT %
1	100% of fundamental
5	0.13% of fundamental
7	0.08% of fundamental
16	5.71% of fundamental
20	4.49% of fundamental
35	3.29% of fundamental
37	3.15% of fundamental
THD %	8.93%

Table 2 Harmonic analysis for the PWM inverter

An analysis of the results presented in tables 1 and 2 shows that the six step produces dominant low order harmonics and the THD produced by the six step method is much higher than the PWM technique. The above results verify that the PWM method produces less harmonics than the six step method. This is the main reason why the PWM method is used for applications of variable speed drives in AC power systems as will be investigated in a succeeding chapter.

In order to validate the above control techniques and the simulation results presented in this chapter, comparison was made with simulation tests carried out by A.McLean [17] for a project sponsored by the power industry (the results of which were validated by using laboratory tests). Validation for the six step and the PWM waveforms that are presented in figure 2.32 can be done by using power electronics reference books such as [8]. Comparison between simulation results presented in this chapter such as the ones in figures 2.26, 2.28 and 2.29 using natural, symmetric and asymmetric sampling PWM with the ones in [17] shows that the inverter drive models presented in this chapter have the appropriate dynamic response. The results show that the currents have the same initial peak form during the start up for the three phases and reach steady state conditions once the rotor speed attains the set value. The speed in both simulations took the required value at steady state conditions due to the correct action of the control systems. Finally although the torque fluctuates at transient conditions, at steady state conditions it attains the required value (i.e. the rated value). It should be mentioned that the dynamic response of the inverter drives is influenced by the action of the control systems described before. For this reason careful consideration regarding the values used for the gains of the individual controllers should be taken into account, in order to use the parameters that will give good dynamic response for the drive. This is a general comment, regardless of the method that is used to control the variable speed drive (six step or natural PWM or symmetric/asymmetric PWM).

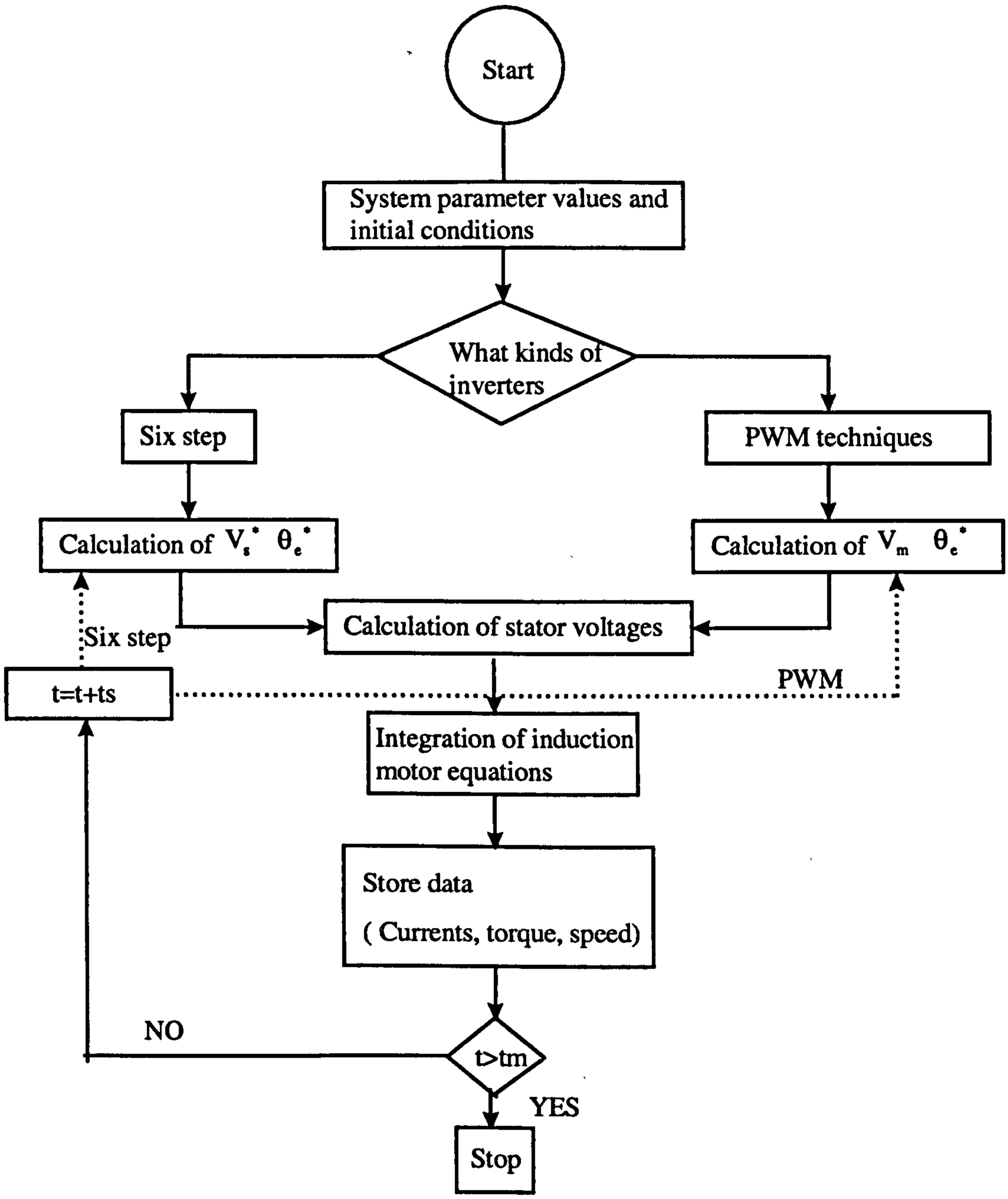

Figure 2.21. A flowchart for the six-step and PWM control of induction motor

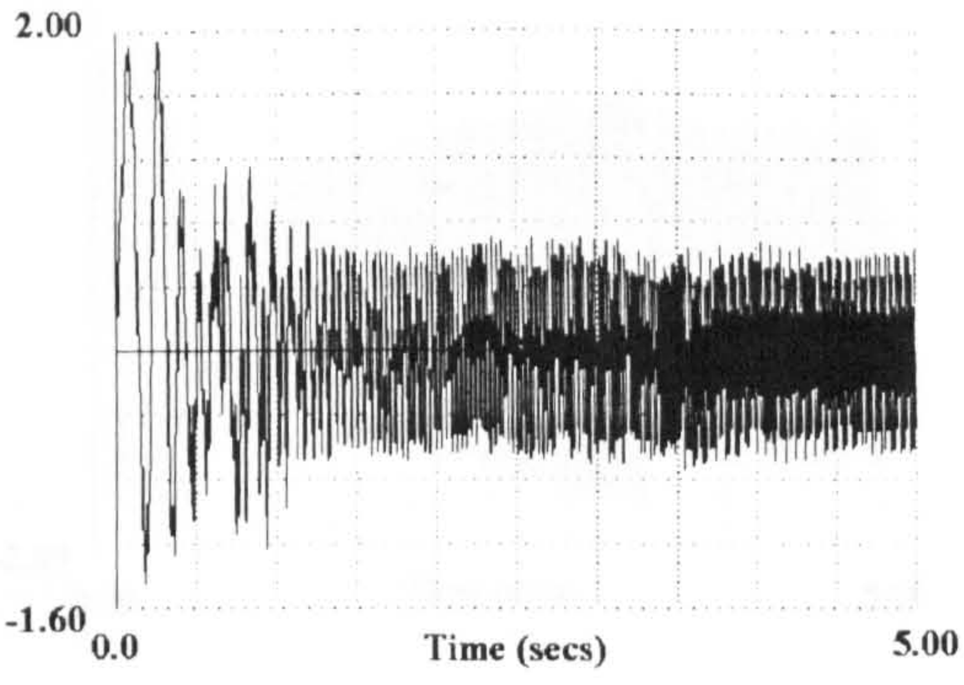

(a) Phase A stator current (pu)

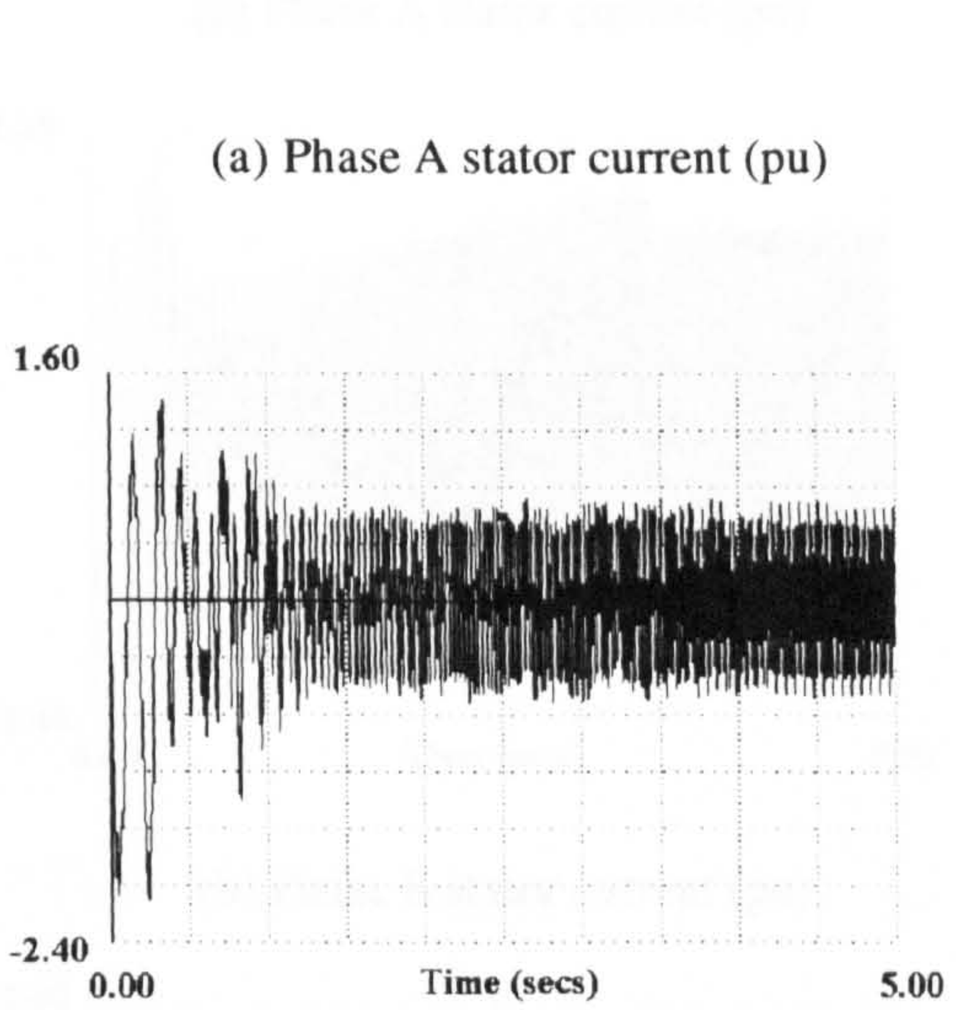

(b) Phase B stator current (pu)

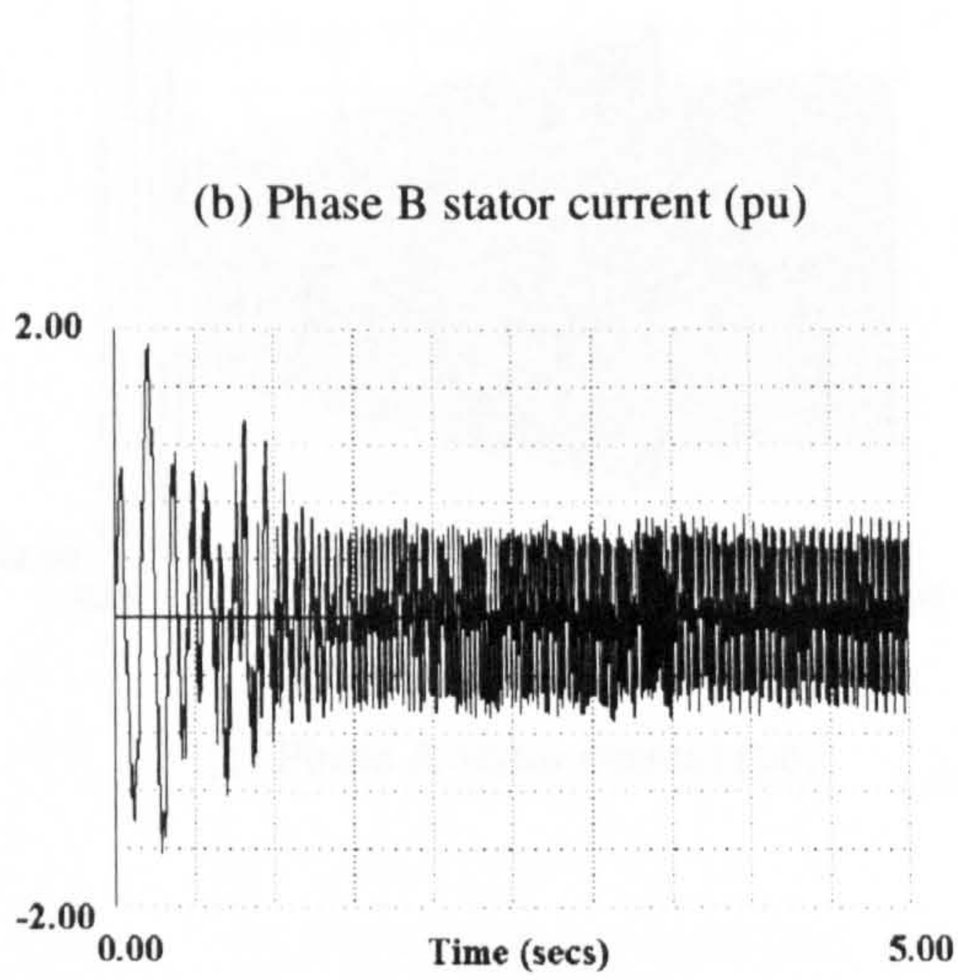

(c) Phase C stator current (pu)

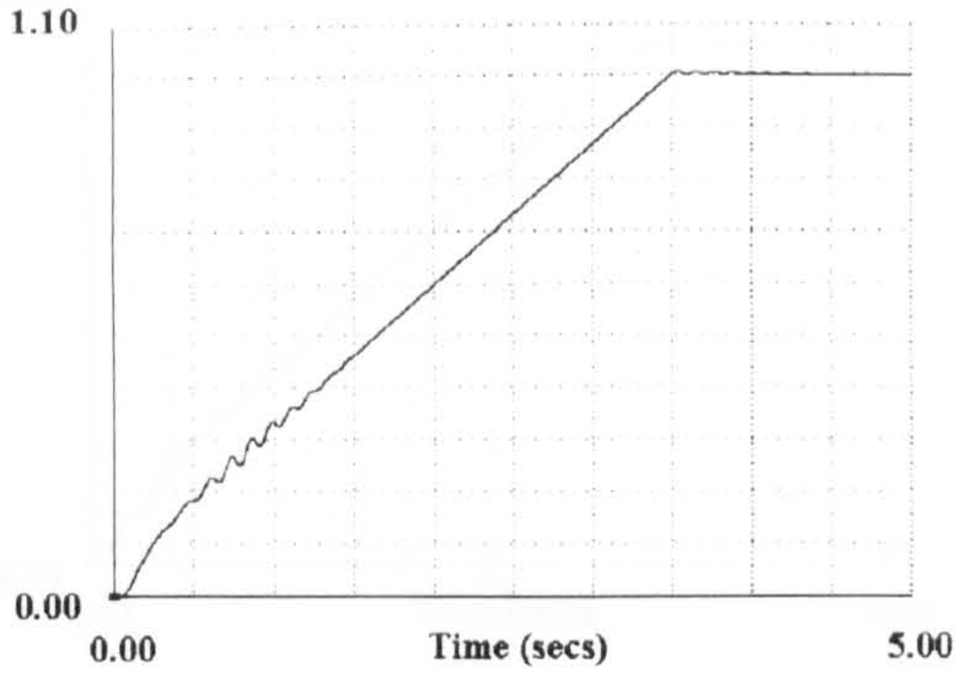

(d) Speed (pu)

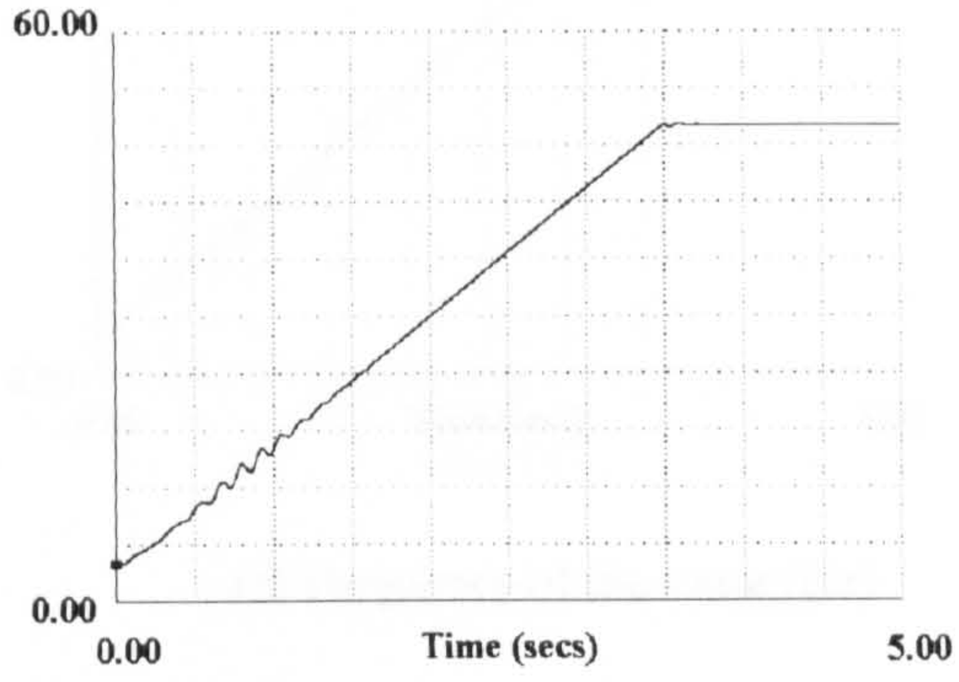

(e) Frequency of the stator (Hz)

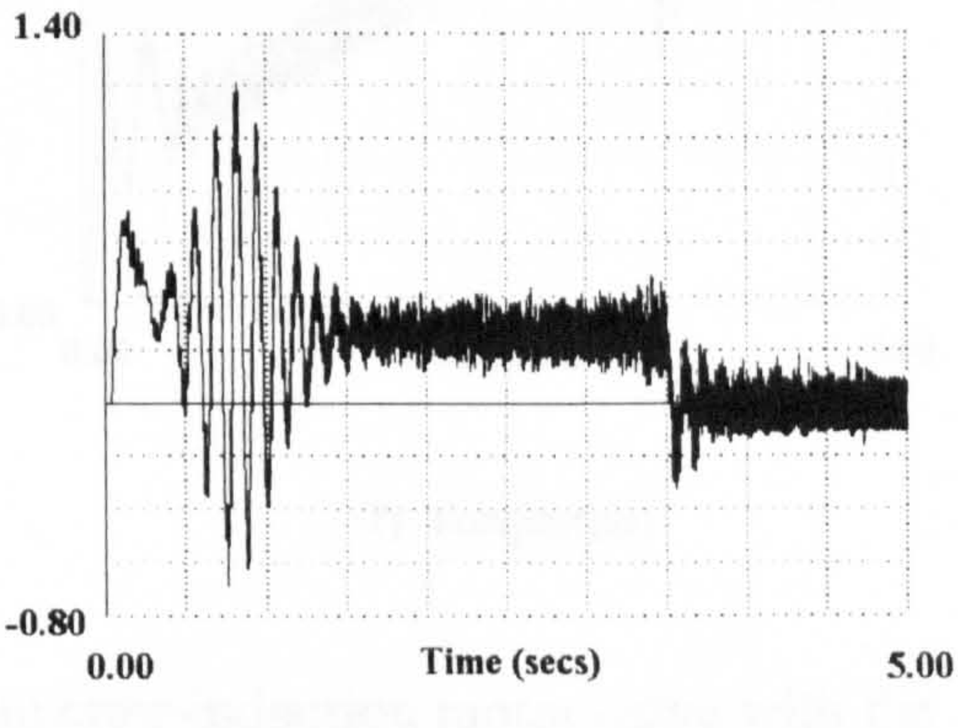

(f) Torque(pu)

Figure 2.22 Dynamic performance of six-step inverter-induction motor drive with the motor unloaded for 1.0 pu speed demand using closed-loop speed control

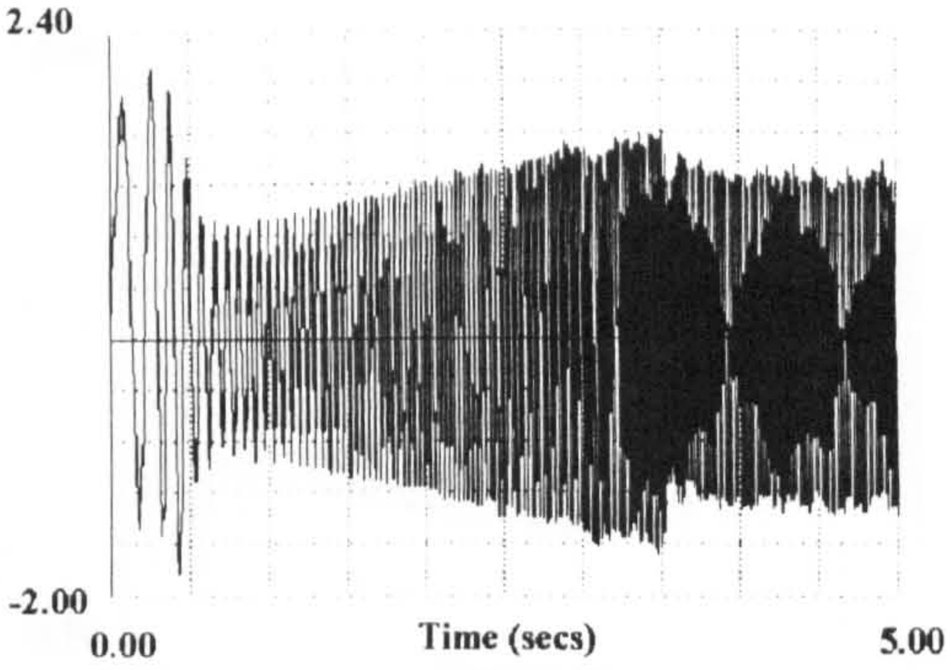

(a) Phase A stator current (pu)

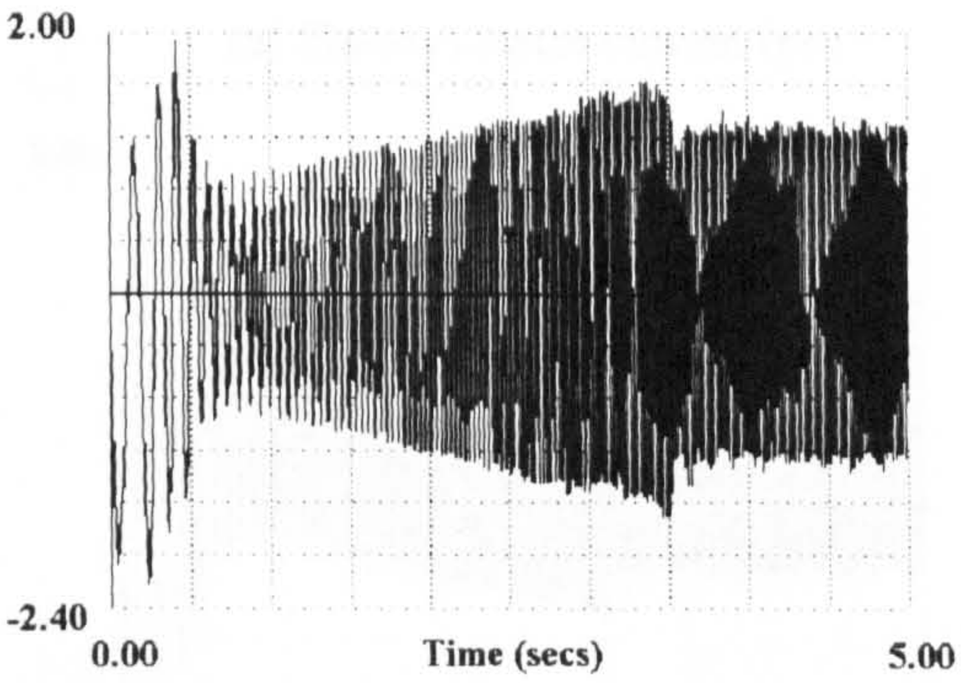

(b) Phase B stator current (pu)

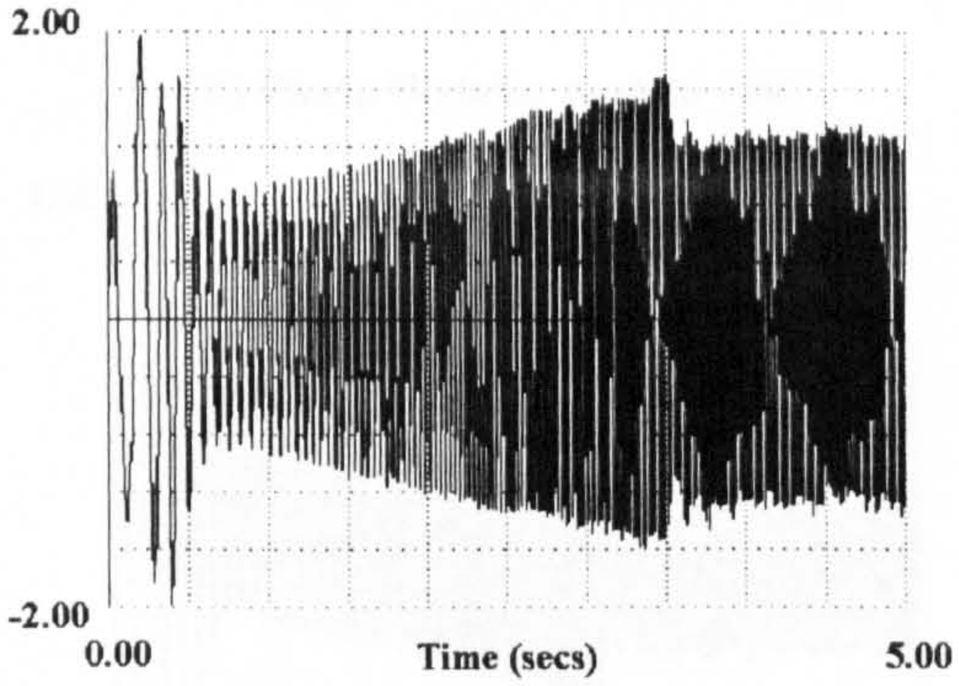

(c) Phase A stator current (pu)

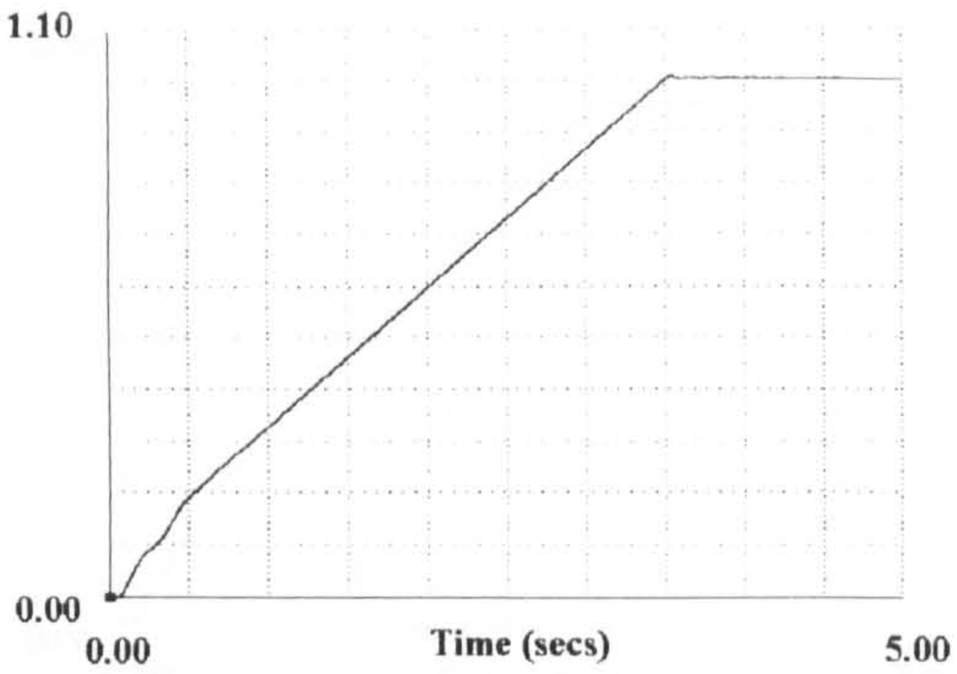

(d) Speed (pu)

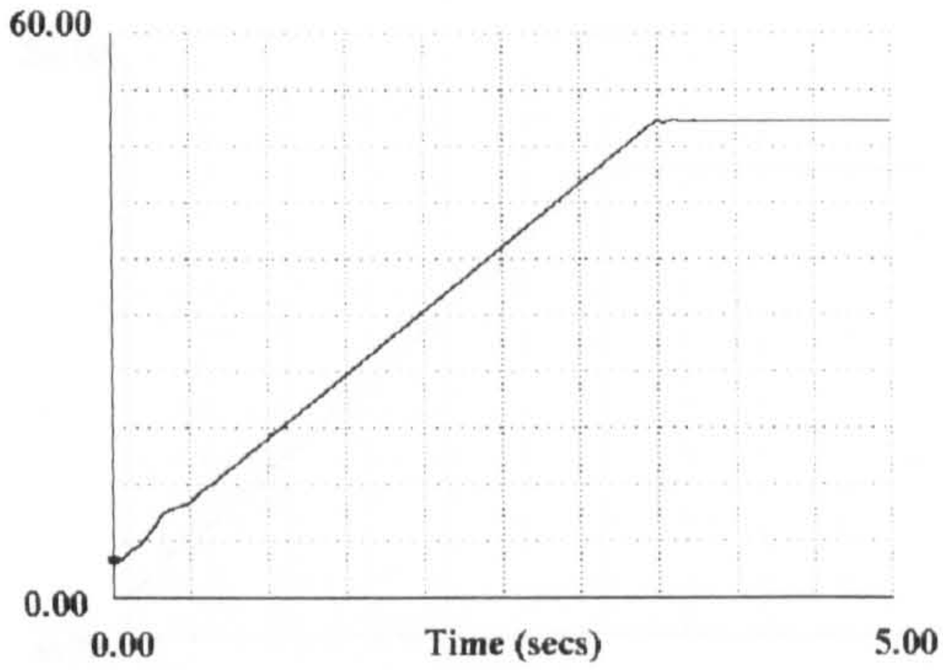

(e) Frequency of the stator (Hz)

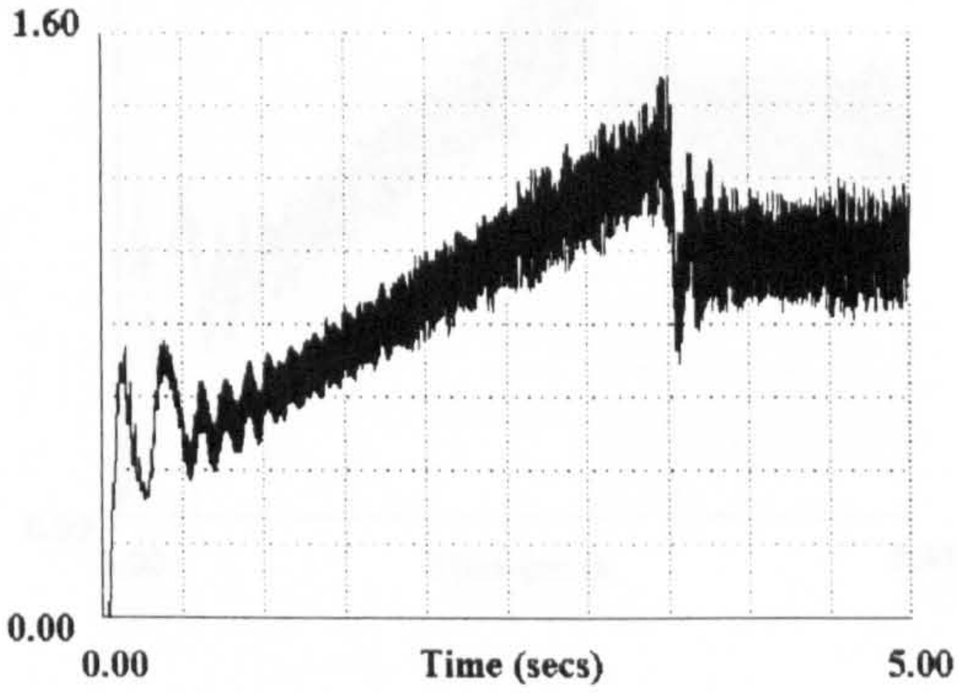

(f) Torque(pu)

Figure 2.23 Dynamic performance of six-step inverter-induction motor drive with the load torque proportional to the motor speed for 1.0 pu speed demand using closed-loop speed control

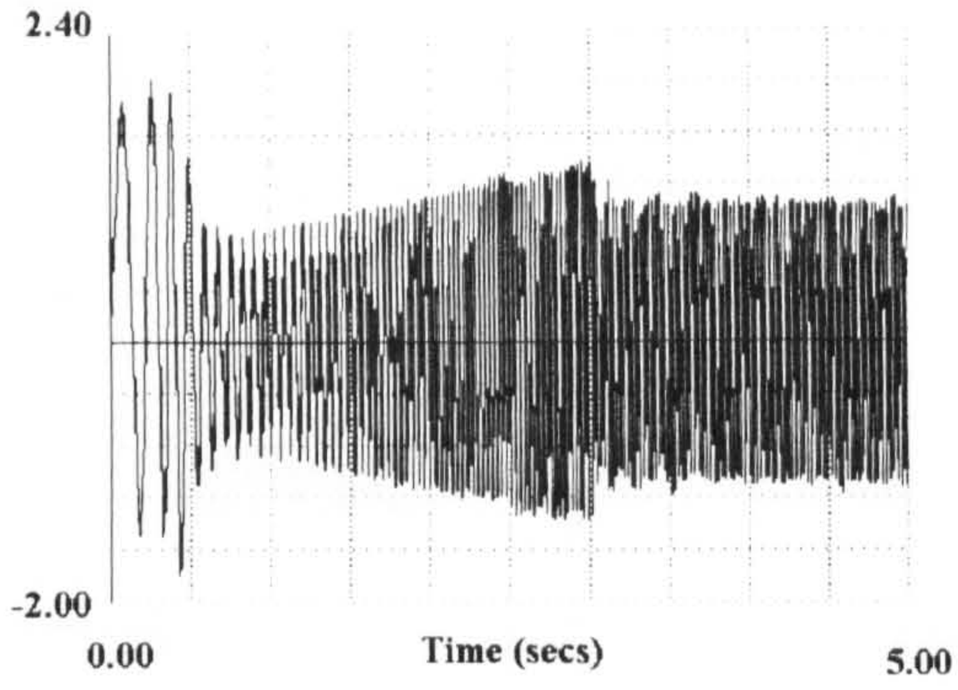

(a) Phase A stator current (pu)

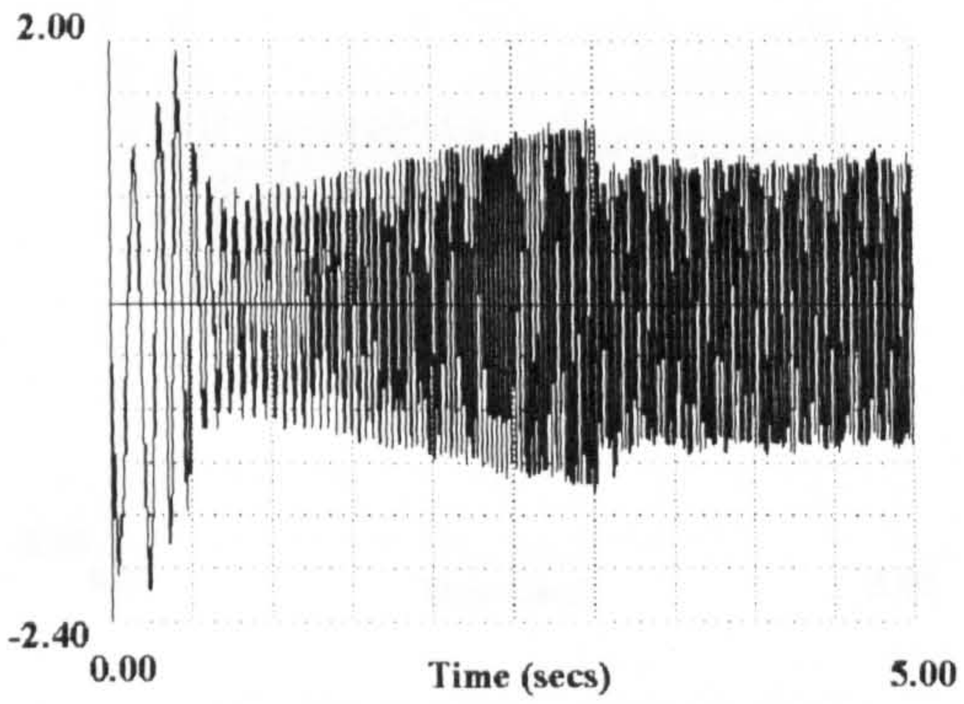

(b) Phase B stator current (pu)

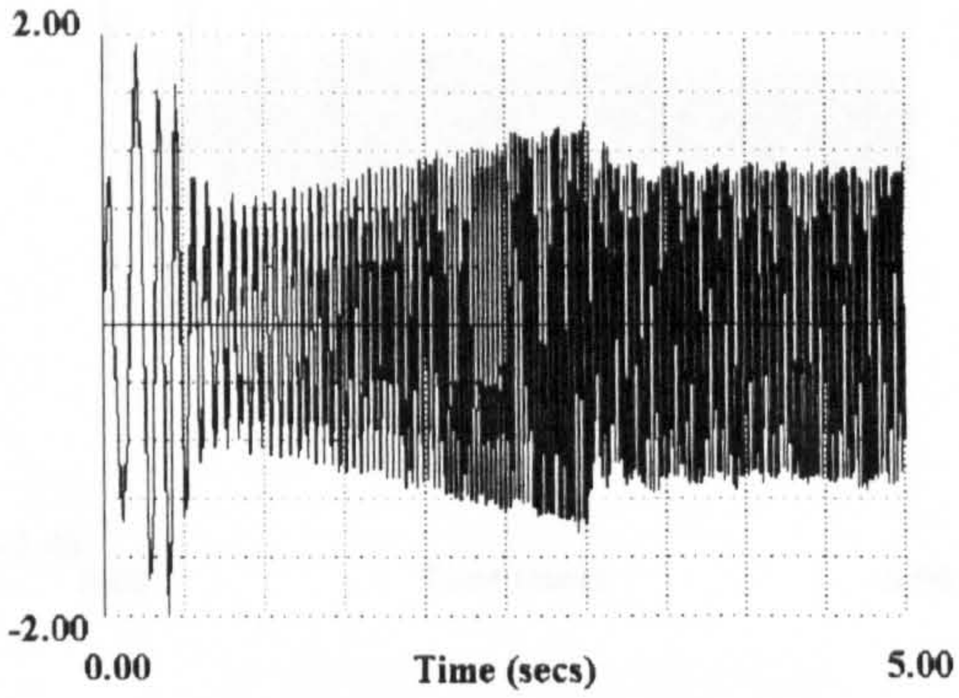

(c) Phase C stator current (pu)

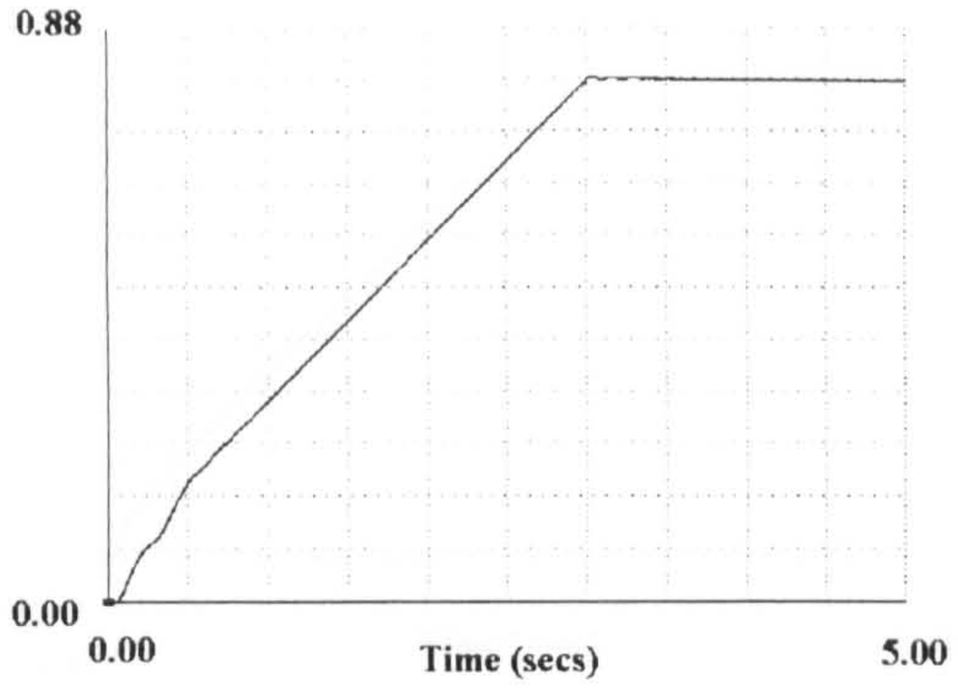

(d) Speed (pu)

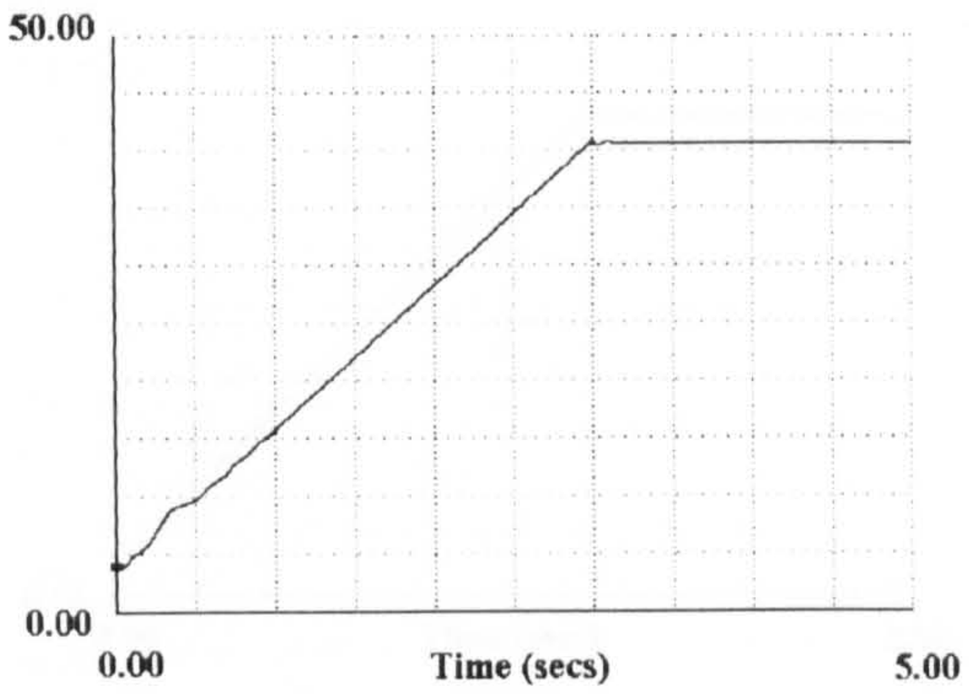

(e) Frequency of the stator (Hz)

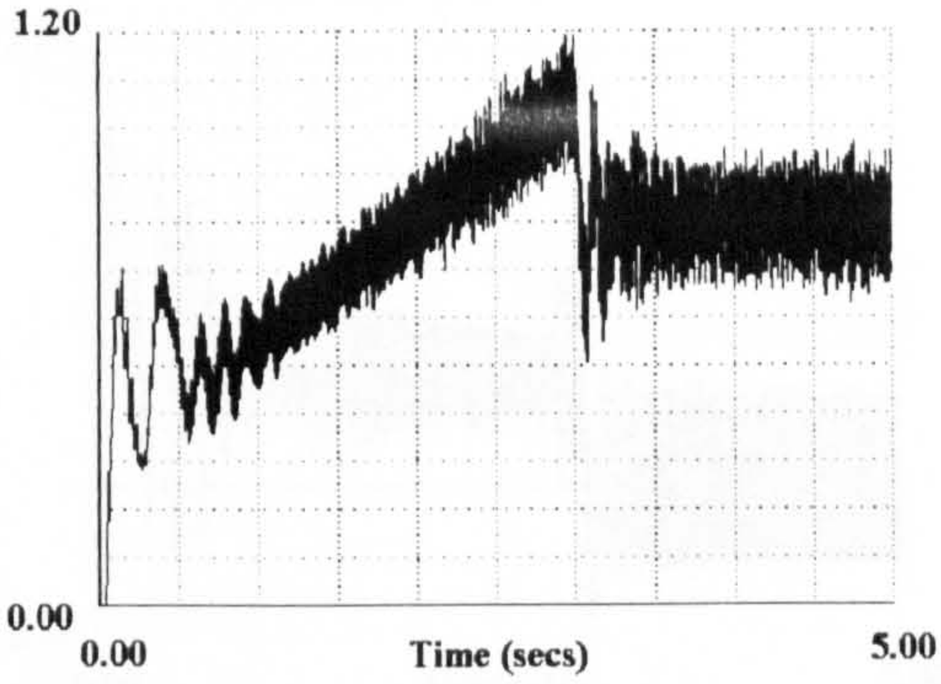

(f)Torque(pu)

Figure 2.24 Dynamic performance of six-step inverter-induction motor drive with the load torque proportional to the motor speed for 0.8 pu speed demand using closed-loop speed control

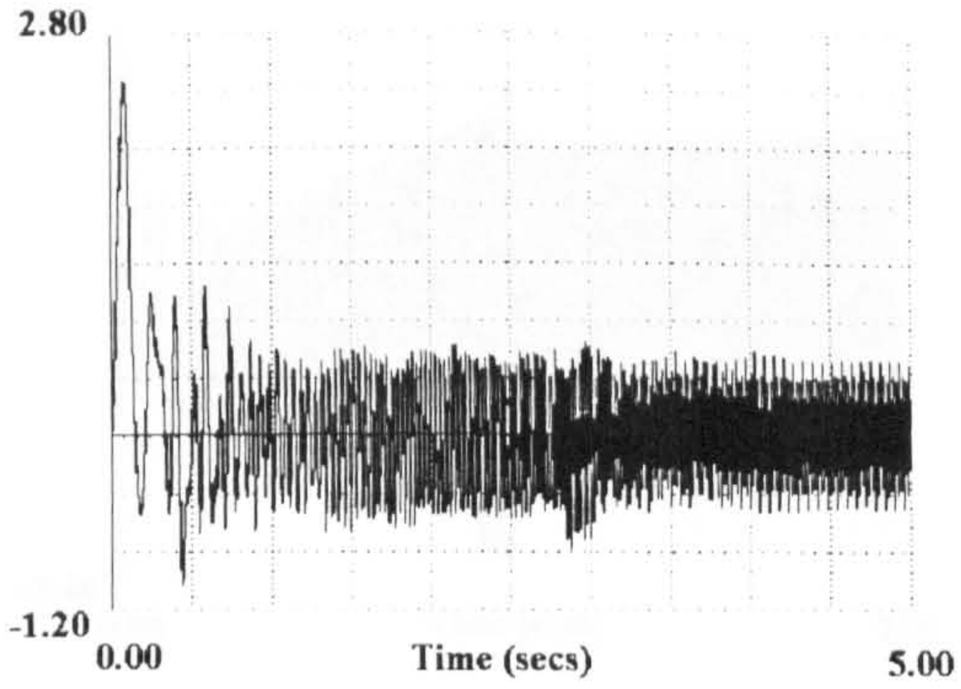

(a) Phase A stator current (pu)

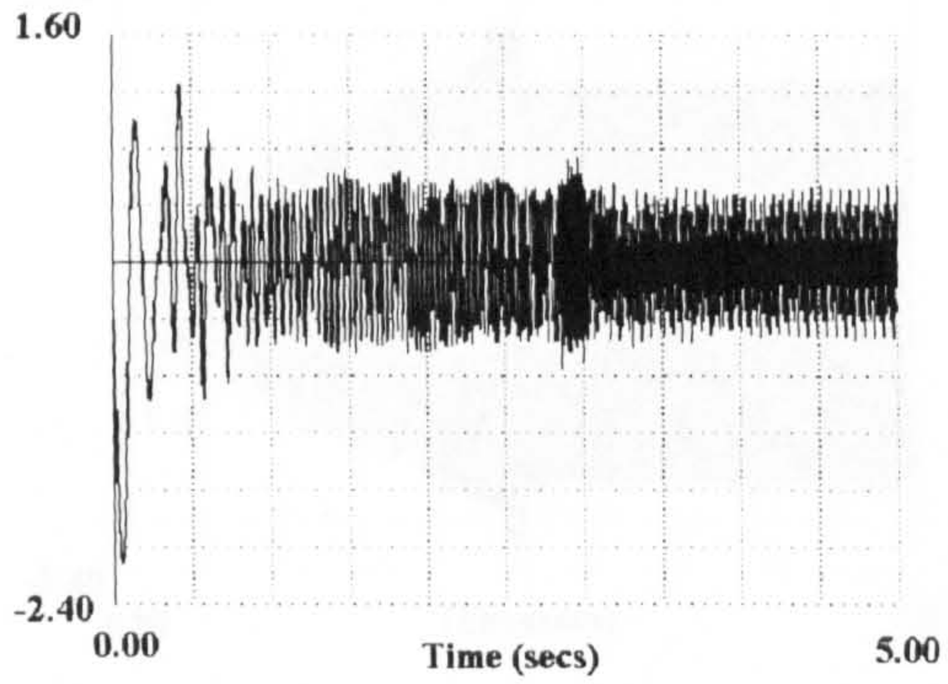

(b) Phase B stator current (pu)

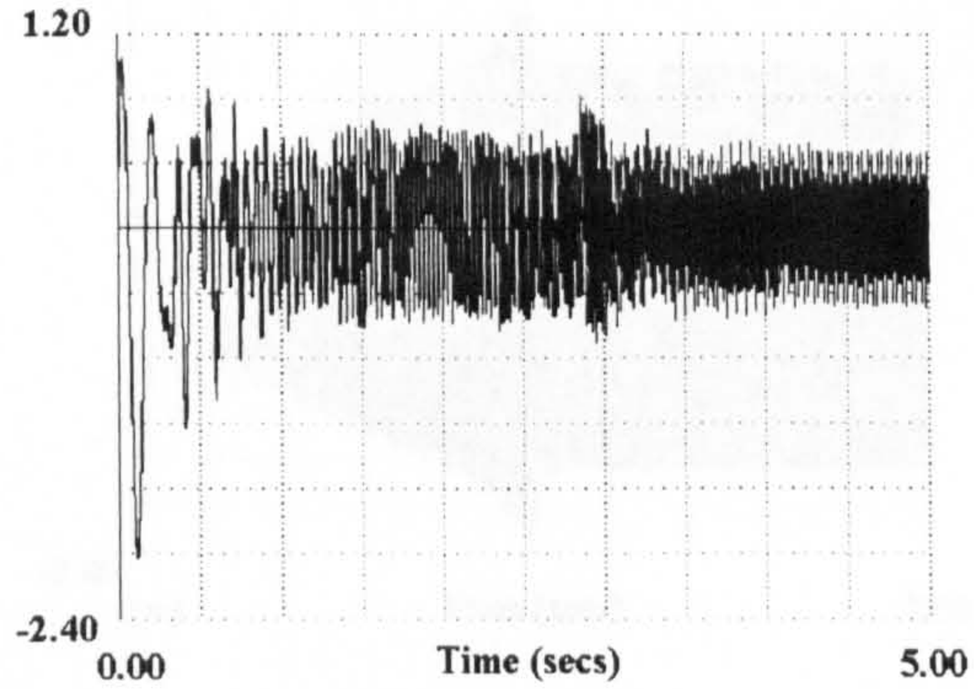

(C) Phase C stator current (pu)

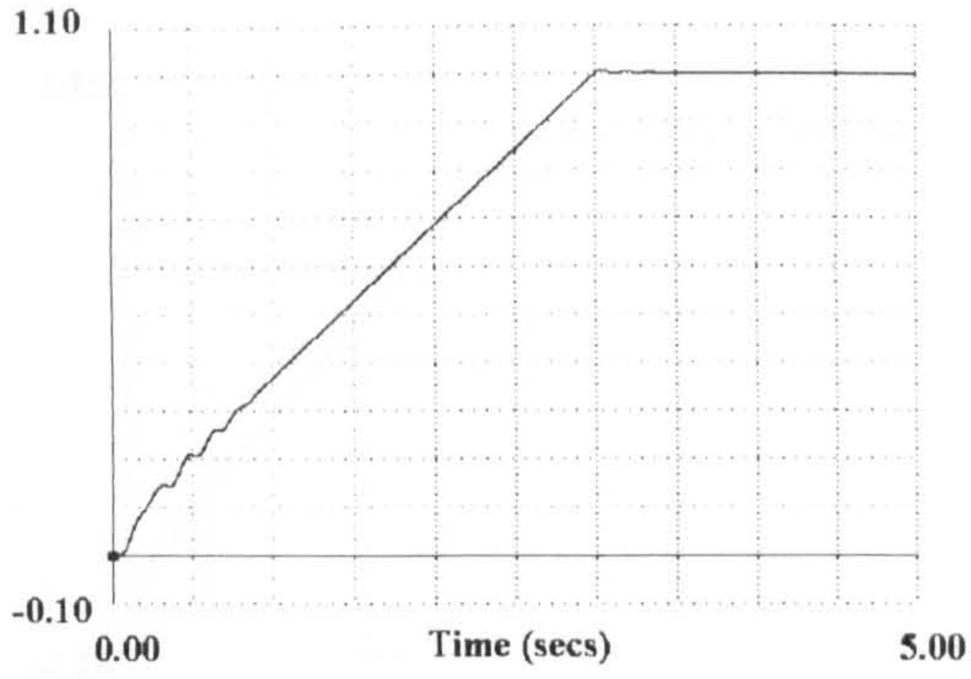

(d) Speed (pu)

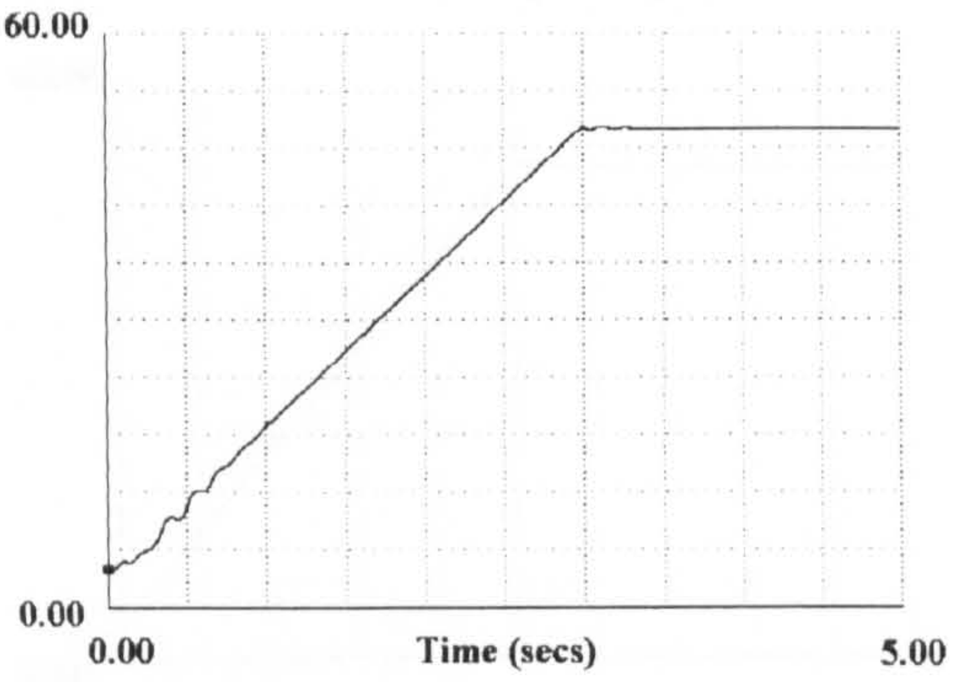

(e) Frequency of the stator (Hz)

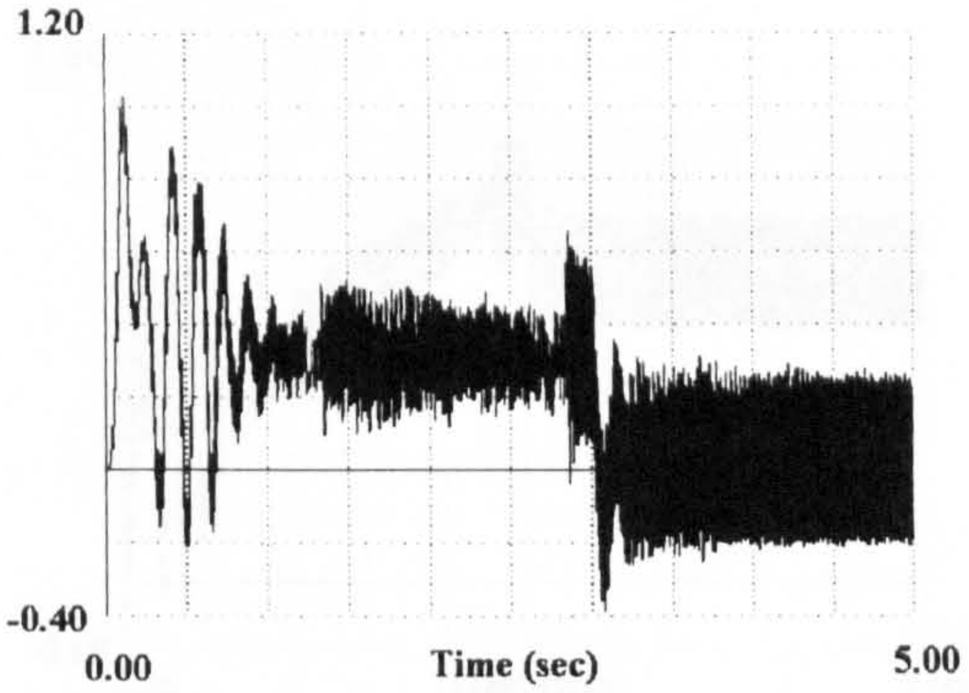

(f) Torque(pu)

Figure 2.25 Dynamic performance of PWM (natural sampling) inverter-induction motor drive with the motor unloaded for 1.0 pu speed demand using closed-loop speed control

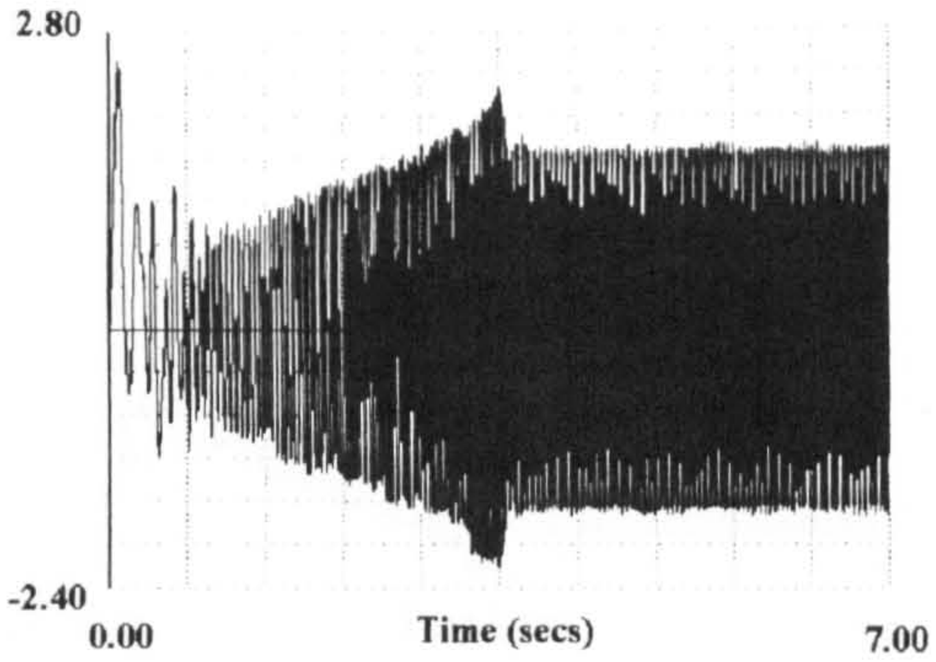

(a) Phase A stator current (pu)

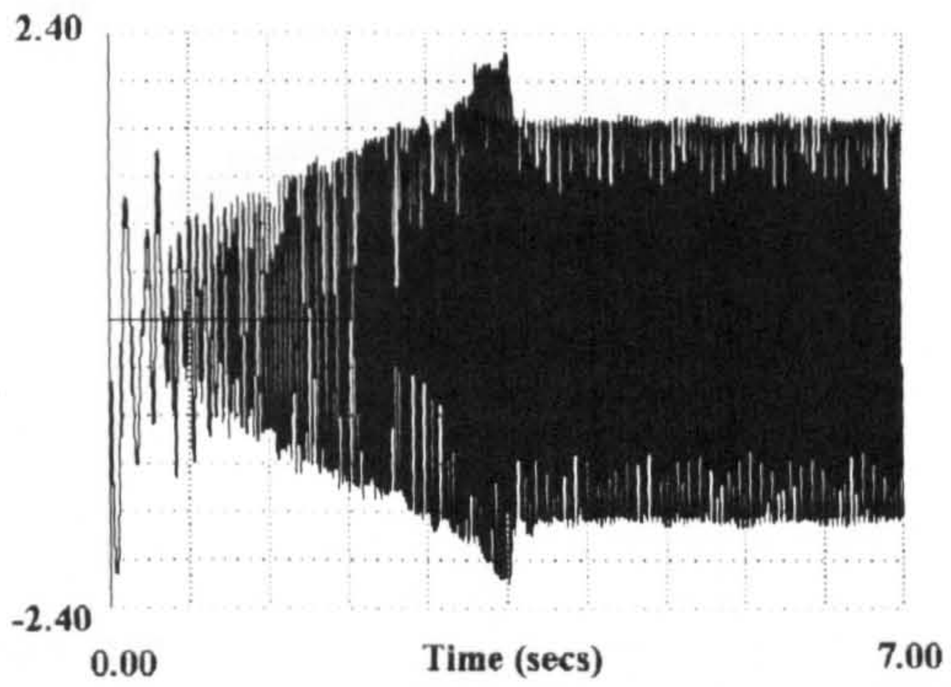

(b) Phase B stator current (pu)

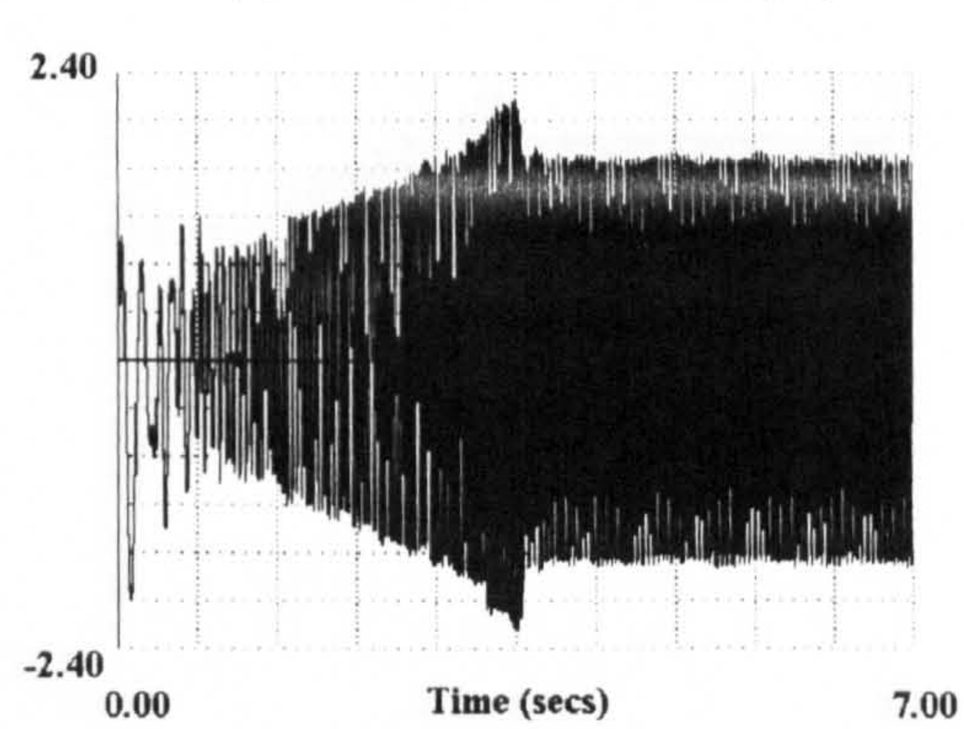

(c) Phase C stator current (pu)

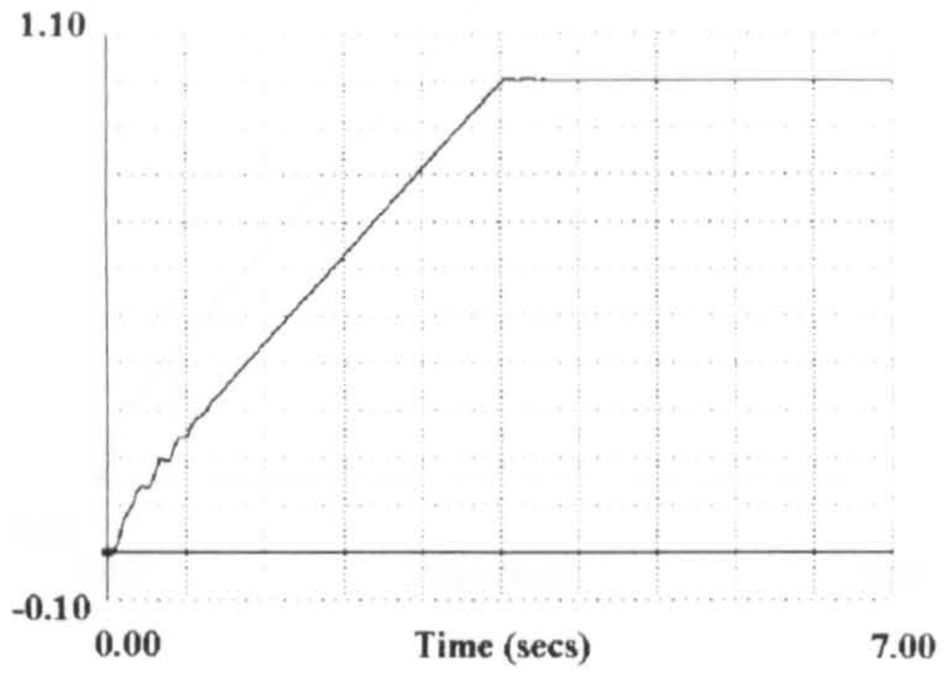

(d) Speed (pu)

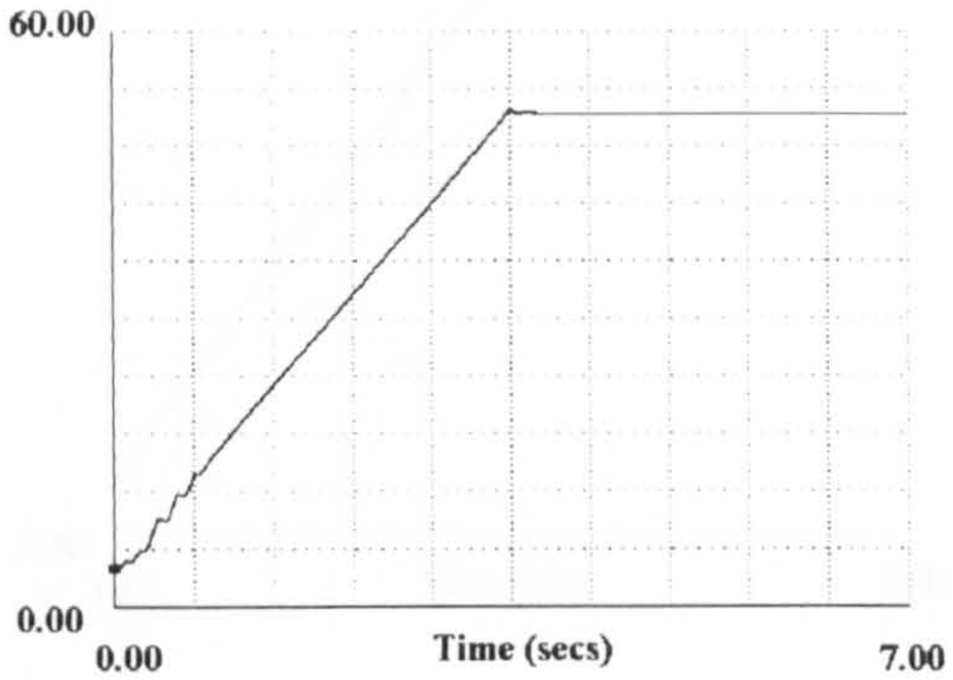

(e) Frequency of the stator (Hz)

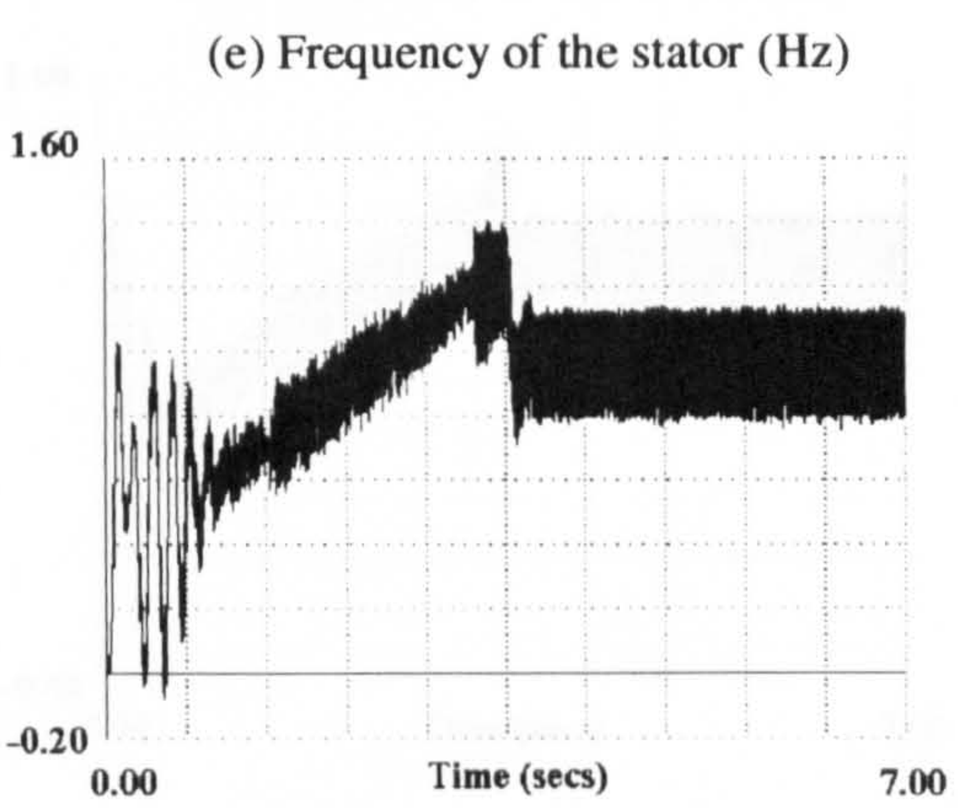

(f) Torque(pu)

Figure 2.26 Dynamic performance of PWM (natural sampling) inverter-induction motor drive with the load torque proportional to the motor speed for 1.0 pu speed demand using closed-loop speed control.

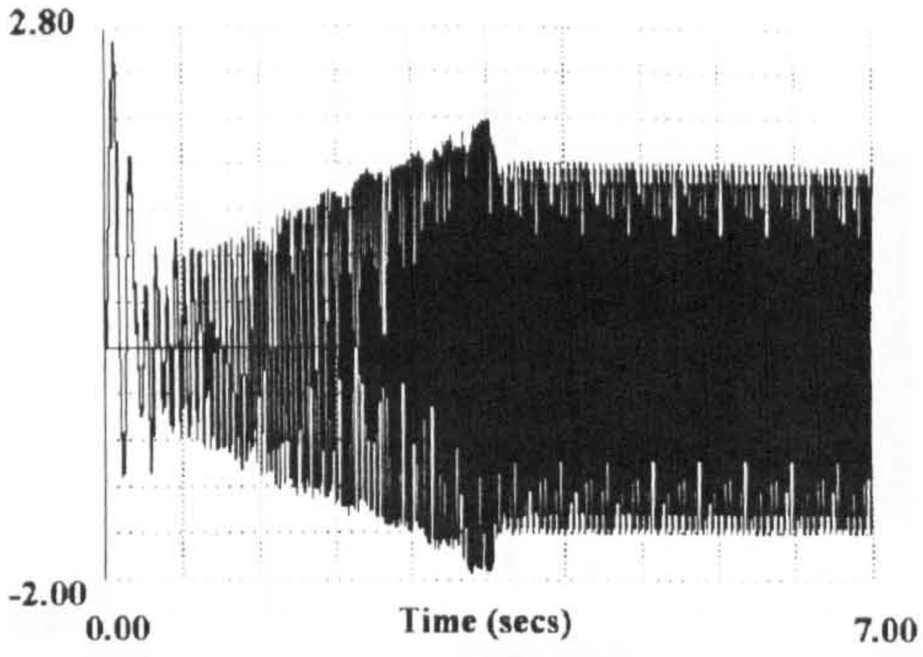

(a) Phase A stator current (pu)

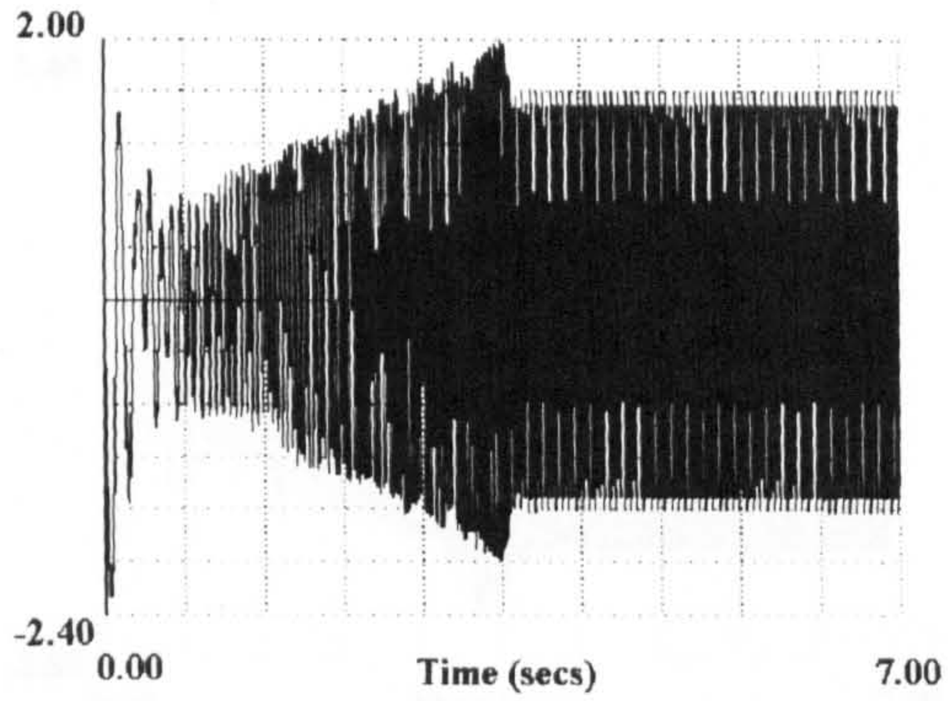

(b) Phase B stator current (pu)

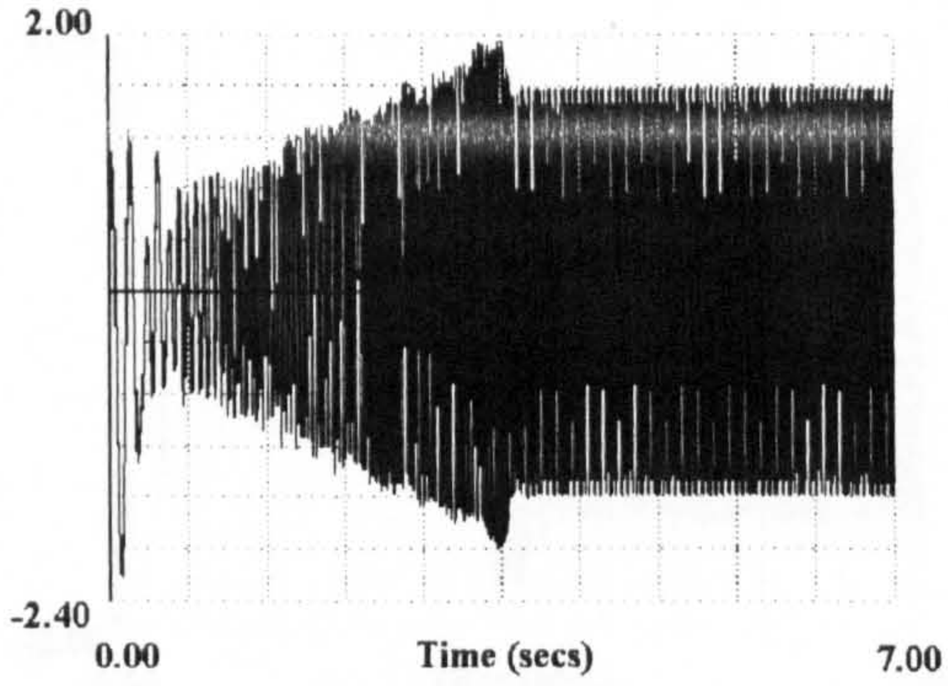

(c) Phase C stator current (pu)

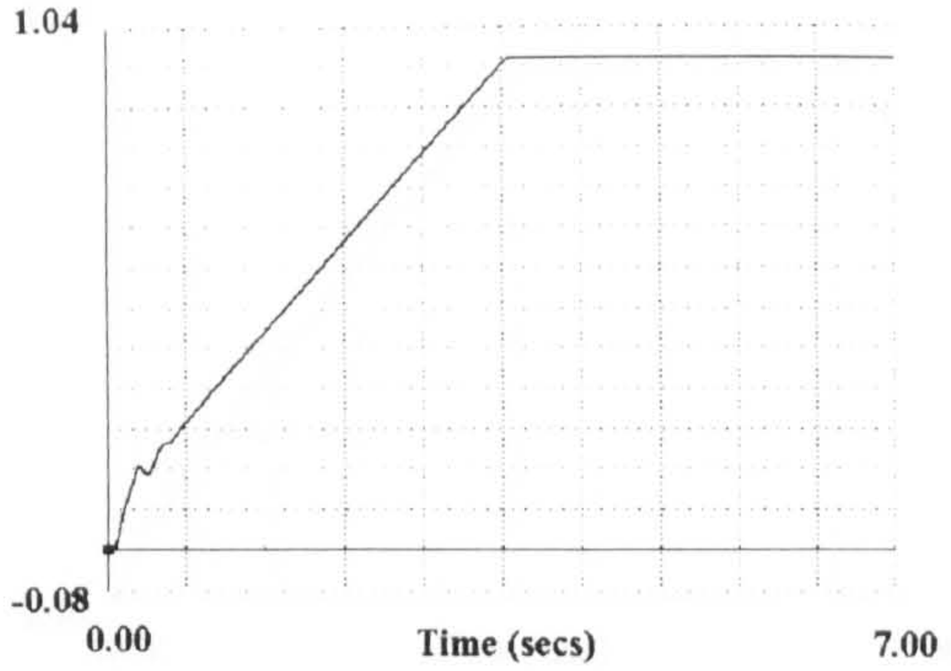

(d) Speed (pu)

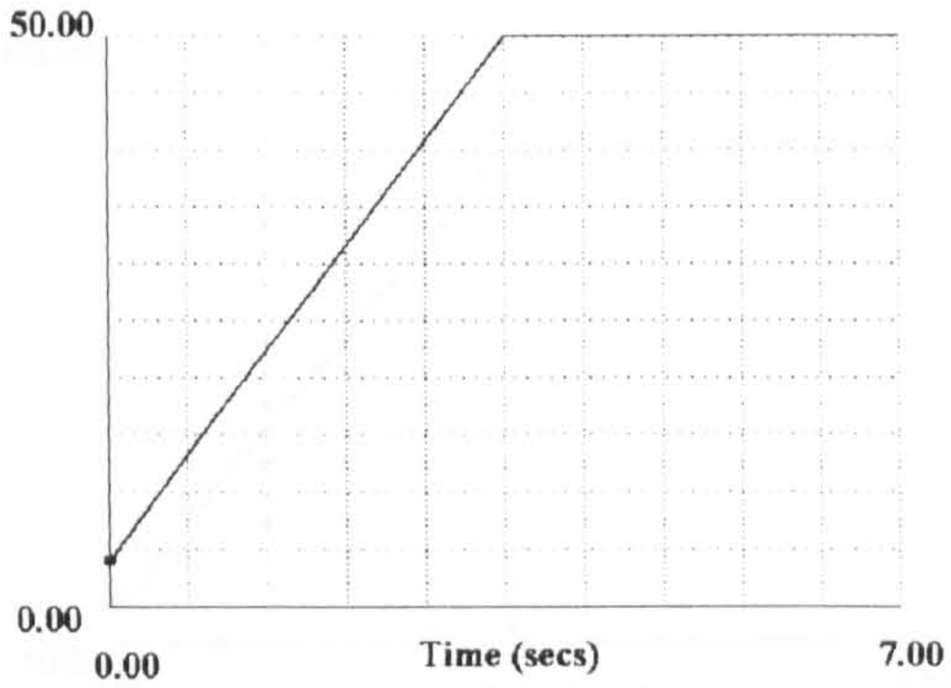

(e) Frequency of the stator (Hz)

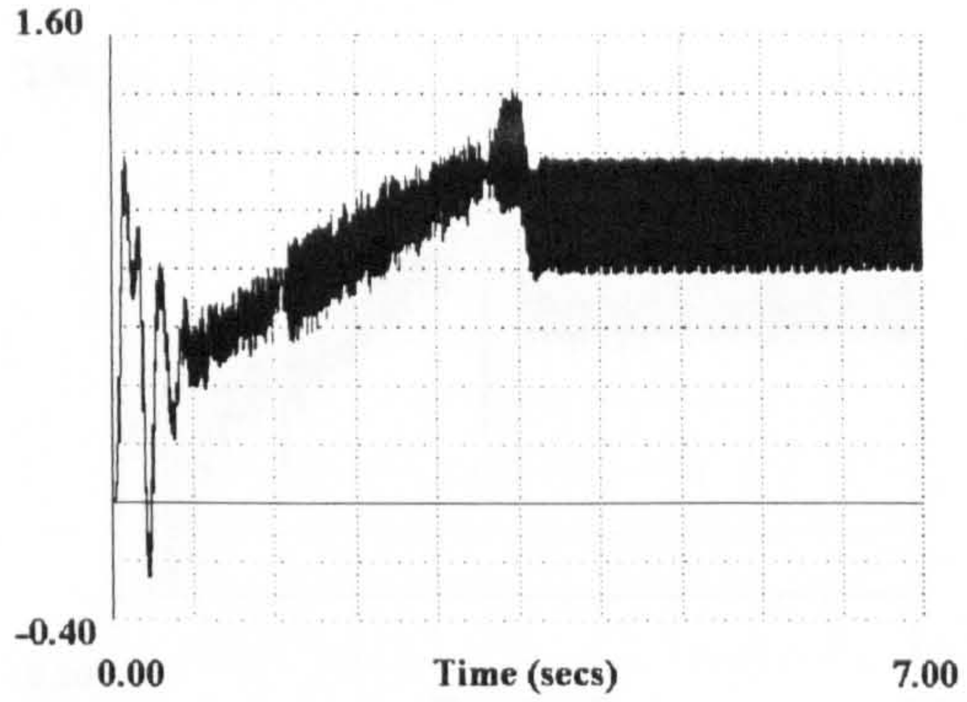

(f) Torque (pu)

Figure 2.27 Dynamic performance of PWM (natural sampling) inverter-induction motor drive with the load torque proportional to the motor speed using open-loop speed control.

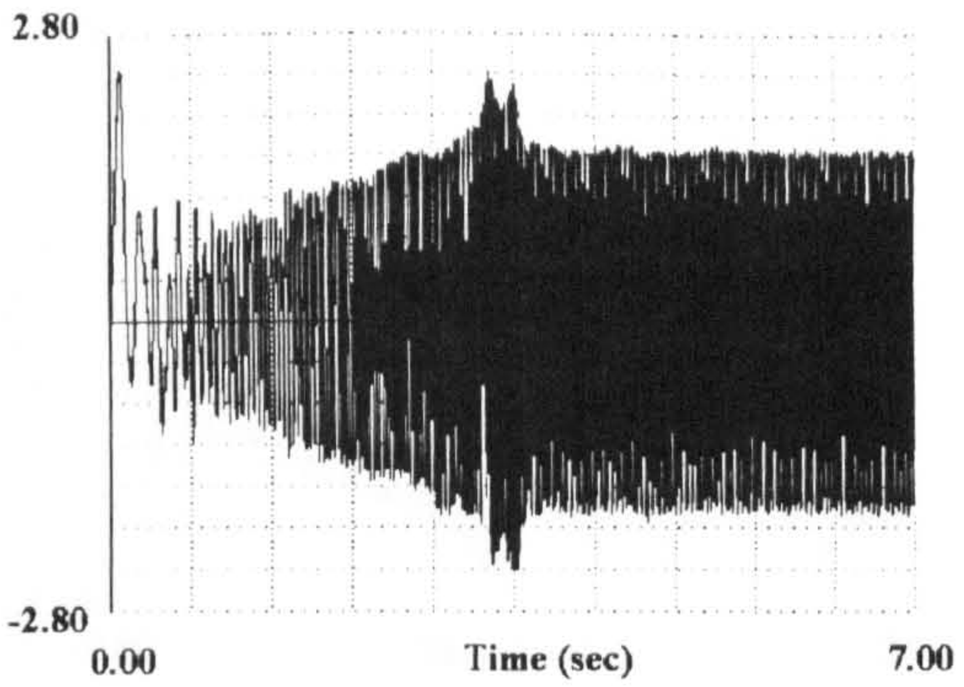

(a) Phase A stator current (pu)

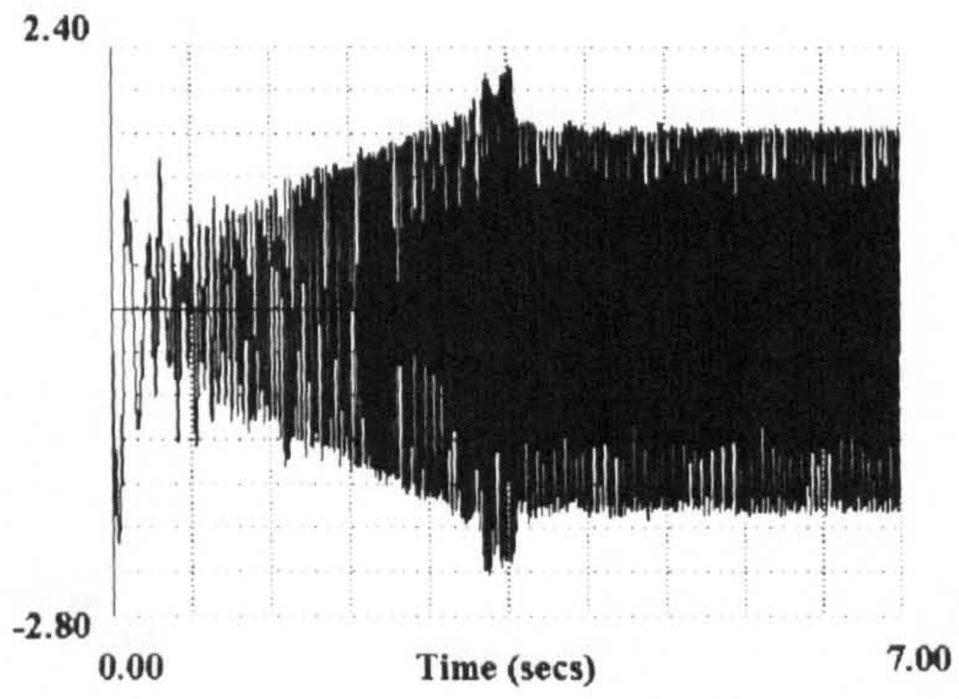

(b) Phase B stator current (pu)

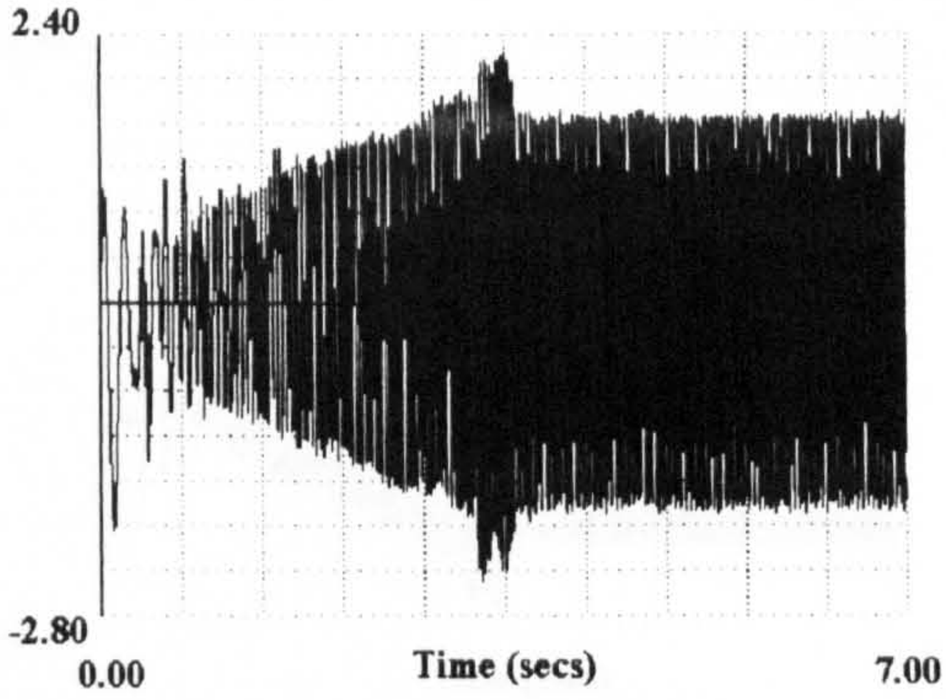

(c) Phase C stator current (pu)

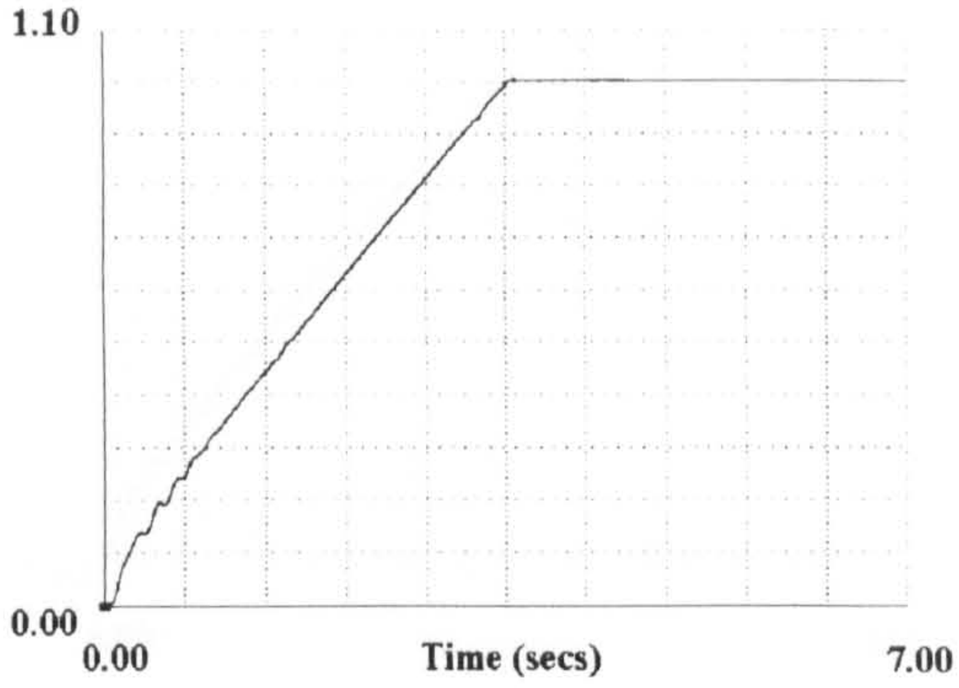

(d) Speed (pu)

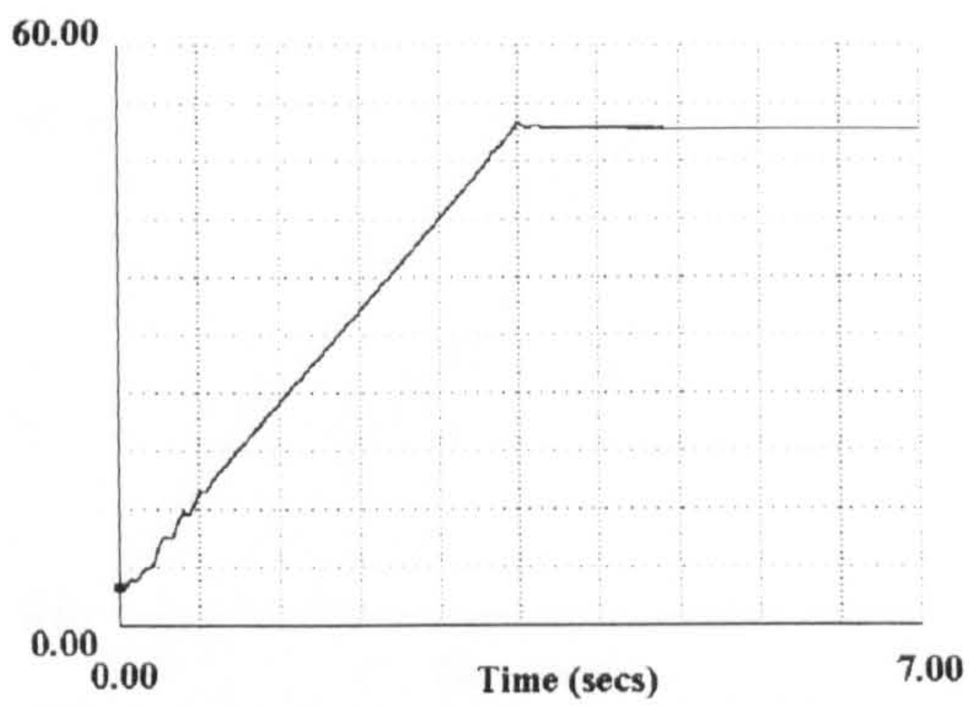

(e) Frequency of the stator (Hz)

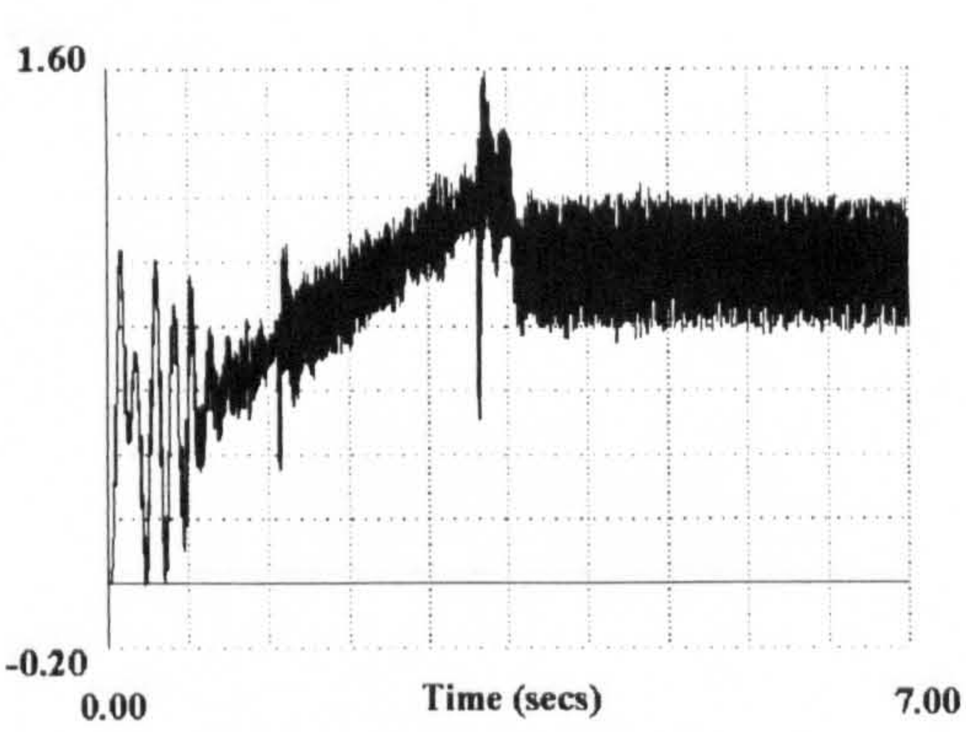

(f) Torque (pu)

Figure 2.28 Dynamic performance of PWM (symmetric regular sampling) inverter-induction motor drive with the load torque proportional to the motor speed for 1.0 pu speed demand using closed-loop speed control.

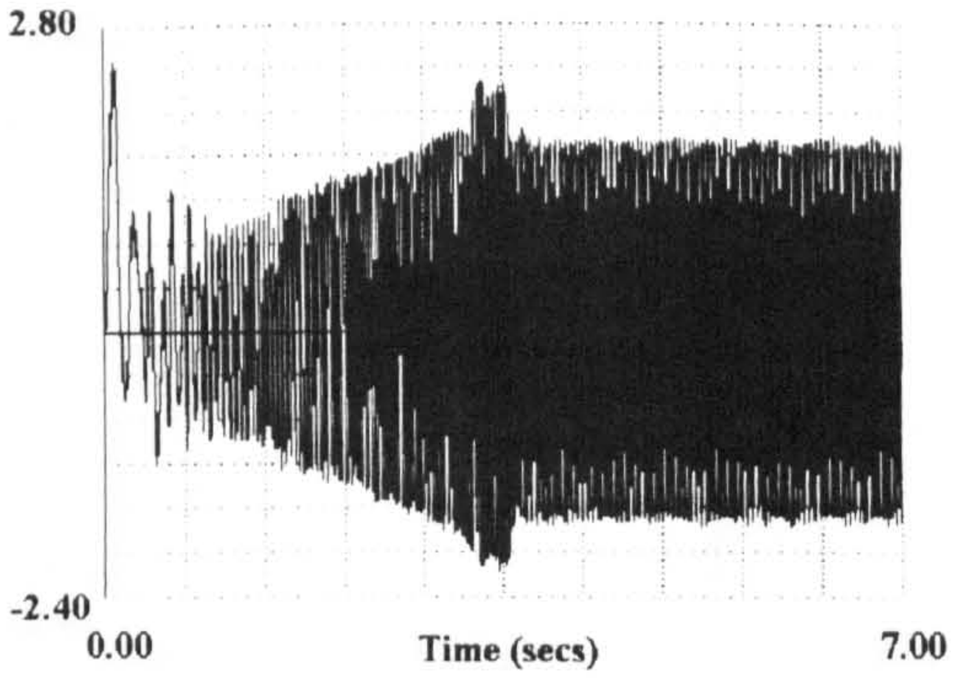

(a) Phase A stator current (pu)

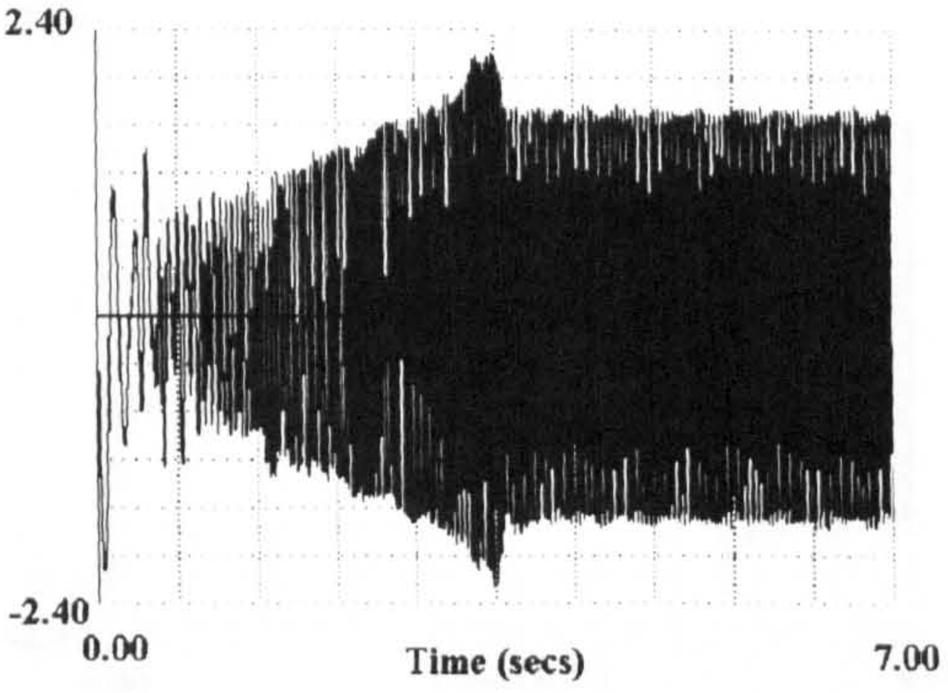

(b) Phase B stator current (pu)

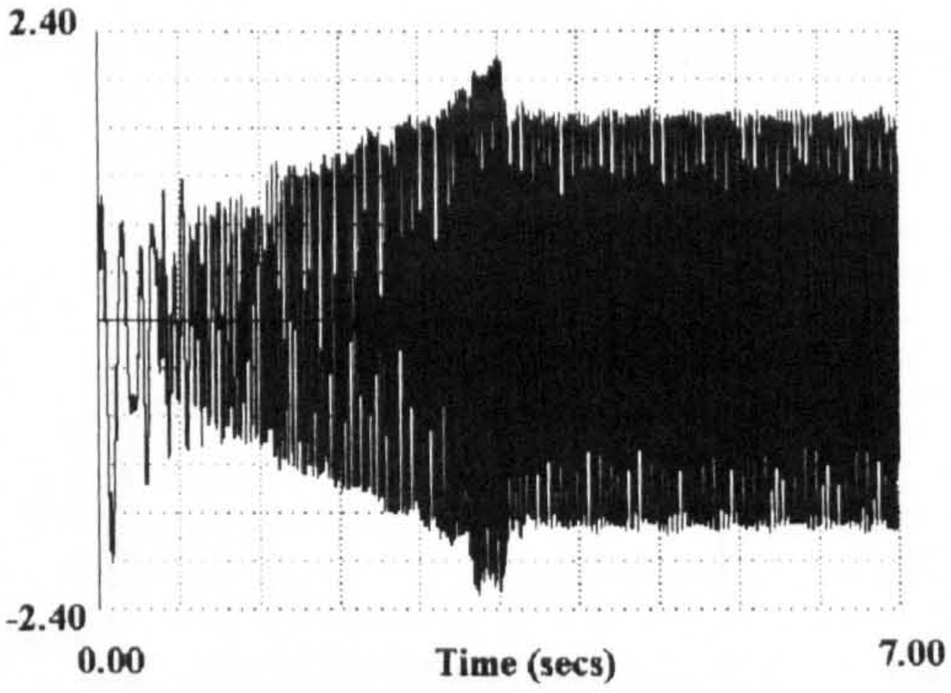

(c) Phase C stator current (pu)

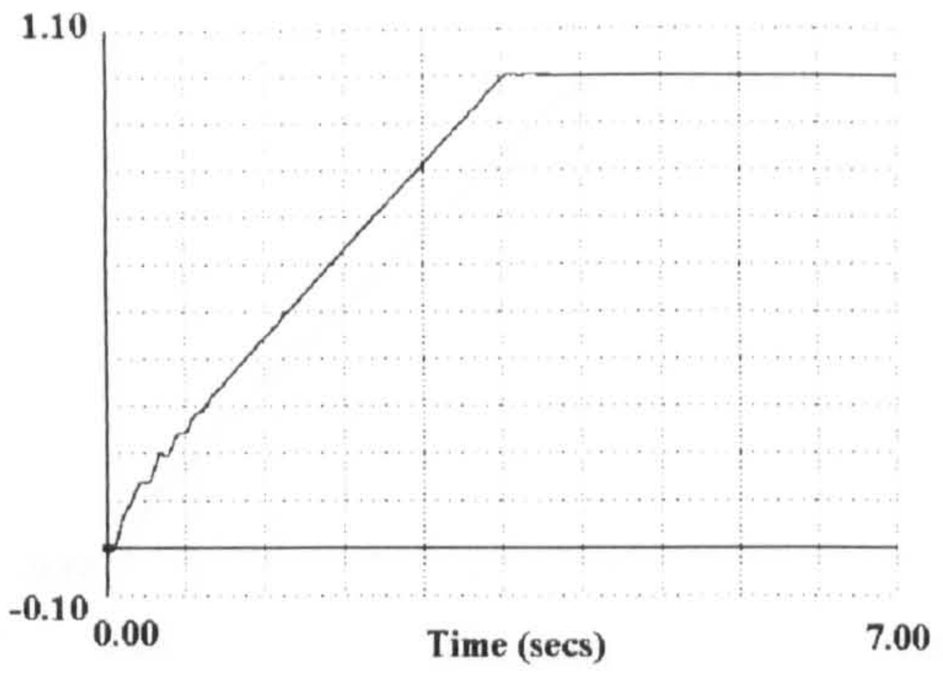

(d) Speed (pu)

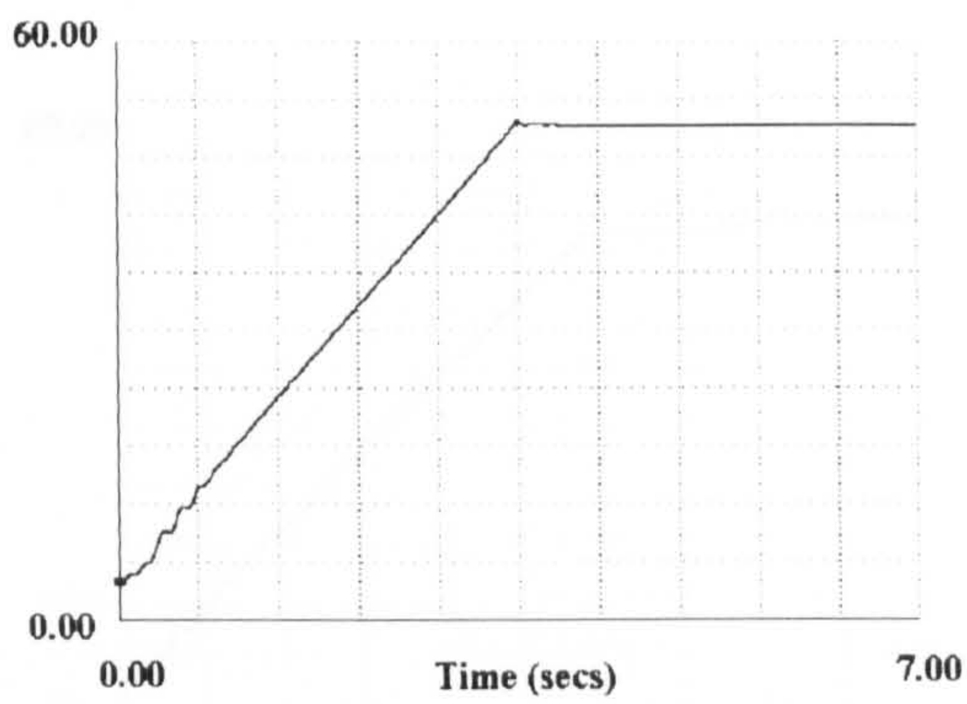

(e) Frequency of the stator (Hz)

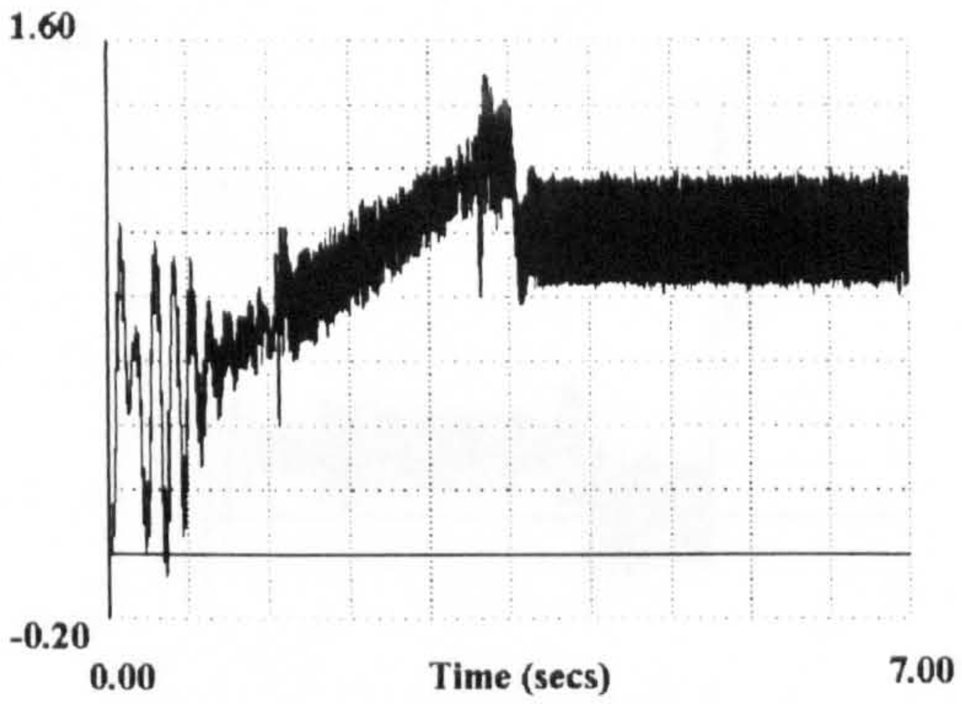

(f) Torque (pu)

Figure 2.29 Dynamic performance of PWM (asymmetric regular sampling) inverter-induction motor drive with the load torque proportional to the motor speed for 1.0 pu speed demand using closed-loop speed control.

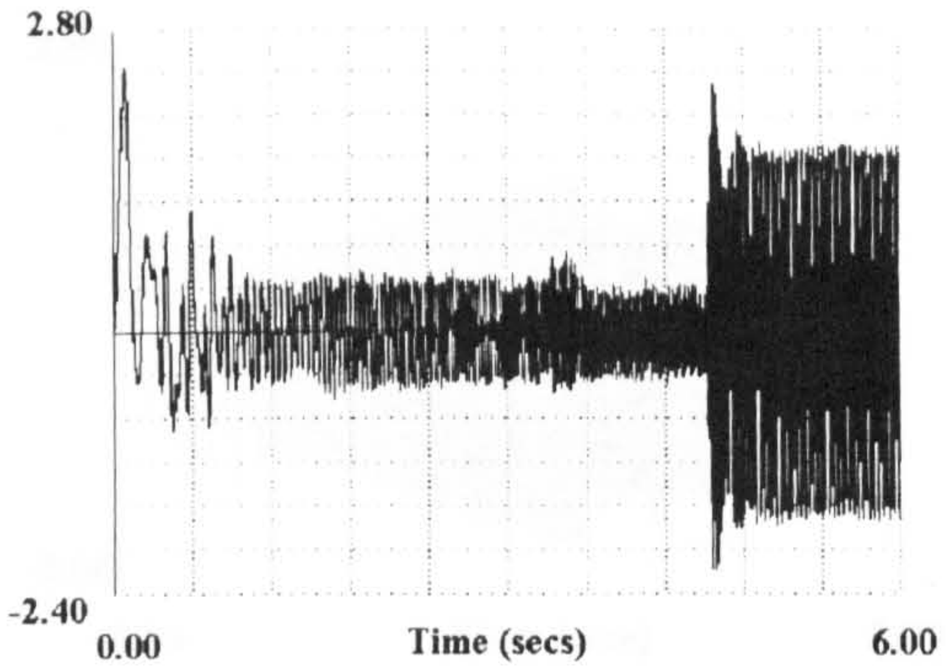

(a) Phase A stator current (pu)

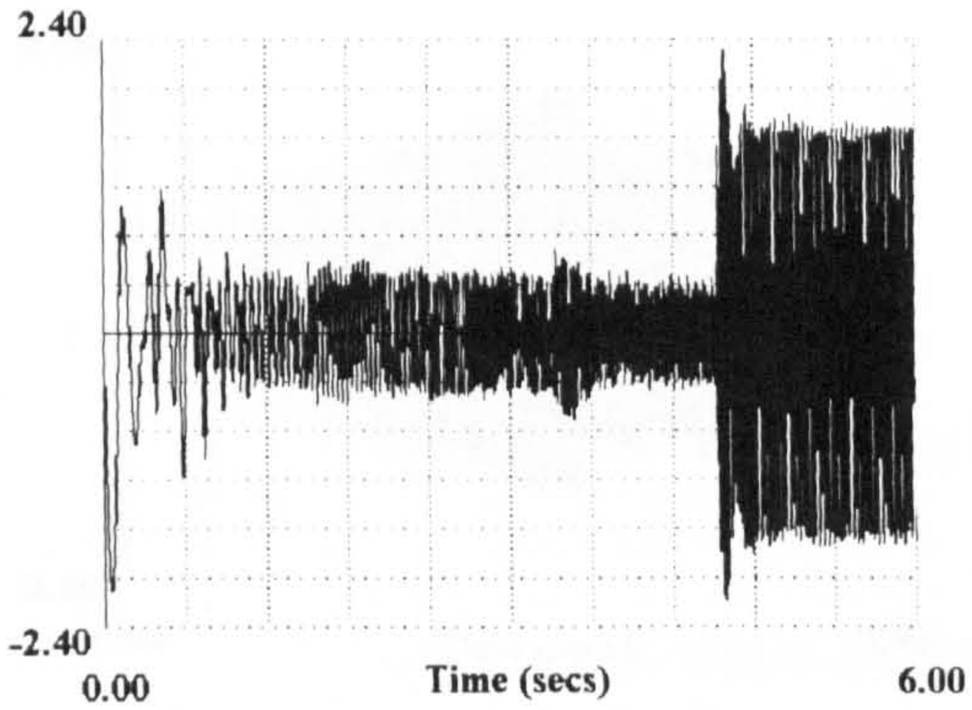

(b) Phase B stator current (pu)

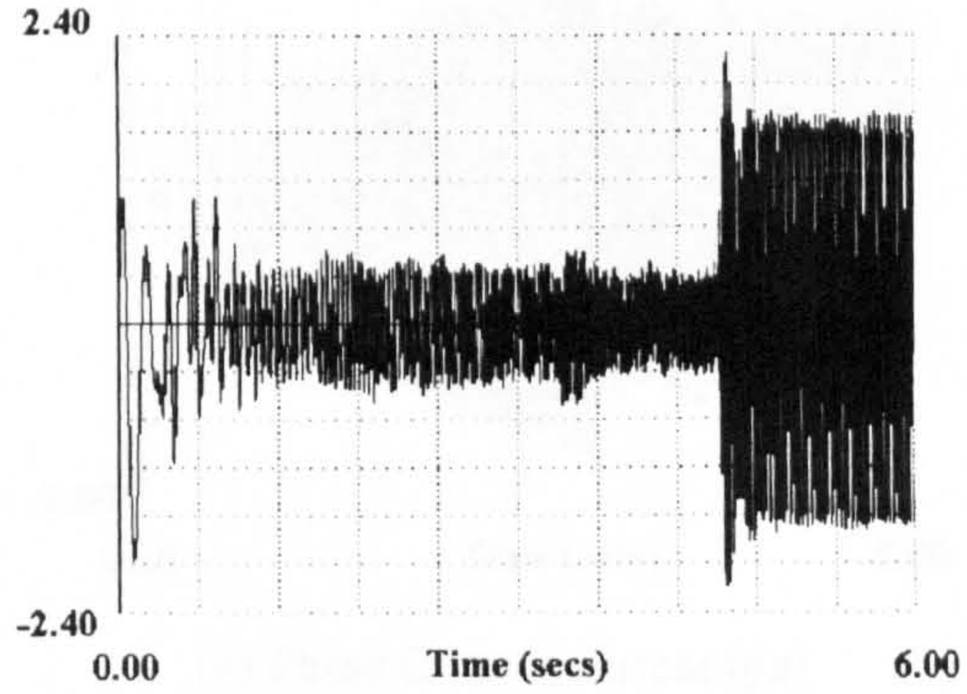

(c) Phase C stator current (pu)

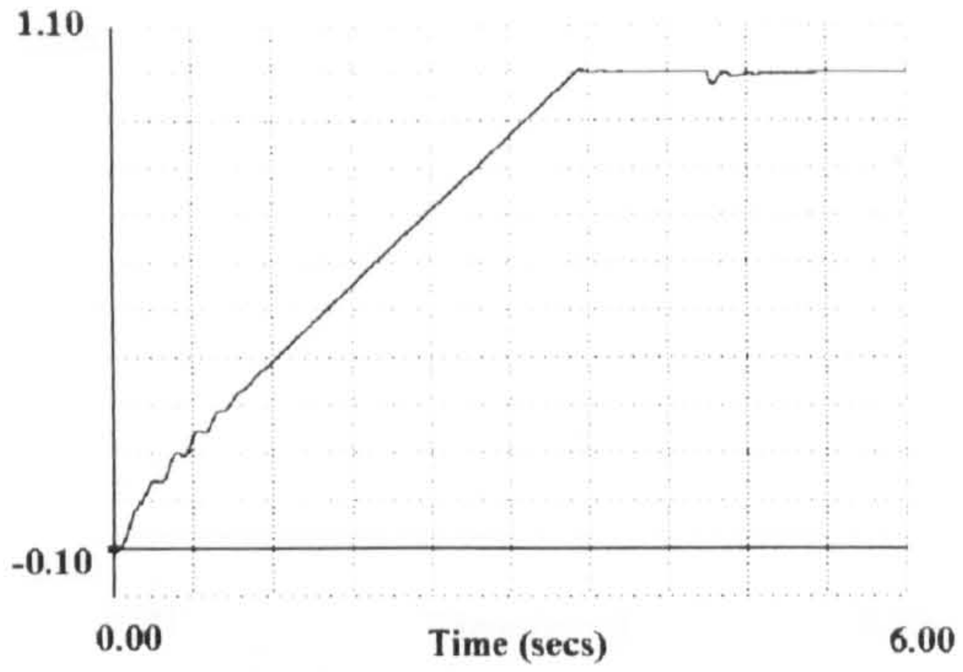

(d) Speed (pu)

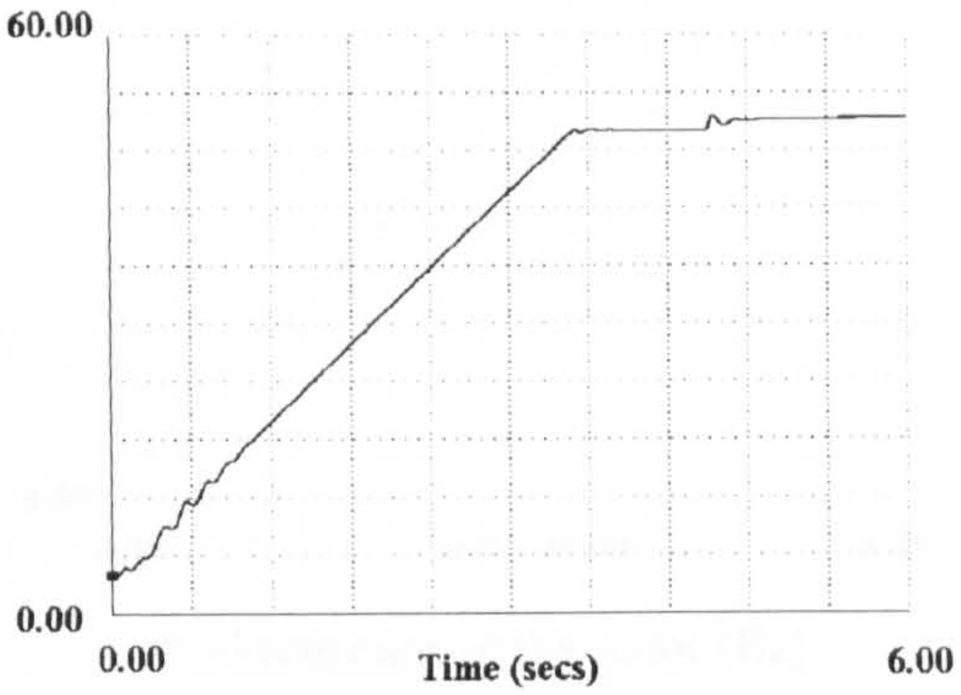

(e) Frequency of the stator (Hz)

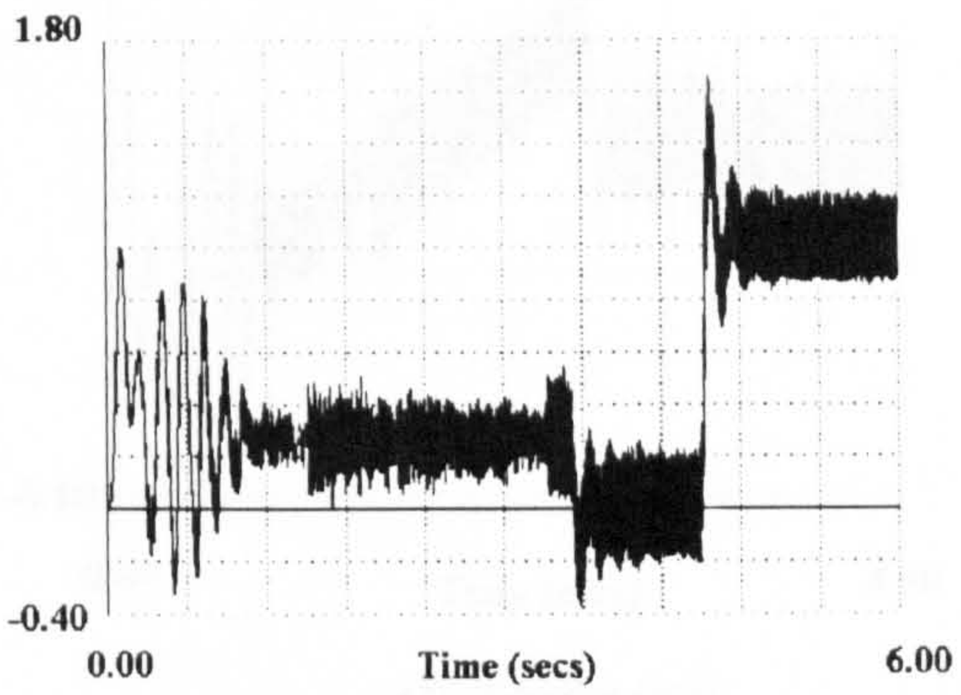

(f) Torque (pu)

Figure 2.30 Dynamic performance of PWM (natural sampling) inverter-induction motor drive with the load torque equal with 1.0 pu from 4.5-6.0 secs for 1.0 pu speed demand using closed-loop speed control.

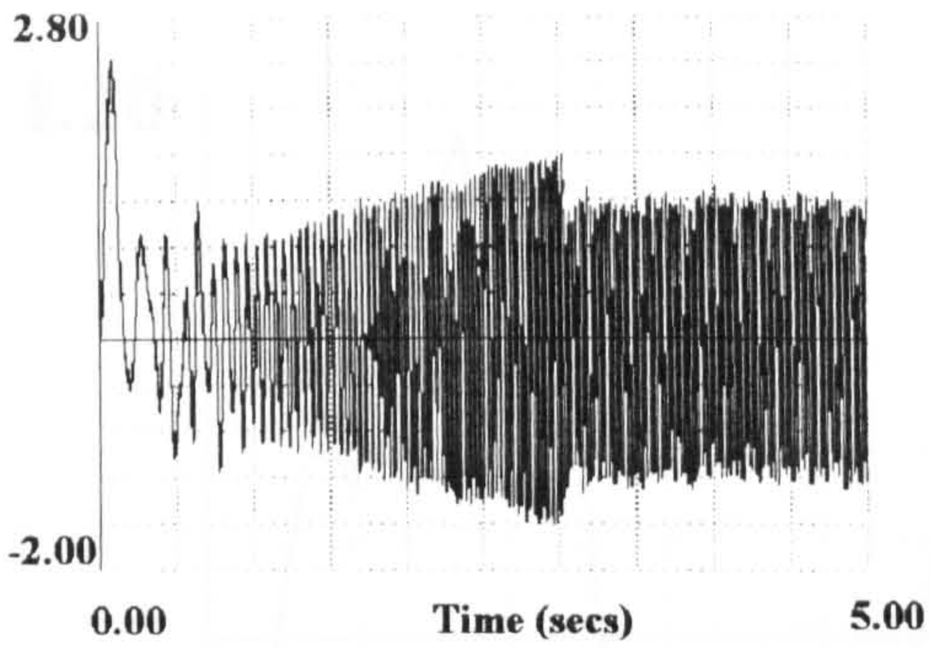

(a) Phase A stator current (pu)

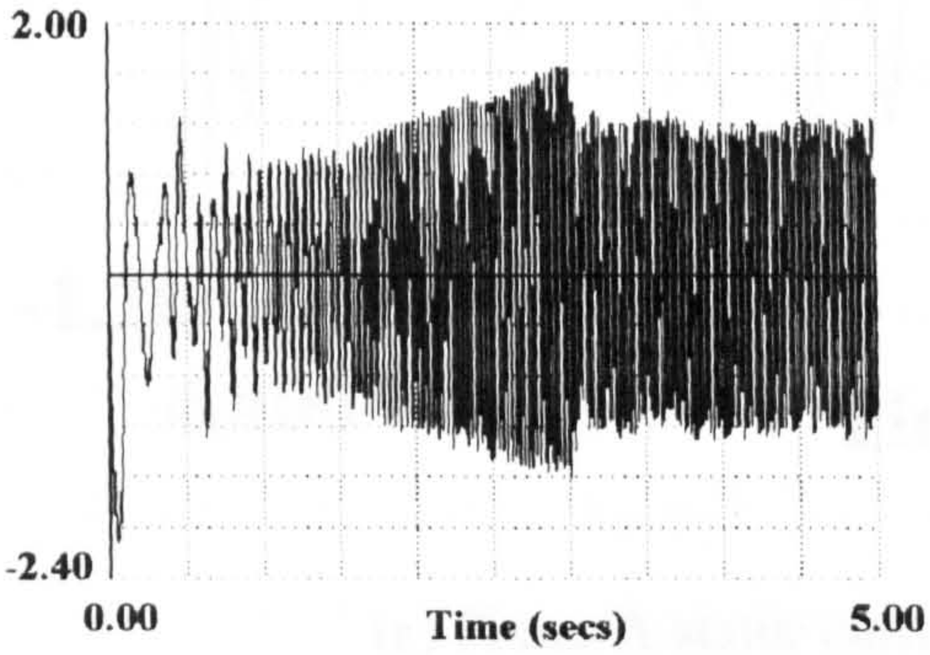

(b) Phase B stator current (pu)

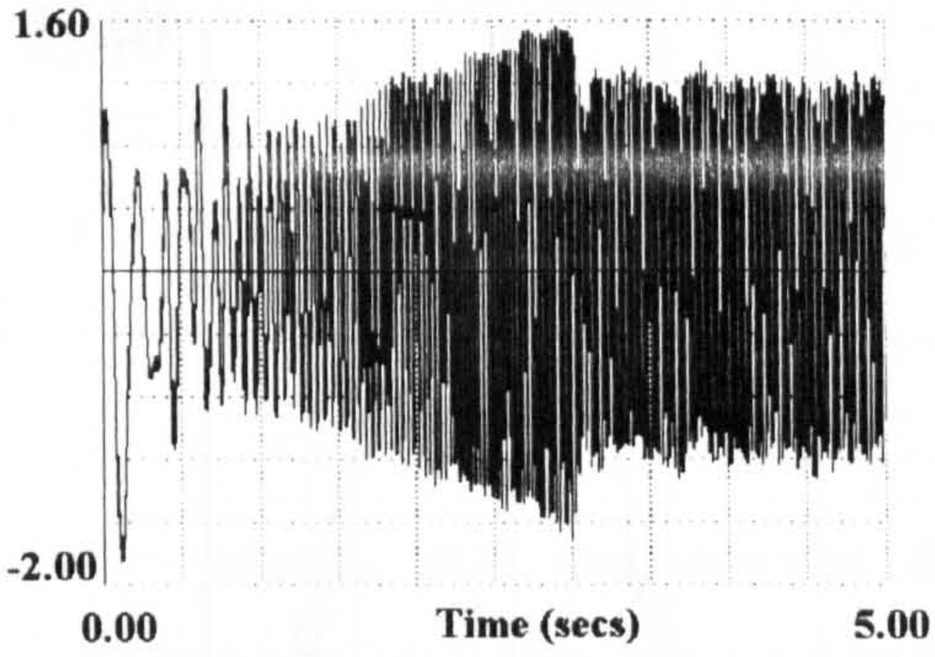

(c) Phase C stator current (pu)

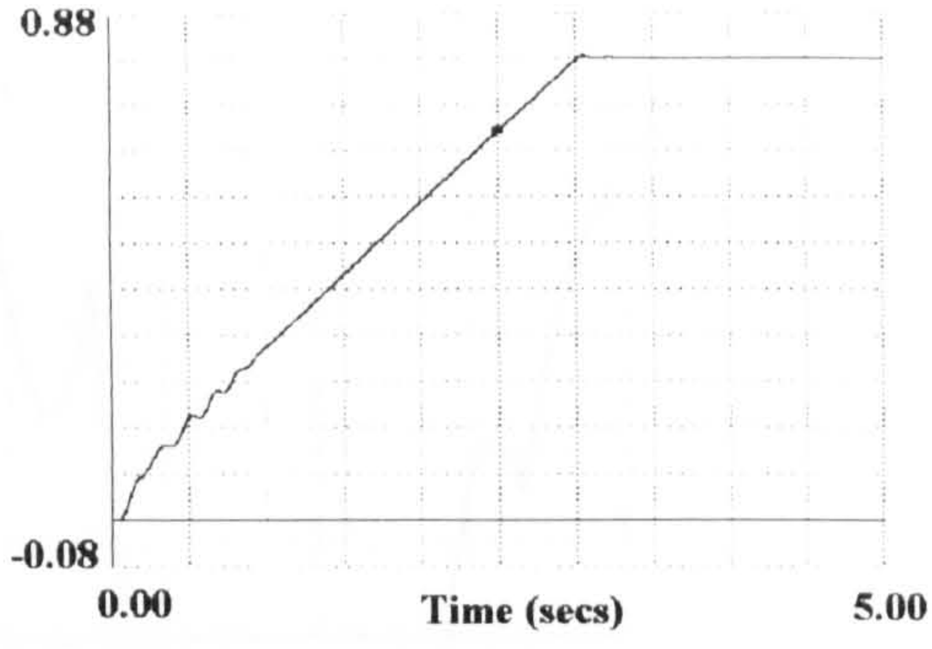

(d) Speed (pu)

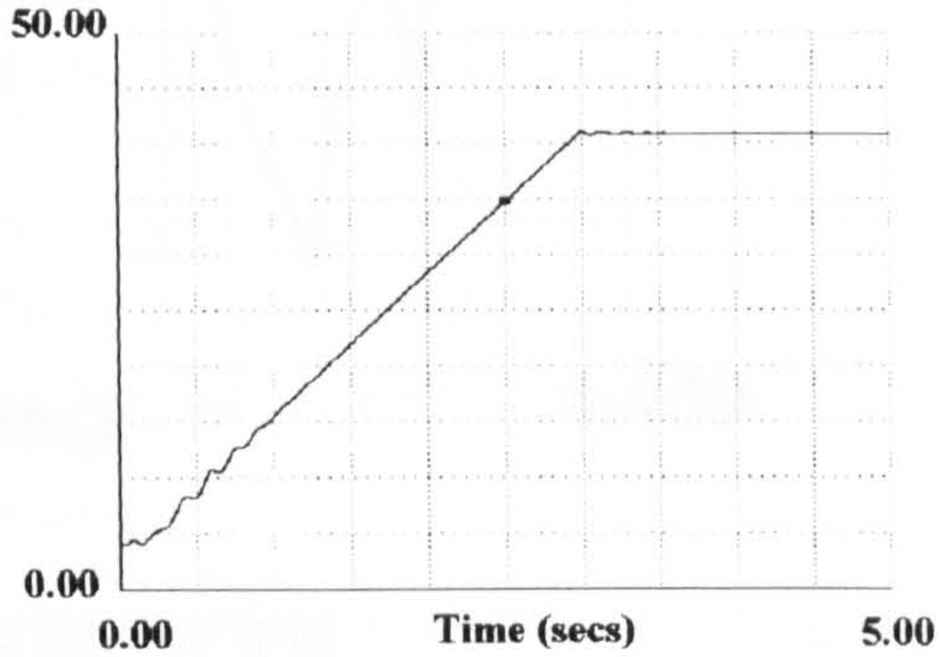

(e) Frequency of the stator (Hz)

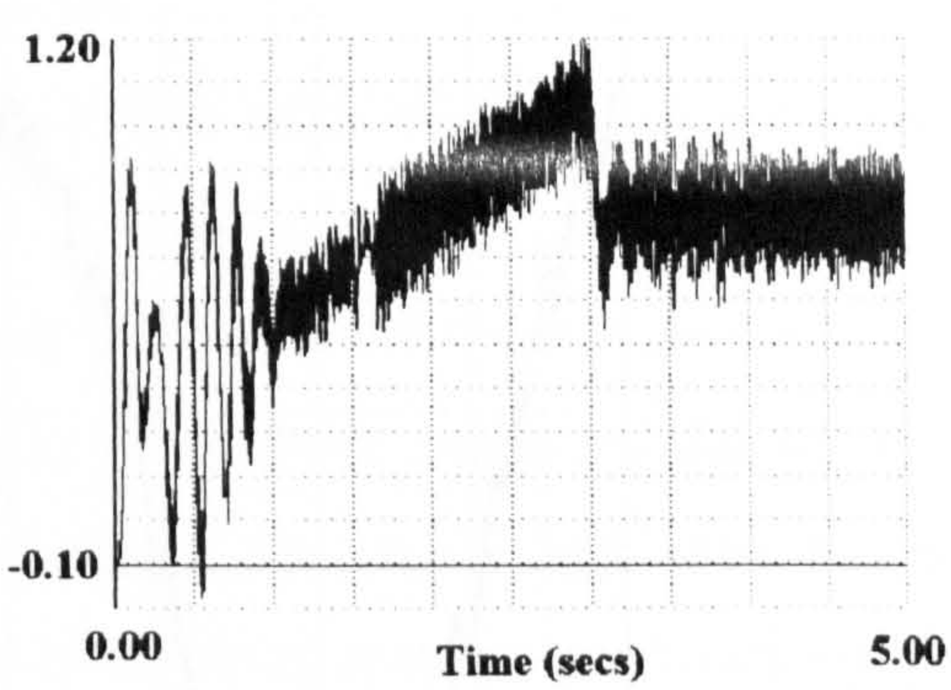

(f) Torque (pu)

Figure 2.31 Dynamic performance of PWM (natural sampling) inverter-induction motor drive with the load torque proportional to the motor speed for 0.8 pu speed demand using closed-loop speed control.

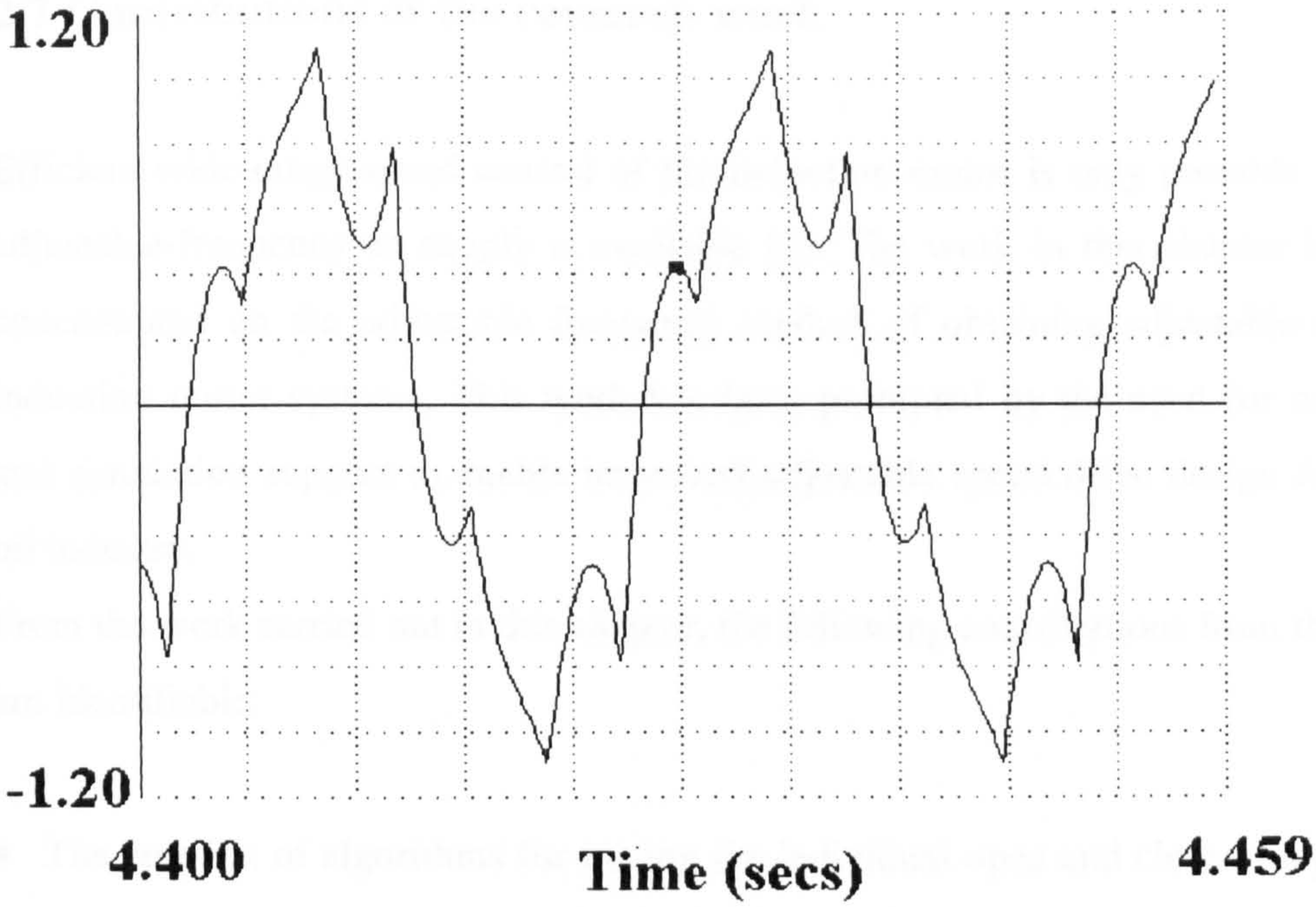

(a) Phase A stator current using six step (pu)

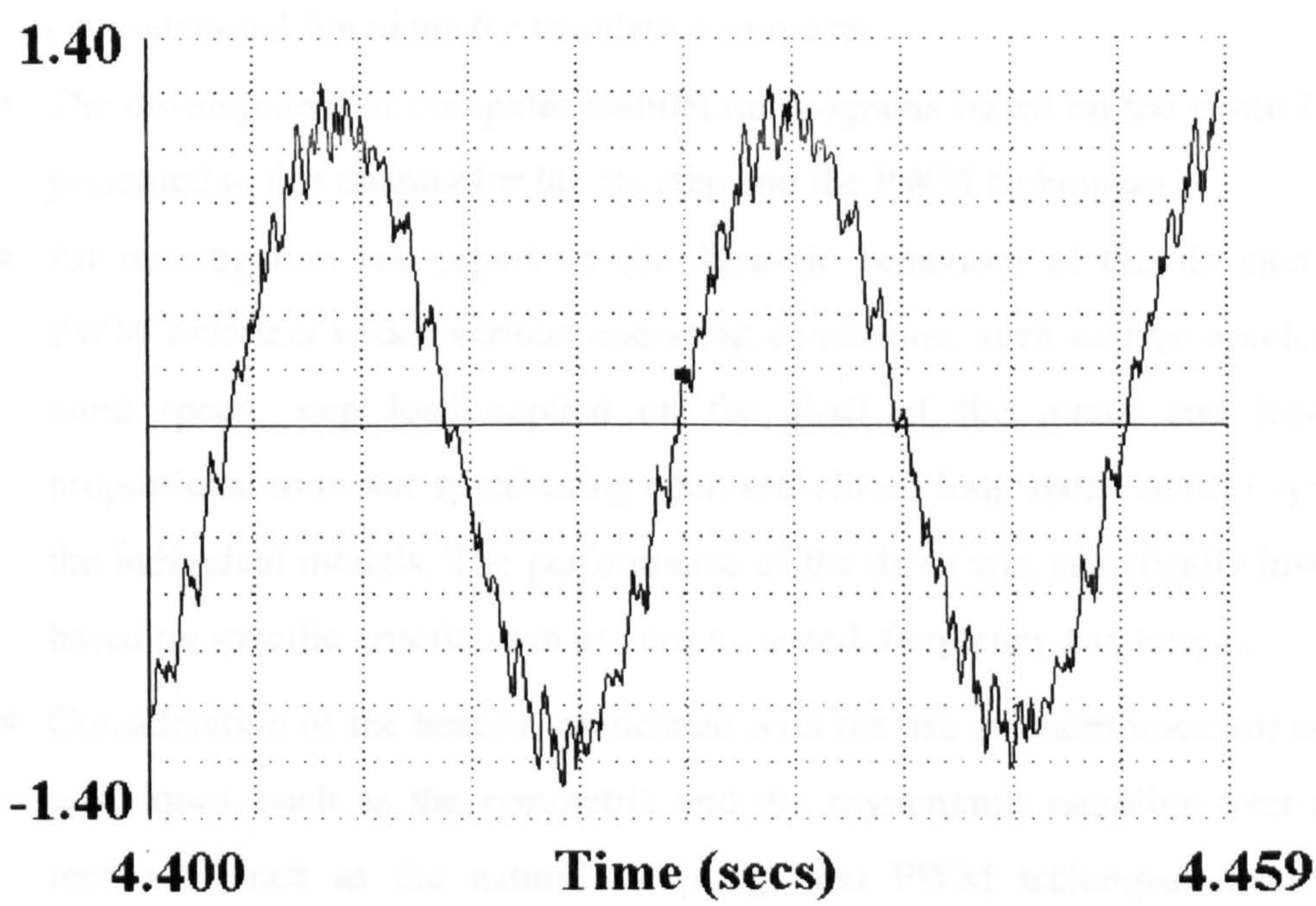

(b) Phase A stator current using PWM (pu)

Figure 2.32

2.7 Contributions of the research work

Efficient wide-range speed control of the induction motor is only possible when an adjustable-frequency ac supply is available [3]. The work in this chapter is largely concentrated on the adjustable frequency method of obtaining adjustable-speed ac induction motor systems. This work has been prompted by the need for modelling and simulation support to enable improved adjustable speed drive design for use in oil industry.

From the work carried out in this chapter, the following contributions from the author are identifiable:

- The creation of algorithms for tracing the individual open and closed loop control systems for the six step and various PWM models.
- The development of mathematical expressions for natural sampling and symmetric/asymmetric sampling PWM methods in order to derive useful computational functions for simulation purposes
- The development of computer simulation programs based on the control systems presented in this chapter for the six step and the PWM techniques
- An investigation and report on the dynamic behaviour of the six step and the PWM inverters under various operating conditions, such as free acceleration to rated speed, step load applied on the shaft of the motor and load torque proportional to motor speed using open and closed loop speed control systems for the individual models. The performance of the drive was analytically investigated based on specific criteria such as current, speed, frequency and torque.
- Consideration of the benefits associated with the use of microprocessor controlled techniques, such as the symmetric and the asymmetric sampling over analogue methods (such as the natural sampling) and PWM techniques over six step inversion

2.8 Conclusions

The work presented in this chapter described the six-step and different PWM inverter control methods of the induction motor. Firstly the fundamentals of the six-step and various PWM techniques were reported and the basic system configurations of these were presented. An analysis of the control systems of the six-step and PWM methods was investigated for both open or closed control systems. Finally extended simulations studies were carried out for a number of different system scenarios.

2.9 References

1. Bose, B. K., "Power electronics and a.c. drives", Prentice-Hall Inc., New Jersey, 1986.
2. Leonard W., "Control of Electrical Machines", Springer-Verlag, 1985.
3. Murphy, J.M.D. and Turnbull, F.G. ,"Power electronic control of a.c. motors," Pergamon Press plc., England, 1988.
4. Bowes, S.R and Mount, M.J : "Microprocessor control of PWM inverters", IEE Proceedings B, 1981, pp 293-305.
5. Bowes, S.R and Bird B.M, "Novel approach to the analysis and synthesis of modulation processes in power convertors", Proceedings IEE 1978, pp 507-513.
6. Mokrytzki, B "Pulse-width modulated inverters for A.C motor drives", IEEE Transactions, 1967, pp 493-503.
7. Casteel, J.B and Hoft, R.G, "Optimum P.W.M waveforms of a microprocessor controller inverter", IEEE Proceedings 1978, pp 243-250.
8. Mohan N, Underland T, Robbins W ,"Power electronics: Converters, Applications and Design", John Wiley and Sons 1995.
9. Krause, P.C. "Analysis of electrical machinery", McGraw-Hill Book Company, New-York, 1987.
10. Abbas, M.A., Christen , R. and Jahns, T.M. "Six step voltage source inverter driven induction motor", IEEE Transactions on Industry Applications, vol IA-20, 1984, pp 1251-1259.
11. Grant, T.L., and Bardon, T.H "Control strategies for P.W.M drives", IEEE Transactions 1980, IA-16, pp 211-215.
12. Zubek, J., Abbondanti, A and Nordby C.J "Pulse-width modulated inverter motor drives with improved modulation", IEEE Transactions 1975, IA-11,pp 695-703.
13. Adams, R.D. and Fox R.S., "Several modulation techniques for the P.W.M inverter", IEEE Transactions, IA-8, 1978, pp 636-643.
14. Namburi, N.R. and Barton, T.H. "Time domain response of induction motors with PWM supplies", IEEE Transactions on Industry Applications, vol. IA-21, 1985, pp. 448-455.

15. Smith J.R. and Chen Meng-Jen, Three-Phase Electrical Machine Systems-computer simulation, Research Studies Press Ltd, 1993.

16. Smith J.R "Response analysis of A.C electrical Machines-computer models and simulation", Research Studies Press Ltd, 1990.

17. McLean A, "A.C Haulage system for coalcutting machine", internal report for Anderson Strathclyde PLC company, November 1990.

CHAPTER 3

MODELLING OF VECTOR CONTROL METHODS

3.1 Introduction

In the scalar control methods of voltage-fed six step and PWM drives, the voltage and frequency are the basic control variables of the ac motor. In a voltage-fed drive, both the torque and air gap flux are functions of voltage and frequency[1,2,3,4,5,6,7]. This coupling effect is responsible for the sluggish response of the ac motor. If, for example, the torque is increased by incrementing the frequency, the flux tends to decrease. However, it is compensated by the sluggish flux control loop feeding in additional voltage. This transient dipping of flux reduces the torque sensitivity with slip and therefore lengthens the response time.

The foregoing limitation can be overcome by applying vector or field-oriented control methods. The aim of field-orientation is to control an ac-machine to obtain the performance characteristics similar to a separately excited dc-machine, providing good efficiency and excellent dynamic performance. Fortunately, dc-motor control is straightforward because the dc-motor has a decoupled control structure with independent control of flux and torque. But it has important limitations caused by the mechanical commutator, and these can be overcome by application of the ac-motor.

In field-oriented control the input stator current of squirrel-cage induction motor is controlled so that it is decoupled into magnetising and torque producing components. Thus the induction motor can have a control structure as in a dc-motor.

In the first part of this chapter, the principles of field oriented control scheme are presented. The basic configuration of a current-controlled PWM inverter drive is implemented, followed by an analysis of the two main vector control methods, the direct and the indirect vector control techniques. A new algorithm has been

developed to permit improved simulation and modelling of an existing indirect field orientation control method. This modelling tool has then been used to simulate system operations for a number of different operating conditions. Finally, the main contributions and general conclusions of this research work are reported.

3.2 Principles of Field-Oriented Control of the Induction Motor

In the vector control method, an ac machine is controlled like a separately excited dc machine[1,8]. This analogy is explained in Fig.3.1 . In a dc machine, the torque is :

$$T_e = K_t' I_\alpha I_f \tag{3.1}$$

where I_α is the armature or torque component of current and I_f is the field or flux component of current.

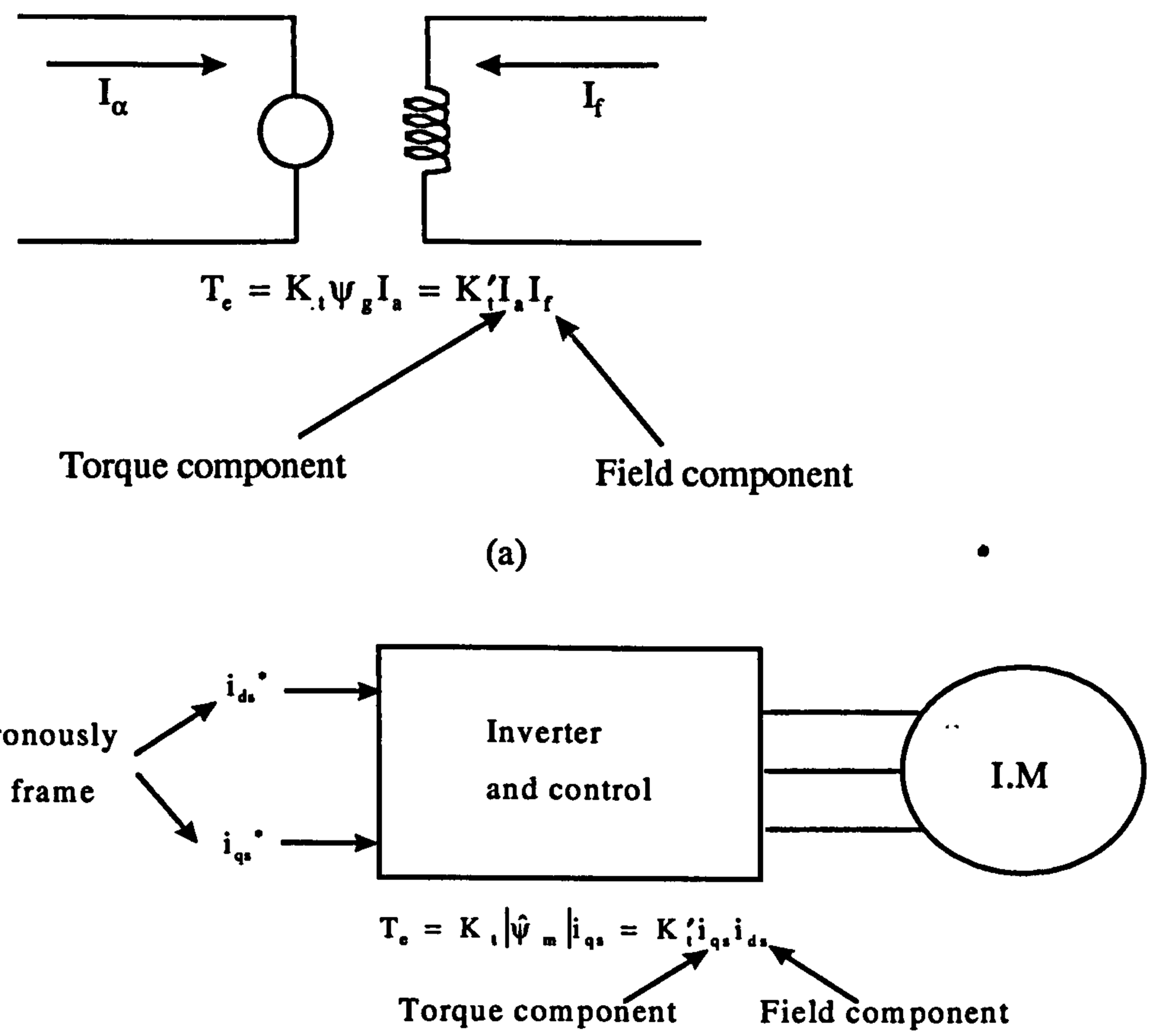

Figure 3.1 Induction motor and dc machine analogy in vector control

In a dc machine, the control variables I_α and I_f can be considered as decoupled vectors. In normal operation, the field current I_f is set to maintain the rated field flux and torque is changed by changing the armature current. Since the current I_f is decoupled from the armature current I_α, the torque sensitivity remains maximum in both transient and steady-state operations. This mode of control can be extended to an induction motor also if the machine operation is considered in a synchronously rotating reference frame where the sinusoidal variables appear as dc quantities. In Fig.3.1 the induction motor with inverter and control is shown with two control inputs, i_{ds}^* and i_{qs}^*. The currents i_{ds} and i_{qs} are the direct-axis component and quadrature-axis component, respectively, of the stator current, where both are in a synchronously rotating reference frame. In vector control, i_{ds} is analogous to the field current I_f and i_{qs} is analogous to the armature current I_α of a dc machine. Therefore, the torque can be expressed as

$$T_e = K_t|\hat{\psi}_m|i_{qs} = K_t' i_{qs} i_{ds} \tag{3.2}$$

The basic concept of how i_{ds} and i_{qs} can be established as control vectors in the vector control method is explained in Fig.3.2 with the help of phasor diagrams in a synchronously rotating $d^e - q^e$ reference frame[3]. For simplicity, the rotor leakage inductance is neglected.

The phasor diagram is drawn with the air gap voltage $\hat{V}_g$ aligned with the q^e axis. The stator current $\hat{I}_s$ lags the voltage $\hat{V}_g$ by $(90-\theta)^\circ$, i.e., $i_{qs} = \hat{I}_s \sin\theta$ is in phase with $\hat{V}_g$ and $i_{ds} = \hat{I}_s \cos\theta$ is in quadrature with $\hat{V}_g$. The current i_{qs} is the torque component of the stator current and the current i_{ds} is the field component of the stator current and is responsible for establishing the air gap flux $\hat{\psi}_m$. From the phasor diagram, the developed torque across the air gap is given by $T_e = K_t|\hat{\psi}_m|i_{qs} = K_t' i_{qs} i_{ds}$, where i_{qs} and i_{ds} are shown in Fig.3.2. The torque

equation is therefore identical to that of a dc machine. For normal operation, the current i_{ds} remains constant and the torque is varied by varying the i_{qs} component.

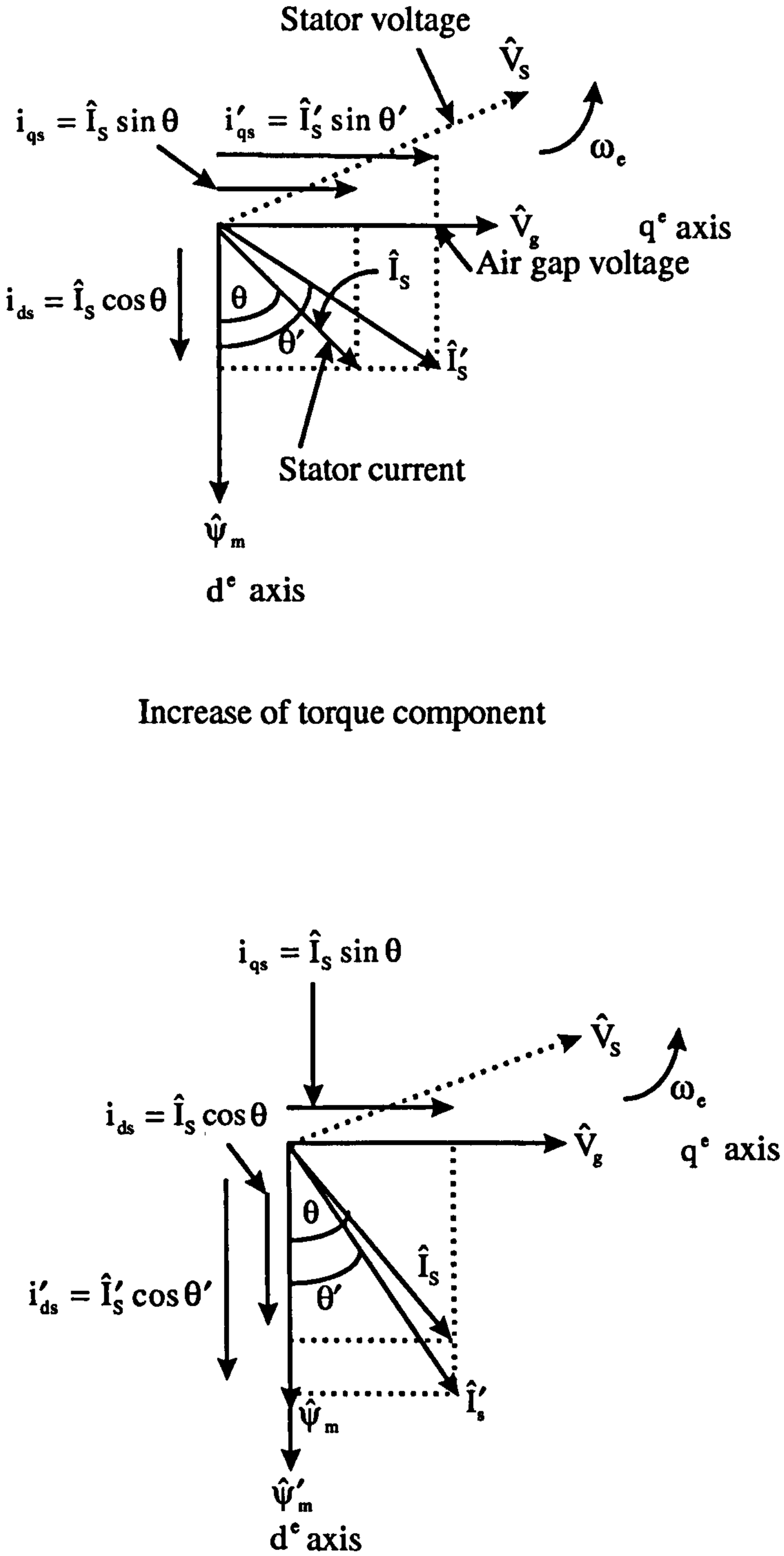

Figure 3.2 Phasor diagrams in direct vector control

3.3 Configuration of Current-Controlled PWM Voltage-fed Inverter

The current regulated voltage source(VS) PWM inverter offers substantial advantages in high performance ac drives and is widely applied in such systems[9,10].

A basic rectifier-inverter(VS-PWM) with current control is shown in Fig.3.3. From this figure it can be seen that the system has three main stages. In the first stage a full diode bridge is used to convert the three-phase voltage input into a dc voltage.

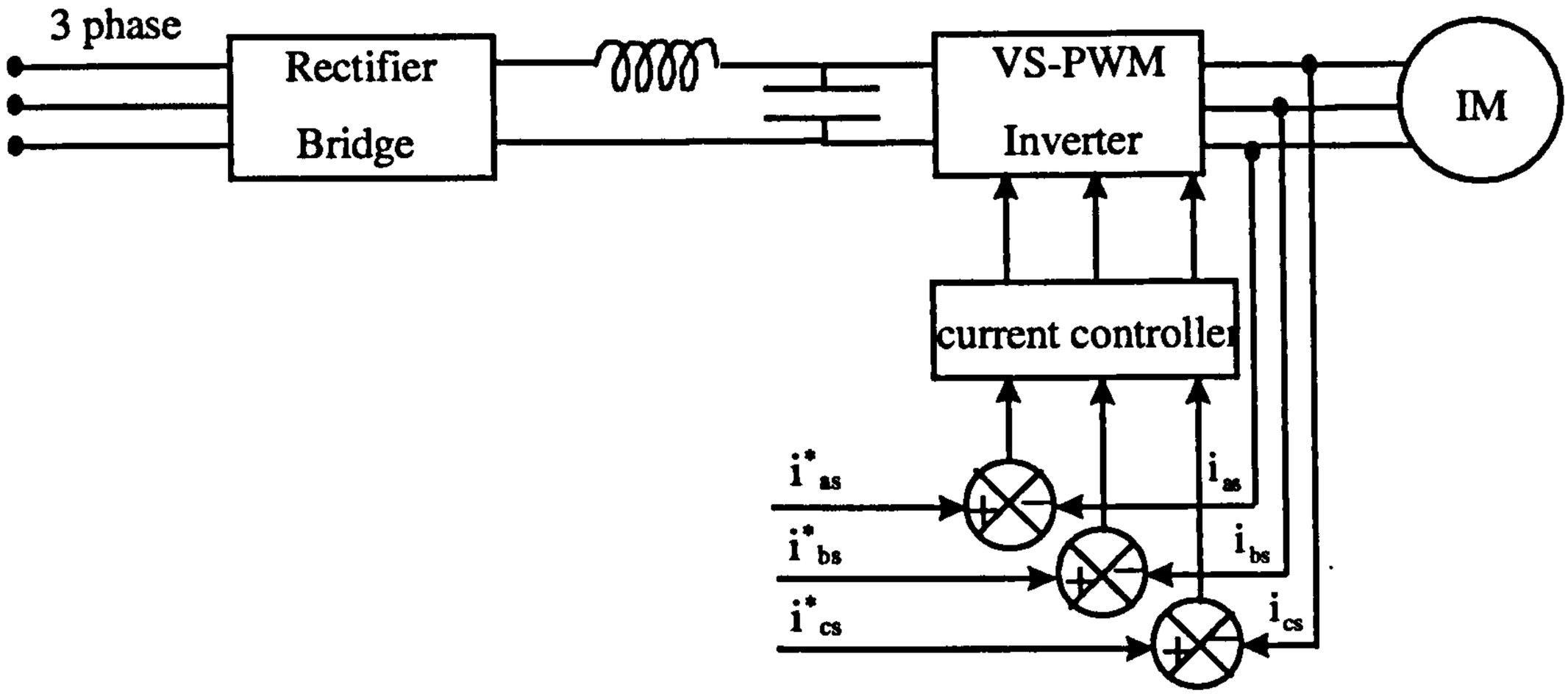

Figure 3.3. Basic system diagram of PWM current controller

Then, a LC circuit filters the voltage ripple and provides a near constant dc bus voltage (V_{dc}) to the inverter. As a last stage the inverter with the current controller impresses stator currents to follow their reference currents.

In this study a hysterisis controller[1], (which is actually three independent controllers, one for each phase) is used. The control of one inverter leg is shown in Fig3.4. The control circuit generates the sine reference current wave of desired magnitude and frequency, which is compared with the actual phase current. If the difference between the reference current and the actual current is positive and greater than the hysterisis value, then the upper transistor in the half-bridge is turn on and the

lower transistor is turned off. If the difference between the reference current and the actual current is negative and greater than the hysterisis value, then the upper transistor is turned off and the lower transistor is turn on. If the difference is less than the hysterisis value then there is no change. A prescribed lock-out time t_L is provided at each transition to prevent a shoot-through fault.

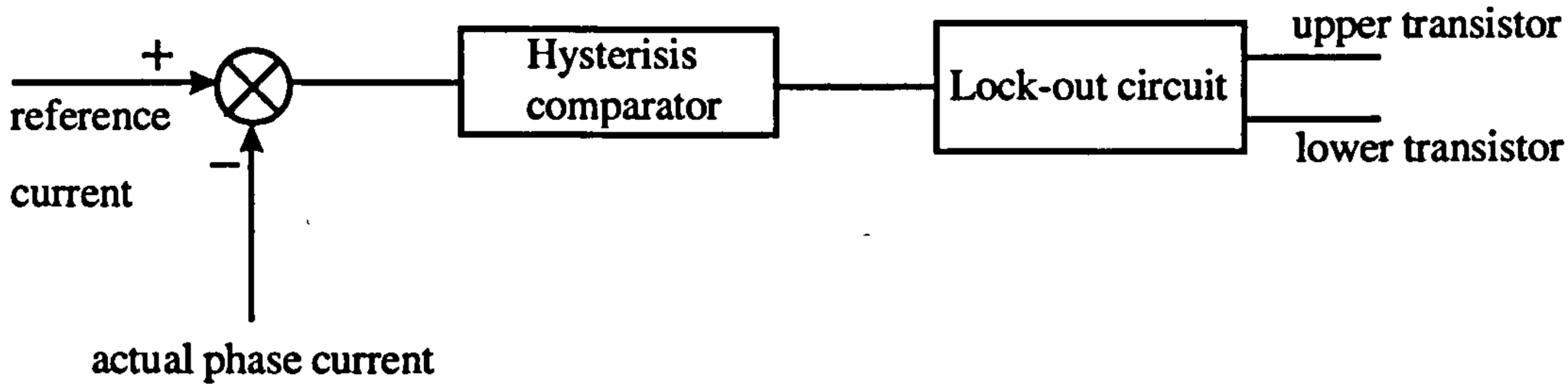

Figure.3.4 Hysterisis control for one phase

Vector control has been criticised as being a complicated approach requiring sophisticated signal processing and complex co-ordinate transformation. This criticism was justified in the past when the implementation was attempted in analog electronics. However, digital control with microprocessors offers significant reductions in processor size and cost[1,3,8].

3.4 Direct Vector Control

Fig. 3.5 shows a simplified block diagram of a vector control scheme using a current-controlled PWM inverter. The two-axis reference currents, i_{qs}^* and i_{ds}^*, are the demanded torque and flux components of stator current, respectively, and are generated by the outer loop. As shown in Fig.3.5 i_{qs}^* and i_{ds}^* undergo a co-ordinate transformation to two-phase stator-based quantities, followed by a two-phase to three phase transformation which generates the stator reference currents $i_{\alpha s}^*, i_{bs}^*, i_{cs}^*$. These reference currents are reproduced in the stator phases by the current-controlled

PWM inverter. The internal action of the motor is to transform the impressed three-phase stator currents to equivalent two-axis currents, i_{qs} and i_{ds}. Thus the external reference currents, i_{qs}^* and i_{ds}^*, are reproduced within the ac motor, and control is executed in term of theses direct and quadrature axis current components to give decoupled control of flux and torque, as in a dc machine.

The control structure is similar to that of a dc drive[3,11,12]. The speed error is fed to the speed controller to generate the torque command, T^*, which is compared with the calculated torque, T, for precise torque control. The torque error generates the quadrature axis reference current, i_{qs}^*. The direct axis reference current, i_{ds}^*, is produced by a rotor flux control loop in which the reference value, ψ_{mr}^* is compared with the actual value ψ_{mr} (calculated at the flux observer block). Below base speed, ψ_{mr}^* is held constant, but field weakening is implemented above base speed by making ψ_{mr}^* inversely proportional to speed as shown in Fig 3.5

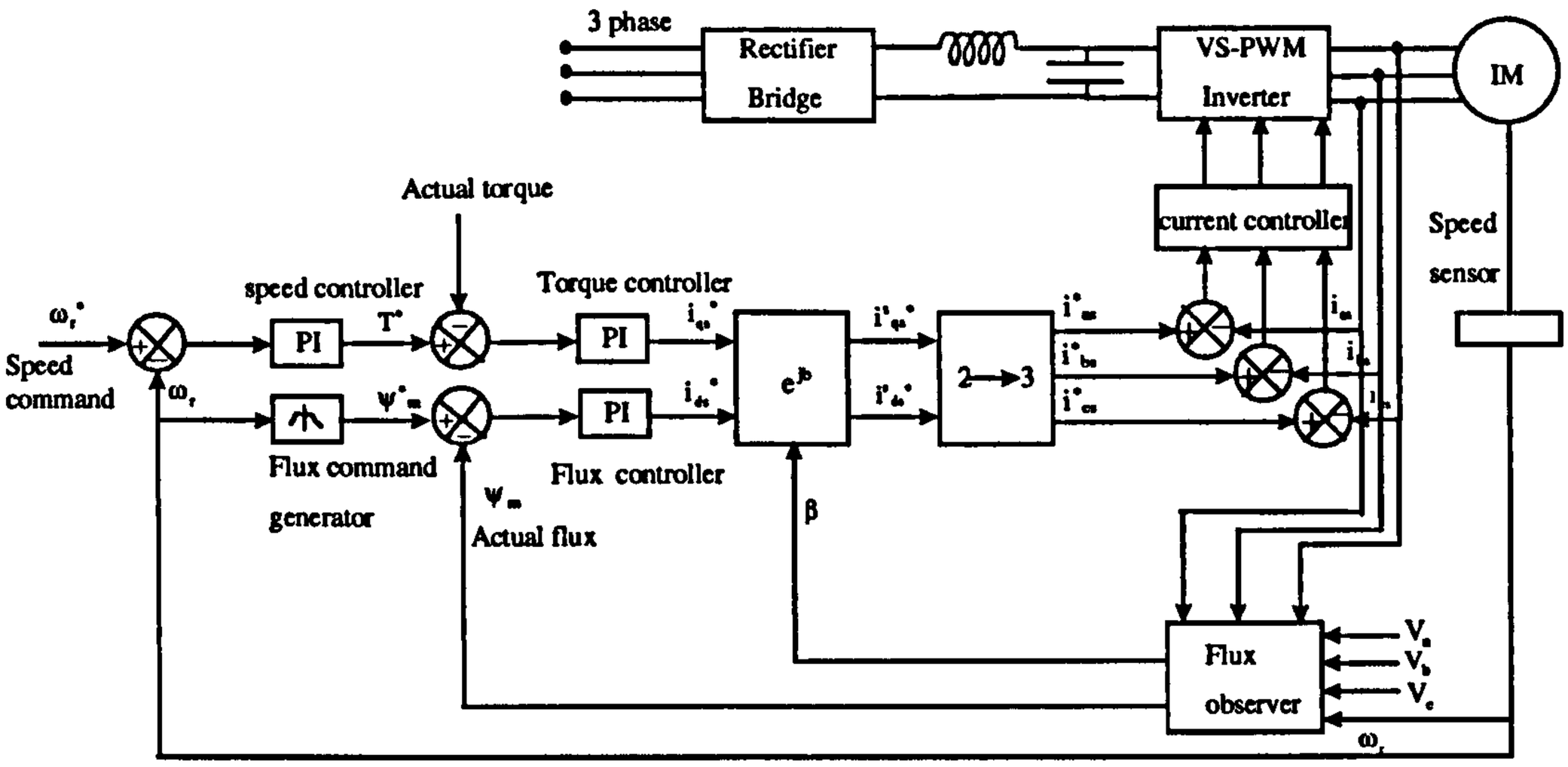

Figure 3.5 AC motor speed control system with direct vector control

3.5 Indirect Vector Control

The indirect methods of vector control eliminate the need for a flux sensor or flux model but require an accurate measurement of shaft position in order to determine the precise location of the rotor flux vector[1,3,13,14]. The indirect vector control principle is explained in Fig.3.6 with the help of a phasor diagram. The $d^s - q^s$ axes are fixed on the stator while the $d^e - q^e$ axes rotate at synchronous angular velocity ω_e. At any instant, the q^e electrical axis is at angular position θ_e with respect to the q^s axis. The angle θ_e is given by the sum of rotor angular position θ_r and slip angular position θ_{sl}. The rotor flux $\hat{\psi}_{mr}$, consisting of the air-gap flux and the rotor leakage flux, is aligned to the d^e axis. Therefore, for decoupling control, the stator flux component of current i_{ds} and the torque component of current i_{qs} are to be aligned to the d^e and q^e axes respectively.

Figures 3.7 and 3.8 shown the D-Q equivalent circuits of an induction motor at the synchronously reference frame.

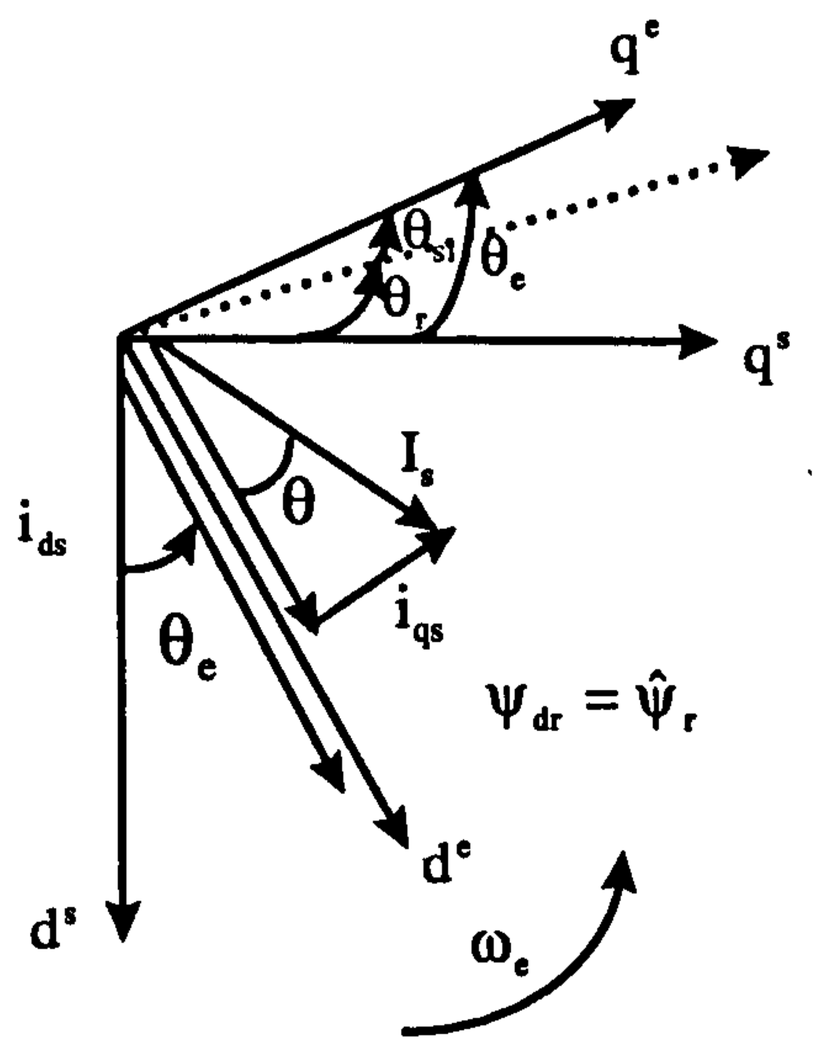

Figure 3.6 Phasor diagram for indirect vector control

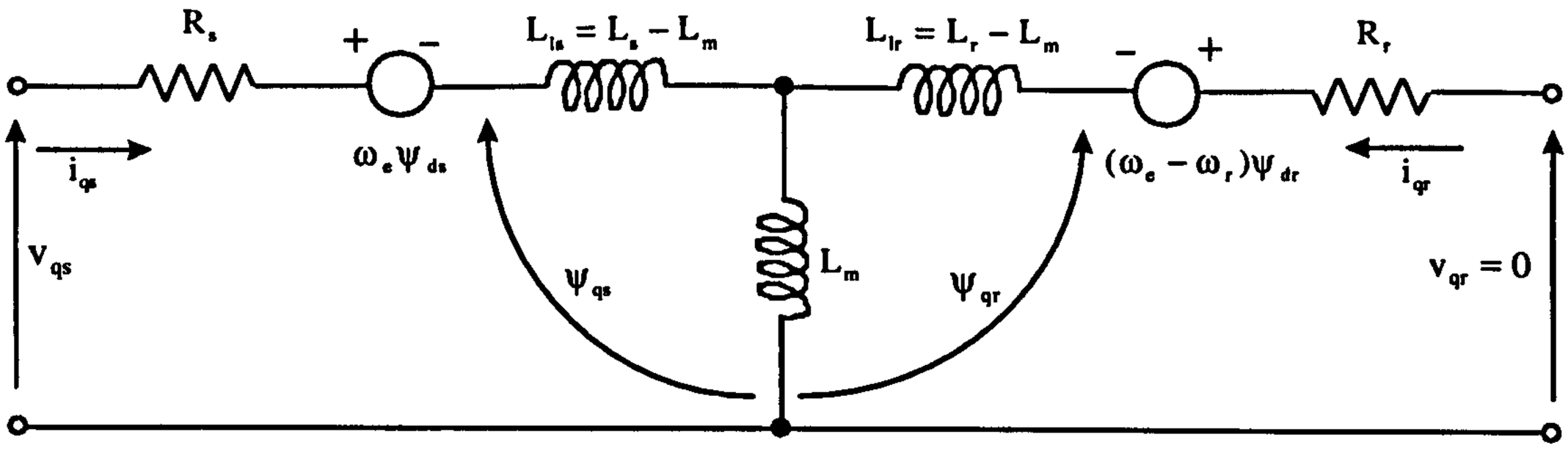

Figure 3.7 q_e - axis equivalent circuit at synchronously rotating reference frame

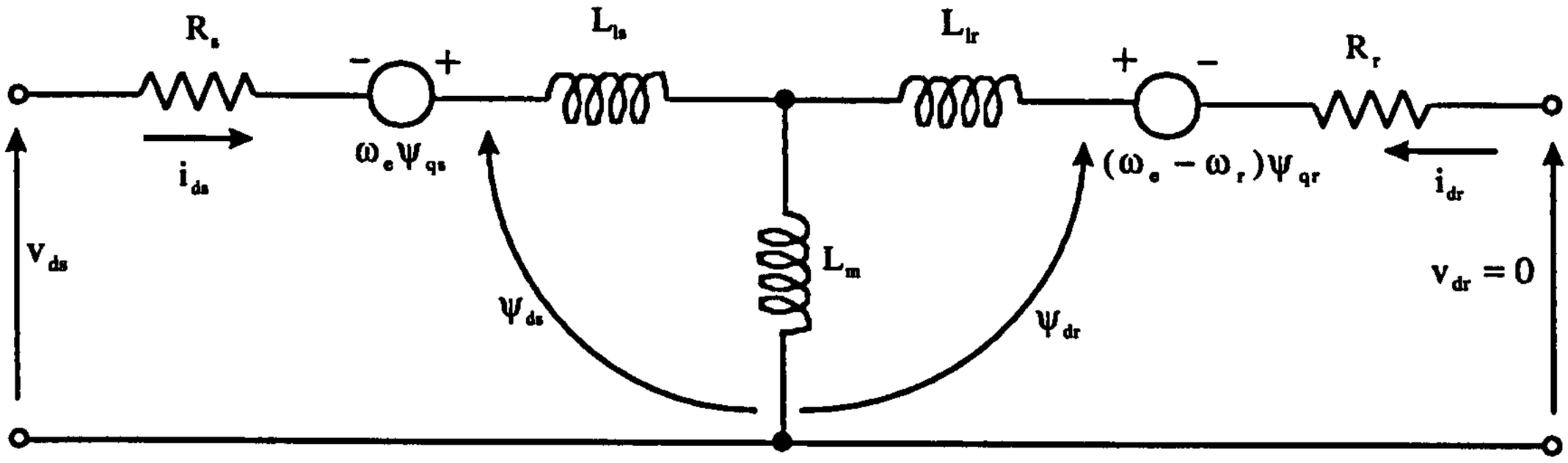

Figure 3.8 d_e - axis equivalent circuit at synchronously rotating reference frame

From the synchronously rotating reference frame, the following equations can be written:

$$\frac{d\psi_{qr}}{dt} + R_r i_{qr} + (\omega_e - \omega_r)\psi_{dr} = 0 \tag{3.3}$$

$$\frac{d\psi_{dr}}{dt} + R_r i_{dr} - (\omega_e - \omega_r)\psi_{qr} = 0 \tag{3.4}$$

Also,

$$\psi_{qr} = L_r i_{qr} + L_m i_{qs} \tag{3.5}$$

$$\psi_{dr} = L_r i_{dr} + L_m i_{ds} \tag{3.6}$$

From equations (3.5) and (3.6) ,

$$i_{qr} = \frac{1}{L_r}\psi_{qr} - \frac{L_m}{L_r} i_{qs} \tag{3.7}$$

$$i_{dr} = \frac{1}{L_r}\psi_{dr} - \frac{L_m}{L_r} i_{ds} \tag{3.8}$$

The rotor currents from equations (3.3) and (3.4) can be eliminated by substituting equations (3.7) and (3.8) as

$$\frac{d\psi_{dr}}{dt} + \frac{R_r}{L_r}\psi_{qr} - \frac{L_m}{L_r} R_r i_{qs} + \omega_{sl}\psi_{dr} = 0 \tag{3.9}$$

$$\frac{d\psi_{qr}}{dt} + \frac{R_r}{L_r}\psi_{dr} - \frac{L_m}{L_r} R_r i_{qs} - \omega_{sl}\psi_{qr} = 0 \tag{3.10}$$

where $\omega_{sl} = \omega_e - \omega_r$.

For decoupling control it is desirable that

$$\psi_{qr} = \frac{d\psi_{qr}}{dt} = 0$$

$$\psi_{dr} = \hat{\psi}_{mr} = \text{ct (constant)}$$

$$\frac{d\psi_{dr}}{dt} = 0$$

Substituting the first two conditions, equations (3.9) and (3.10) can be simplified as

$$\omega_{sl} = \frac{L_m}{\hat{\psi}_{mr}}\left[\frac{R_r}{L_r}\right] i_{qs} \tag{3.11}$$

$$\frac{L_r}{R_r}\frac{d\hat{\psi}_{mr}}{dt} + \hat{\psi}_{mr} = L_m i_{ds} \tag{3.12}$$

The torque as a function of rotor flux and stator current can be derived as follows: the stator flux linkage relations can be written as

$$\psi_{qs} = L_m i_{qr} + L_s i_{qs} \tag{3.13}$$

$$\psi_{ds} = L_m i_{dr} + L_s i_{ds} \tag{3.14}$$

Substituting equations (3.13) and (3.14) in equations (3.5) and (3.6) ,

$$\psi_{qs} = \left[L_s - \frac{L_m^{\,2}}{L_r} \right] i_{qs} + \frac{L_m}{L_r} \psi_{qr} \tag{3.15}$$

$$\psi_{ds} = \left[L_s - \frac{L_m^{\,2}}{L_r} \right] i_{ds} + \frac{L_m}{L_r} \psi_{dr} \tag{3.16}$$

The torque equation as a function of stator currents and stator fluxes is

$$T_e = \frac{3}{2}\left(\frac{P}{2}\right)\left(i_{qs}\psi_{ds} - i_{ds}\psi_{qs}\right) \tag{3.17}$$

Equations (3.15) and (3.16) can be substituted in equation (3.17) to eliminate the stator fluxes. Therefore,

$$T_e = \frac{3}{2}\left(\frac{P}{2}\right)\frac{L_m}{L_r}\left(i_{qs}\psi_{dr} - i_{ds}\psi_{qr}\right) \tag{3.18}$$

Substituting $\psi_{qr} = 0$ and $\psi_{dr} = \hat{\psi}_{mr}$, the torque expression is

$$T_e = \frac{3}{2}\left(\frac{P}{2}\right)\frac{L_m}{L_r} i_{qs}\psi_{mr} \tag{3.19}$$

Electromagnetic torque and rotor flux are independently controlled by appropriately

regulating i_{ds}, i_{qs} and ω_r. The field co-ordinate equations can be used to determine the reference value, i_{ds}^* , i_{qs}^* and ω_r^*, for demanded values of torque, T^*, and rotor flux, ψ_{mr}^*. Thus,

$$L_m i_{ds}^* = \psi_{mr}^* + \tau_r \frac{di_{mr}^*}{dt} \tag{3.20}$$

$$i_{qs}^* = \frac{T^*}{k i_{mr}^*} \tag{3.21}$$

$$\omega_r^* = \frac{i_{qs}^*}{\tau_r i_{mr}^*} \tag{3.22}$$

The basic implementation of a speed control system for a current-controlled PWM inverter drive is shown in Fig.3.9

Figure 3.9 can be modified to incorporate control in the field weakening region. A controller block diagram to extend the operation in the field weakening region is shown in Fig.3.10. Below the base speed, the motor operates at constant $|\psi_{mr}|$ and therefore operation is identical to that shown in figure 3.9. Above the base speed, $|\psi_{mr}|$ is weakened to be inversely proportional to speed. The flux is being controlled in an open-loop manner by solving equation (3.12).

With indirect control the speed can be controlled from zero to the full value. However, a rotor position signal becomes mandatory in this method. The controller is dependent on machine parameters, and for ideal decoupling the controller parameters should track the machine parameters, which is extremely difficult to achieve. The dominant parameter to be considered is the rotor resistance, which can be estimated by an Extended Kalman filter, giving only limited success in ideal decoupling control[10,15,16].

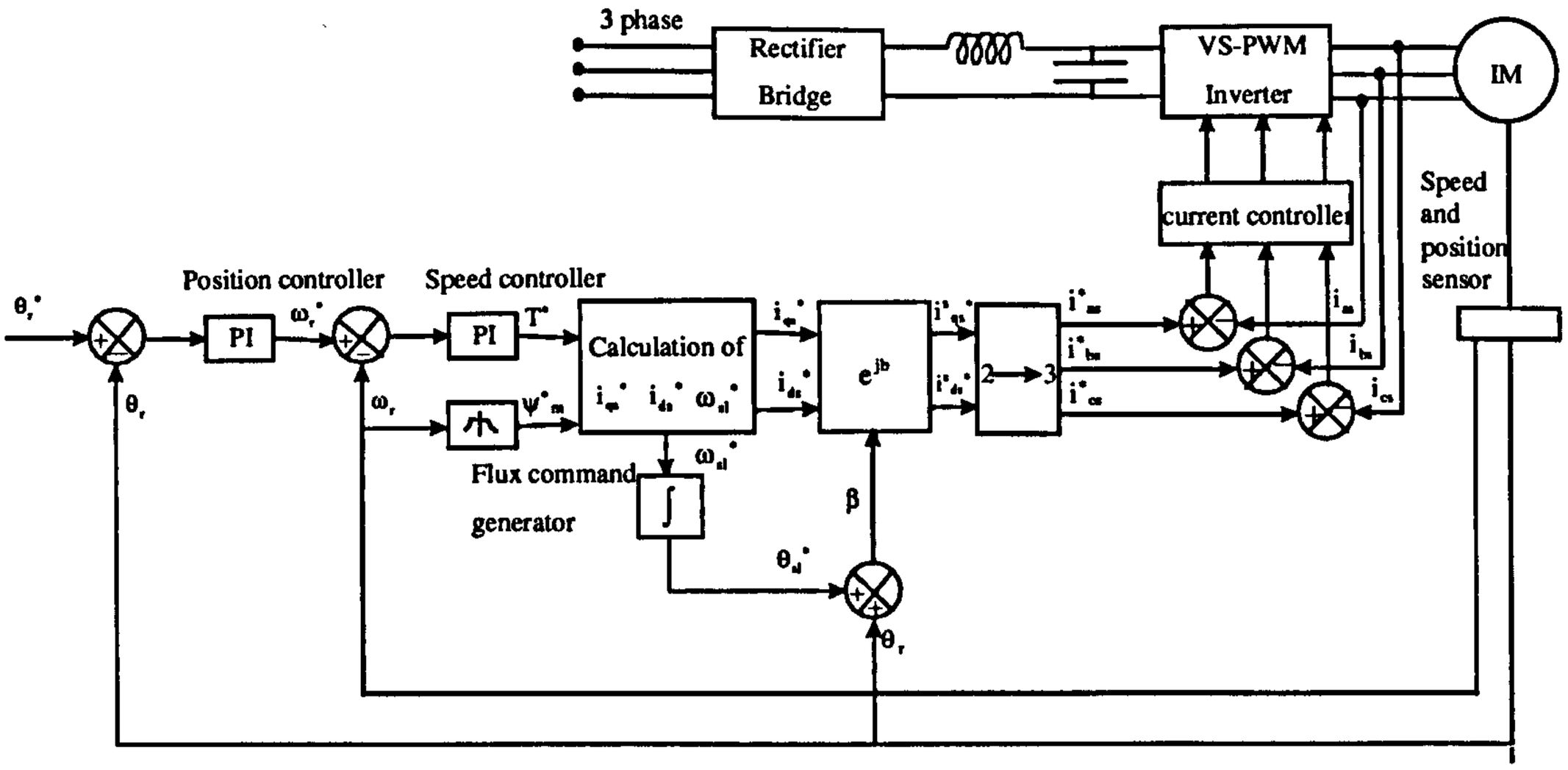

Figure 3.9 AC motor speed control system with indirect vector control

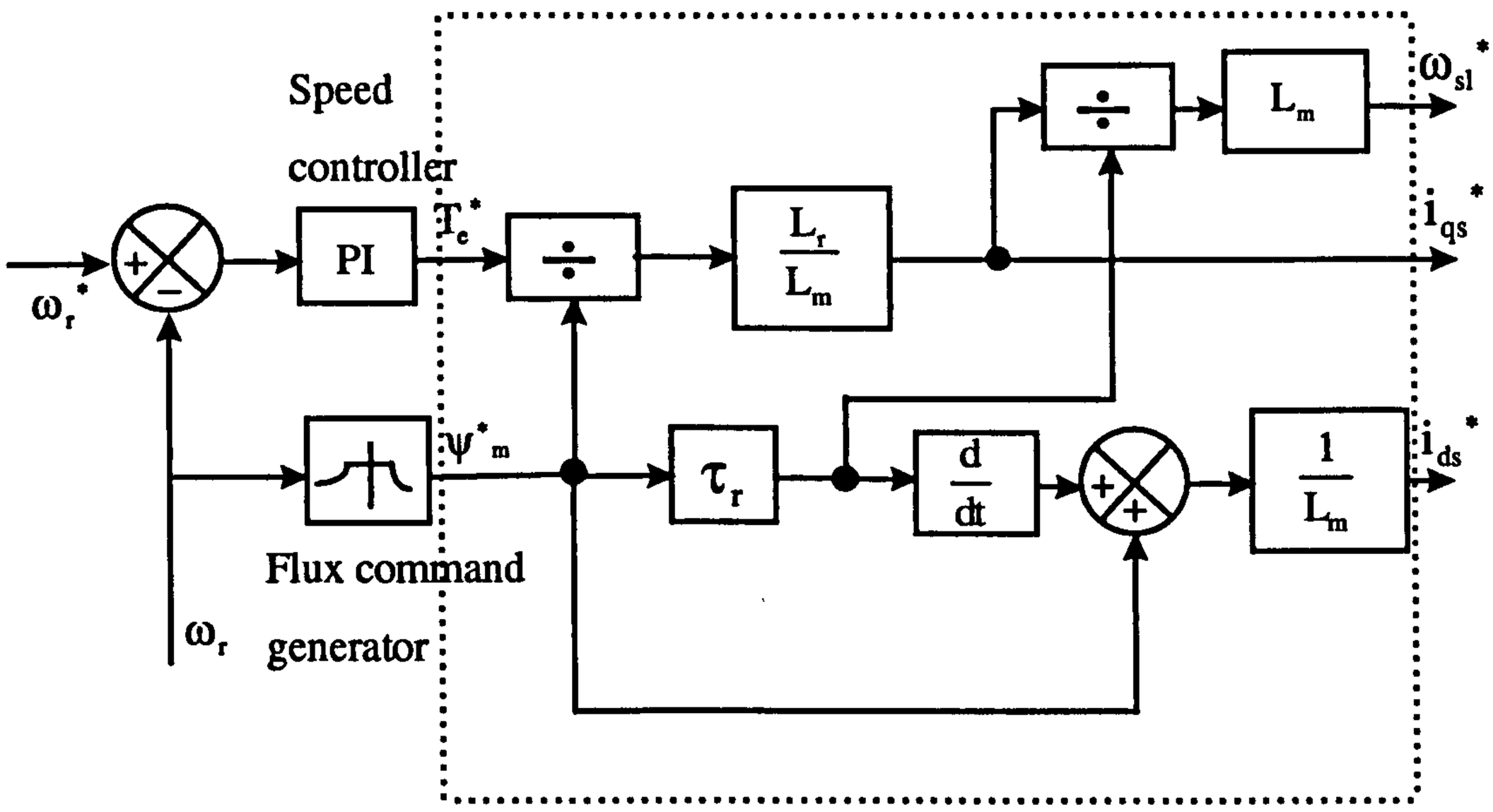

Figure 3.10 Control block diagram to calculate the operation command in field weakening region

3.6 Simulation of indirect field-oriented control of induction motor

A closed-loop speed control system for the induction motor driven by a current-controlled PWM inverter was considered for simulation purposes. The block diagram for such a variable speed drive was given in Fig.3.9. The system parameters used in the simulation are given in appendix 2. A flowchart in Fig 3.11 presents the simulation steps of indirect field-oriented control.

In all the simulations of indirect field-oriented control the motor was initially excited at zero speed for 0.5sec with a dc current flowing through the windings. The dc current fluxes the machine while at rest. This ensures good dynamic response from the motor when a torque demand is received by the control system. For the system illustrated in Fig 3.9 the following parameters were utilised:

(i) the hysterisis band was 0.1pu

(ii) the proportional and integral gains of the PI torque controller were $G_P = 80$ and $G_I = 2$ respectively

(iii) the torque command, which is the output of the PI controller was limited to 1.6 times the rated motor torque

(iv) the simulation time step was 0.1msec.

The gain values for the PI torque controller had been chosen as optimal ones derived from previous runs after extensive simulations. The drive system was simulated with the same motor parameters in the motor model and in the controller for several load and speed conditions.

Firstly, figures 3.12(a)-(f) show simulation results of phase currents, speed, frequency and torque during an acceleration to the rated speed of the unloaded motor. The motor started its acceleration phase from rest to rated speed (1.0 pu). The phase currents have an initial value at no speed and reach steady-state conditions at rated speed.

Figures 3.13(a)-(f) illustrate the motor accelerated to rated speed followed by 1.0 pu step load applied on the shaft of the motor. The drive system successfully achieved

the set speed and demanded torque. The graph of the speed in Fig 3.13(d) shows a slip at the instant when the load is applied and then recovery to 1.0 pu value in a very small time.

To examine the dynamic behaviour of four-quadrant operation, fast speed reversals are carried out with the drive. Figures 3.14(a)-(f) show simulation results during an acceleration and deceleration of the unloaded motor. Smooth transfer between forward and reversed rotation is achieved when the motor started its acceleration from zero to rated speed and then reversed from rated to negative top speed.

The same conditions as in the previous no load case were repeated but with the motor fully loaded (1.0 pu step-load applied on the shaft of the motor). Figures 3.15(a)-(f) display the simulation results. Notice that in Fig 3.15(d) during the crossing of zero-speed the motor delivered rated torque even at zero speed.

As a final study, operation in the field weakening region was performed and the results are depicted in Fig 3.16(a)-(f). The results show that the motor can drive up to twice rated speed. In this mode of simulation the flux was controlled to be constant at rated value for speeds below base speed, and progressively reduced above base speed in the field weakening region.

From these results it was observed that the induction motor model under the field-oriented control using the modelling technique described in this chapter, is capable of meeting the demands of a high performance drive.

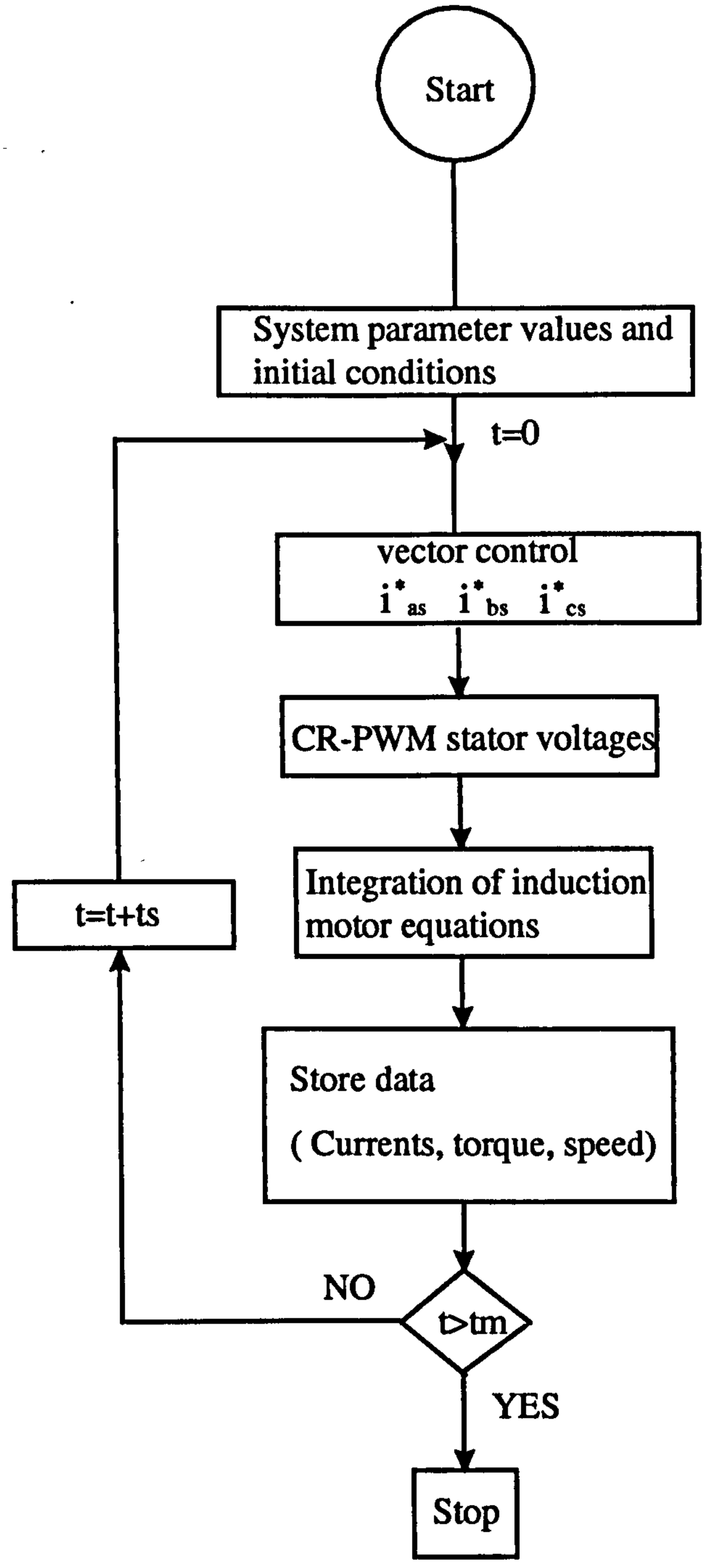

Figure 3.11. A flowchart for the indirect field-oriented control of induction motor

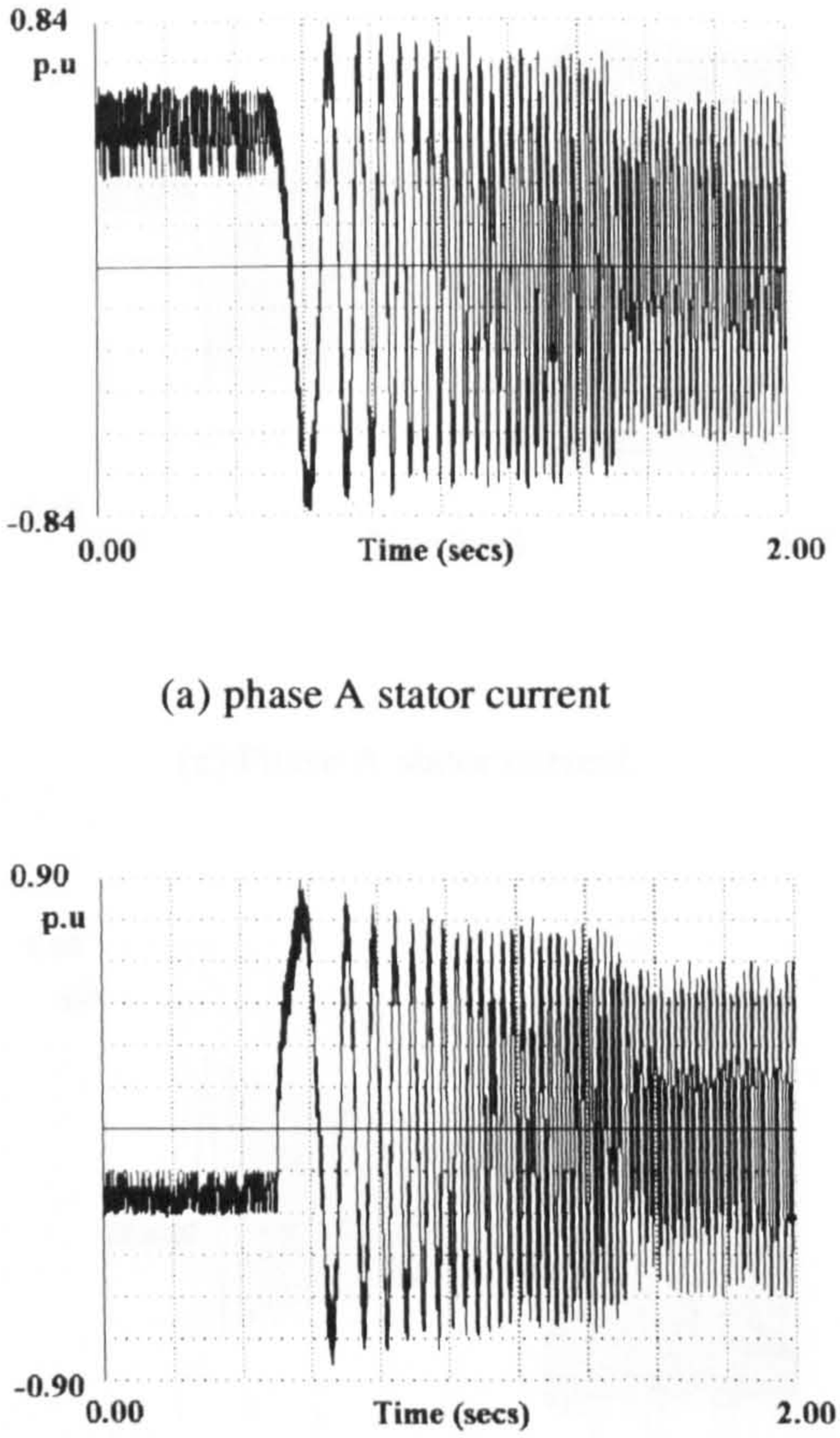

(a) phase A stator current

(b) phase B stator current

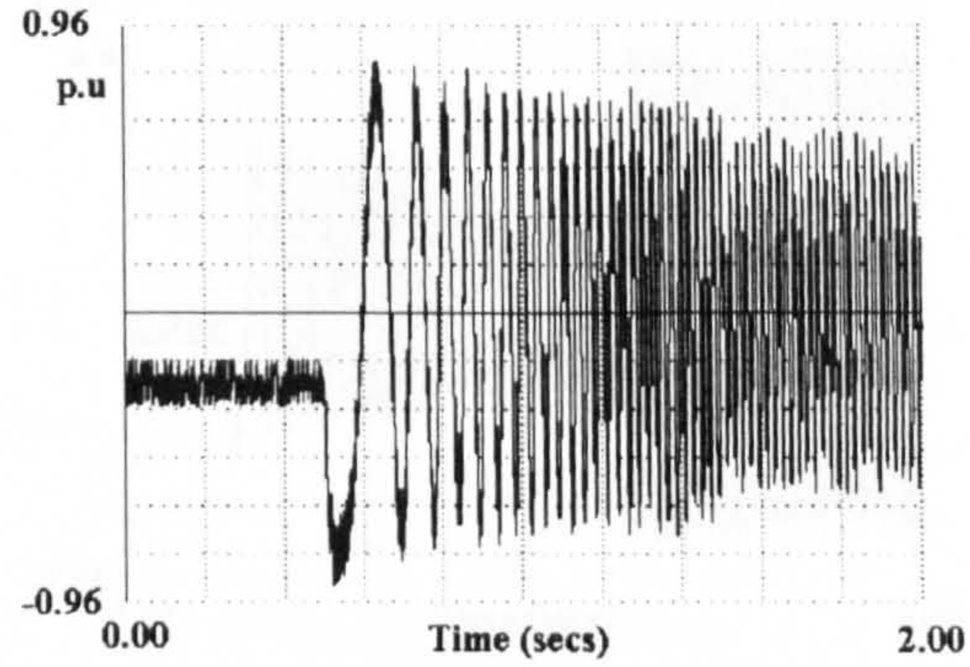

(c) phase C stator current

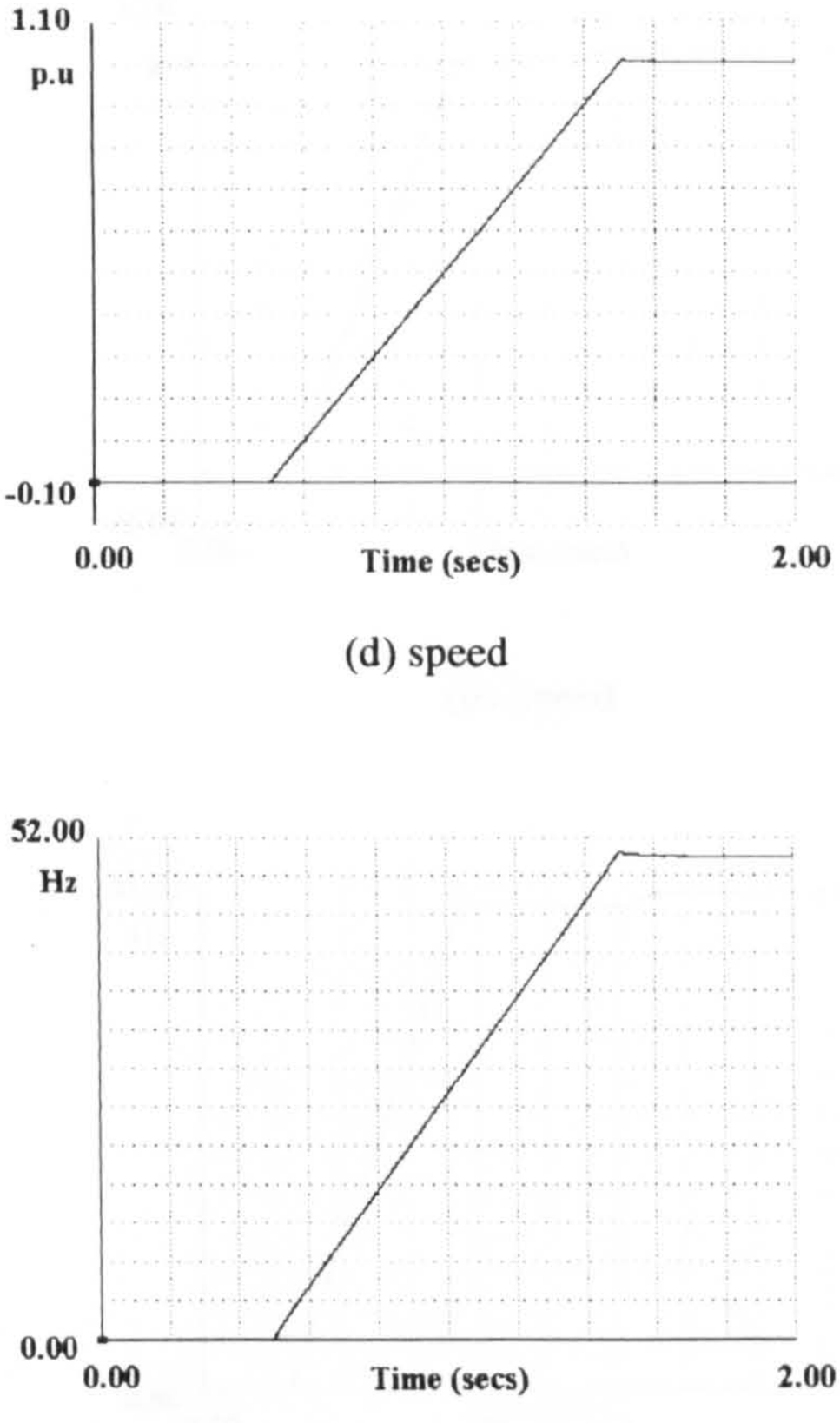

(d) speed

(e) frequency of the stator

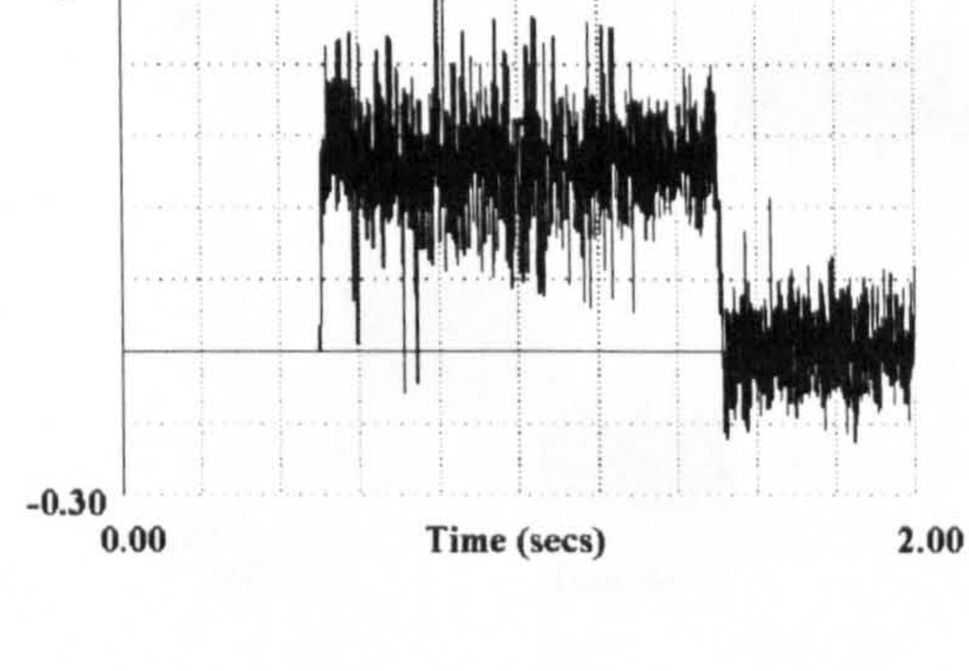

(f) torque

Figure 3.12 Dynamic performance of field-oriented control of the induction motor for 0.5 sec pre-magnetising time followed by free-acceleration to the rated speed.

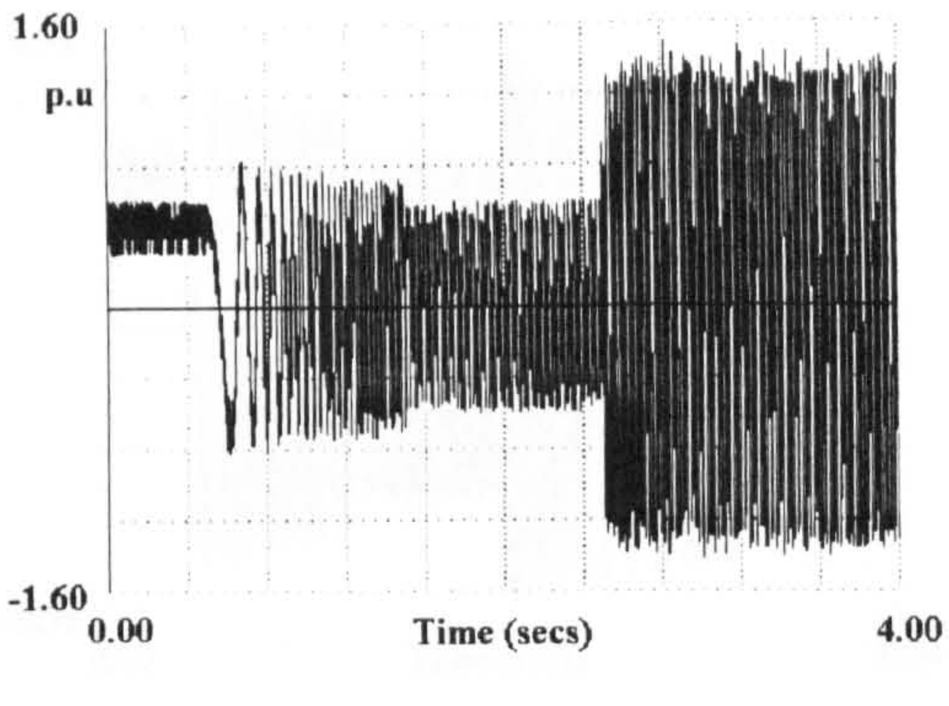

(a) Phase A stator current

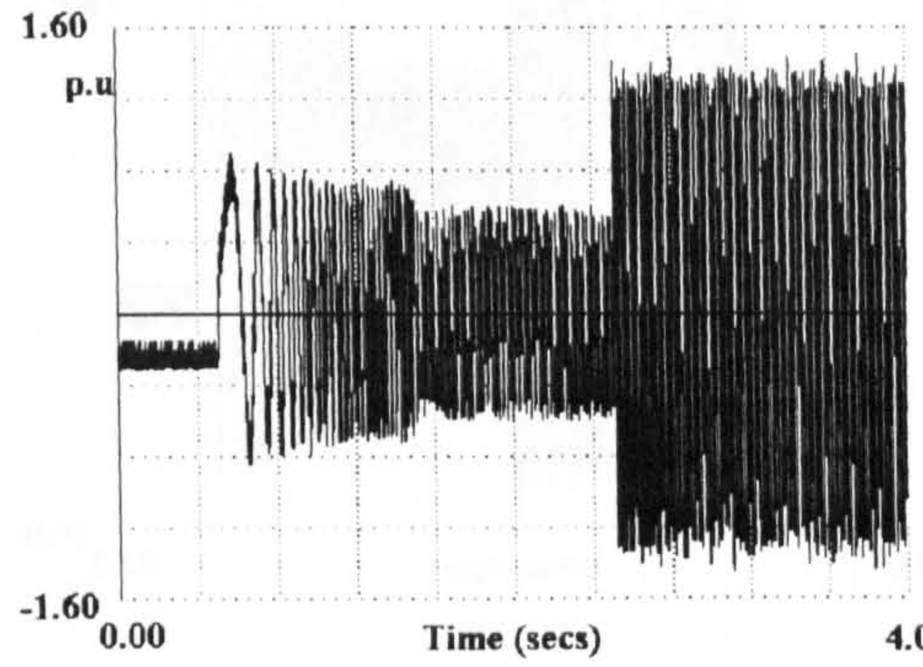

(b) Phase B stator current

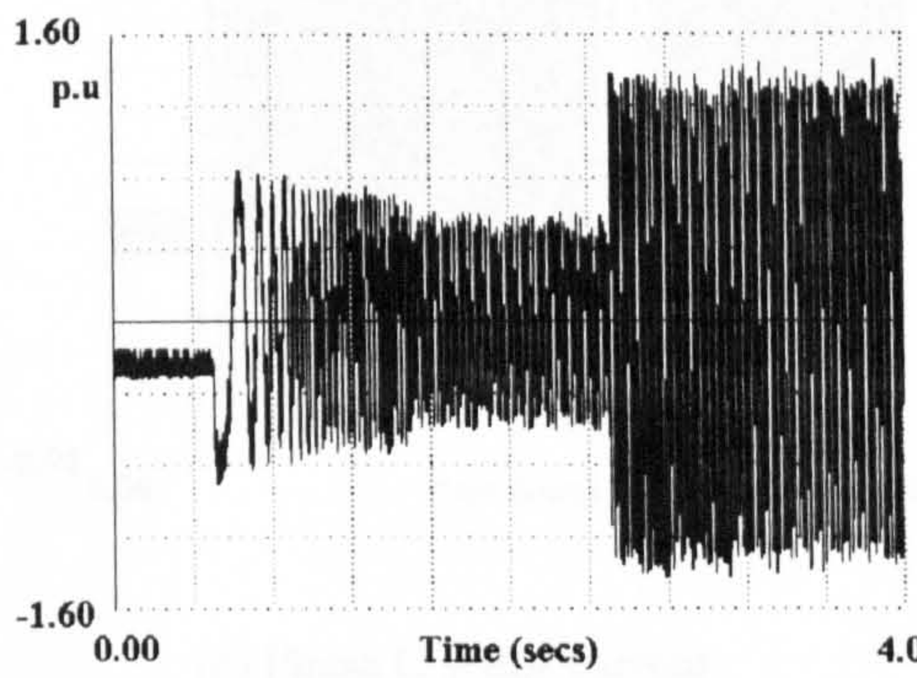

(c) Phase C stator current

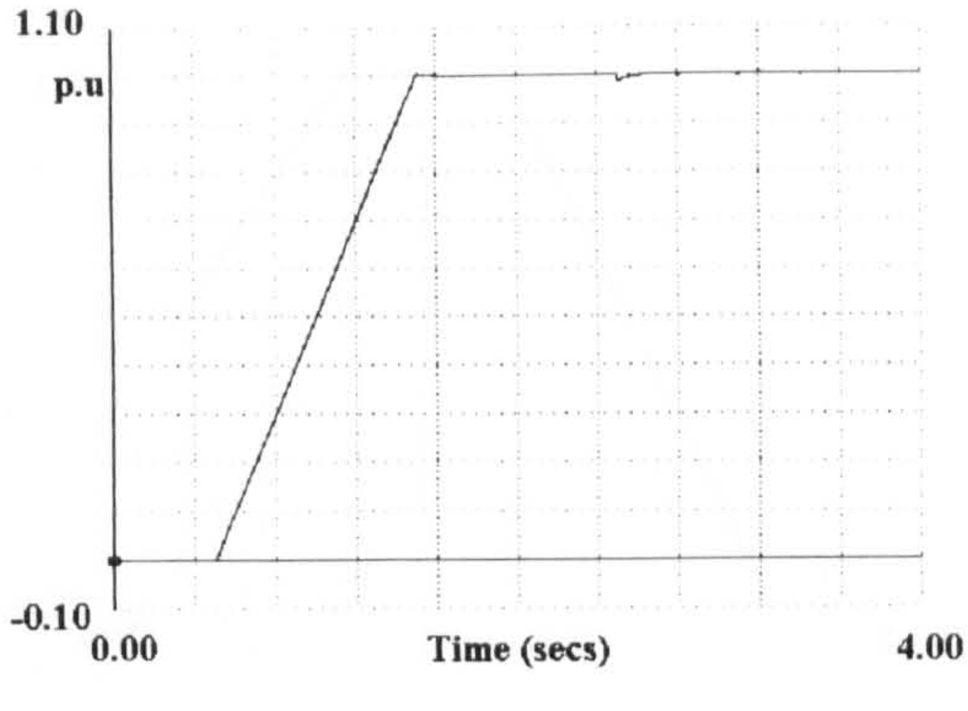

(d) Speed

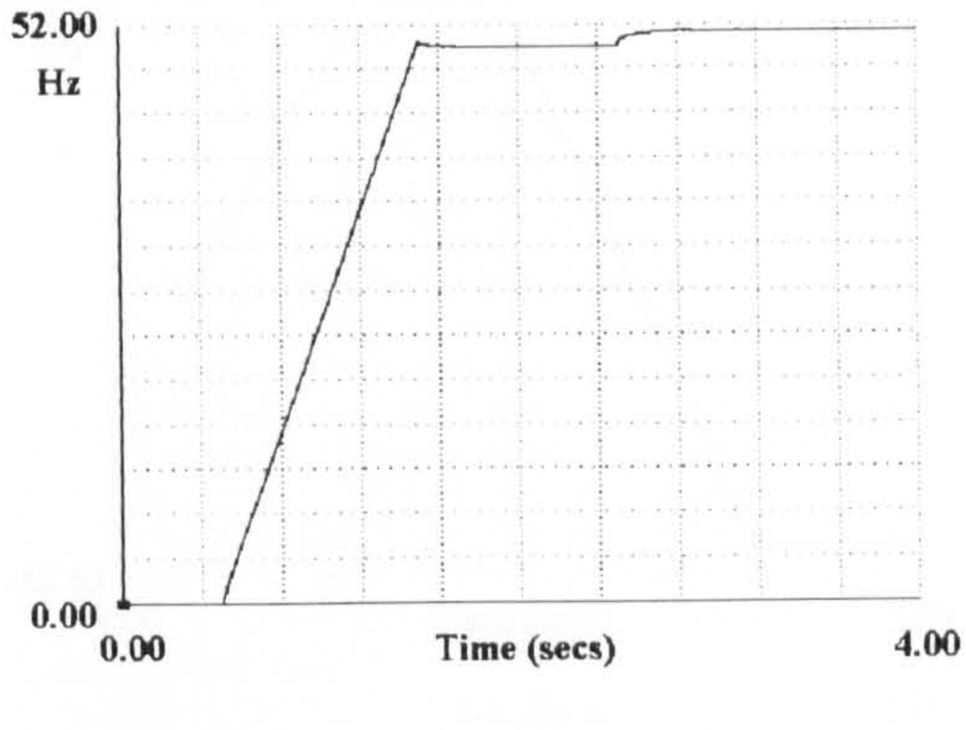

(e) frequency of the stator

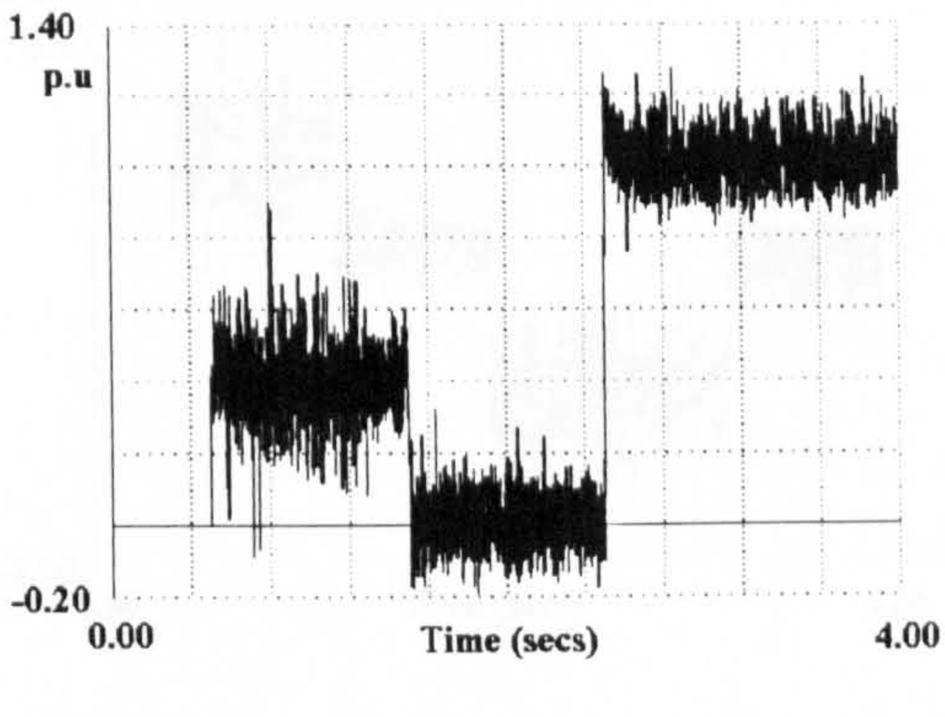

(f) torque

Figure 3.13 Dynamic performance of field-oriented control of the induction motor for 0.5 sec pre-magnetising time followed by free-acceleration to the rated speed and 1.0 pu step load

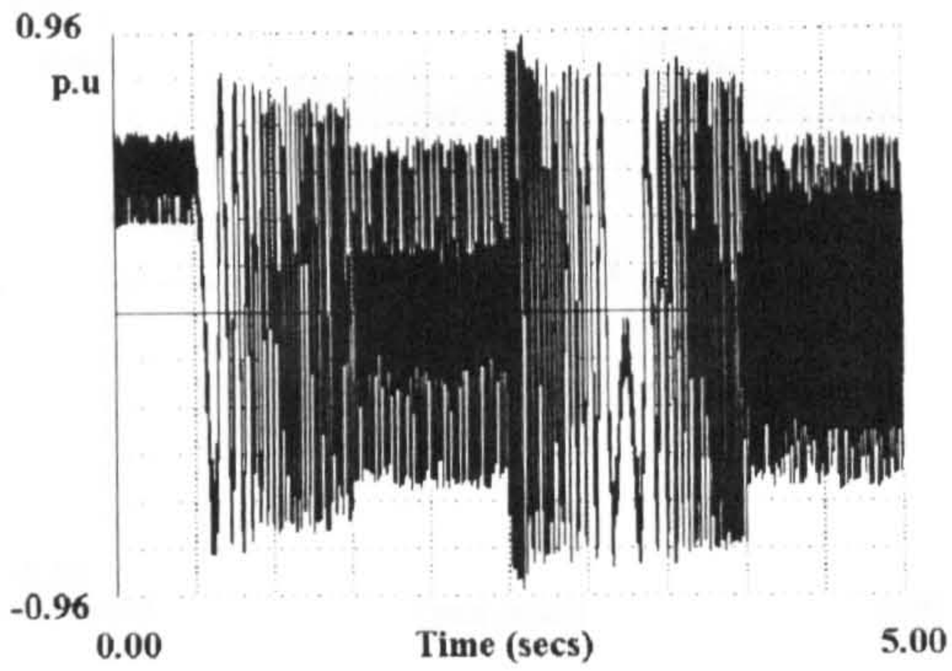

(a) Phase A stator current

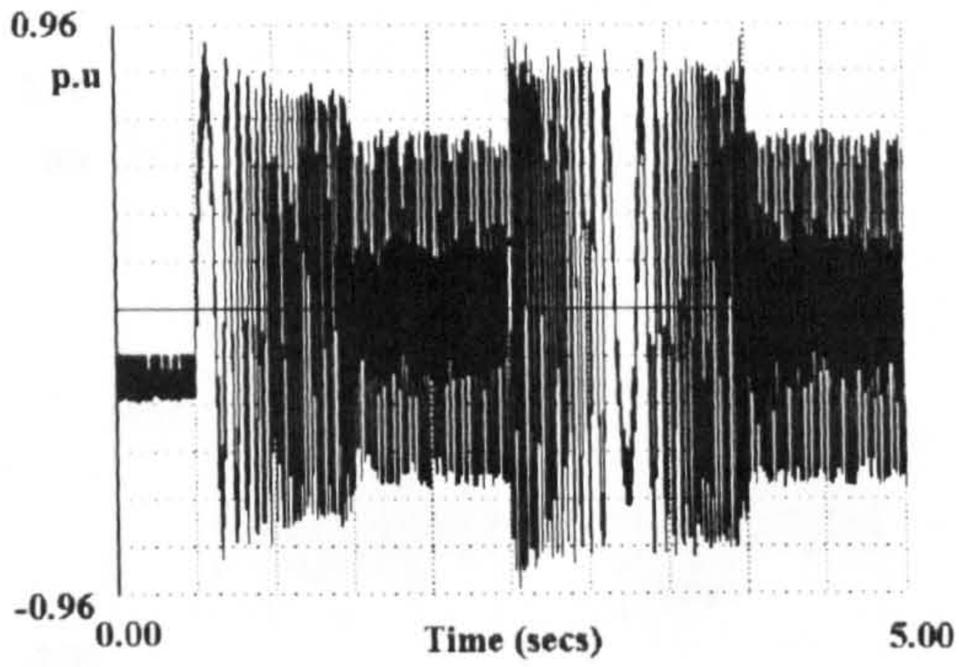

(b) Phase B stator current

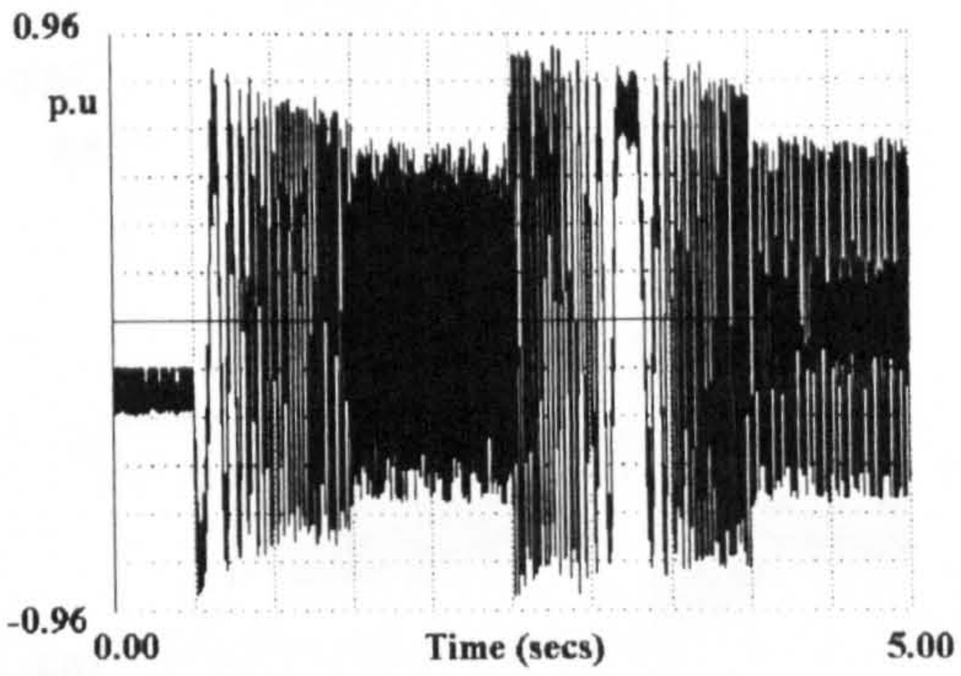

(c) Phase C stator current

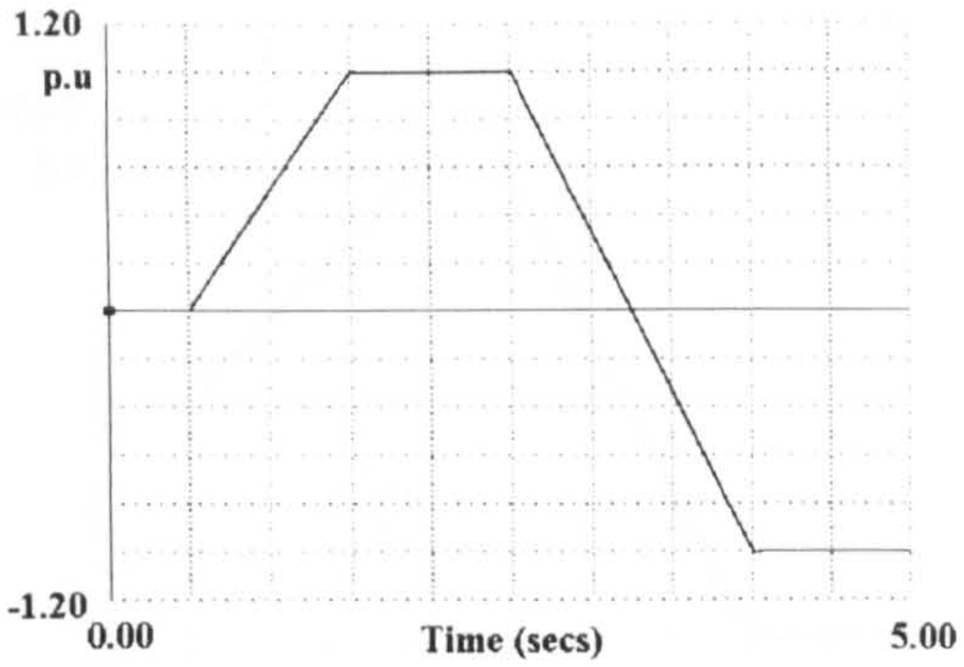

(d) Speed

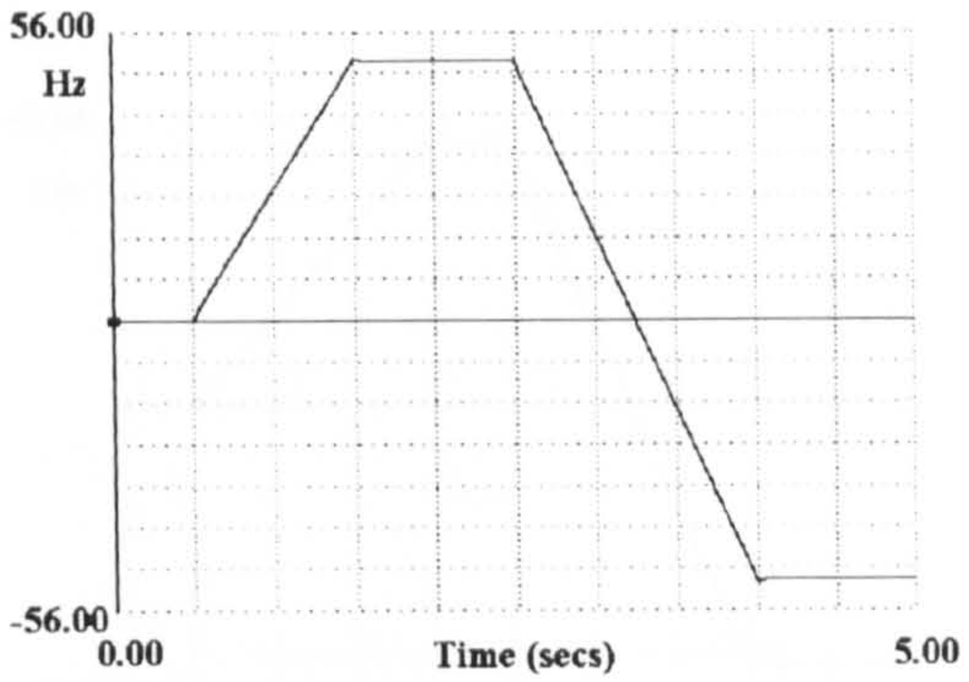

(e) frequency of the stator

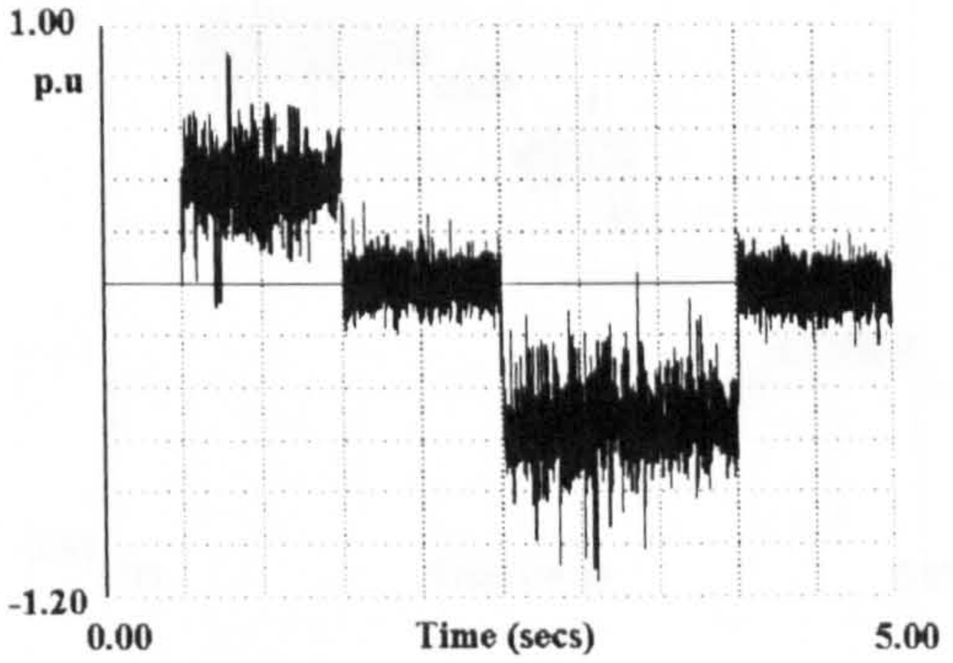

(f) torque

Figure 3.14 Dynamic performance of field-oriented control of the induction motor for 0.5 sec pre-magnetising time followed by free-acceleration to the rated speed and speed reversal

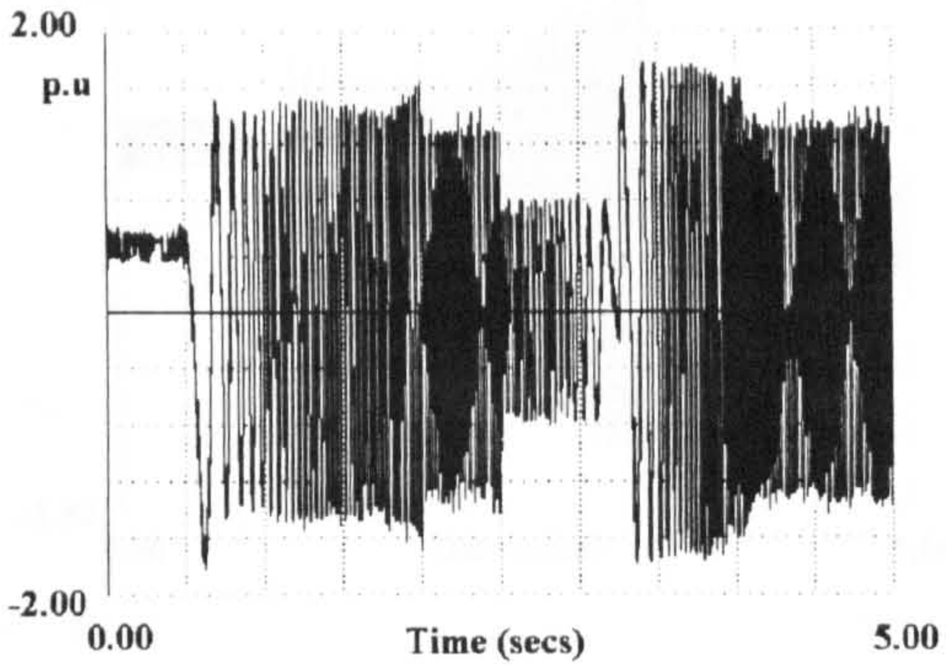

(a) Phase A stator current

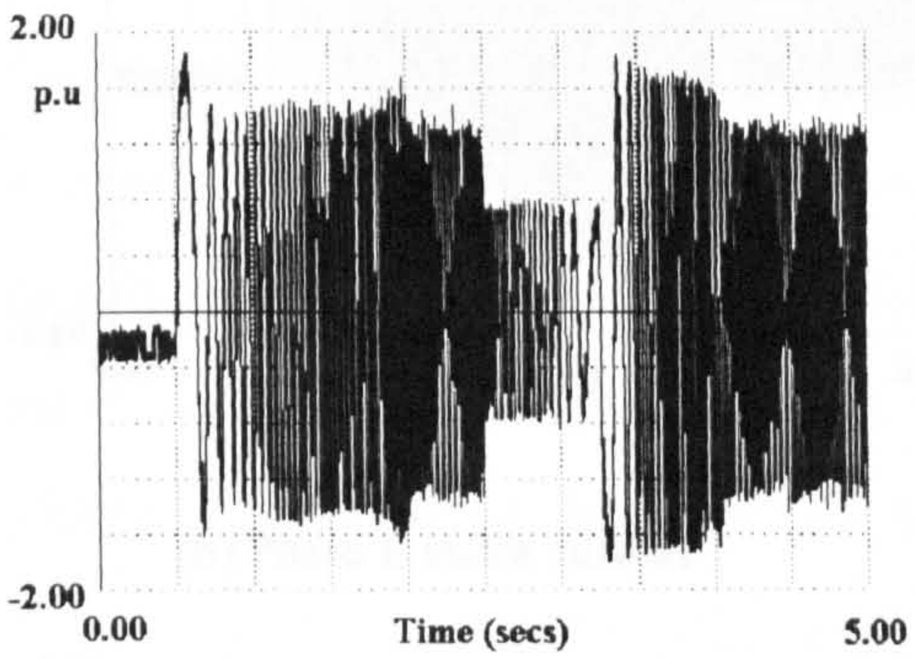

(b) Phase B stator current

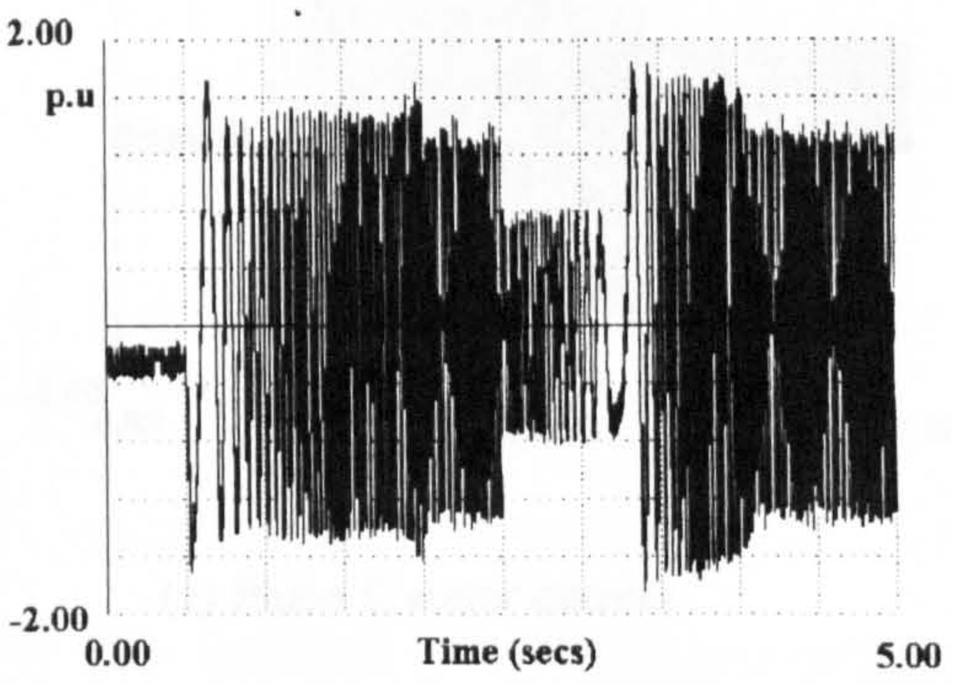

(c) Phase C stator current

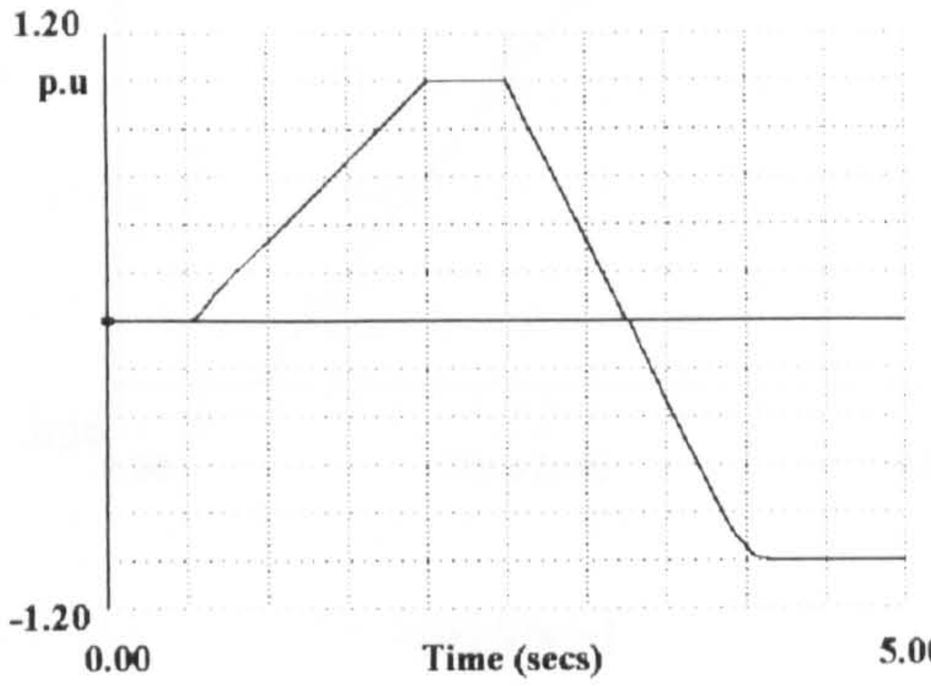

(d) Speed

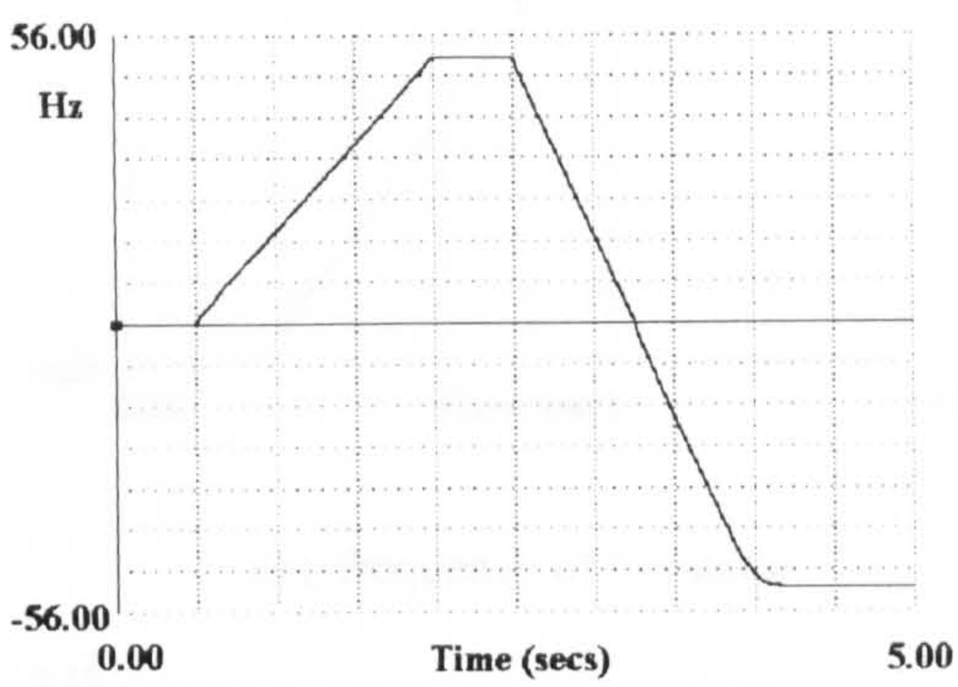

(e) frequency of the stator

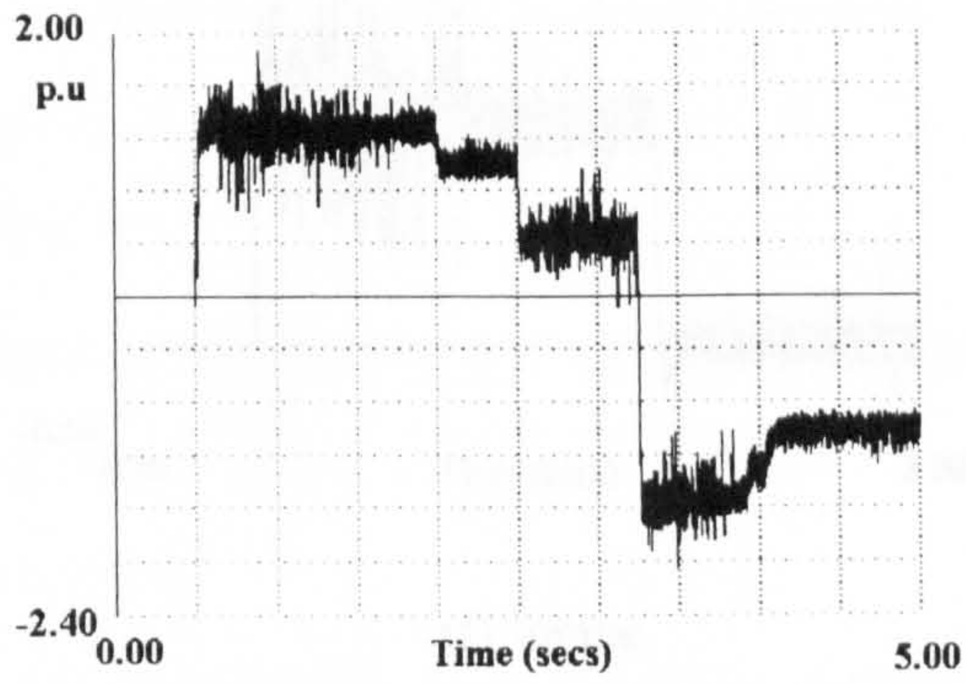

(f) torque

Figure 3.15 Dynamic performance of field-oriented control of the induction motor for 0.5 sec pre-magnetising time followed by acceleration to the rated speed, speed reversal and 1.0 pu step-load torque

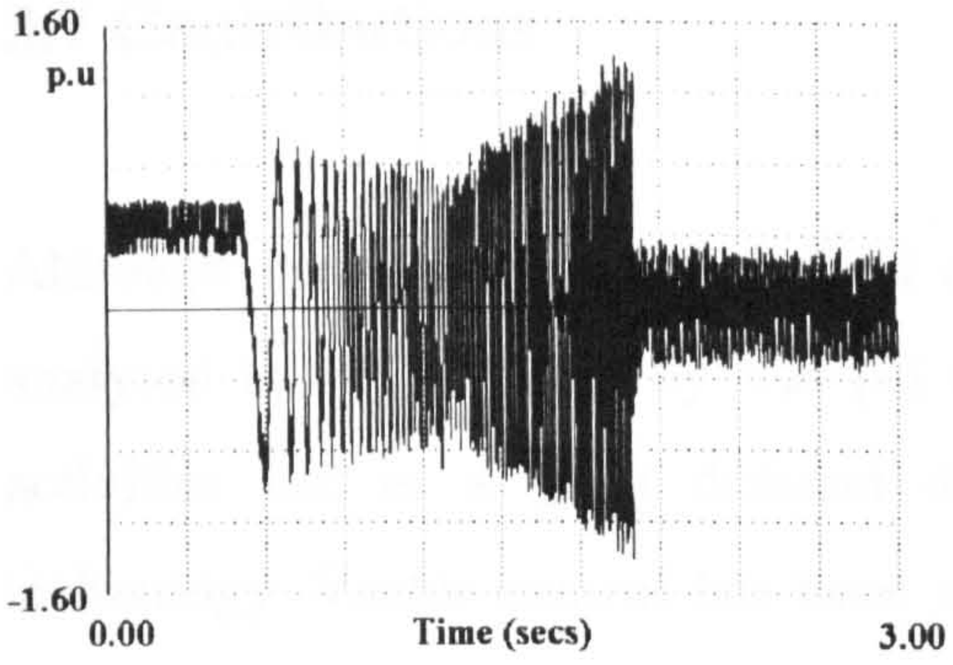

(a) Phase A stator current

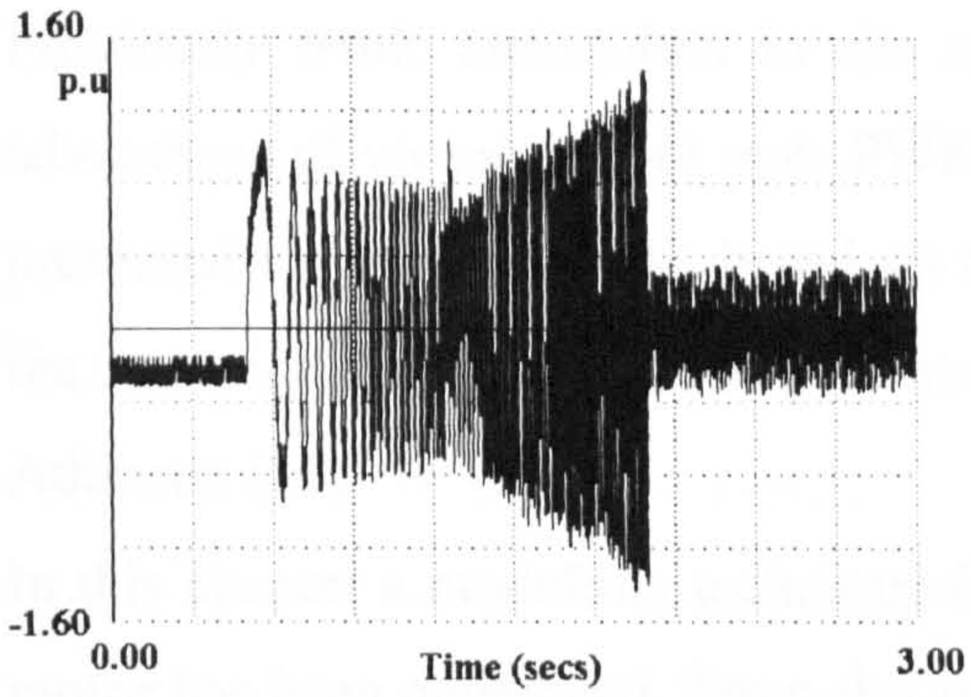

(b) Phase B stator current

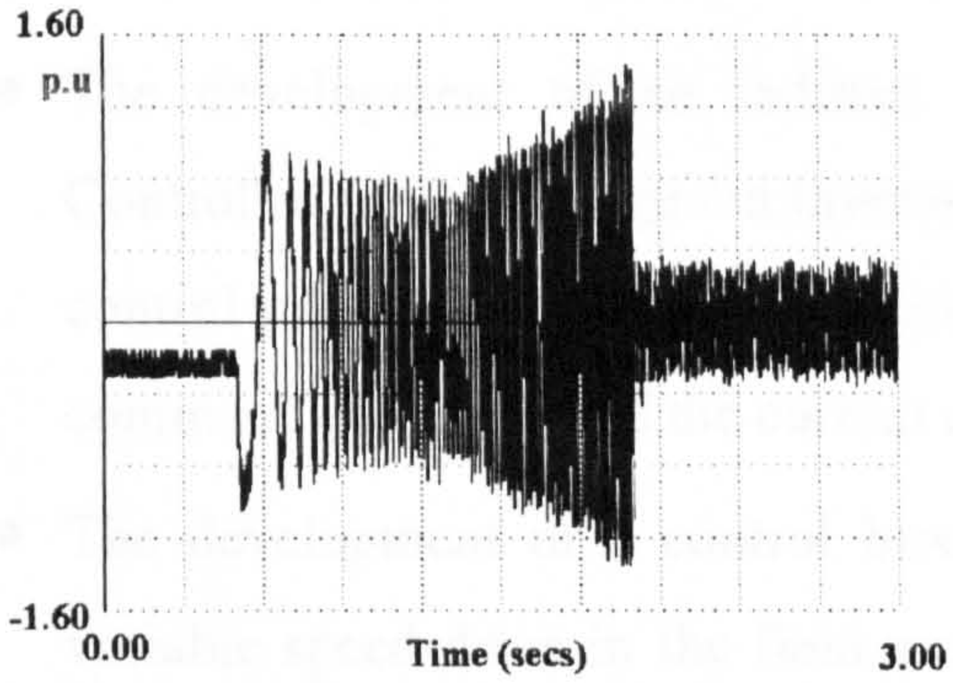

(c) Phase C stator current

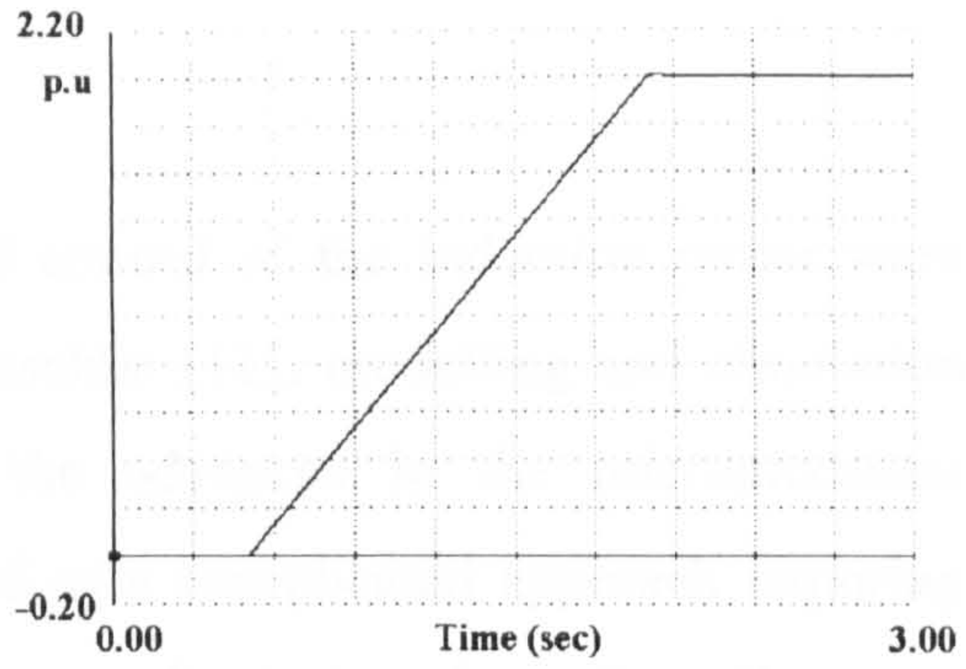

(d) Speed

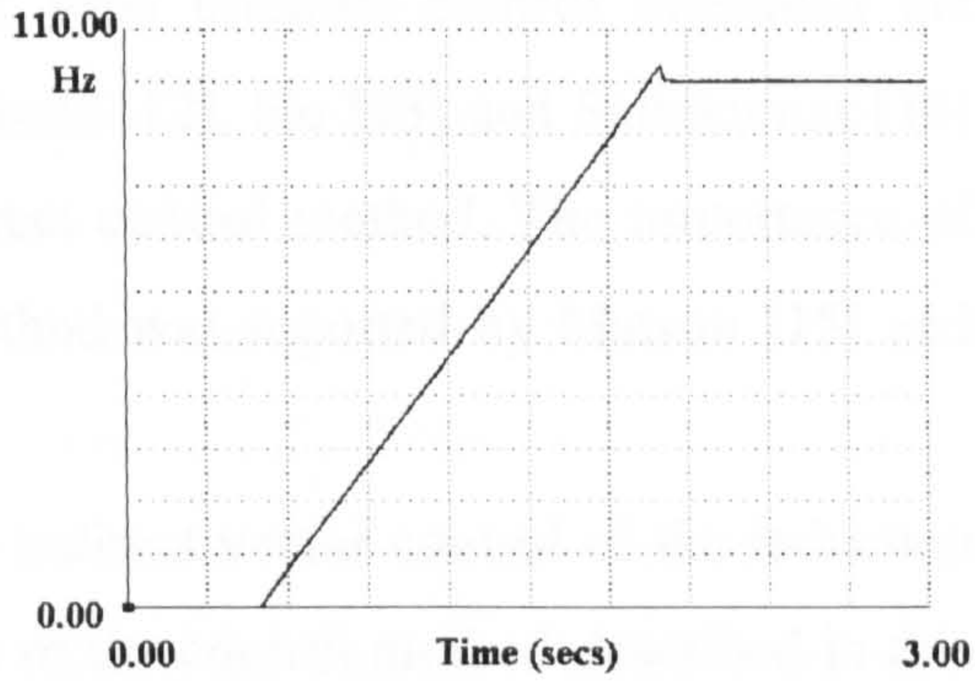

(e) frequency of the stator

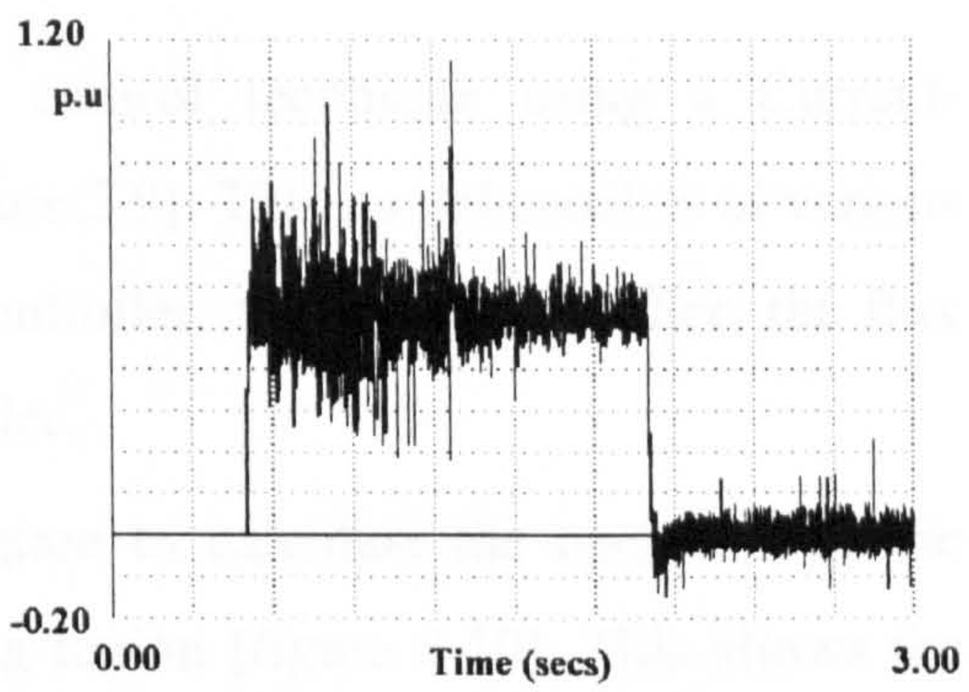

(f) torque

Figure 3.16 Dynamic performance of field-oriented control of the induction motor for 0.5 sec pre-magnetising time followed by free acceleration in the field weakening region.

3.7 Contributions

Although the principles of the field oriented control of the induction motor were analysed in the literature by Vas [8] and Blaschke [11], modelling and simulation activities are in a great demand due to the advances in the microprocessor technology. Vector control has been criticised as a complicated approach requiring sophisticated signal processing and complex co-ordinate transformation. However, digital control with microprocessors offers significant advances [1,3,8].

Previously work undertaken in the area of field oriented control presented the advantages of vector control over PWM methods [12]. Ho [13] and Sathikumar [14] presented simulation results based on the direct control method. The importance of the rotor resistance in the vector control method was reported by Matsuo [15] and Atkinson [16].

In this chapter a modelling technique for the indirect vector control of the induction motor has been developed. From the analysis of the control method described in this chapter the following contributions are identifiable:

- The development of an indirect vector control technique using a Current-Controlled PWM voltage fed inverter [Figure 3.9]. This model consists of various control parameters such as the position controller, the speed controller, the flux command generator and the current controller.
- The development of a control block diagram to calculate the operation of the variable speed drive in the field weakening region [figure 3.10]. This allows the motor to drive up to frequencies greater than rated.
- The creation of a computer program for the closed-loop vector control method coded in the Fortran language.
- An investigation and report on the behaviour of indirect vector control machines under various operating conditions, such as free acceleration to rated speed, step load applied on the shaft of the motor, fast speed reversal and operation in the field weakening region.

- Consideration of benefits and opportunities associated with the use of vector control over scalar control methods (six step and PWM techniques) , such as smooth transfer between forward and reversed rotation and control down to zero speed.

3.8 Conclusions

The work presented in this chapter described field orientation control of the induction motor. At the beginning, an explanation of the fundamentals of field orientation control was presented, followed by an analysis of the operation of a current-controlled PWM inverter model. The two main vector control methods (direct and indirect field orientation control) were reported and simulation studies using indirect field-oriented control were carried out for a number of different system scenarios. The results of the simulations have shown that indirect field-oriented control gives as good a dynamic performance as a dc drive even at zero speed and can used for a number of different applications[5,16,17]. The main contributions of this research work were reported at the end of the chapter.

3.9 References

1. Bose, B. K., "Power electronics and a.c. drives", Prentice-Hall Inc., New Jersey, 1986.
2. Leonard W., "Control of Electrical Machines", Springer-Verlag, 1985.
3. Murphy, J.M.D. and Turnbull, F.G. ,"Power electronic control of a.c. motors," Pergamon Press plc., England, 1988.
4. Mokrytzki, B "Pulse-width modulated inverters for A.C motor drives", IEEE Transactions, 1967, pp 493-503.
5. Mohan N, Underland T, Robbins W ,"Power electronics: Converters, Applications and Design", John Wiley and Sons 1995.
6. Abbas, M.A., Christen , R. and Jahns, T.M. "Six step voltage source inverter driven induction motor", IEEE Transactions on Industry Applications, vol IA-20,1984, pp 1251-1259.
7. Grant, T.L., and Bardon, T.H "Control strategies for P.W.M drives", IEEE Transactions 1980, IA-16,pp 211-215.
8. Peter, V.A.S. "Vector control of a.c machines," Oxford University Press, New York, 1990.
9. Brod, D.M and Novotny, D.W. "Current control of VSI-PWM inverters," IEEE Transactions on Industry Applications, vol. IA-21, May/June 1985, pp 562-570.
10. Bal Gungor, "Performance analysis of field-orientation controlled induction motor with parameter adaptation", PhD thesis, University of Strathclyde, UK,1993.
11. Blaschke F., "The principle of field orientation as applied to the new transvector closed-loop control system for rotating-field machines", Siemens Review XXXIX, No. 5, 1972, pp217-220.
12. Acarnley P.P., Finch J.W., Atkinson D.J., "Field-orientation in AC Drives: State-Of-Art and future prospects", IEE 3rd Int. Conf. On Electrical Machines and Drives, London, Nov.1987, pp 285-289.
13. Ho E.Y.Y., Sen P.C., "Decoupling control of induction motor drives", IEEE Transactions on Industrial Electronics, Vol.35, No.2, 1988, pp253-262.

14. Sathikumar S., Vithayathil J., "Digital simulation of field-oriented control of induction motor", IEEE Transactions on Industrial Electronics, Vol.IE-31, No.2, 1984, pp 141-148.

15. Matsuo T., and Lipo T.A., "A rotor parameter identification scheme for vector-controlled induction motor drives", IEEE Transactions on Industry Applications, vol. IA-21, May/June 1985, pp. 624-632.

16. Atkinson, D. J., Acarrney, P.P. and Finch, J.W. "Application of estimation techniques in vector-controlled induction motor drives", IEE Fourth International Conference on Power Electronics and Variable-speed drives, 1989, pp 358-363.

17. Bose, B.K. "Adjustable Speed AC Drives-A Technology Status Review," Proceedings IEEE, Vol. 70, Feb. 1982, pp 116-135.

CHAPTER 4

MODELLING OF POWER SYSTEM COMPONENTS

4.1 INTRODUCTION

Modelling and simulation of electrical machines and interconnected AC/DC converter stations-variable speed drives has always provided a challenge for power system engineers. Methods of the transient analysis of electrical machines, has in the past, been based on simple models derived using assumptions that were justified in practise for simplified transient stability analysis. In early modelling procedures generators were represented by a voltage source and simple reactance. Loads were either neglected or represented by a static impedance absorbing constant active and reactive power. In the late 1920s, Park introduced a new approach to electric machine analysis [1,2]. He eliminated the time-varying coefficients associated with the representation of the physical machine, due to certain machine inductances which are a function of rotor displacement, by referring the stator variables to a frame of reference fixed in the rotor. Since then this transformation was known as the Park transformation.

With the advent of modern computers, numerical methods can be employed efficiently for solving non-linear differential equations. In such a case, the direct 3-phase model can be used for a more exact study of an electrical machine performance. With direct three phase representation, symmetric and asymmetric conditions, can be simulated with ease. The accurate representation of asymmetrical system operating conditions, due to the use of the direct 3-phase machine models, has

enhanced the viability and quality of various system studies and greatly extended the range of practical studies currently undertaken.

In the last two decades, a number of DC transmission links have been established in various parts of the world. One of the problems associated with the DC transmission is the generation of harmonic currents on both the AC and DC sides. These harmonics affect the AC system adversely and interfere with its operation. Some studies reported in the literature[3-5] use simplified models in which the AC system is represented either by an infinite source[5] or by a simple series impedance which is equal to the short-circuit impedance of the AC system at the converter point.

In practise however, large power systems include synchronous machines, loads, AC and DC transmission lines, AC/DC converters and variable speed drives. In this case a simple representation of the system will not be adequate. In such a case, a detailed representation of these machines is necessary.

For this reason a more general representation of AC/DC system is considered. In order to model such a system, direct-phase quantities are used. The digital computer program, which simulates this system, is developed in such a way to allow the study of various system configurations.

The purpose of this chapter is to develop various direct 3-phase mathematical models of the main components of a modern power system such as synchronous machines, induction machines, three phase transformers and filters. In addition, the chapter covers some essential and common models of automatic voltage regulators, prime movers and also represents the mathematical model of an AC/DC converter station. The modelling technique of a general multi-machine AC/DC power system with converter stations and variable speed drives will be described in the succeeding chapter.

4.2 ELECTRICAL COMPONENT MODELS IN THREE-PHASE AXES

4.2.1 Synchronous machine

Most of the electric power used throughout the world is generated by synchronous generators and many large loads are driven by synchronous motors. These devices operate on the same principle and referred as synchronous machines. Figure 4.1 shows the three-phase salient pole machine with three symmetrical windings on the stator and a field and two damper windings on the rotor. There is an inherent complexity associated with the equations that represent the transient performance of this type of electrical machine. This complexity arises mainly from the non-linear nature of the magnetic circuit of the machine. However without loss of accuracy the following assumptions are made[6]:

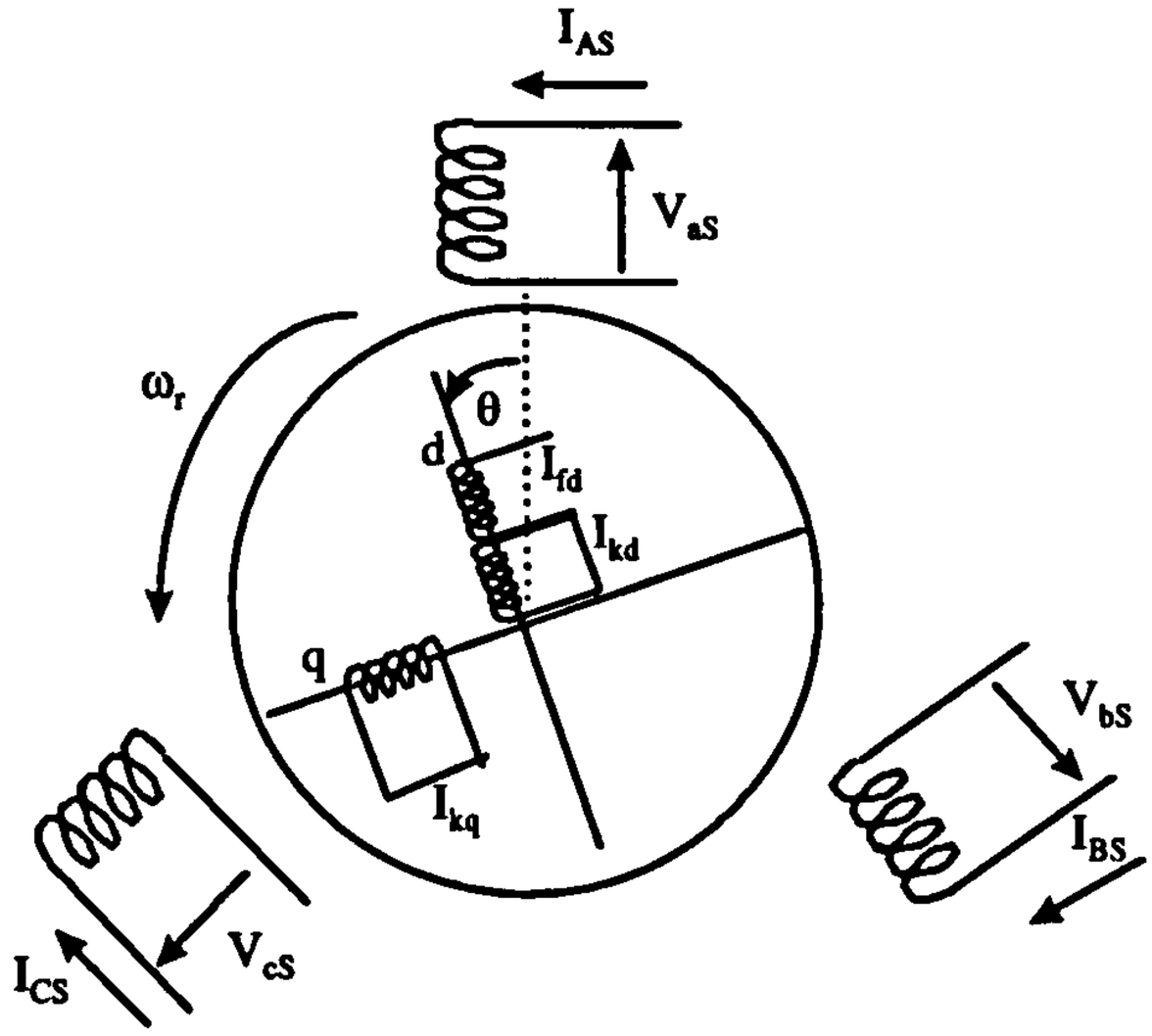

Figure 4.1 Three-phase synchronous machine

i) The distribution of the windings and the shape of the air gap are such that the self mutual inductance of the stator windings contain no Fourier expansion terms greater than $\cos 2\theta$, while the mutual inductance between the stator and rotor

windings vary simply as $\cos\theta$, where θ is the rotor position angle with respect to phase a .

ii) Saturation, hysteresis and eddy current effects are ignored.

4.2.1.1 Machine inductances

(a) Stator Self-inductances

The stator self-inductances are functions of the rotor position and are thus time-varying. They have maximum value when the direct rotor axis is in phase with the corresponding stator phase axis and their minimum when the quadrature rotor axis is in phase with the corresponding stator phase axis. The total self-inductances are given by the following equations[6]:

$$L_{asas} = L_{aa0} + L_{aa2}\cos 2\theta \tag{4.1}$$

$$L_{bsbs} = L_{aa0} + L_{aa2}\cos 2(\theta - \frac{2\pi}{3}) \tag{4.2}$$

$$L_{cscs} = L_{aa0} + L_{aa2}\cos 2(\theta + \frac{2\pi}{3}) \tag{4.3}$$

where

$$L_{aa0} = (L_d + L_q + L_{ls})/3 \tag{4.4}$$

$$L_{aa2} = (L_d - L_q)/3 \tag{4.5}$$

$$L_d = L_{ls} + L_{ad} \tag{4.6}$$

$$L_q = L_{ls} + L_{aq} \tag{4.7}$$

In the previous equations, the stator self-inductances have constant plus second harmonic terms. In a well designed machine higher order harmonic terms are negligible and can be neglected. L_{ls} is the stator leakage inductance and is the same for all three phases. L_d is the d-axis self-inductance and L_q is the q-axis self-inductance. L_{ad} is the d-axis mutual inductance, L_{aq} is the q-axis mutual inductance and θ is the rotor displacement in electrical degrees.

(b) Stator mutual inductances

The mutual inductance between any two stator windings consists of two components. The first component is due to the flux that does not link the rotor and is therefore independent of the rotor position and is always negative because of the windings arrangement. The second component of the mutual inductance varies with the rotor position. The mutual inductances between the stator windings can be expressed as [7]:

$$L_{asbs} = L_{bsas} = -L_{ab0} + L_{aa2}\cos 2(\theta + \frac{2\pi}{3}) \tag{4.8}$$

$$L_{bscs} = L_{csbs} = -L_{ab0} + L_{aa2}\cos 2\theta \tag{4.9}$$

$$L_{csas} = L_{ascs} = -L_{ab0} + L_{aa2}\cos 2(\theta - \frac{2\pi}{3}) \tag{4.10}$$

where

$$L_{ab0} = (L_d + L_q - 2L_{ls})/6 \tag{4.11}$$

(c) Rotor inductances

The self-inductances of rotor circuits and mutual inductances between each other do not vary with rotor position because of the cylindrical structure of the stator. The rotor self-inductances are:

$$L_{fdfd} = L_{lfd} + L_{ad} \tag{4.12}$$

$$L_{kdkd} = L_{lkd} + L_{ad} \tag{4.13}$$

$$L_{kqkq} = L_{lkq} + L_{aq} \tag{4.14}$$

where, L_{lfd}, L_{lkd}, L_{lkq} are the leakage inductances of the field winding, d-axis damper winding and q-axis damper winding respectively. The mutual windings between rotor windings are

$$L_{fdkd} = L_{kdfd} = L_{ad} \tag{4.15}$$

$$L_{fdkq} = L_{kqfd} = L_{kdkq} = L_{kqkd} = 0 \tag{4.16}$$

(d) Stator to Rotor mutual inductances

The stator to rotor mutual inductance varies periodically with the rotor position. With space mmf and air gap flux distribution assumed sinusoidal, the mutual inductance between the stator windings and the excitation winding are:

$$L_{asfd} = L_{fdas} = L_{afd}\cos\theta \tag{4.17}$$

$$L_{bsfd} = L_{fdbs} = L_{afd}\cos(\theta - \frac{2\pi}{3}) \tag{4.18}$$

$$L_{csfd} = L_{fdcs} = L_{afd}\cos(\theta + \frac{2\pi}{3}) \tag{4.19}$$

The mutual inductance between the stator windings and the d-axis amortisseur are:

$$L_{askd} = L_{kdas} = L_{akd}\cos\theta \tag{4.20}$$

$$L_{bskd} = L_{kdbs} = L_{akd}\cos(\theta - \frac{2\pi}{3}) \tag{4.21}$$

$$L_{cskd} = L_{kdcs} = L_{akd}\cos(\theta + \frac{2\pi}{3}) \tag{4.22}$$

The mutual inductance between the stator windings and the q-axis amortisseur are:

$$L_{askq} = L_{kqas} = -L_{akq}\cos\theta \tag{4.23}$$

$$L_{bskq} = L_{kqbs} = -L_{akq}\cos(\theta - \frac{2\pi}{3}) \tag{4.24}$$

$$L_{cskq} = L_{kqcs} = -L_{akq}\cos(\theta + \frac{2\pi}{3}) \tag{4.25}$$

4.2.1.2 Flux Linkage Equations

The flux linkage equations in terms of the machine currents and inductances can be written as follows[7]:

$$[\lambda] = [L][I] \tag{4.26}$$

where

$$[\lambda] = \left[\lambda_{as}\lambda_{bs}\lambda_{cs}\lambda_{fd}\lambda_{kd}\lambda_{kq}\right]^T \tag{4.27}$$

$$[I] = \left[I_{as}I_{bs}I_{cs}I_{fd}I_{kd}I_{kq}\right]^T \tag{4.28}$$

$$[L]=\begin{bmatrix} L_{asas} L_{asbs} L_{ascs} L_{asfd} L_{askd} L_{askq} \\ L_{bsas} L_{bsbs} L_{bscs} L_{bsfd} L_{bskd} L_{bskq} \\ L_{csas} L_{csbs} L_{cscs} L_{csfd} L_{cskd} L_{cskq} \\ L_{fdas} L_{fdbs} L_{fdcs} L_{fdfd} L_{fdkd} L_{fdkq} \\ L_{kdas} L_{kdbs} L_{kdcs} L_{kdfd} L_{kdkd} L_{kdkq} \\ L_{kqas} L_{kqbs} L_{kqcs} L_{kqfd} L_{kqkd} L_{kqkq} \end{bmatrix} \quad (4.29)$$

4.2.1.3 Voltage Equations

The voltage equations of a synchronous machine are given in a matrix notation form as follows:

$$[V]=p[\lambda]+[R][I] \quad (4.30)$$

Where

$$[V]=\left[V_{as} V_{bs} V_{cs} V_{fd} V_{kd} V_{kq}\right]^T \quad (4.31)$$

$$[R]=\mathrm{diag}\left[R_{as} R_{bs} R_{cs} R_{fd} R_{kd} R_{kq}\right] \quad (4.32)$$

Substituting for $p[\lambda]$ from equation 4.26, equation 4.30 can be written as

$$[V]=[R][I]+[L]p[I]+p[L][I] \quad (4.33)$$

$$[V]=[R][I]+[L]p[I]+\omega_r[G][I] \quad (4.34)$$

The matrix [G] is introduced to represent the rotating performance of the electrical machine and is called the rotational inductance matrix. The term p[L] is defined as

$\omega_r[G]$ where ω_r is the rotor speed in electrical radians/sec and p is the differential operator.

4.2.1.4 Torque Equations

If the instantaneous electrical torque of the synchronous machine differs from the prime-mover torque, its speed will vary. At any instant, the input mechanical torque is equal to the electrical torque plus the accelerating torque.

The electromagnetic torque T_e is given [6], in terms of the stator phase quantities, in per unit as follows:

$$T_e = \frac{2}{3\sqrt{3}}\omega_s\left(\lambda_{as}\left(i_{bs}-i_{cs}\right)+\lambda_{bs}\left(i_{cs}-i_{as}\right)+\lambda_{cs}\left(i_{as}-i_{bs}\right)\right) \tag{4.35}$$

The equation of the motion is given in per unit by the following equation:

$$2H\frac{d\omega_r}{dt} = T_m - T_e \tag{4.36}$$

where T_m is the input mechanical torque, ω_r is the per unit rotor speed and H is the per unit inertia constant.

4.2.2 Induction machine

An induction machine has two main groups of windings, namely, those situated on the stator and those associated with the rotor. The stator windings are three indentical sinusoidal distributed windings and are displaced 120 electrical degrees apart. The rotor windings will also be considered as three indentical sinusoidal distributed windings which are displaced 120 electrical degrees apart. Figure 4.2 shows a simple arrangement of windings of a three-phase induction machine. The stator windings are connected to a three-phase supply and the rotor windings are connected together internally forming a closed circuit. Most of the induction machines used are motors

but there is also a small numer of used as generators mostly in remote generation systems.

In developing the model of an induction machine the following assumptions are made in order to simplify the transient analysis[6]:

a) The air-gap of the machine is uniform.

b) Saturation, hysteresis and eddy current effects are neglected.

c) A current in any winding sets up an mmf wave which is sinusoidally distributed in space around the air-gap.

4.2.2.1 Voltage equations

Taking into account the previous assuptions, the basic voltage equations for a three-phase induction machine may be expressed as follows:

$$\begin{bmatrix} V_{as} \\ V_{bs} \\ V_{cs} \\ V_{ar} \\ V_{br} \\ V_{cr} \end{bmatrix} = \begin{bmatrix} R_1 + L_{11}p & pM_{asbs} & pM_{ascs} & pM_{asar} & pM_{asbr} & pM_{ascr} \\ pM_{asbs} & R_1 + L_{11}p & pM_{bscs} & pM_{bsar} & pM_{bsbr} & pM_{bscr} \\ pM_{ascs} & pM_{bscs} & R_1 + L_{11}p & pM_{csar} & pM_{csbr} & pM_{cscr} \\ pM_{asar} & pM_{bsar} & pM_{csar} & R_2 + L_{22}p & pM_{arbr} & pM_{arcr} \\ pM_{asbr} & pM_{bsbr} & pM_{csbr} & pM_{arbr} & R_2 + L_{22}p & pM_{brcr} \\ pM_{ascr} & pM_{bscr} & pM_{cscr} & pM_{arcr} & pM_{brcr} & R_2 + L_{22}p \end{bmatrix} \begin{bmatrix} i_{as} \\ i_{bs} \\ i_{cs} \\ i_{ar} \\ i_{br} \\ i_{cr} \end{bmatrix} \quad (4.37)$$

The mutual inductances between stator and rotor windings vary sinusoidally with the rotor position and are given by the following expressions:

$$M_{asar} = M_{bsbr} = M_{cscr} = \hat{M}\cos\theta \quad (4.38)$$

$$M_{asbr} = M_{bscr} = M_{csar} = \hat{M}\cos(\theta + 120^\circ) \quad (4.39)$$

$$M_{ascr} = M_{bsar} = M_{csbr} = \hat{M}\cos(\theta - 120^\circ) \quad (4.40)$$

and the mutual inductances between stator windings or rotor windings are

$$M_{asbs} = M_{bscs} = M_{ascs} = M_{arbr} = M_{brcr} = M_{arcr} = \hat{M}\cos\frac{2\pi}{3} = -\frac{\hat{M}}{2} \qquad (4.41)$$

where the inductance $\hat{M}$ is the amplitude of the mutual inductance between stator and rotor windings. Also the total stator and rotor self inductances are

$$L_{11} = \hat{M} + L_{ls} \text{ and } L_{22} = \hat{M} + L_{lr} \qquad (4.42)$$

where L_{ls} and L_{lr} are the leakage inductances of the stator and rotor windings, respectively, and p is the differential operator d/dt.

Substituting for the inductances, the voltage equations can be expressed in the form:

$$[V] = [R][i] + [L]p[i] + \omega_r[G][i] \qquad (4.43)$$

where

ω_r is the electrical angular velocity

$$[V] = \left[V_{as}\ V_{bs}\ V_{cs}\ 0\ 0\ 0\right]^T \qquad (4.44)$$

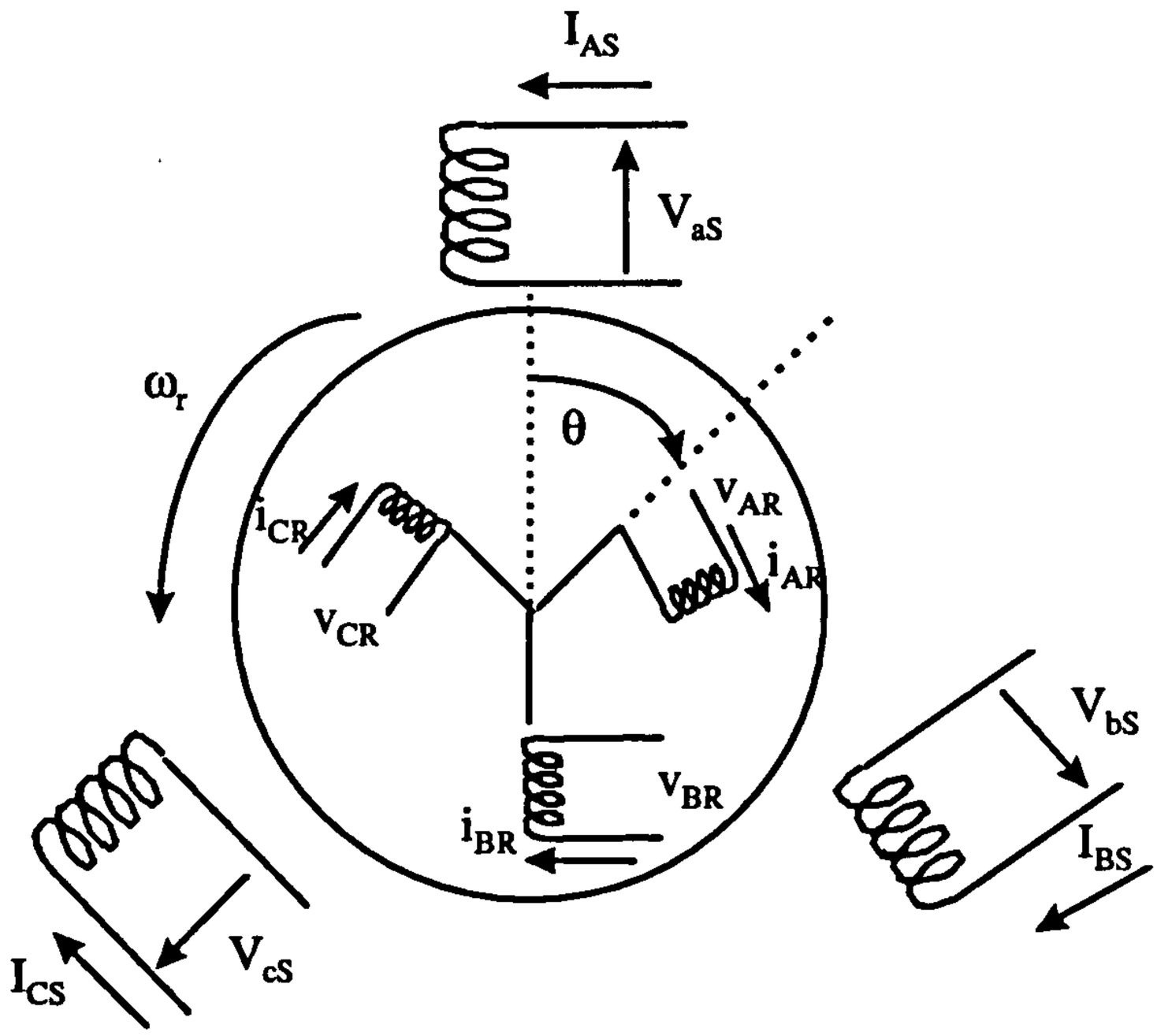

Figure 4.2 Three phase induction machine

$$[i] = [i_{as}\ i_{bs}\ i_{cs}\ i_{ar}\ i_{br}\ i_{cr}]^T \tag{4.45}$$

$$[R] = \text{diag}[R_1\ R_1\ R_1\ R_2\ R_2\ R_2] \tag{4.46}$$

$$[L] = \begin{bmatrix} L_{11} & M_{asbs} & M_{ascs} & M_{asar} & M_{asbr} & M_{ascr} \\ M_{asbs} & L_{11} & M_{bscs} & M_{bsar} & M_{bsbr} & M_{bscr} \\ M_{ascs} & M_{bscs} & L_{11} & M_{csar} & M_{csbr} & M_{cscr} \\ M_{asar} & M_{bsar} & M_{csar} & L_{22} & M_{arbr} & M_{arcr} \\ M_{asbr} & M_{bsbr} & M_{csbr} & M_{arbr} & L_{22} & M_{asar} \\ M_{ascr} & M_{bscr} & M_{cscr} & M_{arcr} & M_{brcr} & L_{22} \end{bmatrix} \tag{4.47}$$

and $$[G] = -\hat{M}\begin{bmatrix} 0 & [g] \\ [g]^T & 0 \end{bmatrix} \tag{4.48}$$

where

$$[g]=\begin{bmatrix} \sin\theta & \sin(\theta+\frac{2\pi}{3}) & \sin(\theta-\frac{2\pi}{3}) \\ \sin(\theta-\frac{2\pi}{3}) & \sin\theta & \sin(\theta+\frac{2\pi}{3}) \\ \sin(\theta+\frac{2\pi}{3}) & \sin(\theta-\frac{2\pi}{3}) & \sin\theta \end{bmatrix} \quad (4.49)$$

4.2.2.2 Torque equations

The torque equation of the induction motor in terms of stator phase equations can be expressed as[7]:

$$T_e=\frac{2}{3\sqrt{3}}\omega_s\left(\lambda_{as}\left(i_{bs}-i_{cs}\right)+\lambda_{bs}\left(i_{cs}-i_{as}\right)+\lambda_{cs}\left(i_{as}-i_{bs}\right)\right) \quad (4.50)$$

where ω_s is the synchronous speed in electrical radians/sec. Also the mechanical equation of the motion may be expressed as :

$$p\omega_r=\left(T_e-T_{load}\right)/2H \quad (4.51)$$

where T_{load} is the load torque and can be expressed as:

$$T_{load}=\alpha_0+\alpha_1\omega_r+\alpha_2\omega_r^{\,2}+\alpha_3\omega_r^{\,3} \quad (4.52)$$

and H is the inertia constant for the motor and the load.

In all the above equations, the subscript s denotes variables and parameters associated with the stator circuit, and the subscript r denotes variables and parameters associated with the rotor circuit.

4.2.3 Three-phase transformer

The three-phase transformer is a very important component in every modern power system, because it is not practically feasible to generate and consume power at high voltages, transformers are utilised throughout, changing the system voltage levels. Figure 3.3 shows the schematic diagram of a three-phase core type transformer with six windings, three primary windings and three secondary windings.

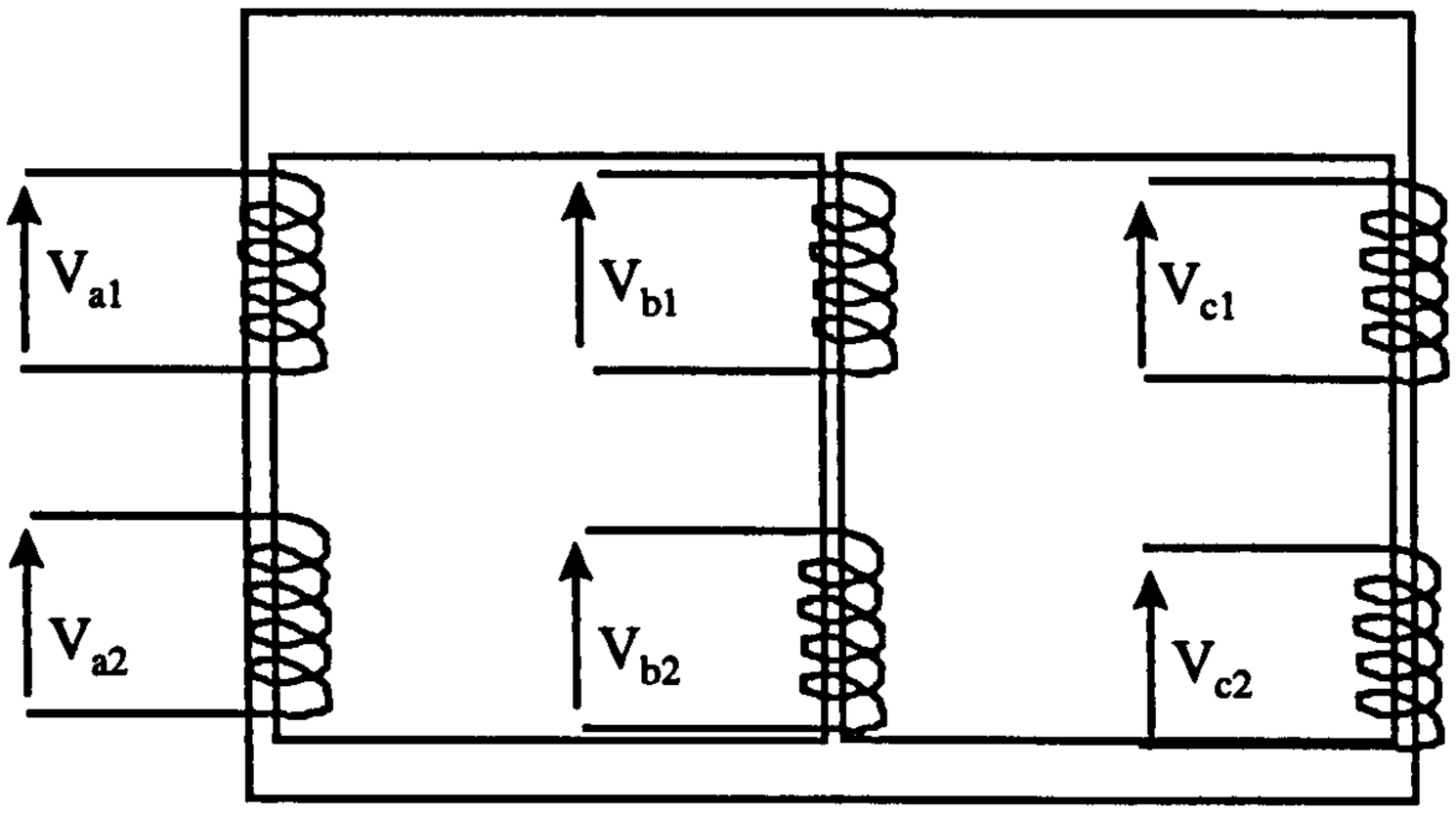

Figure 4.3 Three-phase power transformer

The voltage equations can be expressed as[7]:

$$[V] = p[\lambda] + [R][i] \tag{4.53}$$

where

$$[\lambda] = [L][i] \tag{4.54}$$

and

$$[\lambda] = [\lambda_{a1}\lambda_{b1}\lambda_{c1}\lambda_{a2}\lambda_{b2}\lambda_{c2}]^T \tag{4.55}$$

$$[V] = [V_{a1} V_{b1} V_{c1} V_{a2} V_{b2} V_{c2}]^T \tag{4.56}$$

$$[i] = [i_{a1} i_{b1} i_{c1} i_{a2} i_{b2} i_{c2}]^T \tag{4.57}$$

$$[R] = [R_{a1} R_{b1} R_{c1} R_{a2} R_{b2} R_{c2}]^T \tag{4.58}$$

$$[L] = \begin{bmatrix} L_{a1a1} & L_{a1b1} & L_{a1c1} & L_{a1a2} & L_{a1b2} & L_{a1c2} \\ L_{b1a1} & L_{b1b1} & L_{b1c1} & L_{b1a2} & L_{b1b2} & L_{b1c2} \\ L_{c1a1} & L_{c1b1} & L_{c1c1} & L_{c1a2} & L_{c1b2} & L_{c1c2} \\ L_{a2a1} & L_{a2b1} & L_{a2c1} & L_{a2a2} & L_{a2b2} & L_{a2c2} \\ L_{b2a1} & L_{b2b1} & L_{b2c1} & L_{b2a2} & L_{b2b2} & L_{b2c2} \\ L_{c2a1} & L_{c2b1} & L_{c2c1} & L_{c2a2} & L_{c2b2} & L_{c2c2} \end{bmatrix} \tag{4.59}$$

where the subscripts 1 and 2 denote the primary and secondary quantities, respectively.

4.2.4 Filters

Filters are used to reduce harmonic currents and voltages in the AC systems. They are R-L-C circuits, which are designed to provide a low impedance path for harmonic currents at harmonic frequencies. In figure 4.4 a group of 5^{th}, 7^{th} ,11^{th} and 13^{th} order harmonic filters are connected at the converter AC terminals. The normalised differential equations of these filters can be arranged in a matrix form as follows:

$$p[I_{FLn}] = \left[\frac{1}{L_{FLn}}\right][V] - \left[\frac{1}{L_{FLn}}\right][V_{Cn}] - \left[\frac{R_{FLn}}{L_{FLn}}\right][I_{FLn}] \tag{4.60}$$

$$p[V_{Cn}] = \left[\frac{1}{C_{FLn}}\right][I_{FLn}] \tag{4.61}$$

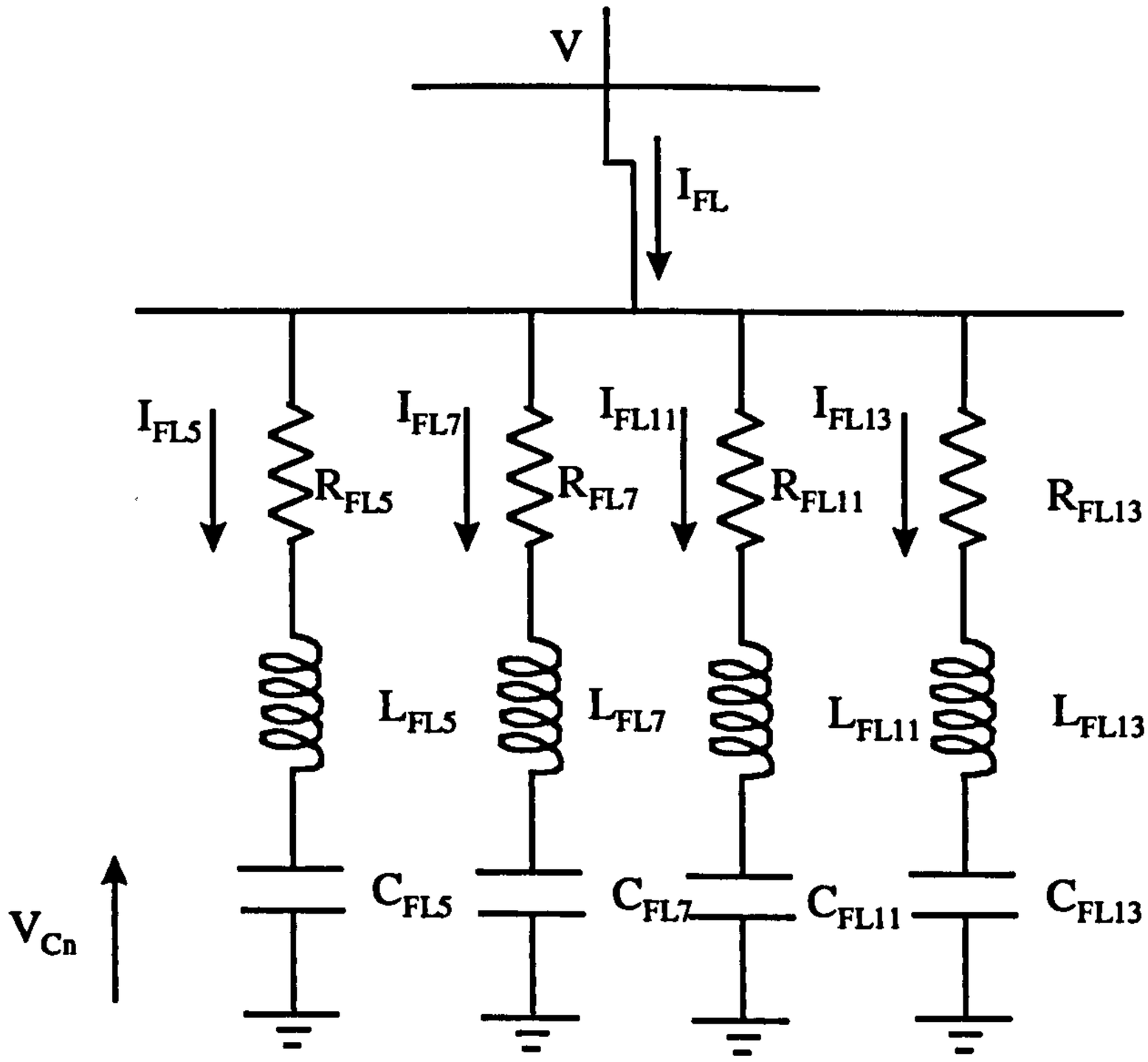

Figure 4.4 Representation of the 5^{th}, 7^{th} ,11^{th} and 13^{th} order harmonic filters

where

$$\left[\frac{1}{L_{FLn}}\right] = \text{diag}\left[\frac{1}{L_{f1n}} \quad \frac{1}{L_{fln}} \quad \frac{1}{L_{fln}} \quad \frac{1}{L_{fln}}\right] \tag{4.62}$$

$$\left[\frac{R_{f1n}}{L_{FLn}}\right] = \text{diag}\left[\frac{R_{f1n}}{L_{f1n}} \quad \frac{R_{fln}}{L_{fln}} \quad \frac{R_{fln}}{L_{fln}} \quad \frac{R_{fln}}{L_{fln}}\right] \tag{4.63}$$

$$\left[\frac{1}{C_{FLn}}\right] = \text{diag}\left[\frac{1}{C_{f1n}} \quad \frac{1}{C_{fln}} \quad \frac{1}{C_{fln}} \quad \frac{1}{C_{fln}}\right] \tag{4.64}$$

$$[I_{FLn}] = \begin{bmatrix} i_{fl_n1} & i_{fl_n2} & i_{fl_n3} & i_{fl_n4} \end{bmatrix}^T \quad (4.65)$$

$$[v_{Cn}] = \begin{bmatrix} v_{c_n1} & v_{c_n2} & v_{c_n3} & v_{c_n4} \end{bmatrix}^T \quad (4.66)$$

n= 5, 7, 11, 13.

4.3 EXCITATION SYSTEM MODELLING

Synchronous generators in power systems operate with automatic voltage regulators(AVRs). The AVR is responsible for the regulation of the terminal voltage of the machine within certain limits. It is also responsible for controlling the reactive power flow through the regulation of the field voltage and therefore the synchronous field current. An important characteristic of an AVR is its ability to respond rapidly to voltage variations during both normal and abnormal operation. While many different types of AVRs are employed in practise, the basic principle of operation may be described in the following; the voltage deviation signal is amplified to produce the signal required to change the exciter field current, which in turn produces a change in exciter output voltage thereby resulting in a new level of excitation for the synchronous generator.

An IEEE Committee[8] recommended two types of AVRs that are representative of the majority of practical regulators and which can be used adequately in system studies. The two types of AVRs are designated "Type 1" and "Type 2".

A typical block diagram of the "Type1" model is shown in figure 4.5. In this model, the generator terminal voltage V_t is applied to the regulator input. T_R is a small time constant representing regulator input filtering. The first summing point determines the voltage error input to the regulator amplifier. The main regulator transfer function is represented as a gain K_A and a time constant T_A. Following this, the maximum and minimum regulator limits are imposed so that large input error signals cannot produce a regulator output exceeding practical limits. The amplifier signal is supplied to the exciter to provide the exciter output voltage or the generator field voltage E_{FD}.

The exciter saturation function S_E is a non-linear function of the exciter output voltage and is subtracted from the regulator output signal. Major loop damping is provided by the feedback transfer function from the exciter output E_{FD} to the second summing point of the block diagram

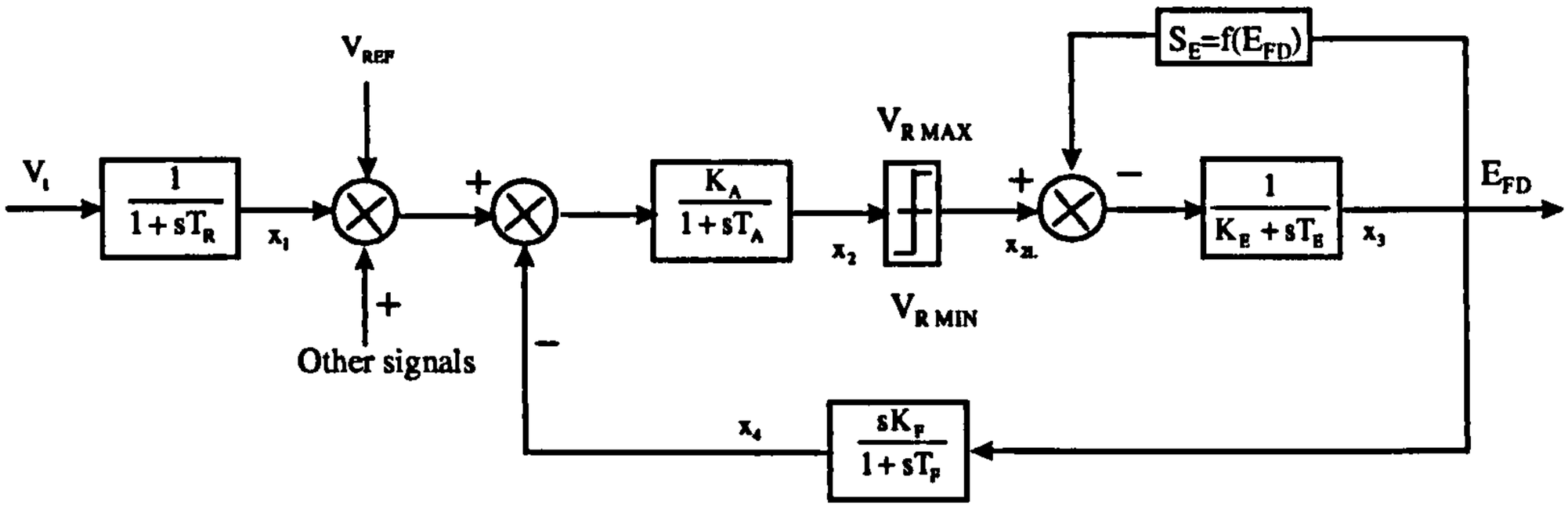

Figure 4.5 IEEE "Type 1" AVR model

The block diagram of "Type 2", is shown in Figure 4.6. As in this type the exciter transfer function is not included in the damping loop, an additional time constant is introduced for compensation. Other characteristics of "Type 2" system are similar to those of "Type 1". The mathematical models for both types may be expressed by the state space equation:

$$\frac{d}{dt}[x]=[A][x]+[B][U] \qquad (4.67)$$

For "Type 1" model

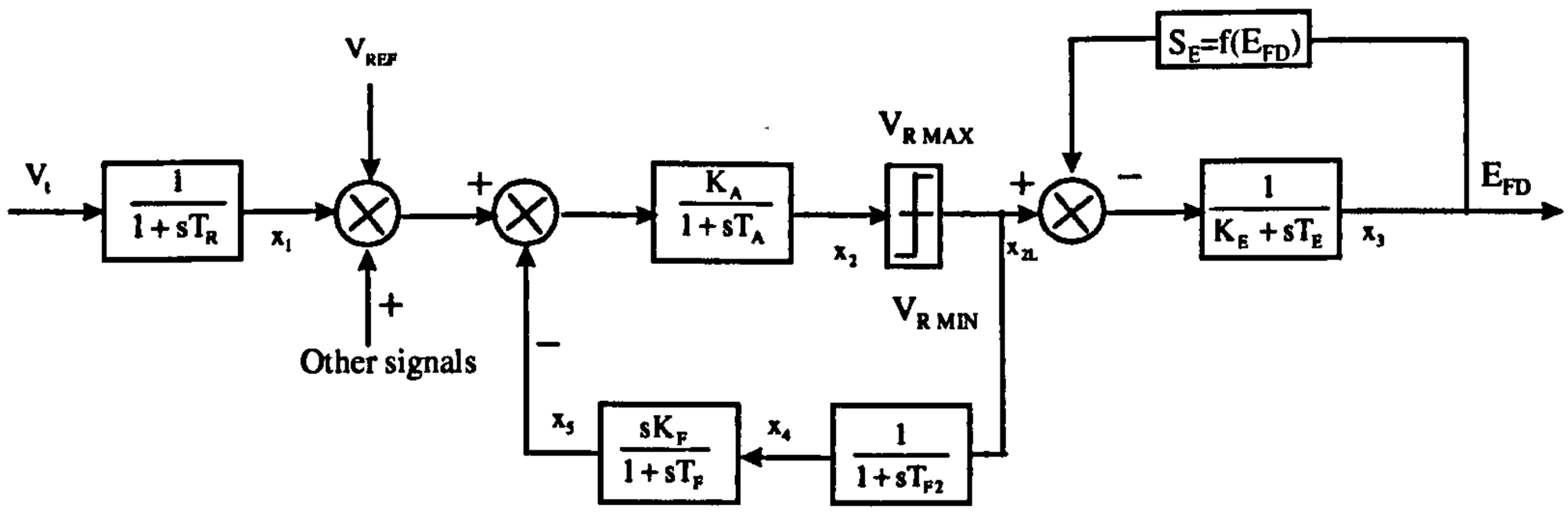

Figure 4.6 IEEE "Type 2" AVR model

$$[x] = [x_1 x_2 x_3 x_4]^T \tag{4.68}$$

$$[U] = [V_t \; V_{REF} \; x_{2L} \; x_{2L}]^T \tag{4.69}$$

$$[B] = \text{diag}\left[\frac{1}{T_R} \quad \frac{K_A}{T_A} \quad \frac{1}{T_E} \quad \frac{K_F}{T_E T_F}\right] \tag{4.70}$$

$$[A] = \begin{bmatrix} -\frac{1}{T_R} & 0 & 0 & 0 \\ -\frac{K_A}{T_A} & -\frac{1}{T_A} & 0 & \frac{-K_A}{T_A} \\ 0 & 0 & -\frac{(K_E + S_E)}{T_E} & 0 \\ 0 & 0 & -\frac{K_F(K_E + S_E)}{T_E T_F} & -\frac{1}{T_F} \end{bmatrix} \tag{4.71}$$

For the "Type 2" model

$$[x] = [x_1 x_2 x_3 x_4 x_5]^T \tag{4.72}$$

$$[U] = [V_t \; V_{REF} \; x_{2L} \; x_{2L} \; x_{2L}]^T \tag{4.73}$$

$$[B] = \text{diag}\left[\frac{1}{T_R} \quad \frac{K_A}{T_A} \quad \frac{1}{T_E} \quad \frac{1}{T_{F2}} \quad \frac{K_F}{T_{F1}T_{F2}}\right] \tag{4.74}$$

$$[A] = \begin{bmatrix} -\frac{1}{T_R} & 0 & 0 & 0 & 0 \\ -\frac{K_A}{T_A} & -\frac{1}{T_A} & 0 & 0 & \frac{-K_A}{T_A} \\ 0 & 0 & -\frac{(K_E + S_E)}{T_E} & 0 & 0 \\ 0 & 0 & 0 & -\frac{1}{T_{F2}} & 0 \\ 0 & 0 & 0 & -\frac{K_F}{T_{F1}T_{F2}} & -\frac{1}{T_{F1}} \end{bmatrix} \tag{4.75}$$

In both types, the output of the AVR represents the input field voltage, in per unit, to the synchronous generator and the output terminal voltage of the generator, in per unit represents the input to the AVR.

4.4 PRIME MOVER SYSTEMS

The prime movers of electrical energy supplied by utilities are the kinetic energy of water and the thermal energy derived from fossil fuels and nuclear fission. The prime movers convert these sources of energy into mechanical energy that is converted to electrical energy by synchronous generators. The function of the prime mover governing systems is to provide a means of controlling power and frequency.

4.4.1 Heavy Type Industrial Gas Turbine

The wide popularity of the industrial gas turbine and their suitability for use as prime movers in isolated situations such as oil fields and offshore installations have increased the demand for providing a simple gas turbine model which can be used for

various power system studies. In addition, at high ratings they have recently found favour with many electricity supply companies world-wide.

The paper written by Rowen [9] provides a simplified mathematical representation of a heavy-duty, simple cycle, single shaft gas turbine that is suitable for use in dynamic power system studies. The control system includes speed control, temperature control, acceleration control and upper and lower fuel limits.

Further simplifications can be introduced into the model, when it is used in most types of power system dynamic studies. The temperature and acceleration controls are eliminated. The simplified block diagram of the model is shown in figure 4.7. The transfer functions represented by blocks in the figure can be transformed to state space equations taking the form.

$$p[X_g] = [A_g][X_g] + [B_g][U_g] \tag{4.76}$$

where

$$[X_g] = [X_1\ X_2\ X_3]^T \tag{4.77}$$

$$[U_g] = [\Delta\omega\ \mathrm{PIL}\ F]^T \tag{4.78}$$

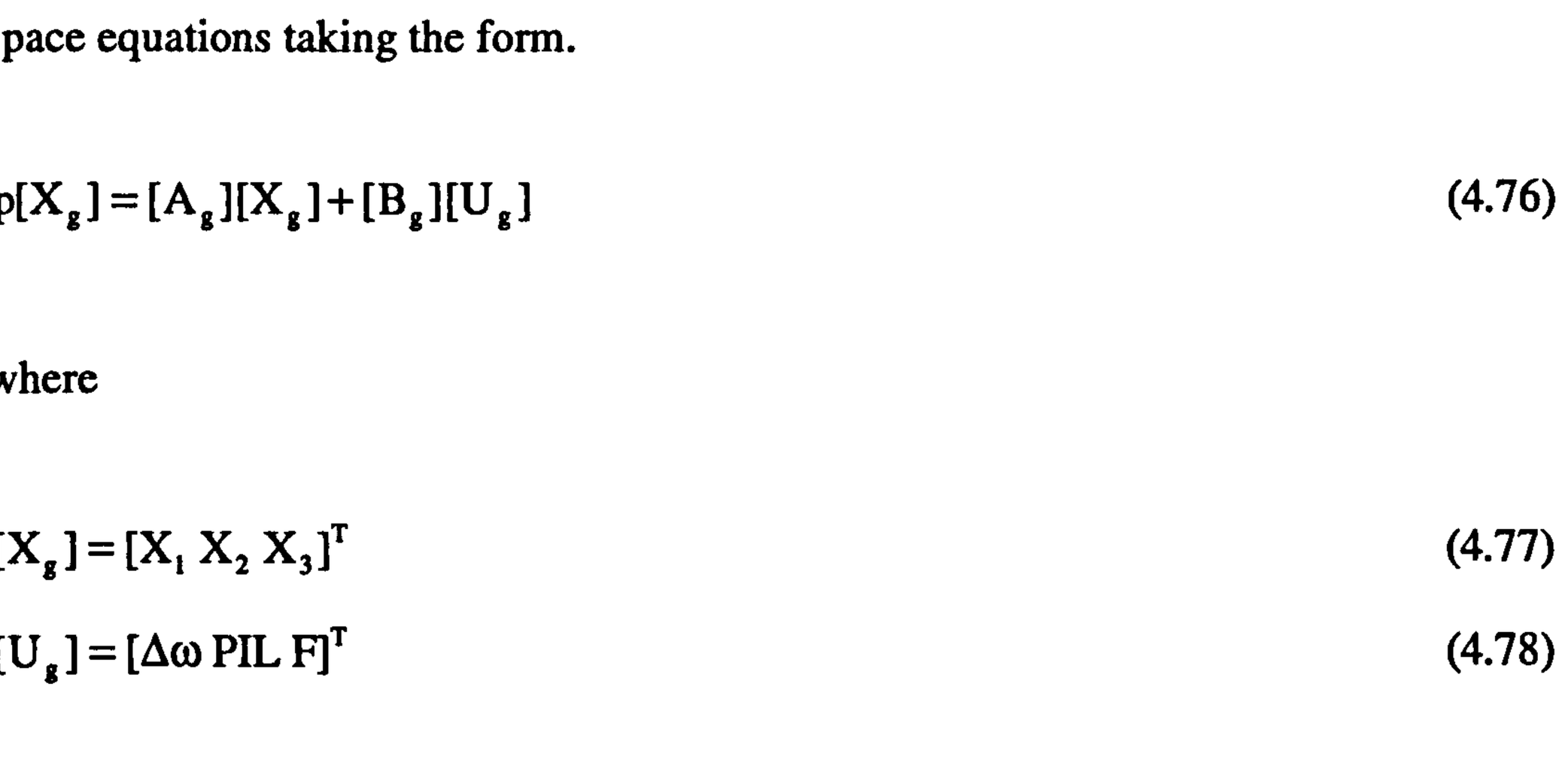

Figure 4.7 Simplified single shaft gas turbine model

$$[A_g]=\begin{bmatrix} -\frac{1}{T_1} & 0 & 0 \\ 0 & -\frac{1}{T_2} & \frac{-K_2K_4}{T_2} \\ 0 & \frac{K_3}{T_3} & -\frac{1}{T_3} \end{bmatrix} \tag{4.79}$$

$$[B_g]=\begin{bmatrix} \frac{K_1}{T_1} & 0 & 0 \\ 0 & \frac{(1-F)K_2}{T_2} & \frac{K_2}{T_2} \\ 0 & 0 & 0 \end{bmatrix} \tag{4.80}$$

4.4.2 Steam turbine

The IEEE Committee [10,11] represented various types of steam turbines, ranging from reheat, tandem compound single and double reheat to cross compound single and double reheat systems, for use in power system studies. The tandem single compound single reheat model is extracted from reference [10] and combined with a linear speed-governing system to form a typical complete model for a steam turbine prime mover as shown in figure 4.8. In the figure the turbine response is adequately modelled by three time constants, the steam chest T3, the re-heater T4, and the crossover T5.

The time constants represent the charging time of associated steam chambers. The coefficients K3 to K5 determine the contributions from various turbine sections. The state space equations for the model given in the figure may be written as:

$$p[X_s] = [A_s][X_s] + [B_s][U_s] \tag{4.81}$$

where

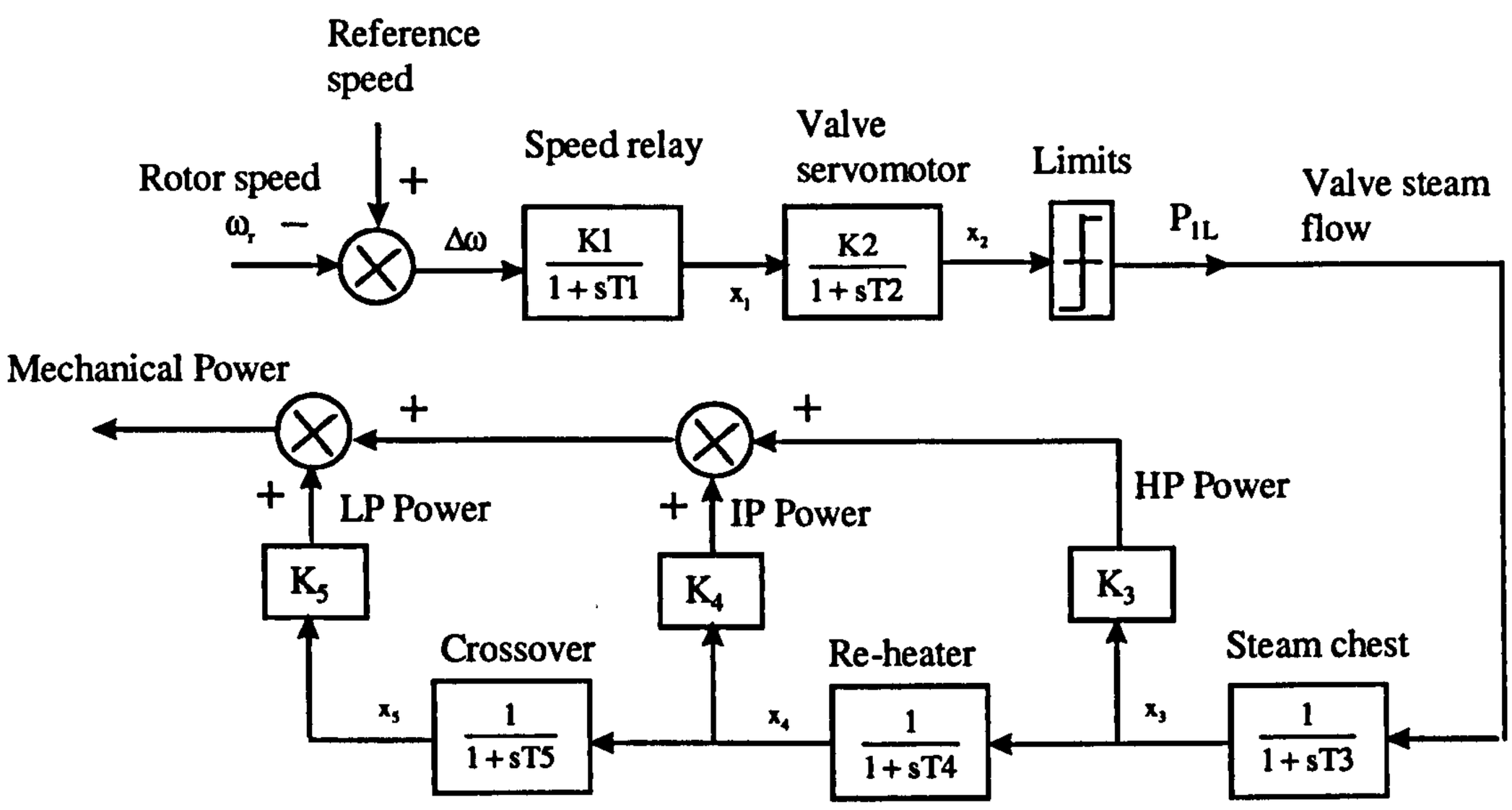

Figure 4.8 Linear speed-governing system with reheat steam-turbine system model

$$[X_s] = [X_1\ X_2\ X_3\ X_4\ X_5]^T \tag{4.82}$$

$$[U_s] = [\Delta\omega\ PIL\ 0\ 0\ 0]^T \tag{4.83}$$

$$[A_S]=\begin{bmatrix} -\frac{1}{T_1} & 0 & 0 & 0 & 0 \\ \frac{K_2}{T_2} & -\frac{1}{T_2} & 0 & 0 & 0 \\ 0 & 0 & -\frac{1}{T_3} & 0 & 0 \\ 0 & 0 & \frac{1}{T_4} & -\frac{1}{T_4} & 0 \\ 0 & 0 & 0 & \frac{1}{T_5} & -\frac{1}{T_5} \end{bmatrix} \quad (4.84)$$

$[B_S]$ is a matrix of 5*5 with only nonzero entities: $B_{11}=\frac{K_1}{T_1}$ and $B_{32}=\frac{1}{T_3}$ (4.85)

4.5 MODELLING OF AN AC/DC CONVERTER STATION

In the operation of a three-phase bridge-connected rectifier, in figure 4.9 either two or three valves are conducting simultaneously. Therefore, twelve different modes of operation exist per cycle. Each mode of the twelve can be represented mathematically by its own differential equations. However it is possible to represent all modes by general equations, since these twelve modes can, in fact, be divided into two main cases. These general equations can be applied to all modes by simply defining the conducting valves in each mode. The general equations in their normalised form are as follows[12]:

$$\frac{di_e}{dt}=[-v_d+v_e(1+\frac{L_d+L}{L_g}K)-v_g\frac{L_d+L}{L_g}K-(-1)^m v_{DC-r}-i_e\{(R_d+R)+R_e+\frac{R_e(L_d+L)}{L_g}K\}-i_g\{(R_d+R)-\frac{R_g(L_d+L)}{L_g}\}K]/[(L_d+L)+L_e+\frac{(L_d+L)L_e}{L_g}K] \quad (4.86)$$

$$\frac{di_d}{dt}=-\frac{di_e}{dt}-K\frac{di_g}{dt} \quad (4.87)$$

$$i_{DC} = (-1)^{m+1} i_d \tag{4.88}$$

$$\frac{di_{DC}}{dt} = (-1)^{m+1} \frac{di_d}{dt} \tag{4.89}$$

$$v_{DC-s} = v_{DC-r} + Ri_{DC} + L\frac{di_{DC}}{dt} \tag{4.90}$$

Subscripts e, d and g are for any of the three phases 1,2 and 3. K and m are constants. R_e, R_d, R_g and L_e, L_d, L_g are the converter transformer resistances and inductances respectively. By varying the subscripts e,d and g and the values K and m according to the conduction condition, equations 4.86-4.90 can be applied to any of the twelve modes of operation.

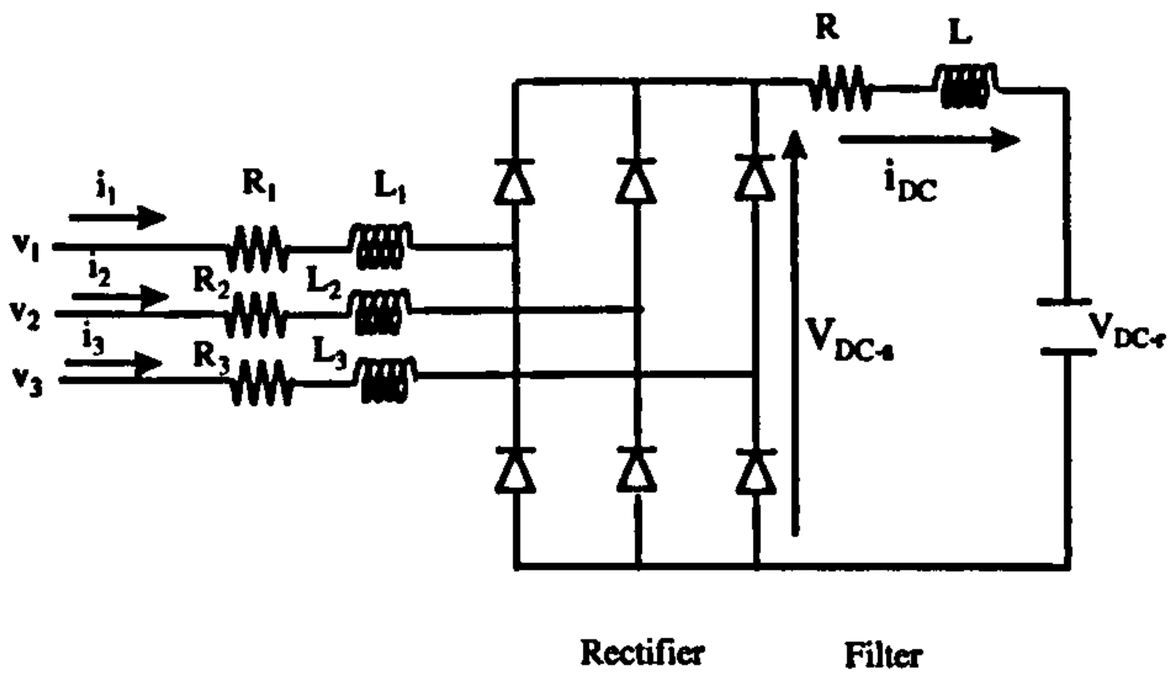

Figure 4.9 Bridge connected rectifier

Several rules for the various modes of operation may be obtained empirically:

(i) If three valves are conducting, then K=1; otherwise K=0.

(ii) If two upper valves are conducting simultaneously, then m=2; otherwise m=1.

(iii) Suffix d always represents the phase number of a current that can be divided into the two other phases. It also represents the phase number having positive phase current with respect to the positive direction of i_{DC} when there are only two conducting phases.

(iv) If a phase is non-conducting, the derivative of its current is zero.

In matrix notation, the derivative vector of the rectifier currents can be written in the form:

$$p[I_{rec}] = F(V, I_{rec}, v_{DC-r}) \tag{4.91}$$

where

$$[I_{rec}] = [i_1 \;\; i_2 \;\; i_3]^T \tag{4.92}$$

$$[V\,] = [v_1 \;\; v_2 \;\; v_3]^T \tag{4.93}$$

4.6 CONLUSIONS

In this chapter, detailed three-phase mathematical models were described for various power system components, such as synchronous and induction machines along with their associated excitation and prime mover systems, three-phase transformers, filters and a mathematical representation of an AC/DC converter station. These models combined together form the basis of a complete multi-machine AC/DC power system, the modelling procedure of which will be described in the succeeding chapter.

4.7 REFERENCES

1. Park, R.H., "Two-Reaction Theory of Synchronous Machines-Generalised Method of Analysis", Part I, AIEE Transactions, Vol 48, 1929, pp.716-727.
2. Park, R.H., "Two-Reaction Theory of Synchronous Machines-Generalised Method of Analysis", Part II, AIEE Transactions, Vol 52, 1933, pp.352-355.
3. Bowles, J.P, "AC System and transformer representation for HVDC transmission studies", IEEE Transactions on PAS, Vol PAS-89, No. 7, Sept/Oct 1970, pp.1603-1608.
4. Owen, R.E., McGranaghan M.F, Vivirito J.R, "Distribution System Harmonics: Controls for large power converters", IEEE Transactions on Power Apparatus and Systems, Vol PAS-101, No 3 March 1982, pp 644-648.
5. Reeve J, and Subba Rao, T. "Dynamic Analysis of Harmonic Interaction between AC and DC Power Systems", IEEE Transactions on PAS, Vol. PAS-93, No.2, March/April 1974, pp. 640-646.
6. Smith J.R. and Chen Meng-Jen, Three-Phase Electrical Machine Systems-computer simulation, Research Studies Press Ltd, 1993.
7. Smith J.R "Response analysis of A.C electrical Machines-computer models and simulation", Research Studies Press Ltd, 1990
8. IEEE Committee Report, "Computer representation of excitation systems", IEEE Transactions, Vol. PAS-87, June 1968, pp. 1460-1464.
9. Rowen W.I. "Simplified Mathematical Representation of Heavy-Duty Gas Turbines", ASME Transactions of Journal of Engineering for Power, Vol 105, 1984, pp 865-869.
10. IEEE Committee Report, "Dynamic Models for steam and hydro turbines in power system studies", IEEE Transactions, Vol PAS-92, November/December 1973, pp 1904-1915.
11. IEEE Working Group Report, "Dynamic Models for fossil fuelled steam units in power system studies, IEEE Transactions, Vol PWRS-6,No.2, May 1991, pp 753-761.

12. Taleb M, Ortmeyer T.H., "Examination of the current injection technique", IEEE Transactions on Power Delivery, Vol 7, January 1992, pp 442-448.

13. Buamud M.S "Dynamic Response Analysis of Large AC Generation systems", Phd thesis, University of Strathclyde, 1995.

14. Weedy B.M "Electric Power Systems", John Wiley & Sons Ltd 1987.

15. Siemens Review : Energy and Automation, Vol 88, 1988.

16. Magnusson P, "Resistively Bridged Harmonic Filter for Power Converters", IEEE Transactions on Power Apparatus and systems, Vol PAS-87, June 1968, pp 1481-1484.

CHAPTER 5

MODELLING AND SIMULATION OF MULTI-MACHINE SYSTEMS WITH AC/DC CONVERTER STATIONS AND VARIABLE SPEED DRIVES

5.1 Introduction

Electric power systems have grown enormously in size and complexity over the past 30 years and the generating units are now additionally given the task to provide increasing demand without corresponding increases in transmission capacity. Modern digital computers, with their increased speed and computing power, make possible the simulation of modern power systems with a degree of accuracy commensurate with the requirements of system planning and current operational procedures. Although electric power systems vary in size and structure and contain various components, they all have the same basic characteristics. They are comprised of three-phase ac systems operating essentially at constant voltage, they use principally synchronous machines for generation of electricity and they transmit power over significant distances to consumers spread over a wide area.

Interaction between AC and DC power systems has always provided a challenge for power system planners [1,2]. Disturbances to supply systems caused by converter loads can only be tolerated within prescribed limits. It is hence important, especially in the case of weak supplies, to predict the levels of expected supply system disturbances so that if necessary appropriate measures can be taken to reduce them. Taking account of the three-phase machine load, converter operation creates harmonic currents that cause additional losses in lines, transformers and machines.

This chapter presents the modelling procedure of a complete general multi-machine AC/DC power system, comprising various generation units and their associated controls and the electromechanical drives, and describes the interconnection method of the system components. The detailed mathematical models of system components, described in the previous chapter, are used extensively here. The modelling technique is applied initially on a small power system with a variable speed drive. Filters are used in order to absorb most of the harmonics that the AC/DC converter station generates and comparative simulation results are presented in order to investigate the impact of harmonic filters on the depth of penetration of the harmonics into the network. Also a very detailed AC/DC multi-machine model is illustrated using two variable speed drives interconnected on the AC system network.

Finally, results are illustrated using the developed computer program for different system configurations.

5.2 Generalised multi-machine system modelling

In this general method, each component connected to the power system is represented by its full three-phase differential equations, as were given in the previous chapter. These equations are combined together, according to the following equation

$$[L]p[i] = [V] - ([R] + [G])[i] \tag{5.1}$$

and solving for the derivatives of the currents,

$$p[i] = [L]^{-1}[V] - [L]^{-1}([R] + [G])[i] \tag{5.2}$$

where the unknowns are the currents and the matrices [R],[L],[G] are a combination of the corresponding matrices of each component connected to the system. Thus the system is considered as an entity and the current and voltage conditions are satisfied at the same time[3-6].

For any system configuration, the nodes are numbered, starting from the generator bus-bars. In figure 5.1, a typical power system node is shown in schematic form, containing m generators and n loads, to help illustrate the method. For that node, for any node of the system starting from the first numbered one, Kirchhoff's voltage law is applied. According to that law, the terminal voltages of all the connected components to the same node are identical. For the typical node, the voltage law may be stated as:

$$V_{g1} = V_{g2} = \ldots = V_{gm} = V_{L1} = V_{L2} = \ldots = V_{Ln} \tag{5.3}$$

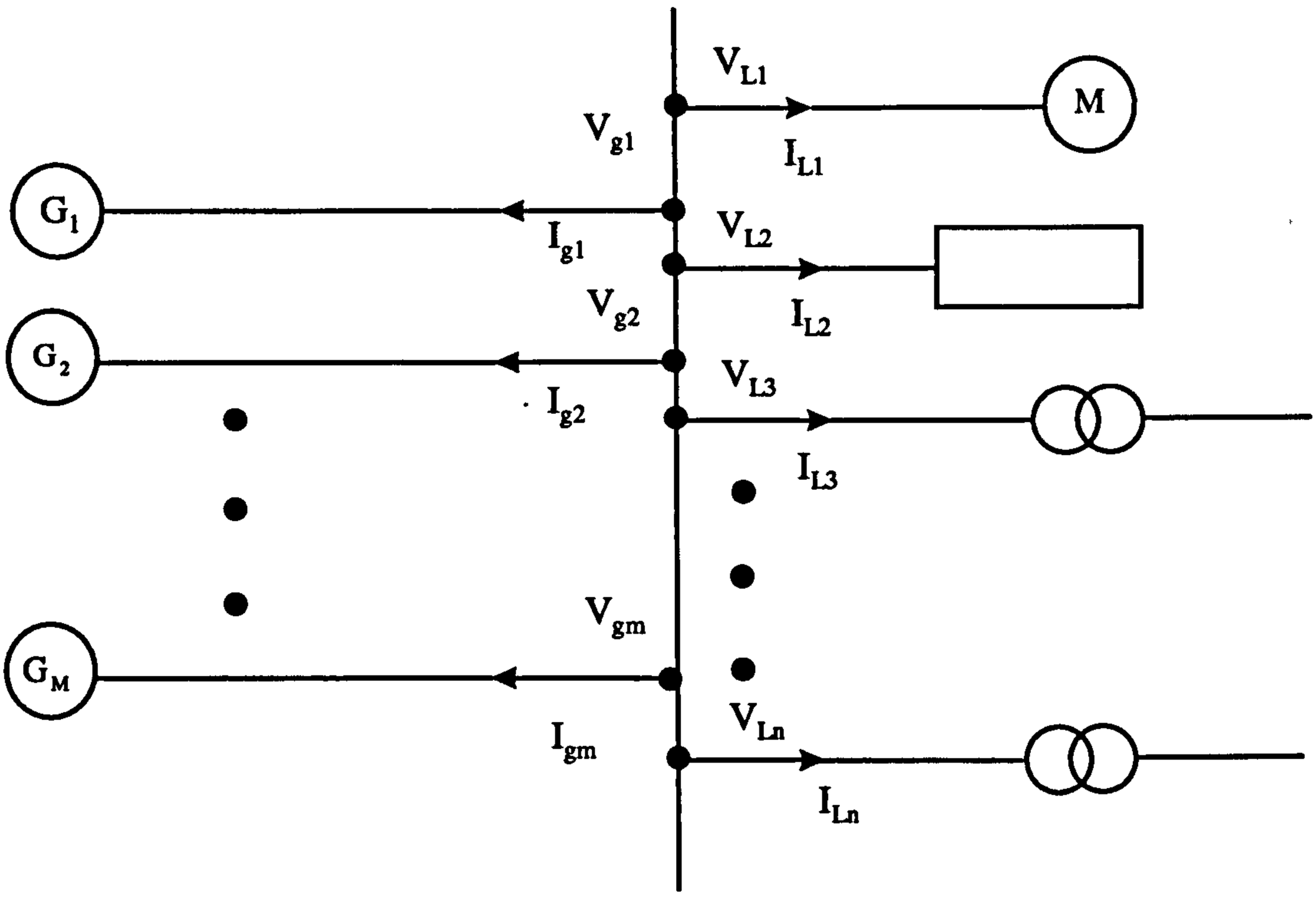

Figure 5.1 Typical power system node

The equations given in the previous chapter treat each component as independent, as if it was not connected to any other component. But clearly this is not the case when

considering a power system, and thus, using these equations in the overall system modelling will result in the system matrices being singular. To rectify that situation Kirchoff's current law is applied at every node and for the typical node in question can be expressed as:

$$\sum_{k=1}^{m} I_{gk} + \sum_{l=1}^{n} I_{Ll} = 0 \tag{5.4}$$

Any one of the three-phase currents can be represented by combinations of the others using the previous equation, thus eliminating one of the unknowns for every node. For consistency, the stator currents associated with one of the generators connected to the bus-bar are eliminated from the overall equations and the value of these currents is obtained from the sum of currents acquired from all other load and generation components connected to this node. The generator or the transformer secondary winding from which currents are eliminated at each node is called the pivotal component.

For every node, the terminal voltage of each component connected to it is equated with the terminal voltage of the selected component, according to Kirchhoff's voltage law. Thus if there are m components connected to a node, there will be (m-1) voltage equations for that node.

The phase voltage equations of various power system components, described in detail in the preceding chapter, are summarised here in the matrix form.

(a) Three-phase synchronous machine

$$V_{sg} = R_{sg} i_{sg} + L_{ssg} p i_{sg} + L_{srg} p i_{rg} + \omega_{rg} G_{ssg} i_{sg} + \omega_{rg} G_{srg} i_{rg} \tag{5.5}$$

$$V_{rg} = R_{rg} i_{rg} + L_{rrg} p i_{rg} + L_{rsg} p i_{sg} + \omega_{rg} G_{rsg} i_{sg} \tag{5.6}$$

(b) Three-phase induction machine

$$V_{sm} = R_{sm} i_{sm} + L_{ssm} p i_{sm} + L_{srm} p i_{sm} + \omega_{rm} G_{srm} i_{rm} \tag{5.7}$$

$$V_{rm} = R_{rm} i_{rm} + L_{rsm} p i_{sm} + L_{rrm} p i_{rm} + \omega_{rm} G_{rsm} i_{sm} \tag{5.8}$$

(c) Three-phase power transformer

$$V_{1T} = R_{1T} i_{1T} + L_{11T} p i_{1T} + L_{12T} p i_{2T} \tag{5.9}$$

$$V_{2T} = R_{2T} i_{2T} + L_{21T} p i_{1T} + L_{22T} p i_{2T} \tag{5.10}$$

(d) Filters

The filters can be modelled as a series combination of resistive, inductive and capacitive impedances. The voltage equations in matrix form can be expressed as:

$$V_{FLn} = L_{FLn}\left(p I_{FLn} + \frac{V_{Cn}}{L_{FLn}} + \frac{R_{FLn}}{L_{FLn}} I_{FLn} \right) \tag{5.11}$$

$$V_{Cn} = \frac{1}{C_{FLn}} I_{FLn} \tag{5.12}$$

(e) Static load

The static load can be modelled as a series combination of resistance and inductance. The voltage equation in matrix form can be expressed as:

$$V_{sl} = R_{sl} i_{sl} + L_{sl} p i_{sl} \tag{5.13}$$

In the previous equations the direction of the current flowing into each component, i.e flowing out of the connected node, is defined as positive.

5.3 Filter circuit configuration-design characteristics

The size of a filter is defined as the reactive power that the filter supplies at fundamental frequency. It is substantially equal to the fundamental reactive power supplied by the capacitors[7,8].

A single tuned filter is a series RLC circuit (as shown in figure 5.2) tuned to the frequency of one harmonic (generally a lower characteristic harmonic).

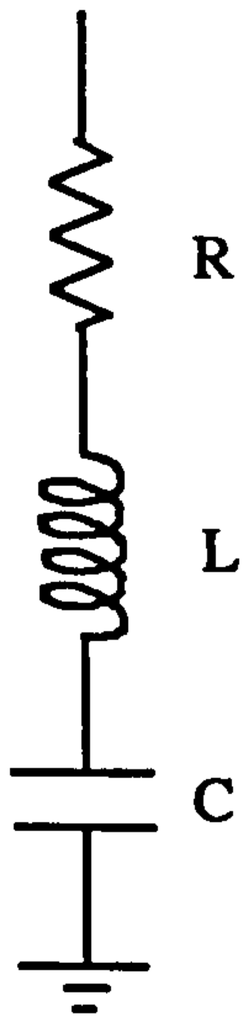

Figure 5.2 Series tuned RLC filter

Its impedance is given by

$$Z_1 = R + j(\omega L - \frac{1}{\omega C}) \tag{5.14}$$

which at the resonant frequency reduces to R. Two basic parameters for the selection of R,L or C are the quality factor and the tuned frequency. The quality factor Q is given by

$$Q = \frac{X_0}{R} \tag{5.15}$$

where

$$X_0 = \frac{1}{\omega_n C} = \omega_n L = \sqrt{\frac{L}{C}} \tag{5.16}$$

and

$$\omega_n = \frac{1}{\sqrt{LC}} \tag{5.17}$$

When choosing and dimensioning filter circuit equipment for a given project, the following points should as a rule be considered:

a) Supply system data (load, compensation devices) of the operator's power system
b) Tolerable harmonic voltages at the point of common coupling (PCC)
c) Total converter load to be connected
d) Possible limitations in terms of reactive power, considering the mode of operation of the drives
e) Economic considerations

5.4 Modelling of a simple AC/DC power system

To illustrate the method of interconnection, described in the previous section, the simple three-node power system shown in figure 5.3 in single line form is employed, comprising one generator, one AC/DC converter station, filters connected to the same busbar with the converter station, a transformer, two induction motors and static loads connected in each busbar. Following the procedure applied in the previous section, the nodes of the system are numbered as shown in figure 5.3. For

every node a pivotal element is selected, allowing the currents associated with it to be eliminated from the differential equations. For node 1 the generator three-phase currents are eliminated and for node 2 the transformer secondary winding three-phase currents are eliminated.

Thus Kirchhoff's current law for the two nodes yields:

$$\text{Node 1:} \qquad i_{sg1} = -i_{sl1} - i_{rec} - i_{fl} - i_{1T} \tag{5.18}$$

$$\text{Node 2:} \qquad i_{2T} = -i_{sm1} - i_{sm2} - i_{sl2} \tag{5.19}$$

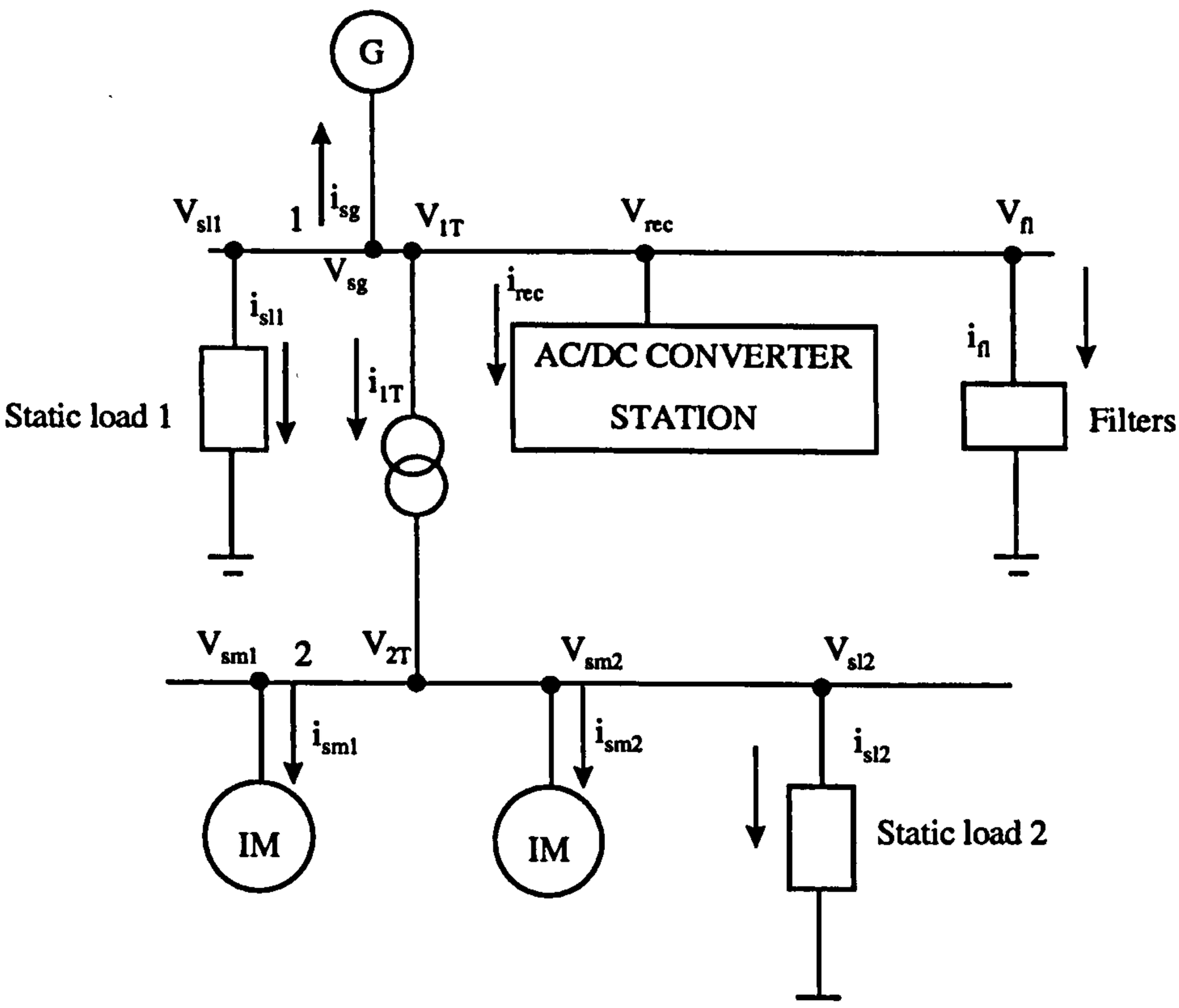

Figure 5.3 Representation of a simple AC/DC power system

For each node the terminal voltage of each component is equated with the terminal voltage of the selected pivotal component. Thus for the system shown in figure 5.3 the three-phase voltage equations for each node, according to Kirchhoff's law, can be expressed as:

Node 1: $$V_{sg1} = V_{sl1} = V_{rec} = V_{fl} = V_{1T} \tag{5.20}$$

Node 2: $$V_{2T} = V_{sm1} = V_{sm2} = V_{sl2} \tag{5.21}$$

Substituting the terminal voltage equations from the previous section in the equations 5.20-5.21 and using the equations 5.18-5.19 to eliminate the selected pivotal components' three-phase currents, the voltage equations, appropriate for solution can be obtained. Rearranging and adding the rotor voltage equations for the generator, the voltage equations for the system in analytical form, can be obtained as follows.

Generator - rotor voltage equation :

$$V_{rg} = R_{rg}i_{rg} + L_{rrg}pi_{rg} - L_{rsg}pi_{sl1} - L_{rsg}pi_{rec} - L_{rsg}pi_{fl} - L_{rsg}pi_{1T} - \omega_{rg}G_{rsg}i_{sl1} - \omega_{rg}G_{rsg}i_{rec} - \omega_{rg}G_{rsg}i_{fl} - \omega_{rg}G_{rsg}i_{1T} \tag{5.22}$$

From equation (5.20) for node 1 we have the following set of equations:

$$0 = (-R_{sg} - R_{sl1})i_{sl1} - R_{sg}i_{rec} - R_{sg}i_{fl} - R_{sg}i_{1T} + L_{srg}pi_{rg} + (-L_{ssg} - L_{sl1})pi_{sl1} - L_{ssg}pi_{rec} - L_{ssg}pi_{fl} - L_{ssg}pi_{1T} + \omega_{rg}G_{srg}i_{rg} - \omega_{rg}G_{ssg}i_{sl1} - \omega_{rg}G_{ssg}i_{rec} - \omega_{rg}G_{ssg}i_{fl} - \omega_{rg}G_{ssg}i_{1T} \tag{5.23}$$

$$0 = -R_{sg}i_{sl1} + (-R_{sg} - R_{rec})i_{rec} - R_{sg}i_{fl} - R_{sg}i_{1T} + L_{srg}pi_{rg} + (-L_{ssg} - L_{rec})pi_{rec} - L_{ssg}pi_{sl1} - L_{ssg}pi_{fl} - L_{ssg}pi_{1T} + \omega_{rg}G_{srg}i_{rg} - \omega_{rg}G_{ssg}i_{sl1} - \omega_{rg}G_{ssg}i_{rec} - \omega_{rg}G_{ssg}i_{fl} - \omega_{rg}G_{ssg}i_{1T} \tag{5.24}$$

$$0 = -R_{sg}i_{sl1} - R_{sg}i_{rec} + (-R_{sg} - R_{fl})i_{fl} - R_{sg}i_{1T} + L_{srg}pi_{rg} - L_{ssg}pi_{rec} - L_{ssg}pi_{sl1}$$
$$+ (-L_{ssg} - L_{fl})pi_{fl} - L_{ssg}pi_{1T} + \omega_{rg}G_{srg}i_{rg} - \omega_{rg}G_{ssg}i_{sl1} - \omega_{rg}G_{ssg}i_{rec} - \omega_{rg}G_{ssg}i_{fl} - \omega_{rg}G_{ssg}i_{1T}$$

(5.25)

$$0 = -R_{sg}i_{sl1} - R_{sg}i_{rec} - R_{sg}i_{fl} + (-R_{sg} - R_{1T})i_{1T} + L_{srg}pi_{rg} - L_{ssg}pi_{rec} - L_{ssg}pi_{sl1}$$
$$- L_{ssg}pi_{fl} + (-L_{ssg} - L_{1T})pi_{1T} + L_{12T}pi_{sm1} + L_{12T}pi_{sm2} + L_{12T}pi_{sl2} + \omega_{rg}G_{srg}i_{rg}$$
$$- \omega_{rg}G_{ssg}i_{sl1} - \omega_{rg}G_{ssg}i_{rec} - \omega_{rg}G_{ssg}i_{fl} - \omega_{rg}G_{ssg}i_{1T}$$

(5.26)

From equation (5.21) for node 2 we have the following set of equations:

$$0 = (-R_{2T} - R_{sm1})i_{sm1} - R_{2T}i_{sm2} - R_{2T}i_{sl2} + L_{21T}pi_{1T} + (-L_{22T} - L_{ssm1})pi_{sm1} - L_{22T}pi_{sm2}$$
$$- L_{22T}pi_{sl2} - L_{srm1}pi_{sm1} - \omega_{rm1}G_{srm1}i_{rm1}$$

(5.27)

$$0 = R_{rm1}i_{rm1} + L_{rsm1}pi_{sm1} + L_{rrm1}pi_{rm1} + \omega_{rm1}G_{rsm1}i_{sm1}$$

(5.28)

$$0 = -R_{2T}i_{sm1} + (-R_{2T} - R_{sm2})i_{sm2} - R_{2T}i_{sl2} + L_{21T}pi_{1T} - L_{22T}pi_{sm1} +$$
$$(-L_{22T} - L_{ssm2})pi_{sm2} - L_{22T}pi_{sl2} - L_{srm2}pi_{sm2} - \omega_{rm2}G_{srm2}i_{rm2}$$

(5.29)

$$0 = R_{rm2}i_{rm2} + L_{rsm2}pi_{sm2} + L_{rrm2}pi_{rm2} + \omega_{rm2}G_{rsm2}i_{sm2}$$

(5.30)

$$0 = -R_{2T}i_{sm1} - R_{2T}i_{sm2} + (-R_{2T} - R_{sl2})i_{sl2} + L_{21T}pi_{1T} - L_{22T}pi_{sm1} - L_{22T}pi_{sm2}$$
$$+ (-L_{22T} - L_{sl2})pi_{sl2}$$

(5.31)

The equations 5.22-5.31 form the complete set of differential equations necessary to solve the system. The preceding equations can be collected together in matrix form according to the following equation:

$$[V] = [R][i] + [L]p[i] + [G][i] \tag{5.32}$$

where the matrices [V],[R],[i],[L] and [G] can be formed as follows:

$$[V] = [V_{rg}\ 0\ 0\ 0\ 0\ 0\ V_{rm1}\ 0\ V_{rm2}\ 0]^T \tag{5.33}$$

$$[R] = \begin{bmatrix}
R_{rg} & 0 & 0 & 0 & 0 & 0 & 0 & 0 & 0 & 0 \\
0 & -R_{sg}-R_{sl1} & -R_{sg} & -R_{sg} & -R_{sg} & 0 & 0 & 0 & 0 & 0 \\
0 & -R_{sg} & -R_{sg}-R_{rec} & -R_{sg} & -R_{sg} & 0 & 0 & 0 & 0 & 0 \\
0 & -R_{sg} & -R_{sg} & -R_{sg}-R_{fl} & -R_{sg} & 0 & 0 & 0 & 0 & 0 \\
0 & -R_{sg} & -R_{sg} & -R_{sg} & -R_{sg}-R_{1T} & 0 & 0 & 0 & 0 & 0 \\
0 & 0 & 0 & 0 & 0 & -R_{2T}-R_{sm1} & 0 & -R_{2T} & 0 & -R_{2T} \\
0 & 0 & 0 & 0 & 0 & 0 & R_{rm1} & 0 & 0 & 0 \\
0 & 0 & 0 & 0 & 0 & -R_{2T} & 0 & -R_{2T}-R_{sm2} & 0 & -R_{2T} \\
0 & 0 & 0 & 0 & 0 & 0 & 0 & 0 & R_{rm2} & 0 \\
0 & 0 & 0 & 0 & 0 & -R_{2T} & 0 & -R_{2T} & 0 & -R_{2T}-R_{sl2}
\end{bmatrix} \tag{5.34}$$

$$[i] = [i_{rg}\ i_{sl1}\ i_{rec}\ i_{fl}\ i_{1T}\ i_{sm1}\ i_{rm1}\ i_{sm2}\ i_{rm2}\ i_{sl2}]^T \tag{5.35}$$

$$[L]=\begin{bmatrix}
L_{rrg} & -L_{rsg} & -L_{rsg} & -L_{rsg} & -L_{rsg} & 0 & 0 & 0 & 0 & 0 \\
L_{srg} & -L_{ssg} & -L_{sll} & -L_{ssg} & -L_{ssg} & 0 & 0 & 0 & 0 & 0 \\
L_{srg} & -L_{ssg} & -L_{ssg} & -L_{rec} & -L_{ssg} & 0 & 0 & 0 & 0 & 0 \\
L_{srg} & -L_{ssg} & -L_{ssg} & -L_{ssg} & -L_{fl} & 0 & 0 & 0 & 0 & 0 \\
L_{srg} & -L_{ssg} & -L_{ssg} & -L_{ssg} & -L_{ssg} & -L_{1T} & L_{12T} & 0 & L_{12T} & 0 & L_{12T} \\
0 & 0 & 0 & 0 & L_{12T} & -L_{22T} & -L_{ssm1} & 0 & -L_{22T} & 0 & -L_{22T} \\
 & & & & & & -L_{srm1} & & & & \\
0 & 0 & 0 & 0 & 0 & L_{rsm1} & L_{rrm1} & 0 & 0 & 0 \\
0 & 0 & 0 & 0 & L_{12T} & -L_{22T} & 0 & -L_{22T} & -L_{ssm2} & 0 & -L_{22T} \\
 & & & & & & & -L_{srm2} & & & \\
0 & 0 & 0 & 0 & 0 & 0 & 0 & L_{rsm2} & L_{rrm2} & 0 \\
0 & 0 & 0 & 0 & L_{12T} & -L_{22T} & 0 & -L_{22T} & 0 & -L_{22T} & -L_{sl2}
\end{bmatrix}$$

(5.36)

$$[G]=\begin{bmatrix}
0 & -\omega_{rg}G_{rsg} & -\omega_{rg}G_{rsg} & -\omega_{rg}G_{rsg} & -\omega_{rg}G_{rsg} & 0 & 0 & 0 & 0 & 0 \\
\omega_{rg}G_{srg} & -\omega_{rg}G_{ssg} & -\omega_{rg}G_{ssg} & -\omega_{rg}G_{ssg} & -\omega_{rg}G_{ssg} & 0 & 0 & 0 & 0 & 0 \\
\omega_{rg}G_{srg} & -\omega_{rg}G_{ssg} & -\omega_{rg}G_{ssg} & -\omega_{rg}G_{ssg} & -\omega_{rg}G_{ssg} & 0 & 0 & 0 & 0 & 0 \\
\omega_{rg}G_{srg} & -\omega_{rg}G_{ssg} & -\omega_{rg}G_{ssg} & -\omega_{rg}G_{ssg} & -\omega_{rg}G_{ssg} & 0 & 0 & 0 & 0 & 0 \\
\omega_{rg}G_{srg} & -\omega_{rg}G_{ssg} & -\omega_{rg}G_{ssg} & -\omega_{rg}G_{ssg} & -\omega_{rg}G_{ssg} & 0 & 0 & 0 & 0 & 0 \\
0 & 0 & 0 & 0 & 0 & 0 & -\omega_{rm1}G_{srm1} & 0 & 0 & 0 \\
0 & 0 & 0 & 0 & 0 & \omega_{rm1}G_{rsm1} & 0 & 0 & 0 & 0 \\
0 & 0 & 0 & 0 & 0 & 0 & 0 & 0 & -\omega_{rm2}G_{srm2} & 0 \\
0 & 0 & 0 & 0 & 0 & 0 & 0 & \omega_{rm2}G_{srm2} & 0 & 0 \\
0 & 0 & 0 & 0 & 0 & 0 & 0 & 0 & 0 & 0
\end{bmatrix}$$

(5.37)

Summary of method

The numerical solution sequence for any system configuration can be summarised in the following steps:

1) The nodes of the system are numbered starting from the generator ones and a pivotal component is selected for each node. Then the matrices [R], [L] and [G]

of the equation 5.32 are constructed using the equations for each component described in the preceding sections.

2) The initial state variables are derived from specified operational conditions at t=0 and the system equation acquires the matrix form of equation 5.1 . The 'Gaussian elimination' method is employed to put the equation 5.1 into the form of equation 5.2.
3) Using the 4^{th} order Runge-Kutta numerical integration method, the new values of state variables, i.e the three-phase currents, are obtained at t=0+h, where h is the integration step-length, solving the set of first-order differential equations of equation 5.2
4) New values of excitation, prime mover input power and variables associated with the DC converter station (such as node voltages) can be obtained by solving the differential equations of the excitation controller, prime mover and the DC converter station, respectively.
5) The simulation time is increased by a step-length and the steps (2) to (4) are repeated, until the total simulation time is reached.

5.5 Simulation results of a simple AC/DC power system

For the purpose of illustrating the previous simplified AC/DC power system, simulations were conducted in order to study the dynamic performance of that system.

One of the most interesting challenges that power planners have to face in power systems is the interaction between the AC and the DC systems [2-22]. The rectifier current in such an AC/DC system contains fundamental current and harmonic frequency components of the order $6k \pm 1$, where k is an integer [12]. For the system in figure 5.3 because of these rectifier currents, the three-phase armature currents of the synchronous machine are not sinusoidal. They contain harmonic current components, the most prominent of which are of the order $6k \pm 1$ (k is an integer). These harmonic currents are flowing from the rectifier to the machine. The rotor currents have a harmonic component as well. The existence of the harmonic currents

of the order 6k in the rotor windings is due to the presence of the harmonic current components of the order $6k \pm 1$ in the stator winding [23]. The stator harmonics of the order 6k+1 create an MMf with the same sense of rotation as that of the rotor, figure 5.4.a. Therefore the relative velocity of such an MMf with respect to the rotor is 6k times that of the rotor. On the other hand, the harmonic components of the stator phase currents of the order 6k-1 create an MMf which has also a relatively velocity with respect to the rotor of the same value as those of the 6k+1 harmonics but of opposite direction as shown in figure 5.4.b. These two MMfs rotating in opposite directions result in an elliptical field, as shown in figure 5.4.c, and they induce harmonic currents of the order 6k in the rotor circuits.

Moreover the existence of harmonic currents flowing in the stator and rotor windings of a synchronous machine gives rise to pulsating torque and thus to vibration [23].

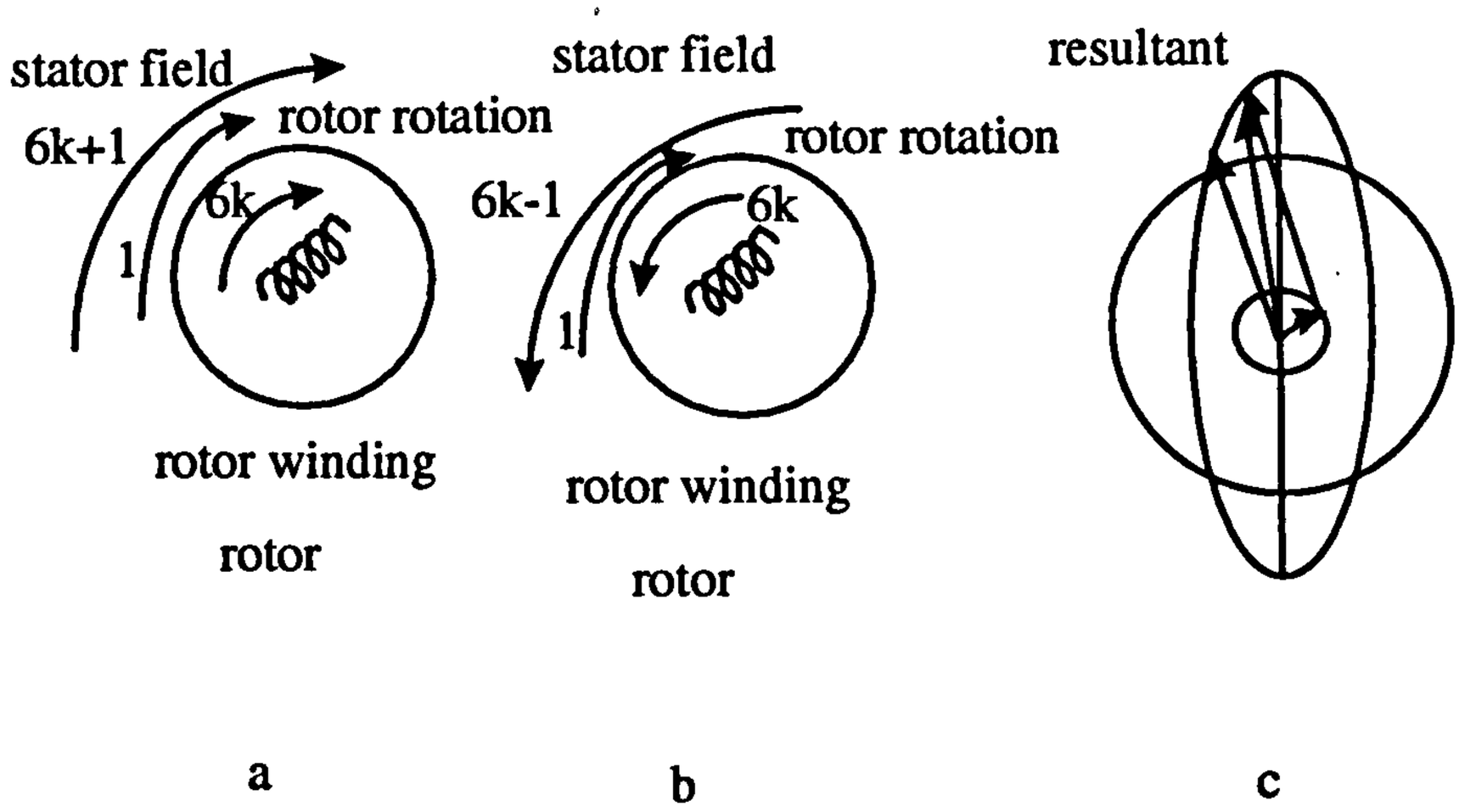

Figure 5.4

The use of harmonic filters solves many of the problems addressed before. These filters absorb most of the harmonic components of the 5^{th} ,7^{th} 11^{th} and 13^{th} order of the rectifier currents [7,8]. This is because the filters in the system offer a low impedance path to the harmonic currents of the rectifier. Therefore the harmonics in

the stator windings and as a consequence those induced in the rotor windings are less than in the case of a system without filters.

Despite the presence of the filters in the present case the current and voltage waveforms will not be perfectly sinusoidal. This is because these filters are of the 5^{th}, 7^{th}, 11^{th} and 13^{th} order only and their impedances still have definite values at their resonant frequencies. Thus the corresponding harmonic current will not be completely short-circuited by these filters.

Also it should be pointed out that careful consideration should be taken in the design of synchronous machines operating near AC/DC converter stations so that can withstand the extra heating due to the flow of the harmonics in their windings. This is true even if filters are installed in the station [7].

Simulations carried out later in this chapter show the effect of using filters on the voltage and current waveforms throughout the power system network.

For the system in figure 5.3 the generator is rated at 10 MVA and uses a single gas turbine and governing system illustrated in figure 4.7. The generator is also equipped with the IEEE 'Type 2' model as described in chapter 3 and shown in figure 4.6. The transformer associated with the generator is a delta-star and the induction motors are switched on to the supply in sequence. Instead of a DC converter station, a variable speed drive was used. The variable speed drive consists of a AC/DC converter station connected to an induction motor as was described in previous chapters. Parameters for the variable speed drive, the filters associated with it, as well as all the previous power system components are given in the appendix 3.

The system is expressed by a set of first-order differential equations, using the methodology described in the previous section.

The total simulation time was 20 seconds. The sequence of events is given below.

1) At 0.1 seconds the static load and the filters (when there are included in the analysis) are connected to the generating system.
2) At 0.1 seconds the motor that is not connected near to the static load (1) is connected as well.

3) At 5.1 seconds the second motor (the motor located near to the load (2)) is connected to bus 2.
4) At 11.1 seconds the variable speed drive is connected to bus 1.
5) At 20.0 seconds is the end of the simulation.

For the variable speed drive the natural sampling PWM method was used as was discussed in previous chapter.

Selected results of the simulation, showing the generator response, the induction motor responses and the bus-bars terminal voltages, along with the primary current of the transformer and also variables that illustrate the variable speed drive response are given in figures 5.5-5.10. As can be seen from the graphs, the switching of the motors to the supply caused voltage dips at the generator bus and generator speed drops. After a short delay the voltage began to recover due to the action of the excitation systems and speed governors. Every time an induction motor is switched on, a fluctuation of bus voltage and frequency was imposed on the system. The same thing applies when the variable speed drive is connected, however the drops are lower due to the fact that the voltage across the drive stator terminals is only proportional to the voltage at rated speed. However the use of the variable speed drive causes harmonics at the generator currents, torque and field voltage and current.

One important issue in power system analysis is system stability. The stability of a system of interconnected dynamic components depends on its ability to return to normal or stable operation after having been subjected to some form of disturbance. The study of stability is one of the main concerns of the control engineer whose methods are applied to electric power systems. The main form of instability in power systems is the loss of synchronism in synchronous machines. The angle δ (rotor angle) gives an estimation of the stability of a power system [24,25] and is used for steady state and transient stability. With an isolated machine supplying its own load and when the voltages at the machine and load terminals are known the angle δ between the voltage phasors is the load angle and is dependent on the power input

from the turbine shaft. In this case the power required can be dictated and hence the load angle is known; when connected to an infinite-busbar system, however, the power delivered by the machine is no longer directly dependent on the connected load. By changing the turbine output, and hence δ, the generator can be made to take on any load that the operator desires subject to economic and technical limits. The power systems analysed in this chapter are assumed to be stable with the generators feeding various load components and with no major system disturbances. For this reason the issue of power system stability will not be investigated and the angle δ will not be analysed in detail.

As it was addressed before, the filters absorb most of the harmonics generated by the AC/DC power system. The impact of the harmonic filters on the performance of the AC/DC power system can be investigated by using comparative simulation results and by performing harmonic analysis at steady state conditions with and without filters for the system described above.

For this reason simulations and harmonic analysis were carried out using the system in figure 5.3 with and without harmonic filters. Figure 5.11 shows simulations of the voltage waveform of phase A where the drive is connected (bus 1) with and without filters at steady state conditions (at 18.00secs). Similar waveforms can be obtained for the remaining phases B and C. These results show sudden jumps in the voltage waveform in figure 5.11 (a) which are due to the sudden changes in the rectifier current at the end of the commutation periods. From the graph of figure 5.11 (b) is obvious that the waveform with filters is much less distorted than the one without and it approaches the sinusoidal. The harmonic analyses in tables 5.1 and 5.2 shows that the filters absorb most of the unwanted harmonics and the total harmonic distortion (THD) is reduced significantly. It should be mentioned that the level of acceptable THD for the harmonic voltages and currents is 5% [23,27]. The use of filters brings the voltages and the currents through the network well below this limit giving an acceptable system response.

ORDER OF HARMONICS	CONTENT %
1	100% of fundamental
5	4.00% of fundamental
7	2.77% of fundamental
11	1.21% of fundamental
13	1.08% of fundamental
THD %	5.62 %

Table 5.1 Harmonic analysis for the voltage at bus 1 (phase A) without filters

ORDER OF HARMONICS	CONTENT %
1	100% of fundamental
5	0.90% of fundamental
7	0.70% of fundamental
11	0.06% of fundamental
13	0.08% of fundamental
THD %	1.36 %

Table 5.2 Harmonic analysis for the voltage at bus 1 (phase A) with filters

The effect of filtering can also be demonstrated by using other simulation results such as the generator stator currents in figure 5.12. The 3-phase currents are approaching the sinusoidal shape in comparison with those without the filters connected. The three phase stator currents of the synchronous machine are not sinusoidal. They contain harmonic current components, the most prominent of which are of the order $6k \pm 1$. These harmonic currents are flowing from the rectifier to the

machine (figure 5.12 (a)). The use of filters absorbs most of the harmonics, however there is still an amount of harmonics for reasons that have been discussed before. The harmonic analysis in tables 5.3 and 5.4 shows a significant reduction in the harmonic currents and an improvement in the total harmonic distortion.

ORDER OF HARMONICS	CONTENT %
1	100% of fundamental
5	8.06% of fundamental
7	3.92% of fundamental
11	1.14% of fundamental
13	0.81% of fundamental
THD %	9.12 %

Table 5.3 Harmonic analysis for the stator current (phase A) without filters

ORDER OF HARMONICS	CONTENT %
1	100% of fundamental
5	2.99% of fundamental
7	1.64% of fundamental
11	0.22% of fundamental
13	0.20% of fundamental
THD %	3.77 %

Table 5.4 Harmonic analysis for the stator current (phase A) with filters

The effect of filtering can also be demonstrated by using other simulation results such as the transformer currents (phase A) in figure 5.13 and the motor currents (phase A)in figure 5.14. Harmonic analysis for this waveforms are presented in tables 5.5, 5.6, 5.7 and 5.8.

ORDER OF HARMONICS	CONTENT %
1	100% of fundamental
5	4.41% of fundamental
7	2.21% of fundamental
11	0.52% of fundamental
13	0.38% of fundamental
THD %	5.04 %

Table 5.5 Harmonic analysis for the transformer current (phase A) without filters

ORDER OF HARMONICS	CONTENT %
1	100% of fundamental
5	1.24% of fundamental
7	0.69% of fundamental
11	0.07% of fundamental
13	0.04% of fundamental
THD %	1.52 %

Table 5.6 Harmonic analysis for the transformer current (phase A) with filters

ORDER OF HARMONICS	CONTENT %
1	100% of fundamental
5	3.97% of fundamental
7	2.01% of fundamental
11	0.52% of fundamental
13	0.40% of fundamental
THD %	4.74 %

Table 5.7 Harmonic analysis for the motor current (phase A) without filters

ORDER OF HARMONICS	CONTENT %
1	100% of fundamental
5	1.56% of fundamental
7	0.84% of fundamental
11	0.19% of fundamental
13	0.16% of fundamental
THD %	2.27 %

Table 5.8 Harmonic analysis for the motor current (phase A) with filters

The simulation results and the harmonic analysis presented before demonstrate the claims that were addressed in this chapter for the less distorted voltage and current waveforms through the power system network due to filtering.

Waveforms that illustrate the variable speed drive operation are presented in figure 5.10(a)-(i). Figures 5.10 (g)-(i) show the phase voltages at the node where the variable speed drive is connected at steady state conditions. The drive will reach steady state conditions after approximately 3.5 seconds after the start up.

For validation purposes results from the dynamic simulations based on the modelling technique presented in this chapter were compared with results from the reference [26]. In this reference an AC power system is connected to a AC/DC converter station and a number of simulation results were illustrated. For the same operating conditions in both studies the comparison shown that there was a very good similarity (in the voltage and current waveforms for the generators, motors, AC/DC converter station) and the same conclusions for the response of the integrated AC/DC power system were drawn. The complete system analysed in this section is of course more complicated and it contains a variable speed drive instead of an AC/DC converter station. The dynamic response of a PWM variable speed drive was analytically investigated in chapter 2.

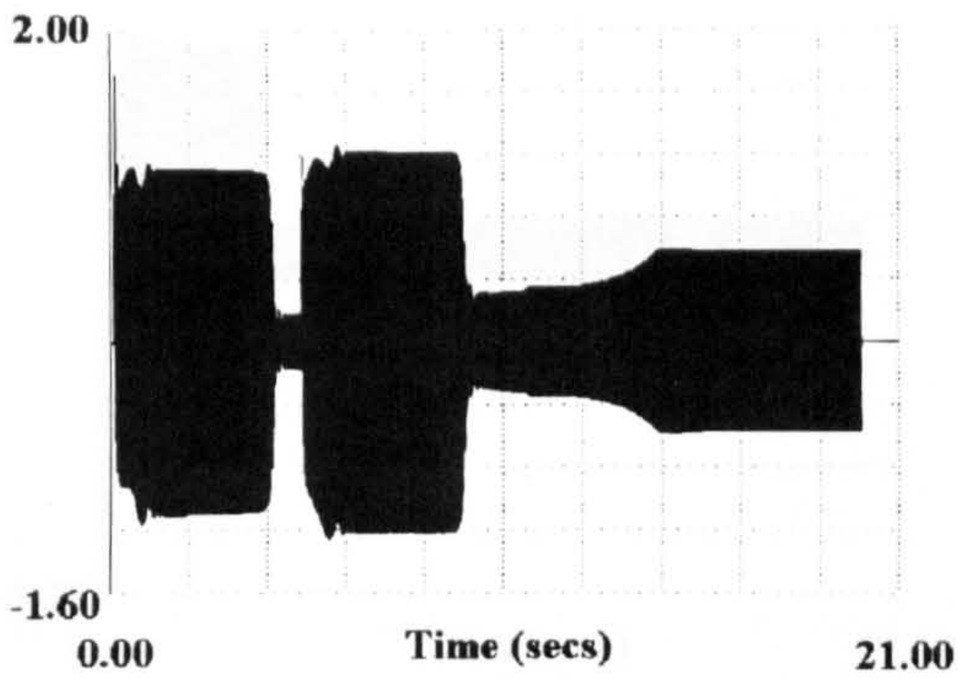

(a) Stator current phase-a (pu)

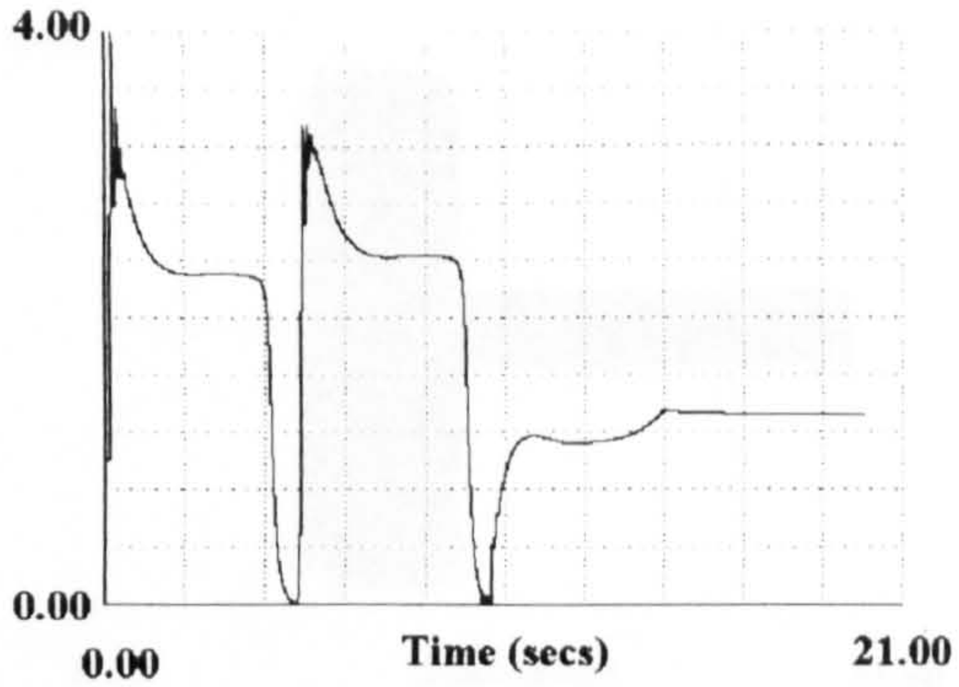

(b) Field voltage (pu)

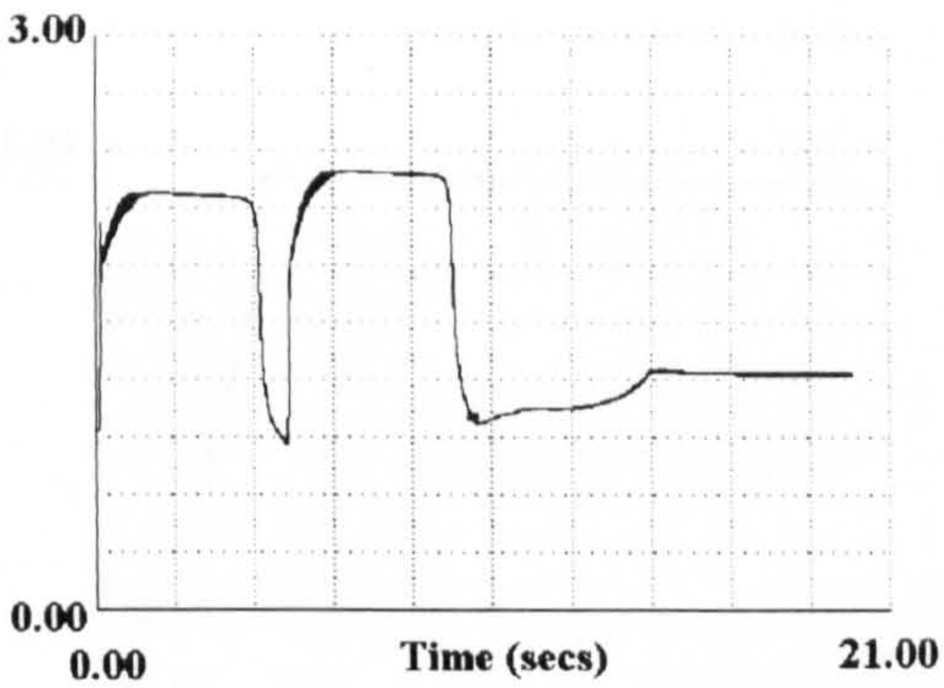

(c) Field current (pu)

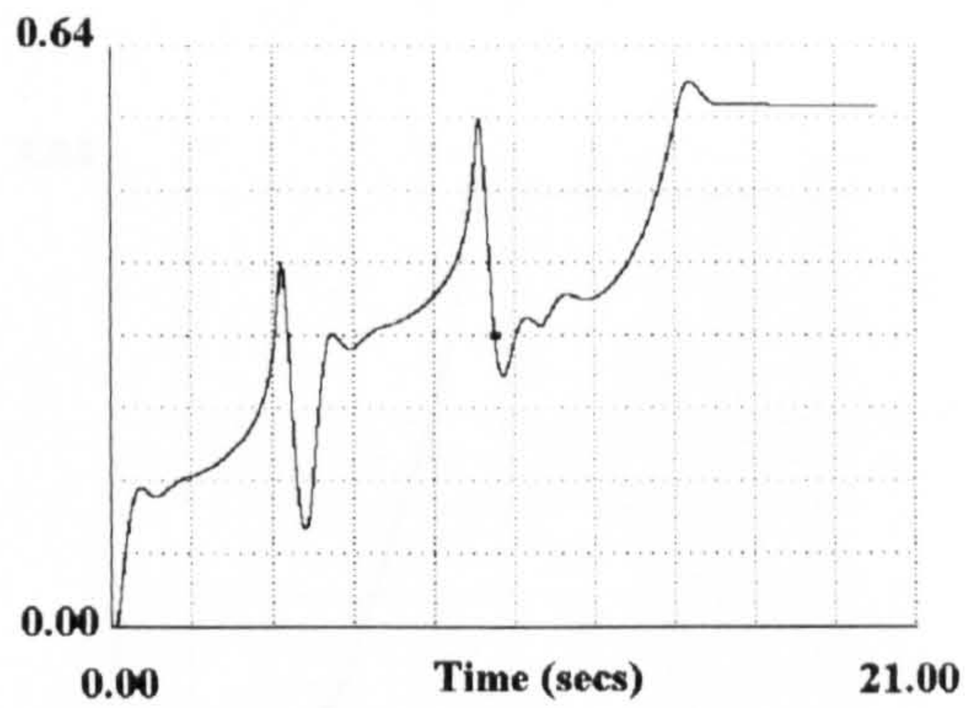

(d) Input power from prime mover(pu)

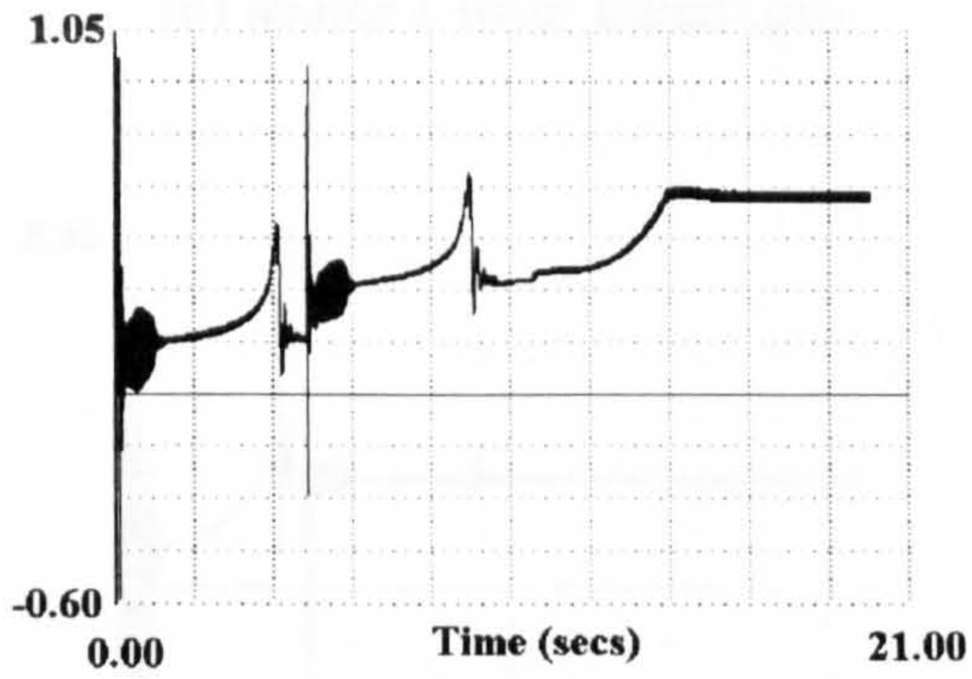

(e) Electromagnetic torque (pu)

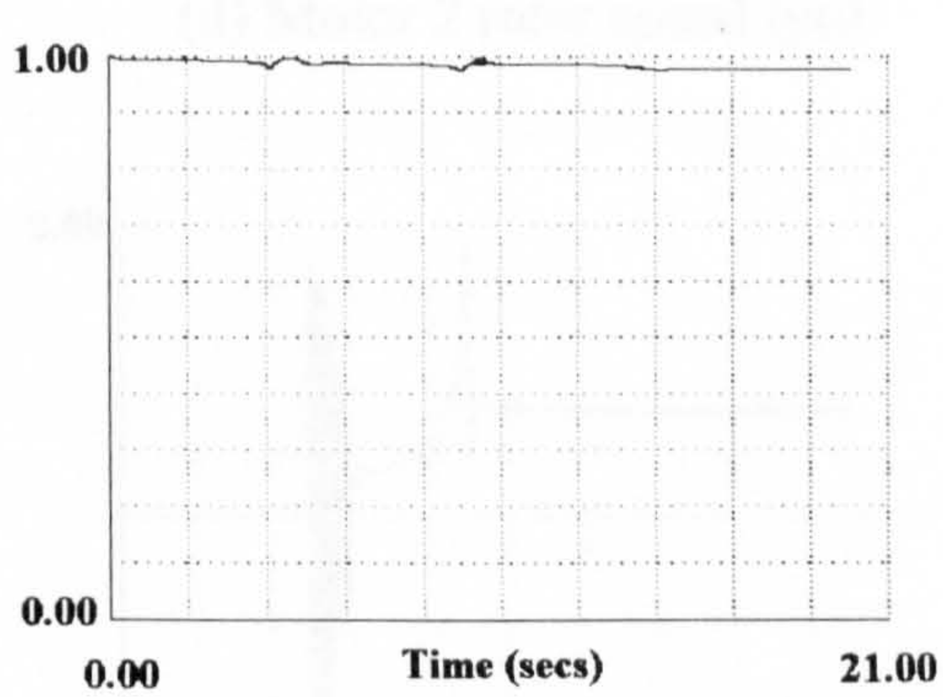

(f) Rotor speed (pu)

Figure 5.5 Generator response

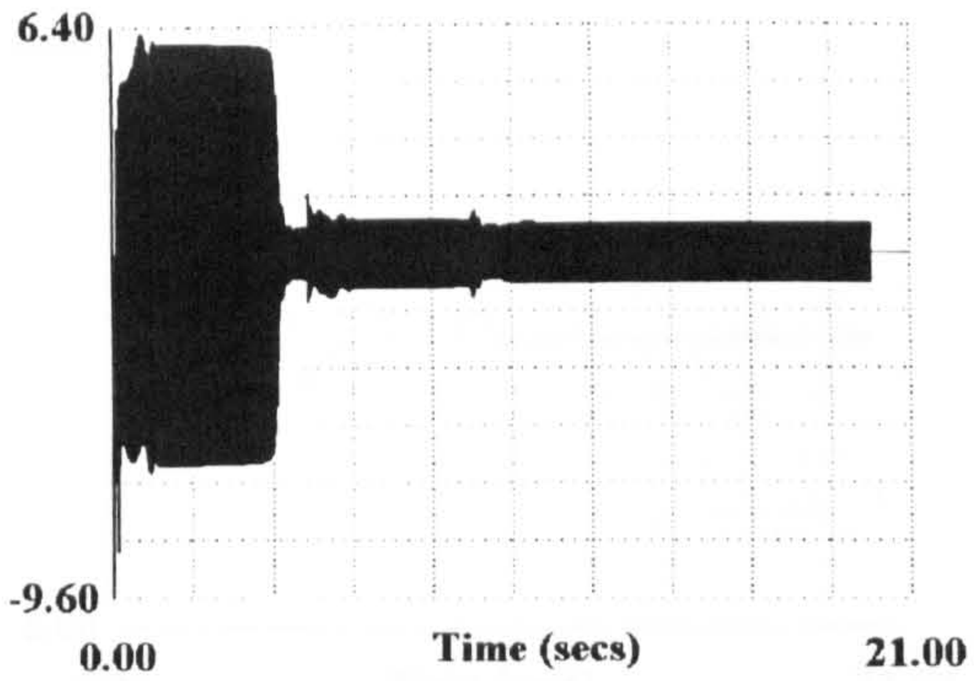

(a) Motor 1 stator current (pu)

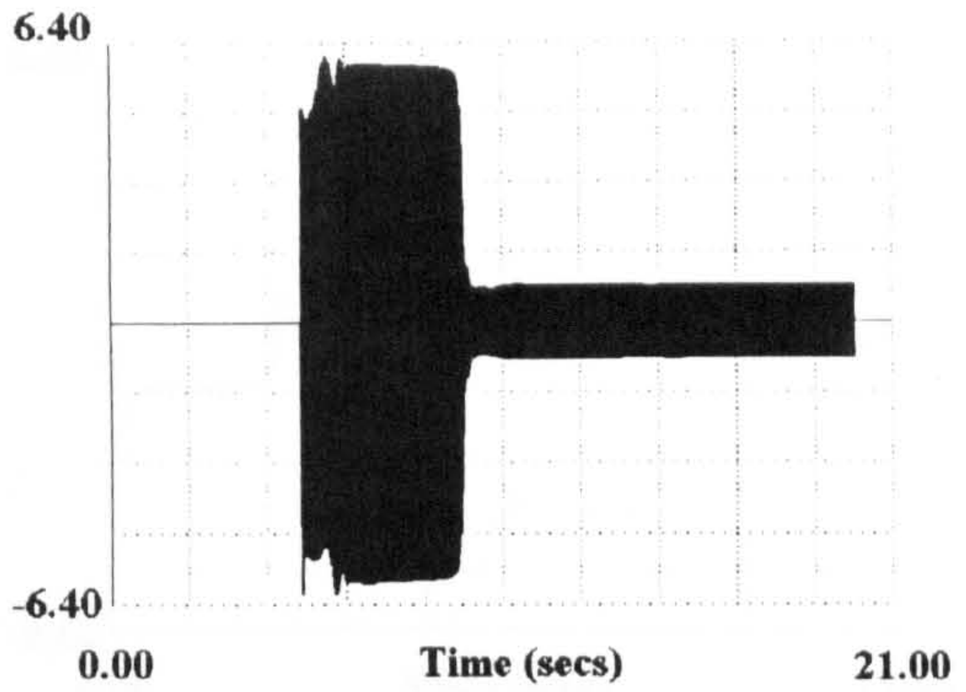

(b) Motor 2 stator current (pu)

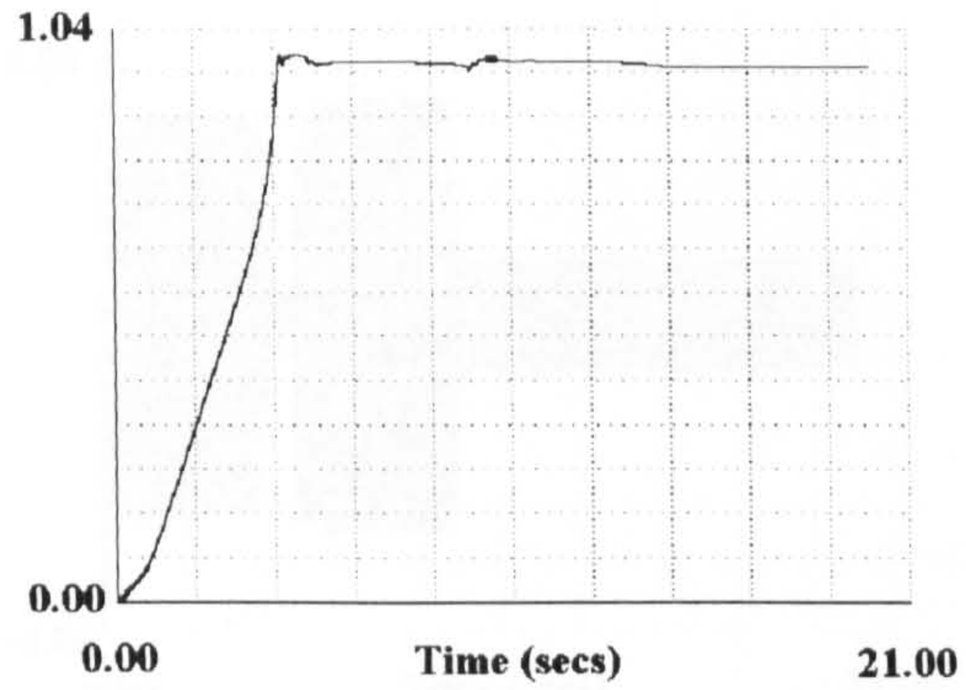

(c) Motor 1 rotor speed (pu)

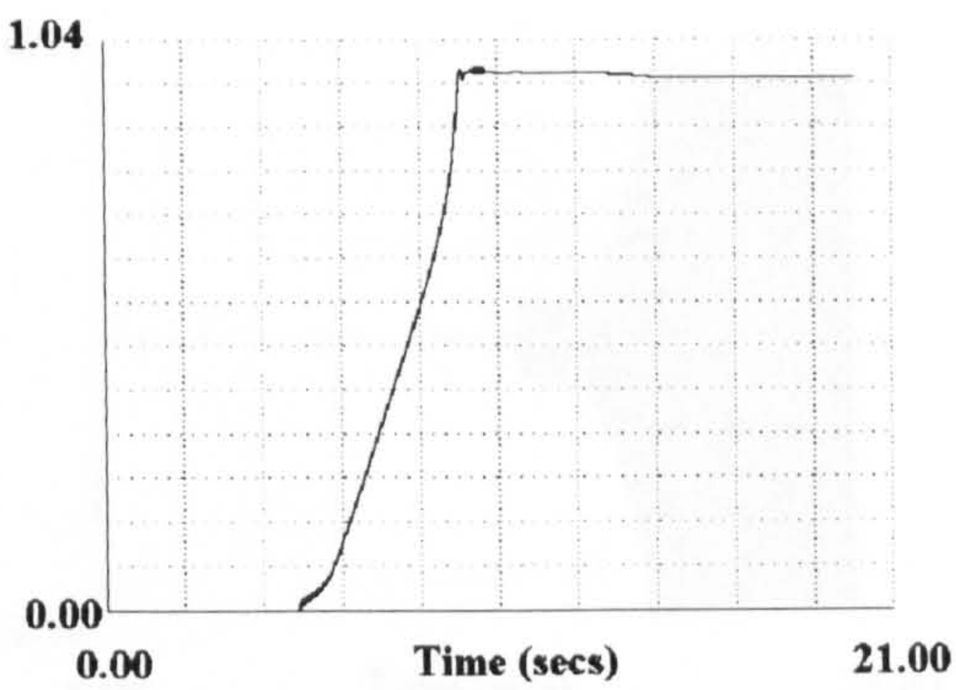

(d) Motor 2 rotor speed (pu)

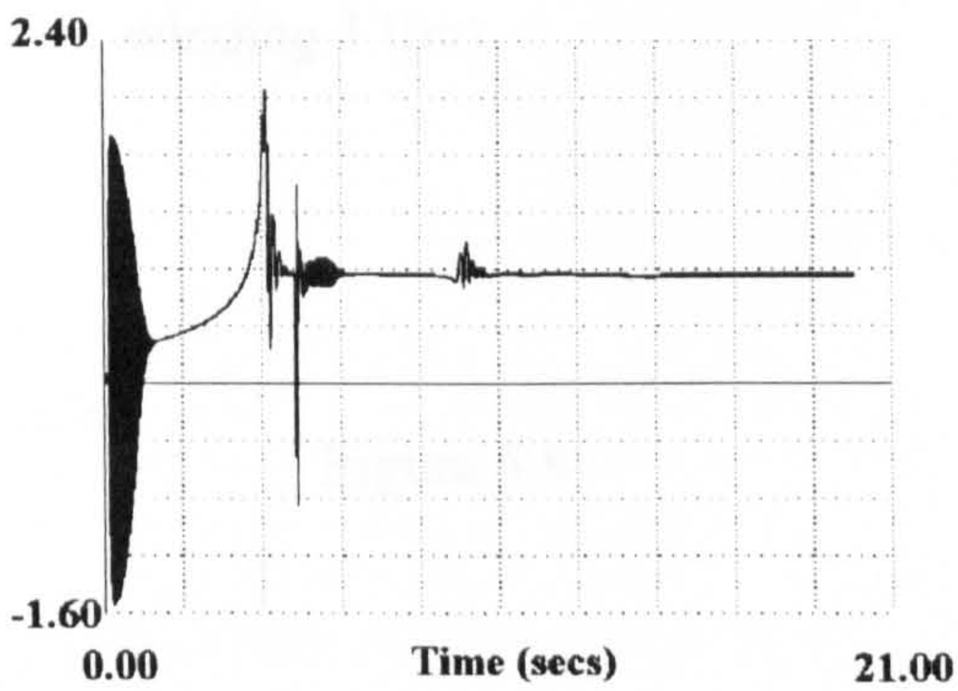

(e) Motor 1 speed torque (pu)

Figure 5.6 Motor 1 response

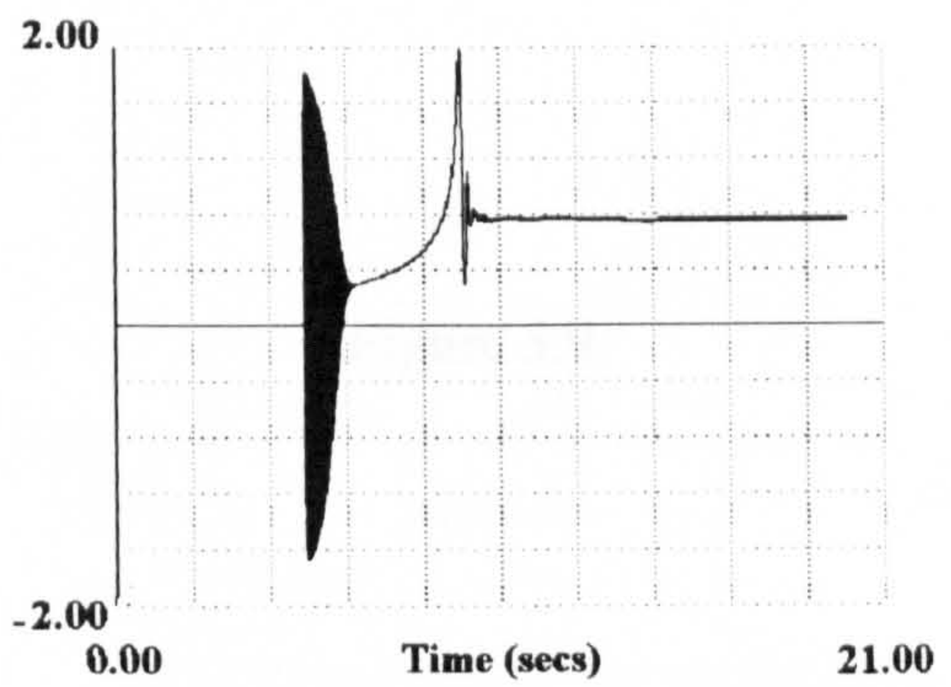

(f) Motor 2 speed torque (pu)

Figure 5.7 Motor 2 response

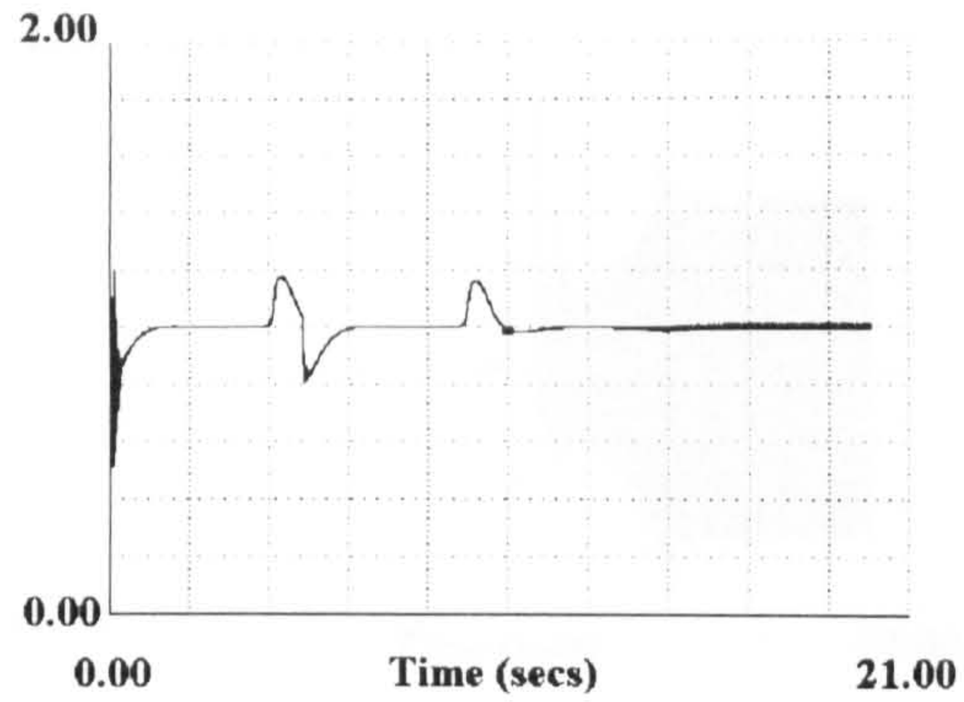

(a) Voltage at bus 1 (pu)

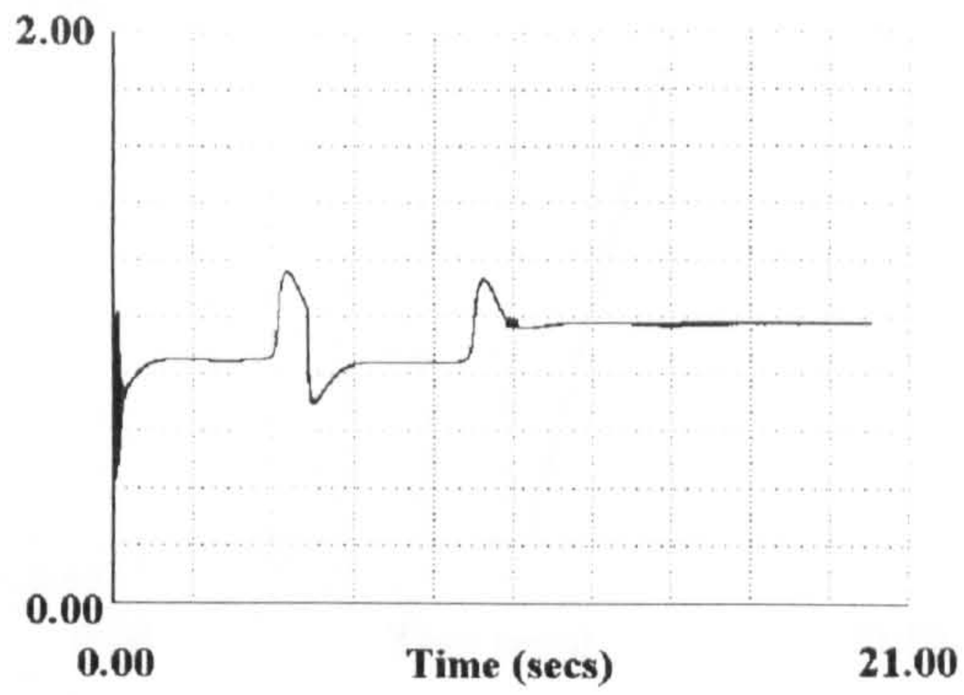

(b) Voltage at bus 2 (pu)

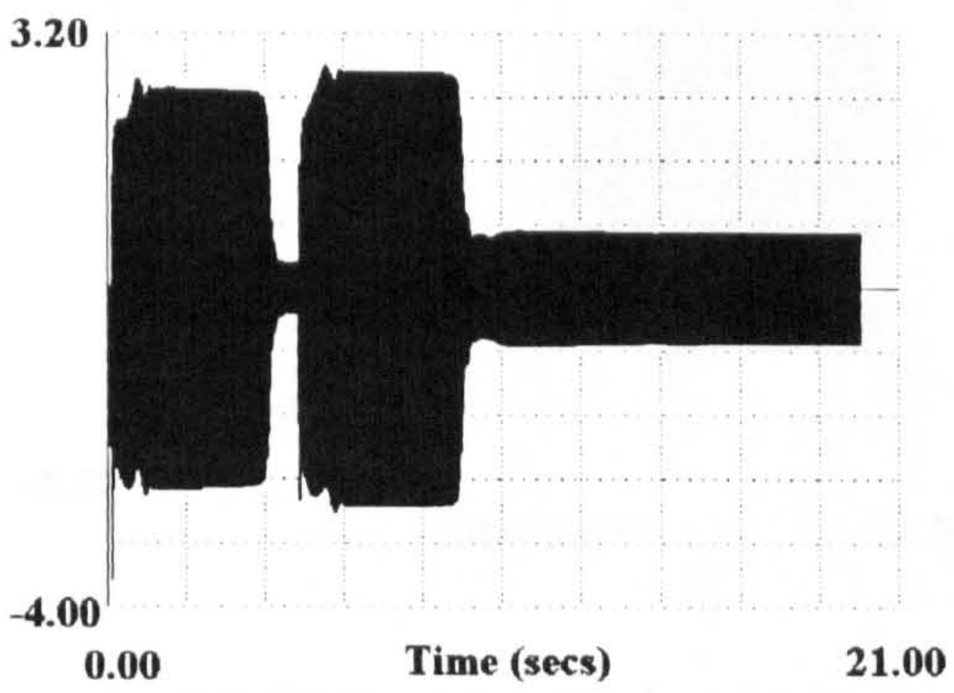

(c) Transformer current on winding 1 (pu)

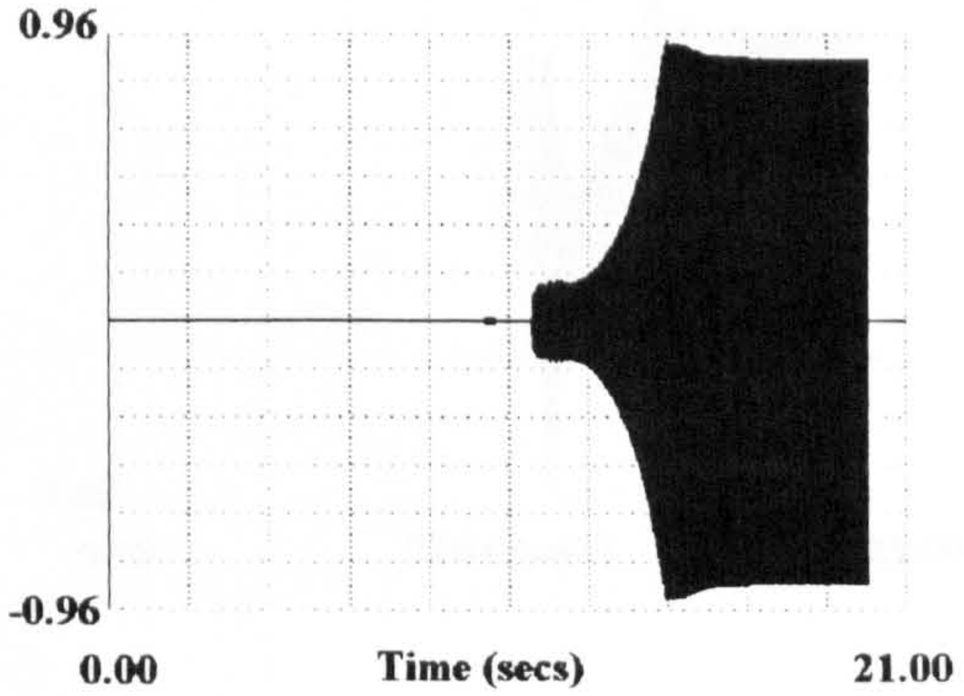

(d) Rectifier current (pu)

Figure 5.8

Figure 5.9

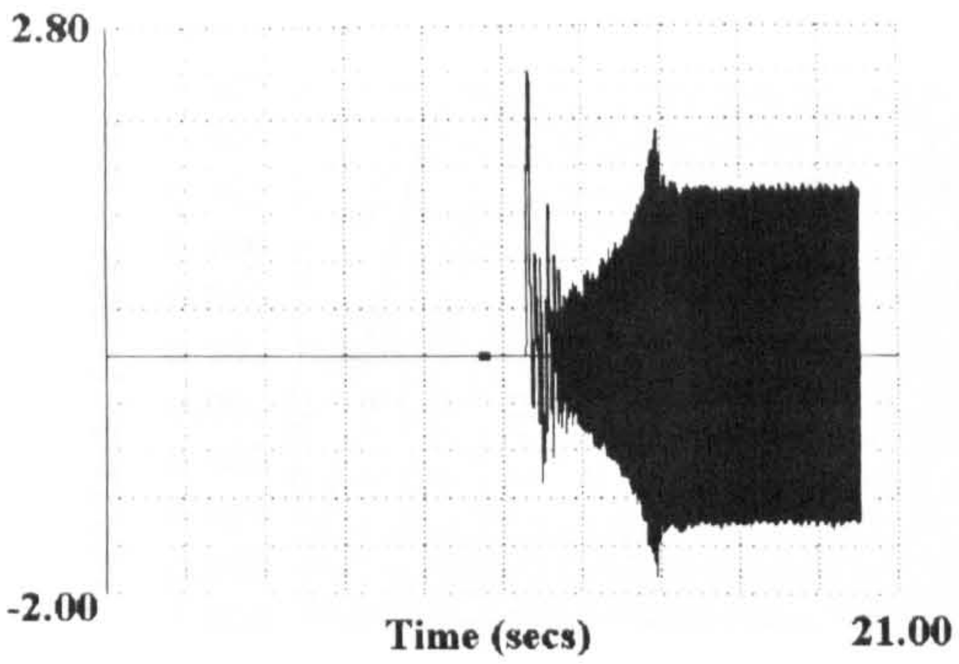

(a) Stator current phase-a (pu)

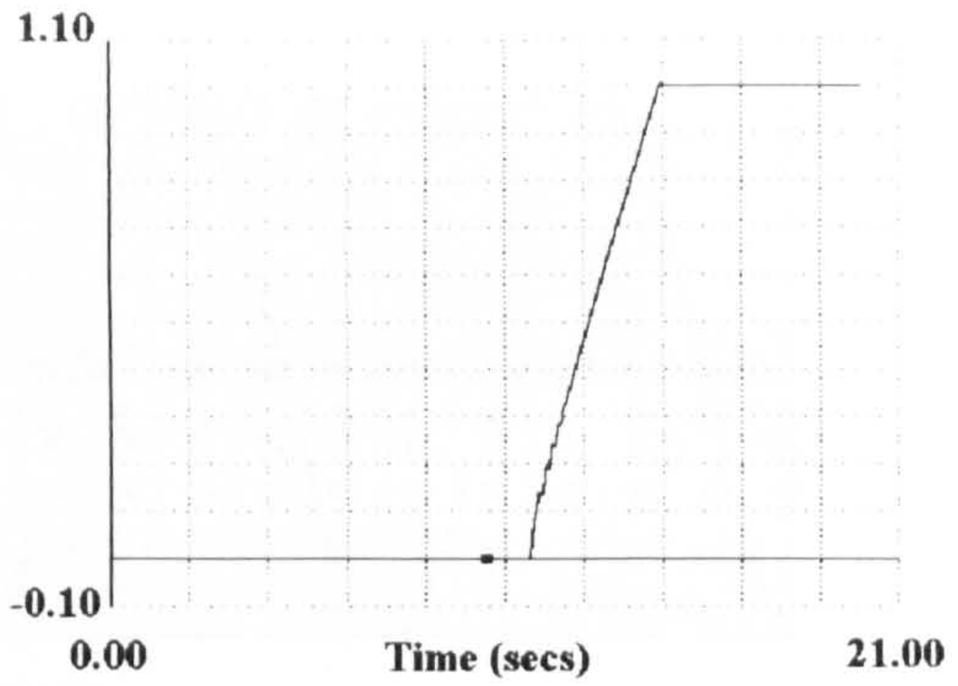

(b) Rotor speed (pu)

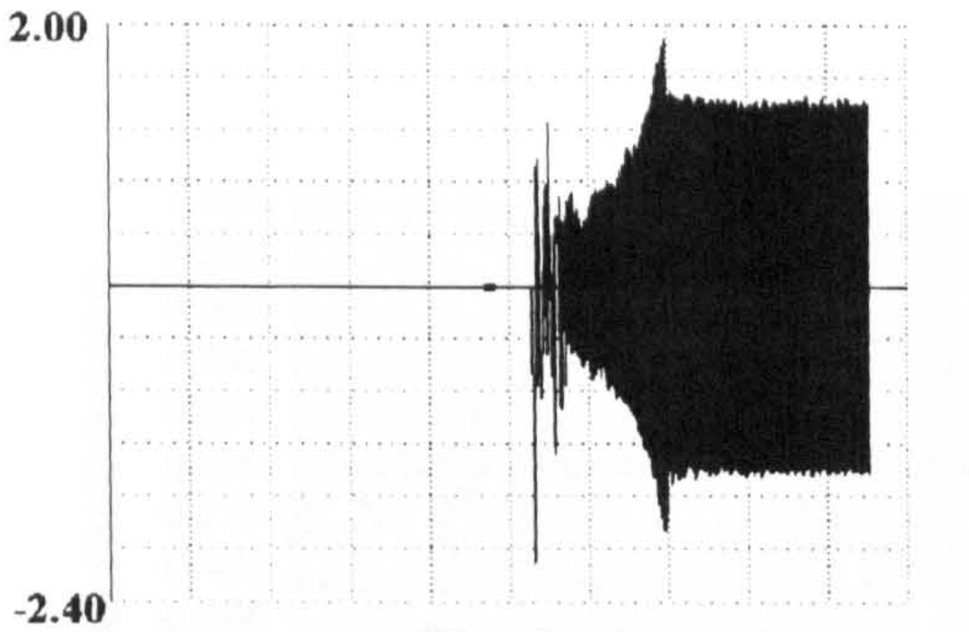

(c) Stator current phase-b (pu)

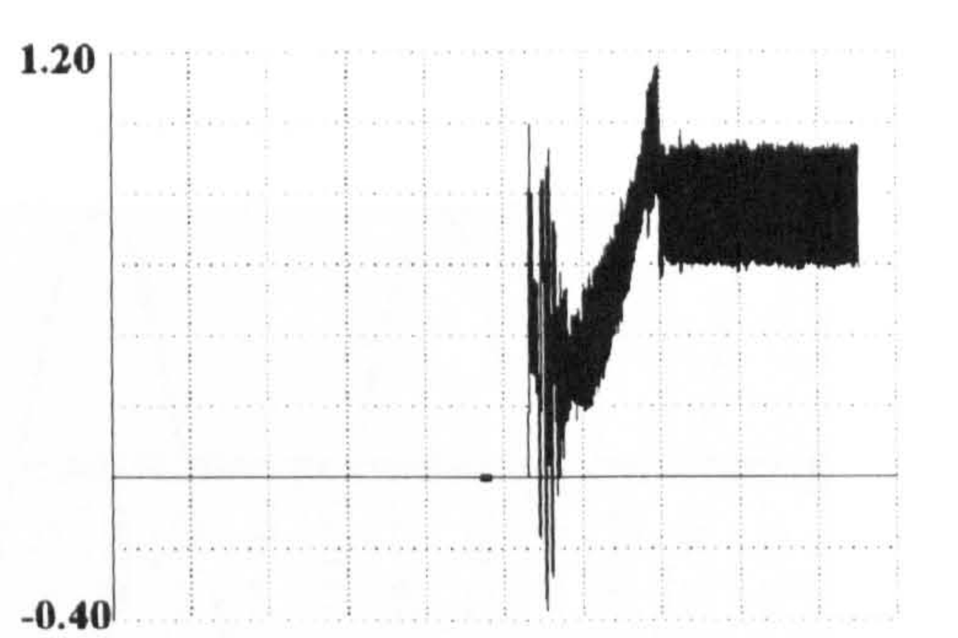

(d) Electromagnetic torque (pu)

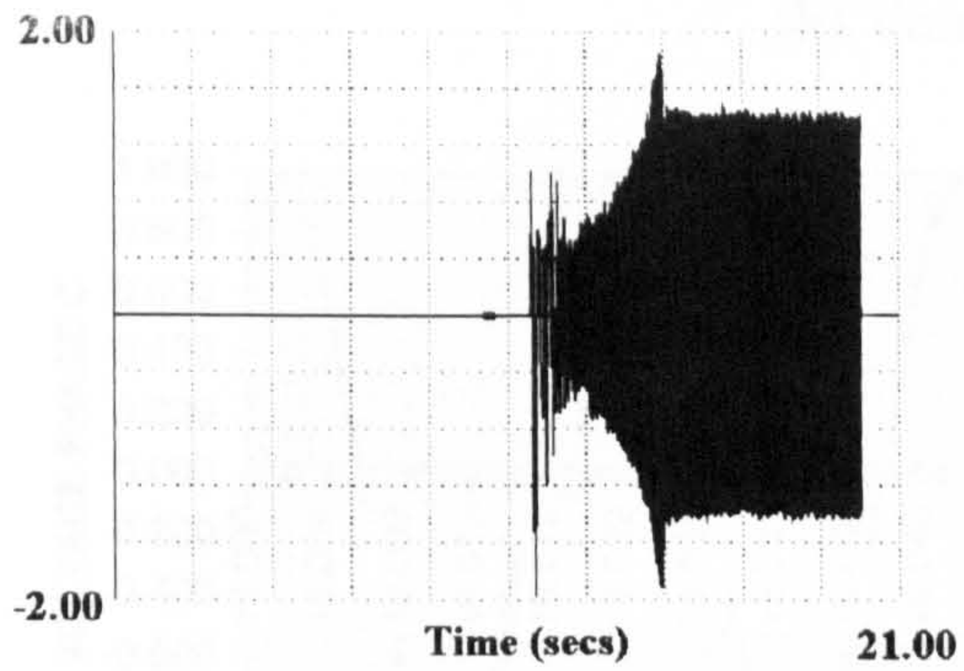

(e) Stator current phase-c (pu)

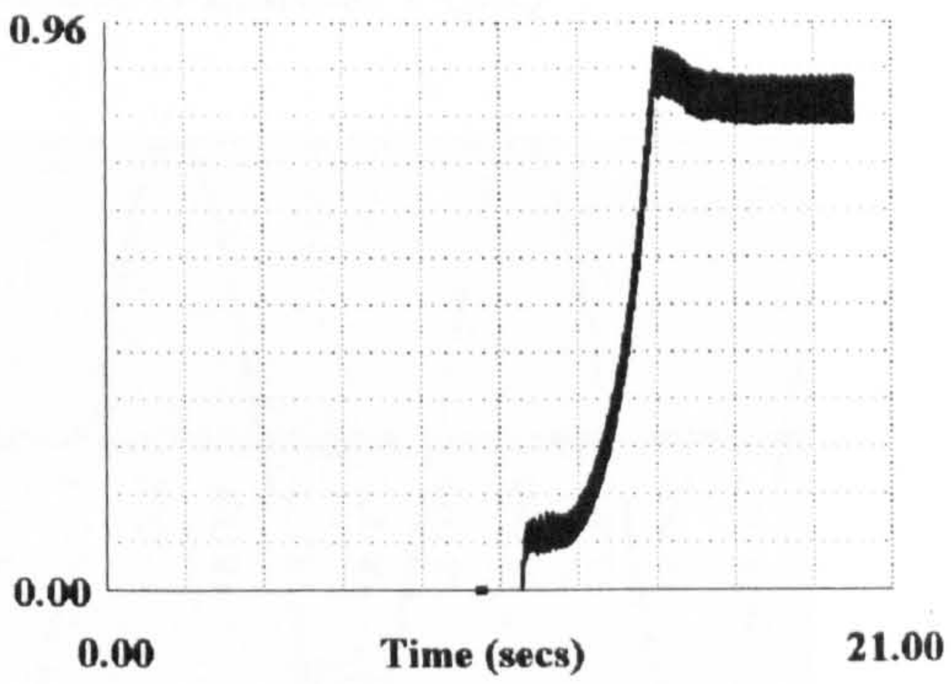

(f) DC current of the rectifier(pu)

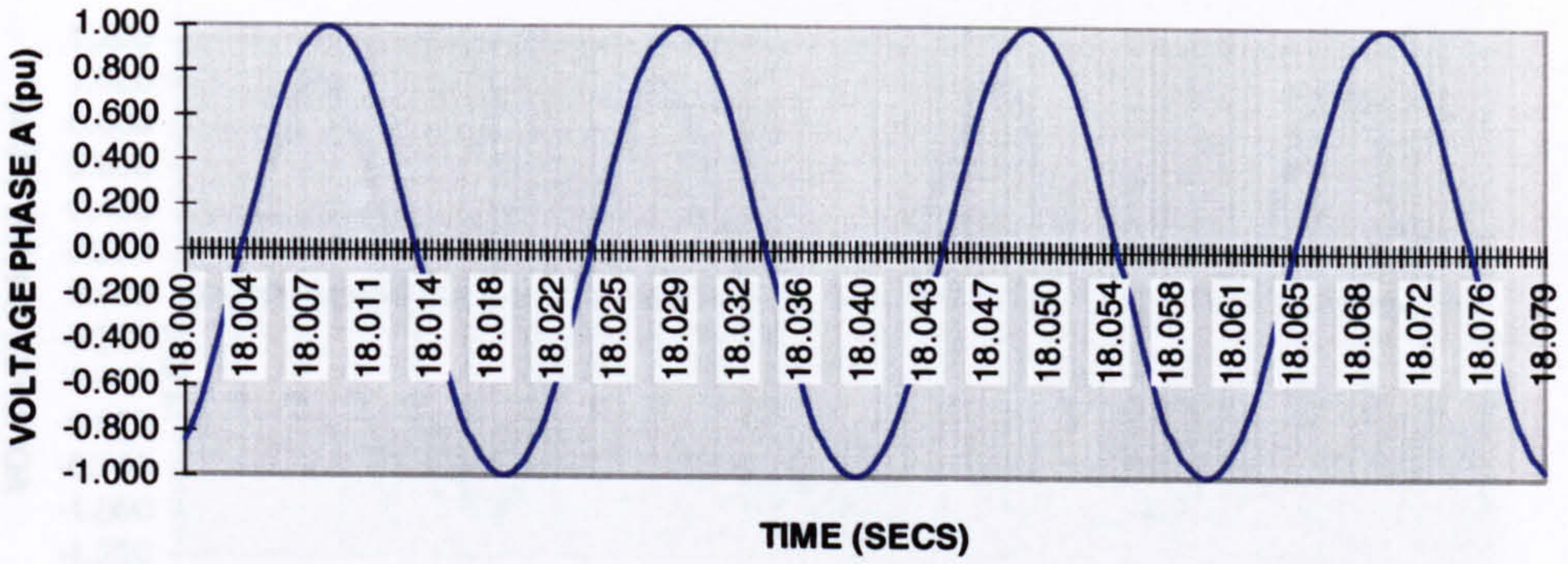

(g) Voltage of phase A at node 1 (pu)

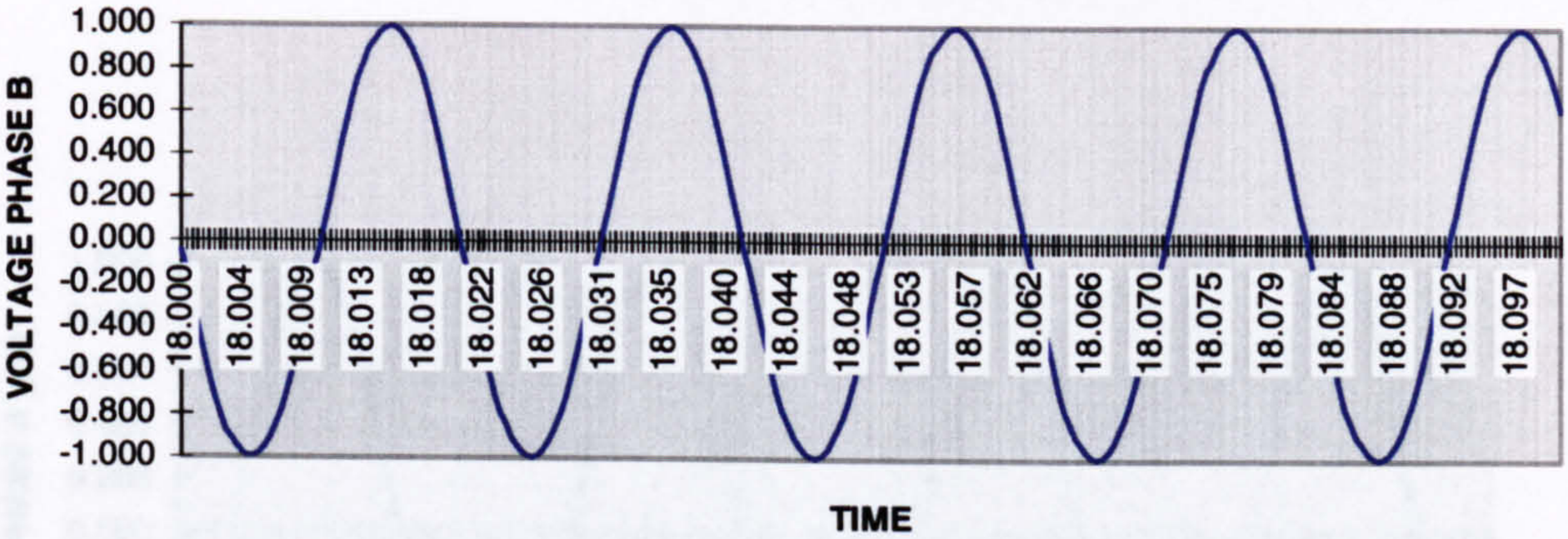

(h) Voltage of phase B at node 1 (pu)

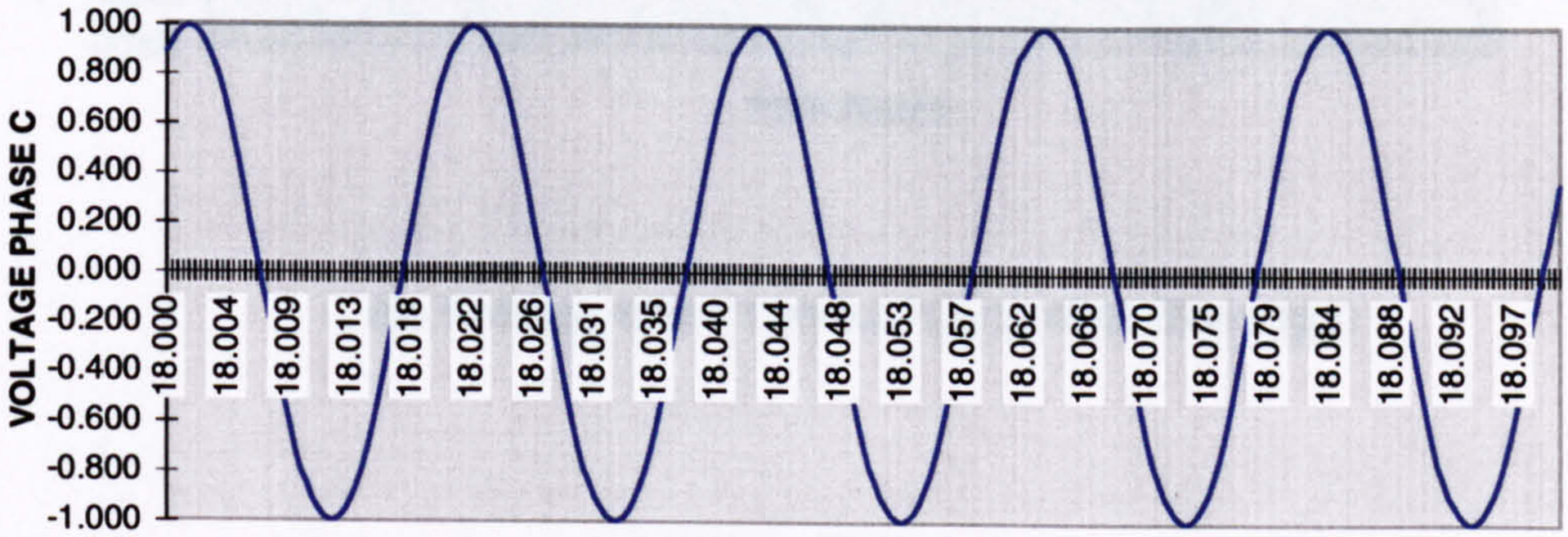

(i) Voltage of phase C at node 1 (pu)

Figure 5.10 Response of the variable speed drive

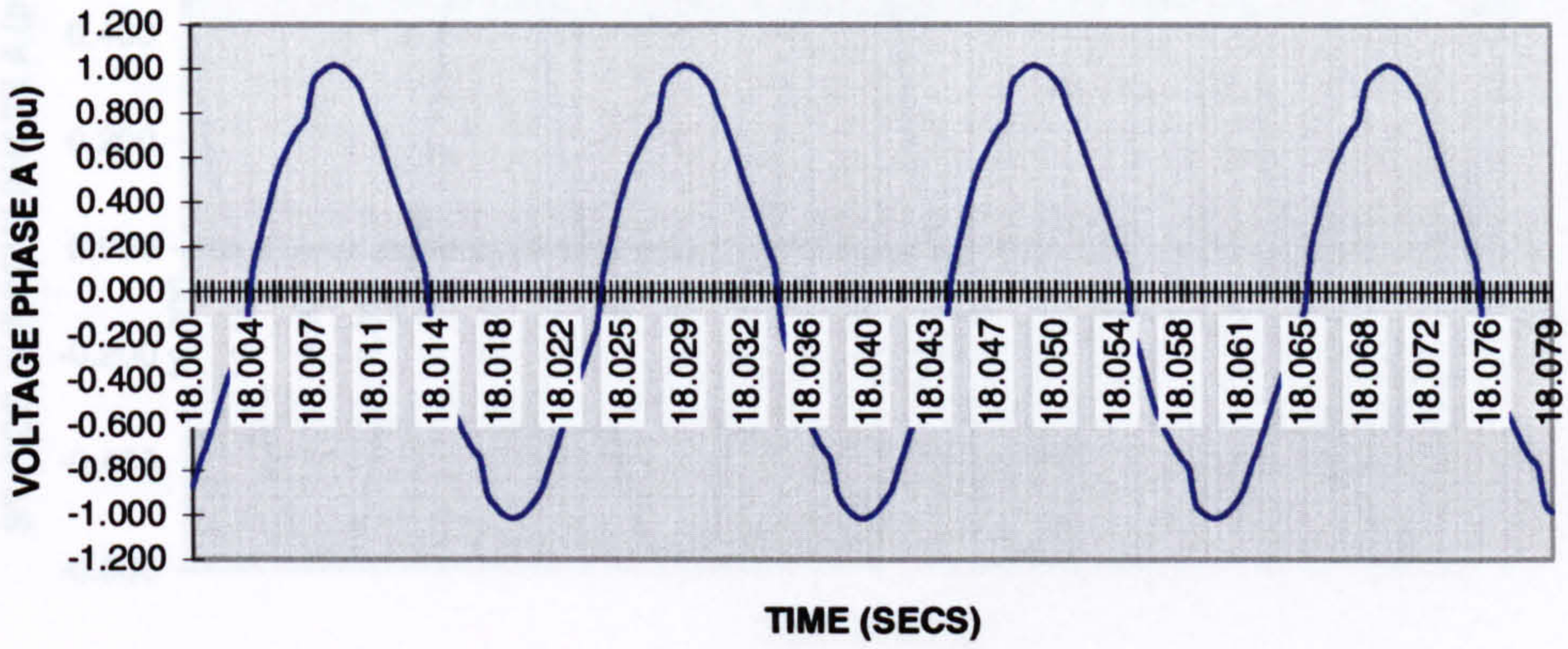

(a) Voltage at bus 1 phase A (pu) without filters (pu)

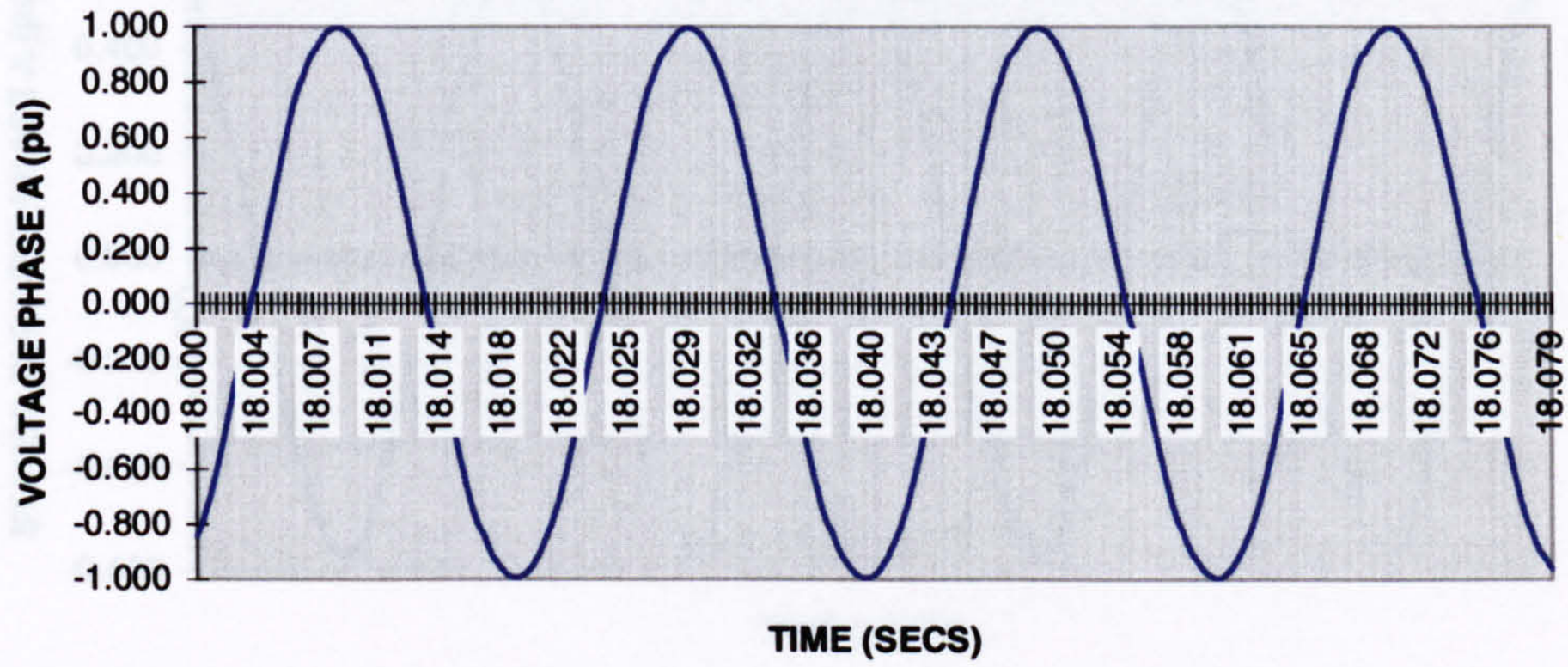

(b) Voltage at bus 1 phase A (pu) with filters (pu)

Figure 5.11

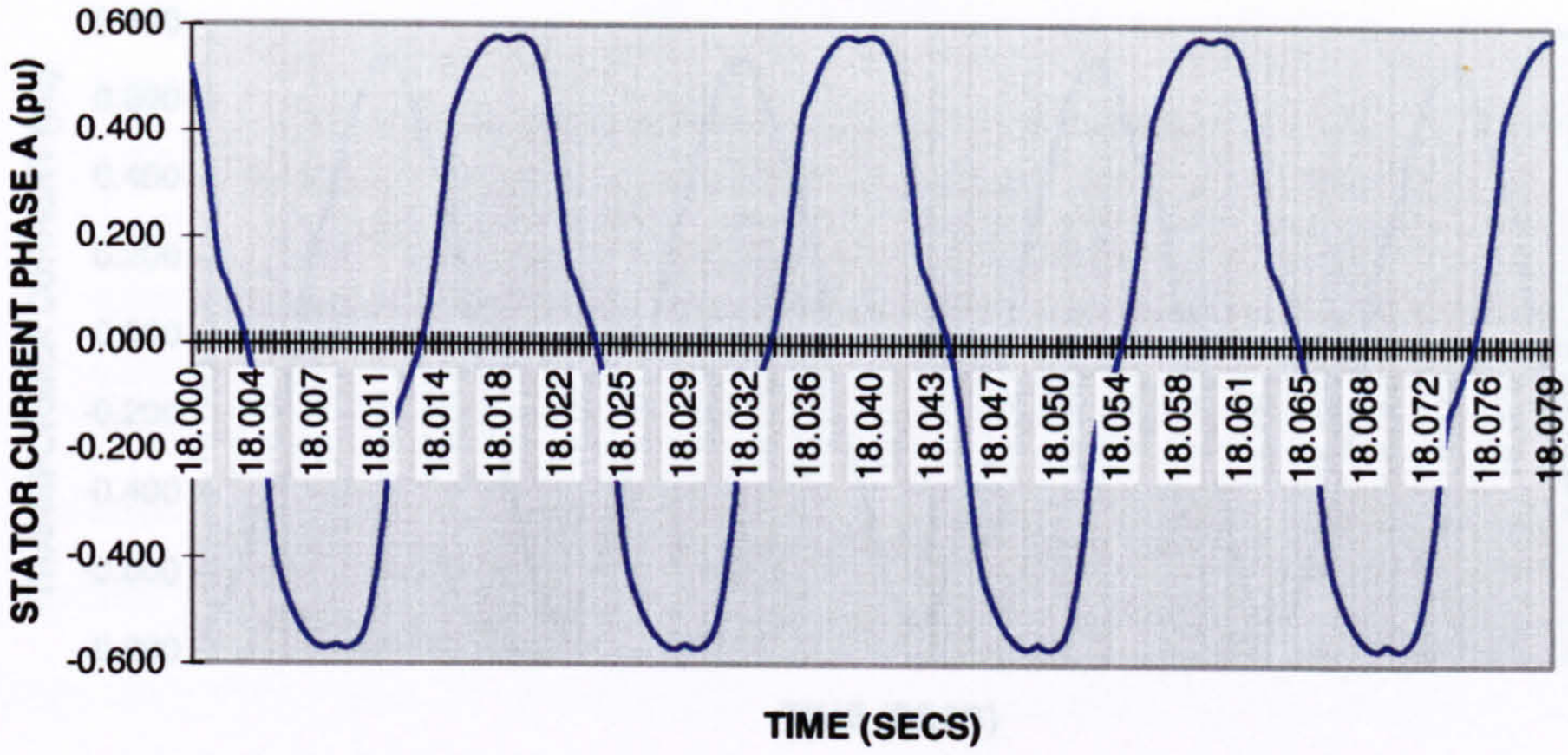

(a) Stator current phase A without filters (pu)

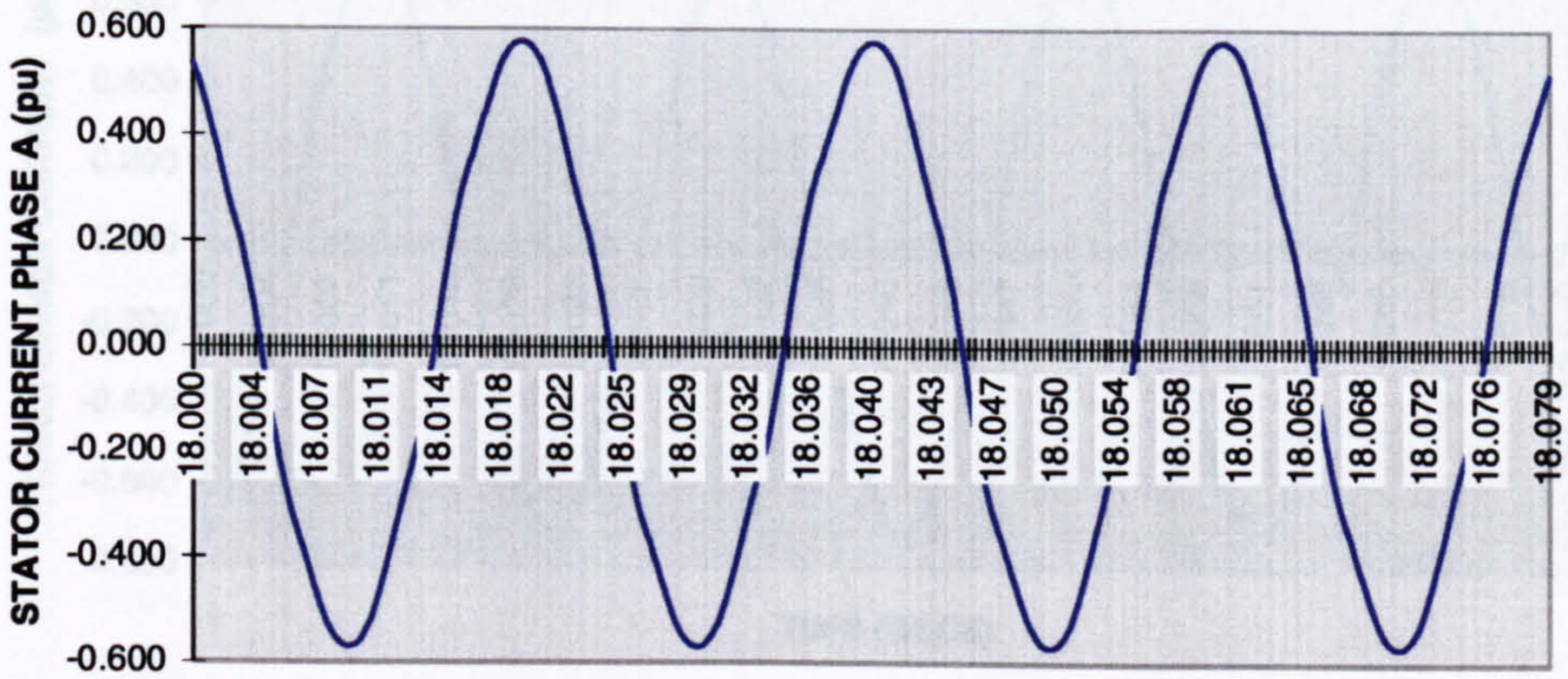

(b) Stator current phase A with filters (pu)

Figure 5.12

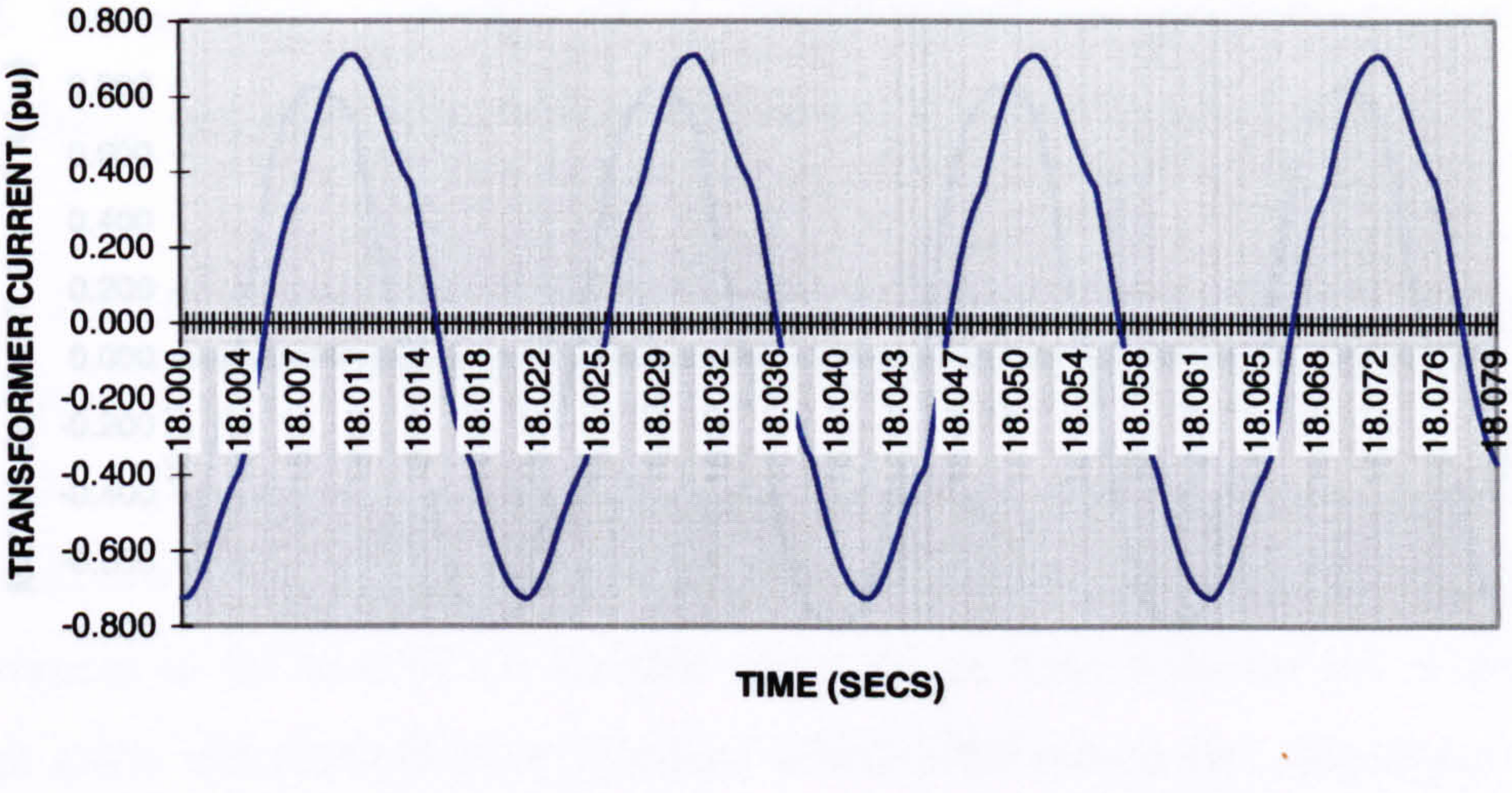

(a) Transformer current phase A without filters (pu)

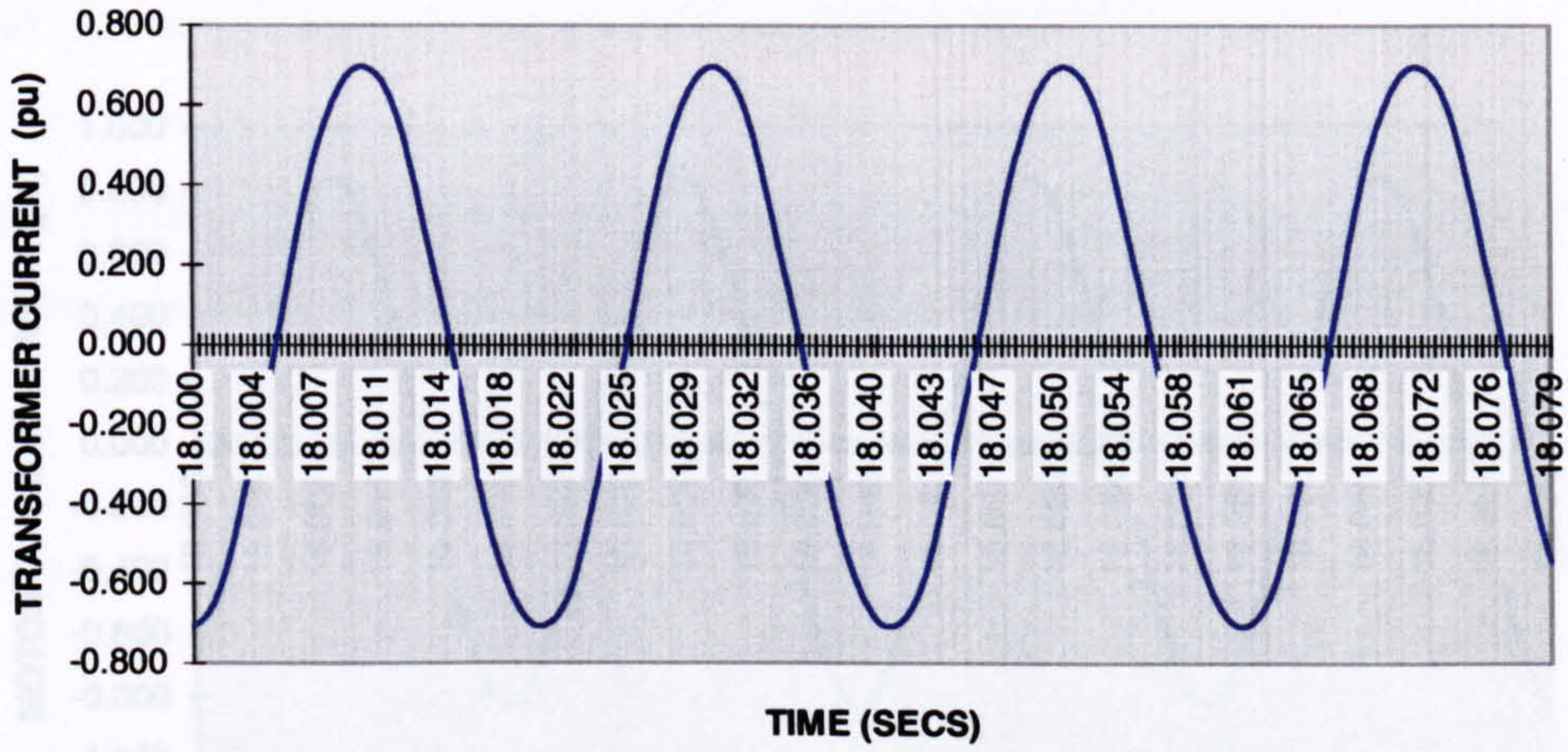

(b) Transformer current phase A with filters (pu)

Figure 5.13

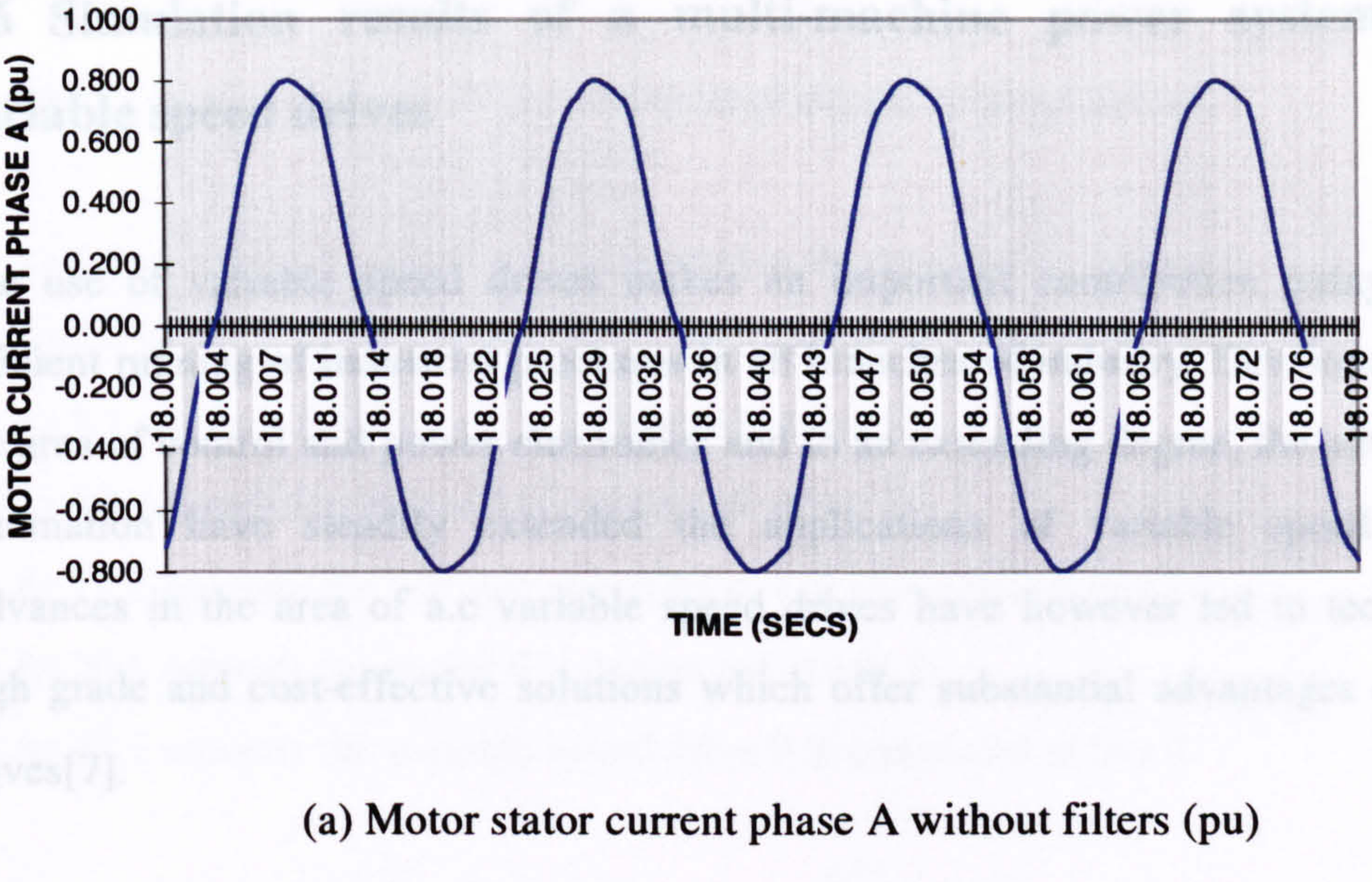

(a) Motor stator current phase A without filters (pu)

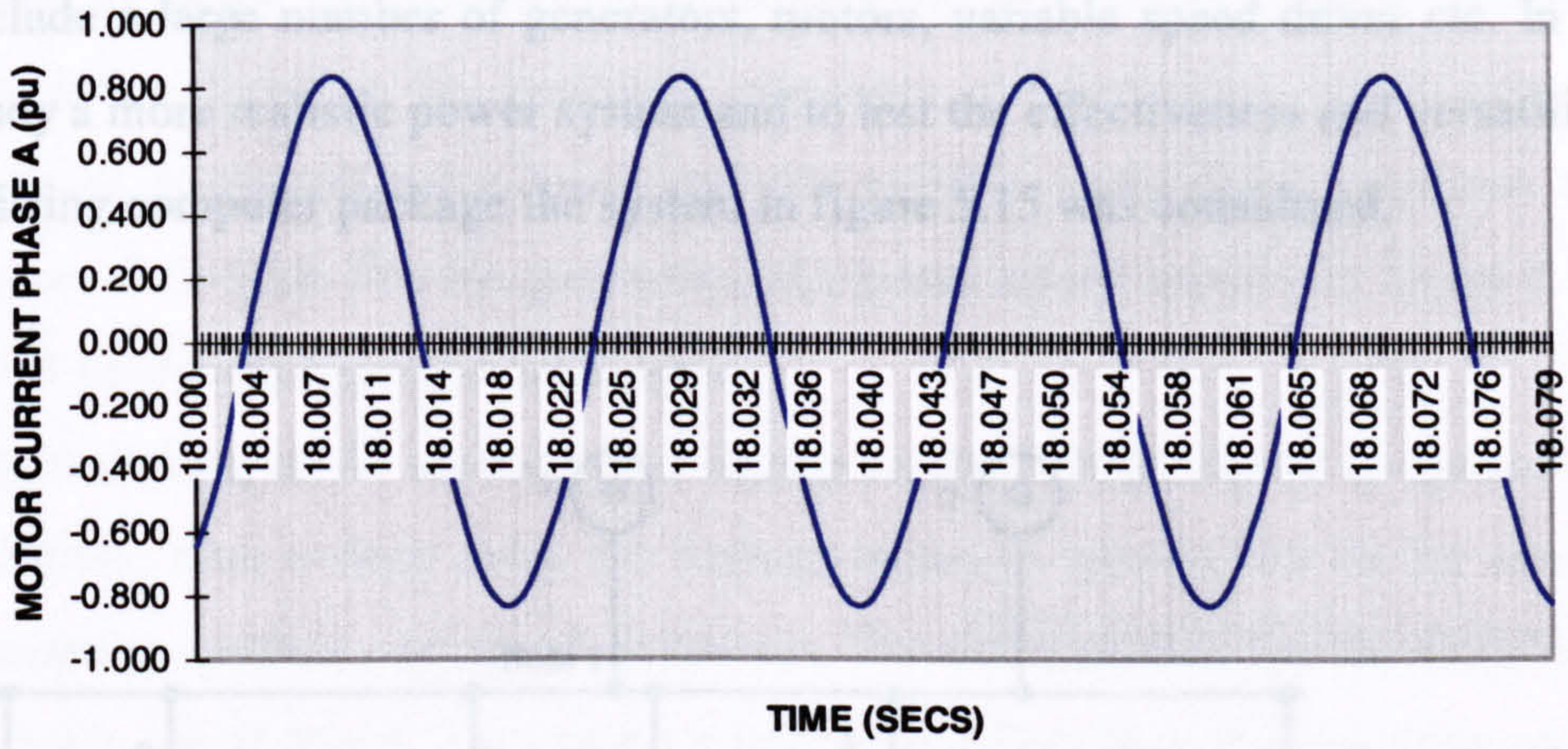

(b) Motor stator current phase A with filters (pu)

Figure 5.14

5.6 Simulation results of a multi-machine power system with variable speed drives

The use of variable speed drives makes an important contribution today to the efficient running of industrial processes in all branches of industry. Developments in the area of control and power electronics and to an extending degree, the advance of automation have steadily extended the applications of variable speed drives. Advances in the area of a.c variable speed drives have however led to technically high grade and cost-effective solutions which offer substantial advantages over d.c drives[7].

Real power systems are far more complicated than the system at figure 5.3. They include a large number of generators, motors, variable speed drives etc. In order to study a more realistic power system and to test the effectiveness and versatility of the existing computer package the system in figure 5.15 was considered.

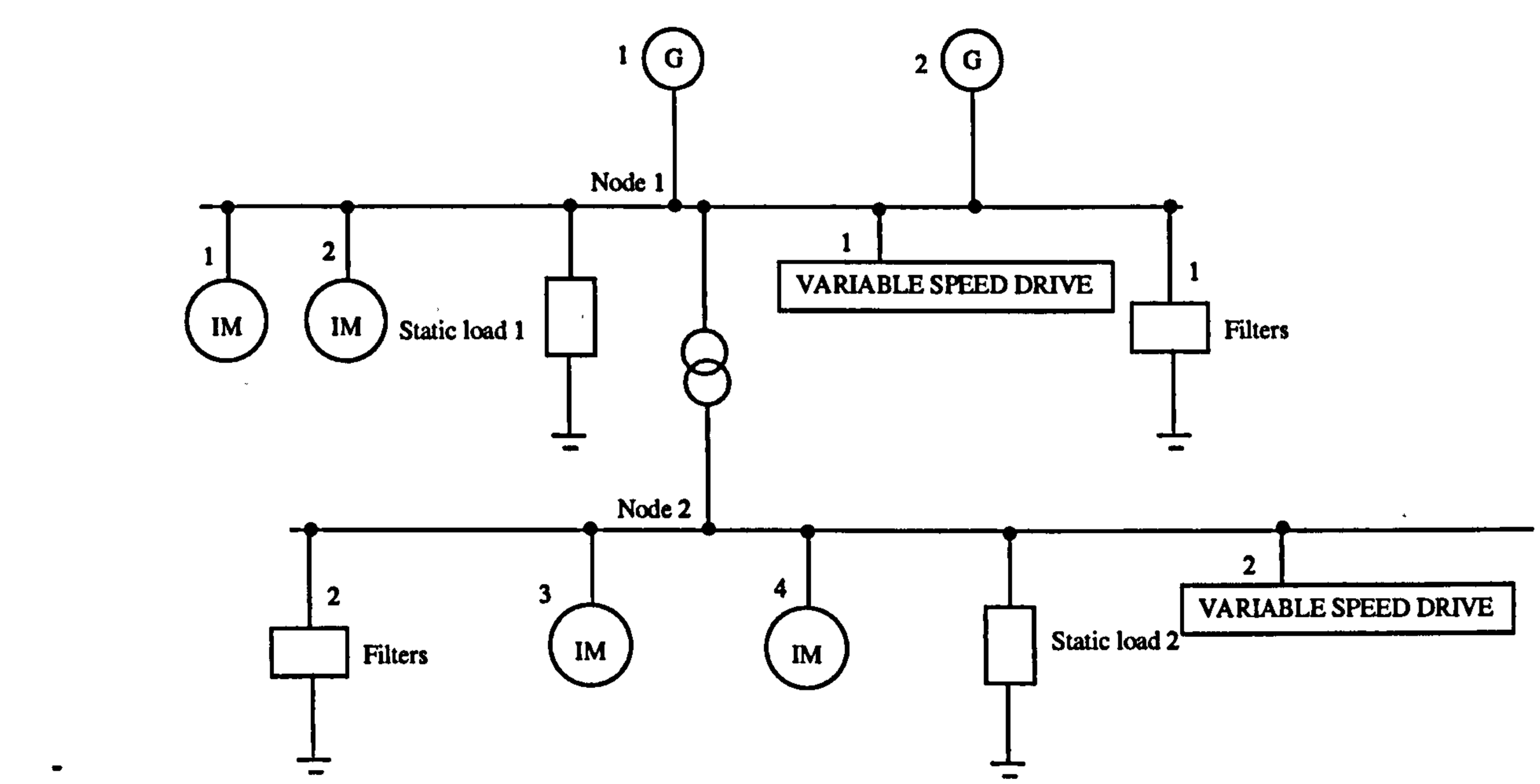

Figure 5.15 Representation of a multi machine AC/DC power system with variable speed drives

For the system of figure 5.15 the sequence of events is given below:

1) At 0.1 seconds the motor 1 is connected to the generating system.
2) At 0.1 seconds the filters in buses 1 and 2 are connected to the generating system.
3) At 5.1 seconds the motor 2 is connected at bus 1.
4) At 9.1 seconds the motor 3 is connected at bus 2.
5) At 15.1 seconds the variable speed drive 1 is connected at bus 1.
6) At 20.1 seconds the motor 4 is connected at bus 2.
7) At 27.1 seconds the variable speed drive 2 is connected at bus 2.

For this multi-machine AC/DC system we obtain a number of simulation results in order to study the dynamic performance of the power system. Results of the simulation showing the generator responses, the induction motor responses, the voltages at the generator buses and the variable speed drive responses are given figures 5.16-5.23. For the generators, the prime mover models in figure 4.7 and the AVR models in figure 4.6 were used.

The switching of the motors to the supply causes voltage dips at the generator buses, however, after a short delay the voltage began to recover due to the action of the excitation systems and speed governors. The same applies for the switching of the variable speed drives. They cause a voltage dip (less than the induction motors) and also produce a number of harmonics polluting the entire network. In order to avoid these unwanted harmonics a number of filters are connected at the generator buses. These filters will absorb most but not all the harmonics, as can be seen from the generator and motor waveforms. The variable speed drive waveforms show that each drive will reach steady state conditions after 3.5 seconds. The operation of its drive is greatly affected from the switching of other components of the system such as induction motors. This is due to the fact that the switching of a motor causes a voltage dip where the motor is located therefore a change in the variable speed drive variables.

A complete set of data for the overall simulated system is given in appendix 4.

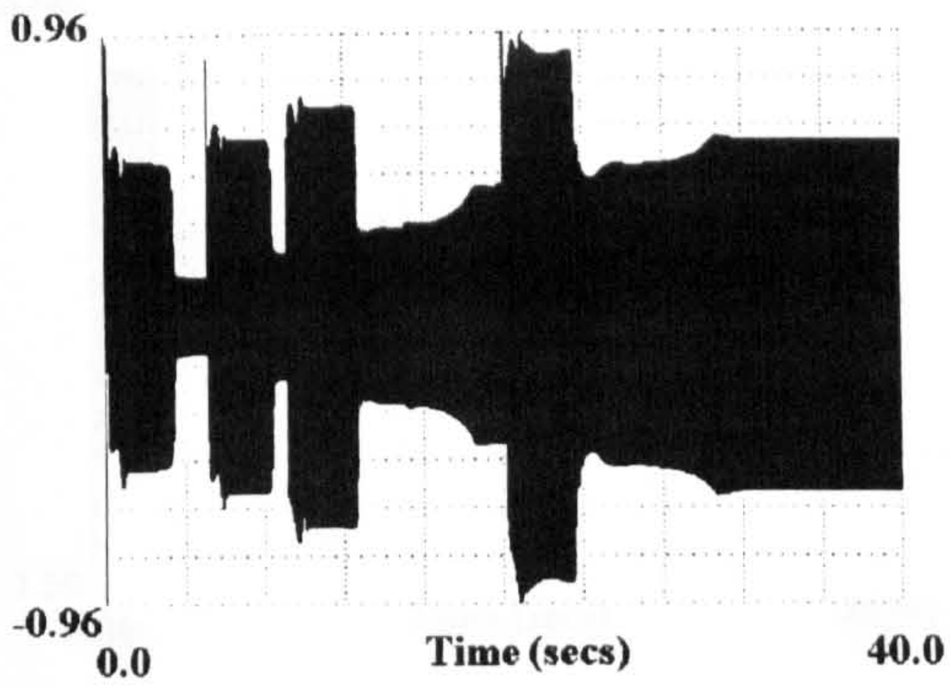

(a) Stator current phase-a (pu)

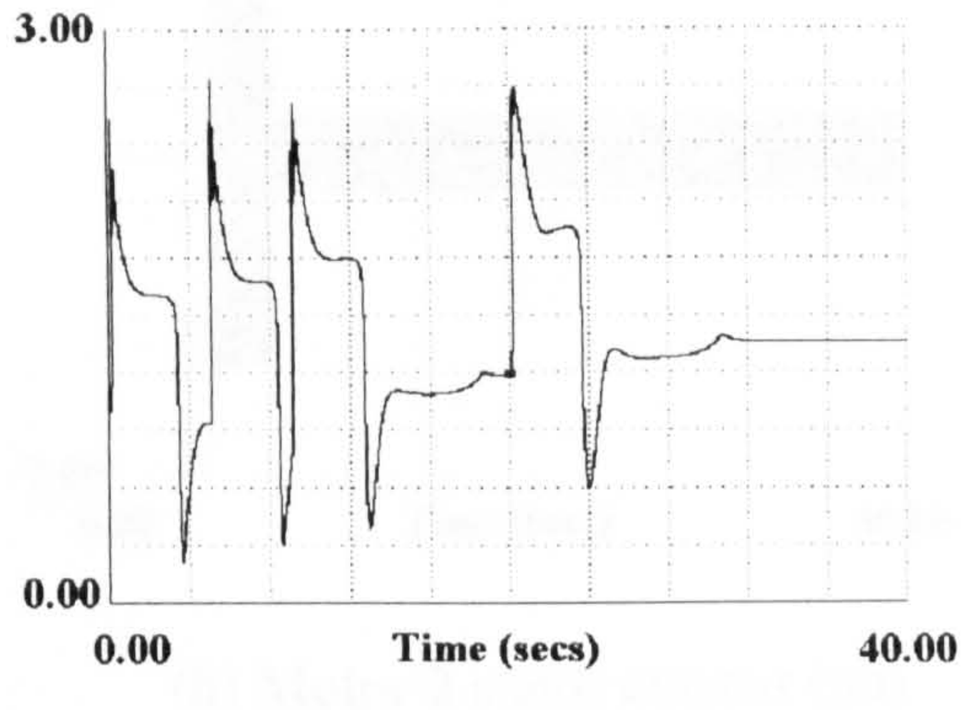

(b) Field voltage (pu)

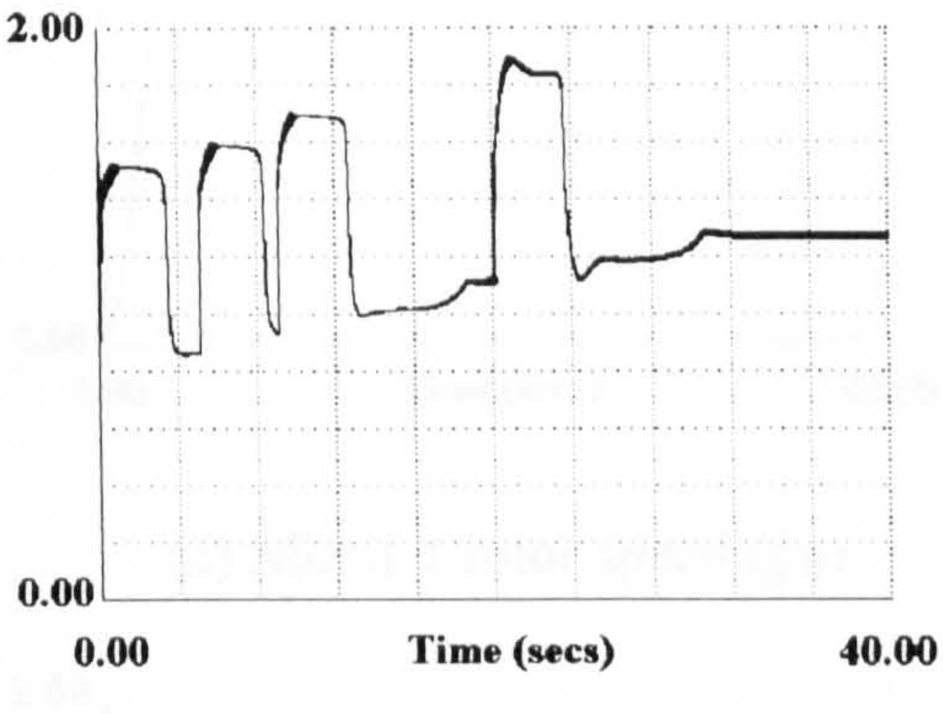

(c) Field current (pu)

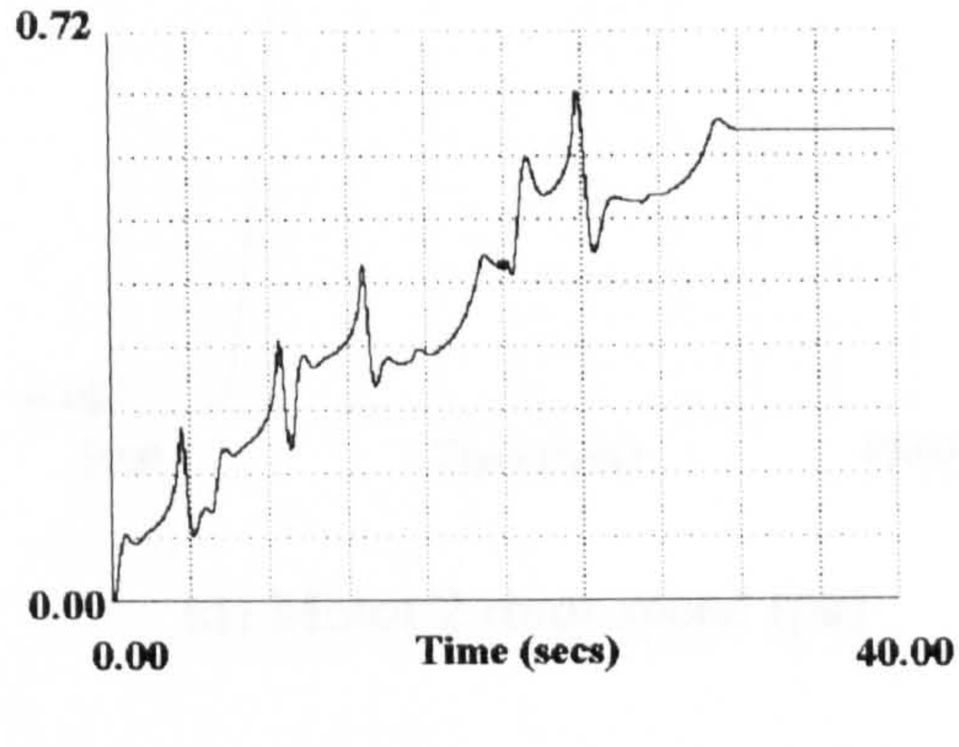

(d)Input power from prime mover(pu)

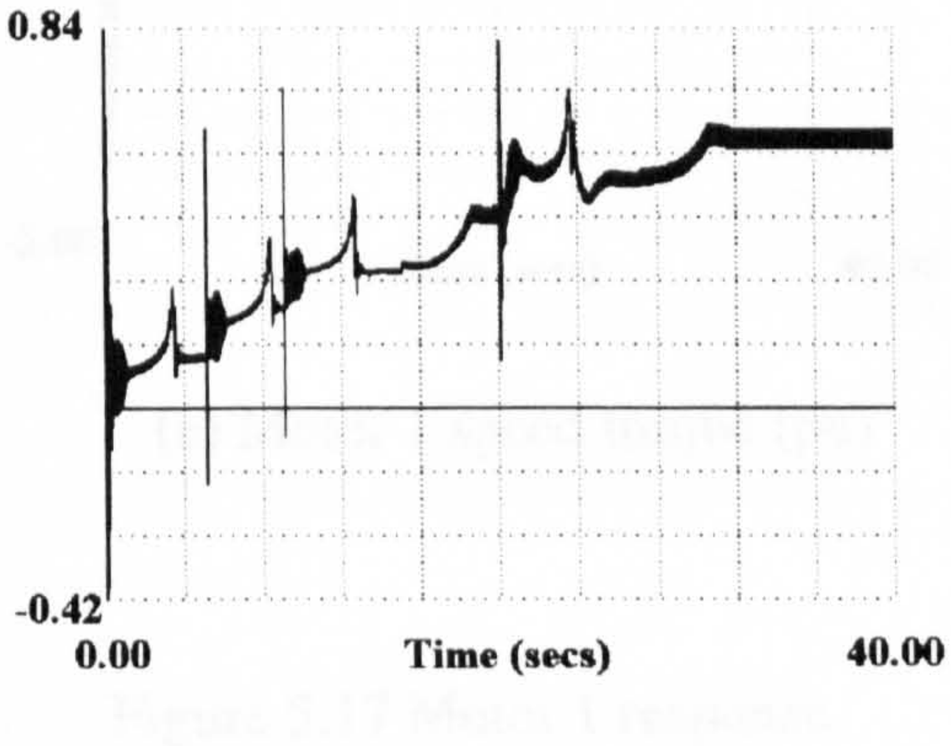

(e) Electromagnetic torque (pu)

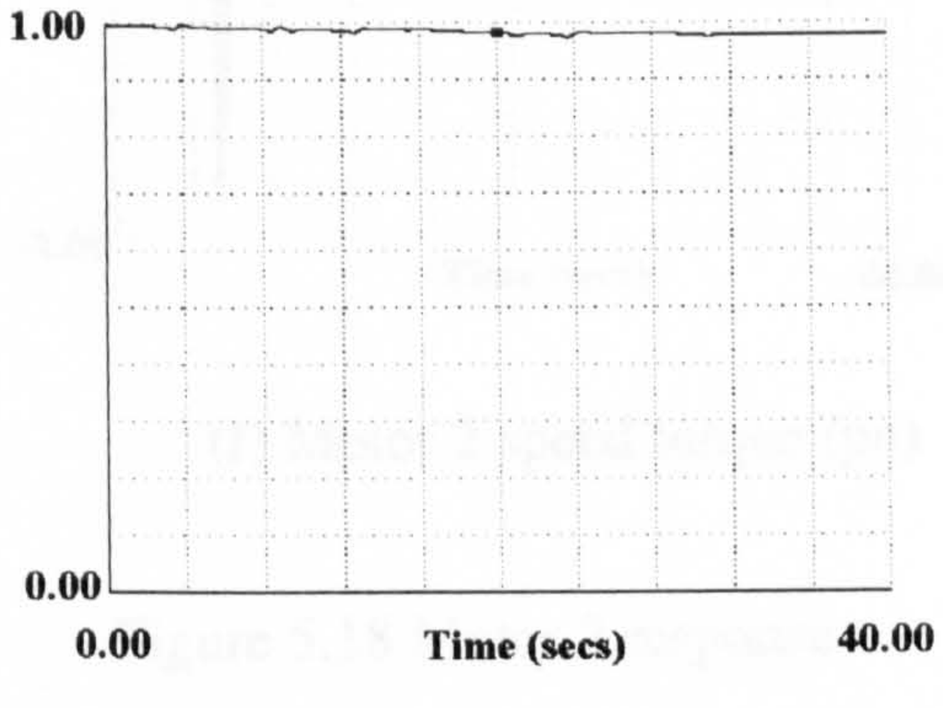

(f) Rotor speed (pu)

Figure 5.16 Generators 1 and 2 responses

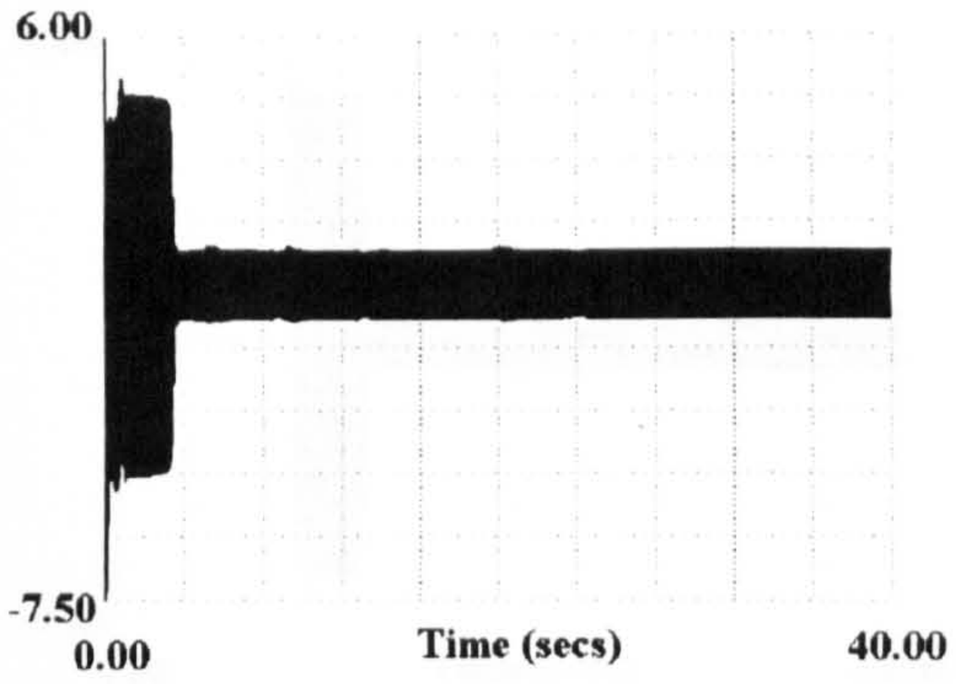

(a) Motor 1 stator current (pu)

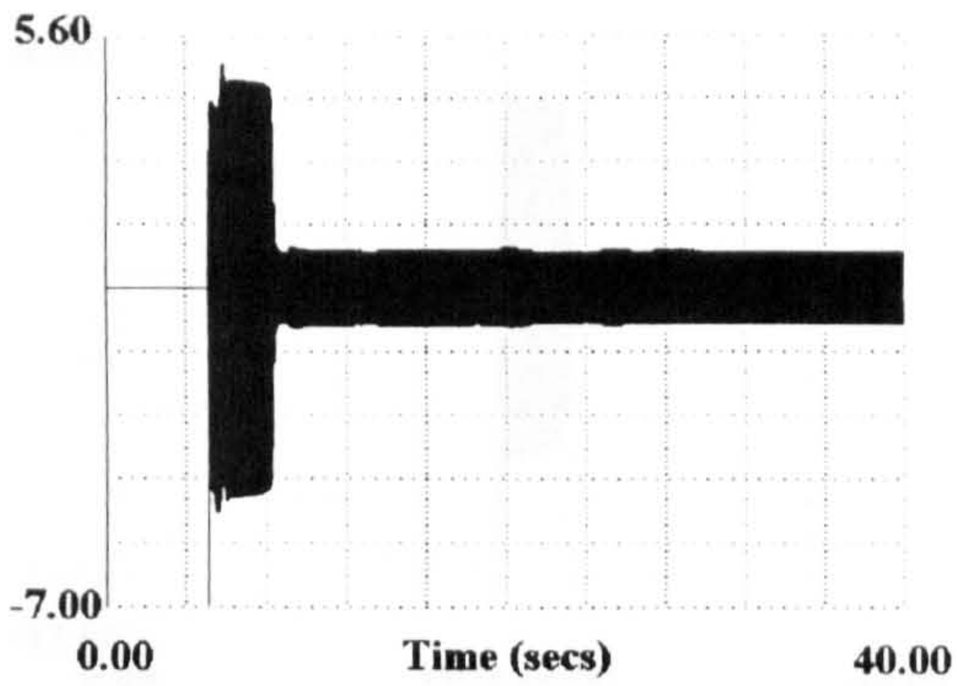

(b) Motor 2 stator current (pu)

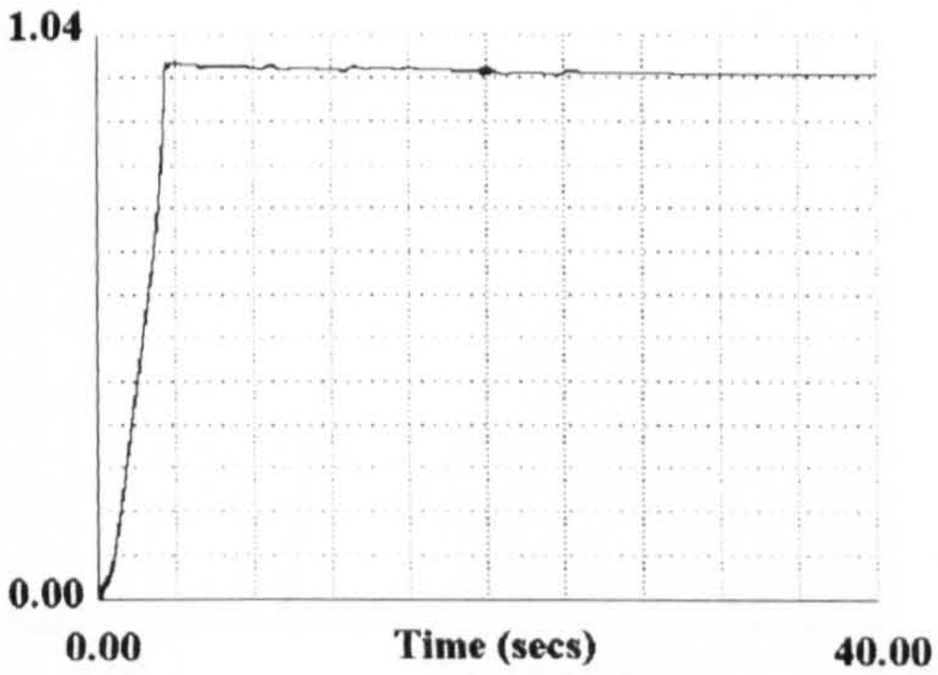

(c) Motor 1 rotor speed (pu)

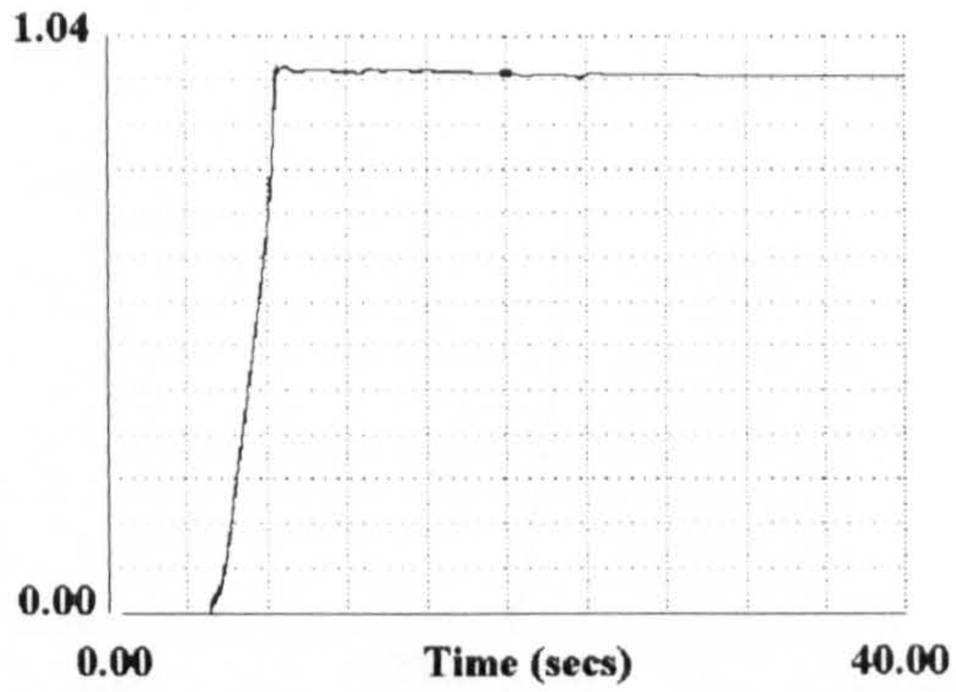

(d) Motor 2 rotor speed (pu)

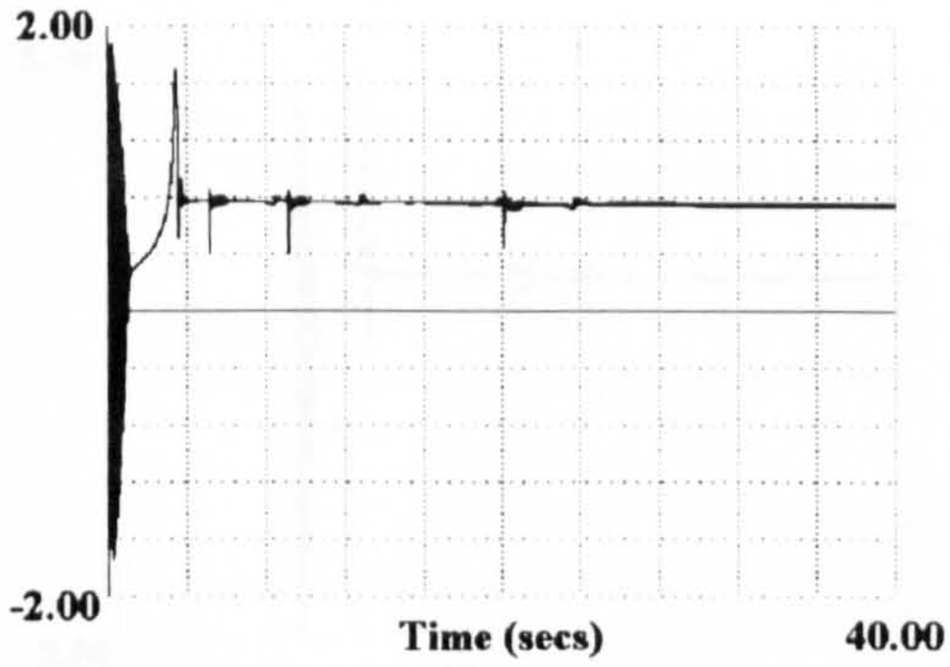

(e) Motor 1 speed torque (pu)

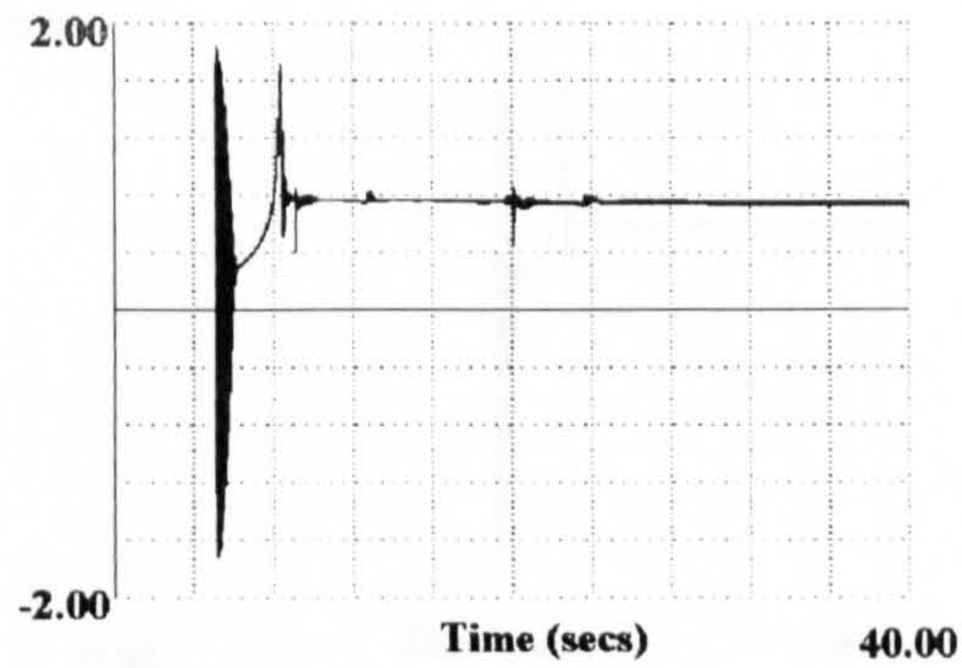

(f) Motor 2 speed torque (pu)

Figure 5.17 Motor 1 response

Figure 5.18 Motor 2 response

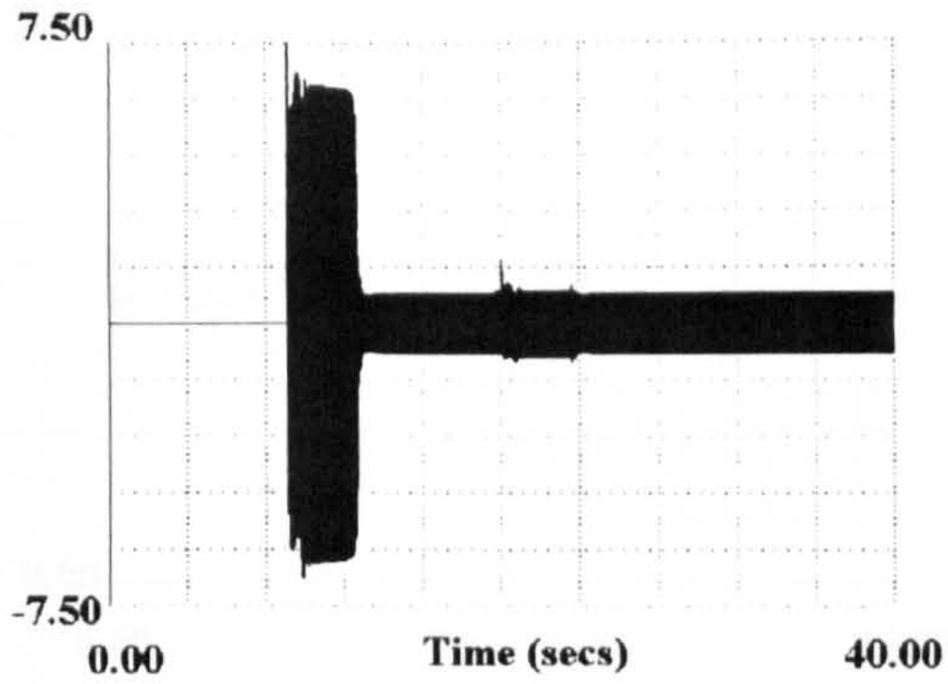

(a) Motor 3 stator current (pu)

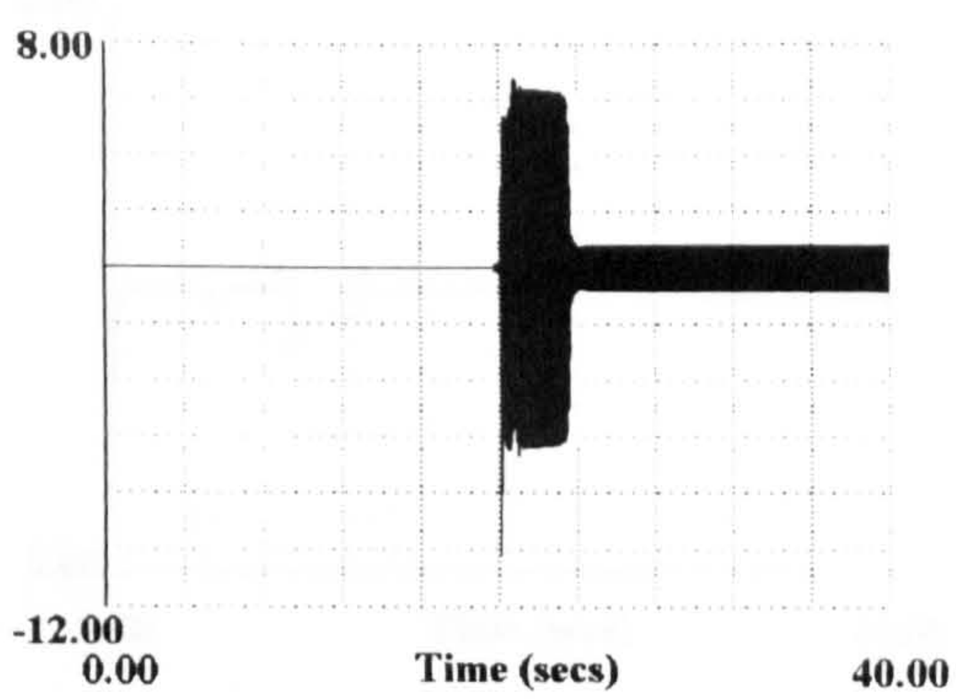

(b) Motor 4 stator current (pu)

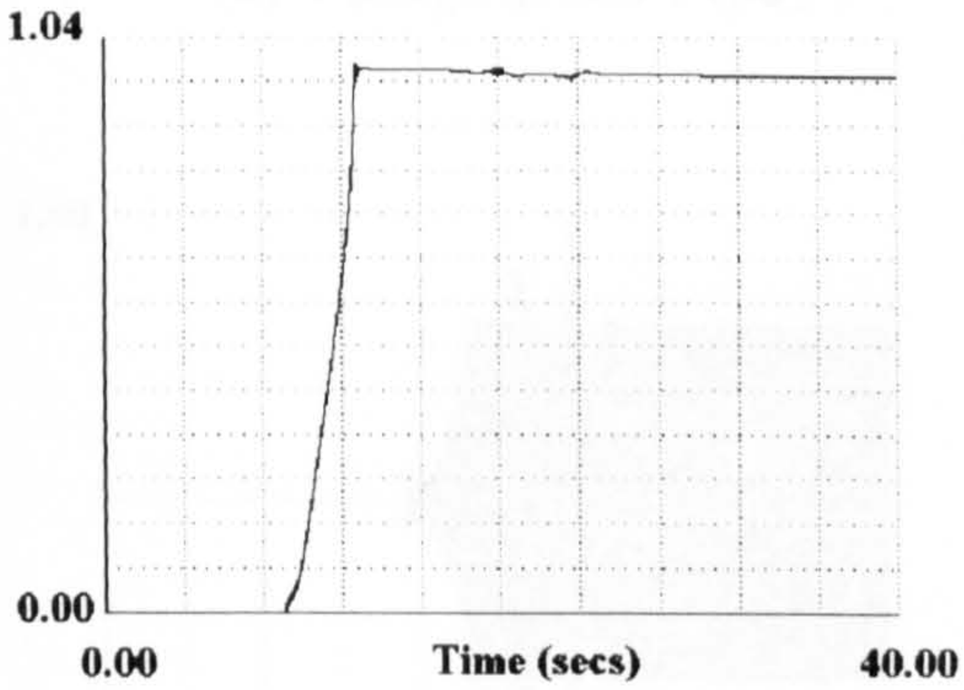

(c) Motor 3 rotor speed (pu)

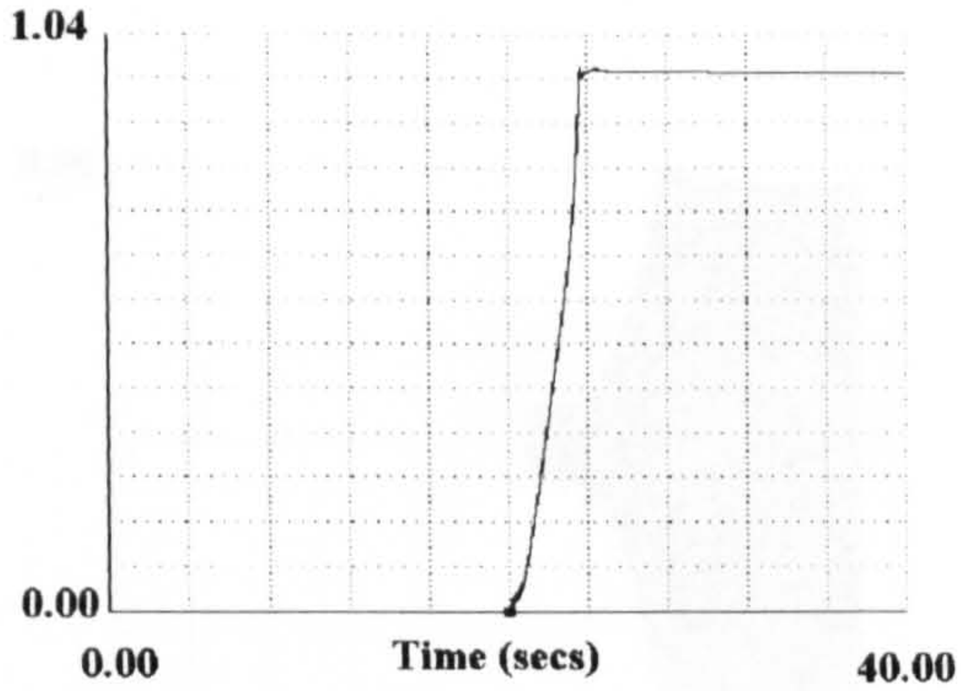

(d) Motor 4 rotor speed (pu)

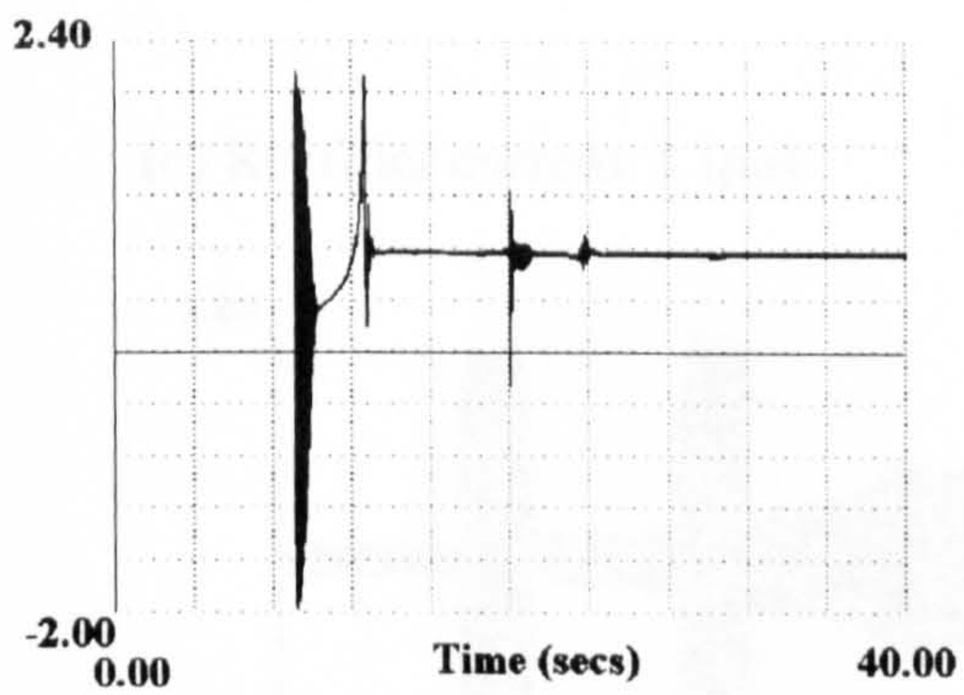

(e) Motor 3 speed torque (pu)

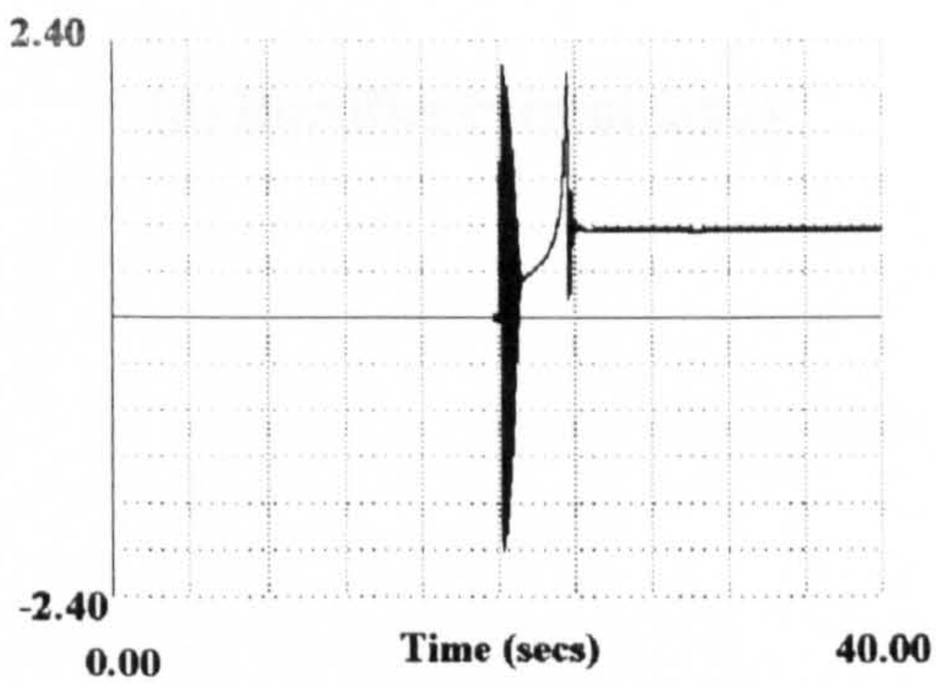

(f) Motor 4 speed torque (pu)

Figure 5.19 Motor 3 response

Figure 5.20 Motor 4 response

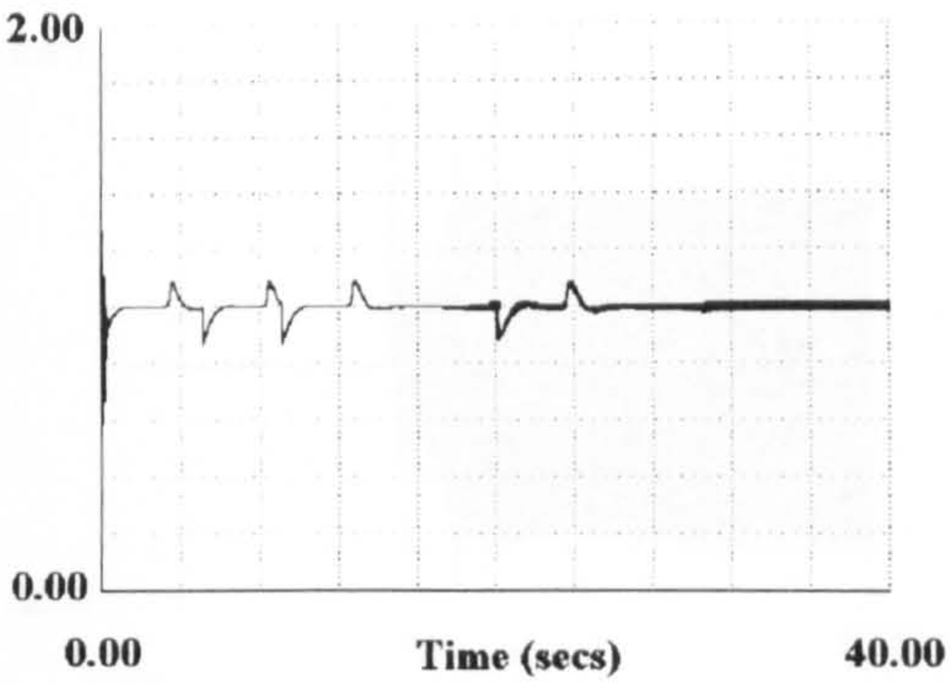

(a) Voltage at bus 1 (pu)

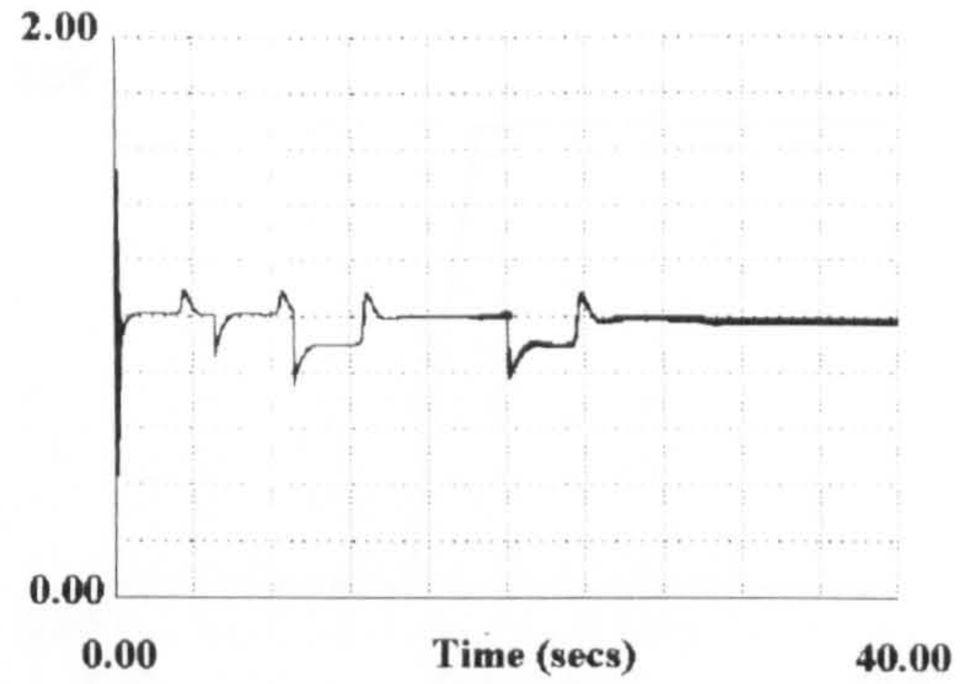

(b) Voltage at bus 2 (pu)

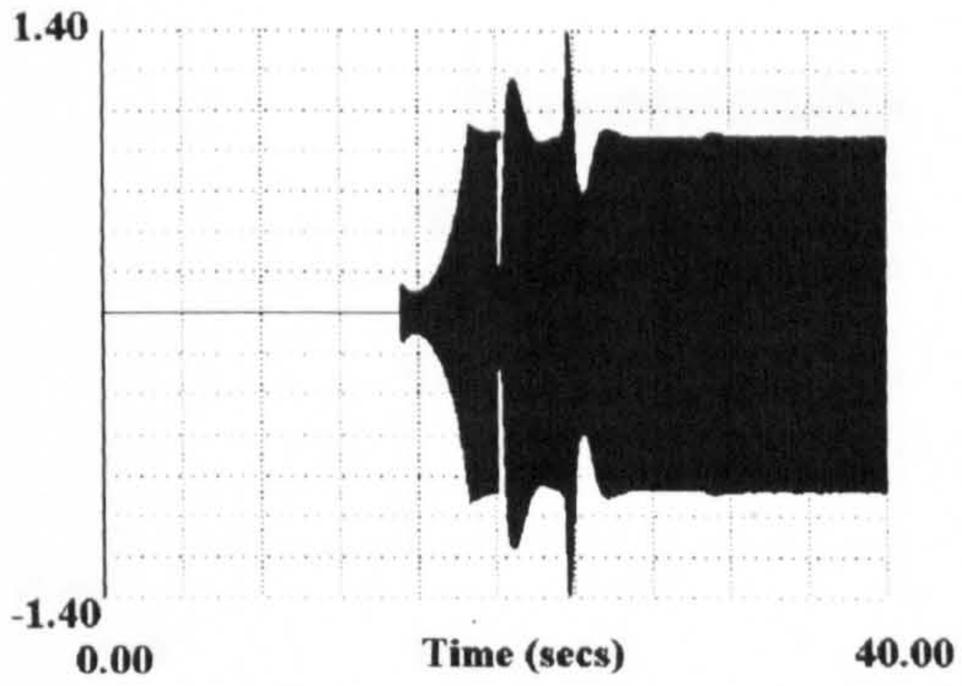

(c) Rectifier current 1 (pu)

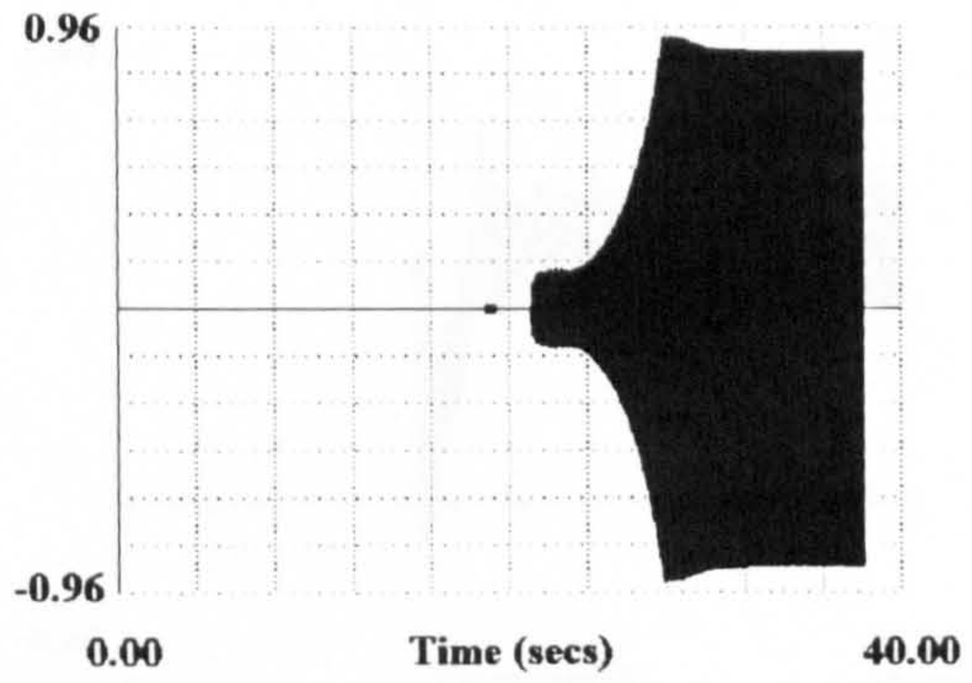

(d) Rectifier current 2(pu)

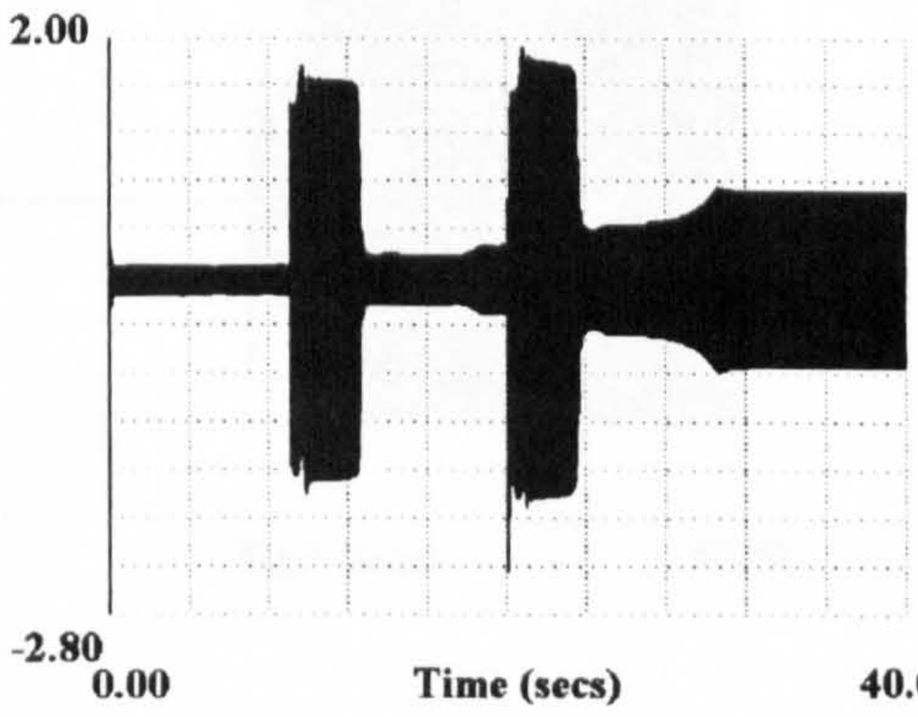

(e) Transformer current on winding 1 (pu)

Figure 5.21

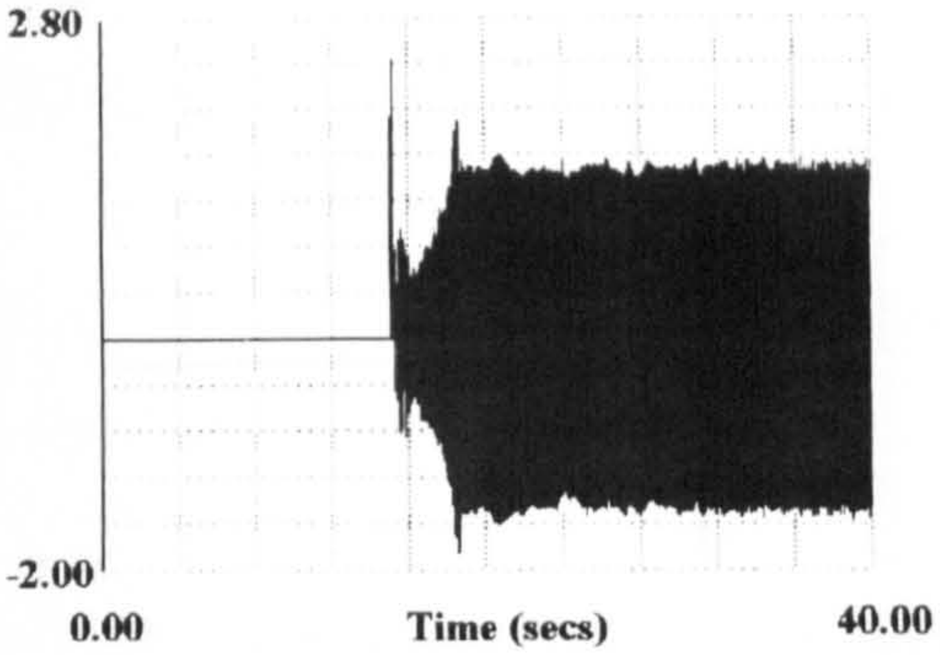

(a) Stator current phase-a (pu)

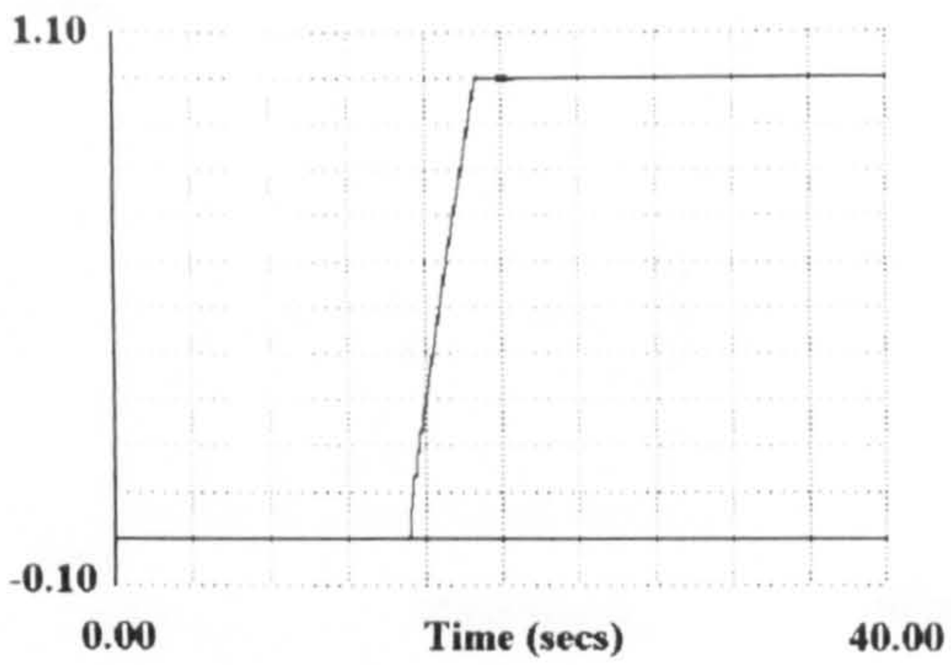

(b) Rotor speed (pu)

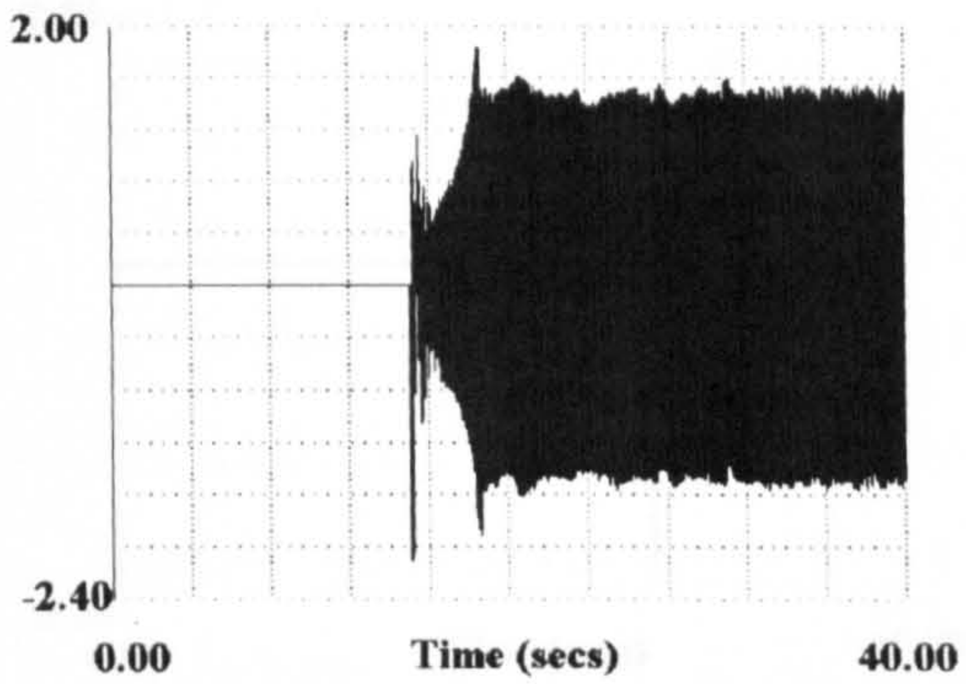

(c) Stator current phase-b (pu)

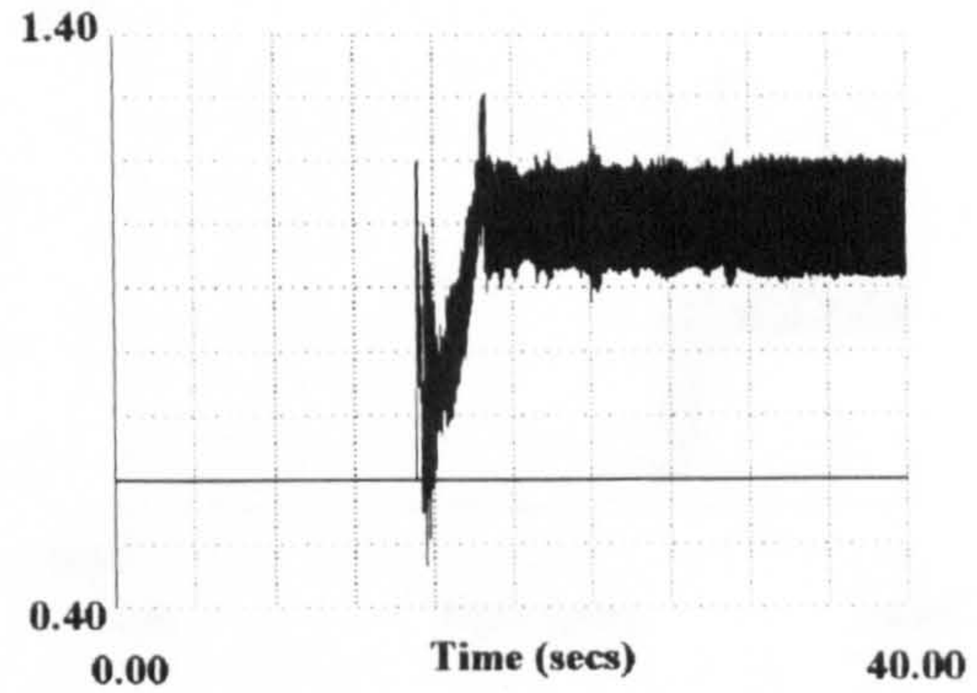

(d) Electromagnetic torque (pu)

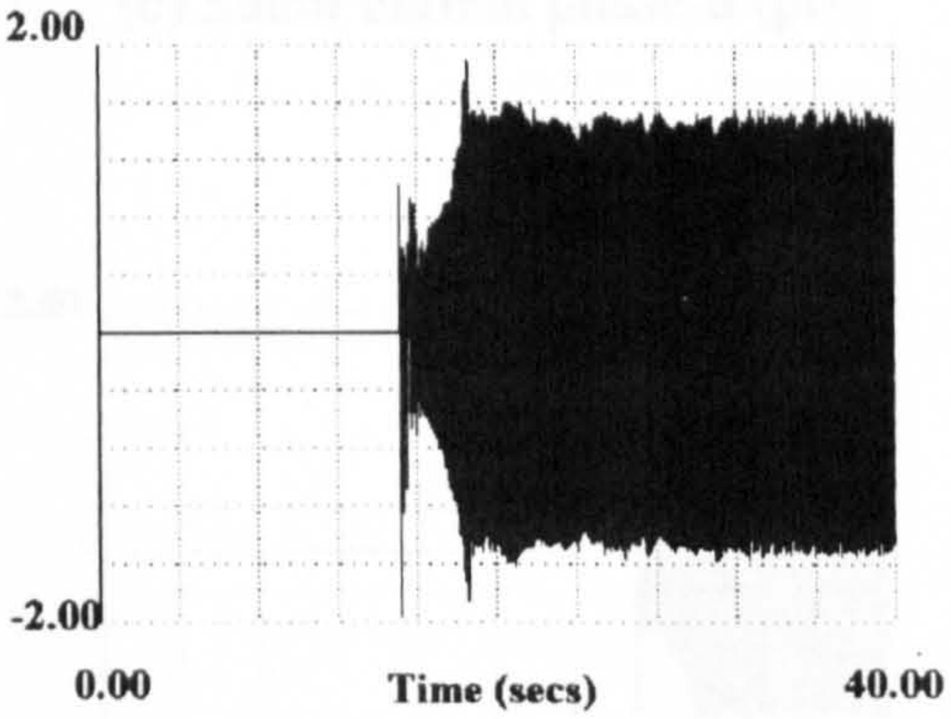

(e) Stator current phase-c (pu)

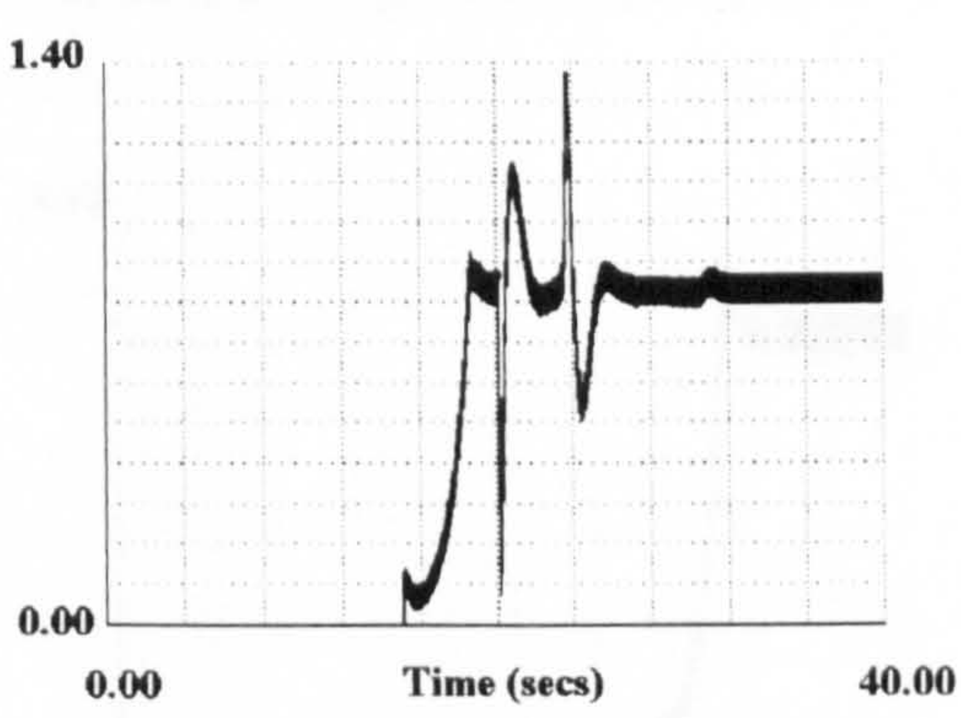

(f) DC current of the rectifier (pu)

Figure 5.22 Response of the variable speed drive 1

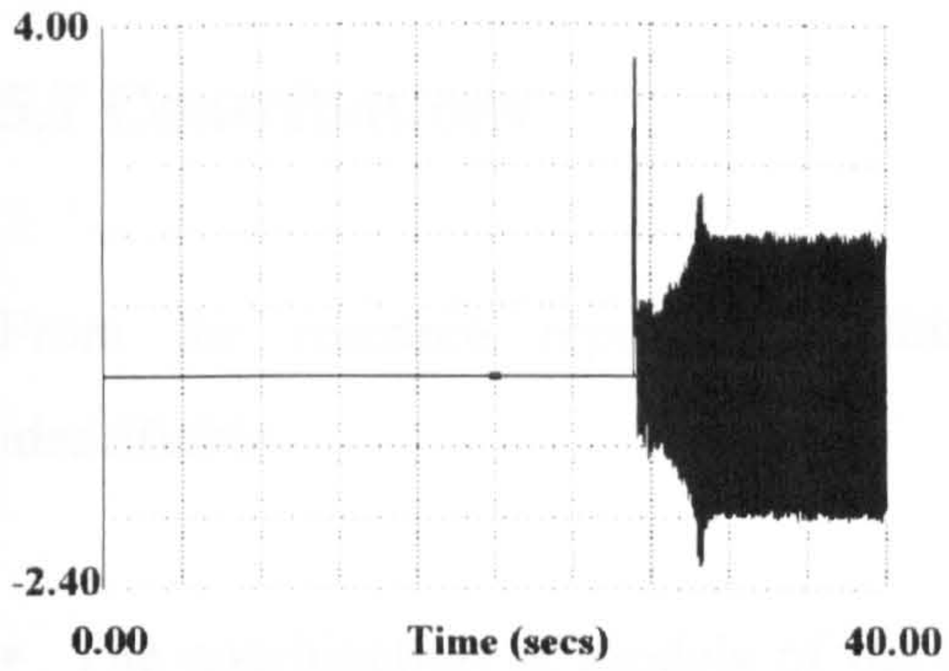

(a) Stator current phase-a (pu)

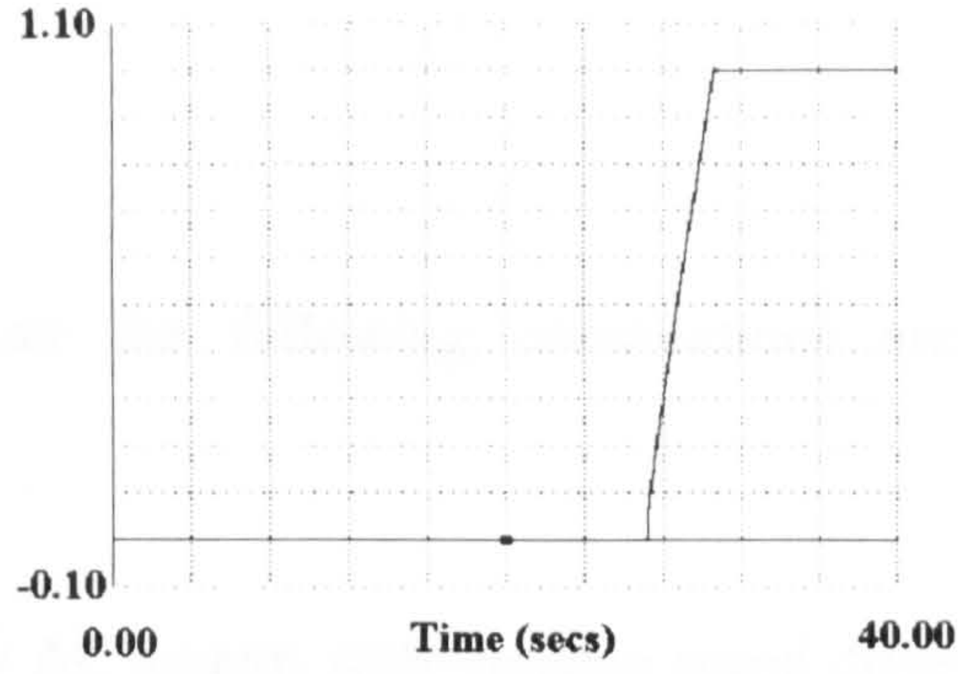

(b) Rotor speed (pu)

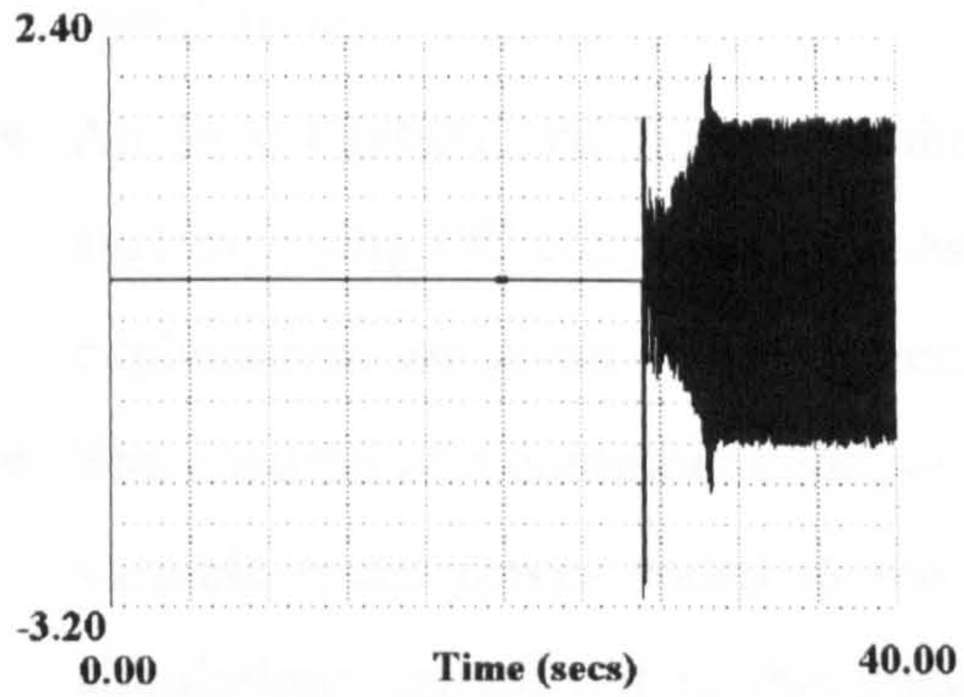

(c) Stator current phase-b (pu)

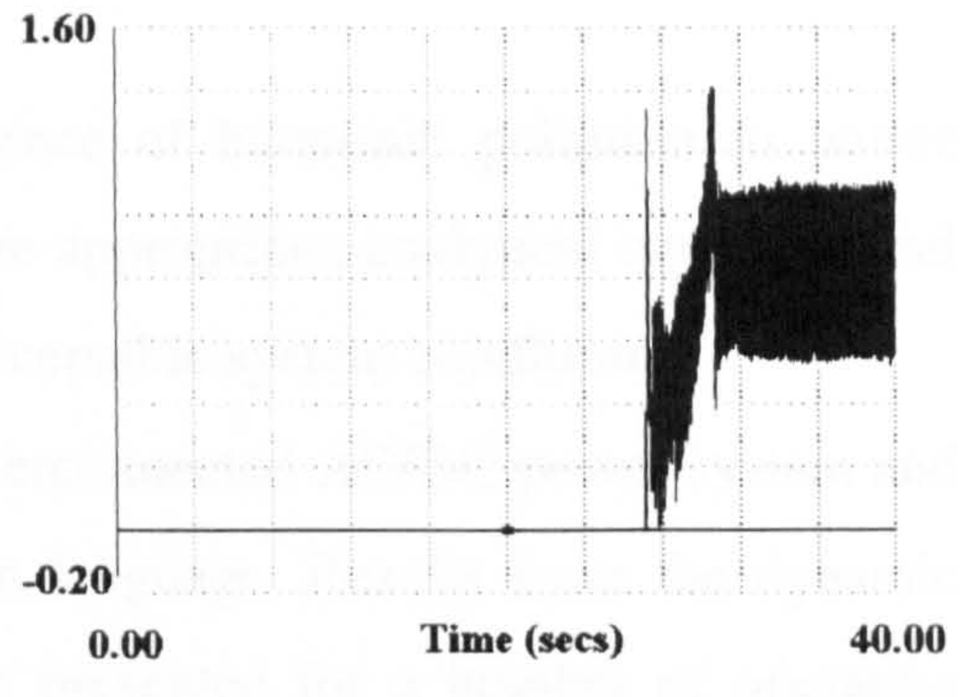

(d) Electromagnetic torque (pu)

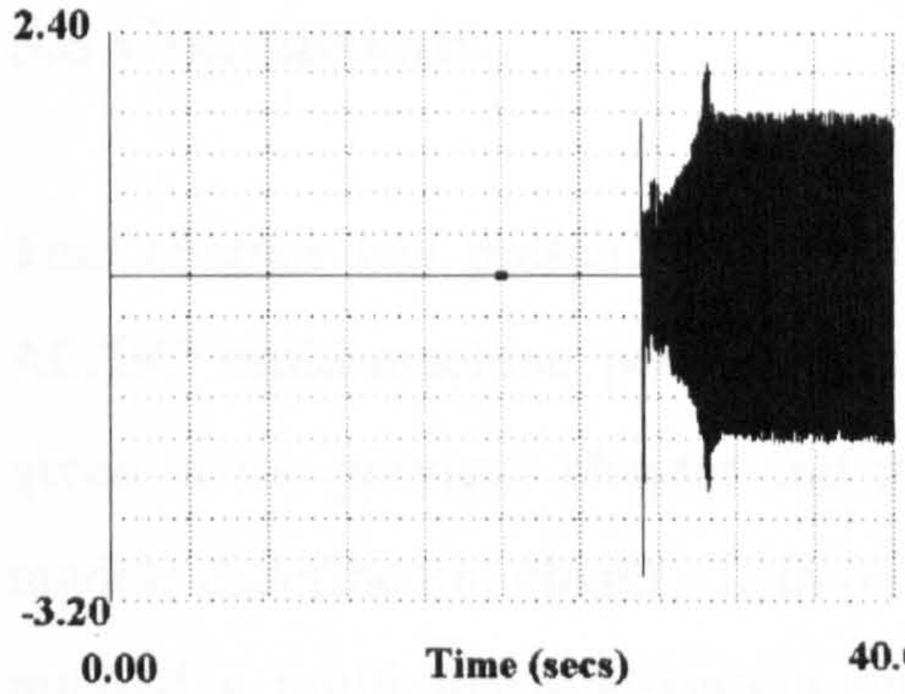

(e) Stator current phase-c (pu)

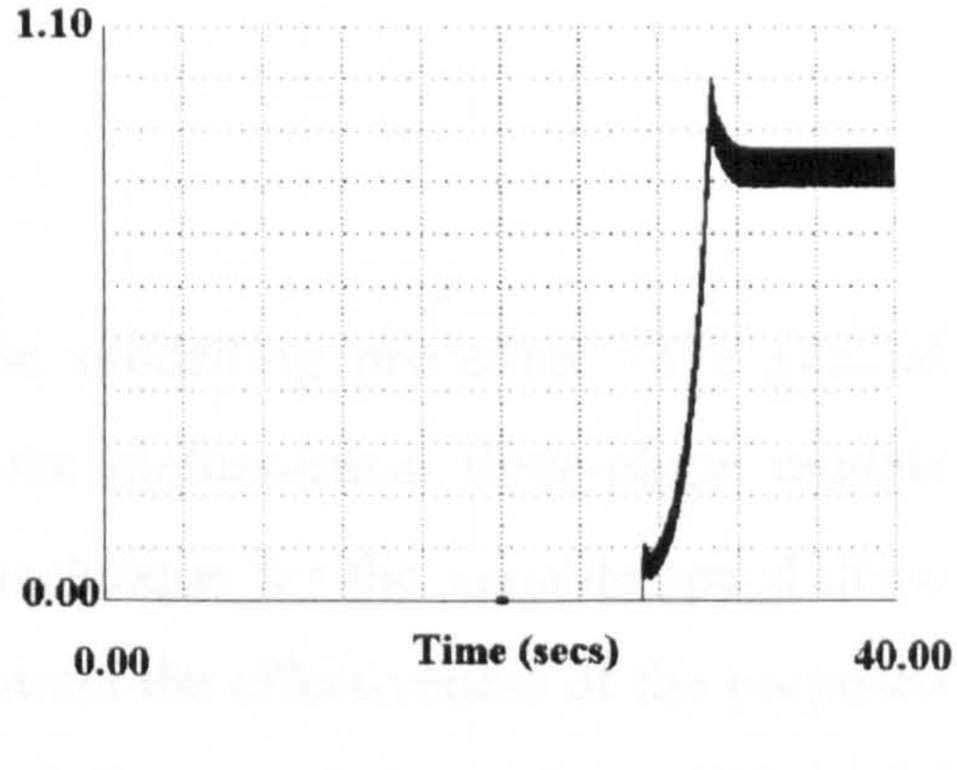

(f) DC current of the rectifier (pu)

Figure 5.23 Response of the variable speed drive 2

5.7 Contributions

From the research reported in this chapter the following contributions are identifiable:

- The combination of models of the primary AC system with variable speed drive models
- The development of a new generalised approach to power system modelling, which incorporates modelling of AC systems with DC converter stations/variable speed drives
- An investigation and report on the influence of harmonic pollution to power systems using DC converter stations. Where appropriate, analytical equations and explanations are given which will ensure acceptable system conditions
- The creation of a computer code for the interconnected AC/DC power system and variable speed drives coded in the Fortran language. Results from the dynamic simulations carried out in this chapter are presented for a number of operating conditions
- Consideration and investigation of the technical benefits associated with the use of filters for use in AC/DC power systems (in terms of less harmonic distortion).

5.8 Conclusions

This chapter has presented and described the modelling procedure of a general AC/DC multi-machine power system, using the mathematical three-phase models given in the previous chapter and the PWM technique for the variable speed drive models described in chapter 1. In order to illustrate the effectiveness of the proposed method a multi machine-system was used and the set of three-phase differential equations, needed to solve the system was described. Finally, the developed computer program was used to simulate examples of multi-machine AC/DC power systems (with or without filtering) using variable speed drive models.

The simulation results show that the developed computer program is capable of simulating various types of generation, load systems and variable speed drives with different configurations when subjected to various operating conditions.

5.9 References

1. Mohan N, "A novel approach to minimise line-current harmonics in interfacing power electronics equipment with 3-phase utility systems", IEEE Transactions on Power Delivery, Vol.8 , No. 3, July 1993, pp 1395-1403.
2. Alves J, Pilotto L, Watanabe E, "An adaptive digital controller applied to HVDC transmission", IEEE Transactions on Power Delivery, Vol. 8, October 1993, pp 1851-1859.
3. Smith J.R "Response analysis of A.C electrical Machines-computer models and simulation", Research Studies Press Ltd, 1990
4. Say M.G. "Alternating Current Machines", Longman Scientific & Technical 1983
5. Buamud M.S "Dynamic Response Analysis of Large AC Generation systems", PhD thesis, University of Strathclyde, 1995.
6. Weedy B.M "Electric Power Systems", John Wiley & Sons Ltd 1987
7. Siemens Review : Energy and Automation, Vol 88, 1988
8. Magnusson P, "Resistively Bridged Harmonic Filter for Power Converters", IEEE Transactions on Power Apparatus and systems, Vol PAS-87, June 1968, pp 1481-1484.
9. Taleb M, Ortmeyer T.H., "Examination of the current injection technique", IEEE Transactions on Power Delivery, Vol 7, January 1992, pp 442-448.
10. Emanuel A, Yang M, "On the harmonic compensation in nonsinusoidal systems", IEEE Transactions on Power Delivery, Vol 8, January 1993, pp 393-399.
11. Mohan N, Rastogi M, Naik R, "Analysis of a new power electronics interface with approximately sinusoidal 3-phase utility currents and a regulated dc output", IEEE Transactions on Power Delivery, April 1993, pp 540-546.
12. Grotzbach M, Frankkenberg W, "Injected currents of controlled AC/DC converters for harmonic analysis in industrial power plants", IEEE Transaction on Power Delivery, Vol 8, April 1993, pp 511-517.
13. Woodford D, "Secondary arc effects in AC/DC hybrid transmission", IEEE Transactions on Power Delivery, 1992, pp 704-711.

14. Carpinelli G., Gagliardi F., Russo M., Sturchio A., "Steady state mathematical models of battery storage plants with line-commutated converters", IEEE Transactions on Power Delivery, Vol. 8, No.2, April 1993, pp 494-501.

15. Hingorani N.G., Hay J.L, Crosbie R.E., "Dynamic simulation of h.v.d.c transmission systems on digital computers", Proceedings of IEE, May 1966, pp 793-805.

16. Htsui J.S.C., Shepherd W., "Method of digital computation of thyristor switching circuits", Proceedings of IEE, August 1971, pp 239-242.

17. Rumph E., Ranade S., "Comparison of suitable control systems for HVDC stations connected to weak ac systems. Part II. Operational behaviour of the HVDC transmission", IEEE Transactions on Power Delivery, May 1971, pp 555-564.

18. Hingorani N, Burbery F., "Simulation of AC system impedances in HVDC system studies", IEEE Transactions on Power Apparatus and Systems, May 1970, pp 819-826.

19. Rumph E., Ranade S., "Comparison of suitable control systems for HVDC stations connected to weak ac systems. Part I. New control systems" Transactions on Power Delivery, May 1971, pp 549-555.

20. Bowles, J.P, "AC System and transformer representation for HVDC transmission studies", IEEE Transactions on PAS, Vol PAS-89, No. 7, Sept/Oct 1970, pp1603-1608.

21. Owen, R.E., McGranaghan M.F, Vivirito J.R, "Distribution System Harmonics: Controls for large power converters", IEEE Transactions on Power Apparatus and Systems, Vol PAS-101, No 3 March 1982, pp 644-648.

22. Reeve J, and Subba Rao, T. "Dynamic Analysis of Harmonic Interaction between AC and DC Power Systems", IEEE Transactions on PAS, Vol. PAS-93, No.2, March/April 1974, pp 640-646.

23. Mohan N, Underland T, Robbins W ,"Power electronics: Converters, Applications and Design", John Wiley and Sons 1995.

24. Krause, P.C. "Analysis of electrical machinery", McGraw-Hill Book Company, New-York, 1987.

25. Smith J.R. and Chen Meng-Jen, Three-Phase Electrical Machine Systems-computer simulation, Research Studies Press Ltd, 1993.

26. Serafi E, Shehata S, "Digital simulation of an AC/DC system in direct-phase quantities", IEEE Transactions on Power Apparatus and Systems, Vol PAS-95, No 2, 1976, pp 731-742.

27. IEEE Recommended Practices and Requirements for Harmonic Control in Electrical Power Systems, April 1993.

CHAPTER 6

FACTS APPLICATIONS AND BENEFITS IN AC TRANSMISSION SYSTEMS

6.1 Introduction

High voltage transmission systems are increasingly stressed because of the increase in demand and because of restrictions on building new lines due to environmental and cost concerns. Also bulk power transfers over substantial distances are on the increase in highly interconnected networks. Less new transmission capacity means that more generation resources would be required locally which may not be economical. Significant enhancements are therefore needed to transmission capabilities, but they have to be acceptable to the public environmentally as well as be received with enthusiasm by planners in publicly or privately owned utilities. [1,2,3].

The operation of an AC power transmission network is generally constrained by limitations on one or more specific plant items, even though plant in other parallel transmission lines may have adequate capability to carry additional amounts of power. This is a consequence of the free flow mode of operation of AC transmission networks which results in the power flow on individual transmission circuits being determined by the relevant characteristics of the transmission network itself. (Kirchhoff's Law).

This free flow mode of transmission network operation can be contrasted with a vision of a controlled power flow mode of operation where the power flow through one or more transmission lines is controlled in a predetermined manner. This vision can be achieved, and the natural behaviour of the network modified, through the application of power flow control devices at strategic locations. The use of such devices could reduce the need for additional network facilities by improving the utilisation and performance of existing facilities.

FACTS is an acronym for flexible AC transmission systems[3,4]. The philosophy of FACTS is to use power electronic controlled devices to control power flows in a transmission network, thereby allowing transmission line plant to be loaded to its full capability. The significant impact that FACTS devices will make on transmission systems arises from their ability to effect high-speed control. Currently, the main control actions in a power system, such as changing transformer taps, switching current or governing turbine steam pressure, are achieved through the use of mechanical devices which necessarily impose a limit on the speed at which control action can be made. FACTS devices are based on solid-state control and so are capable of control actions at far higher speed. The three parameters that control transmission line power flow are line impedance, magnitude and phase of line end voltages[5,6]. Conventional control of these parameters, although adequate during steady-state and slowly changing load conditions, cannot, in general be achieved quickly enough to handle dynamic system conditions. The use of FACTS technology will change this situation.

The objective of this chapter is to review potential FACTS applications in transmission systems, to present the advantages and benefits of power electronics based FACTS technology and to describe the circuitry of the main FACTS devices.

6.2 Structure of power systems

In practice, power systems operate at various voltage levels separated by transformers. From voltage-level point of view, a power network can be classified into the following subsystems :

1. Transmission system
2. Sub-transmission system
3. Distribution system

The transmission system interconnects all major generation stations and main load centres in the system. It operates at the highest voltage level(typically, 230kV and above) and handles large amount of power.

The sub-transmission system transmits smaller amount of power from transmission substations to distribution substations. Large industry customers are served directly by the sub-transmission system. Typically, voltage varies between 11kVand 132kV.

The distribution system represents the final stage in the transfer of power to the individual customers. The primary distribution voltage is typically between 4kV and 34.5 kV. Small industrial customers are supplied by primary feeders at this voltage level. The second distribution feeders supply residential and commercial at 120/240V.

6.3 Requirement for new solutions in transmission systems

Power system planners and operators are aware of the limitations imposed on electric transmission networks. The present situation is characterised by the following :

1. Increase in consumption of electrical power

In developing countries, there is a rapidly rising demand for electricity created by industrialisation and urbanisation coupled to population increase. In industrial countries the electricity fraction of the total energy consumption is also increasing, because electricity is important to achieve productivity increases.

2. Growing public concern

Although electricity is being increasingly used, there is a concern at the impact of new transmission facilities. Biological effects of electrical magnetic fields are being investigated.

3. Regulatory constrains

Obtaining right-of-way licences for construction of new transmission lines is becoming difficult and time consuming.

4. Improved utilisation of existing facilities

In this aspect, an increase in power transfer capability in existing transmission routes would be very beneficial. The economic advantage offered by deferring large and difficult investments in new facilities is also obvious.

By analysing the above mentioned transmission market environment and needs, one can draw the conclusion that the market will require new solutions in transmission systems.

Phase shifting of a given bus can be achieved using a force-commutated converter that adds a voltage of controlled magnitude and angle in series with the line.

Amplitude control of bus voltage can be performed by using a Static Var Compensator, using conventional thyristor technology.

6.4 FACTS -Custom power technology

Power systems are at the beginning of a significant change that is technology and market driven by microelectronics (computers and microprocessors), communications and power electronics. The combined impact of these technologies

is important for both transmission and distribution, by making them more reliable, controllable and efficient.

FACTS (Flexible Alternating Current Transmission Systems)- the use of high-power electronics to enhance the controllability and capacity of utility transmission systems.

Custom power- customised electric service for industrial and commercial customers through the application of power electronics on utility distribution networks.

Facts and custom power technologies can be utilised respectively to improve the utilisation of ac networks and the quality of the supply of ac power. Developments in each of these applications areas are conditioned heavily by advances in power semiconductor devices, whether thyristors or fully controlled devices.

6.5 Potential FACTS applications

a. Parallel power flow

For the power system shown in Fig. 6.1, if we consider the flow of power from

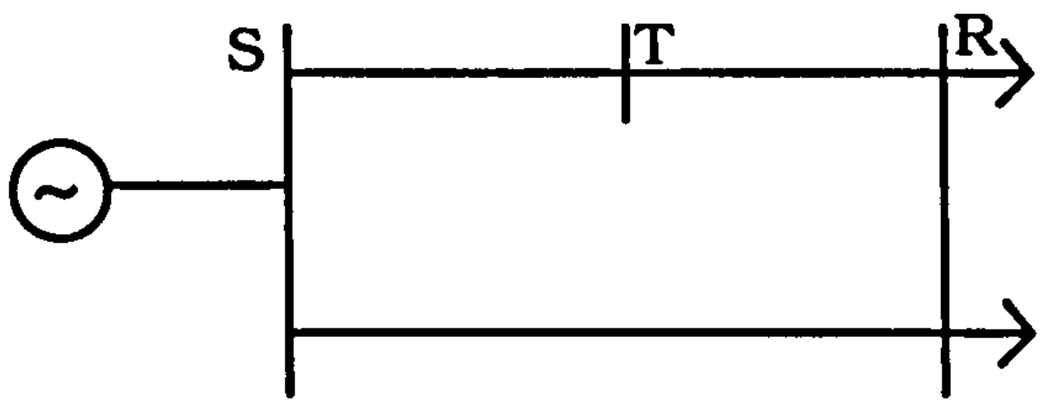

Figure 6.1

busbar S to busbar R, there is no way of individually setting the power flow through each circuit, either directly from S to R, or via T. The load sharing is entirely governed by the line impedances, i.e. it is inflexible. If the impedances are dissimilar, one circuit may never realise its full thermal capacity when operating in parallel with the other circuit. One possible way of controlling the load sharing between circuits is by the use of HVDC schemes as shown in Fig.6.2

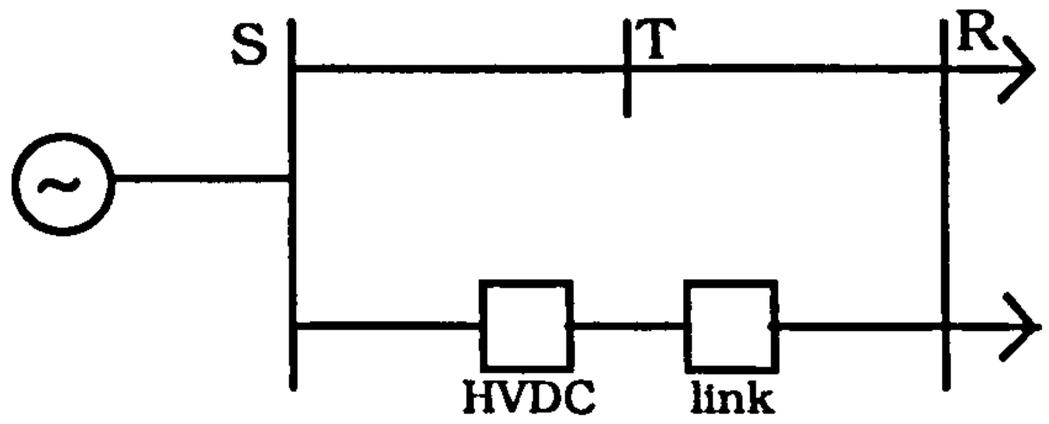

Figure 6.2

The power flowing along the HVDC path can be electronically controlled by adjusting converter firing angles; it is thus possible to load each circuit separately. However, the use of HVDC schemes is unlikely to be an economic solution to the problem of improving circuit utilisation since it requires the installation of costly converter equipment on one circuit and rebuilding of the overhead lines or cables.

The use of FACTS technology is a more attractive option since FACTS devices can be fitted retrospectively to existing AC transmission routes, thus providing an economic solution[7-11]. For this case, a FACTS device, e.g. controlled series capacitor or phase shifter, is fitted in the circuit and provides control over system electrical parameter as shown in Fig. 6.3.

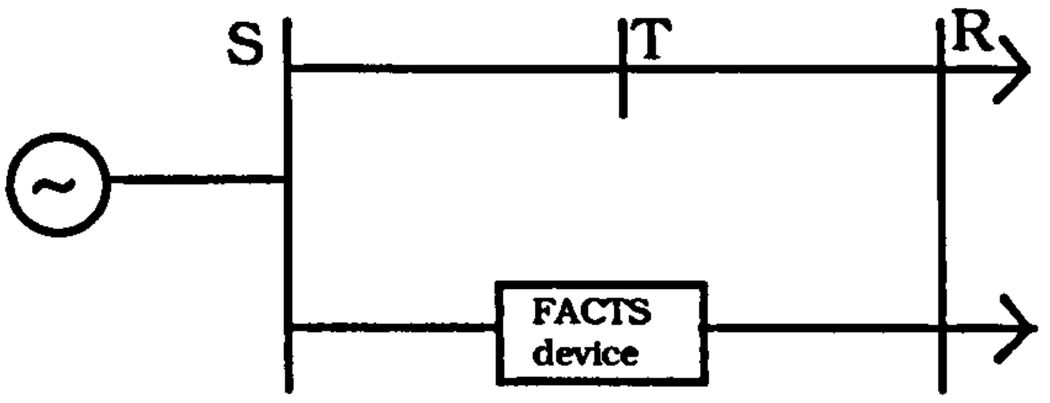

Figure 6.3

It is important to appreciate that FACTS control of AC transmission is effective not only during steady-state conditions, but also during system transient conditions, such as caused by unexpected line outages, where it may be important for the stability of the system to control power flow through a critical circuit in the power system.

b. Voltage limits

Voltage control to avoid overvoltages or undervoltages is achieved by injection or absorption of reactive power(using power electronic converters) into the network [2-4]. Conventionally used methods are generator reactive power adjustment by excitation control, mechanical tap changers on transformers, and shunt reactors or capacitors which may be fixed or mechanically switched by circuit breakers (or load switches).

c. Stability limits

Power flow along a transmission line is a function of the sending and receiving end voltages, as shown in Figure 6.4.

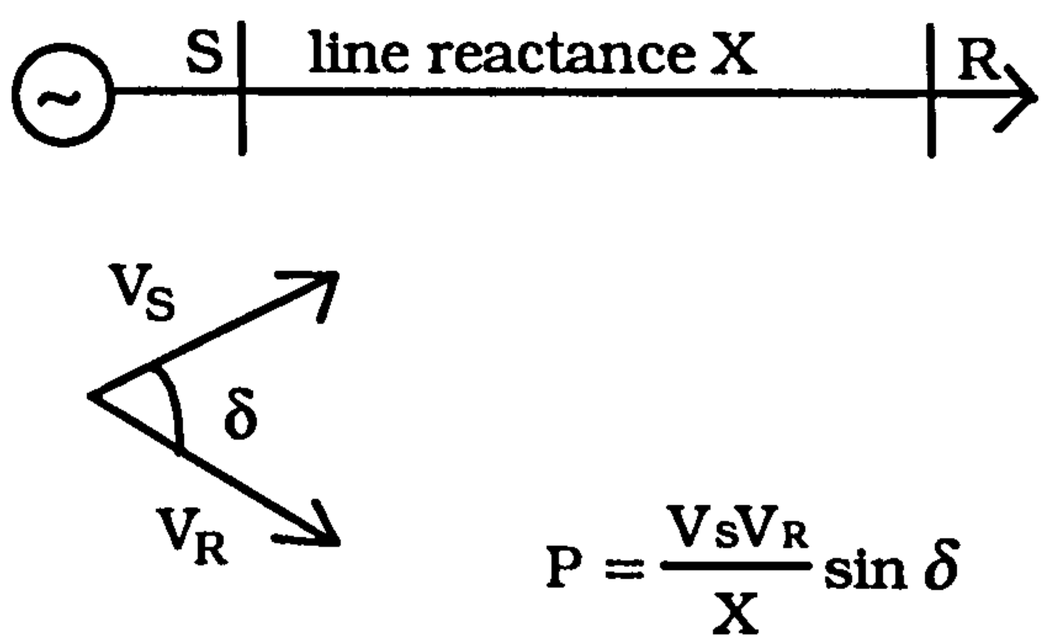

Figure 6.4

Assuming that busbar magnitudes are maintained at fixed levels, in order to increase power flow, we must increase δ, the angle between V_S and V_R. However, increasing δ increases the rise of transient and voltage stability problems if a fault were to occur along the line. Since power systems are far more complex than Fig. 6.4, so too is the problem of stability and more complicated techniques need to be sought to assess stability in highly interconnected systems. In the case of some unexpected 'shock' to

the system, such as unscheduled out-load switching or a line fault, a generator is subject to an instantaneous loading change.

Shocks to the systems may lead to a oscillation which slowly build up over a period of time to result in pole slipping and loss of synchronism. FACTS technology can 'alleviate' both transient and dynamic instability problems. FACTS devices inherently increase stability margins, thus allowing greater circuit loading before the stability constraint is met. The high-speed control action of FACTS devices helps to dampen down power oscillations that would otherwise cause loss of synchronism.

d. Thermal limits

On-load temperature rise of conductors, transformers, reactors, series, capacitors etc. is an inherent limitation on the power transfer capability of a transmission system. Lines are typically operated well below their thermal limits in order that a substantial margin is available for outage contingencies following a disturbance. FACTS devices allow secure loading of transmission lines to their thermal limits, while avoiding overloading.

6.6 Main benefits of FACTS

(a) Cost: Due to the high capital cost of transmission plant, cost considerations frequently outweigh all other considerations. Compared to alternative methods of solving transmission loading problems FACTS technology is often the most economic alternative.

(b) Convenience: All FACTS devices can be retrofitted to existing AC transmission plant with varying degrees of ease. Compared to HVDC or six-phase transmission schemes, solution can be provided without widescale system disruption and within reasonable timescale.

(c) Environmental impact: It is common for environmental opposition to frustrate attempts to establish new transmission routes. FACTS technology however, allows greater throughput over existing routes.

6.7 Semiconductor technology

The main workhorse of FACTS technology is the thyristor. One fundamental limitation to the use of the conventional thyristor is that the device can only be turned off at the next current zero crossing. The only turn-on, turn-off device currently available in sizes large enough to be used in FACTS devices is the gate-turn-off thyristor (GTO).

The GTO is a gated thyristor which can be turned off by a negative gate current pulse. However, further developent is needed before GTOs find widespread application due to high losses, high gate currents and low operating frequencies. Several prototype FACTS devices have however, been developed using GTOs[12-16].

The high switching losses associated with GTOs limit their use to relatively low frequencies, typically up to about 1 kHz.

Although not yet available in ratings comparable with GTOs and thyristors, the IGBT has much lower switching losses that the GTO and is therefore much better suited to applications involving switching frequencies in excess of about 1 kHz. IGBTs have minimal gate drive and snubbing requirements; moreover, voltage and current ratings of IGBTs have recently been increasing rapidly.

6.8 Typical FACTS devices

After the FACTS operation concepts in transmission systems have been reviewed, it comes to the conclusion that FACTS technology can be presently utilised in

transmission systems using high power electronic devices. Some FACTS devices such as SVC, STATCON and TCSC have been implemented in practical systems and more experiences of FACTS operations have been obtained. The following sections will illustrate those power electronic based FACTS devices which have been used or will soon be installed in practical systems.

a. Static Var Compensators

Figure 6.5 shows the fundamental circuit configurations for SVC systems which can be divided into two basic categories:

- Systems with fixed capacitors and thyristor-controlled reactors(FC - TCR types);
- Systems with thyristor-switched capacitors and thyristor-controlled reactors (TSC/TCR types).

The fixed capacitors in the FC/TCR system may be omitted, switched by circuit breakers or integrated into the filters provided to absorb the current harmonics generated by the TCR.

The combination of thyristor-controlled capacitors and reactors makes it possible to set any desired operating point over a predetermined VAr range within its capacitive and inductive limits.

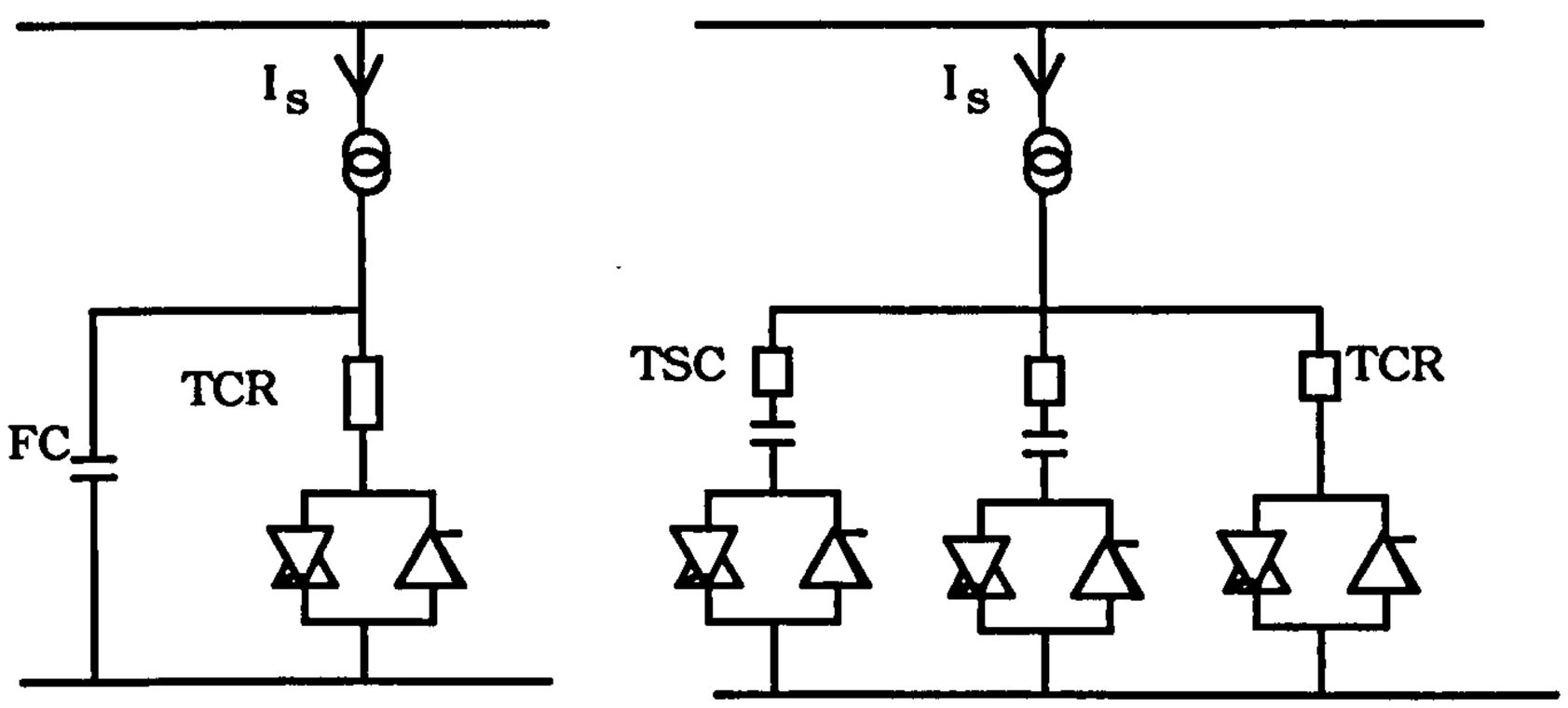

a. b.

Figure 6.5

For applications in high voltage networks, a step-down transformer is required for matching the optimised electrical data of the semiconductor devices. For both schemes a 12-pulse connection through two wye-delta connected transformer secondaries eliminates a large portion of harmonics.

Which arrangement is actually more economical depends upon the particular system in question, with account being taken of:

- loss characteristic over the control range;
- damping of the harmonics generated by the TCR;
- equipment layout;
- protection scheme for the thyristor valves.

In general, in a SVC with proper coordination of the capacitor switching and reactor control, the Var output can be varied continuously between the capacitive and inductive rating of the equipment.

A complete SVC model with its associated controls will be presented in a succeeding chapter.

b. Static Condeser (STATCON)

The Advanced Static Var Compensator (known also as a static condeser or STATCON) consists of a GTO-based power converter (inverter) whose DC side is connected to a capacitor. Its AC side is connected to the line through a transformer. Fig. 6.6 illustrates a STATCON.

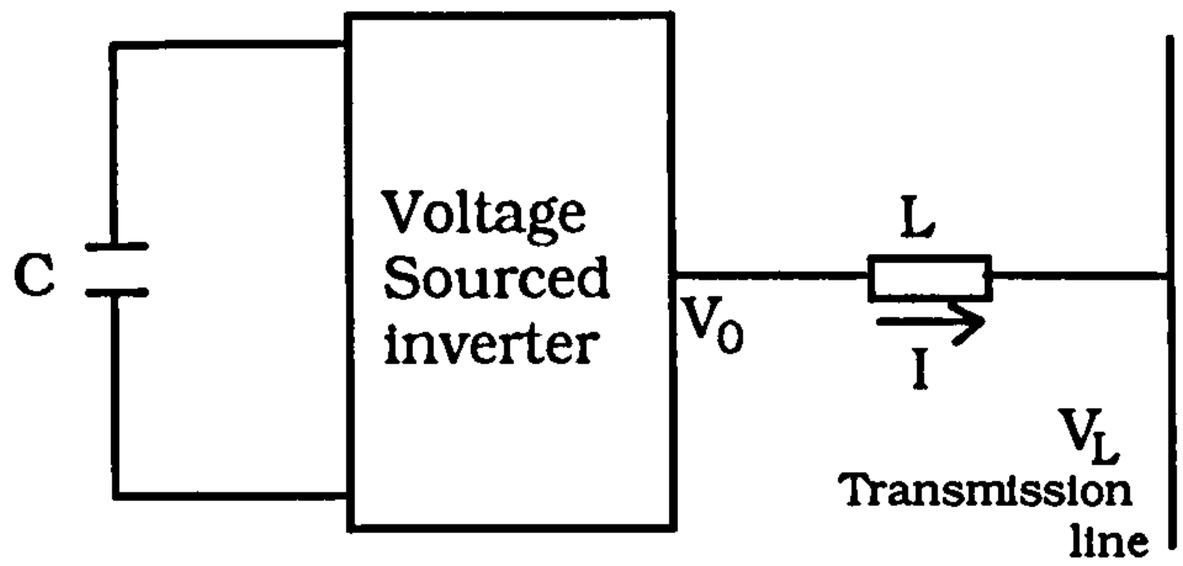

Figure 6.6

By controlling the inverter output voltage, leading or lagging reactive current can be drawn from the line. The steady state characteristics of the equipment are very similar to those of rotating synchronous condenser.

As there are no sizeable power sources or sinks associated with the inverter and its DC-side components, the real power must be actively controlled to a value which is zero on average and which departs from zero only to compensate for the losses in the system.

A STATCON model connected to a power system will be presented and analysed in a following chapter.

c. Thyristor controlled series compensator (TCSC)

The TCSC is normally operated in the capacitive region[17,18]. Control of the TCSC is possible within its reactance limits. Hence the control for the TCSC is essentially meant to vary the reactance of the TCSC to meet a particular objective. Here, the constant angle control is proposed which is aimed at regulating the voltage drop across the line. The objective is to regulate the power flow in the parallel paths particularly during contingency conditions.

The figure under study is:

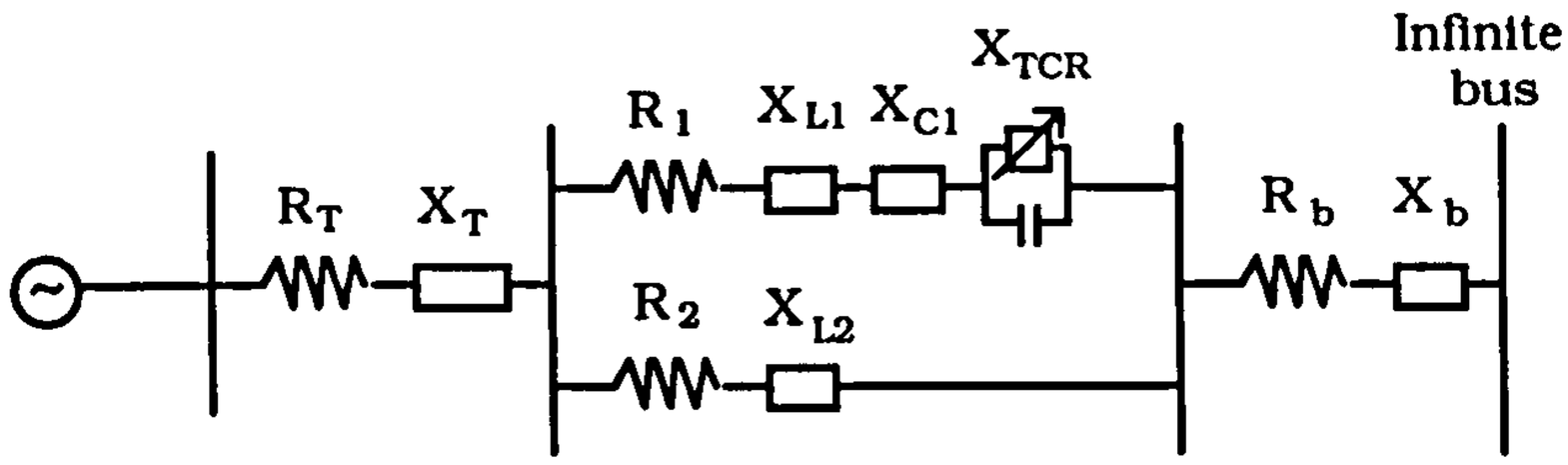

Figure 6.7

If $\hat{V}$ is the voltage across the line(which includes $R_1, X_{L1}, X_{C1}, X_{TCR}$) and $\hat{I}_L$ is the current flowing through the line, X_L the line reactance $(X_{L1} + X_{C1})$ and $\hat{V}_{TCSC}$ the voltage across the TCSC, then neglecting the line resistance, the control objective is

$$V = \left| I_L \cdot X_L + V_{TCSC} \right| = K \text{ (constant)} \quad (6.1)$$

Hence, $I_L = \left(K - V_{TCSC}\right) / X_L = I_{TCSC}$, V_{TCSC} is assumed to be positive in the inductive region and negative in the capacitive region. Therefore, if we choose a slope $S_K = -1 / X_L$, in the control characteristic then the voltage across the line can be kept at a constant. This type of control is expected to reduce power angle swings.

The controller for the TCSC is shown in Figure 6.8.

The TCSC current, I_{TCSC} and the voltage across the TCSC, V_{TCSC} weighted by a factor of S_K representing the voltage drop are fed to the reference junction. T_t represents the transducer time constant assumed equal for voltage and current measurements. The error signal I_e (the difference between the sensed current and the reference current I_{REF}) is integrated. This results in a change of the firing angle of the thyristor to appropriately correct the effective reactance of the TCSC. The limits X_{CMIN} and X_{CMAX} represent the minimum and the maximum values of the TCSC reactance.

A typical TCSC is illustrated in figure 6.9.

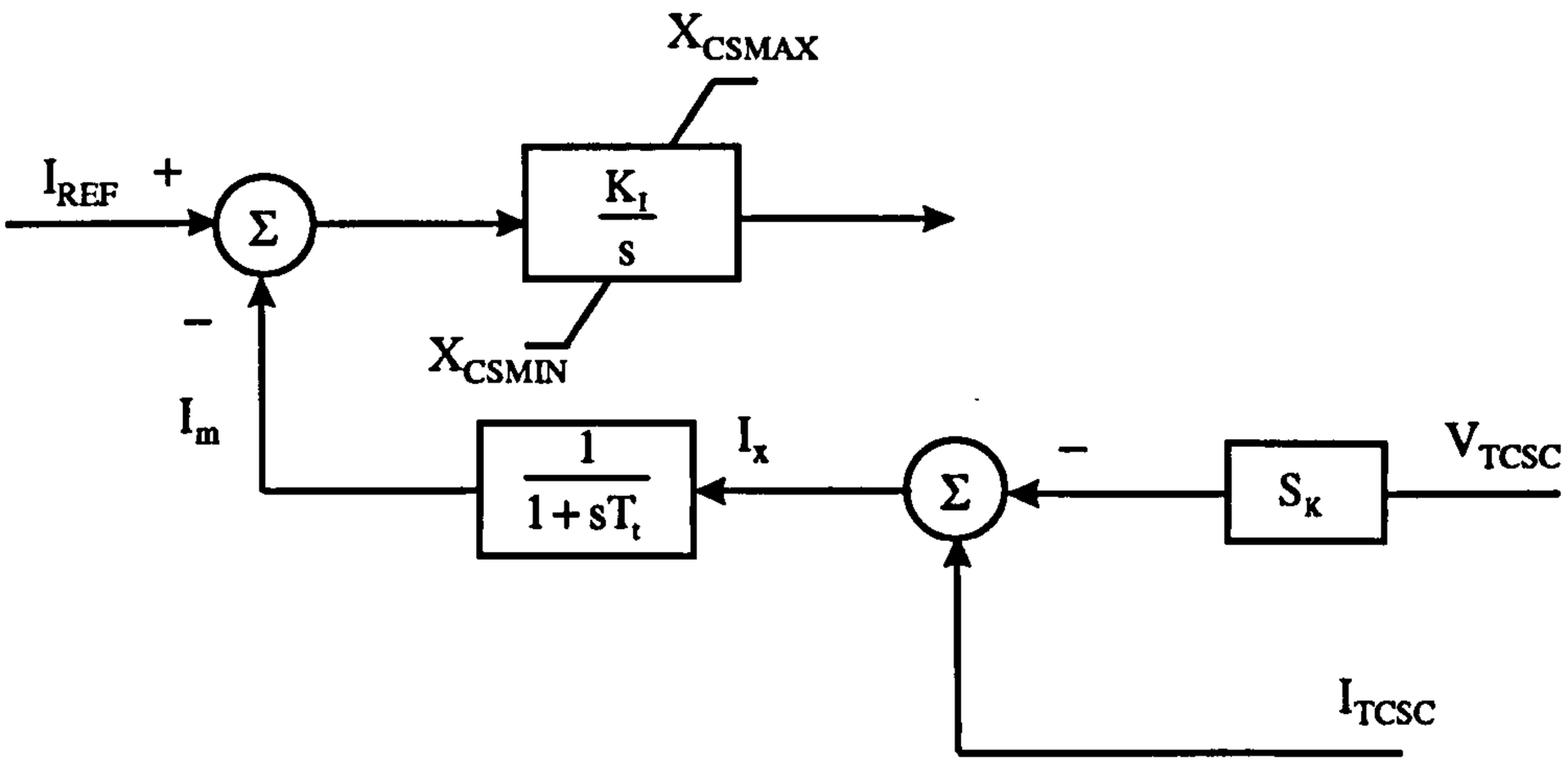

Figure 6.8

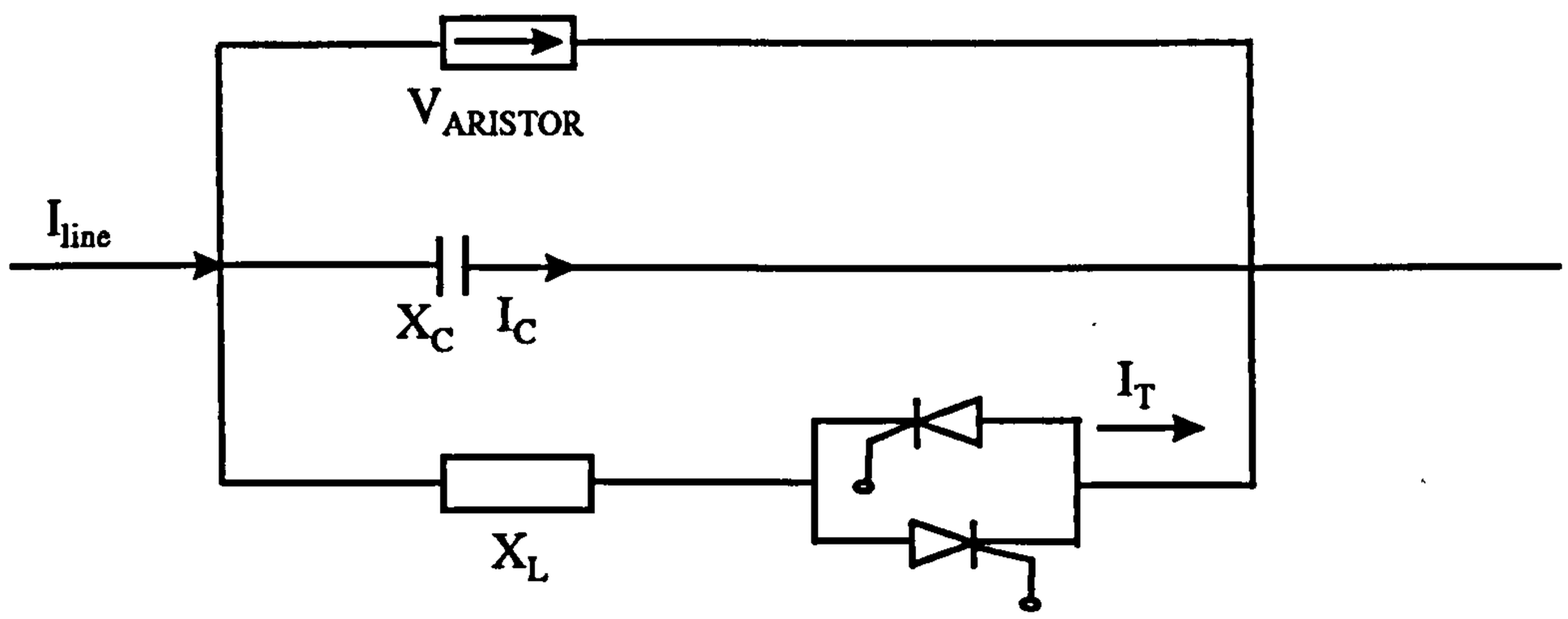

Figure 6.9

The varistor is used for the protection of the capacitor.

From the known value of the susceptance a TCSC circuit we can calculate the firing angle by using a non-linear relationship. The output of the pulse generator goes to the thyristor valves, controlling in this way the TCSC circuit[18].

d. Unified power flow controller (UPFC)

The Unified Power Flow Controller (UPFC) consists of two switching inverters, which in the implementation considered are voltage-sourced inverters using gate turn-off (GTO) thyristor valves, as illustrated in Figure 6.10.

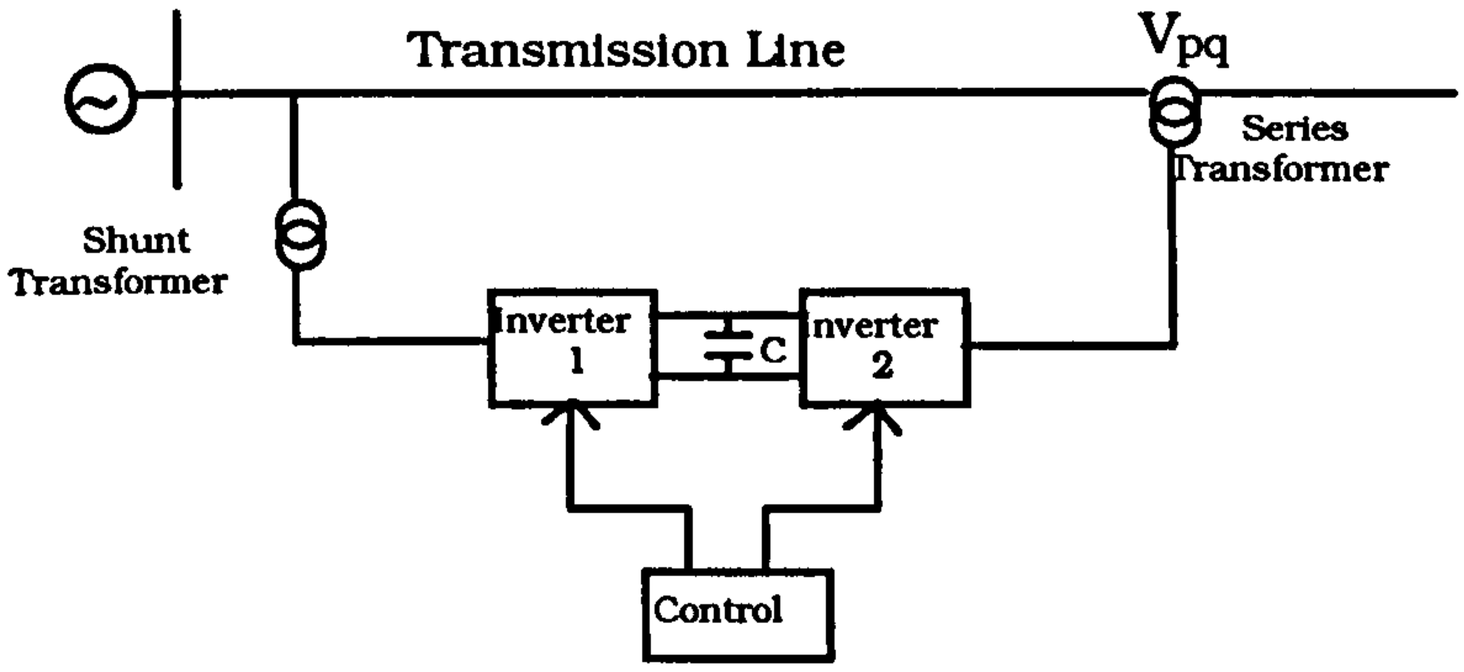

Figure 6.10

These inverters, labelled 'Inverter 1' and Inverter 2' in the figure, are operated from a common dc line provided by a dc storage capacitor. This arrangement functions as an ideal ac to ac power converter in which the real power can freely flow in either direction between the ac terminals of the two inverters and each inverter can independently generate (or absorb) reactive power at its own ac output terminal.

Inverter 2 provides the main function of the UPFC by injecting ac voltage V_{pq} with controllable magnitude V_{pq} and phase angle at the power frequency, in series with the line via an insertion transformer. This injected voltage can be considered essentially as a synchronous ac voltage source. The transmission line current flows through this voltage source resulting in real and reactive power exchange between it and the ac system. The real power changed at the ac terminal (ie at the terminal of the insertion transformer) is converted by the inverter into dc power which appears the dc line as positive or negative real power demand. The reactive power exchanged at the ac terminal is generated internally by the inverter. The basic function of Inverter 1 is to supply or absorb the real power demanded by Inverter 2 at the common dc link. This dc link power is converted back to ac and coupled to the transmission line via shunt-connected. Inverter 1 can also generate or absorb controllable reactive power, if it is desired, and thereby it can provide independent shunt reactive compensation for the line. It is important to note that whereas there is a closed 'direct' path for the real power negotiated by the action of series voltage injection through Inverters 1 and 2

back to the line, the corresponding reactive power exchange is supplied or absorbed locally by Inverter 2 and therefore it does not flow through the line. Thus, Inverter 1 can be operated at a unity power factor or be controlled to have a reactive power exchanged with the line independently of the reactive power exchanged by Inverter 2. This means that there is no continuous reactive power flow through the UPFC[19-25].

The PWM method is used to control both converters. A UPFC model connected to a power network will be presented and analysed later in the thesis.

6.10 Conclusions

This chapter described the potential applications of a new established power electronics technology, Flexible Alternating Current Transmission Systems(FACTS). The advantages and benefits of power electronic based FACTS technology were summarised. The main FACTS devices were presented and an analysis into their operating principles were reported. This chapter provided a background for further discussion on FACTS devices in the following chapters.

6.11 References

1. IEE: Flexible AC Transmission Systems (FACTS) - "The Key to Increased Utilisation of Power Systems", IEE Colloquium Digest, January, 1994, London, No .087, p. 10/1p.
2. Thanawala, H.L., "Voltage Control and Stability and Improved Quality of Electricity Supply", Symposium of Power Engineering Innovations and Environment, Nov. 1992, Hong Kong.
3. Lavsey, E., Weaver, T. IEEE-CIGRE Working Groups Joint Document: "FACTS Overview", IEEE Publication April, 1995, pp 95-108.
4. Le Du A. Toutini, "Which FACTS Equipment for Which Need? ",CIGRE Winfield, Paris, France, 1992, Paper 14/37/38-08.
5. Gyugyi, L., "Unified Power-flow Control Concept for Flexible AC Transmission Systems", IEE Proceedings, Vol. 139. No. 4, July, 1992, pp 478-483.
6. Gyugyi, L. "Reactive power Generation and Control by Thyristor Circuits", IEEE Trans. Ind. Appl. 1979, pp A1-A15.
7. Schauder, C. "Vector Analysis and Control of Advanced Static VAR Compensators" IEE Proceedings - C, Vol. 140, No. 4, July 1993, pp.299-306.
8. Paserba, John, "A Thyristor Controlled Series Compensation model for Miller, N.Power System Stability Analysis IEEE Transactions on PowerDelivery, Vol. 10, No. 3, July 1995, pp 743-751.
9. Mohan N "A novel approach to integrate computer exercises into teaching of utility-related applications of power electronics", IEEE Transactions on Power systems", February 1992, pp 359-364.
10. Schauder, C. "Development of a ±100 MVAR Static Condenser for Voltage Control of transmission systems", IEEE Transactions on Power Delivery, Vol 10., No3, July 1995, pp 1486-1493.
11. J Y Liu, Y H Song, A M Foss "Digital studies and simulation of the PWM UPFC using EMTP", Proceedings of the sixth IEE AC/DC International Conference IEE, London,1996, pp 351-356.

12. Tenorio A.R.M., Ekanayake J.B., Jenkins N, "Modelling of FACTS devices", IEE AC/DC Power transmission, 1996, pp 340-346.

13. Menzies R.W., Zhuang Y, "Advanced static compensation using a multilevel gto thyristor inverter", IEEE Transactions on Power Delivery, No.2, April 1996, pp 732-738.

14. Akagi H, Kanazawa Y, Nabae A, "Instantaneous reactive power compensators comprising switching devices without energy storage components", IEEE Transactions on Industry Applications, May-June 1984, pp 625-632.

15. Ooi B, Dai S, Wang X, "Solid state capacitive reactance compensators", IEEE Transactions on Power Delivery, April 1992, pp 914-921.

16. Jacobson D.A.N., Menzies R.W. "Comparison of thyristor switched capacitor and voltage source GTO inverter type compensators for single phase feeders", IEEE Transactions on Power Delivery, April 1992, pp 776-783.

17. Godart T, Imerce A, Chebli E, "Feasibility of thyristor controlled series capacitor for distribution substation enhancements", IEEE Transactions on Power Delivery, January 1995, pp 203-208.

18. Zhu W, Spee R, Mohler R.R., Alexader G.C, "An EMTP study of SSR mitigation using the thyristor controlled series capacitor", IEEE Transactions on Power Delivery, Vol 10, July 1995, pp 1479-1485.

19. S.D Round, Q.Yu, L.E. Norum, T.M Undeland, "Performance of a unified power flow controller using a d-q control system", AC and DC Power Transmission, 29 April-3 May 1996, No.423 1996, pp 357-362.

20. Q.Yu, S.D. Round, L.E. Norum, T.M. Underland, "A new control strategy for a unified power flow controller", EPE'95 pp 2.901-2.906.

21. L.Gyugyi, "Dynamic Compensation of AC Transmission Lines by Solid-State Synchronous Voltage Sources", IEEE Transactions on Power Delivery, Vol 9, No.2 April 1994, pp 904-911.

22. L.Gyugyi, "Unified power flow control concept for flexible AC transmission systems", IEE Proceedings Vol.139, No 4, July 1992, pp 323-331.

23. L.Hu, R.E.Morrison, "Simulation Study of a transmission system containing two unequally rated parallel lines and a UPFC", AC and DC Power Transmission, No.423,1996, pp 343-350.

24. Joncquel E, Lombard X, "A unified power flow controller model for the electromagnetic transients program" , EPE 1995, pp 2.173-2.178.

25. Yacamini R, Paschoareli D, "A unified power flow controller using space vector modulation control", EPE 1995, pp 2.540-2.545.

CHAPTER 7

MODELLING OF STATIC VAR COMPENSATOR

7.1 INTRODUCTION

In power systems, controlling the voltage throughout the network, as well as damping power and frequency oscillations, presents a continuous challenge to power system planners and operators. In order to run the integrated generation-transmission-distribution system in the most economic and reliable fashion and prevent it from collapse under all possible operating conditions, new control techniques are always in great demand. Advances in power electronics have introduced powerful tools to the electric energy transmission and distribution industry.

One of the major products is the Static Var Compensator (SVC). The excellent performance of such an economic and versatile device has been proven in the field[1]. SVCs have been successfully applied to power factor correction, load balancing and for dynamic voltage control[2,3,4]. Today the electric energy industry is facing a great challenge in meeting the increased load demand with highest reliability and by minimum transmission expenditure. With the availability of highly flexible and reliable micro-processor based controllers, it is now possible to introduce new algorithms to enable Static Var Compensators to enhance power system stability directly. In this regard, the basic issues which must be addressed are:

- system dynamic and transient stabilities
- increasing power transmission capacity
- damping power oscillations
- maintaining network voltage

This chapter describes the modelling of Static Var Compensator, a FACTS device that meets the above requirements. Firstly, a description of the modes of operation of the SVCs is given as well as a formulation of SVC voltage and current equations. Next an overview of previous work on SVCs is reported followed by a brief discussion of a SVC model for electromagnetic transient studies. Modelling of the main parts of the SVC is also presented and a number of case studies under steady state and transient conditions have been investigated. Finally comparison of the control and firing methods proposed in this chapter with other control methods and firing systems (such as the Phase Locked Loop) method is presented.

7.2 OPERATION MODES OF SVCs

Static Var compensators (SVCs) are shunt connected devices applied to power systems to solve a variety of problems. They are characterised by fast response, high reliability and flexibility. The response time of SVCs is in the range of 2-3 cycles.

The most prevalent types of compensators are the thyristor controlled reactor-fixed capacitor (TCR-FC) and the thyristor controlled reactor with thyristor-switched capacitor (TCR-TSC). The fixed capacitors in the TCR/FC system may be omitted, or integrated into the filters provided to absorb the current harmonics generated by the TCR. The combination of thyristor-controlled or fixed capacitors and thyristor controlled reactors makes it possible to set any desired operating point over a predetermined Var range within its capacitive and inductive limits. The only constraints are that the TCR rating can fully compensate the capacitive rating or that a switchable capacitor bank is graded accordingly. Figure 7.1 shows single phase arrangements of SVC models:

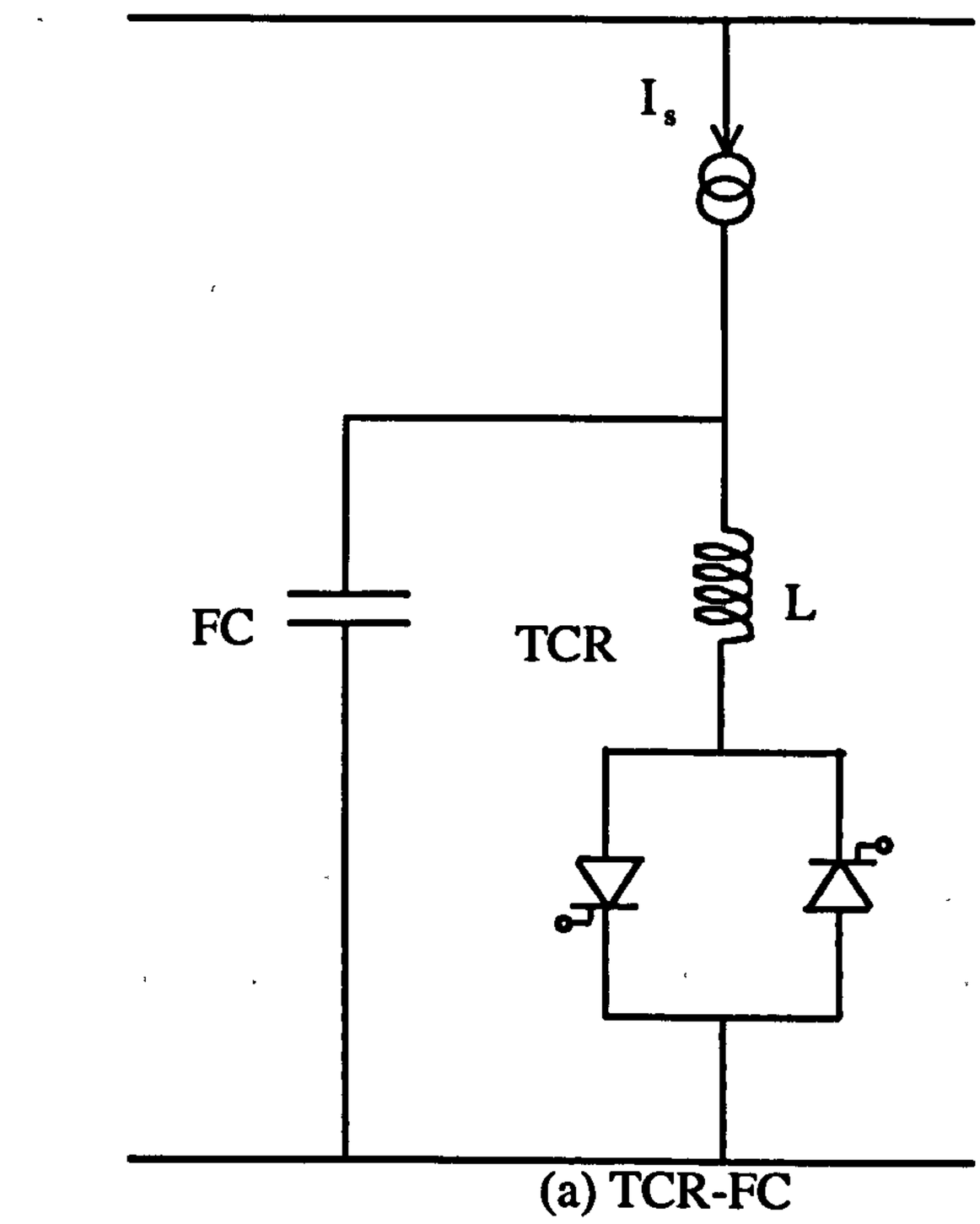

(a) TCR-FC

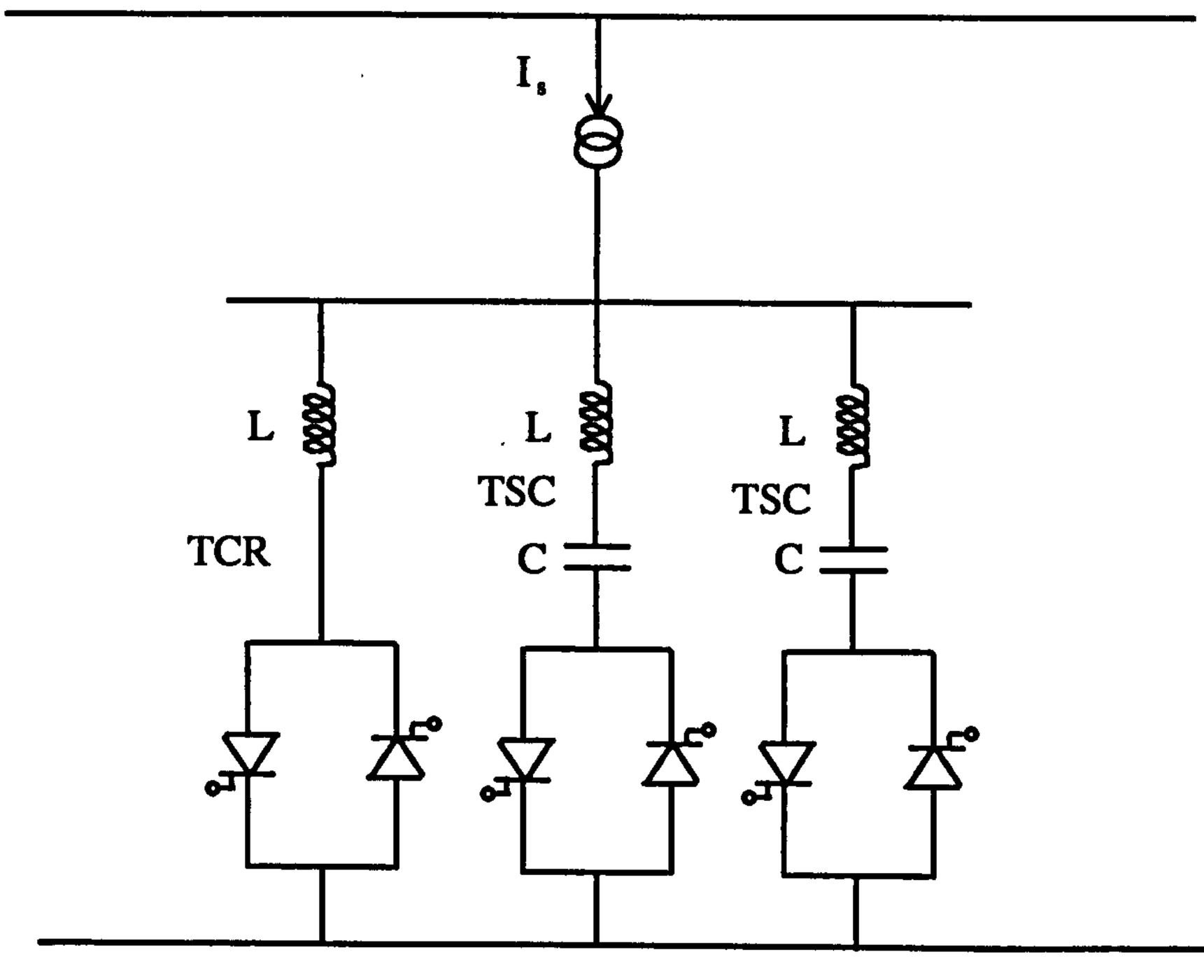

(b) TCR-TSC

Figure 7.1. Different types of SVC models

For applications in high voltage networks, a step-down transformer is required for matching the optimised electrical data of the semiconductor valves. For both schemes a 12-pulse connection through two Y and Δ connected transformer secondaries eliminates a large portion of harmonics.

7.2.1 Operation modes of Thyristor Controlled Reactors (TCRs)

In the thyristor controlled reactors (Fig 7.2) the thyristors conduct on alternate half-cycles of the supply frequency. The current flow in the inductor L is controlled by adjusting the conduction interval of the back to back connected thyristors. This is achieved by delaying the closure of the thyristor switch by an angle α (referred to as the firing angle), in each half cycle with respect to the voltage zero.

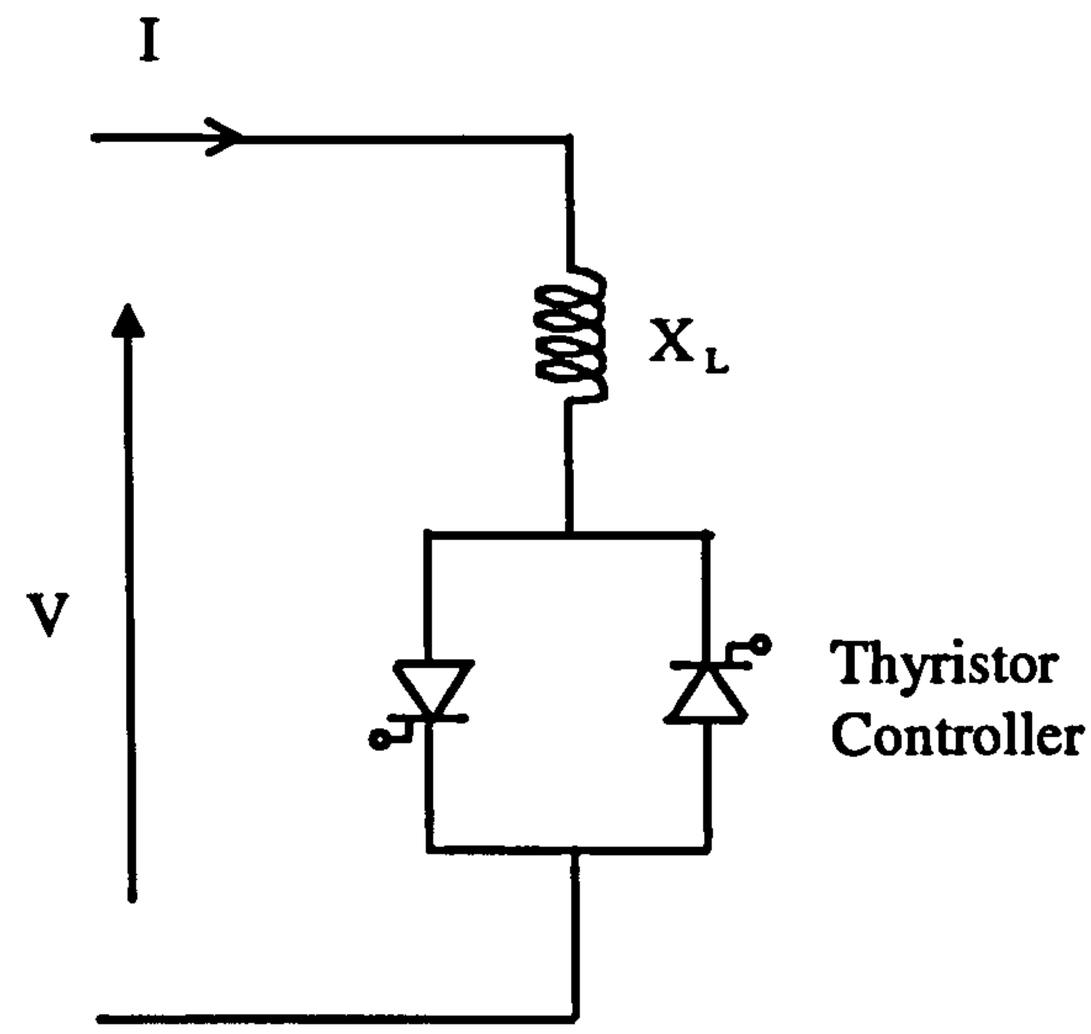

Figure 7.2. Thyristor controlled reactor

7.2.2. Operation modes of Thyristor Switched Capacitors (TSCs)

The basic elements of a TSC are a capacitor in series with a bidirectional thyristor pair and a small reactor as shown in Fig 7.3(a). The purpose of the reactor is to limit switching transients, and to form a filter for harmonics coming from the power

system or from any parallel connected SVCs. A one line diagram of a TSC scheme is shown in Fig 7.3(b). The susceptance is adjusted by controlling the number of parallel capacitors connected in shunt. Each capacitor always conducts for an integral number of half cycles. The total susceptance thus varies in a stepwise manner. In principle the steps can be made as small or numerous as desired, by having sufficient number of individually switched capacitors. This degree of flexibility is not usually sought in power systems compensators because of the resulting cost and complexity of the controls.

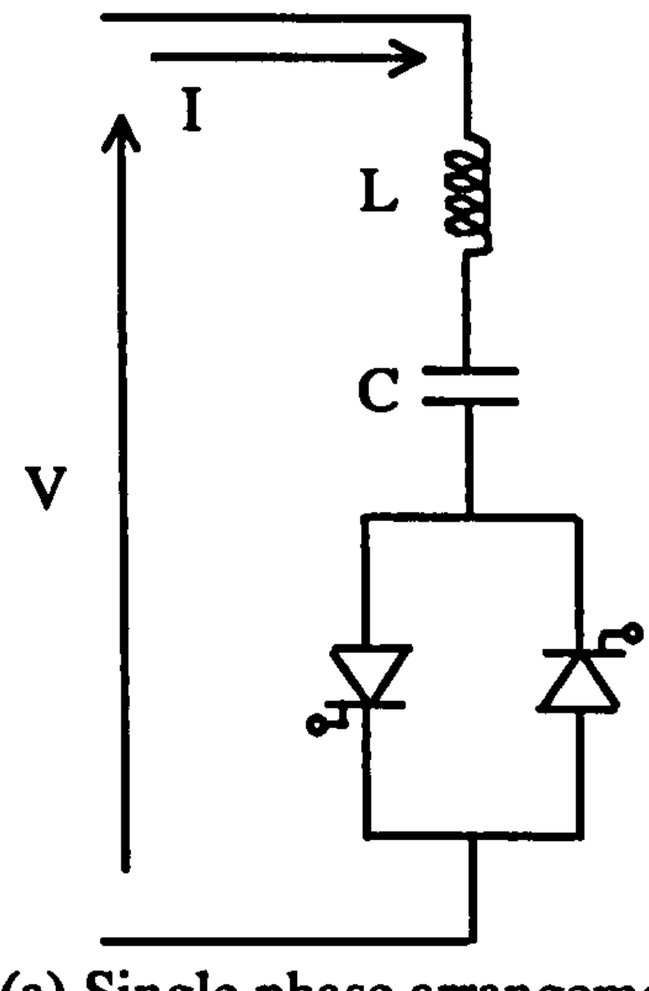

(a) Single phase arrangement of a TSC

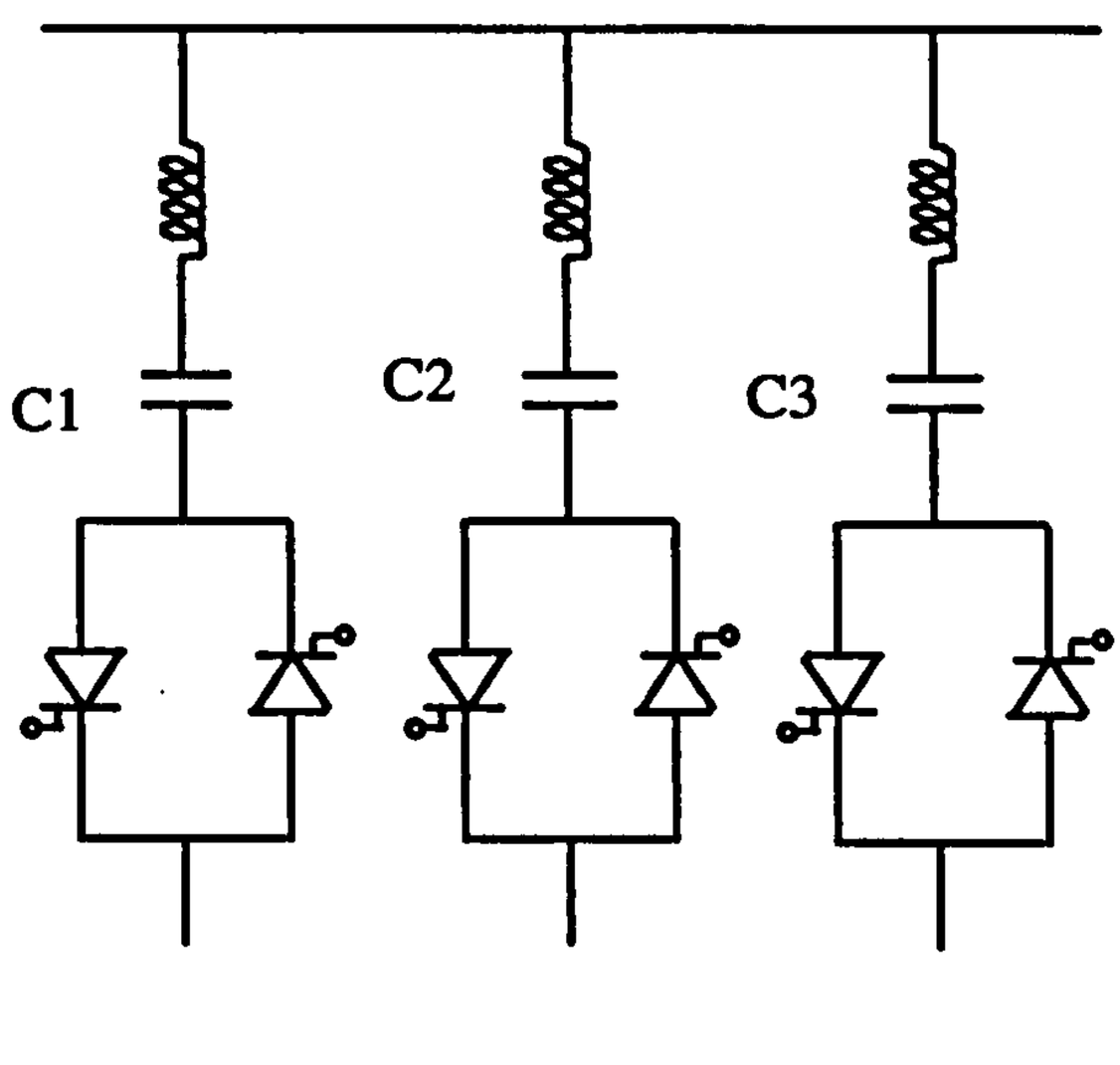

(b) One line diagram of a TSC scheme

Figure 7.3 Thyristors switched capacitors (TSC)

7.3 CURRENT AND VOLTAGE EQUATIONS OF THE SVC

This section presents the SVC steady state impedance characteristic at fundamental frequency. In addition, the concepts of the SVC harmonics performance are discussed.

7.3.1 Susceptance of the TCR element of an SVC at fundamental frequency[5]

An elementary thyristor controlled reactor (TCR) consists of a fixed reactor and a bidirectional thyristor valve. The current in the TCR can be controlled continuously from maximum (thyristor valve in full conduction , $\alpha = 90°$) to zero (thyristor valve blocked, $\alpha = 180°$) by the method of phase angle control.

Considering the equivalent circuit of a TCR shown in figure 7.4 and assuming a negligible resistance, it is possible to write the following:

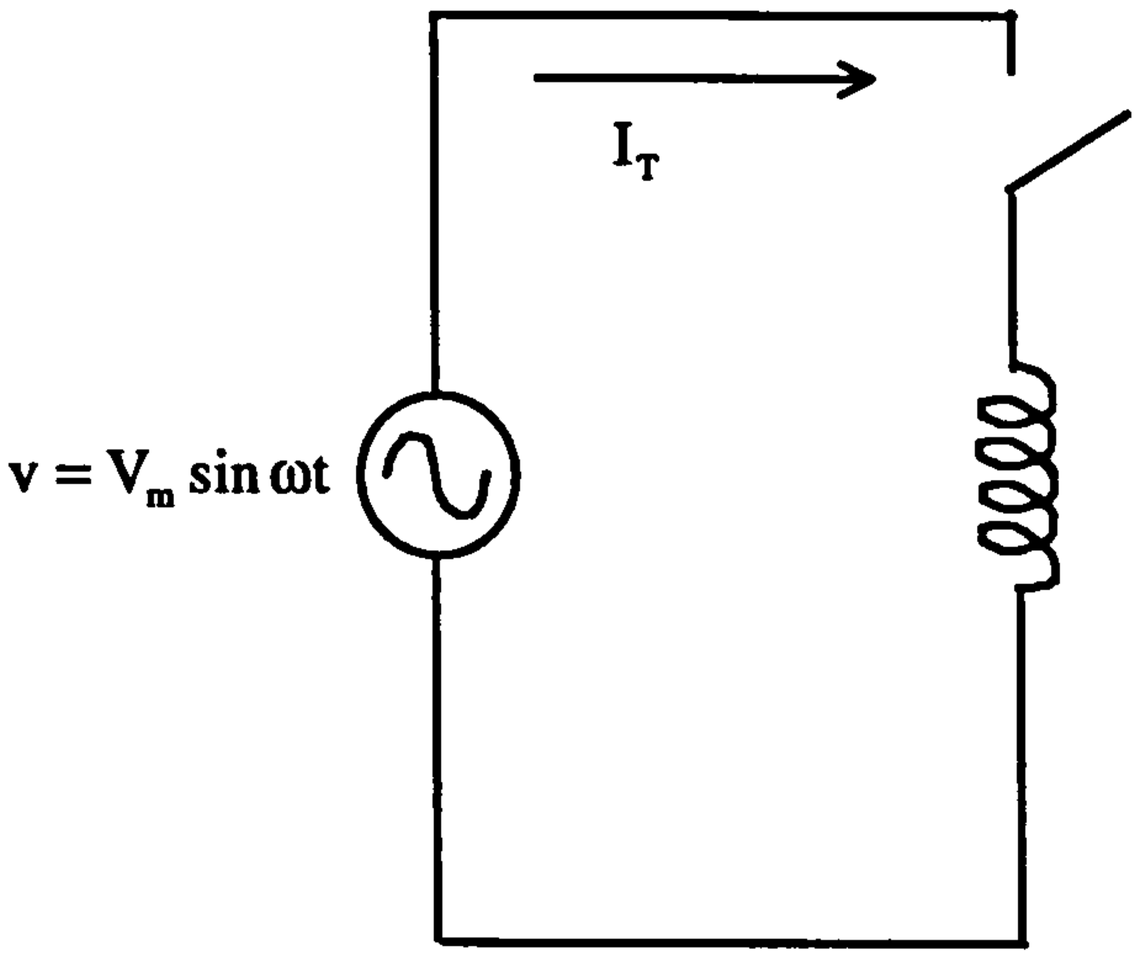

Figure 7-4: One line diagram of a TCR

$$L\frac{di_T}{dt} = V_m \sin \omega t \tag{7.1}$$

Then,

$$i_T = \frac{V_m}{L}\int_0^t \sin \omega t dt + C = -\frac{V_m}{\omega L}\cos \omega t + C\,, \text{ where C is a constant} \tag{7.2}$$

When $\omega t = \alpha$, the thyristor current is equal to zero, then

$$i_T(\omega t = \alpha) = 0 = -\frac{V_m}{\omega L}\cos \alpha + C\,, \qquad \text{where } C = \frac{V_m}{\omega L}\cos \alpha \tag{7.3}$$

Hence,

$$i_T = -\frac{V_m}{\omega L}(\cos \omega t - \cos \alpha) \text{ for } \alpha \le \omega t \le 2\pi - \alpha \tag{7.4}$$

By a similar procedure, the equations for the thyristor current for the interval between 0 and π rads are established as follows:

$$i_T(\omega t) = -\frac{V_m}{\omega L}(\cos \omega t + \cos \alpha), \text{ for } 0 \le \omega t \le \pi - \alpha \tag{7.5}$$

$$i_T(\omega t) = 0 \tag{7.6}$$

$$i_T(\omega t) = -\frac{V_m}{\omega L}(\cos \omega t - \cos \alpha), \text{ for } \alpha \le \omega t \le \pi \tag{7.7}$$

Where α varies in the range between $\pi/2$ and π rads. The waveshape of the thyristor current is shown in figure 7.5

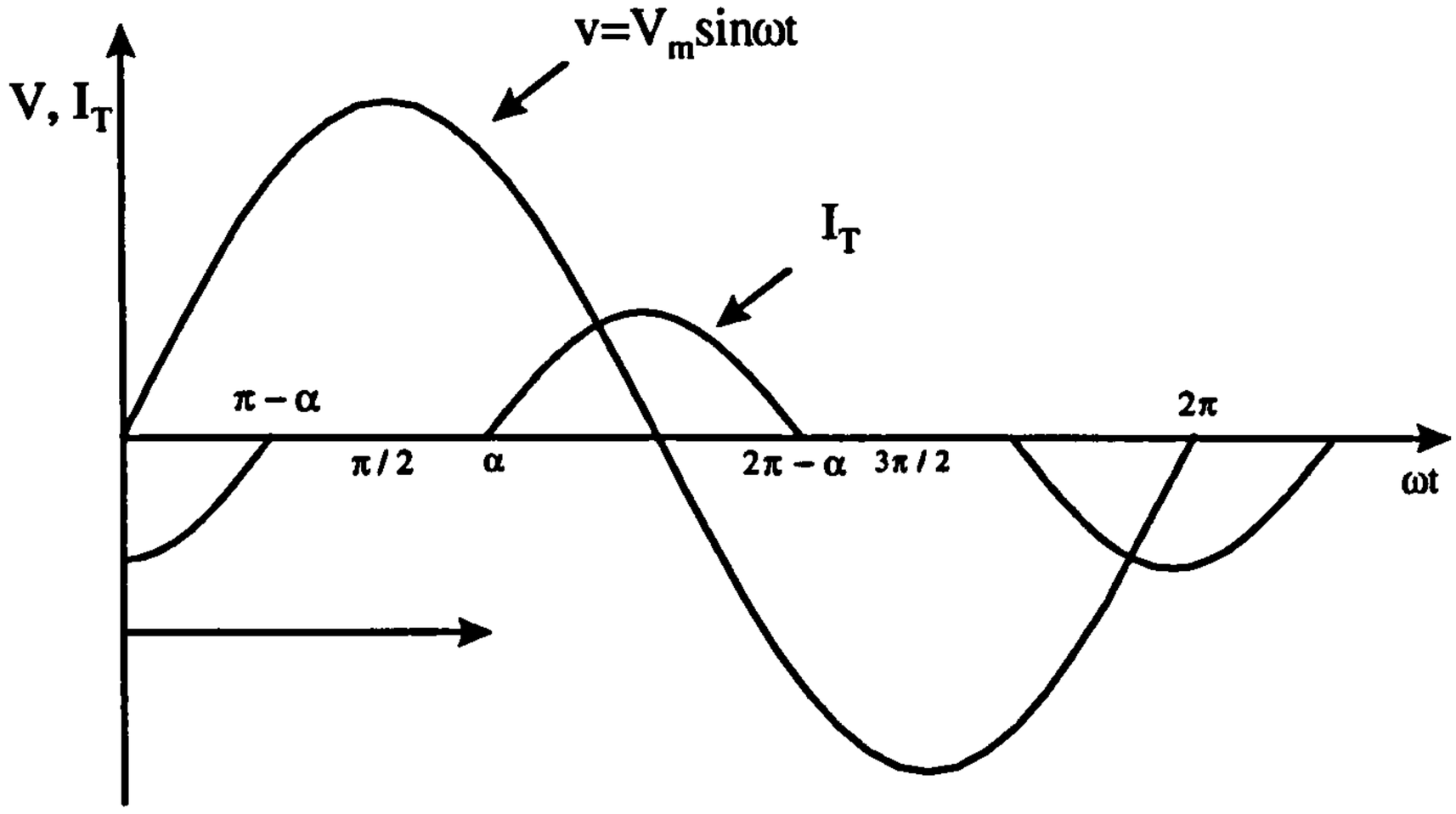

Figure 7.5. Waveshape of a TCR current

As can be seen, the TCR current is symmetric about $0, \pi, 2\pi$ ....Therefore, i_T is an even and periodic function (period of 2π) and consequently it can be analysed in Fourier series, as follows:

$$i_T(\omega t) = \frac{\alpha_0}{2} + \sum_{k=1}^{n} \alpha_k \cos k\omega t \qquad (7.8)$$

By symmetry α_0 is equal to zero, and α_n is given by :

$$\alpha_n = \frac{2}{\pi} \int_0^{\pi} i_T(\omega t) \cos n\omega t d(\omega t) \quad \text{for } n = 1,2,3,.... \qquad (7.9)$$

For the fundamental frequency (n=1), equation (6.9) can be written as

$$\alpha_1 = \frac{2}{\pi} \int_0^{\pi} i_T(\omega t) \cos \omega t d(\omega t) \qquad (7.10)$$

Substituting equation (7.5) into (7.10), α_1 can expressed as :

$$\alpha_1 = \frac{2}{\pi}\int_0^{\pi-\alpha} -\frac{V_m}{wL}(\cos\omega t + \cos\alpha)\cos\omega t d(\omega t) + \frac{2}{\pi}\int_\alpha^{\pi} -\frac{V_m}{\omega L}(\cos\omega t - \cos\alpha)\cos\omega t d(\omega t)$$

hence,

$$\alpha_1 = \frac{V_m}{\omega L}\left[\frac{2(\pi-\alpha)+\sin 2\alpha}{\pi}\right] \tag{7.11}$$

Therefore, seen from fundamental frequency i_T is expressed as:

$$i_{T(1)} = \frac{V_m}{\omega L}\left[\frac{2(\pi-\alpha)+\sin 2\alpha}{\pi}\right]\cos\omega t = I_{T(1)}\cos\omega t \tag{7.12}$$

If the thyristor current peak $\left(V_m / \omega L\right)$ is taken as the base, the magnitude of the thyristor current $I_{T(1)}$ can be written as:

$$I_{T(1)} = \left[\frac{2(\pi-\alpha)+\sin 2\alpha}{\pi}\right]\text{pu} \tag{7.13}$$

Consequently, the TCR susceptance (B) is equal to the fundamental thyristor current in per unit as follows:

$$B = \left[\frac{2(\pi-\alpha)+\sin 2\alpha}{\pi}\right]\text{pu} \tag{7.14}$$

The fundamental component of the current $I_{T(1)}$ from equation (7.13) can be rewritten by:

$$I_{T(1)} = \frac{\sigma - \sin\sigma}{\pi X_L} V \tag{7.15}$$

where

V is the rms voltage across the TCR

X_L is the fundamental frequency reactance

σ is the conduction angle, related to α by the following equation:

$$\sigma = 2(\pi - \alpha) \tag{7.16}$$

Figure 7.6 shows the fundamental component of the current versus the conduction angle(σ).

Then equation (7.14) can be written as:

$$B(\sigma) = \frac{\sigma - \sin\sigma}{\pi X_L} \tag{7.17}$$

The maximum value of $B(\sigma)$ is $(1/X_L)$, obtained with $\sigma = \pi$ that is full conduction in the thyristor controller. The minimum value is zero, obtained with $\sigma = 0$. This control principle is called phase control. It follows that with phase control, the effective impedance of the TCR is continuously variable.

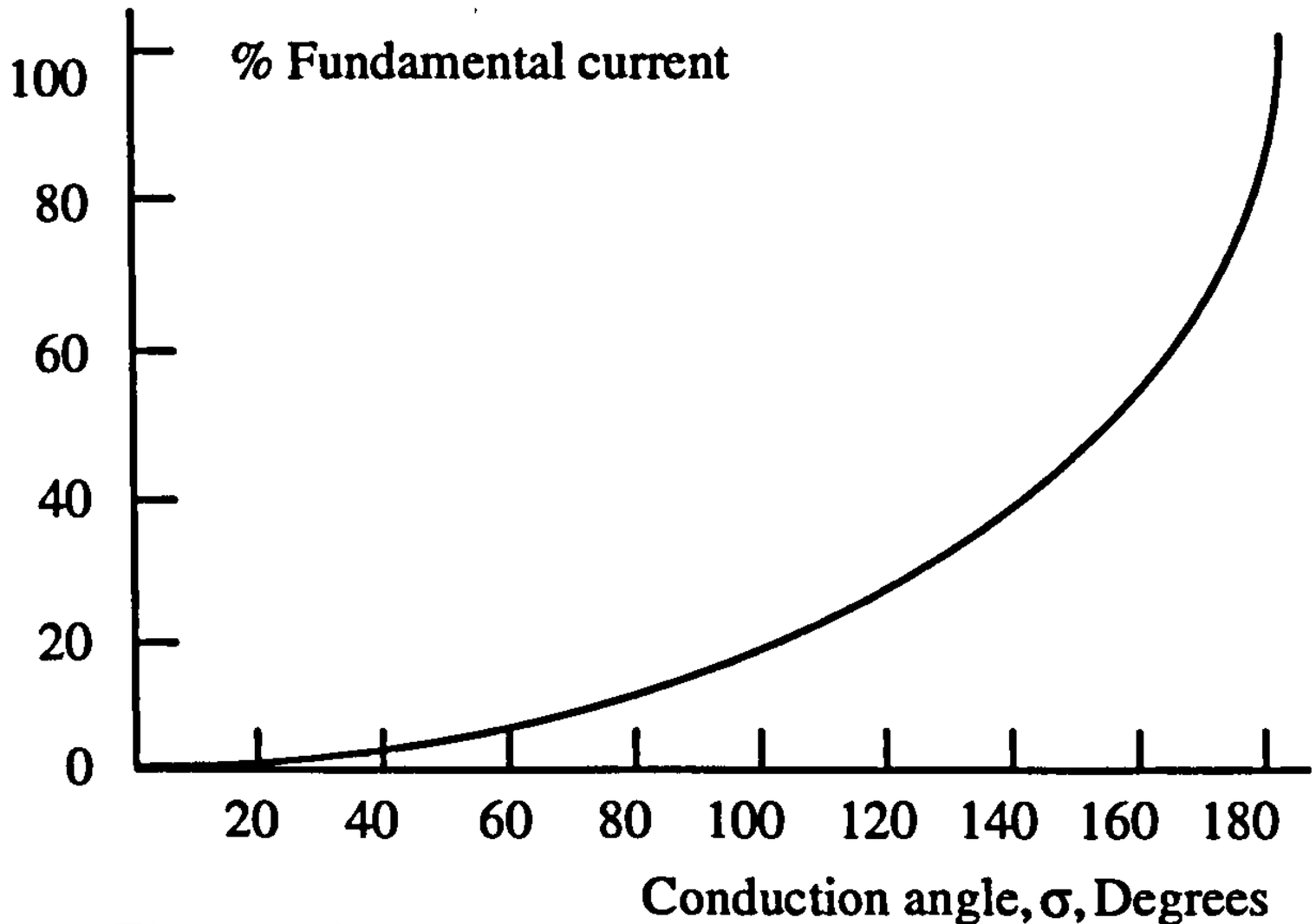

Figure 7.6. Fundamental current as a function of the conduction angle

7.3.2 Harmonics of the TCR-FC model

Under phase control, the TCR generates harmonics. If the gating angles are balanced, all the odd harmonics are generated and the rms value of the n_{th} harmonic component is given by:

$$I_n = \frac{4V}{\pi X_L}\left[\frac{\sin(n+1)\alpha}{2(n+1)} + \frac{\sin(n-1)\alpha}{2(n-1)} - \frac{\cos(\alpha)\sin(\alpha)}{n}\right] \qquad (7.18)$$

where n=3,5,7.....

In three phase applications, the basic TCR elements are connected in star or delta though a transformer. The transformer is necessary for matching the mains voltage to the thyristor valve voltage. The delta connection of the basic reactor arrangement is most suitable because the third harmonic which is produced is cancelled out. The transformer can then be connected in a star-star configuration as shown in Figure 7.7

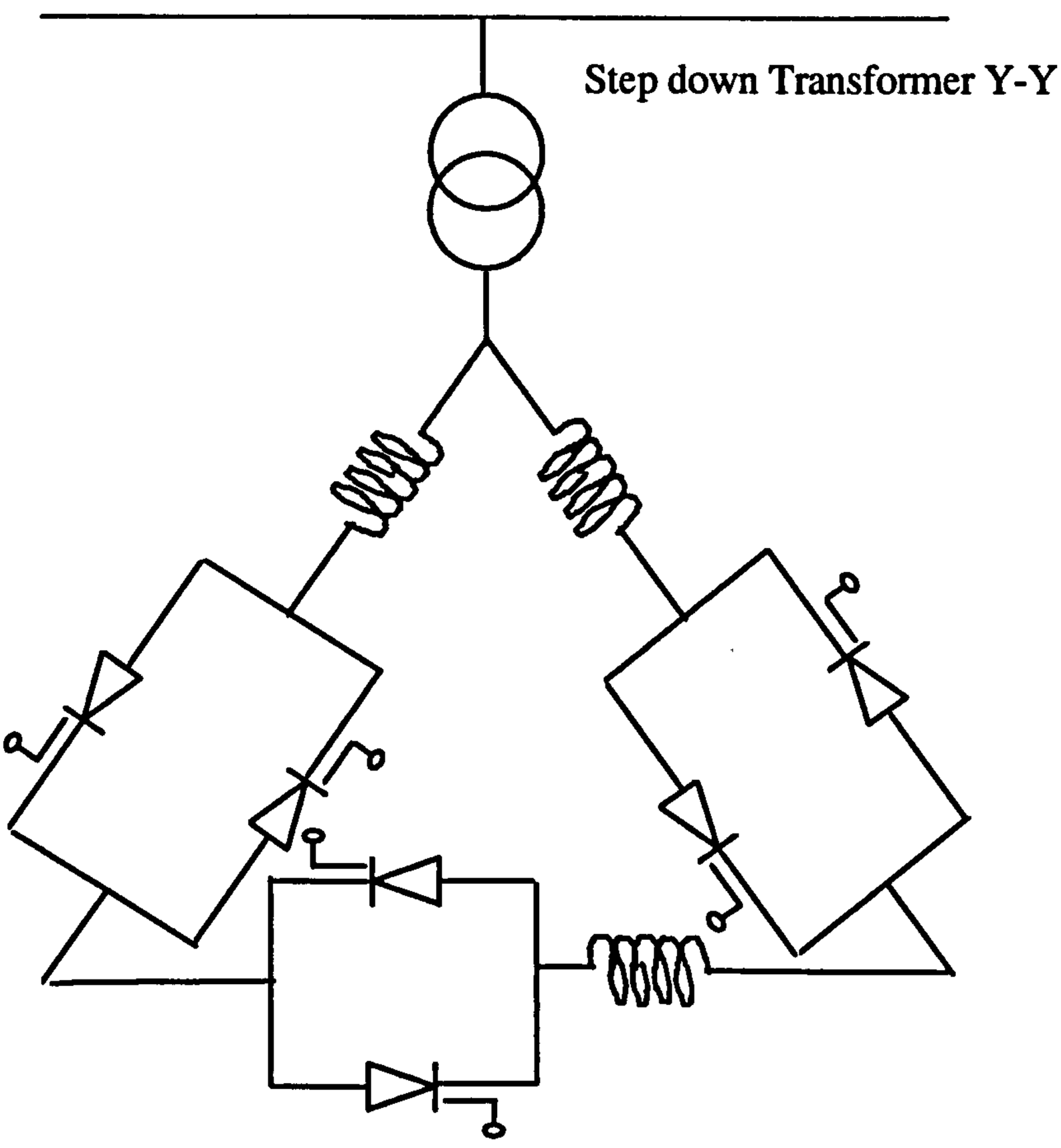

Figure 7.7 Six pulse TCR

In this arrangement harmonics of the order $6n \pm 1$ (where n=1,2,3) exist in the line currents. The harmonics in the line current can be reduced by replacing the fixed capacitors, associated with reactive power generation, with a filter network. The filters can be designed to draw the same fundamental current as fixed capacitors at the system frequency and provide low-impedance shunt paths at the harmonic frequencies.

7.3.3 Fundamental Voltage/Current characteristic of the TCR-FC model

A TCR, in the extreme condition of its thyristors continuously conducting, behaves simply as a linear reactor giving a characteristic OGH in Fig 7.8.

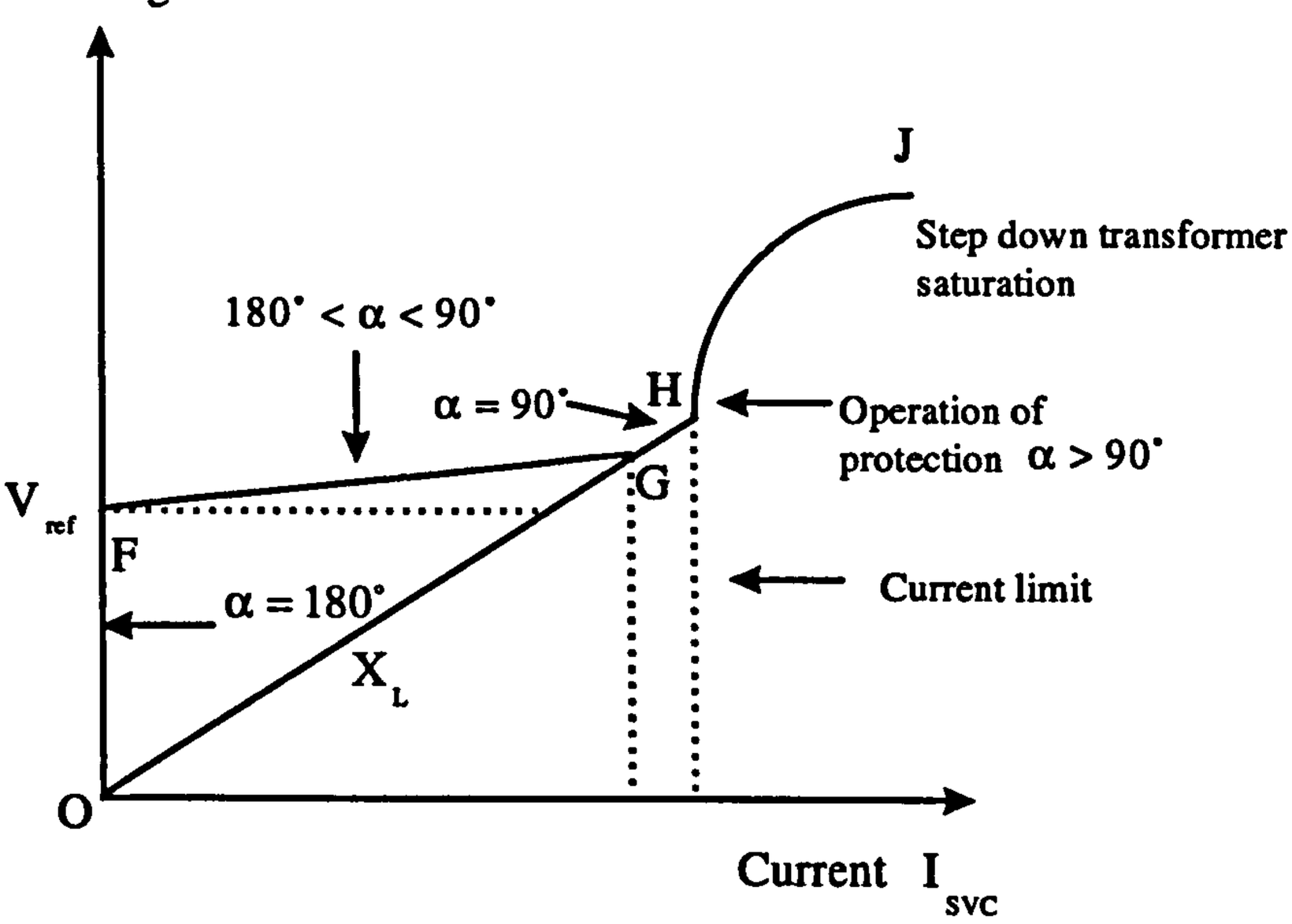

Figure 7.8. Output characteristic of a TCR

The characteristic from F to G can be obtained by phase control of the thyristor firing angle. The TCR control system has to determine the gating instants to obtain the required characteristic from F to G. The basic overload characteristics of a TCR is the line GH, as for an uncontrolled reactor[6]. There may be a limitation due to the thyristors, which have a small thermal time constant. Overcurrent protection can be provided by adding a current limit to the characteristic of HJ, but then the thyristor must be rated to withstand the excess voltage. Generally, if an appreciable overload rating is required, a higher thyristor cost is inevitable. It is important to note that the TCR current can be varied continuously, without step, between zero and a maximum value corresponding to full conduction. The current is always lagging so that the reactive power can only be absorbed. However, the TCR compensator can be biased by shunt capacitors so that its overall power factor is leading and reactive power is generated into the external system. The output characteristic of a TCR with fixed or switched capacitor(s) is given in Fig 7.9

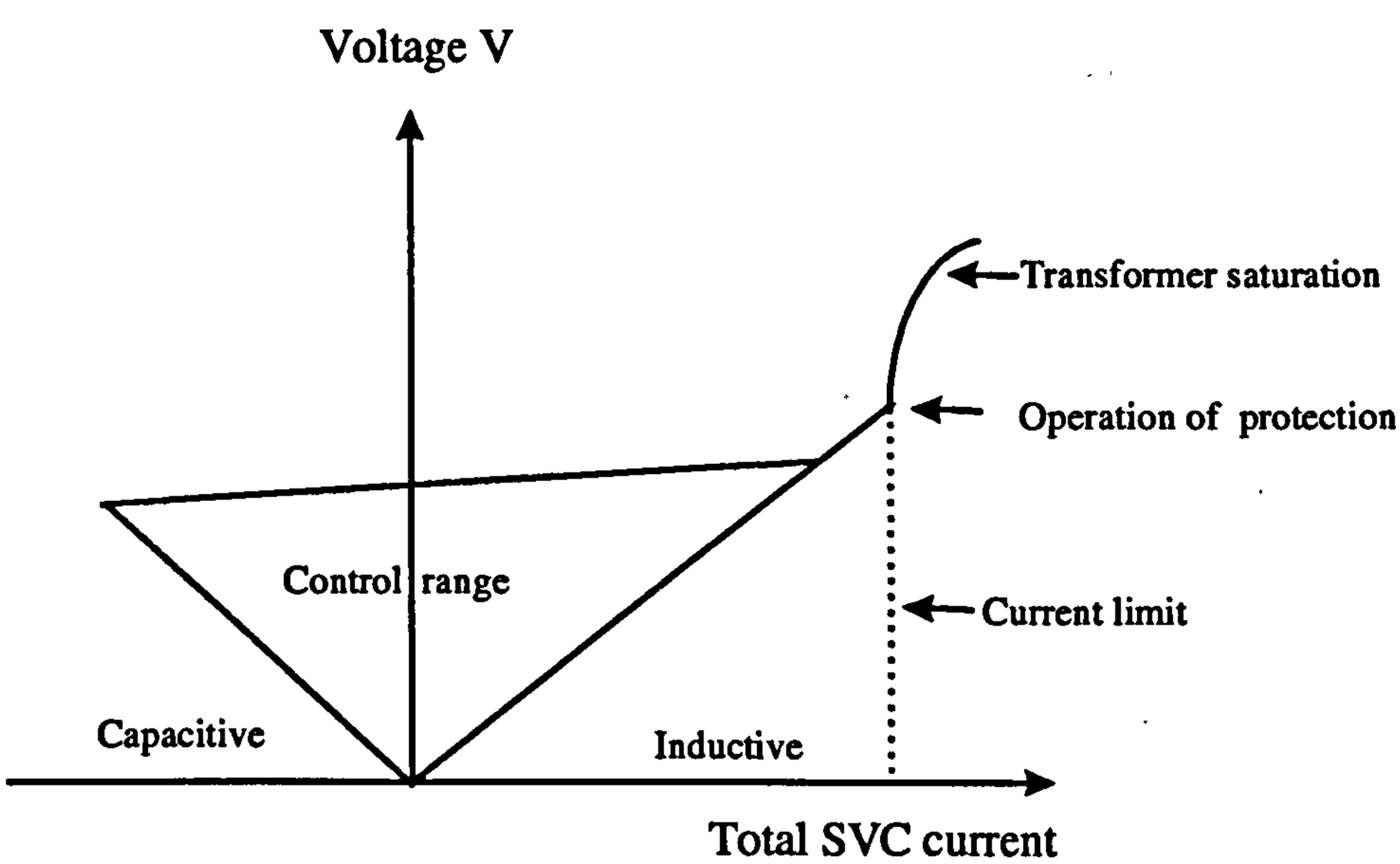

Fig 7.9 Output characteristics of a TCR with shunt capacitor(s)

7.4 OVERVIEW OF PREVIOUS WORK

The use of Static Var compensators to increase power transfer capacity, improve system damping, transient stability and reduction of temporary overvoltages has long been recognised and several schemes have been implemented using both TCR-FC and TCR-TSC models.

A.M.Gole and V.K.Sood [2] describe the design and operation of an 167 lead/100 lag TSC-TCR (2 stages of 83MVA capacitance) in a 500MW back to back HVDC system. The SVC was modelled using the EMTDC package and tested under steady state and voltage sag conditions. Guidelines for using a variable timestep in order to achieve greater accuracy under thyristor switching were also provided. Modelling of the firing system of the SVC was presented using the Phase Locked Loop method (PLL). Modelling of a similar model based on the same firing technique (PLL) will be presented later in this chapter and comparison will be made with the firing method presented in this chapter. In this publication a novel technique of modelling the thyristor switched capacitors was used. The basic concept of this method is that the switching on and off of the capacitors depends on the value of firing angle. A standard control system was used for the regulation of the SVC and the system dynamic analysis was performed under voltage sag conditions. The simulation results presented in this paper are similar to the ones that were obtained during the course of this thesis using the same basic principles for the control and the synchronising systems.

A.M.Vasconcelos and A.J.P Ramos in 1992 [7] describe the design and operation of an 200 lead/140 lag TSC-TCR (2 stages of 100MVA capacitance) using a more complicated control system than the one in [2] using synchronisation filters in order to determine the zero crossings of the voltage. The pulse generating unit in this system is based on the detection of the zero-crossing of the synchronisation signal. The model was tested under single phase fault conditions in the busbar where the SVC is connected. Despite the relative good response of that system under imbalance

conditions the firing method based on the detection of the zero-crossing of the synchronisation signal causes some problems such as the existence of subsynchronous harmonics as reported in [8].

Exposito and Mitchell designed a microprocessor based control system for a SVC using optimal load compensation in 1992 [4]. Using an optimisation technique based on load compensation the firing angles of a TCR/FC model were calculated, stored in the memory and called by the microprocessor to control the SVC. A similar model to this one was developed by J.A.Martinez [9].

SVC control strategies for damping power system oscillations were reported in 1986 by A.E Hammad [6]. In this paper a basic TCR/FC model was used and an optimal damping control strategy was developed to control the SVC. The prime objective of this technique was that the system analysed should recover promptly from a severe transient and return to a stable condition as rapidly as possible. For this reason optimisation control techniques were used in order to calculate the appropriate firing angles for the TCR.

The effect of the SVC in transient stability and voltage compensation studies and a comparison with other FACTS controllers has been carried out by Nelson and Rietman [10],using a +50/-50 MVAr SVC. Simplified models for the control of the SVC were used based on the concept of the variable susceptance. A similar analysis showing the improvement of power system performance using SVCs was reported in 1996 by Y.Besanger and J.Passelergue [11].

Ainsworth in [12], presented a thyristor controlled reactor model and investigated the response of the Phase Locked Loop control system (PLL) under various disturbances in comparison to elementary firing control methods.

Analysis of a grid control system using d-q-z transformation for static compensator systems was investigated in 1989 by A.Gole,V.K Sood and L.Mootoosamy[13]. In this system the basic principles of the Phase Locked Loop (PLL) method were reported for the first time for use within static compensator systems. This firing technique has to solve the problem of establishing accurate firing in systems vulnerable to harmonics and voltage synchronisation. A control system for static compensator systems based on the d-q-z transformation was modelled and tested under various disturbance conditions, such as loss of synchronising voltages (single and three phase faults) and harmonic distortion in the synchronising voltages. A simple AC system was analysed using a 12 pulse SVC model similar to the one proposed in [2] and the dynamic response of that system under small disturbance conditions (load disconnection) was investigated. A similar study is performed later in this chapter following the modelling techniques analysed in this paper and a comparison is made with the results taken from the firing and the control methods that are proposed in this thesis.

Harmonics interactions on the operation of Static Var Compensators were investigated by R.H.Lasseter, Y.Shern and S.G. Jalali in 1995 [14]. In [3] a basic description and the operating principles of Static Var Systems are presented and general control algorithms are reported in order to regulate SVC models.

Detailed modelling of SVCs was developed by Sang Y.Lec and Subroto Bhattachavya using a TCR-TSC model in 1992 [15]. The test system in this paper is a 345-kV transmission system fed by a 345/18 kV step down transformer. The SVC is a combined TCR/TSC type consisting of three TSCs rated 121 MVar each, one TCR rated at 163 MVar and harmonic filters. The control system includes undervoltage and overvoltage strategies and power modulation controls. The Phase Locked Loop method was used in order to achieve accurate firing pulses for the TCR valves. The system was tested under fault conditions and the response of the system is significantly rapid to bring the voltage back to its pre-fault level in a reasonable timescale.

A static compensator model was proposed by Lefebvre and Gerin in 1992 for the Hydro-Quebec system [16]. This model consists of a generic six-pulse TCR/FC model and the firing and synchronising units follow the principles of finding the firing pulses of the TCRs using a method where the only information is needed is the conduction or not of the thyristor current in the TCR branches and by taking the advantage of the 90° phase shift between the voltage and the current. In this system the only information required is the state of the conduction of the thyristors. This makes the firing method insensitive to harmonics and transients on the voltage waveform. The firing method for the SVC model described in this chapter is based on this technique. Simulation results showing the effectiveness of this approach are presented later in this chapter and demonstrate that accurate firing can be achieved in a reasonable timescale similar to the Phase Locked Loop method.

A detailed SVC model was also developed by Dickmander and Thorvaldsson in 1992 [17]. This model consists of various control functions such as overcurrent and overvoltage limiter, undervoltage strategies and other supplementary control function for the SVC regulator. The PLL (Phase Locked Loop) method was used for the firing system of the thyristor control reactor and the system was analysed under voltage unbalance conditions. The results show that the system is basically immune to severe voltage distortions.

For the SVC model presented in this chapter useful information was taken using the previously described publications, such as the firing method which is based on the technique used in [16]. For the control system the modelling technique has many similarities with the one in [2], however despite the common objective that both techniques have (which is to derive the required susceptance through the regulation of the voltage) in the technique described in this thesis the function of the voltage controller is to derive the appropriate conduction angle by using a non-linear relationship [12], where in [2] the aim is to derive the firing angle and to switch on/off capacitor banks according to the value of the firing angle. These different approaches are basically due to the different firing systems that are used to generate

the pulses for the thyristors (such as firing method based on the conduction or not of the thyristors versus the Phase Locked Loop method). The use of TCRs in a power system results in harmonics which penetrate into the AC network. As harmonics currents flow through system impedances by various paths, harmonic voltages are formed all over the system. In the process they may excite resonances polluting the entire network. In the work reported here AC filters are installed to absorb these harmonics. These filters are generally shunt-connected branches that present a low impedance path to ground for harmonics. They also appear as large capacitors at fundamental frequency, providing the needed reactive power compensation. For the studies analysed in this thesis, AC filters have been used with their values taken according to the network power flow. Useful guidelines for the filter parameters were taken from Kimbark's book [18]. The TCR-FC is identified as a basic building block for high power SVC applications and the following investigations are carried out for this configuration. To :

- study in detail the behaviour of SVC under steady state power system conditions
- investigate the performance of SVC under various system disturbances(variable loads-faults)
- mathematically analyse the control system of the SVC.
- produce a reliable computer model to assist in the design of a SVC and filters.

From the research work that will be analysed in this chapter the following contributions are identifiable:

- An efficient and realistic method to model the Static Var Compensator (SVC), using comprehensive control and firing systems has been developed in this thesis, along with guidelines for designing the harmonic filters. The SVC is considered to be a continuously variable-shunt susceptance which is adjusted in order to achieve a specified voltage magnitude

- The development of mathematical expressions for the control and the firing systems of the Static Var Compensator in order to derive useful computational functions for simulation purposes
- The creation of a computer code for the Static Var Compensator (SVC) model coded in the TACS language using the EMTP simulation package
- An investigation and report on the behaviour of the Static Var Compensator (SVC) under various operating conditions, such as variable load, phase shift, single phase fault and three phase fault
- Comparison of the control and firing methods proposed in this chapter with other control methods and firing systems (such as the Phase Locked Loop) method. Similar results of the PLL and the control methods proposed in [2] and [13] will be obtained in this chapter using the EMTDC modelling package and various case studies will be analytically investigated and compared with the ones using the control and firing methods proposed in this chapter. The validation of the techniques that will be presented in this thesis demonstrates that the proposed SVC controller gives a very good representation of a practical system. The results that will be presented using the proposed firing method prove the effectiveness of the technique that is used in this chapter, show that is insensitive to voltage waveform distortion and capable of establishing accurate firing timing in a timescale similar to using the Phase Locked Loop method; consequently it can be used as an alternative to the PLL method for the control of Static Var Compensator models. Moreover, by using the firing technique presented in this thesis the problem caused by using the PLL method as reported in [8], which is that the dynamics of the PLL require a very small time step which demands a high CPU time, can be avoided.

7.5 THE BASIS OF A SVC MODEL FOR ELECTROMAGNETIC TRANSIENT STUDIES

When a new technology is first researched with the objective of being employed in different power systems, one natural problem arises; the lack of reliable models for

representing it. In this sense, the correct development of FACTS device models is essential. Moreover, time domain simulations provide a means of analysing the dynamic behaviour of these devices. Time domain simulations are actually one of the most important tools for power system analysis.

SVCs and other fast acting devices potentially respond to higher frequency (above 5 Hz) electromagnetic oscillations. For high frequency oscillations, the network resonant frequencies start to have an impact and must be considered in the transient analysis. This means that the network phasor approach is not entirely valid and an electromagnetic transient analysis must be undertaken. This transient analysis is to verify the SVC electromagnetic performance and coordination with other devices.
For this reason, an SVC model for the electromagnetic transient program (EMTP/ATP) is a very useful tool for evaluating the performance of this piece of equipment in higher frequency phenomena.

7.5.1 THE EMTP/ATP PROGRAM

The existence of powerful, computational efficient programs such as EMTP/ATP allows complex and detailed modelling of the FACTS devices for practically all kinds of electromagnetic transient in a power system. Representation of the real relationship between control systems and power system is then possible though Transient Analysis of Control Systems-TACS/EMTP or even in the more recently developed MODELS/EMTP[19].
The SVC model will be developed for the EMTP/ATP program. Its control system will be developed using TACS. TACS is quite a useful tool for power system analysis, since it allows control system representation in addition to that of the network. Signals can be exchanged between the electric network and TACS and vice versa.
FACTS devices have characteristics that allow them to interact with power systems modifying their transient behaviour. Therefore, a SVC model for transient purposes

is a useful tool for analysing this piece of equipment and establishing its importance as a means of improving power system performance.

7.5.2 ASSUMPTIONS FOR MODELLING A SVC

The approach will consider an SVC controlled by a conventional control system. The control acts directly on the thyristor firing angle.

In a conventional approach, the thyristor valve is controlled through the firing angle, i.e. the thyristors work in a phase controlled mode, in order to control the SVC reactance leading towards a zero error of the controlled variable in the steady-state. It is conventional for the controlled variable to be the voltage at the point of connection of the SVC with the rest of the power system. During faults the voltage tends to decrease rapidly and the control system tries to decrease the conduction angle, consequently decreasing the admittance of the TCR.

Most control systems will generate a required reactive current value which is converted to the conduction angle using a non-linear interface.

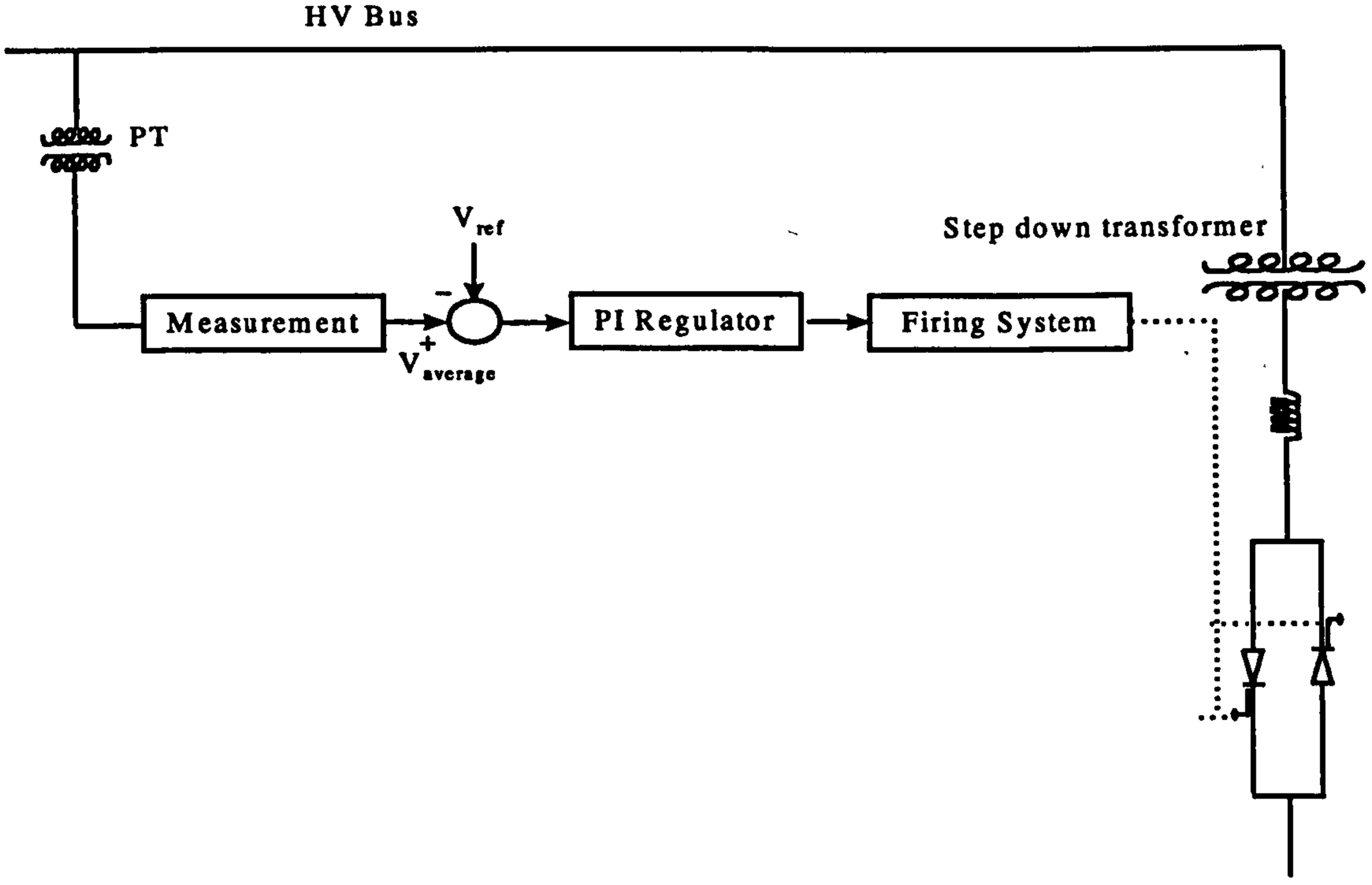

Figure 7.10 Typical control system based on PI regulator

A typical control system operating in closed loop configuration is outlined in figure 7-10.

This figure shows a simplified diagram of an SVC voltage regulator. The main objective of this regulator is to keep the voltage controlled by a PI controller that sends an admittance order to a pulse generating unit. The pulse generating unit (also called the firing system), issues firing pulses that permit a thyristor controlled reactor to operate in a thyristor phase controlled mode, i.e. each thyristor is fired once per cycle to control the effective reactance. Other modes of operation exist and a detailed diagram will be present later.

7.5.3 OUTLINE OF SVC MODEL FOR ELECTROMAGNETIC PURPOSES

With the objective of modelling an SVC, its circuits were grouped into three distinct systems or modules, namely : power circuit; measurement and control systems; firing system. The SVC model is shown in figure 7-11.

The power circuit is composed of filters in parallel with a thyristor controlled reactor. In terms of the modelling task, the power circuit's components are represented with the conventional models available in the EMTP.

The measurement circuit is composed of a measurement device that converts a sinusoidal signal into a DC one. The control system comprises a PI regulator whose main function is to keep at zero the steady-state error and a non-linear interface which provides the conduction angle. The firing system consists of a pulse generating unit that is responsible for issuing firing pulses to the thyristor valves. Next the detailed modelling of each module will be described and its main specifications.

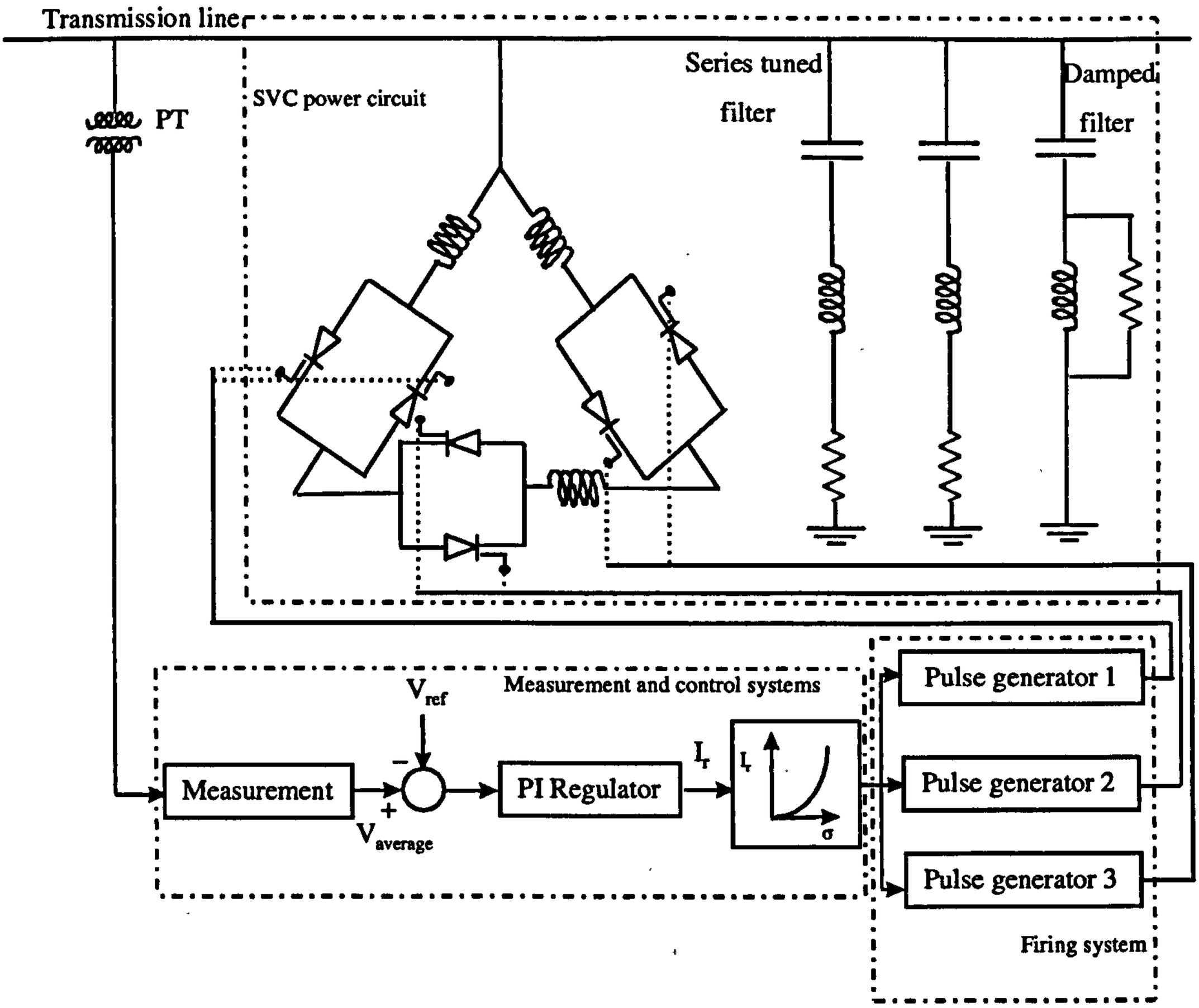

Figure 7.11. Structure of a SVC for modelling purposes

7.6 MODELLING THE MAIN PARTS OF A SVC IN THE EMTP

The main parts of a three-phase SVC will be presented using EMTP built-in models and TACS models specially developed for implementing the functions of a SVC voltage regulator. For modelling purposes the SVC is divided into three main parts, as follows: power circuit; measurement and control systems; firing system. The modelling was developed using version ATP 6.0 of the EMTP program.

7.6.1 Power circuit

The SVC power circuit comprises reactors, thyristor valves and filters. Basically, the power circuit components were represented in the EMTP through the conventional, built-in EMTP models. The capacitor and reactor were represented through their capacitance and inductance respectively. A resistance was added in the filters to account for their losses.

The filters were used in order to prevent harmonic currents from entering the AC network. For this purpose, the per-phase filters are commonly used. The series-tuned filters are used for the low-order harmonics. A high-pass filter is used to eliminate the rest of the higher order harmonics. Definitions of tuned frequency and quality factor of AC filters can be found in Kimbark's classic textbook[18]. The filters also appear as large capacitors at fundamental frequency providing the needed reactive compensation. The filters were represented in the EMTP using the simplified R-L-C model.

With respect to thyristor valves, they are usually represented in EMTP as ideal AC switches in series with small resistors that account for part of the conduction losses. In EMTP thyristors are modelled as type-11 TACS controlled switches. A thyristor can be modelled as an open-circuit when not conducting. Then when conducting, it may be modelled by a simple equivalent circuit as shown in figure 7.12.

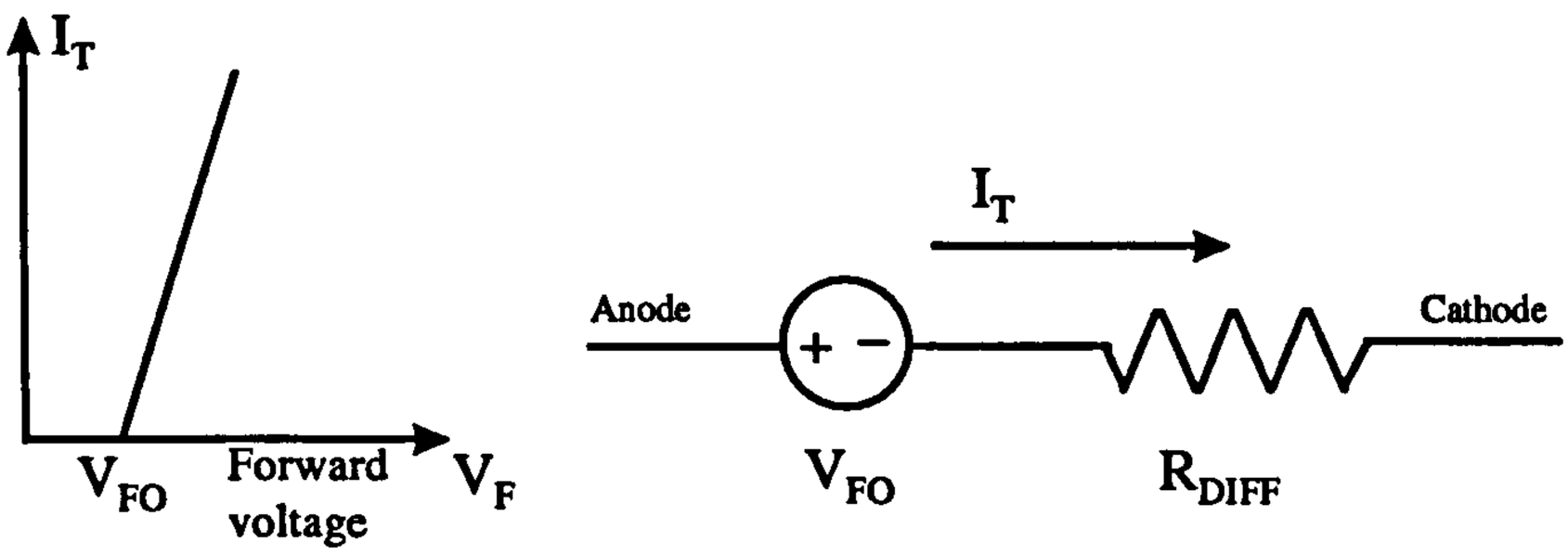

Figure 7-12 Equivalent circuit for a thyristor when conducting.

As can be seen, thyristors start conducting when the forward voltage is greater than the " on voltage drop " (V_{FO})and there is a positive pulse as a gate signal. The on state voltage drop is typically around one volt and it accounts for part of the thyristor losses. On state voltage drop is not easily implemented in a program like EMTP. However, it is commonly accepted to neglect this voltage in the representation of thyristor valves for the EMTP program. The modelled thyristor will present losses less than the real thyristors, but this simplification that is assumed as a reasonable approximation.

The recovery current is an important characteristics of thyristors. Recovery current occurs during the time when the thyristor is changing from conducting to nonconducting state. In loop-time simulations, the EMTP program only identifies a current zero-crossing in the time-step after the current reverses its polarity or alternatively when the current is within a defined "current margin". In order to represent approximately the recovery voltage transient, a current margin equal to zero is assumed. In this case, if a proper time-step (Δt) is chosen and a snubber circuit is added to the thyristor valves, the recovery voltage transient may be roughly represented. The recovery current transient across the thyristor valve as represented in the EMTP is shown in figure 7.13

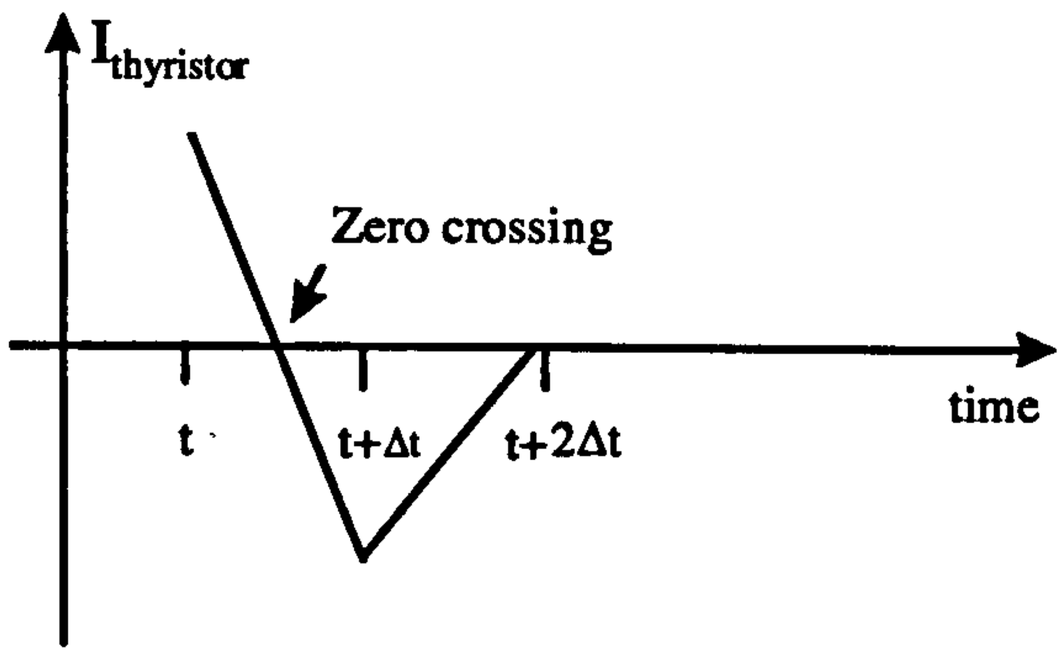

Figure 7-13:Recovery transient current across the thyristor as modelled in the EMTP

In the actual thyristor valves an RC snubber circuit must be added to limit the recovery voltage transient peak to acceptable levels. In terms of modelling, the snubber is represented by an equivalent RC circuit across the type-11 TACS controlled switch and the resistor. The snubber circuit provides a path for the current when the thyristor ceases conducting. The representation of the snubber circuit improves the thyristor valve modelling and avoids numerical oscillations associated with the switching of the inductive currents. Both suitable time-step and values of the RC snubber components are required to avoid numerical instability.

The general diagram of the SVC power circuit for the EMTP program is shown in figure 7.14

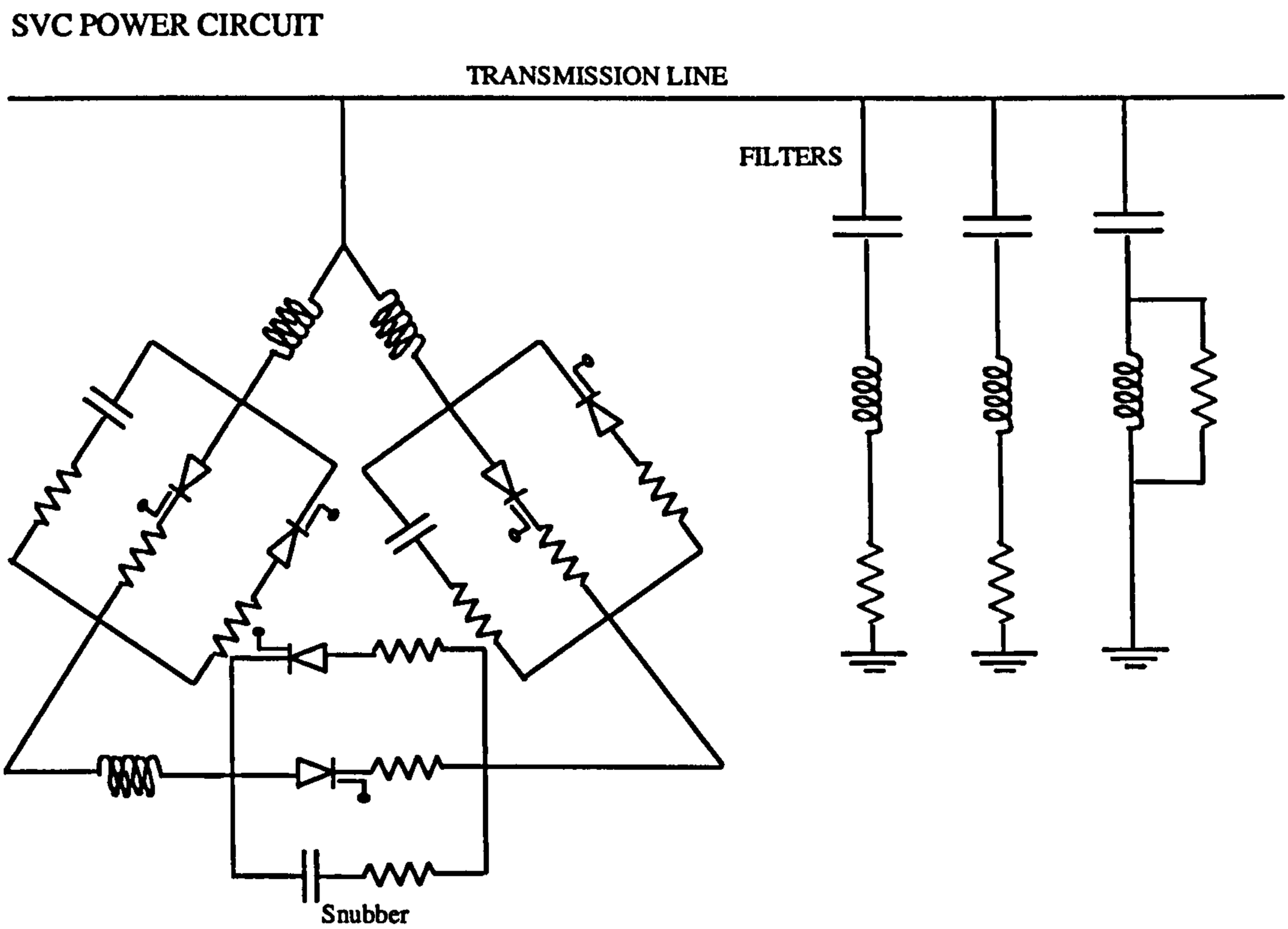

Figure 7.14 EMTP diagram for the SVC power circuit

7.6.2 Measurements and control systems

The measurement system comprises a RMS voltage calculator, the output of which is the input of the SVC control system. The control system is based on a PI regulator. Figure 7.15 shows the block diagram of the measurement and control systems.

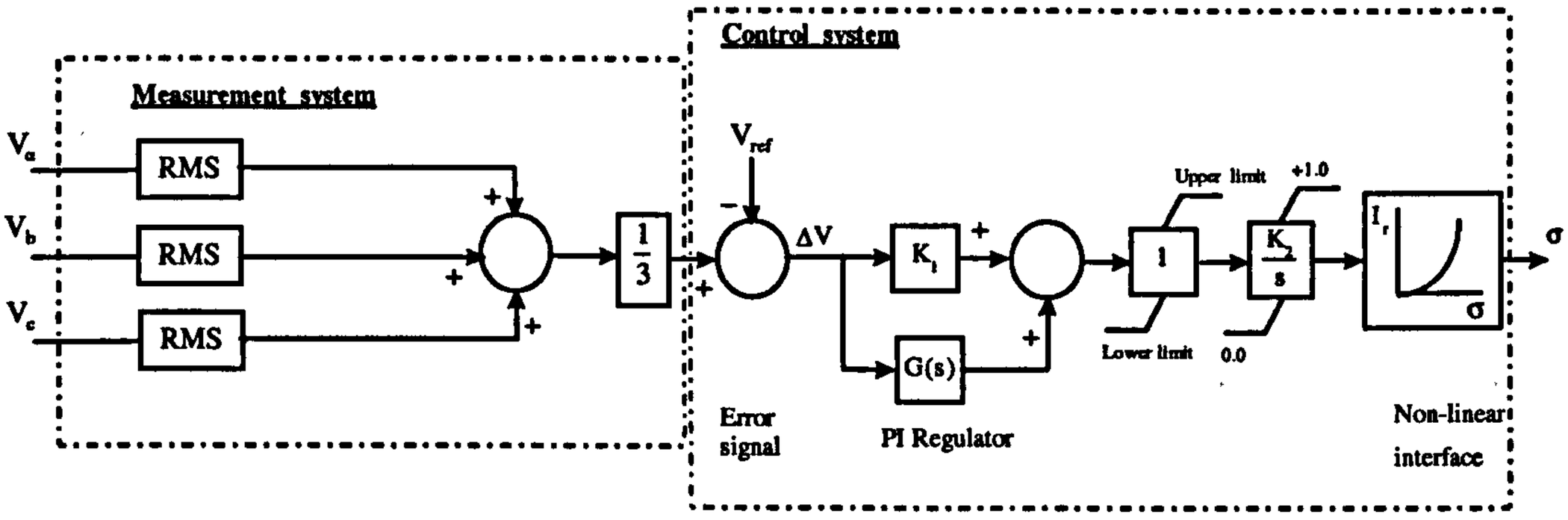

Figure 7.15 Diagram of the measurement and control systems.

a) Measurement system

The SVC control system must see the voltage as a DC signal in order to calculate the error compared to a set reference. The measurement system plays an important role in this process. It is responsible for the conversion from an AC signal to a DC one.

The input signals to the measurement systems are the three line-to neutral bus voltages to be regulated. Each of these phase voltages is fed to RMS transducers which calculate the RMS value on a continuous basis. The RMS calculation includes not only the fundamental, but also all of the harmonic components of the input signal. The three RMS voltages are scaled and averaged to provide per unit output. In terms of modelling the type-66 device was used to get the RMS value in the EMTP. A schematic diagram was given in figure 7.15.

b) Control system

In order to study the dynamic performance under small and large disturbances in the power systems using EMTP or any other simulating device the control circuit needs to be closed with a regulator. In this case, the regulator controls the average voltage of the three RMS phase voltages. This control scheme is adequate to handle three phase symmetrical changes and different kinds of disturbances. The regulator could have other functions like compensating reactive current demand, etc.

There are three functional elements in the control loop: the error signal, the regulator and the non-linear interface. The SVC control system was illustrated in figure 7.15. The signal from the measurement system is compared with a reference to produce a voltage error signal ΔV for input to the regulator. The regulator comprises a PI (proportional-integral) regulator that operates continuously to reduce to zero its input error (voltage error). The regulator provides a proportional path with a gain of K_1. This is a principle small gain for the regulator. For large changes there is a rate feedback with transfer function G(s) which allows fast response during high $\Delta V/\Delta t$ events. The rate feedback loop controls fast changes while having minimum affects on steady-state regulation. The small signal or steady-state gain, which is the product of K_1 and K_2, determines the steady-state response. If this gain is too large, the SVC output will undergo damped oscillations in approaching the final value. If this gain is too small, the system will take too long to compensate for small changes in the voltage.

The outputs from the proportional and the feedforward path are combined and inserted in to an integrator which calculates the corresponding reactive current. The maximum magnitudes of the input signal to the integrator are clamped by a pair of fixed limits. These limits, combined with the gain of the integrator, control the maximum rate of change of the reactive current request I_r for any input signal. If there were no limiters, large disturbances would change the reactive power too fast and cause instability problems. For this system the maximum rate of change of I_r is 1 p.u. in one cycle. The integrator gain is shared by both the steady-state and transient control, and any change in this gain has effects on both responses. The reactive

current request is bounded by an upper limit of 1.0 which requires the TCR to be fully on, and a lower limit of 0.0 which requires the TCR to be fully off.

I_r is the input for the non-linear interface which calculates the correct conduction angle through a current/conduction angle curve that will send a firing angle order to the pulse generating unit.

In general, the reactive current from the static Var compensator will have harmonics for any operation point with an α greater than 90°. For many transient studies it is possible to ignore these harmonics[2,7,13]. For cases where the harmonics can be neglected a simple fundamental current model can be used. Equation (7.15) shows the relationship between the fundamental current and the conduction angle, and figure 7.6 illustrates the non-linear interface between them.

In terms of modelling, Fortran expressions with the supplemental 99,88,98 devices were used to obtain all the transfer function blocks, and the number 56 device was used for the non-linear interface.

7.6.3.1 Firing system of the proposed SVC model

The firing system consists of the gate pulse generator which purpose is to provide firing pulses to the thyristors. The regulator calculates the conduction angle σ, which is passed to the gate pulse generator as a control signal. It is the function of the gate pulse generator to generate the correct firing pulses to achieve the requested conduction angle, σ. It should be noted here that σ is the time the thyristor conducts, while the firing point relative to the voltage across the thyristor is normally indicated by α. These two variables are related by $\sigma+2\alpha=2\pi$.

A typical gate pulse generator would calculate the firing angle α from the point of zero voltage crossings. To achieve this firing at a requested α, the controller could consist of an integrator that starts integrating at zero voltage and resets when it reaches a controlled threshold. At this point, a firing command would be generated for the appropriate thyristor. Control would be achieved by changing the value of the threshold. This type of system acts correctly if the points of zero voltage crossing are

accurately known. This is not the case since both harmonics and transients are expected.

For the case of a TCR this problem can be solved by taking advantage of the 90° phase shift between the current and the voltage. This insures that the conduction angle σ is centered about the zero crossing of the voltage. In that case, the conduction current can be used to locate the zero crossings of the voltage without the problems associated with harmonics. This is illustrated in figure 7.16.1

In this figure NCON is the input logic signal, which is high when there is no conduction in either thyristor. This is added to a signal with a value of unity. The resultant signal is shown in curve (c). The value is 2.0 when there is no conduction and 1.0 during conduction. When this signal is integrated the result is an output which looks like a gain change at the point where conduction stops.

Another advantage of this scheme is that the only information needed is whether the thyristors are conducting or not conducting. There is no need for accurate measurement of voltage or current. NCON is the only input to the gate pulse generator. This signal is increased by unity and integrated. The output of the integrator is subtracted by V_A as shown in figure 7.16.1(d). The control signal has a range from 0 to V_A.

This signal is then input to a zero plus detector (Z.P.D.) which issues the firing pulse whenever the signal becomes positive. The integrator is also reset at this point. The firing pulses are illustrated in figure 7.16.1(e).

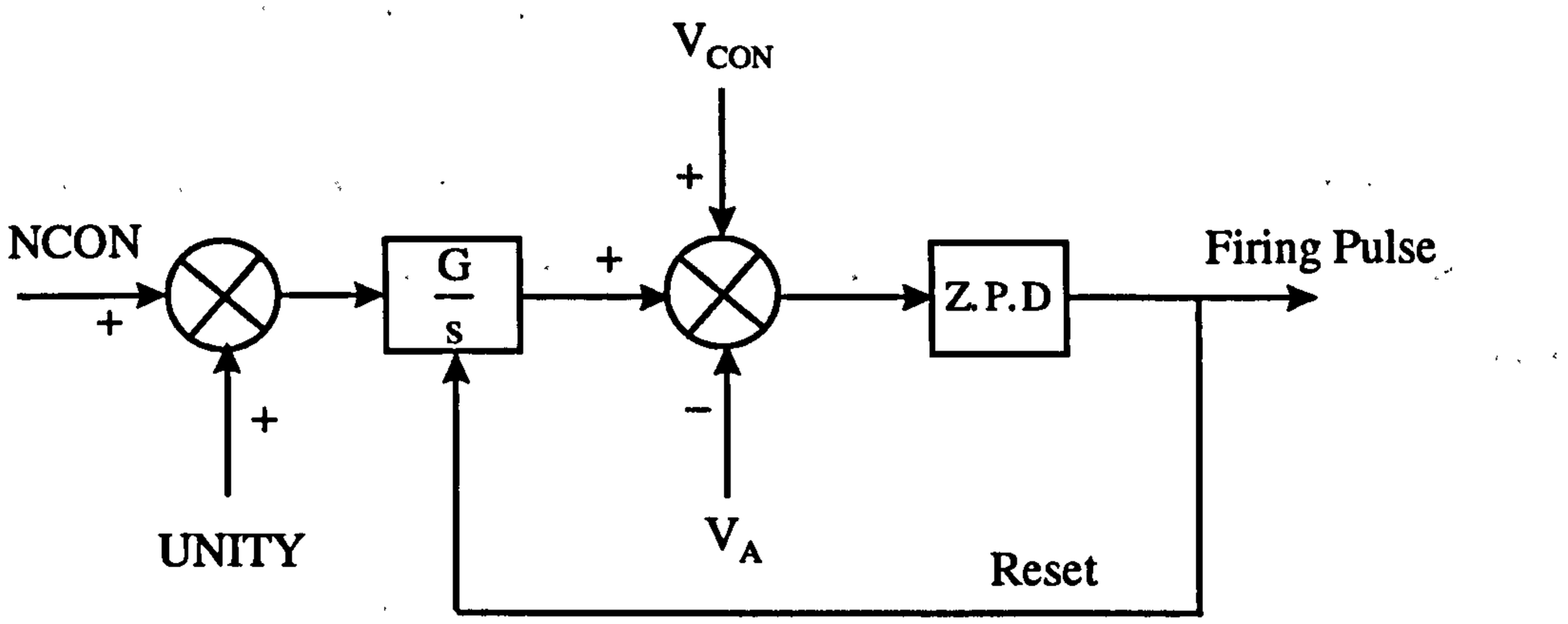
V_{CON}
+
NCON
+
+
G
s
+
Z.P.D
Firing Pulse
+
−
UNITY
V_A
Reset

a)

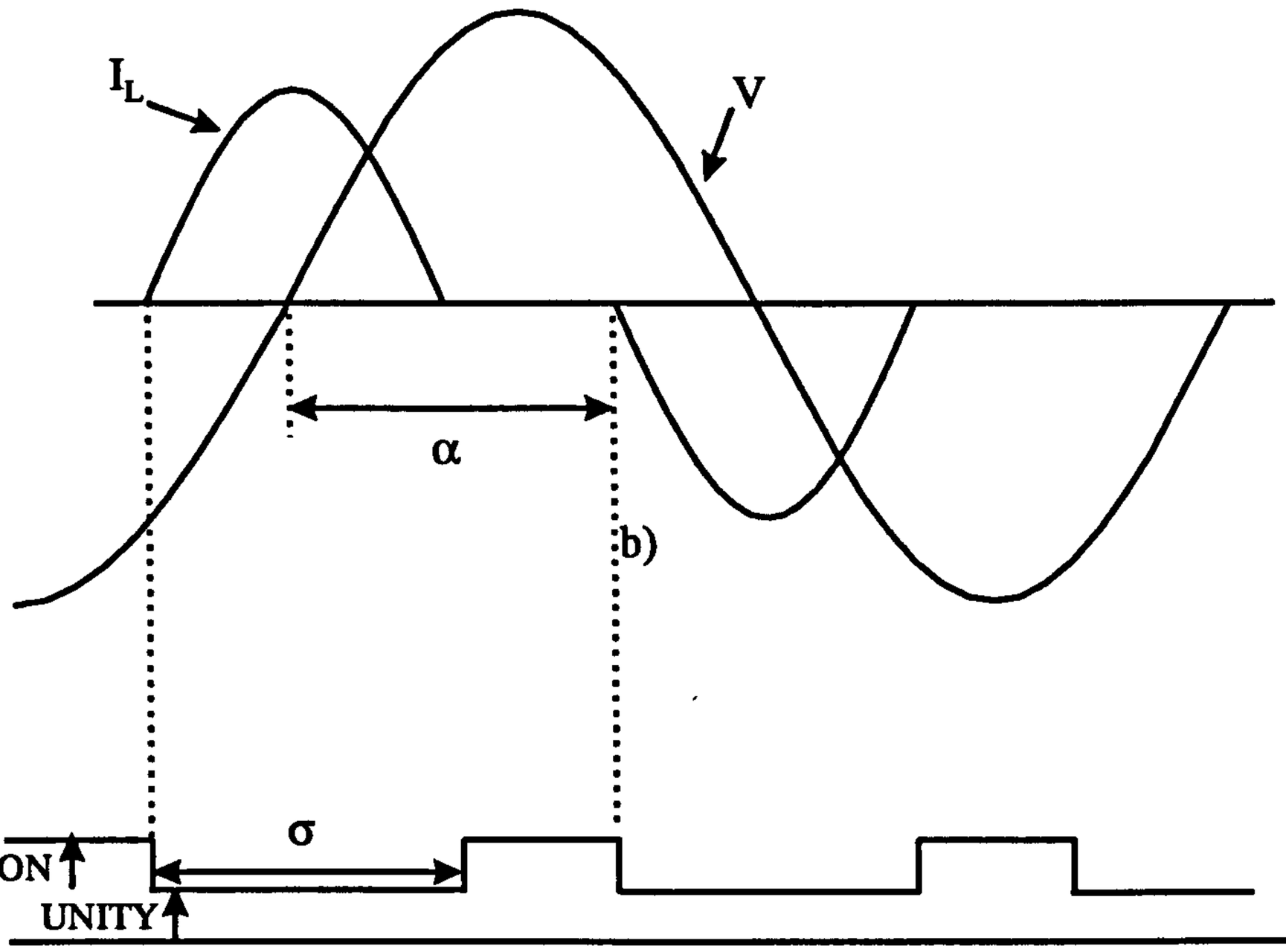
I_L
V
α
b)
σ
NCON
UNITY

c)

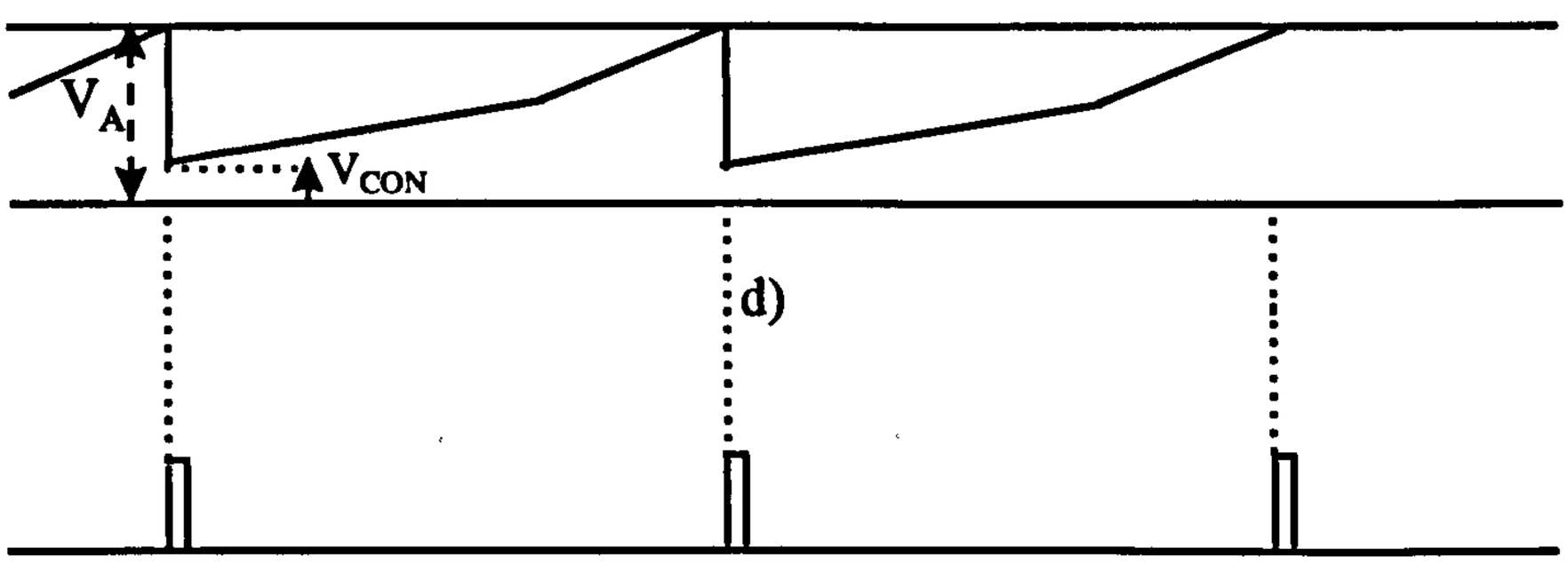
V_A
V_{CON}
d)

e)

Figure 7.16.1 Gate pulse generator with waveforms

Upon increasing the magnitude of V_{CON} the value of α would decrease and therefore σ would increase. This results in a gate pulse generator where σ is proportional to V_{CON}. From figure 7.16.1(d) it follows that V_A is related to V_{CON} through the gain G and the two regions of conduction and non-conduction. This can be expressed in the following equations:

$$\int_0^{\omega} Gdt = \frac{G\sigma}{\omega} \tag{7.19}$$

$$\int_0^{\frac{\alpha-\frac{\sigma}{2}}{\omega}} Gdt = 2G\left(\frac{\alpha-\frac{\sigma}{2}}{\omega}\right) \tag{7.20}$$

$$V_A = V_{CON} - \frac{G\sigma}{2\pi f} + \frac{G}{f} \tag{7.21}$$

using $\alpha = \pi - \frac{\sigma}{2}$

then

$$V_A = V_{CON} - \frac{G\sigma}{2\pi f} + \frac{G}{f} \tag{7.22}$$

If the values G, f and V_A are :

$G=50$

$F=50$ Hz

$V_A = 1.0$

then $V_{CON} = \frac{\sigma}{2\pi}$

From this expression it follows that for $\sigma = 180^\circ$ and for $\sigma = 0^\circ$, $V_{CON} = 0.0$.

In addition to being able to fire at the correct point, the gate pulse generator must also correct for changes in voltage synchronisation. For example, on systems where a line to ground fault would cause a phase shift in the voltage across a Δ configured TCR,

the gate pulse generator must correct the firing for this phase shift. Studies later on will show that using the above model synchronisation is achieved in a very reasonable time scale.

To build in the above model of the firing system in the EMTP, TACS models were used such as type 93 for the input sources, type 58 for the integrator, type 52 for the Z.P.D. , and FORTRAN based expressions for the block devices.

Using EMTP the gate pulse generator can produce firing pulses for the requested conduction angles. Up to this point we have been concerned with the function of the TCR. The ac system has been assumed to be a perfect voltage source. Of course, the greater power of digital simulation is the ability to look at the interaction between the thyristor controlled reactor and the ac power system. This dynamic interaction will be studied next.

7.6.3.2 Phase Locked Loop (PLL) method

As discussed before a typical gate pulse generator would calculate the firing angle α from the point of zero voltage crossings of the commutating bus. This type of system acts correctly if the points of zero voltage crossing are accurately known. This is not the case since both harmonics and transients are expected. Distortion on the commutating bus may shift or produce multiple zero crossings. An imbalance in the three phase voltages may result in the zero crossings being more (or less) than 120° apart. The net result is that individual phase firing techniques are very susceptible to harmonic instability.

One alternative method to the one that was described before in section 7.6.3.1 is the Phase Locked Loop (PLL) method. A PLL generates a fundamental frequency waveform which is in phase with the positive sequence component of the commutating bus voltages. The PLL generally uses a feedback control system to follow changes in the frequency of the commutating bus. This technique prevents the need to observe zero crossings and is effective in combating harmonic instability.

The phase locked loop was first introduced for AC/DC convertors in 1968 [20]. Later with significant improvements, PLL-based systems were introduced in HVDC

control. The first PLL's principle for controlling TCRs was reported by Ainsworth [12]. Gole, Sood and Mootoosamy in 1989 [13] introduced the PLL method for controlling Static Var Compensator Systems. A similar model was developed by the Gole, and Sood in 1990 [2] using the Electromagnetic Transients Program EMTDC. A Static Var Compensator model will be developed later in this chapter based on the principles of the above two papers [2] and [13]. According to [2] a built -in-dq0-transformation based PLL is provided as the basic PLL model. Figure 7.16.2 shows a block diagram of this type of PLL.

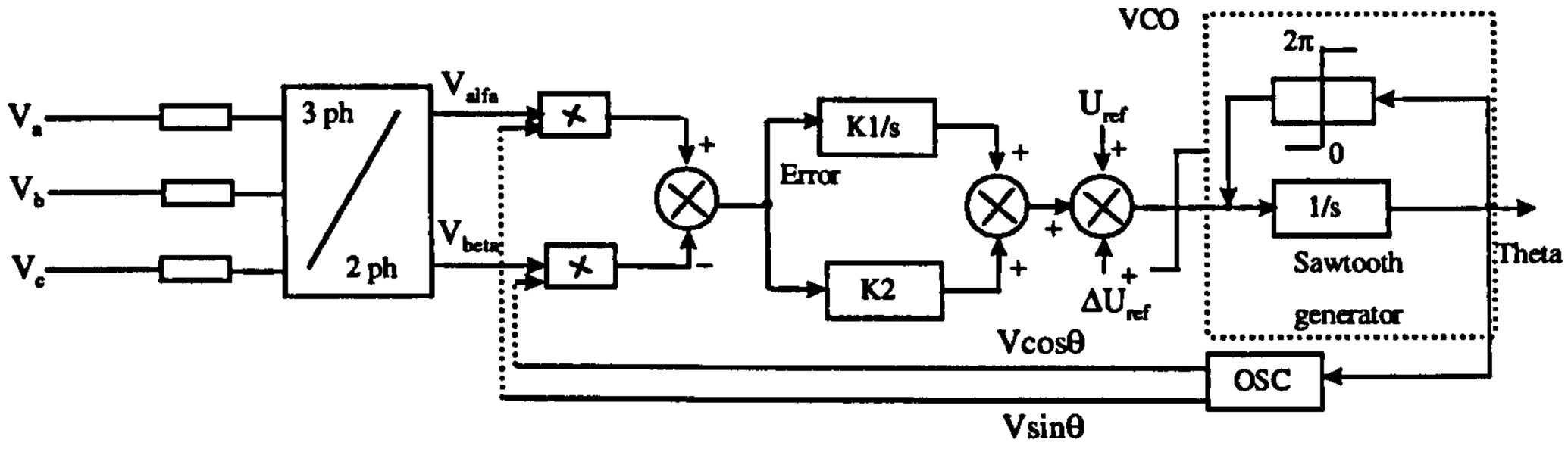

Figure 7.16.2 Phase Locked Loop Oscillator

The three phase synchronising voltages derived from the commutating bus are V_a, V_b and V_c. Using a 3-phase to 2-phase transformation, the direct and quadrature axes voltages, V_{alfa} and V_{beta} respectively, are derived according to the following equations:

$$V_{alfa} = (2/3)V_a - (1/3)V_b - (1/3)V_c \tag{7.23}$$

$$V_{beta} = (1/\sqrt{3})(V_b - V_c) \tag{7.24}$$

An error signal is generated according to the following equation:

$$\text{Error} = V_{alfa} V \sin\theta - V_{beta} V \cos\theta \tag{7.25}$$

where θ is the output of the Voltage Controlled Oscillator (VCO).

The error signal is acted upon by a PI controller with proportional gain K2 and integral gain K1. This is followed by a VCO to derive a control signal Theta θ for a Sine-Cosine Oscillator; the nominal frequency of the VCO is controlled by a reference voltage U_{ref}; dynamic modulation of this reference voltage can be accomplished by the input ΔU_{ref}. The output of the VCO, which is limited between 0 and 180 degrees, generates the timing Sawtooth waveform with value θ, which is utilised to derive the firing pulses for the valves of the compensator :

$$\theta = [(K1/s + K2)(error) + U_{ref} + \Delta U_{ref}]/s \qquad (7.26)$$

where s is the differential operator $\frac{d}{dt}$. The outputs of the Sine-Cosine Oscillator, $V\sin\theta$ and $V\cos\theta$, are fed back as indicated in equation (7.25). The output θ is a ramp which is synchronised to the Phase A commutating bus line to ground voltage. The output signal is then phase shifted by simply adding a constant angle to the ramp to generate the firing ramp for a valve. The ramps of the other valves are generated by adding 60° increments to the previous valve.

The actual firing is accomplished for each valve by comparing the alpha order to the value of the ramp.

Simulation results presented later in this chapter will demonstrate a SVC controller with the control method presented in [2] using the Phase Locked Loop firing method for various system conditions. A comparison will also be made with results taken from the control and the firing method proposed in this chapter. The validation of the results using the SVC controller presented in this chapter prove the effectiveness of the control method and the ability of the firing system to establish accurate firing timing in a timescale similar to the PLL method.

7.7 COMPUTER SIMULATION OF THE SVC

The development of an SVC model for the EMTP program has been previously presented. The working of this SVC model in power systems will now be demonstrated. The SVC model will be connected to different power systems and typical waveshapes will be shown. Aspects of the initialisation process of the EMTP program will also be discussed.

7.7.1 Power systems under investigation

The two power systems to be simulated with the SVC system are shown in figures 7.17 and 7.18. For the system in figure 7.17 a network equivalent system with short-circuit contribution of 4.2 GVA has been represented and it accounts for the source and its impedance in bus 1, interconnected by a 230kV transmission line. The transmission line has a length of 200km and in the middle of it, the SVC with the filters are connected. The source is represented using number 14 of the TACS devices in the EMTP, and the transmission line from bus 1 to 2, and from 2 to 3 was modelled using the distributed line model. The transformer between bus 3 and bus 4 was represented by a series inductance referred to as the 230kV line, followed by a load. Finally, the load was represented by a R-L simple model.

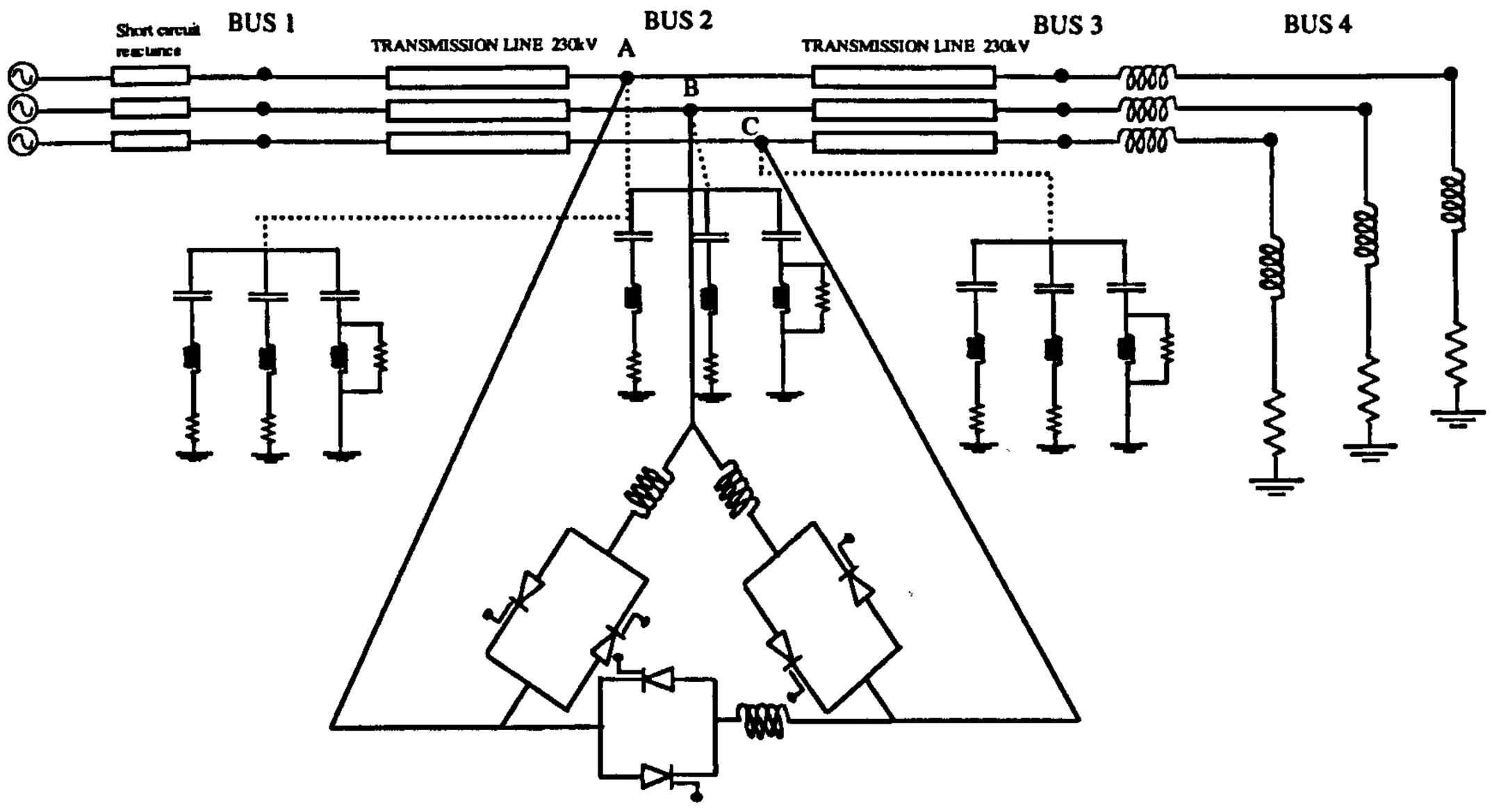

Figure 7.17 Diagram of power system 1

For the system in the figure 7.18 the network equivalent systems in buses 1 and 3 were represented as in figure 7.17, with short-circuit contribution of 4.2 GVA each, interconnected by the 230kV transmission line model as before. The SVC with the filters are connected to the middle of the transmission line. Although the power systems are simple, they are capable of demonstrating several problems of large interconnected systems without the loss of generality.

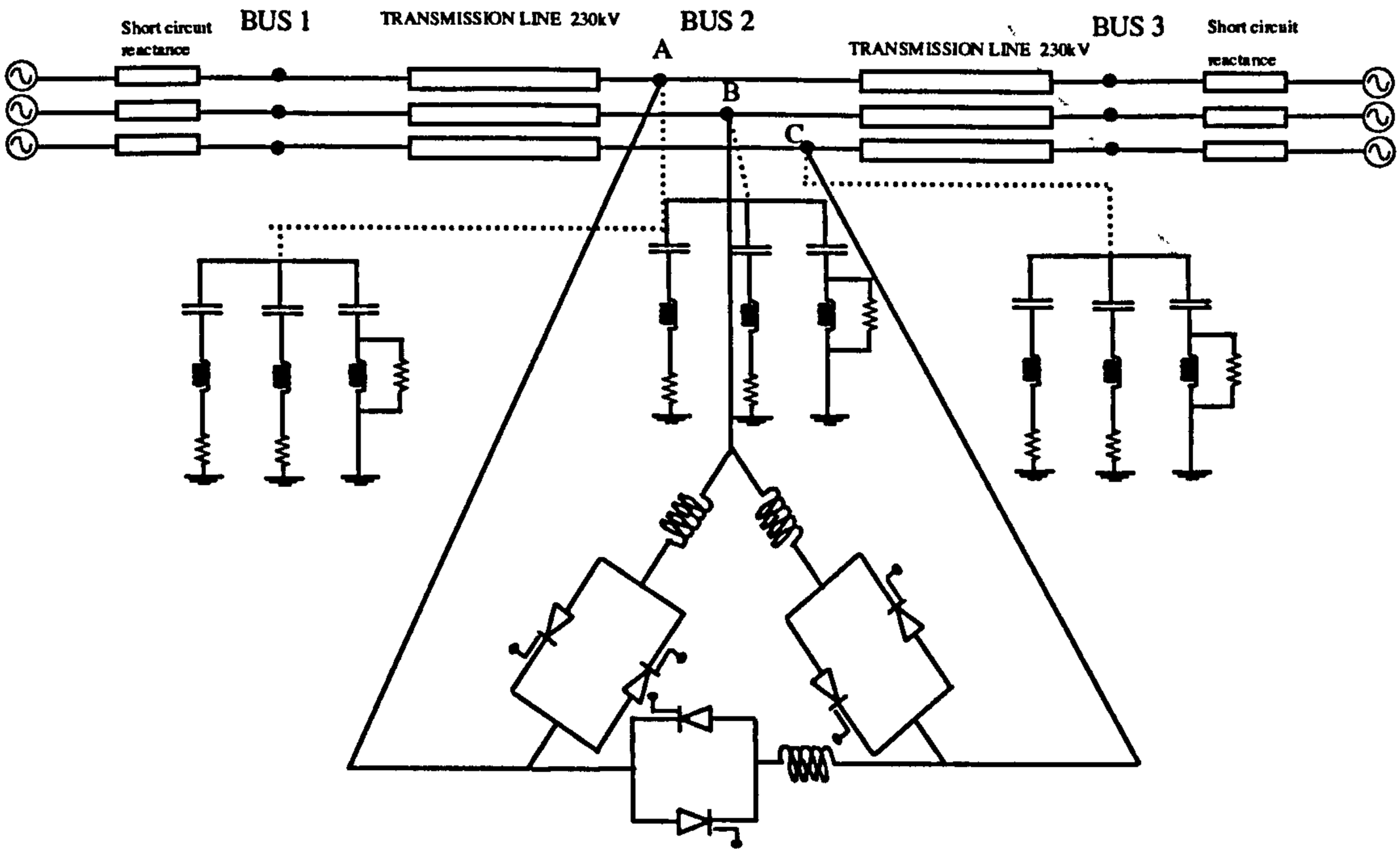

Figure 7.18 Diagram of power system 2

7.7.2 Advantages of SVCs over traditional voltage control systems

Reactive power support is a traditional way of voltage control in power systems. For this reason fixed capacitor banks have been used in the past, in order to provide voltage support under different power system arrangements. However, this method of control is inflexible; if a light load is used, the use of capacitors results in overvoltage. Using SVCs this problem no longer exists, since they provide voltage control for a wide range of load changes by exchanging reactive power with the network they are connected to.

For the system in figure 7.17, figure 7.19 illustrates the RMS value of phase A of the voltage in bus 2, when the TCR is out, and the filters in bus 2 have been represented by their capacitance only. In this case a light load was used in bus 4. Using a 230kV line to line voltage at bus 1, an RMS value of 132kV is almost expected. However, with the use of capacitors the voltage is about 155 kV, an overvoltage of 20%.

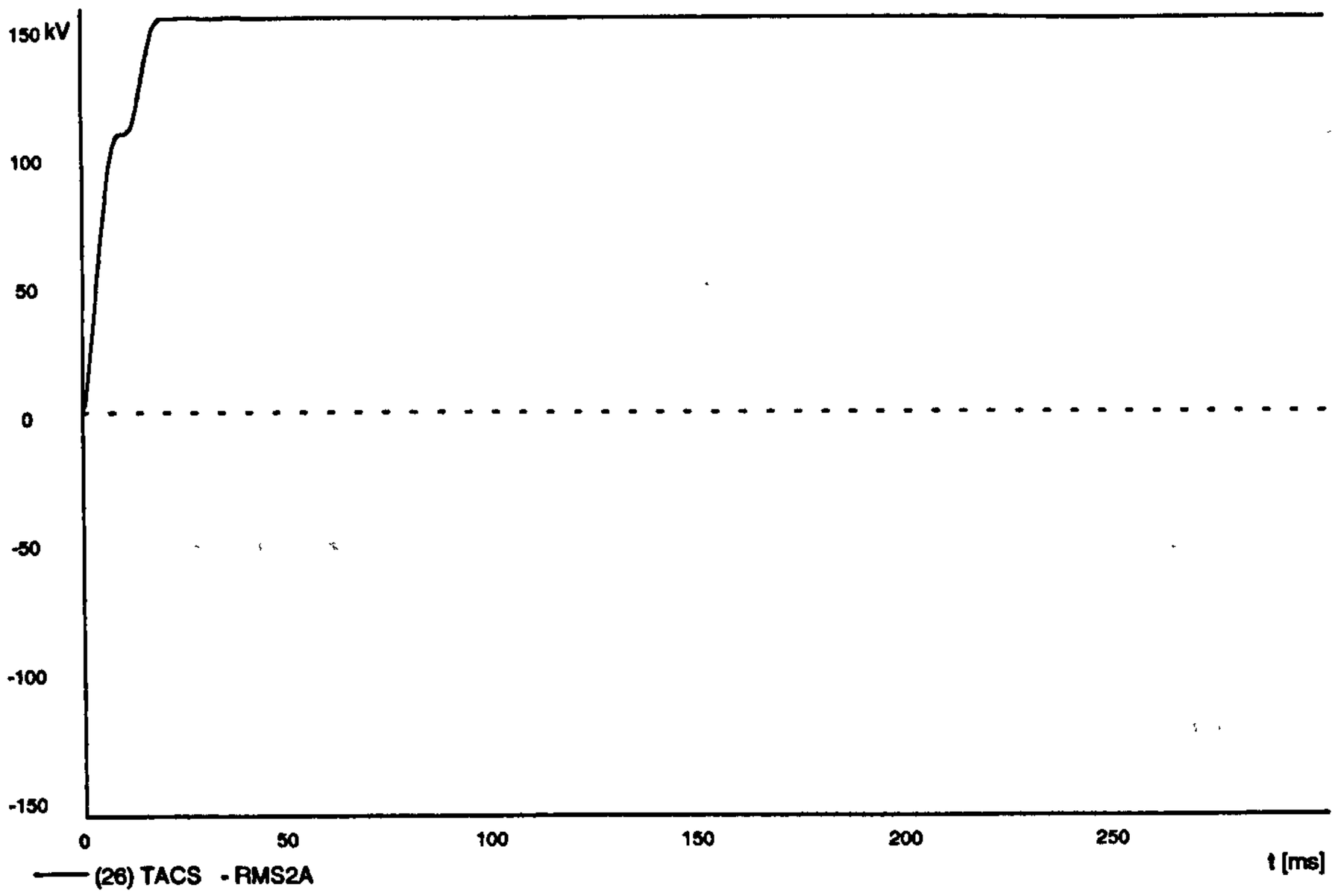

Figure 7.19 RMS voltage at bus 2 without the TCR

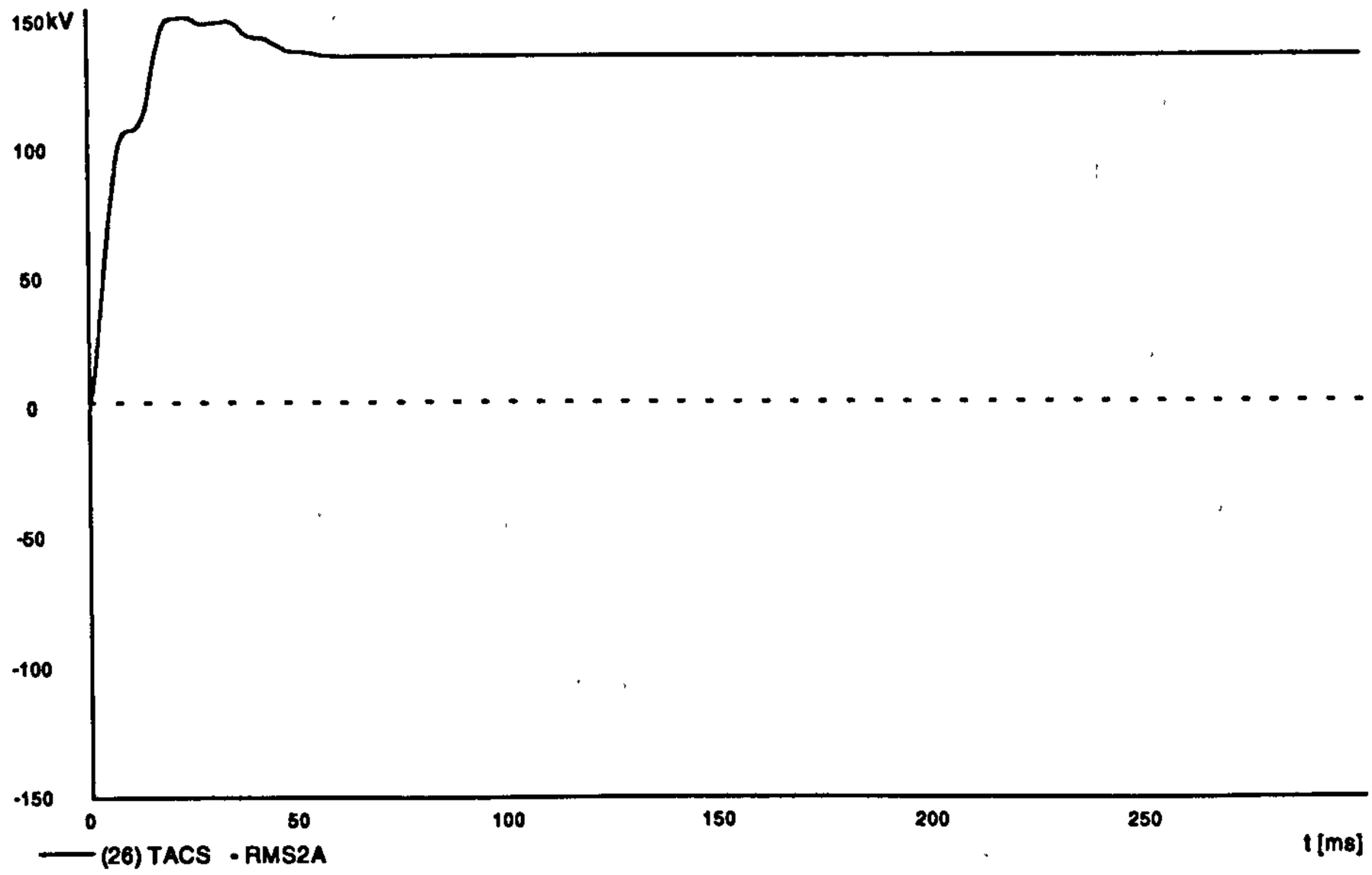

Figure 7.20 RMS voltage at bus 2 with the TCR

Figure 7.20 shows the same model with the TCR connected. In this case, as can be seen from the graph the voltage at bus 2 is almost 132kV, which is the voltage that expected.

This result shows that the SVC is a very powerful tool in transmission systems since it has the ability to maintain a constant voltage at its terminals, compared to other traditional methods that were used in the past.

7.7.3 Initialisation of the SVC model in the EMTP program

The EMTP simulations take place in two different stages, namely : steady-state simulation and loop-time simulation. The steady-state initialisation is just a single-frequency initialisation, i.e. a phasor solution at the fundamental frequency. The initialisation process is a key feature of the digital model[19]. It is important to carry over initialisation to approach steady-state condition with minimum cpu time. If the initialisation is not carefully done abnormal modes of operation may occur, or the system can take too long to achieve steady-state condition.

The best way to deal with the initialisation problem is to give initial pulse, which must be between the floating and the TCR full conduction angles. This strategy is adopted and used in both power systems in figures 7.17 and 7.18. The initialisation process will be tested using the power system 1. For this system a small load in bus 4 was used (P=9kW,Q=3kVAR). As in the previous case the filters have been replaced by their equivalent capacitance. For the initialisation process, we must take into consideration that some blocks of the SVC control system need time to be initialised correctly. In our case an initial pulse for $\sigma = 120^{\circ}$ was given. In figure 7.21(a) the reference source voltage is shown, and in figure (b) the three currents at the branches of the delta connected SVC are illustrated. At figures (c) ,(d) and (e) the voltages at bus 2 where the SVC is connected, were plotted. From the graphs we can see, that after the first two cycles the SVC is working as required. From the graphs (c),(d),and (e) it is shown that the voltages across the SVC are normalised, having the correct phase sequence. This happens due to the correct firing from the SVC branches

illustrated in graph (b). This graph illustrates that after the first 30 ms the currents have the correct sequence, and only one thyristor is active per cycle. Initialisation is a very important process and its correct operation is vital, before analysing the system's steady-state and transient behaviour.

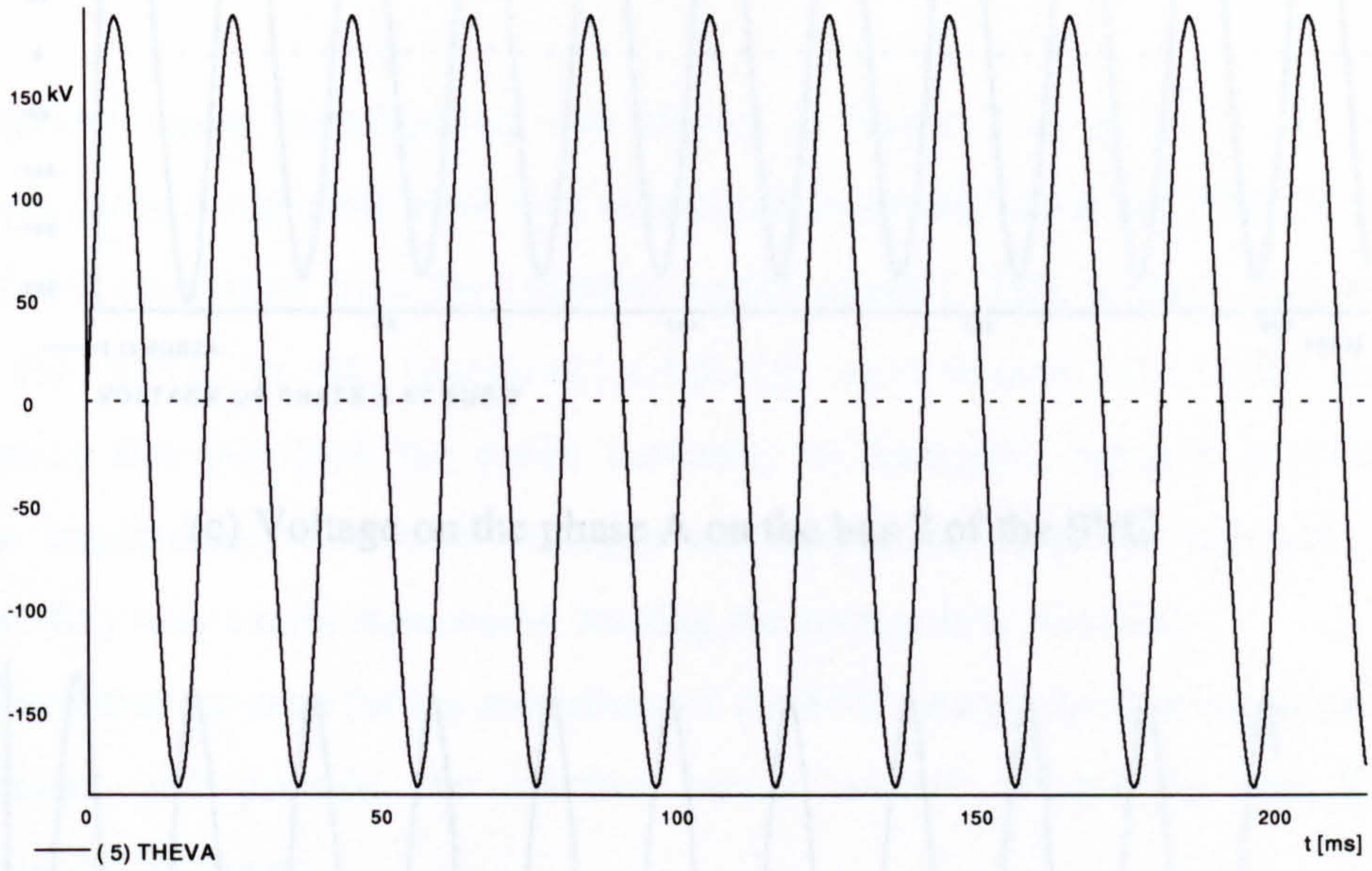

(a) Voltage of phase A of the voltage source

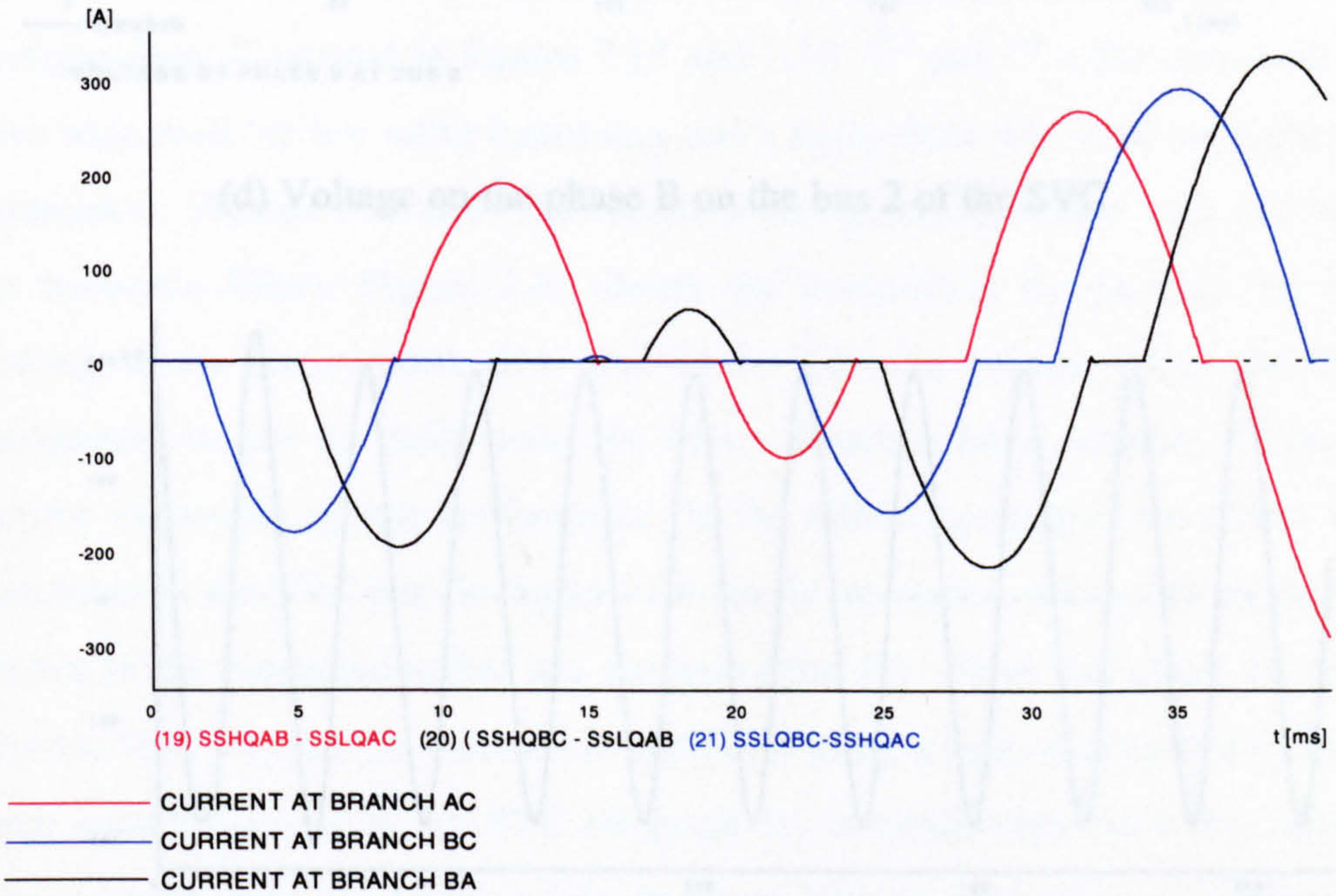

(b) Currents on the SVC branches

Figure 7.21

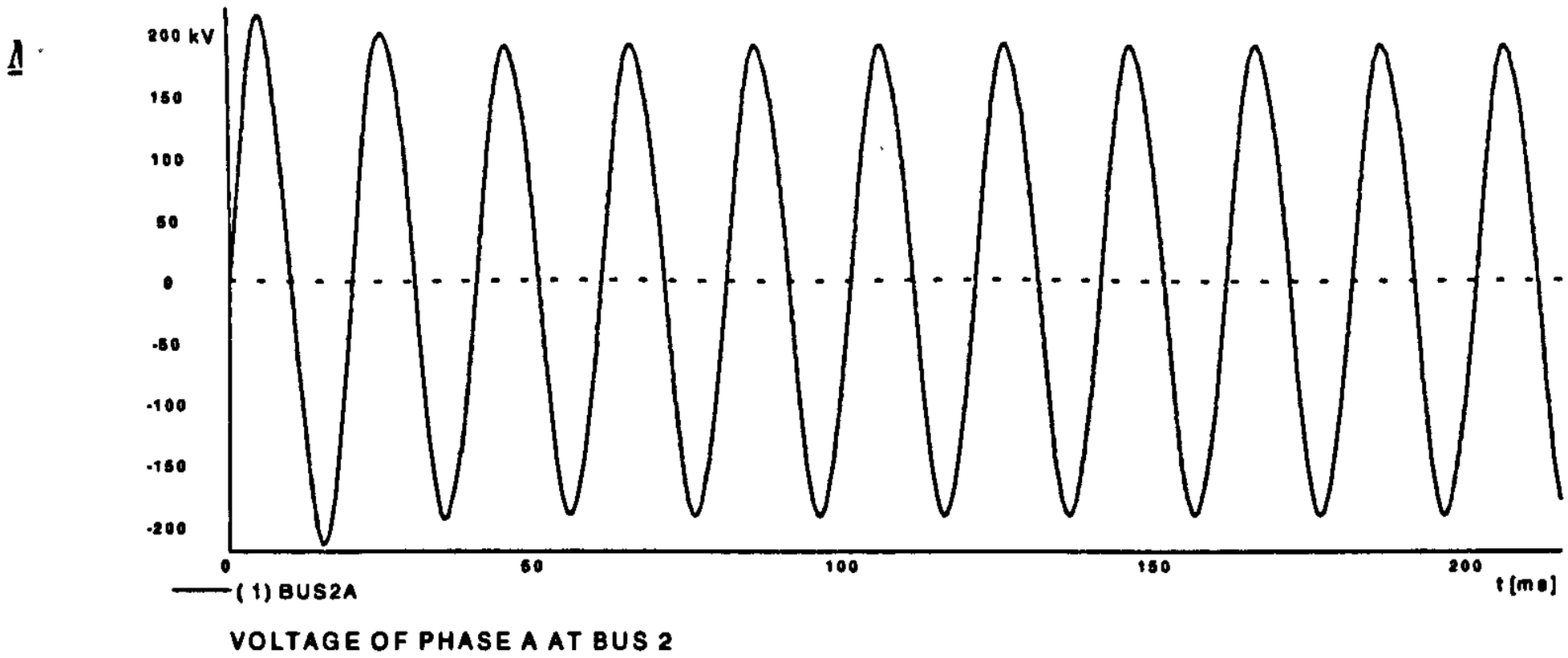

VOLTAGE OF PHASE A AT BUS 2

(c) Voltage on the phase A on the bus 2 of the SVC

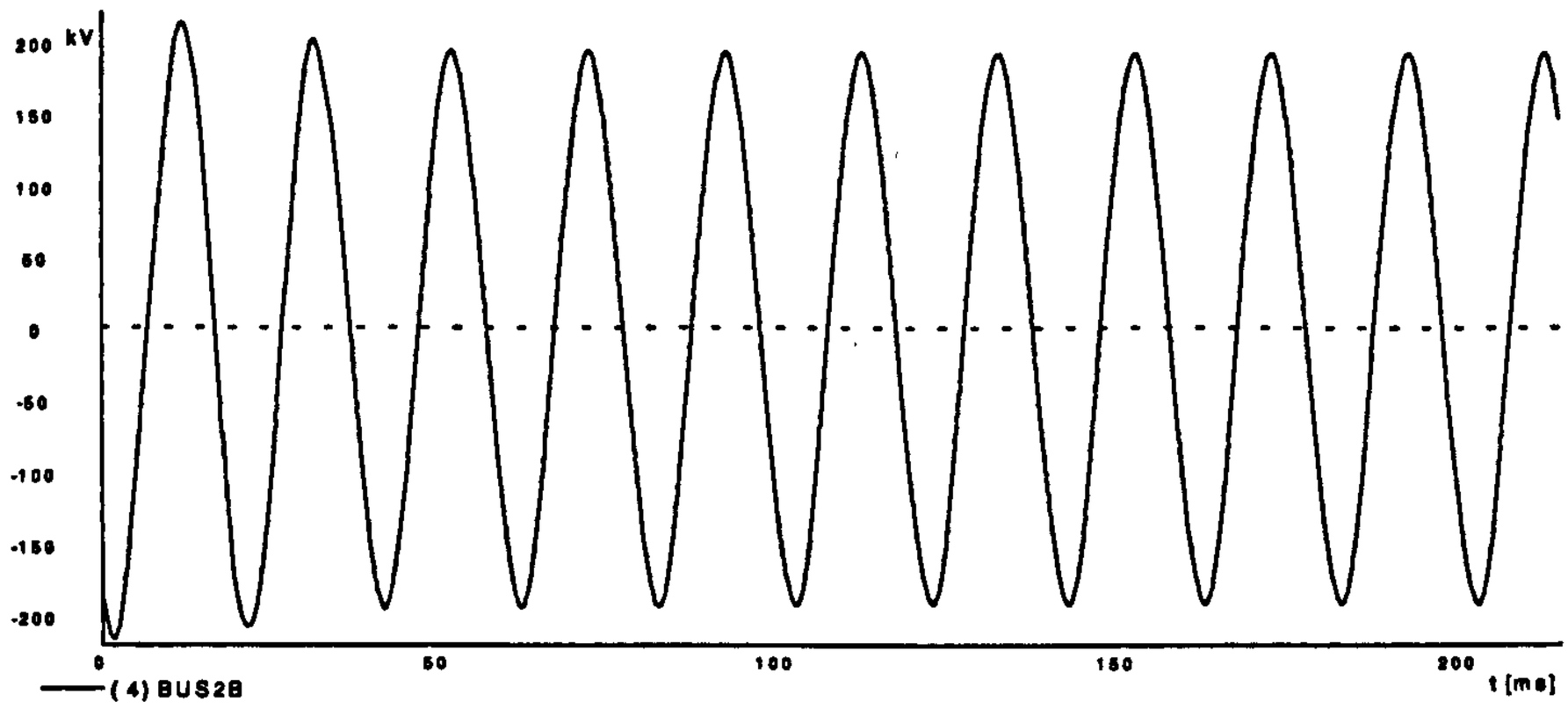

VOLTAGE OF PHASE B AT BUS 2

(d) Voltage on the phase B on the bus 2 of the SVC

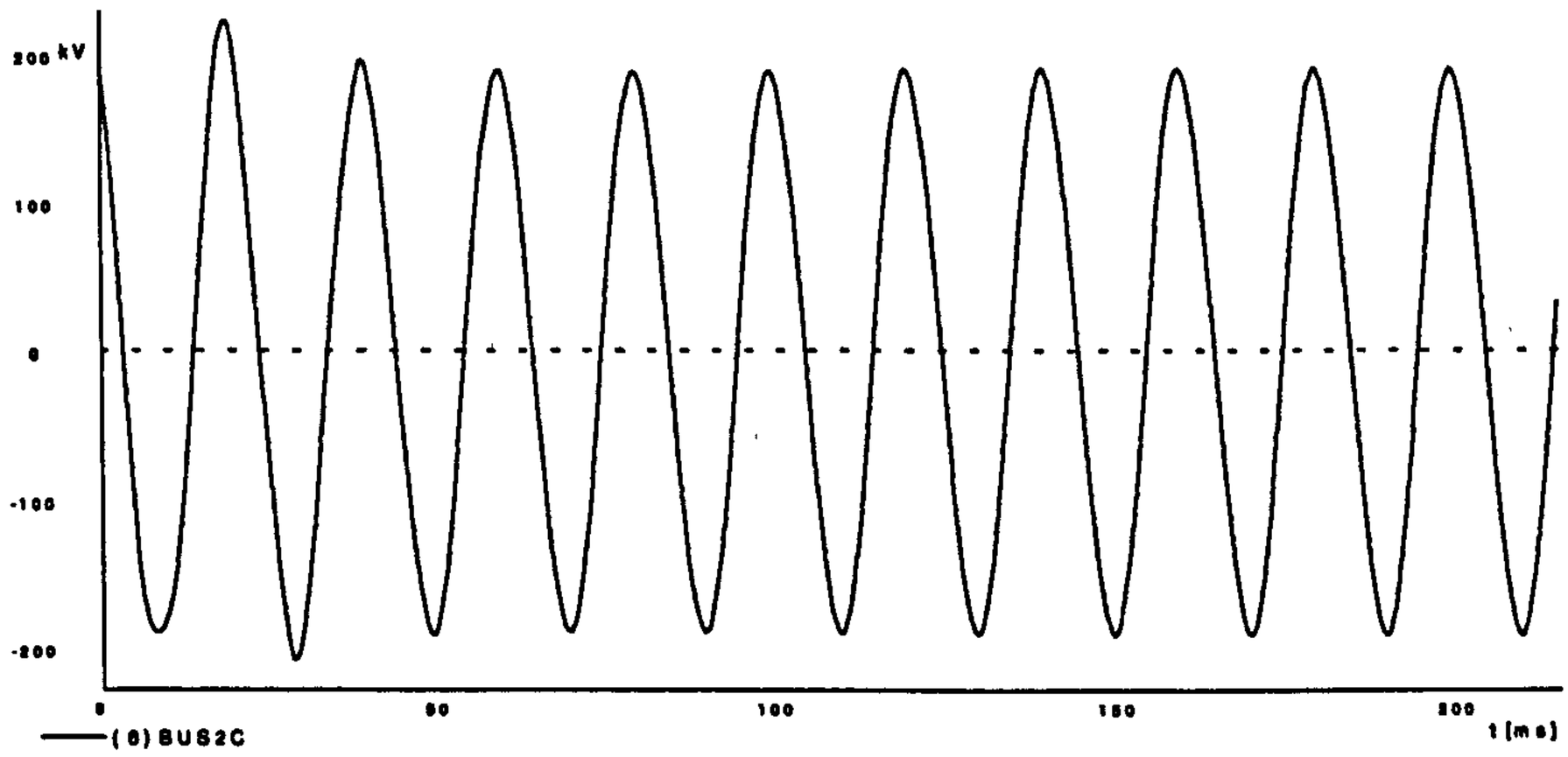

VOLTAGE OF PHASE C AT BUS 2

(e) Voltage on the phase C on the bus 2 of the SVC

Figure 7.21

7.7.4 Steady-state operation of power system 1

The system under investigation was shown in figure 7.17 in 7.7.1. In the two previous cases a capacitor bank was connected in parallel with the SVC in order to supply the capacitive Vars for reactive power control. This method was reported most for SVCs in the literature[1,4,6,9,13], nevertheless, the TCR produces harmonics that penetrate the entire network. As harmonic currents flow through system impedances, harmonic voltages are formed all over the network. In the process they may excite resonances, leading the system into instability.

The filters that are used for the modelling of the SVC absorb these harmonics at high frequencies and provide the reactive power control needed for the SVC at fundamental frequency.

The capacitive range for the SVC is determined through a set of load flow studies. Once this range is determined the inductive reactive power can be found. From the capacitive rating, the capacitance of the filters is calculated, and according to [18] the resistance and reactance of the filters can be obtained. In both power system configurations illustrated in figures 7.17 and 7.18 5^{th} and 7^{th} order harmonic filters have been used for low order harmonics and a damp filter was used for higher order harmonics . Figures 7.22 and 7.23 illustrate the system operation with and without the harmonic filters. Figure 7.22 shows the comparison by plotting the current flowing in the transmission line, and figure 7.23 the voltage where the SVC is connected. As can be easily seen the filters absorb a large amount of harmonics thereby improving system performance. In the following analysis the filters will be connected at the SVC bus. In figure 7.24 for the reference voltage of graph (a), the current of the transmission line has the waveform (b) . From this graph we see, that after the first 2 cycles the current has stabilised using a load of 120kW/40 kVar. The three branch currents of the SVC on graph (c) at steady-state have the symmetry required for a large conduction angle. In figure 7.25 the three phase voltages at bus 2 after the first two cycles have stabilised giving a constant voltage at the SVC terminals. In figure 7.26(a) the active power of the load has been plotted ,followed by the conduction angle which reaches a steady-state value in a reasonable timescale.

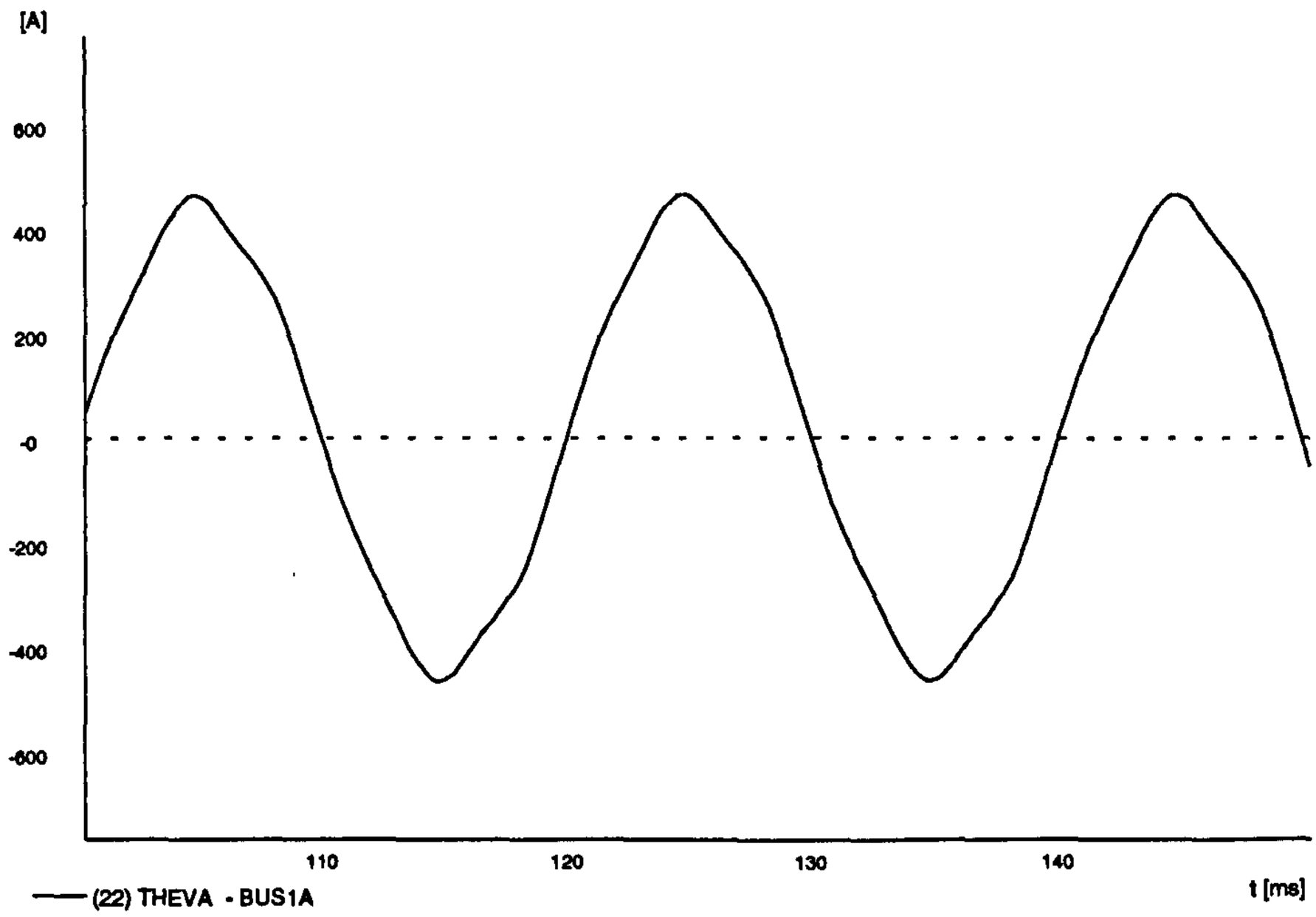

CURRENT BETWEEN THE AC SOURCE AND BUS 1

(a) Current flowing in the transmission line, phase A without filters

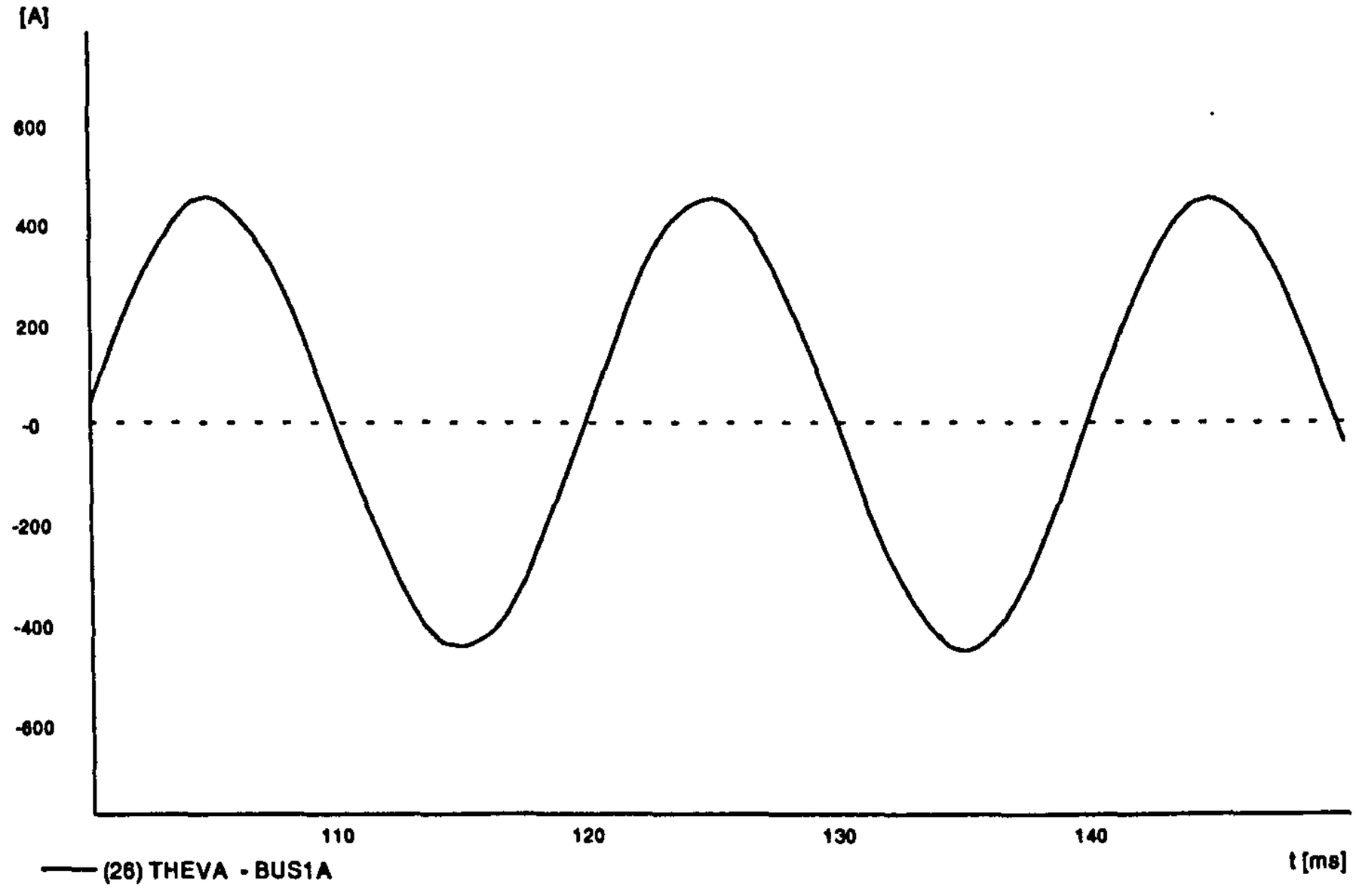

CURRENT OF PHASE A BETWEEN THE SOURCE AND BUS 1

(b) Current flowing in the transmission line, phase A with filters

Figure 7.22

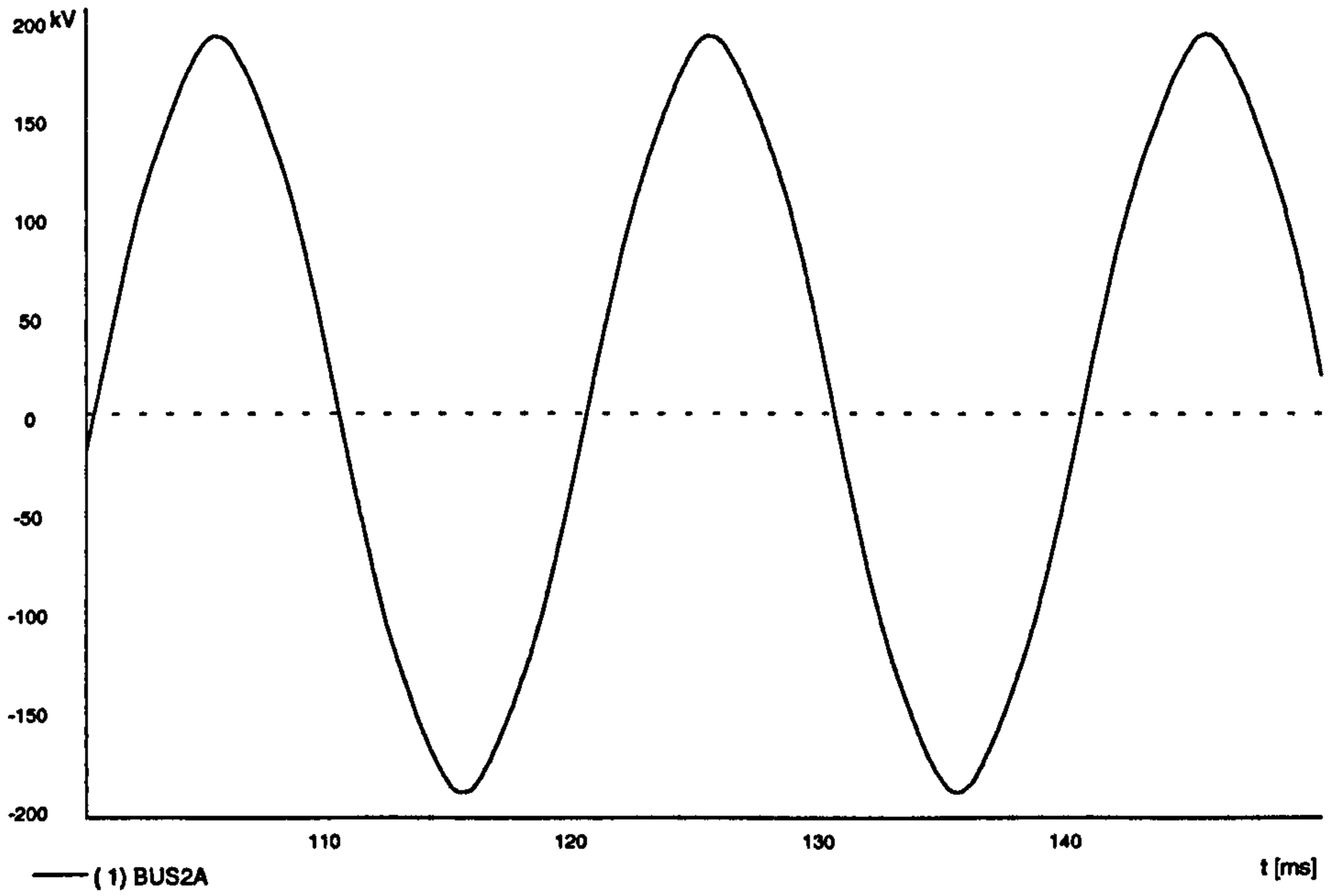

(a) Voltage of phase A at bus 2 without filters

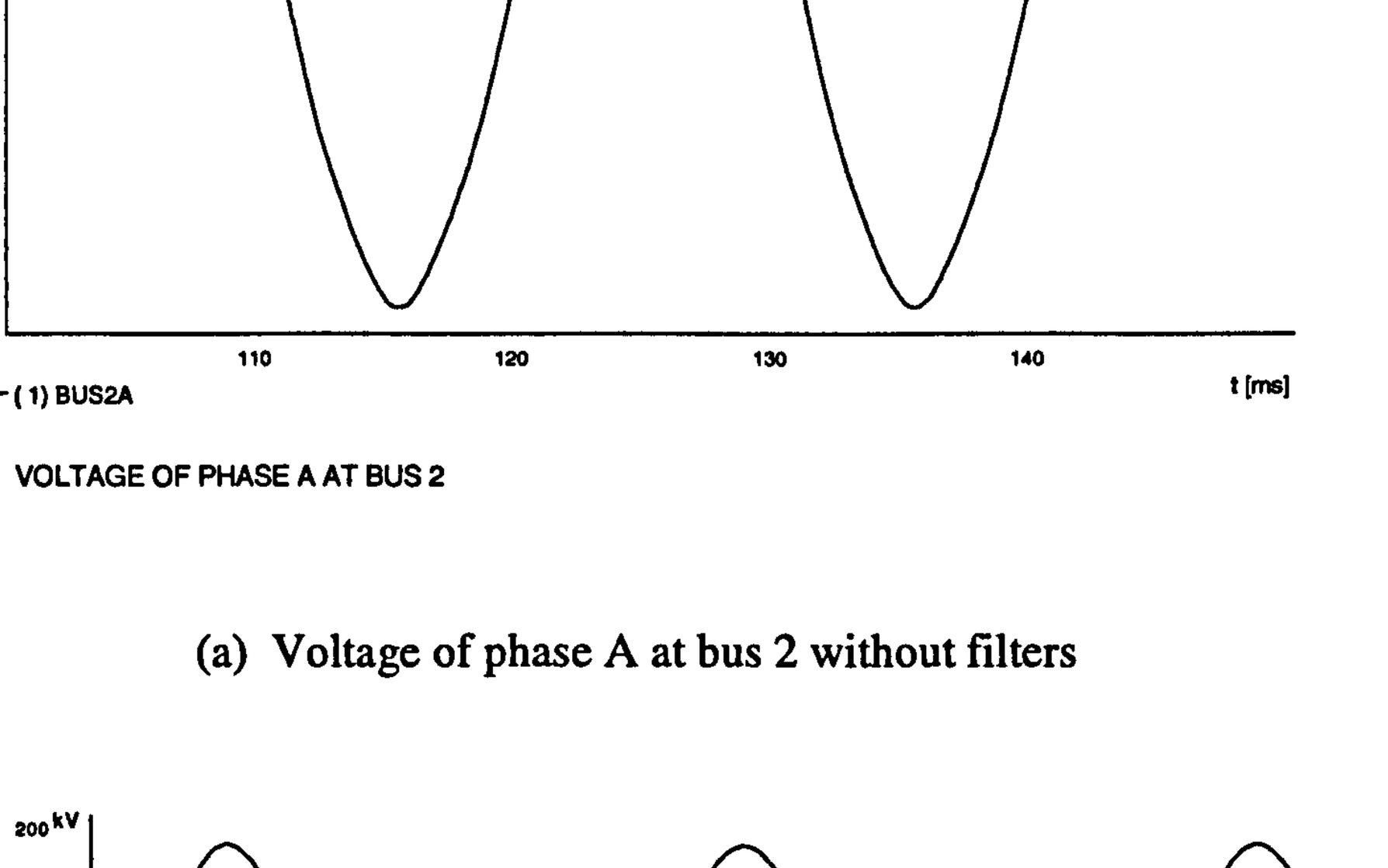

(b) Voltage of phase A at bus 2 with filters

Figure 7.23

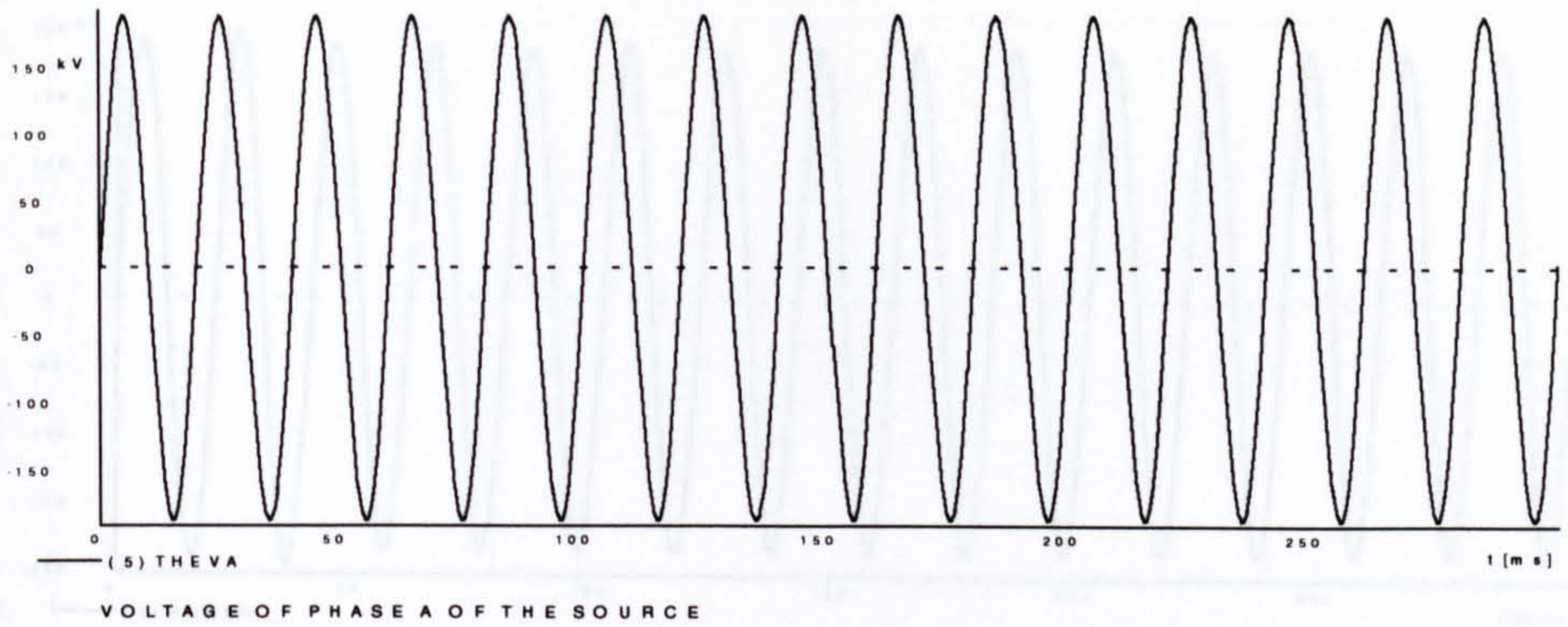

(a) Voltage of phase A of the source

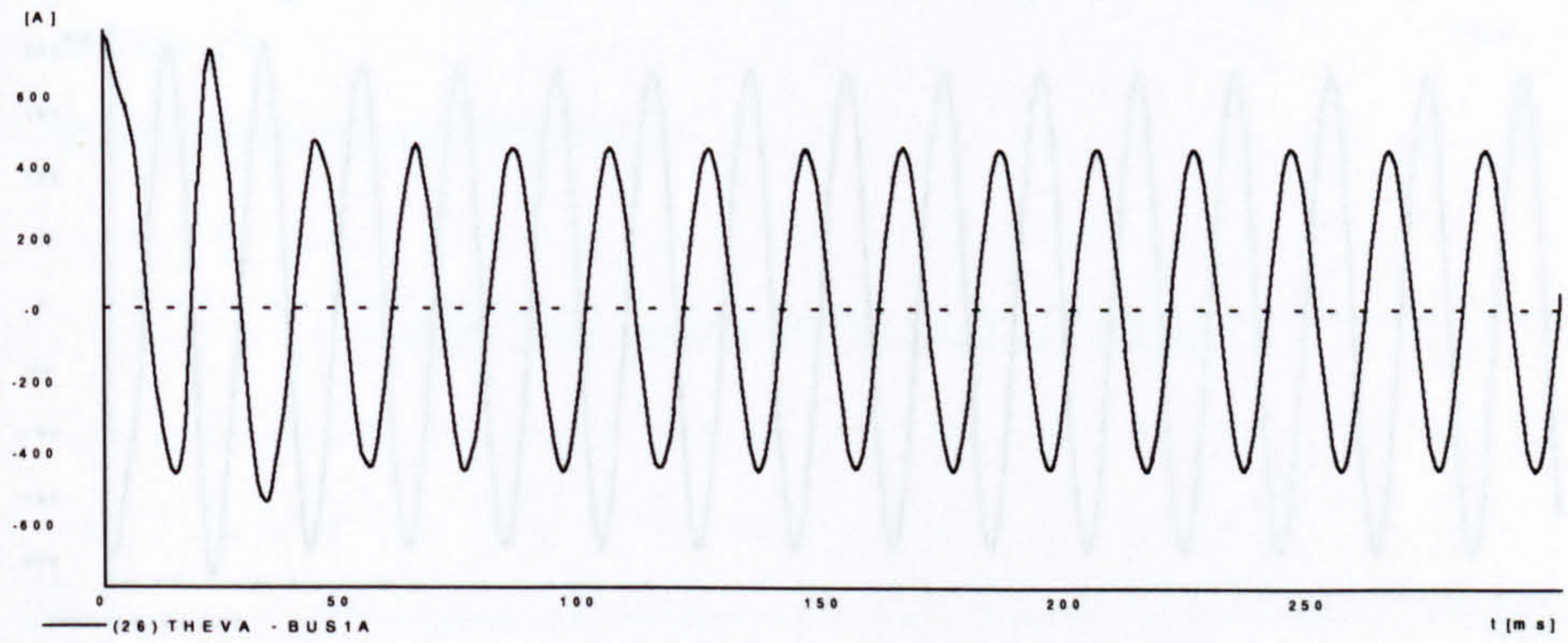

(b) Current of phase A between the source and bus 1

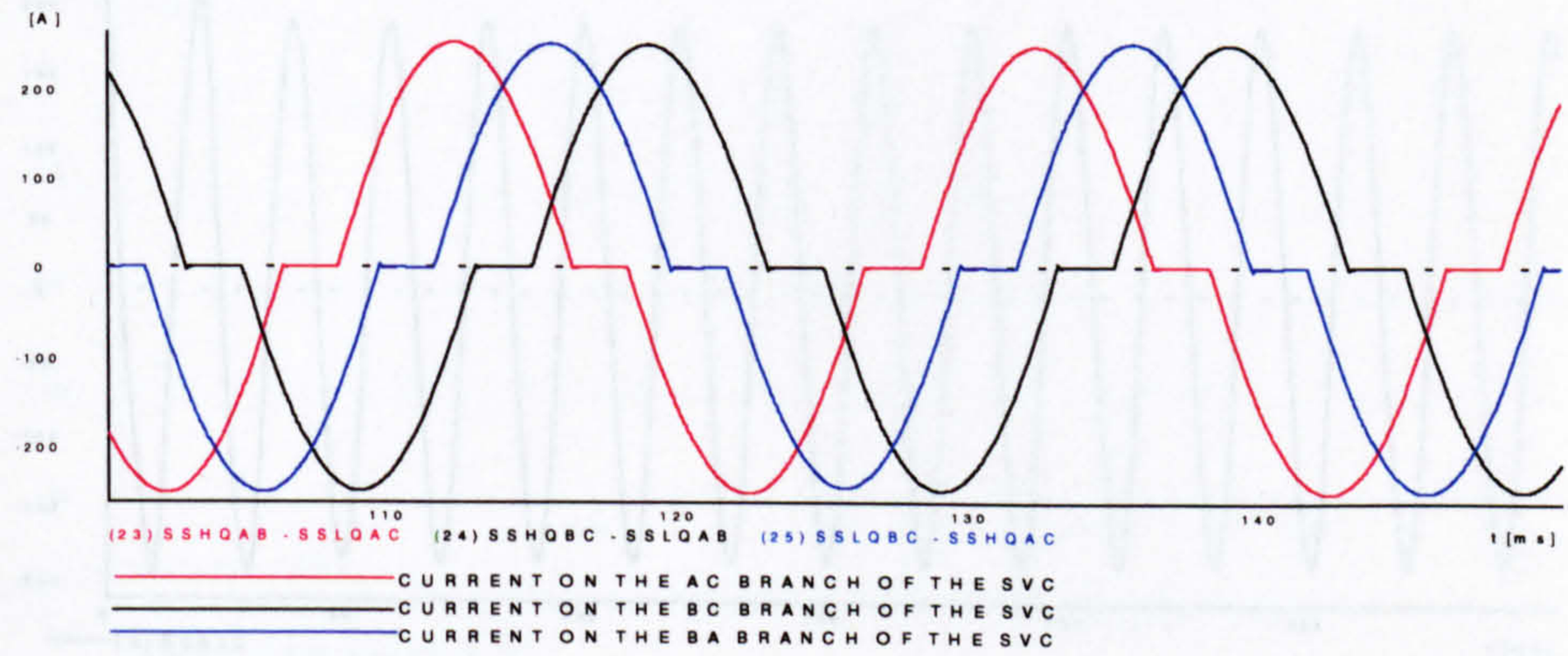

(c) Currents on the branches of the SVC

Figure 7.24

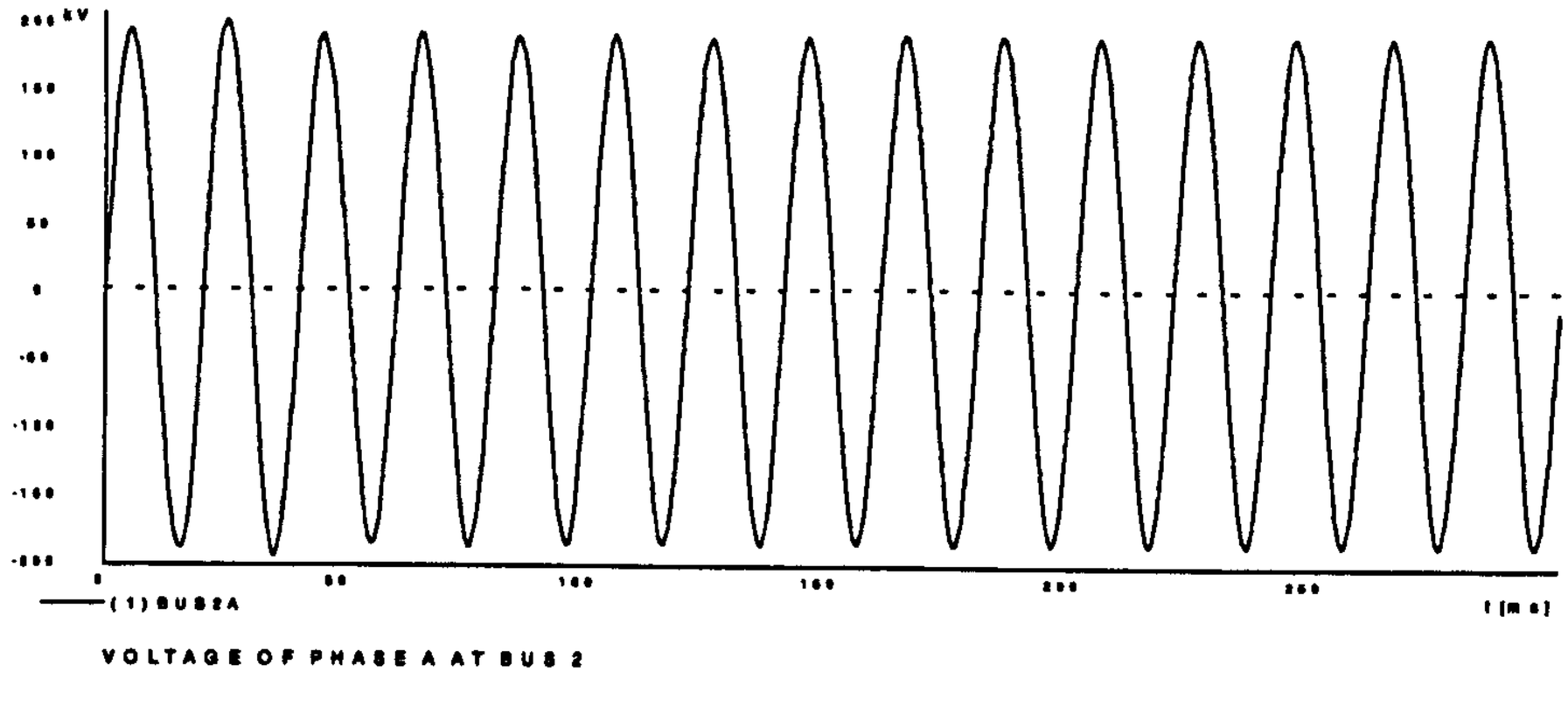

(a) Voltage of phase A at bus 2

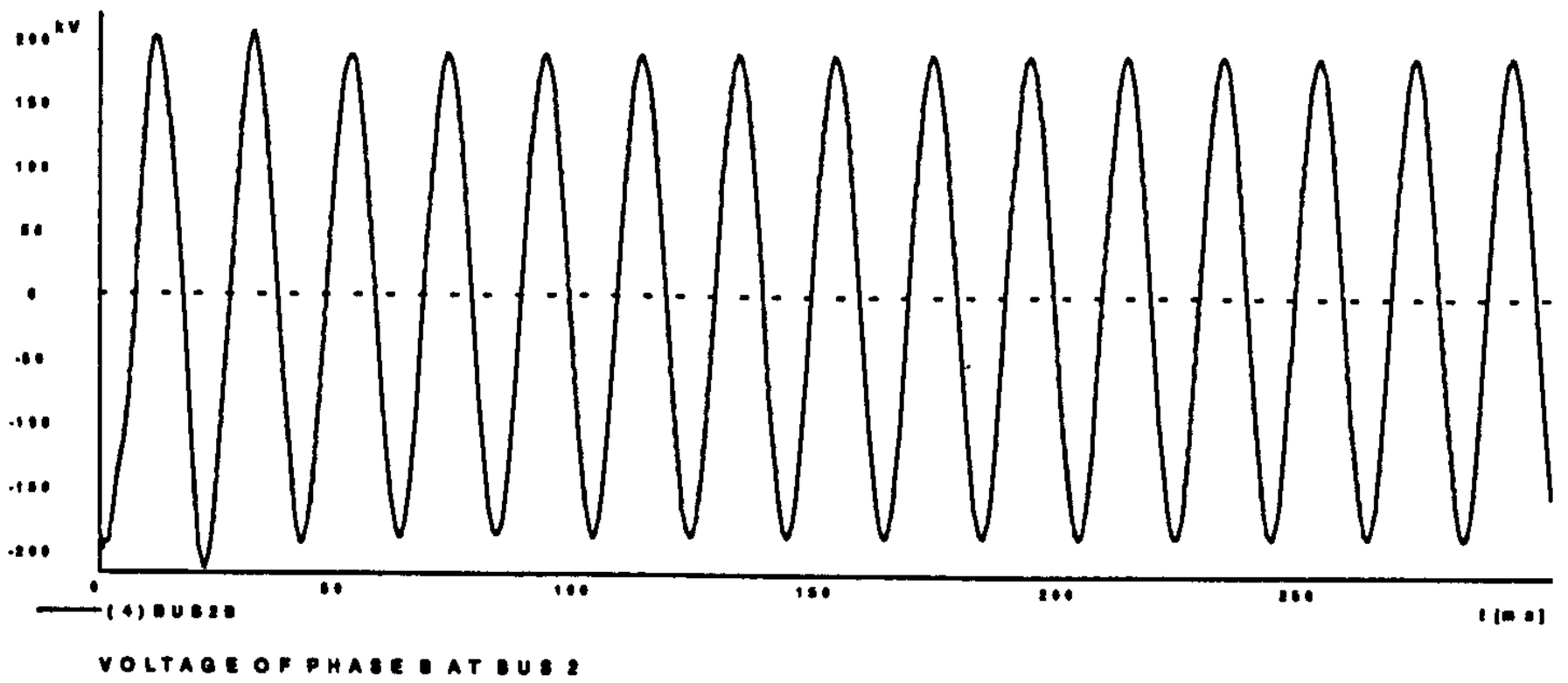

(b) Voltage of phase B at bus 2

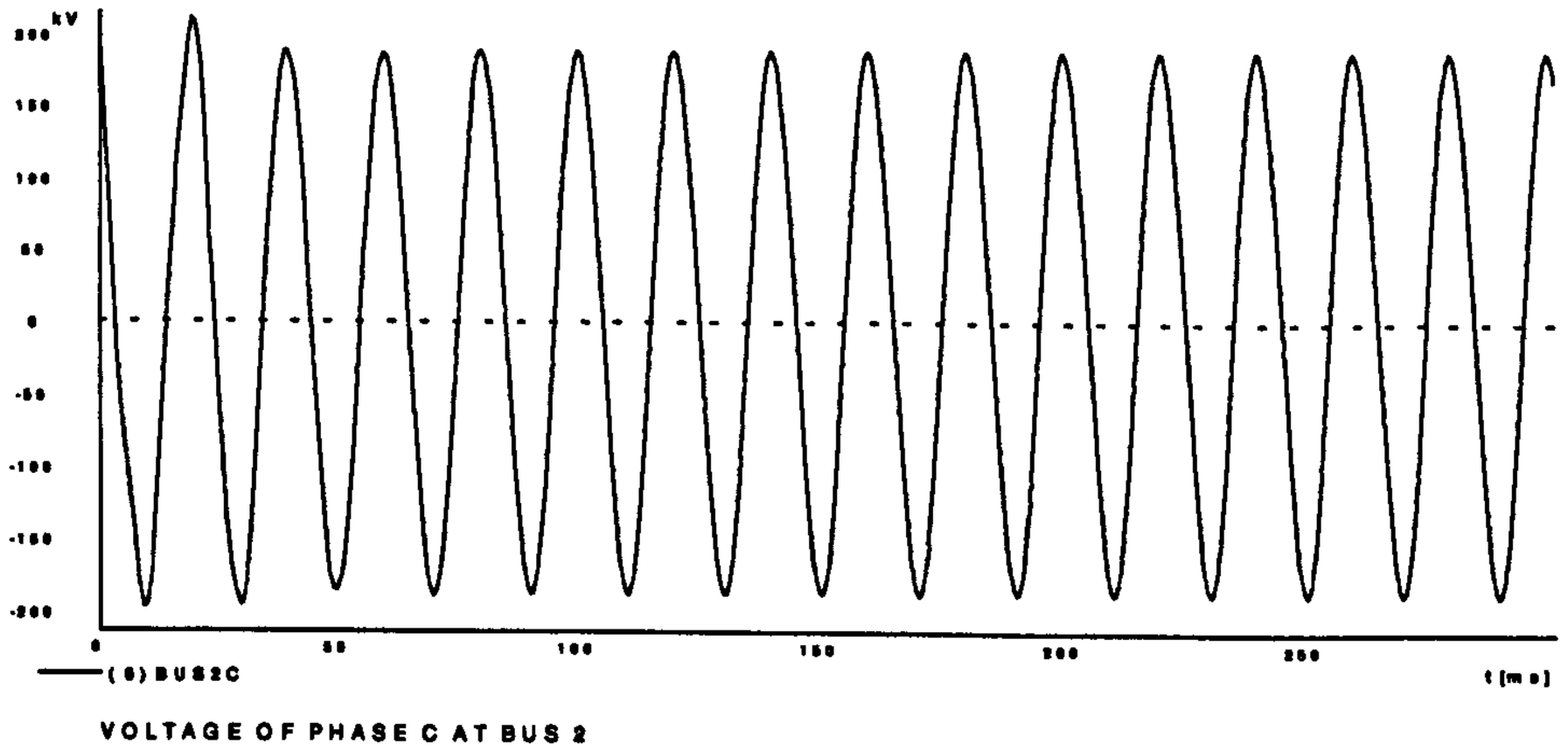

(c) Voltage of phase C at bus 2

Figure 7.25

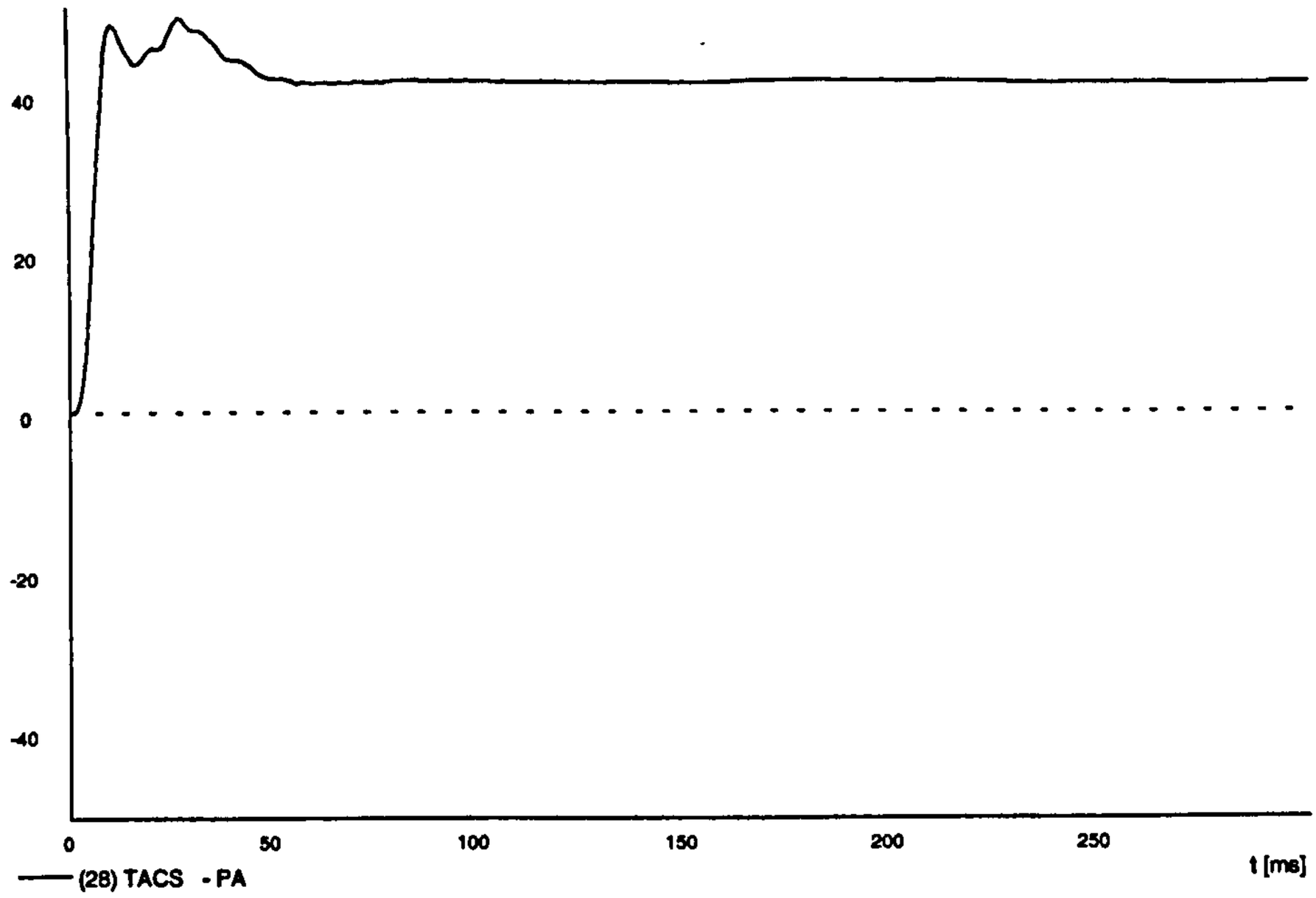

(a) Real power of the load per phase

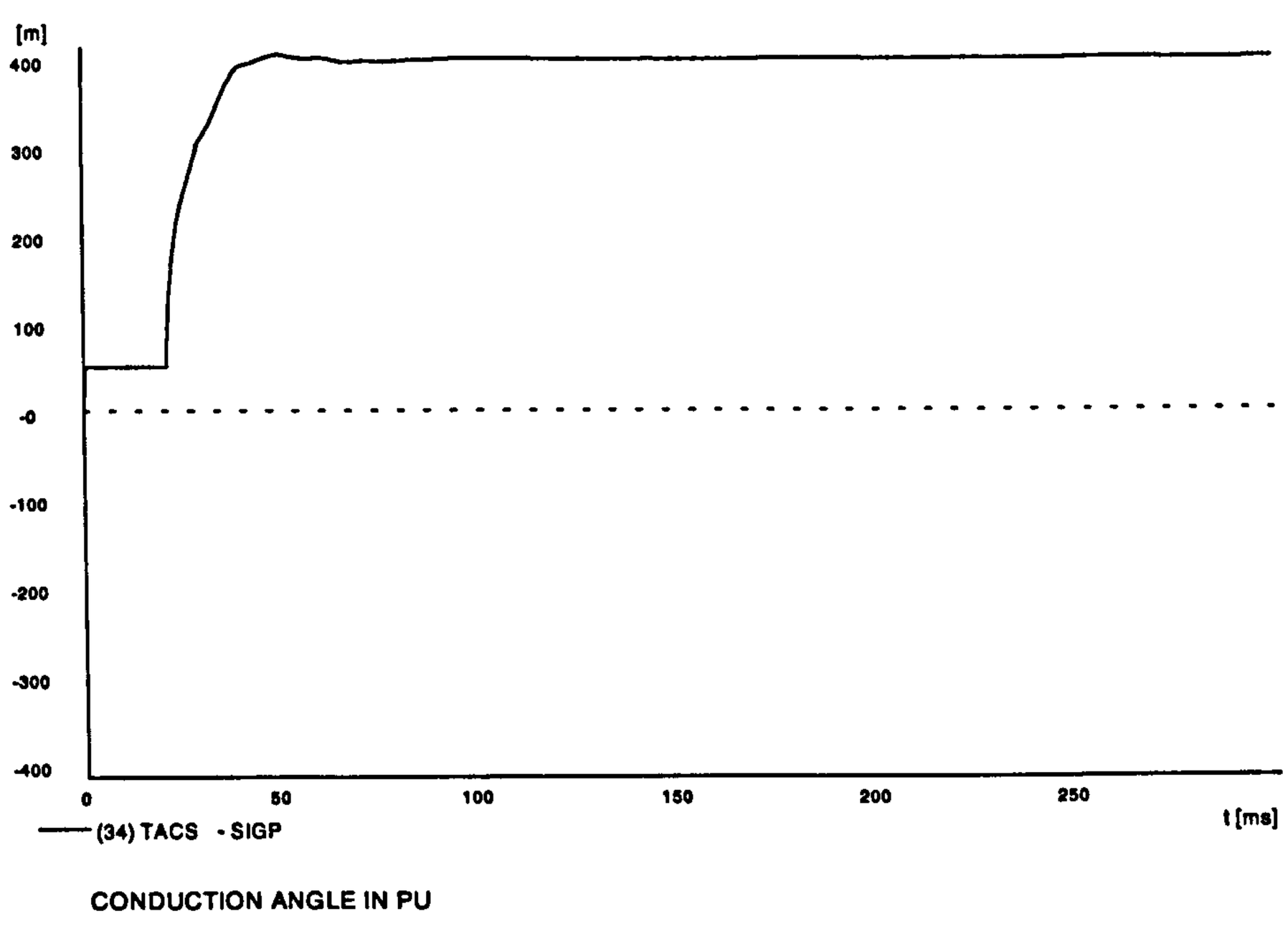

(b) Conduction angle in pu of the SVC

Figure 7.26

7.7.4 Transient behaviour of power system 1

With the objective of studying the interaction between the SVC and the power system in a disturbance condition, the following subsections will show the SVC response in a power system under variable load conditions, phase shift and different fault conditions.

a) SVC response using a variable load

In order to study the system response to small disturbances a variable load was used at bus 4 of figure 7.17. This load can be represented with a simple R-L model with a fixed P/Q ratio. The load change takes place at 100msec, as it is illustrated in figure 7.27(a) by its per phase active power. Due to the load increase there is a voltage decrease, which is corrected in 2 cycles as it is seen from graph 7.28(a). In figure 7.28(b) although there is a voltage drop in the load voltage due to the high load that is used, the voltage at the SVC terminals has the same magnitude with the source voltage at steady state conditions. When the load change occurs, an undervoltage at the SVC terminals takes place; the function of the SVC is to keep the voltage constant. Therefore, the conduction angle changes rapidly to a small value (figure 7.29(a)) ,allowing the SVC to operate in the capacitive range and so increasing the voltage. The inductive currents on the TCR branches also have a very small value as they are plotted in figure 7.29(b). Due to the load increase the current in the transmission line is also increased (figure 7.29(b)). From the above figures it is obvious that the SVC responds fast and effectively in a reasonably timescale (2 cycles) to small system disturbances by controlling the conduction angle of the SVC.

b) SVC response using phase shift at the voltage source

In addition to being able to fire at the correct point, the firing system must be also correct changes in voltage synchronization. When a phase shift in the voltage across

the SVC occurs, the gate pulse generator must correct the firing for this phase shift. In order to study this phenomenon a phase shift in the voltage source of figure 7.17 of 25°, happens at 0.14 sec for all the three phase voltages and it is illustrated in figure 7.30(a). After the change in voltage phase, there is an excess amount of current in the SVC branches which is shown in figure 7.30(b). The increase in the current is due to an increase in the conduction angle, which happens when the phase shift occurs as plotted in figure 7.31(a). The control system acts immediately to the phase variation as can be seen from the graph of the current between the source and bus 1(figure 7.31 (b)) . The voltage at bus 2 comes back to steady state conditions again after two cycles in figure 7.31(c). From the above graphs it can be observed that the system has synchronised successfully itself to new voltage phasing in a reasonable time, due to the correct operation of its control system.

c) SVC response to balance and unbalance faults

There is a great diversity of possible types of short circuit faults in power systems. However, the more representative among them are the three-phase and single-phase to ground. Short circuits impose stresses on the power system, since they reduce the electrical power consequently creating an accelerating power (difference between mechanical and electrical power), which after fault clearing causes electromechanical oscillations. In addition to this, severe overvoltages and overcurrents can arise depending upon the type of fault and power system earthing conditions. This section is intended to study balanced and unbalanced faults from the standpoint of electromagnetic oscillations and the associated SVC interaction, since these faults can excite several resonances existing in power systems.

SVC response to single-phase to ground short circuit

The single-phase to ground is probably the most common fault in power systems. It is regarded as a standard fault for assessing the power system's performance in unbalanced conditions. In the power system 1 of figure 7.17 a single-phase to ground

fault is applied in phase A, between the voltage source and its equivalent reactance, at 0.18 sec, and cleared at 0.21sec. Figure 7.32(a) shows the voltage source and figure 7.32(b) illustrates the voltage of phase A at bus 2. After the voltage collapse on phase A because of the fault, there is a voltage recovery in a small period of time. The conduction angle during the fault, reduced in order to assess the voltage to recover (the SVC operates in the capacitive mode in this period). Figure 7.33(a) shows the conduction angle waveform. It can also be noted from this waveform, and from the waveform of the current between the source and bus 1 (Figure 7.33(b)), that after the fault has been cleared it took almost 3 cycles to get back to the conditions before the fault. In figure 7.34(a) the currents on the SVC branches have been plotted. These currents are almost negligible in the fault and 3 cycles after the fault period, due to the small conduction angle. However as can be observed from the graph, the current on branch AC gets a very large value just after the fault has cleared. This is due to the incorrect synchronisation that takes place in that period. The current starts to conduct almost when the voltage becomes positive; (figure 7.34(b)) giving in this way a very large current. This problem, 3 cycles after the fault clearance, no longer exists, the SVC has synchronised itself successfully, as can be noticed from figure 7.34(a).

SVC response to three-phase to ground short circuit

Although less frequent than single-phase faults, three phase faults are very severe for the power system and, therefore, they are usually studied as a system performance criterion.

A three-phase fault was applied between the voltage source and its equivalent reactance at 0.180sec and cleared at 0.210sec. This disturbance causes an almost complete voltage collapse at the SVC terminals during the fault period as can be observed in figure 7.35(a). However the control system acts immediately by decreasing the conduction angle, thereby allowing the SVC to operate in the capacitive mode in order to increase the voltage of the SVC. In the graph 7.35(b) can be seen that during the fault the conduction angle is sustained and after the clearing

of the fault, when the system lost synchronism, the conduction angle is kept at low level and as soon as the voltage starts to stabilise the conduction angle approaches its specified condition. From this graph can also be noted that after the fault has been cleared it took almost 180msec to get back to the conditions before the fault, more enough than the single-phase case that was discussed earlier. The latter can also be observed from the waveform of the current flowing between the voltage source and bus 1 in figure 7.35(c). In figure 7.36 the three currents on the SVC branches have been plotted and also the voltage across them have been illustrated. In figures 7.36(a) and (b) we notice that the current on the SVC branches is trapped in the system during the period of collapse voltage. This follows since there is insufficient voltage to turn off the thyristors. By looking at the reactor's current in figure 7.36(c) we see that the trapped current is opposite polarity with the voltage returning in such a way to increase this current, causing some cycles of oscillation after the voltage returns. This indicates an extra type of duty that the thyristors might be subject to which cannot be controlled through any control strategy. It is totally dependent upon on the phasing of the voltage when it returns.

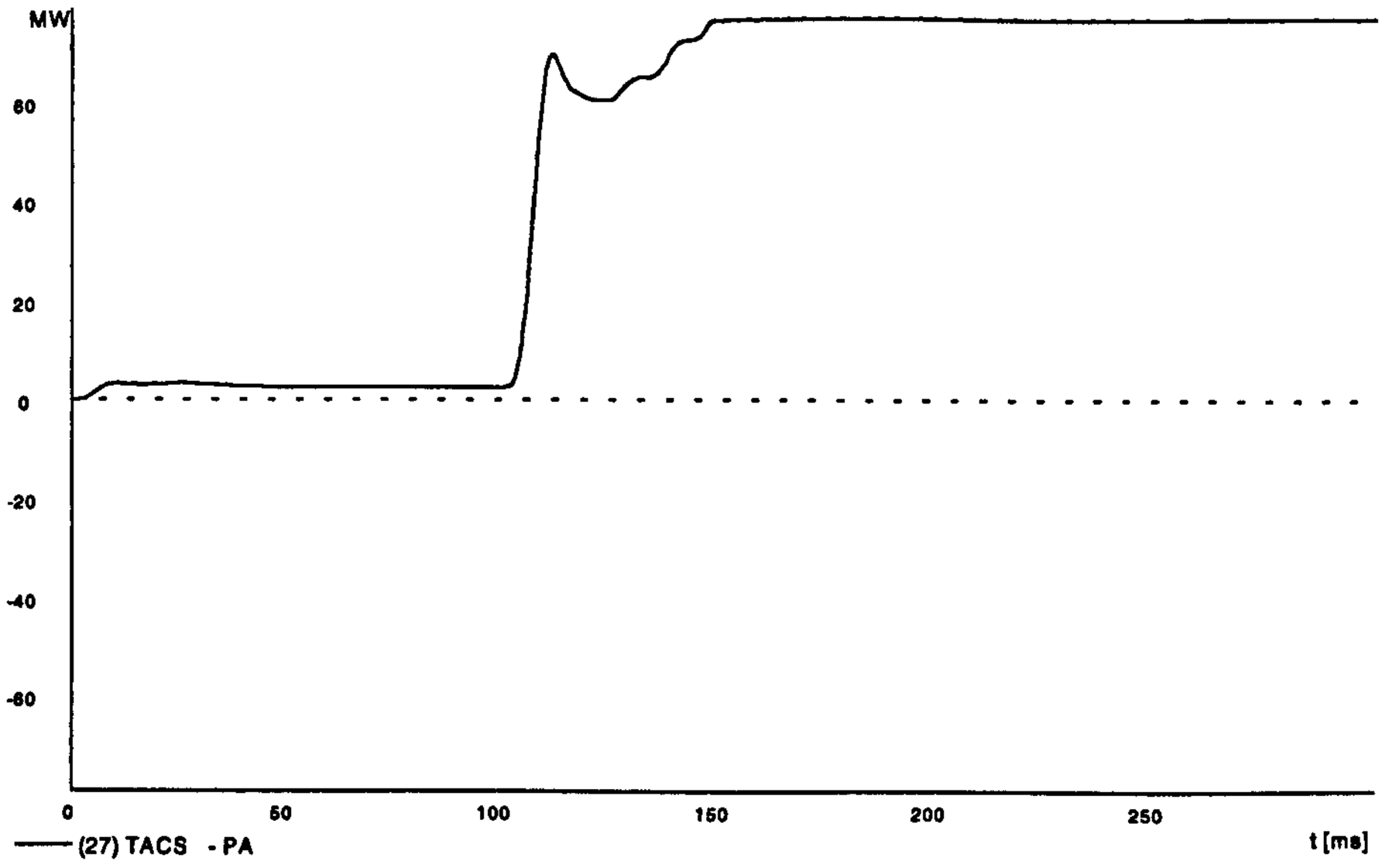

(a) Real power per phase of the load

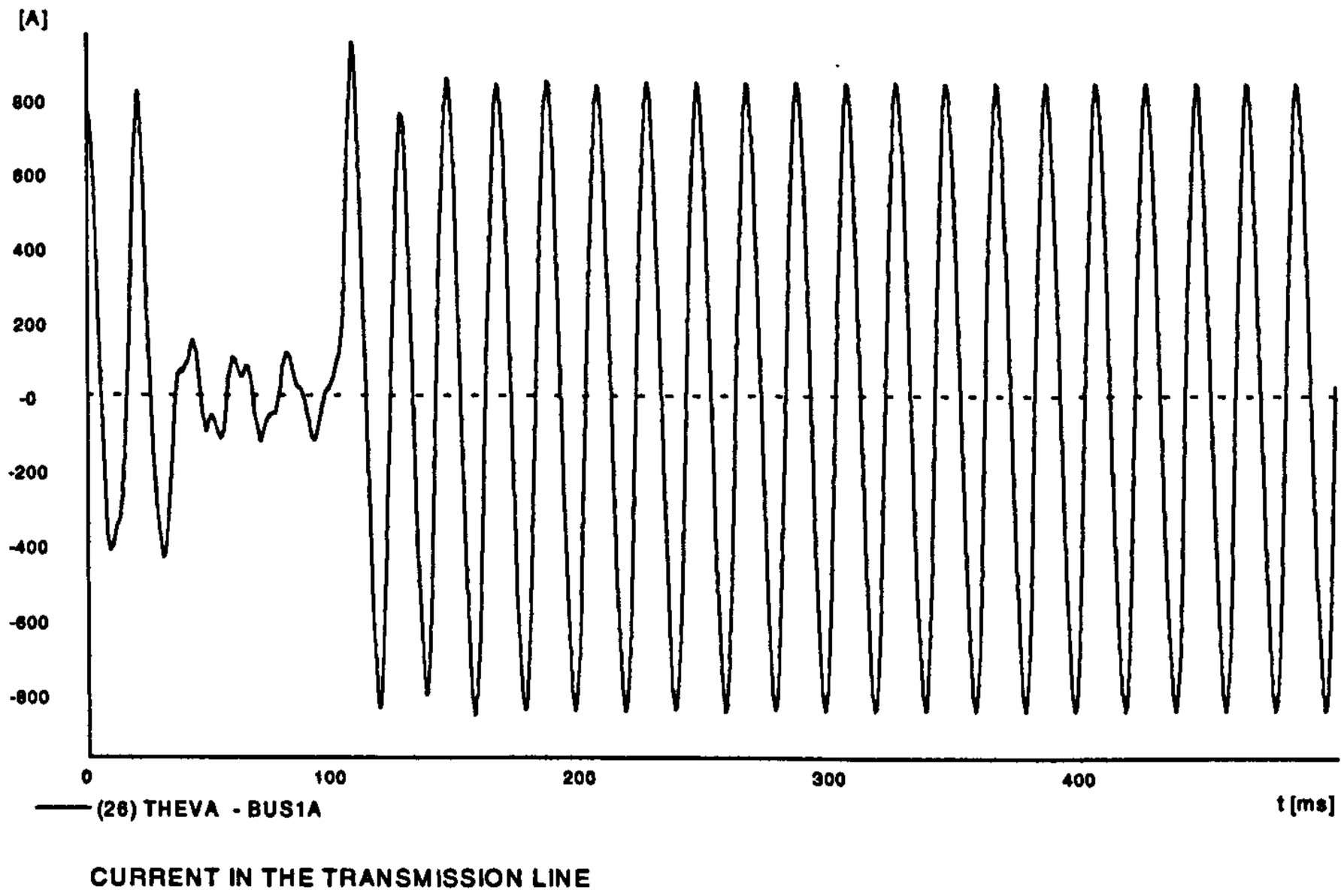

(b) Current in the transmission line

Figure 7.27

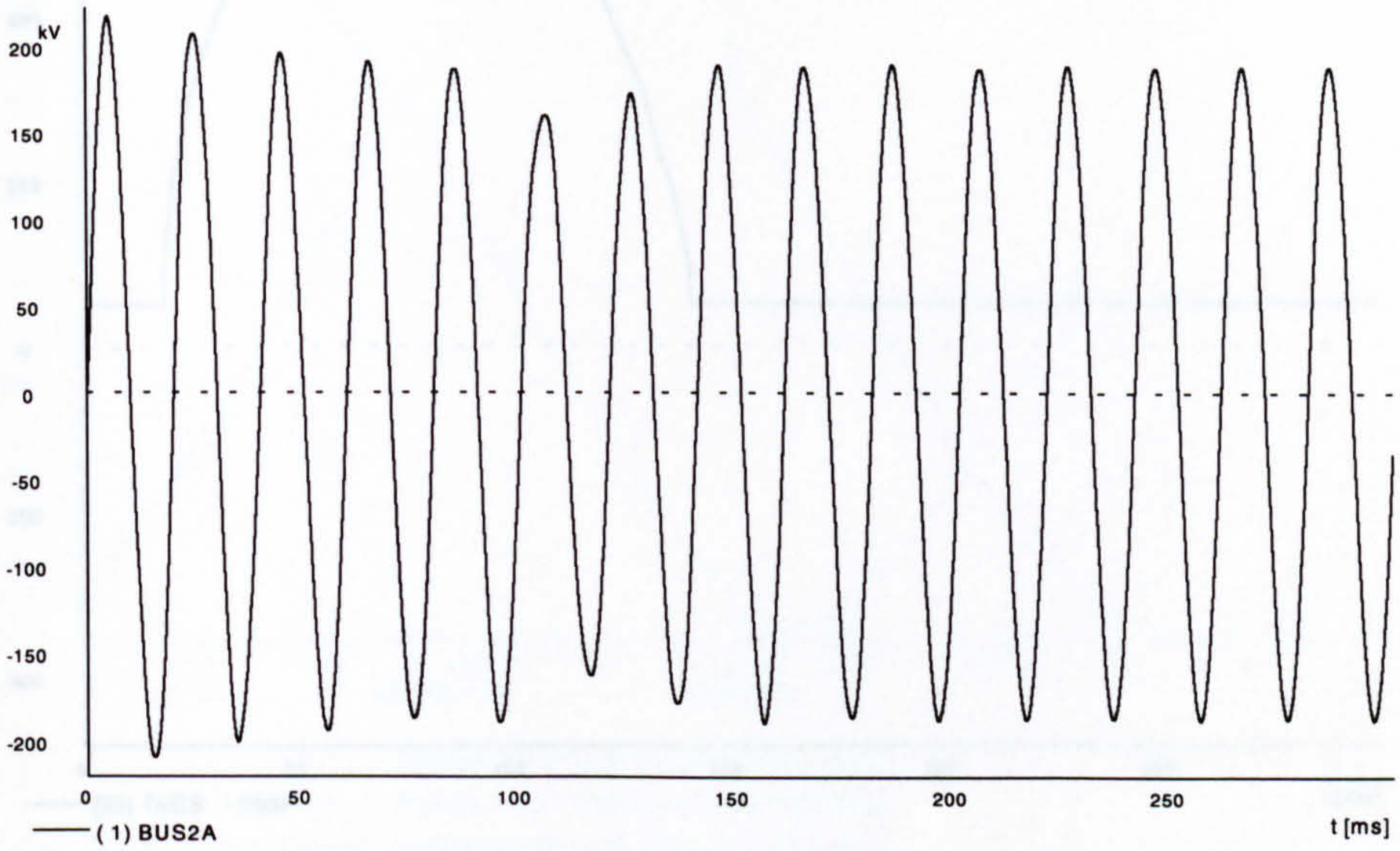

(a) Voltage of phase A at bus 2

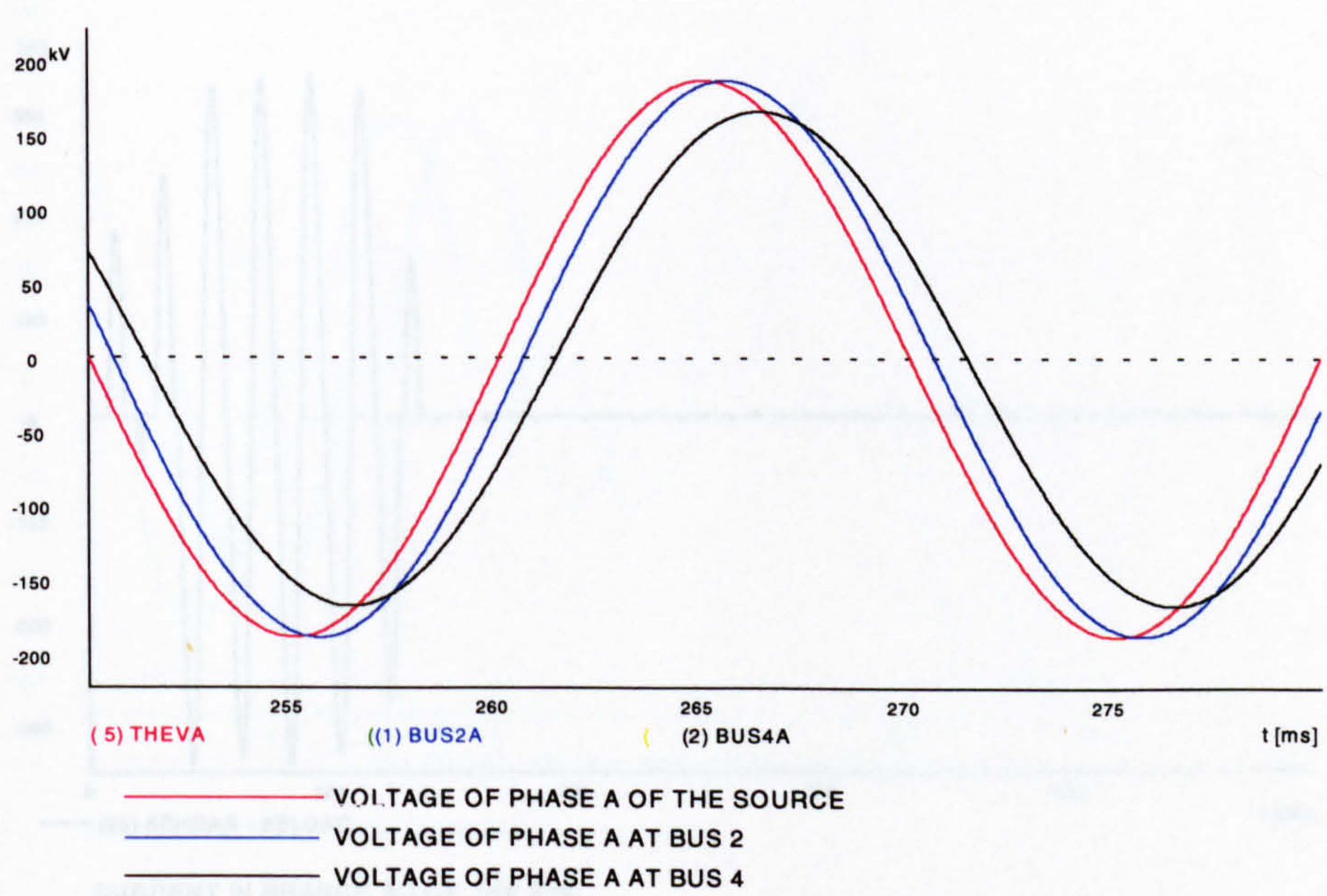

(b) Comparison between the source voltage and voltages of buses 2 and 4

Figure 7.28

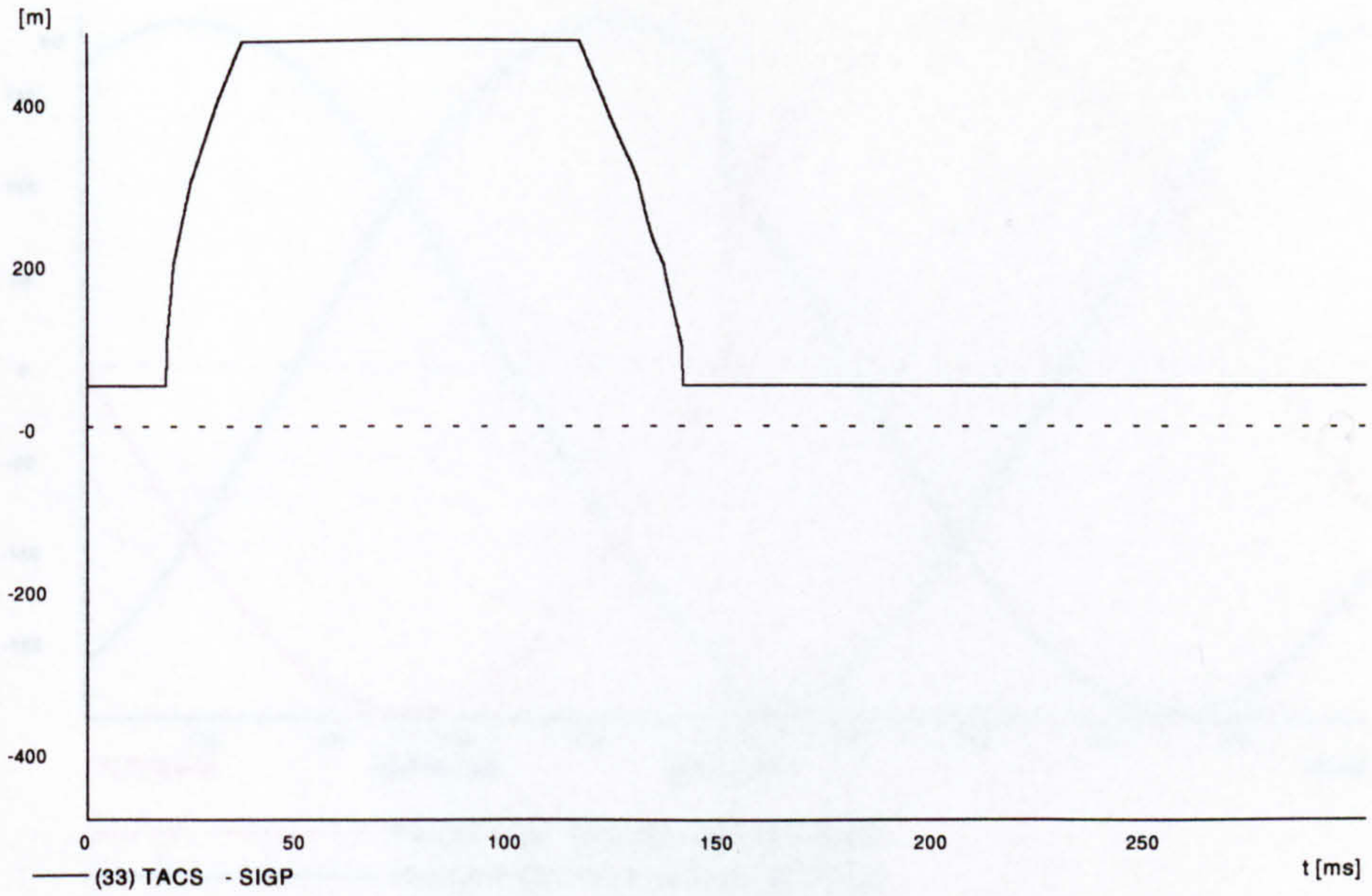

(a) Conduction angle of the SVC

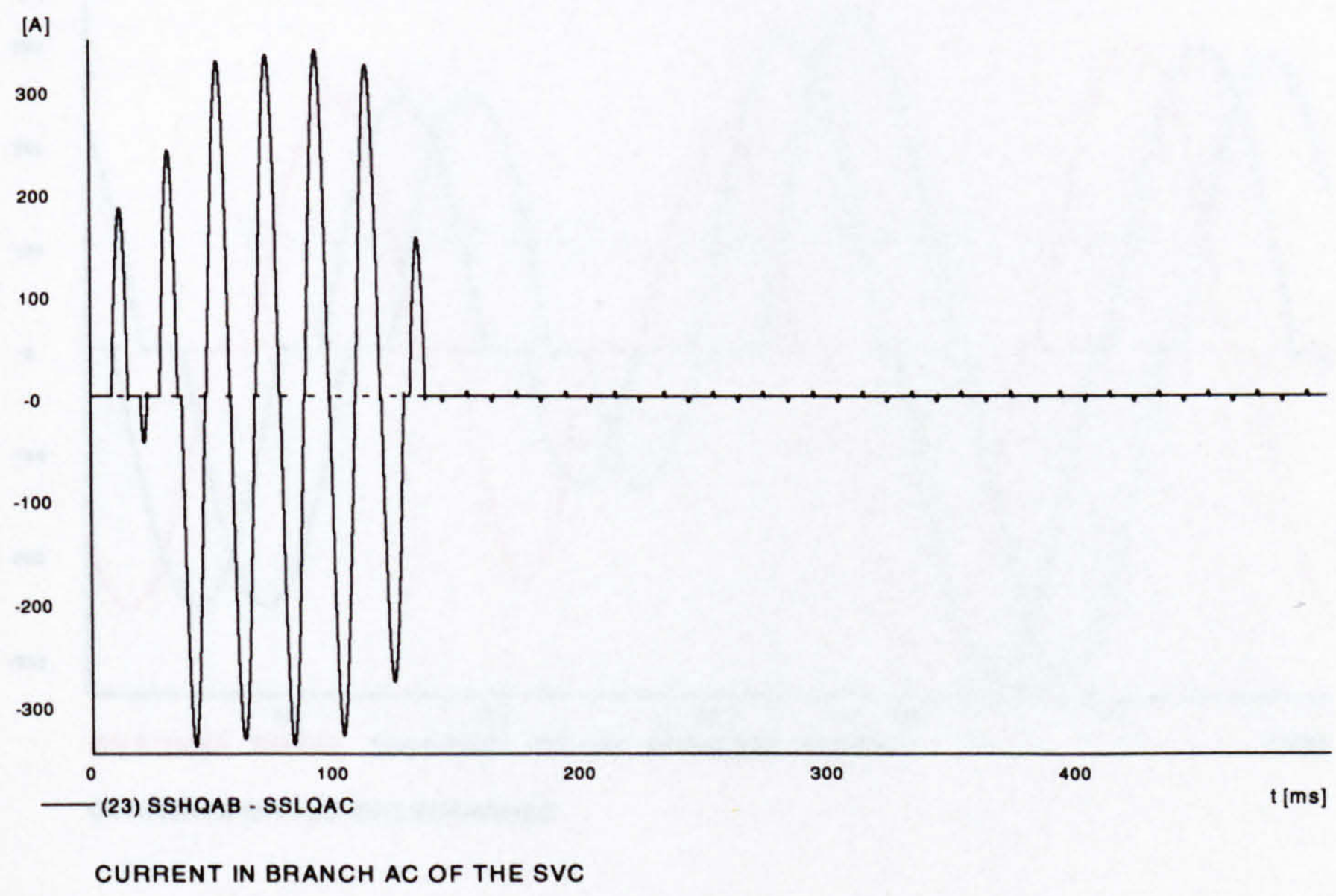

(b) Current in branch AC of the SVC

Figure 7.29

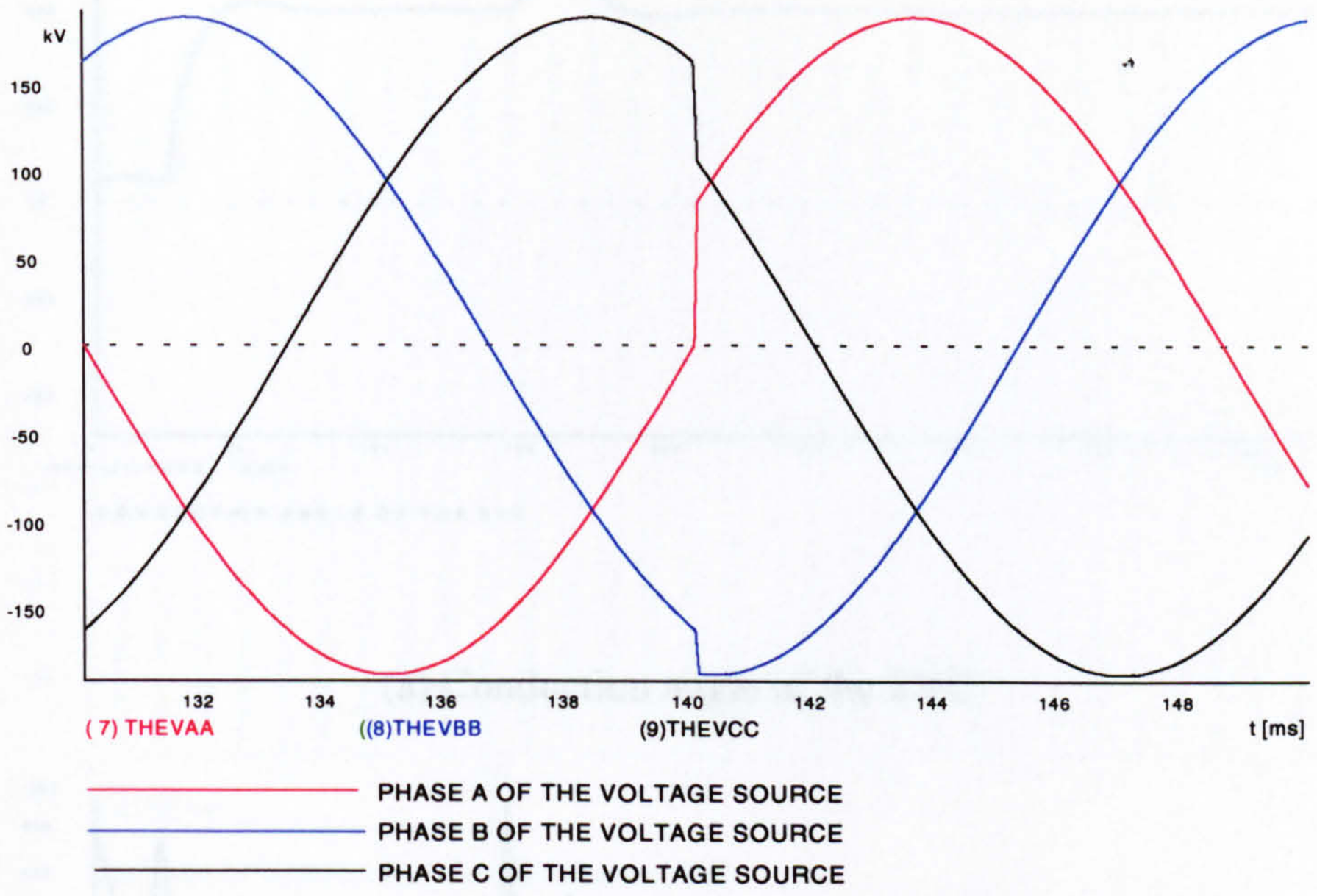

(a) Voltages of the three phases on the AC source

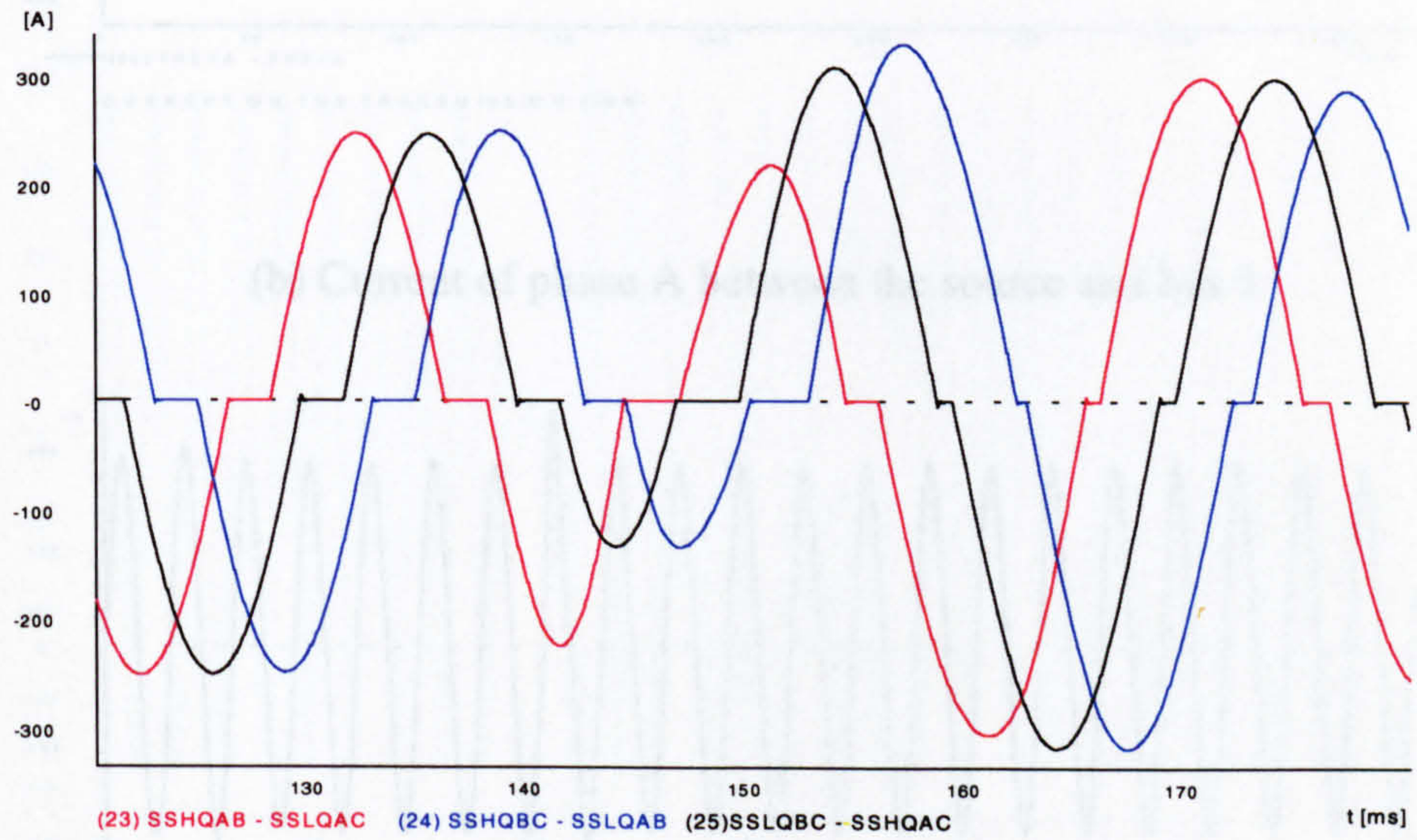

(b) Currents on the SVC branches

Figure 7.30

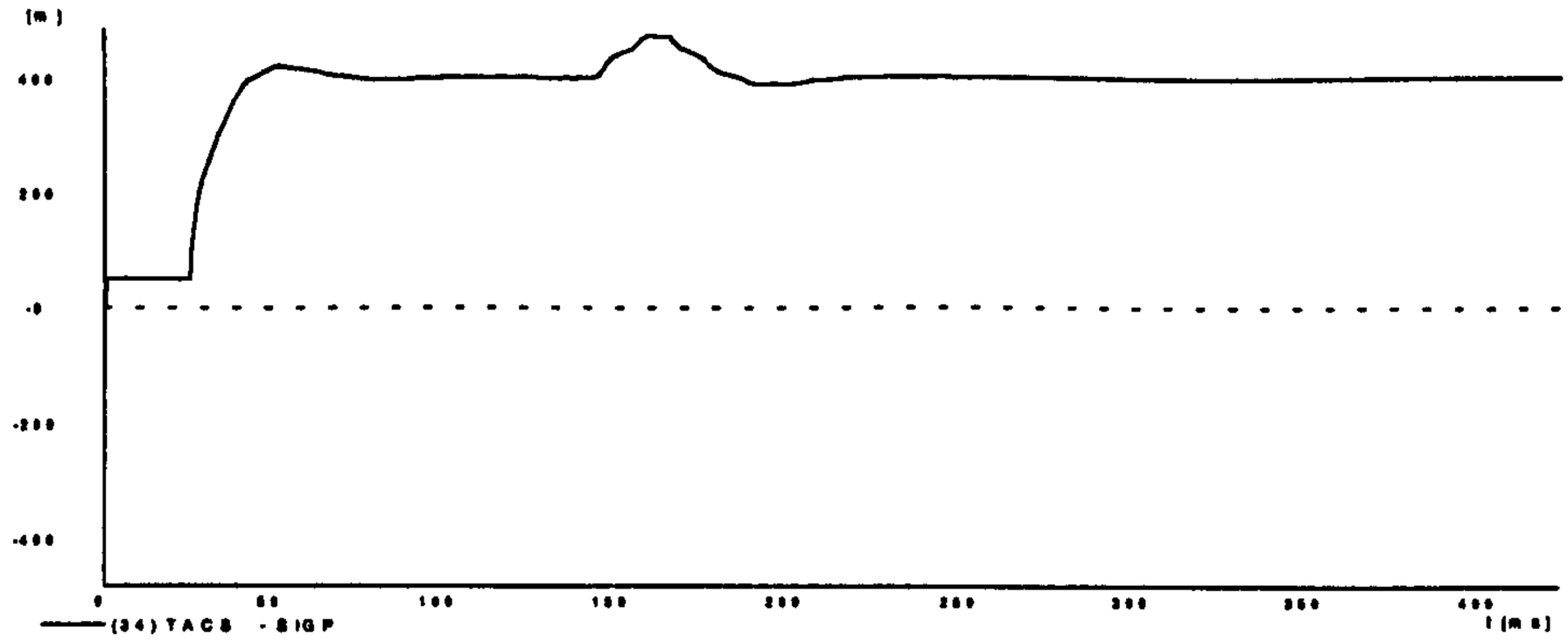

CONDUCTION ANGLE OF THE SVC

(a) Conduction angle of the SVC

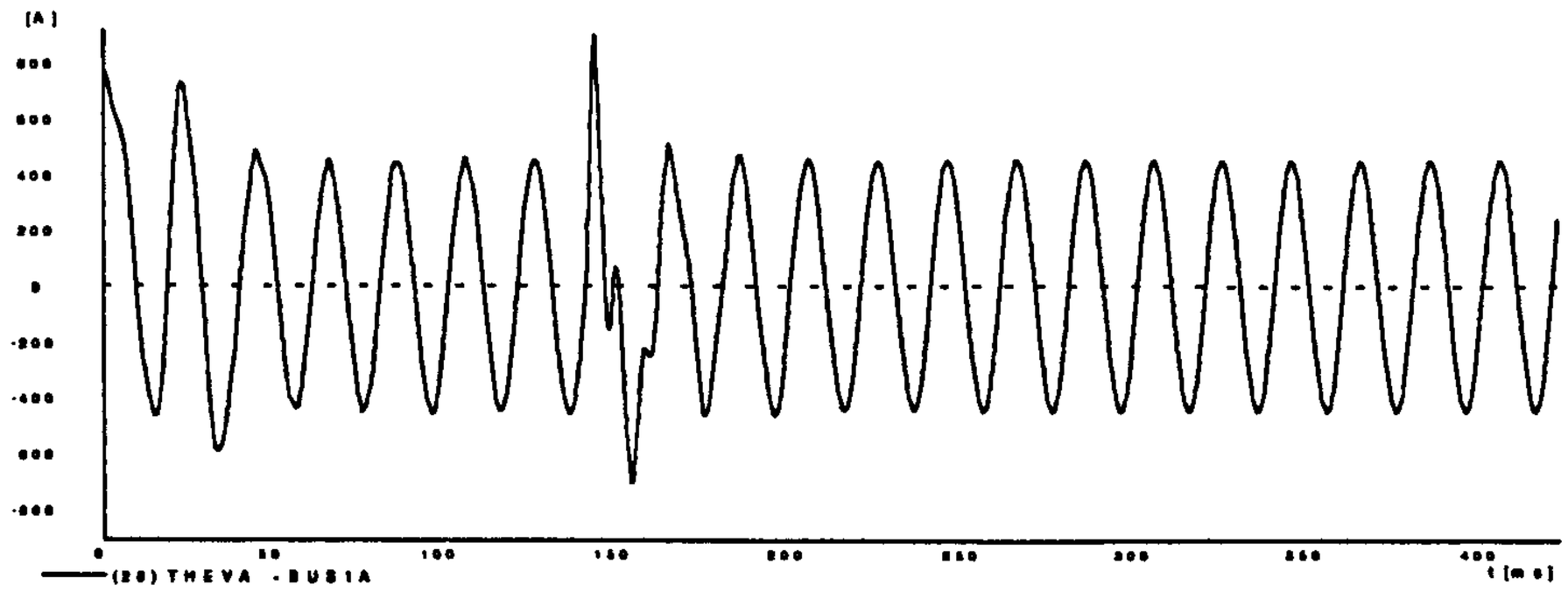

CURRENT ON THE TRANSMISSION LINE

(b) Current of phase A between the source and bus 1

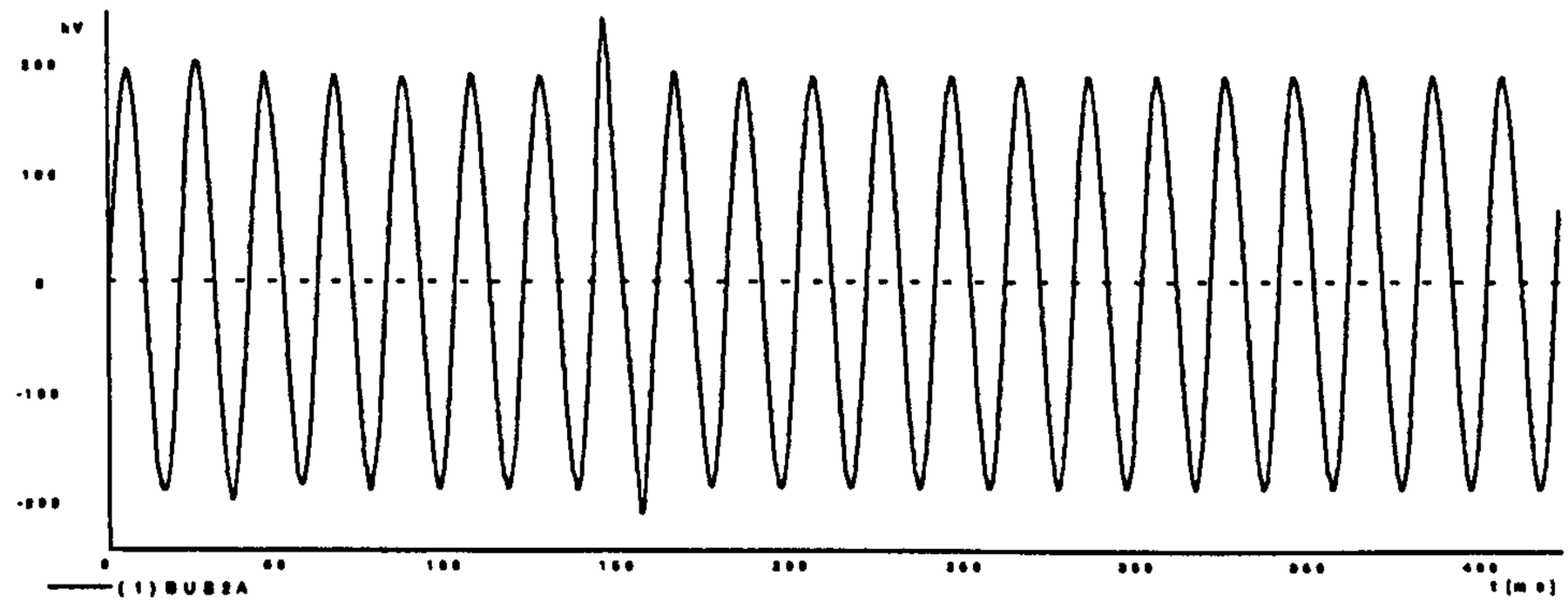

VOLTAGE OF PHASE A AT THE SVC TERMINALS

(c) Voltage of phase A at the SVC terminals

Figure 7.31

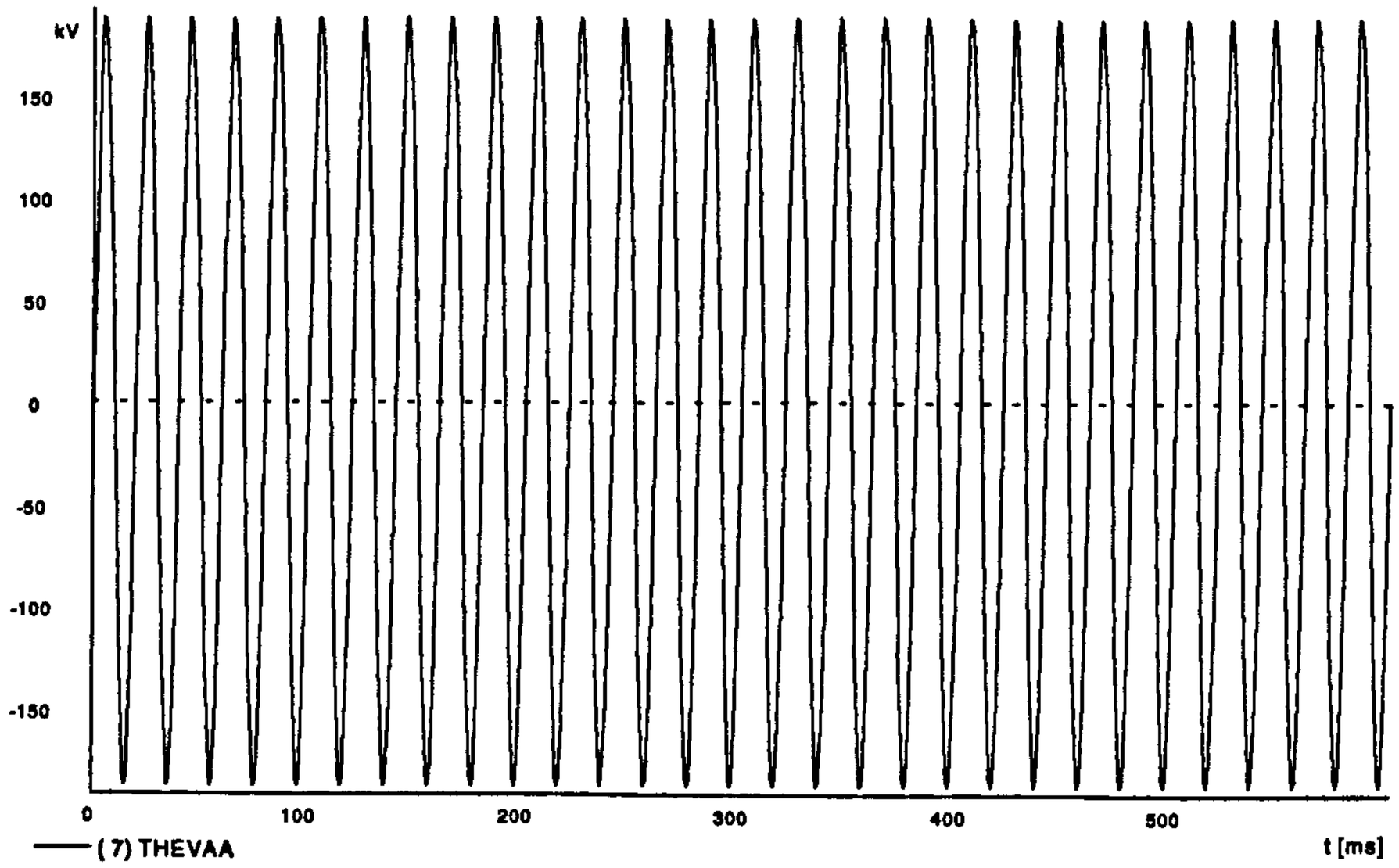

VOLTAGE OF PHASE A ON THE VOLTAGE SOURCE

(a) Voltage of phase A on the voltage source

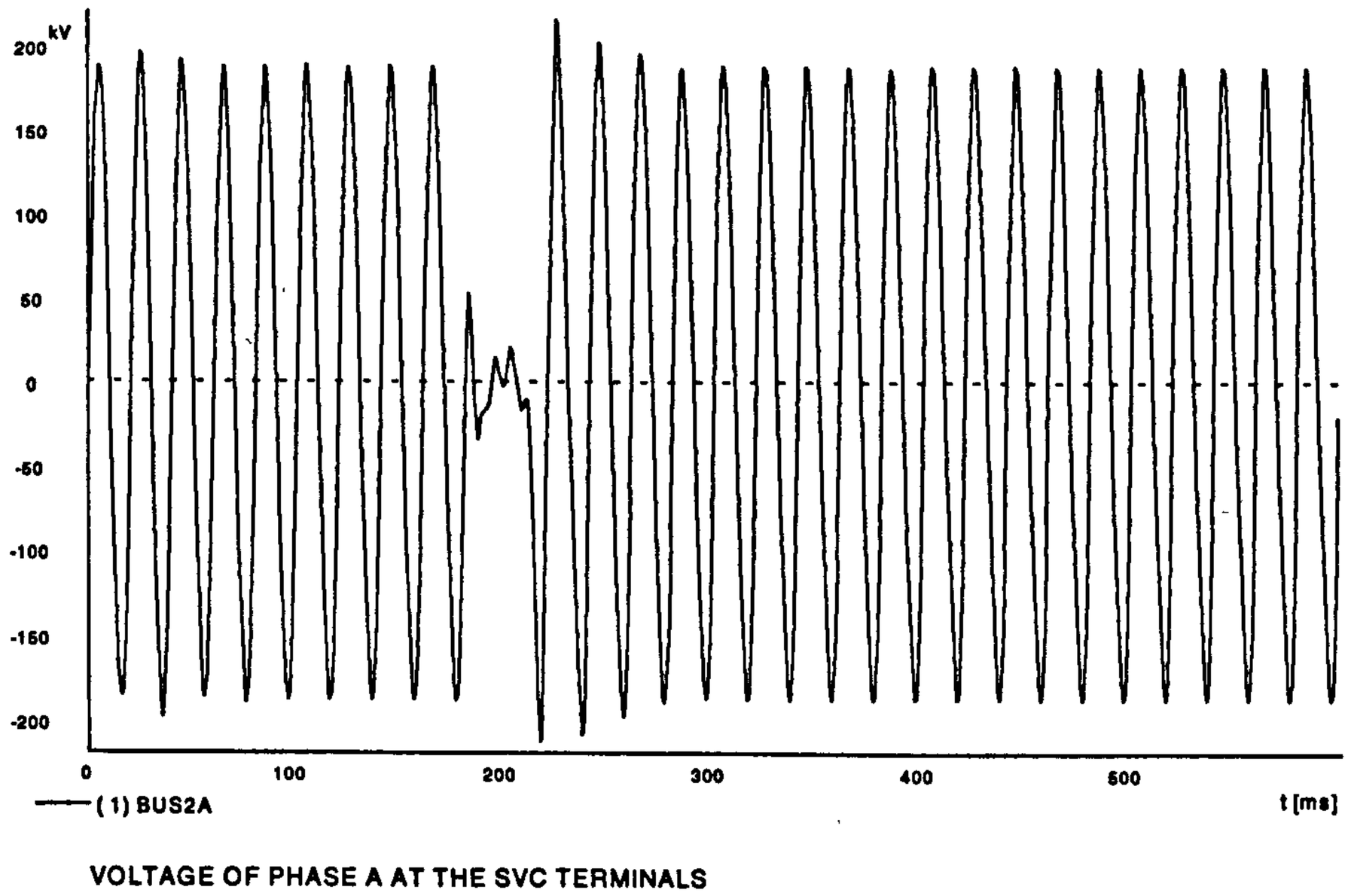

VOLTAGE OF PHASE A AT THE SVC TERMINALS

(b) Voltage of phase A on the SVC terminals

Figure 7.32

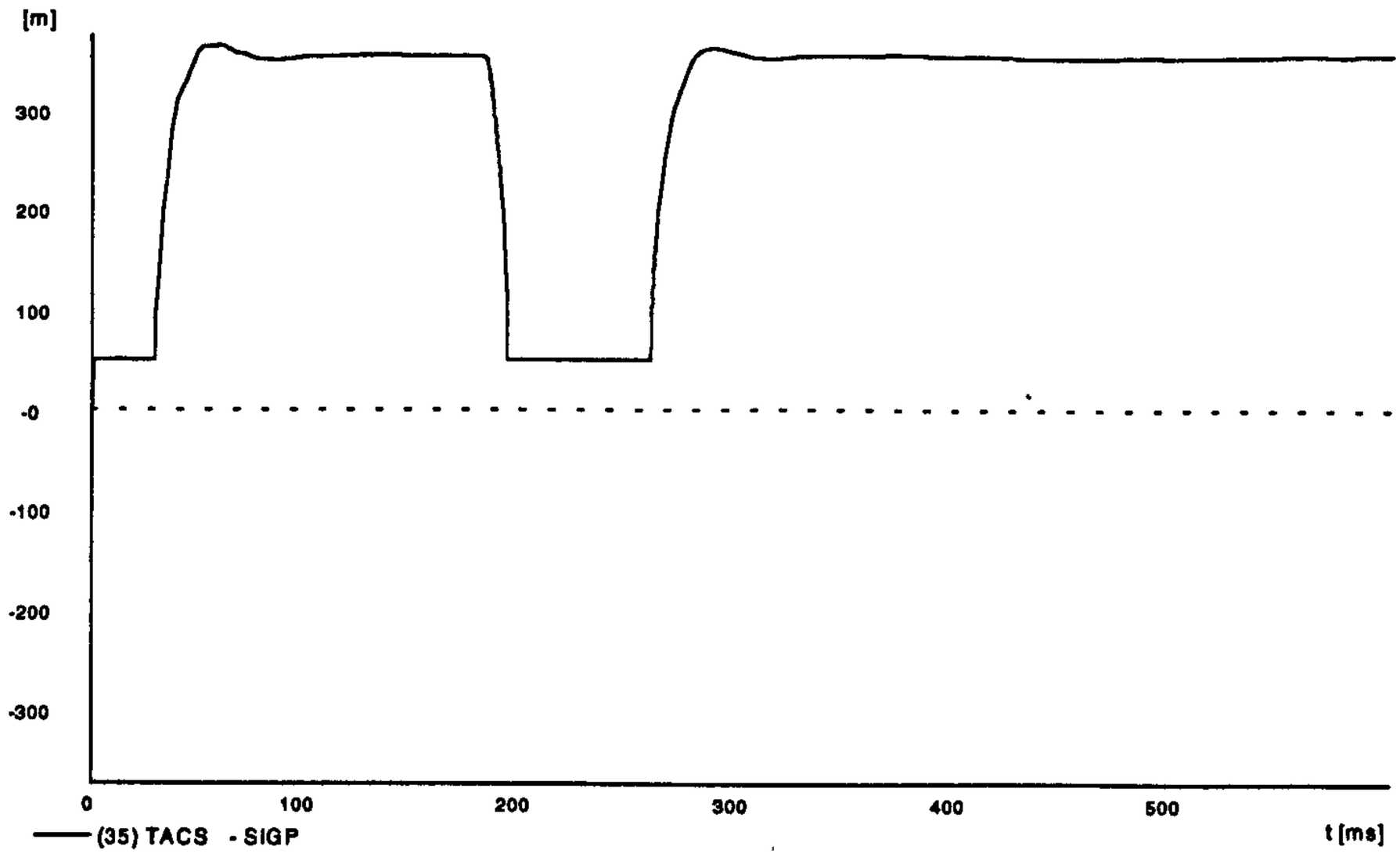

CONDUCTION ANGLE OF THE SVC

(a) Conduction angle of the SVC

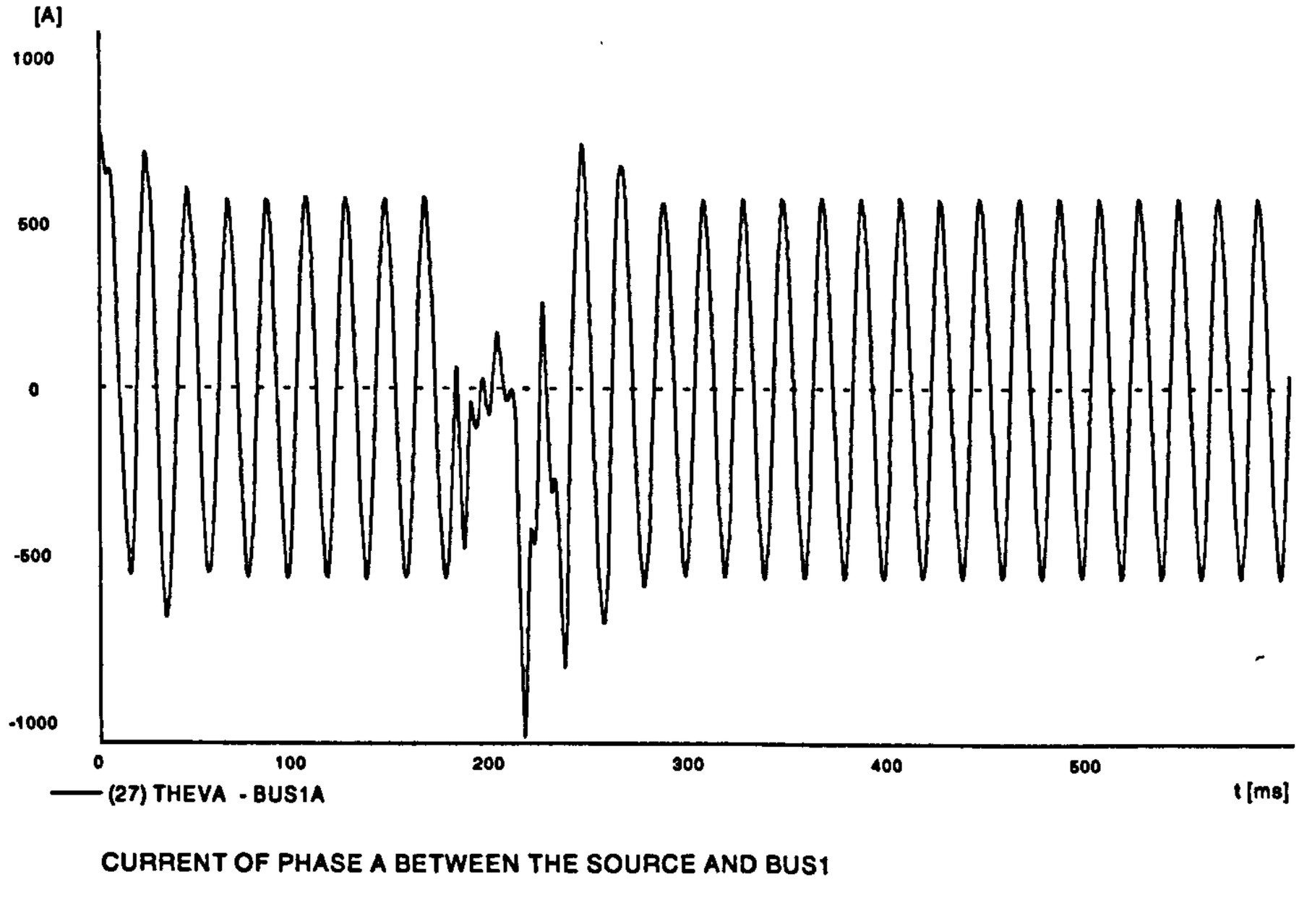

CURRENT OF PHASE A BETWEEN THE SOURCE AND BUS1

(b) Current of phase A between the source and bus 7

Figure 7.33

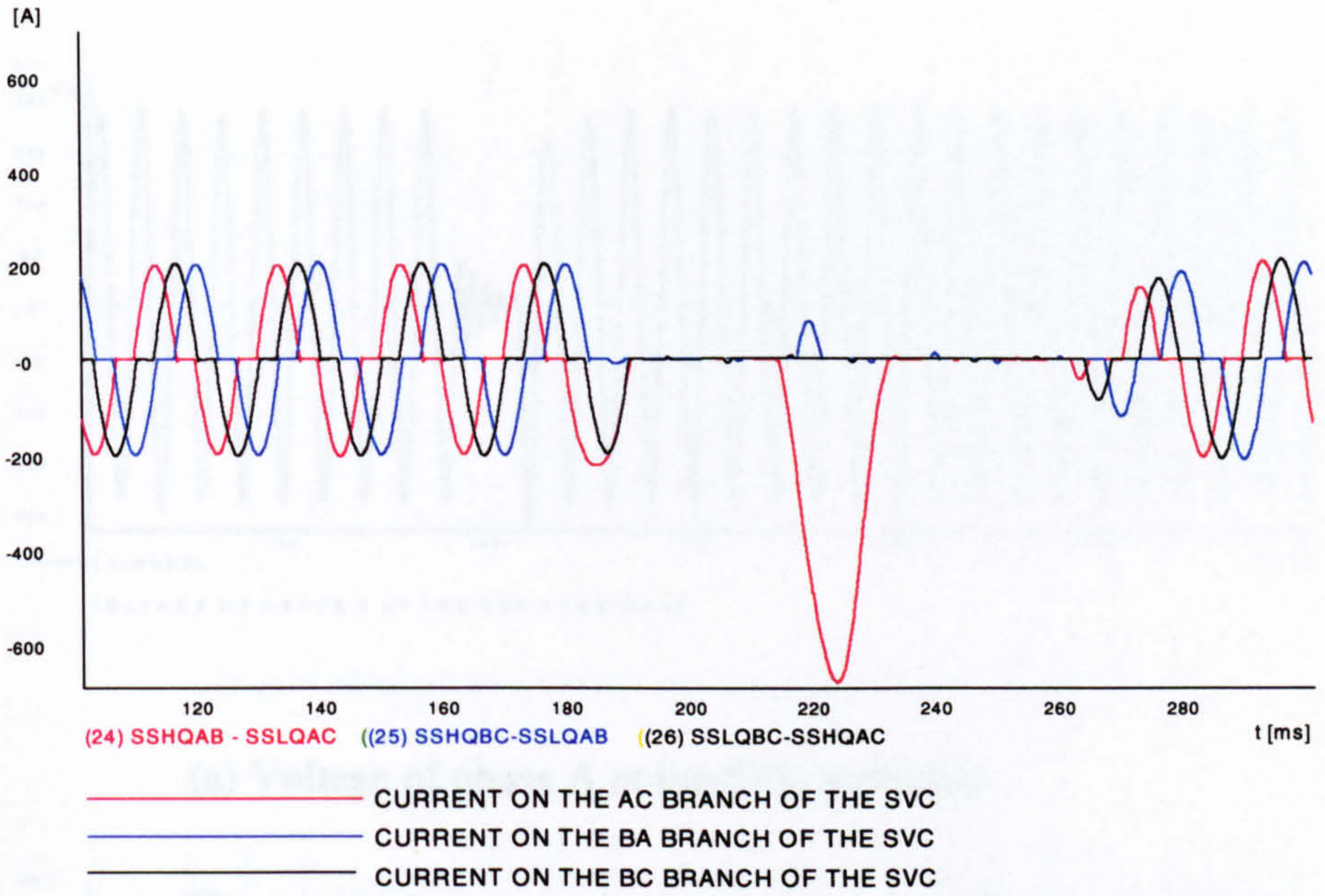

(a) Currents on the SVC branches

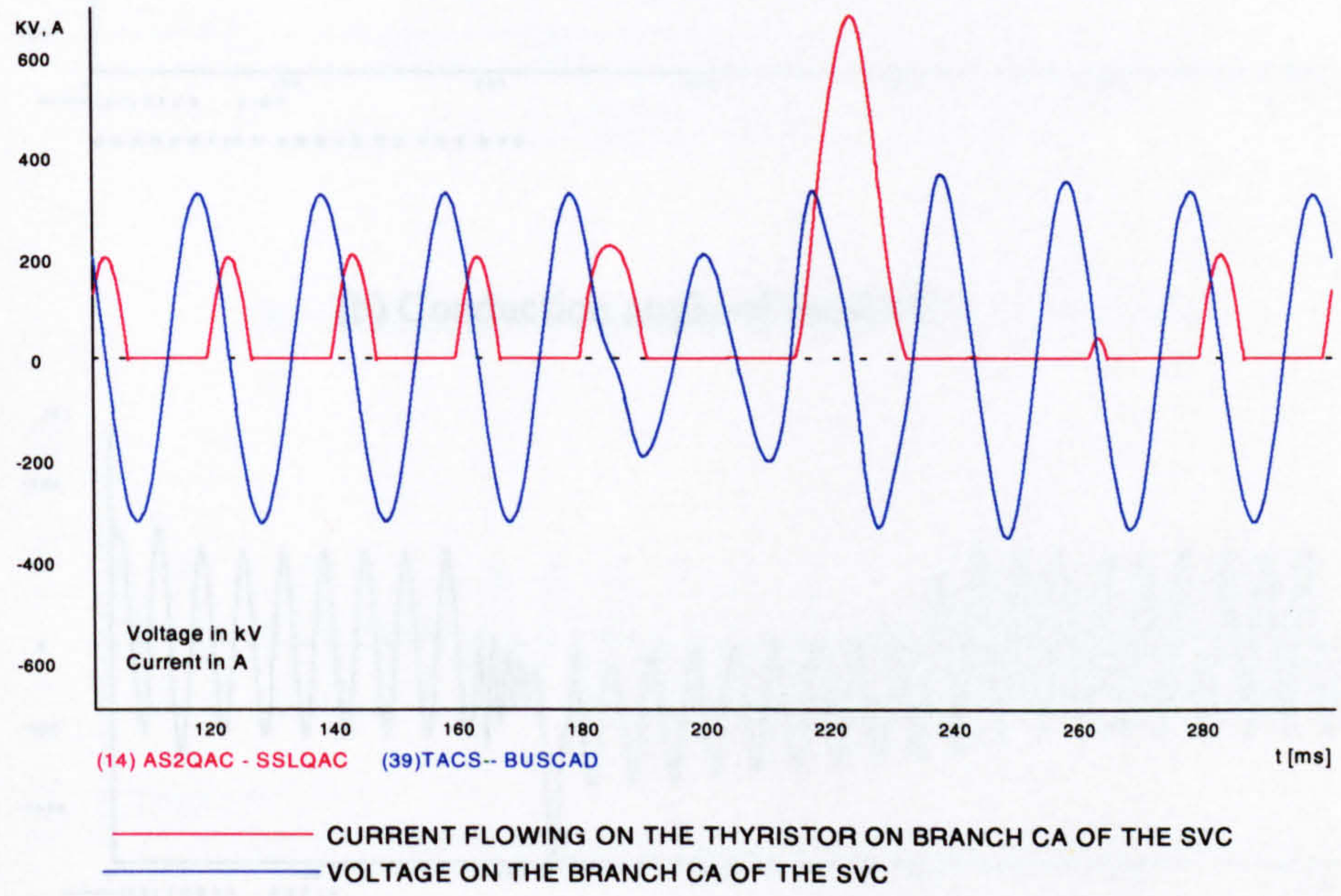

(b) Current and voltage waveforms on the thyristor on branch CA of the SVC

Figure 7.34

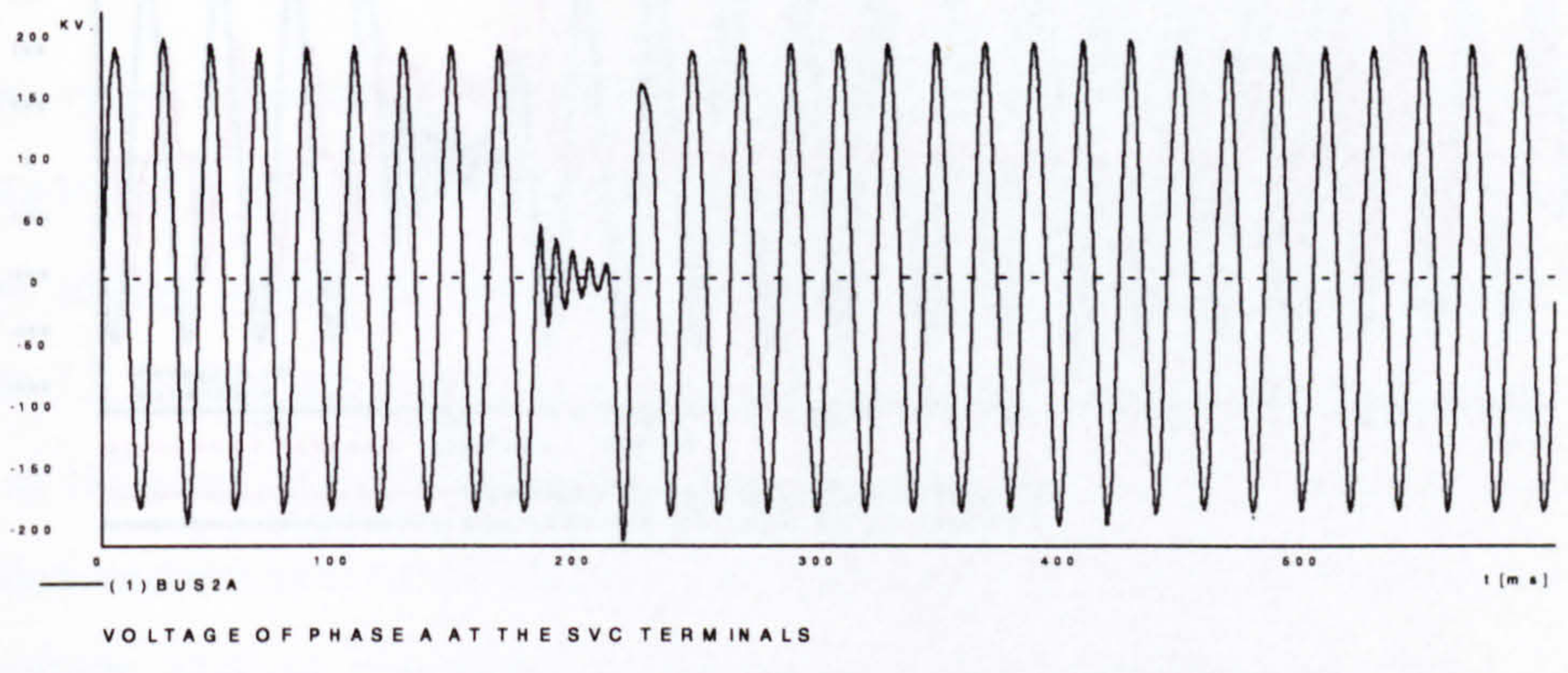

(a) Voltage of phase A at the SVC terminals

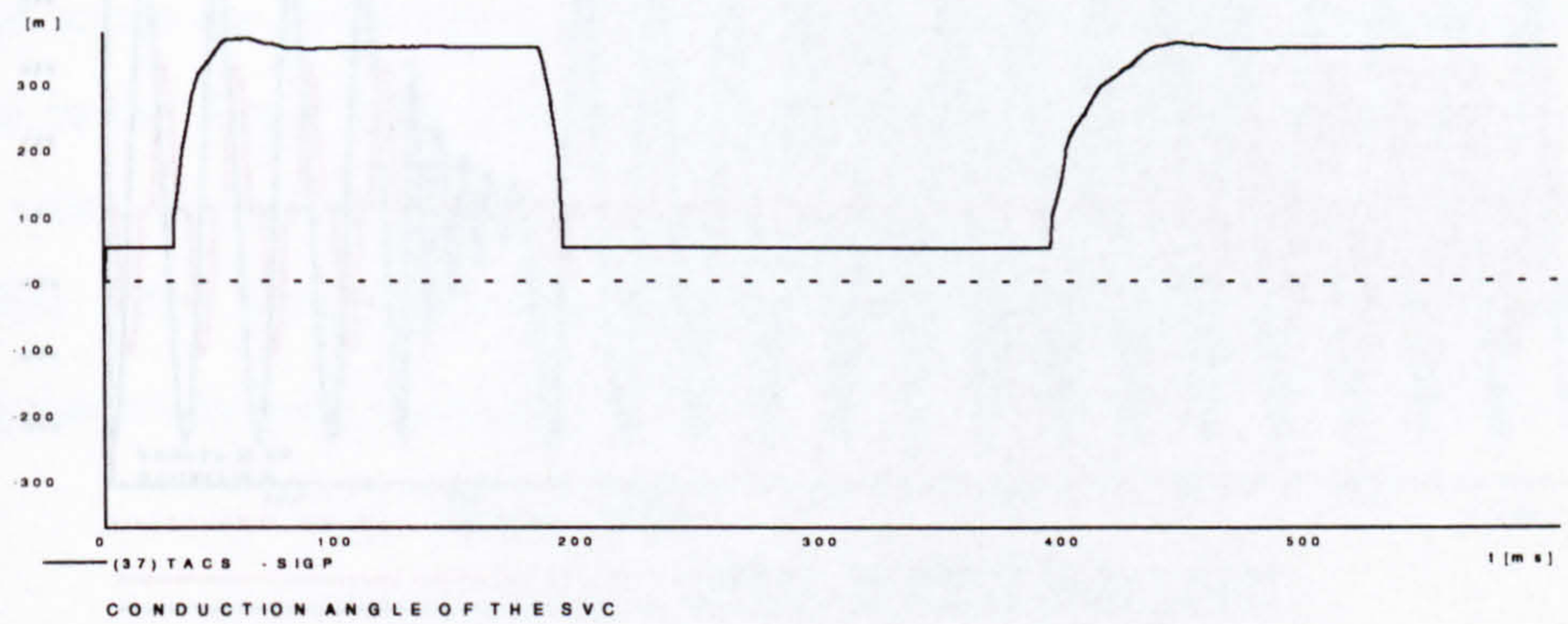

(b) Conduction angle of the SVC

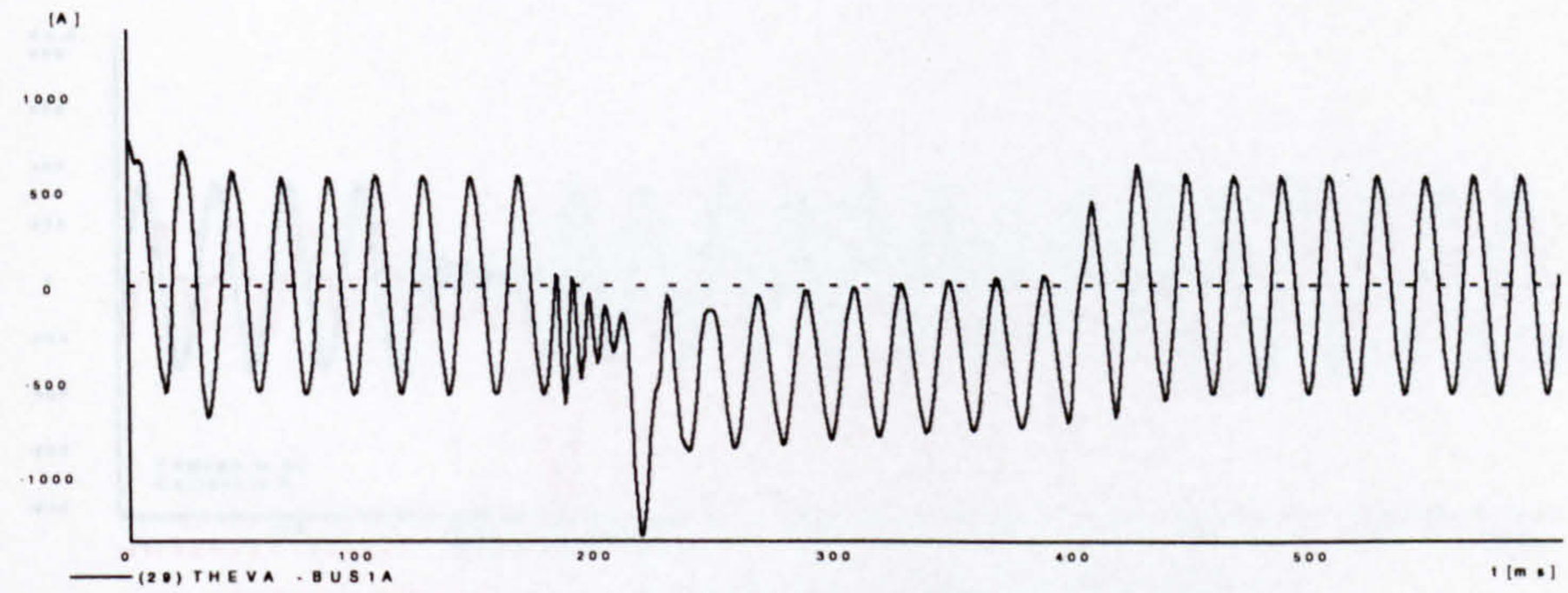

(c) Current of phase A flowing between the source and bus 1

Figure 7.35

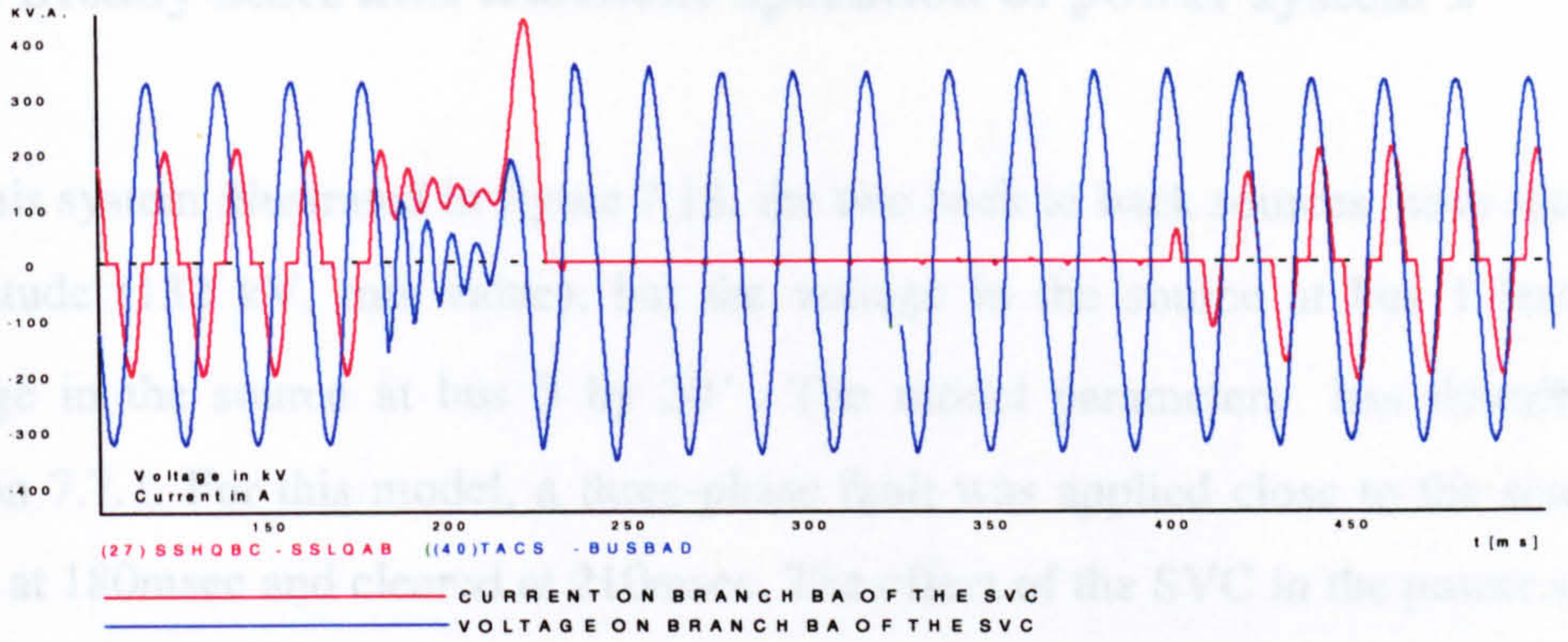

(a) Voltage and current on the branch BA of the SVC

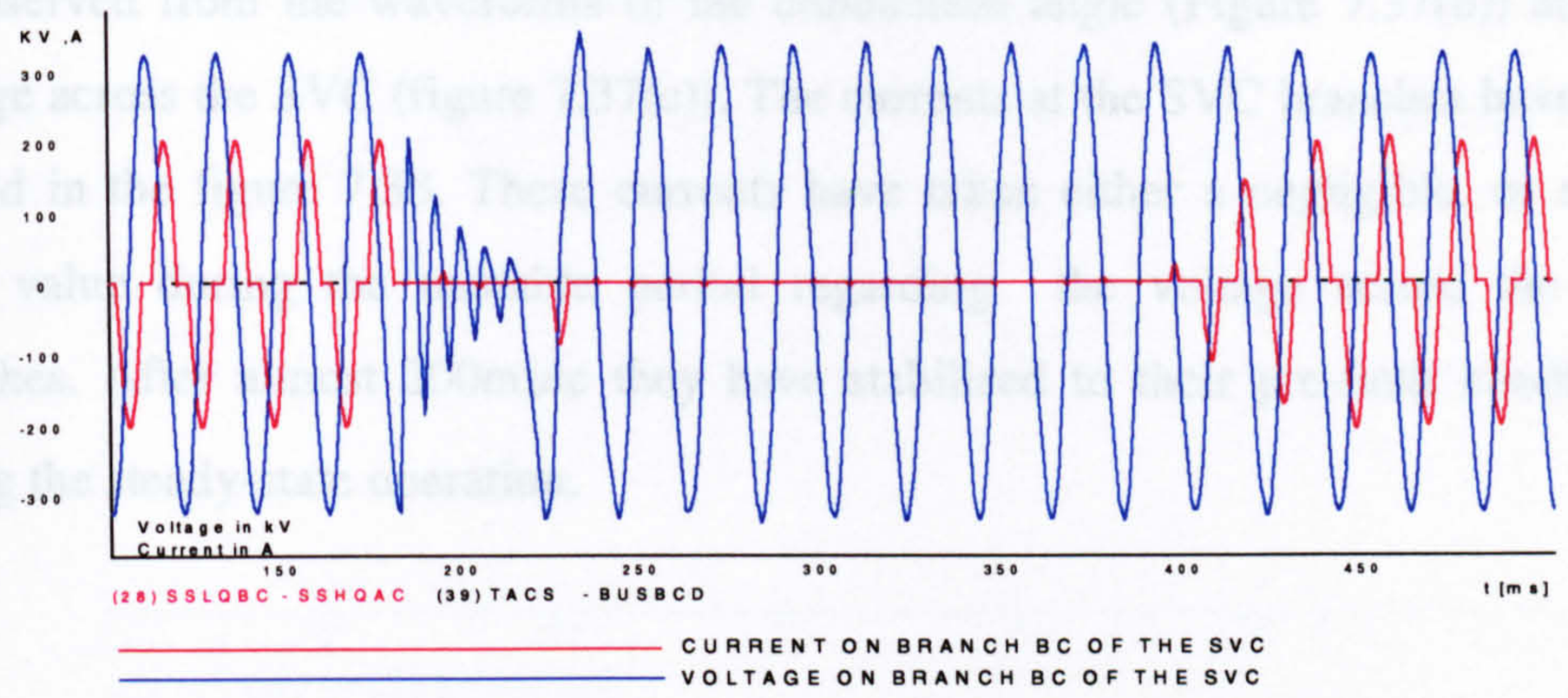

(b) Voltage and current on the branch BC of the SVC

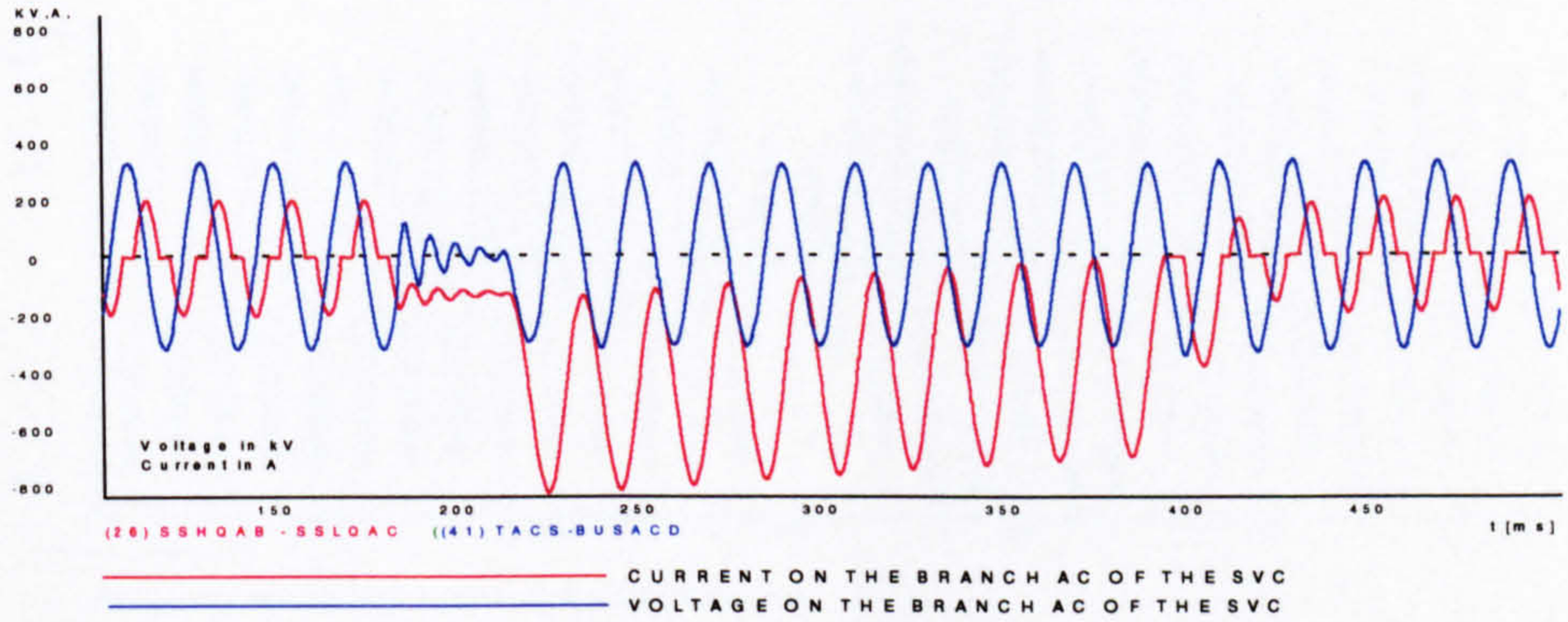

(c) Voltage and current on the branch AC of the SVC

Figure 7.34

7.7.5 Steady-state and transient operation of power system 2

For this system illustrated in figure 7.18, the two back to back sources have the same amplitude (132 kV, rms value), but the voltage in the source at bus 1 leads the voltage in the source at bus 3 by 30°. The model parameters has described in section 7.7.1. For this model, a three-phase fault was applied close to the source at bus 1 at 180msec and cleared at 210msec. The effect of the SVC in the power system operation under transient conditions is of major concern. Figure 7.37(a) illustrates the two voltage sources connected at the buses 1 and 3 respectively. After the fault occurrence it took almost 200msec to return to the conditions before the fault, as can be observed from the waveforms of the conduction angle (Figure 7.37(b)) and the voltage across the SVC (figure 7.37(c)). The currents at the SVC branches have been plotted in the figure 7.38. These currents have taken either a negligible, or a very large value during the unstable period regarding the voltage across the SVC branches. After almost 200msec they have stabilised to their pre-fault conditions, giving the steady-state operation.

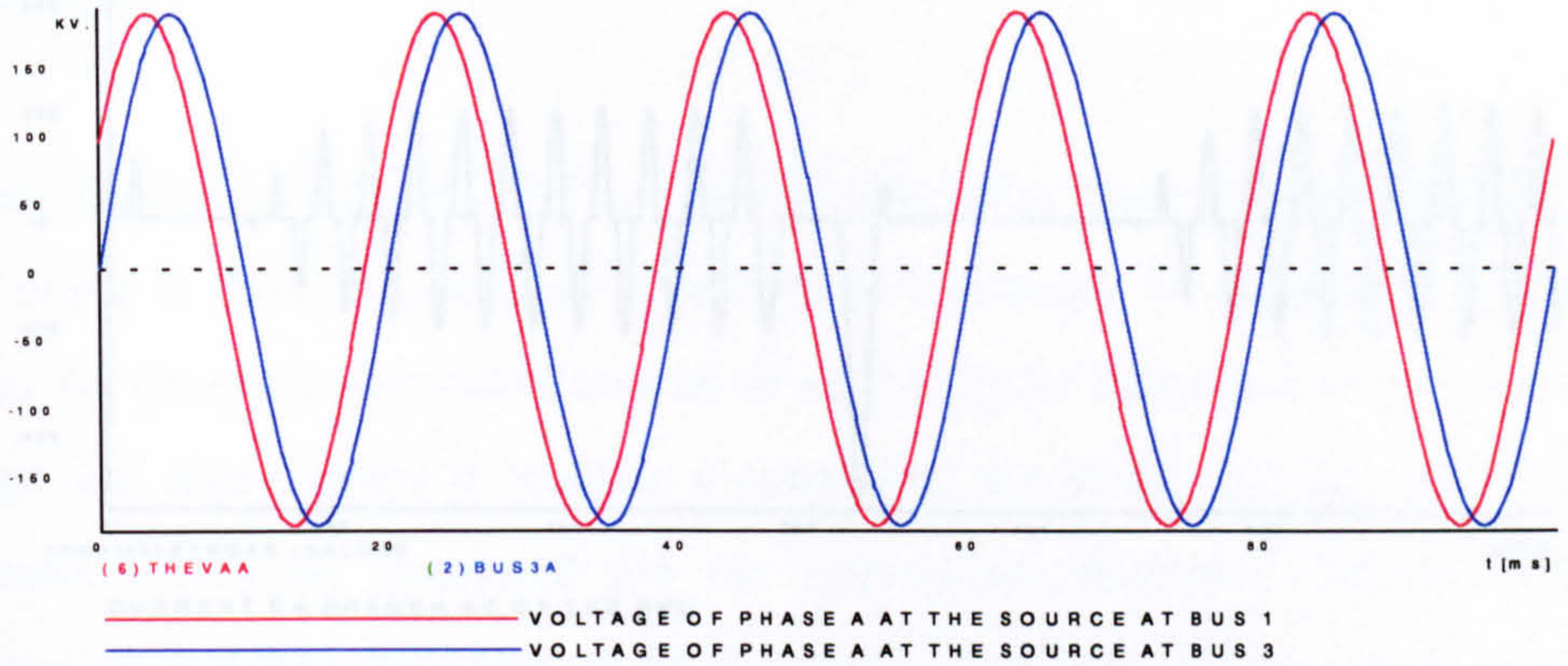

(a) Voltages of phase A at buses 1 and 3

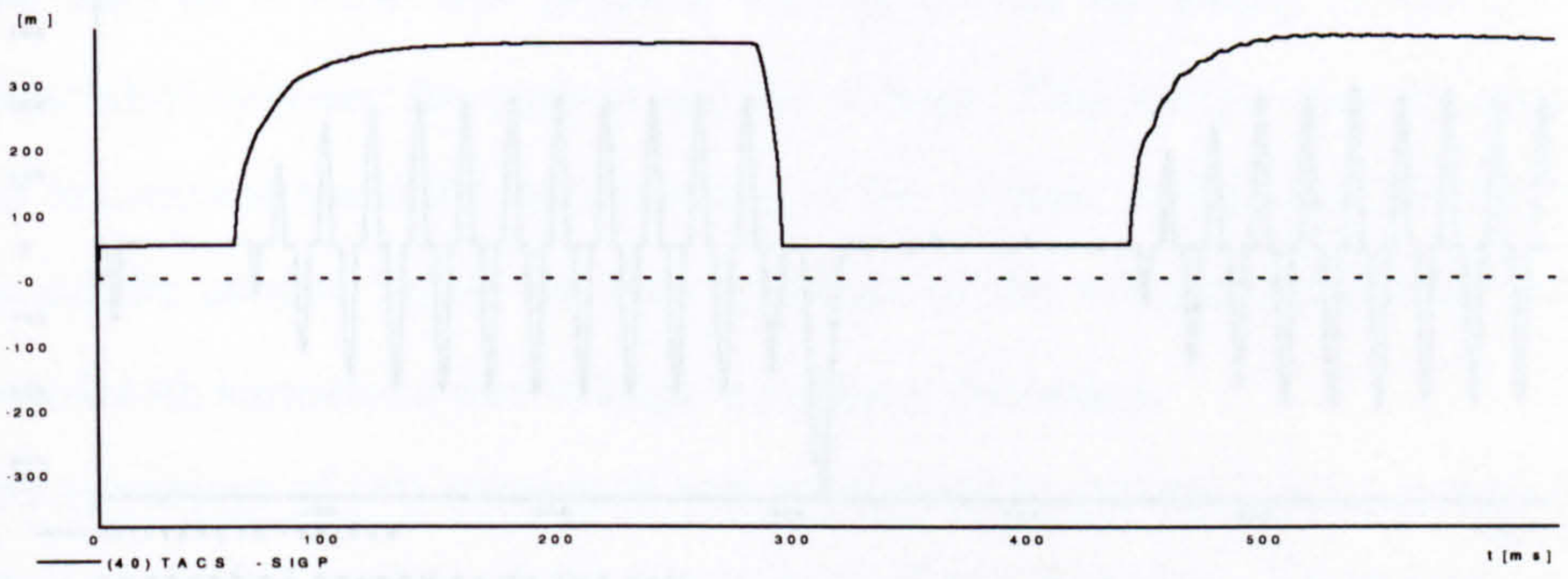

(b) Conduction angle of the SVC

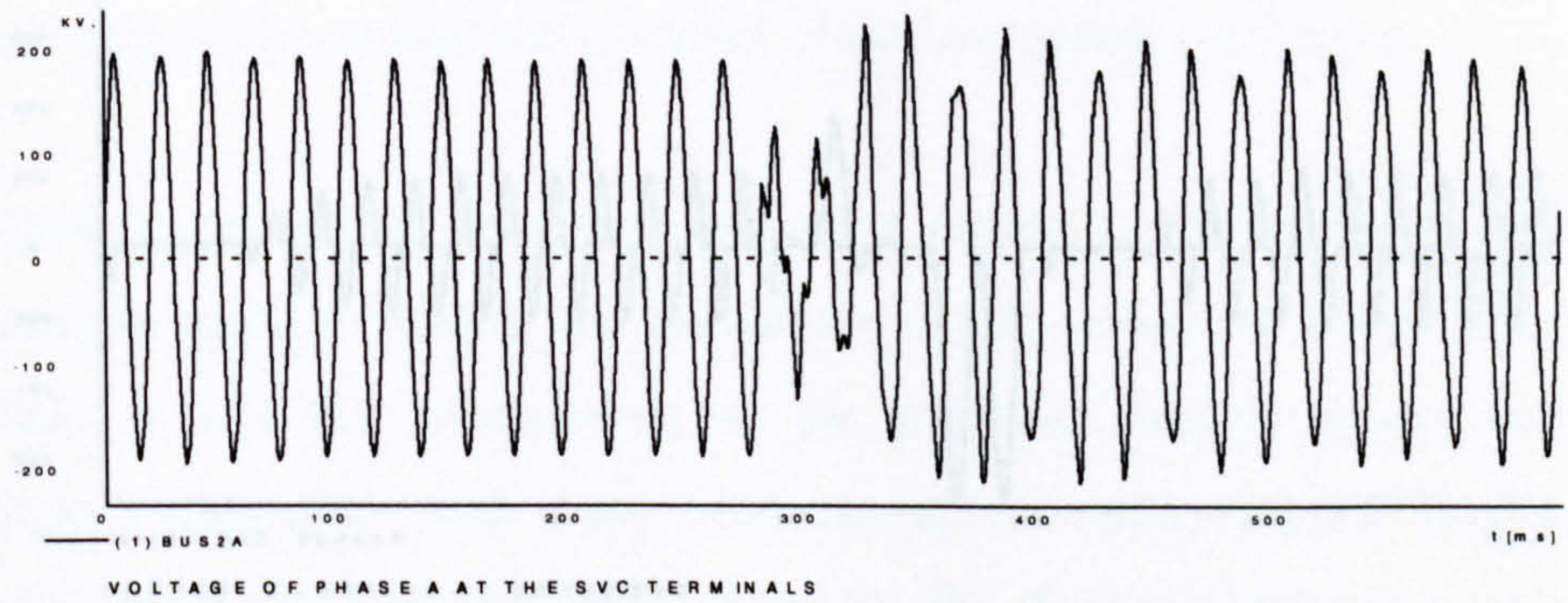

(c) Voltage of phase A at the SVC terminals

Figure 7.37

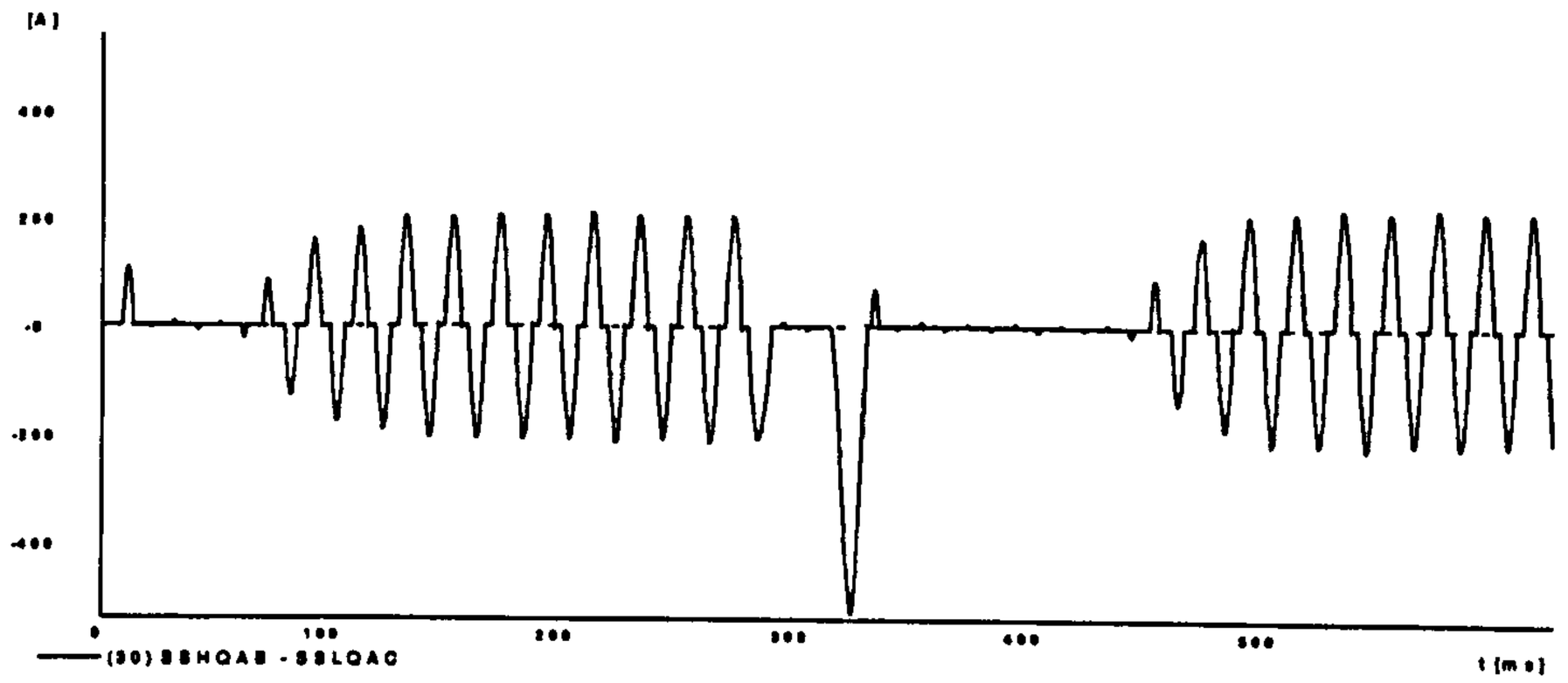

CURRENT ON BRANCH AC OF THE SVC

(a) Current on branch AC of the SVC

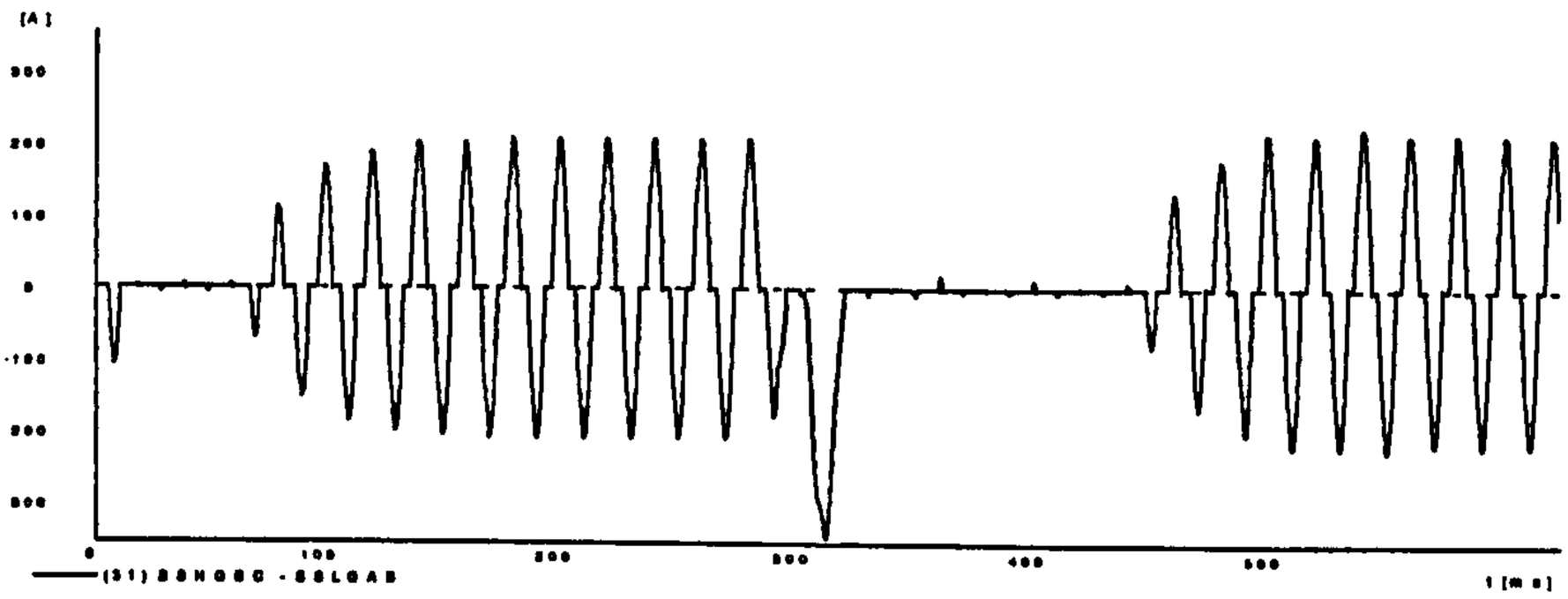

CURRENT ON BRANCH BA OF THE SVC

(b)Current on branch BA of the SVC

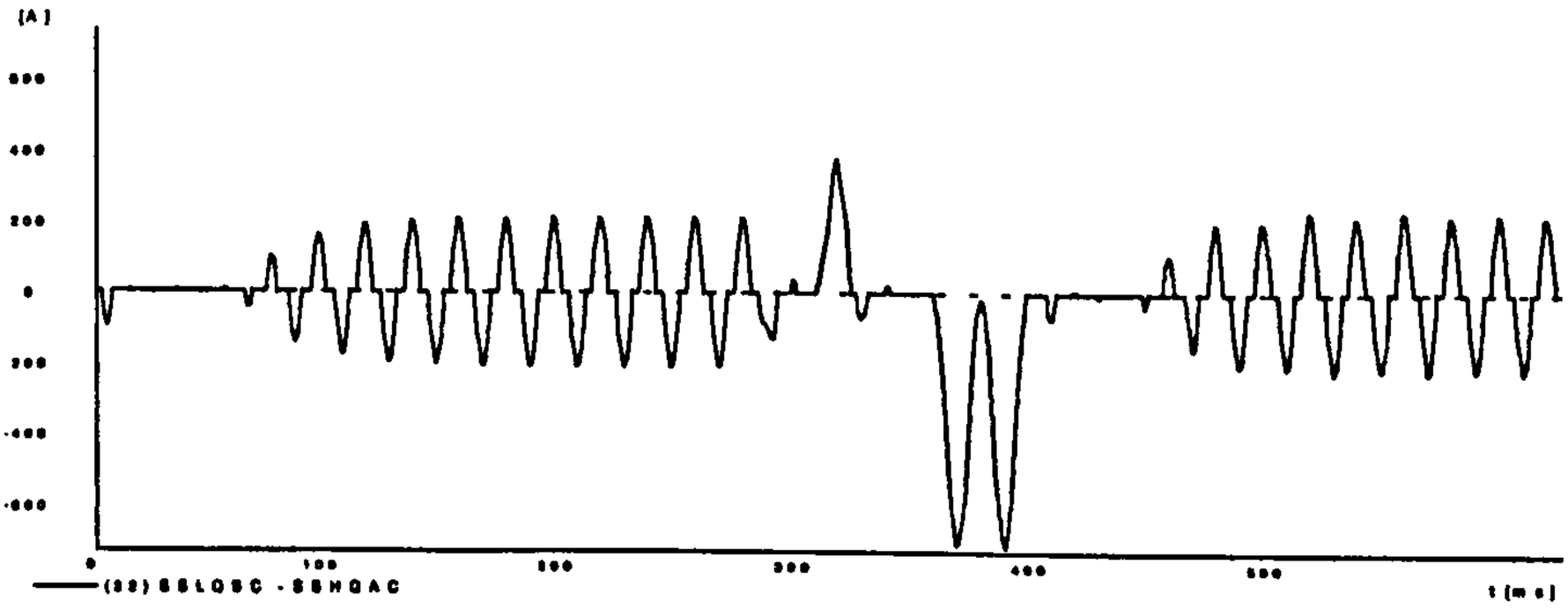

CURRENT ON BRANCH BC OF THE SVC

(c) Current on branch BC of the SVC

Figure 7.38

7.8 Validation and comparative simulation results using the PLL method

As was reported in section 7.6.3.1. a typical gate pulse generator would calculate the firing angle α from the point of zero voltage crossings. To achieve this firing at a request α, the controller could consist of an integrator that starts integrating at zero voltage and resets when it reaches a controlled threshold. At this point, a firing command would be generated for the appropriate thyristor. Control would be achieved by changing the value of the threshold. This type of system acts correctly if the points of zero voltage crossing are accurately known. This is not the case since both harmonics and transients are expected.

For the case of a TCR this problem can be solved by taking advantage of the 90° phase shift between the current and the voltage. This insures that the conduction angle σ is centered about the zero crossing of the voltage. In that case, the conduction current can be used to locate the zero crossings of the voltage without the problems associated with harmonics and voltage waveform distortion.

Another advantage of this scheme as was mentioned in section 7.6.3.1 is that the only information needed is state of the conduction of the thyristors. There is no need for accurate measurement of voltage or current. The system is insensitive to harmonics and transients on the voltage waveform. The effectiveness of this firing method will be tested in this section by using comparative simulation results with the Phase Locked Loop (PLL) method for a number of various system conditions.

Validation is considered as a very important aspect in power system simulation programs. In order to validate the simulation results carried out in this chapter and especially to test the effectiveness of the proposed control system and firing technique a comparison was made with simulation results obtained from an SVC controller that is using a control method and the PLL firing technique presented in [2] and [13].

For the above reasons various case studies using the SVC controller presented in this chapter will now be examined. In this case an AC system, represented by three phase

voltage source BUS1 (rated close to 120 kV L-L rms voltage depending on the study that is being investigated) and an R-L equivalent system impedance (3.58 ohms for the series resistance, 0.0358 H for the inductance and 1000 ohms for the parallel resistance) is feeding a resistive load of 144 ohms (1.0 pu load). The circuit diagram is shown in figure 7.39.

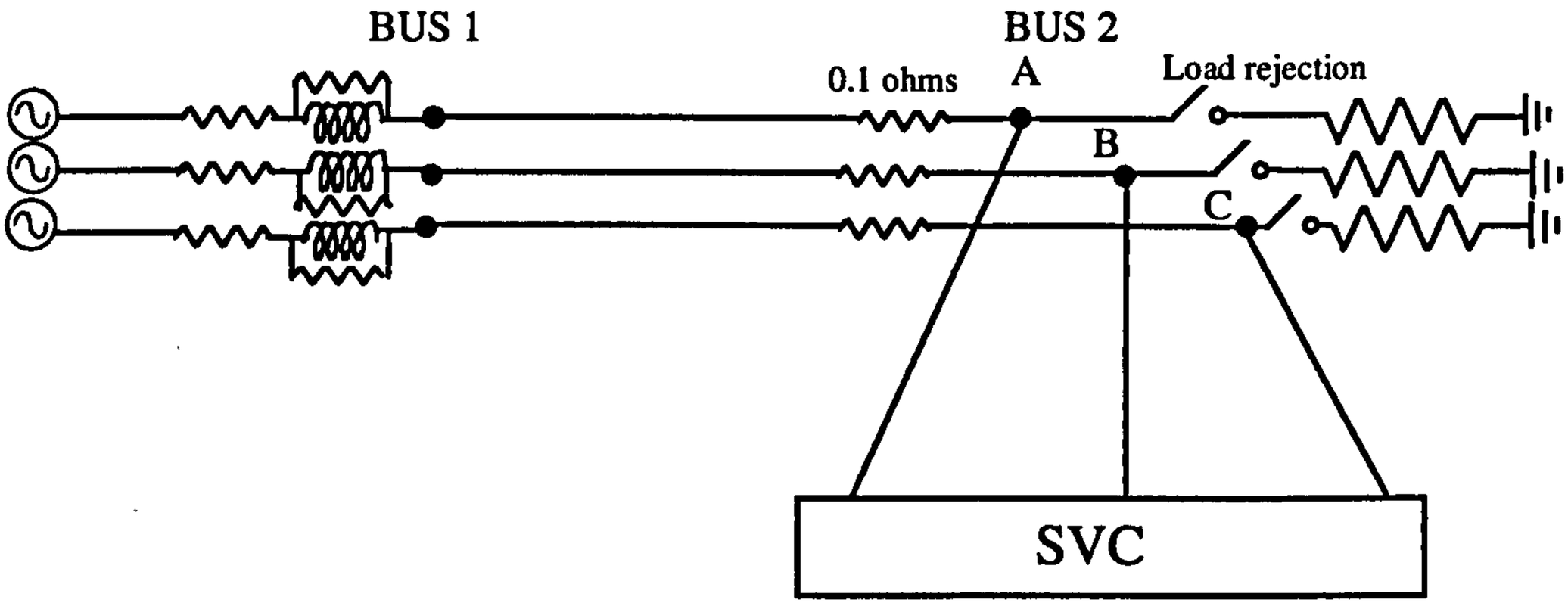

Figure 7.39

In the above system it is desired to control the voltage at bus 2 to 120 kV by the addition of the SVC under various system disturbances. Results using the models presented in this chapter will be compared with results taken by using the EMTDC simulation package using the control method and the firing technique (PLL) presented in the [2] and [13] using the same rating for the SVC model. The EMTDC model for the above system is illustrated in figure 7.40. The parameters for this SVC model and the control systems are similar to the ones used in [2] and [13]. The SVC consists of a 120/12.65 kV $Y/\Delta - Y$ transformer feeding a 12 pulse TCR/TSC (Thyristor controlled reactor/Thyristor switched capacitor) with the thyristor controlled reactor elements connected in delta and the thryristor switches modelled as changing resistances. The thyristor controlled capacitors are switched on/off according to a control demand.

The SVC controller for this example can be based on the following principles:

- to compare the measured voltage where the SVC is connected with the reference voltage (both in p.u)
- pass the error signal through a PI controller to produce the alpha (firing angle) order
- use the alpha order signal to trigger control signals to switch capacitors:

  when $\alpha > 3.1$ radians, switch on one capacitor stage (signal NDIR=1 in figure 7.40)

  when $\alpha < 1.6$ radians, switch off one capacitor stage (signal NDIR=-1 in figure 7.40)

The complete controls for this type of SVC are illustrated in figure 7.40. The instant of valve firing for the TCR is determined when a reference angle derived from a phase locked loop (PLL) equals to the order angle. A built -in dq0- transformation based PLL is used using the principles described in 7.6.3.2. In order to test the effectiveness of the control and the firing methods presented in this chapter a number of case studies were investigated for the two SVC models:

a) Disconnected load

For that case the three phase source in figure 7.39 is rated at 123kV and a load rejection takes place at 0.5 secs for the three phases at bus 2. The rating of the SVC is 110 MVA inductive and 73 MVA capacitive. In this case only one capacitor stage was used (with a rating of 73 MVA). Figures 7.41-7.43 show the responses of the two SVC models. The total load rejection causes AC bus over-voltages at bus 2 resulting in reducing the α (firing angle) order in graphs 7.42. The new adjustment of α brings the voltage at bus 2 to 1.0 p.u in a very short term. The results in the previous graphs show very good similarity and prove the effectiveness of the modelling methods used in this chapter. These results are also similar to the ones demonstrated in [13] using the control and firing systems presented in figure 7.40 for the same system conditions.

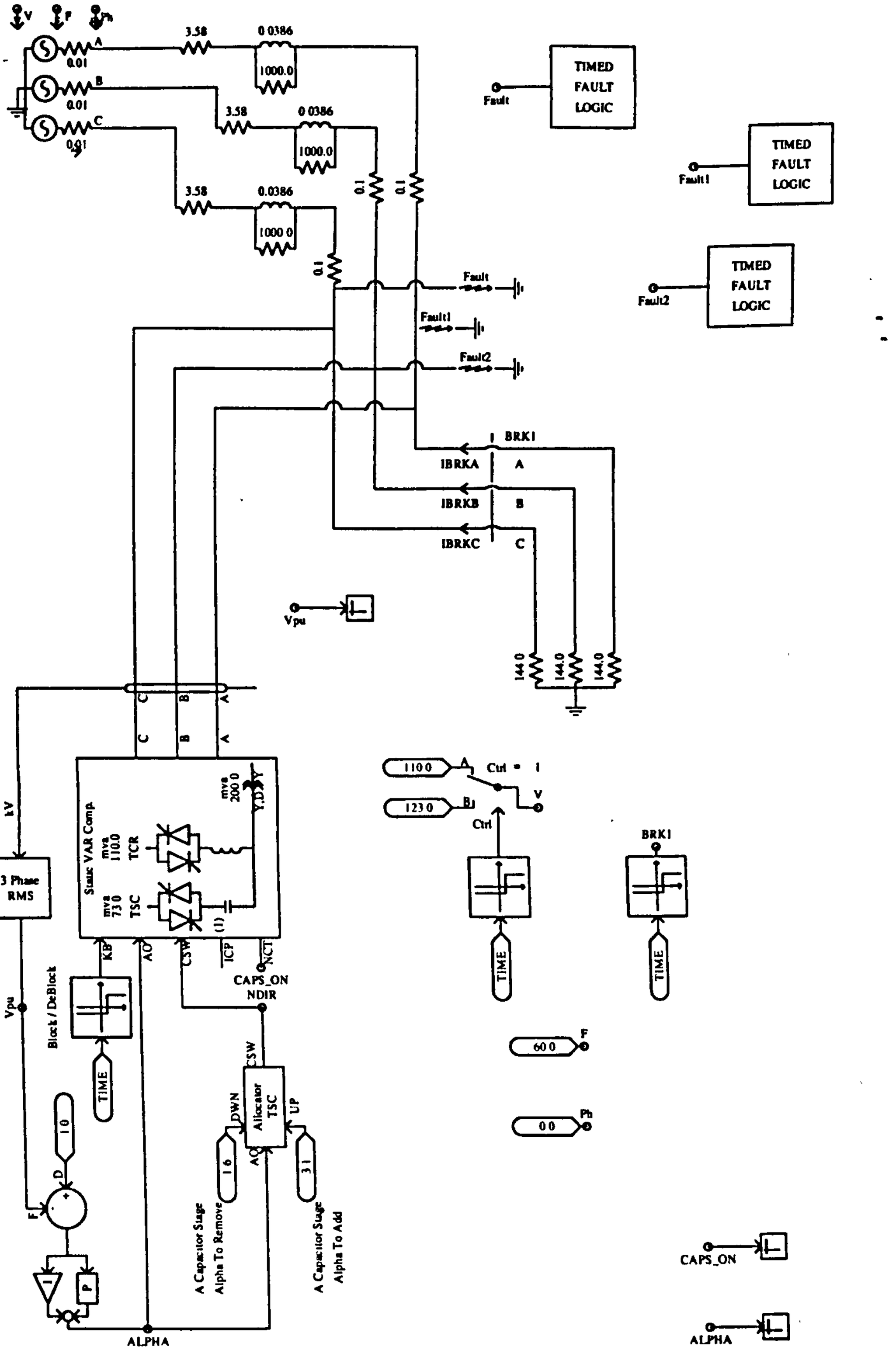

Figure 7.40 SVC model using the EMTDC simulation package

In order to test the effectiveness of the firing method proposed in this chapter simulation results are presented in figures 7.43 (a)-(b) and compared with results found in [13].

For the results in figure 7.43 (a) it is clear that from the graphs of the thyristor currents and the generated sawtooth waveform (used for the firing of thyristors) for one on the TCR branches, the response of the system to a load rejection (at 0.5 secs) is practically stabilised in one cycle. A similar response is illustrated for the same conditions using the Phase Locked Loop (PLL) method by examining the thyristor currents in [13] . The firing method for the system presented in [13] is the same with the one used in figure 7.40. In figure 7.43 (b) the generated firing pulses of two TCR branches are plotted. From these results is obvious that despite the sudden change in the system conditions at 0.5 secs (load rejection) firing pulses are being generated with a 60° interval between the TCR branches for every half cycle (one pulse is generated for each branch every 180°). This is due to the immediate response of the firing system to the change in system conditions in a way similar to the PLL method.

b) Voltage drop

For this case study the three phase voltage source in figure 7.39 is rated at 120kV with a voltage reduction of 8% (from 120 kV down to 110 kV) occuring for this voltage at 0.5 secs for the three phases. The rating of the SVC is 100 MVA inductive and 167 MVA capacitive. For this case two capacitor stages were used (with a rating of 83 MVA each). A control signal is responsible for the switching on/off of the capacitor stages depending on the value of the firing angle α as was addressed in section 7.8. The SVC model presented in figure 7.40 is identical with the one used in [2] and was tested for the same system conditions. Figures 7.44-7.47 show the responses of the SVC models presented in figures 7.11 and 7.40. By examining the previous graphs it is clear that the source voltage reduction at 0.5secs causes the voltage at bus 2 to drop below 1.0 p.u and the firing angle α to increase up to level of switching in two capacitor stages (figure 7.46 (b)). After this only a small adjustment

of α (or σ in figure 7.46 (a)) brings the voltage back to 1.0 p.u. The switching on/off of the capacitor stages due to the value of the firing angle α can also be observed during the start up on the above figures. In that case because the voltage at bus 2 is less than the reference in figure 7.40 α is held at π radians and according to the technique described in the section 7.8 two capacitor stages are switched on. When the measured voltage at bus 2 exceeds 1.0 p.u then α is reducing and after a certain value one capacitor stage is switched off.

The comparison of the results plotted in figures 7.44 (a) and 7.45 (a) with the ones in 7.44 (b) and 7.45 (b) shows that the modelling techniques presented in this chapter are capable and accurate enough to control SVC models. These results are also similar to the ones presented in [2] using the control method and the PLL firing technique presented in figure 7.40 for the same system conditions.

From the results of the thyristor currents and the generated sawtooth waveforms (responsible for the firing of thyristors) in one of the TCR branches in figure 7.46 (a) it can be noticed that the system has stabilised itself in 2-2.5 cycles following the disturbance at the voltage source. This is due to the correct action of the control system (regulation of σ) and the firing method (accurate firing timing) used for the SVC model. In figure 7.46 (b) the response of the firing system can be detected by examining the generated pulses in two TCR branches. From these results it is shown that the firing system has synchronised itself shortly after the disturbance at about 25 mseconds (within 2 cycles) giving the correct firing sequence for the thyristor pulses (firing pulses are generated with a 60° interval between the TCR branches for every half cycle). This example illustrates the effectiveness of the technique that was used in this chapter and shows that is insensitive to transients on the voltage waveform; consequently it can be used as an alternative to the PLL method for the control of Static Var Compensator models.

c) Three phase fault

In this case there is a complete loss of the synchronising voltages where the SVC is connected at bus 2 at 0.38seconds with a duration of 30msecs. The three phase voltage source in figure 7.39 is rated at 120kV and the rating of the SVC is 100 MVA inductive and 83.0 MVA capacitive (only one capacitor stage is used with a rating of 83.0 MVA). Because only one capacitor stage is used in the analysis the control system does not include the function for the switching on/off of capacitor stages due to the value of the firing angle as was described in before in section 7.8. Figures 7.48-7.50 show the responses of the SVC models presented in figures 7.11 and 7.40. By looking at these graphs we notice that the very severe drop at the voltage bus 2 (figures 7.48(a) and (b)) causes the firing angle to increase up to a maximum value and then gradually to drop back to its pre-fault conditions bringing in this way the voltage back to 1.0 p.u in a short timescale. The results in the previous graphs show very good similarity and prove the effectiveness of the control and firing methods used in this chapter in comparison with the ones used in figure 7.40.

From the results of the current and the generated sawtooth waveforms in one of the TCRs branches in figure 7.50 (a) we notice that the system has stabilised itself about 90mseconds after the fault. This is mainly due to the time that the firing angle needs in order to come back to its pre-fault conditions as can be seen in figures 7.48. Immediately after the fault the firing system is out of synchronisation as can be seen from the graph of the current in one of the TCR branches in 7.48 (b). This results in the first half cycle of the current having a very large conduction angle, much greater than 180°. The second half cycle in the positive plane has a significant smaller conduction angle, where the third one is close to the requested value (obtained by the control system).

According to the results presented in [13] the response of the Phase Locked Loop method under similar system conditions (complete voltage collapse at the SVC terminals) is within 2 cycles after the fault has cleared. Synchronisation of the fundamental component of the voltage and the signal that is used by the PLL method

for the firing of thyristors has occurred within the same period. The pulses that are being generated have symmetry (come at exactly 60°) within 2 cycles after the clearance of the fault.

In figure 7.50 (c) the generated pulses of two TCR branches are plotted. From these results it can be shown that the firing system has synchronised itself shortly after the voltage collapse at about 25-30 mseconds (within 2 cycles) giving the correct firing sequence for the pulses in the TCR branches (equidistant pulse firing has been achieved, the pulses come at 60° intervals). By comparing the above results with the response taken by using the PLL method in [13] it can be concluded that the firing technique is effective and gives similar results to the ones obtained by using the PLL method for the control of SVC models.

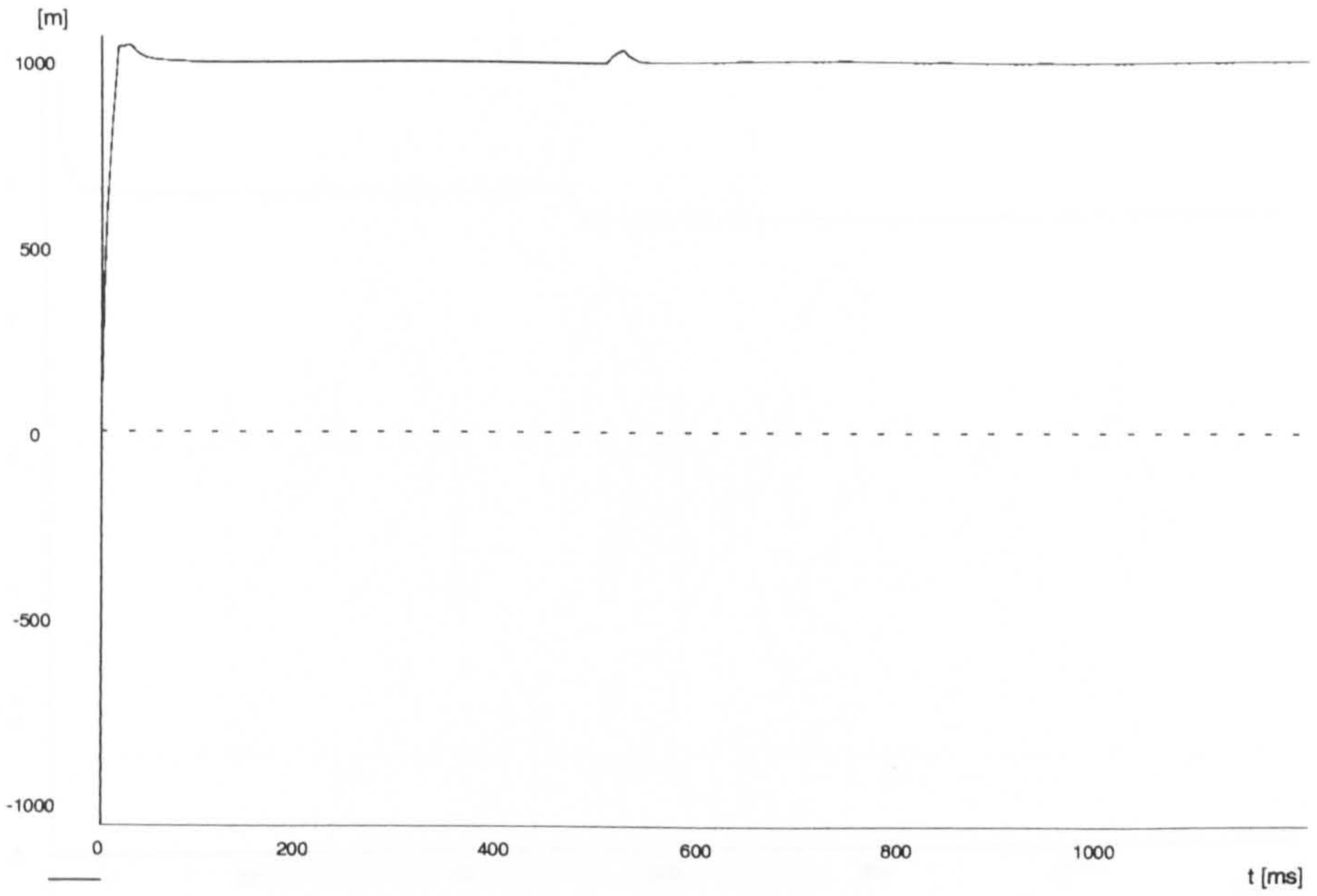

(a) Voltage at bus 2 in p.u using the SVC model described in figure 7.11

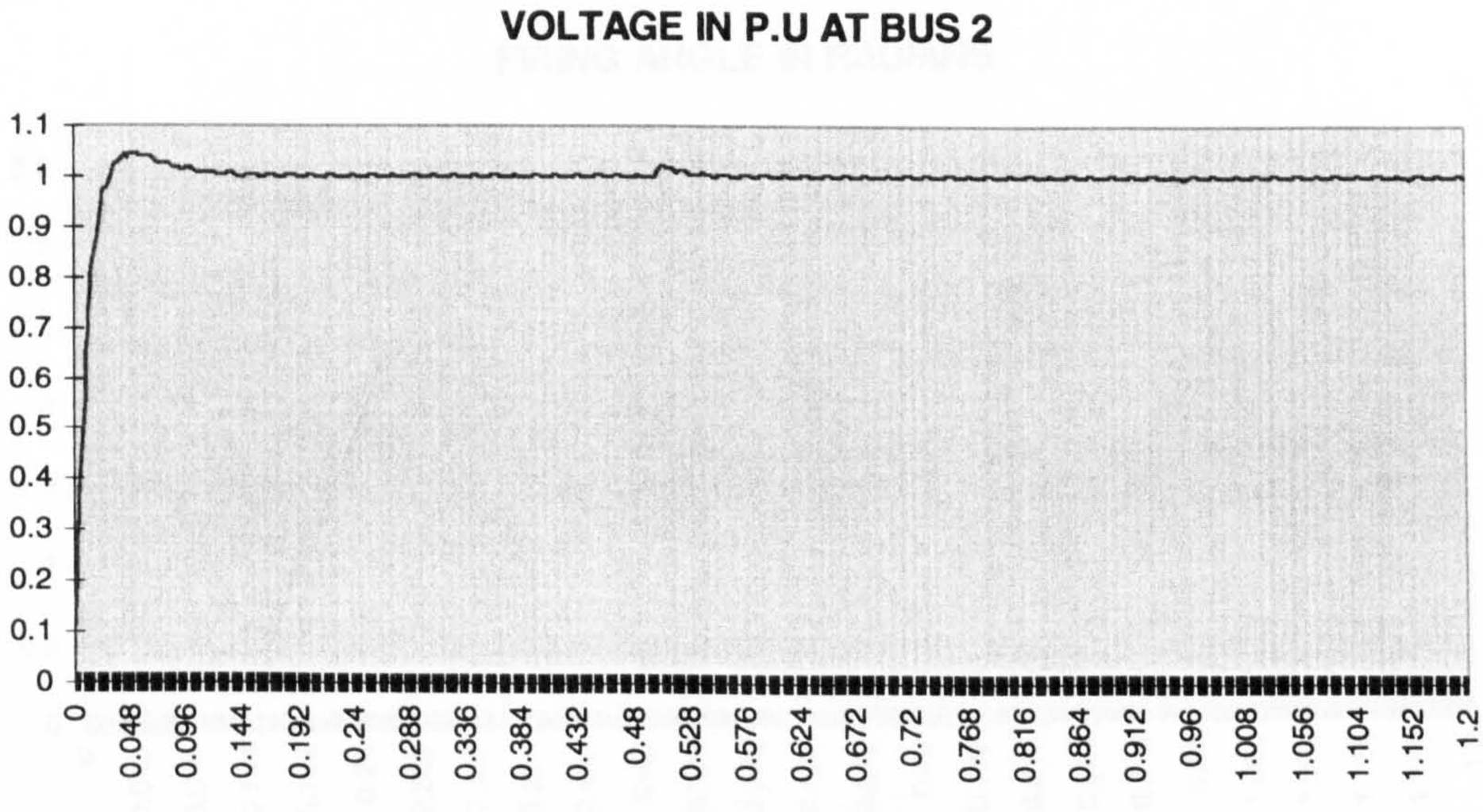

(b) Voltage at bus 2 in p.u using the SVC model described in figure 7.40

Figure 7.41

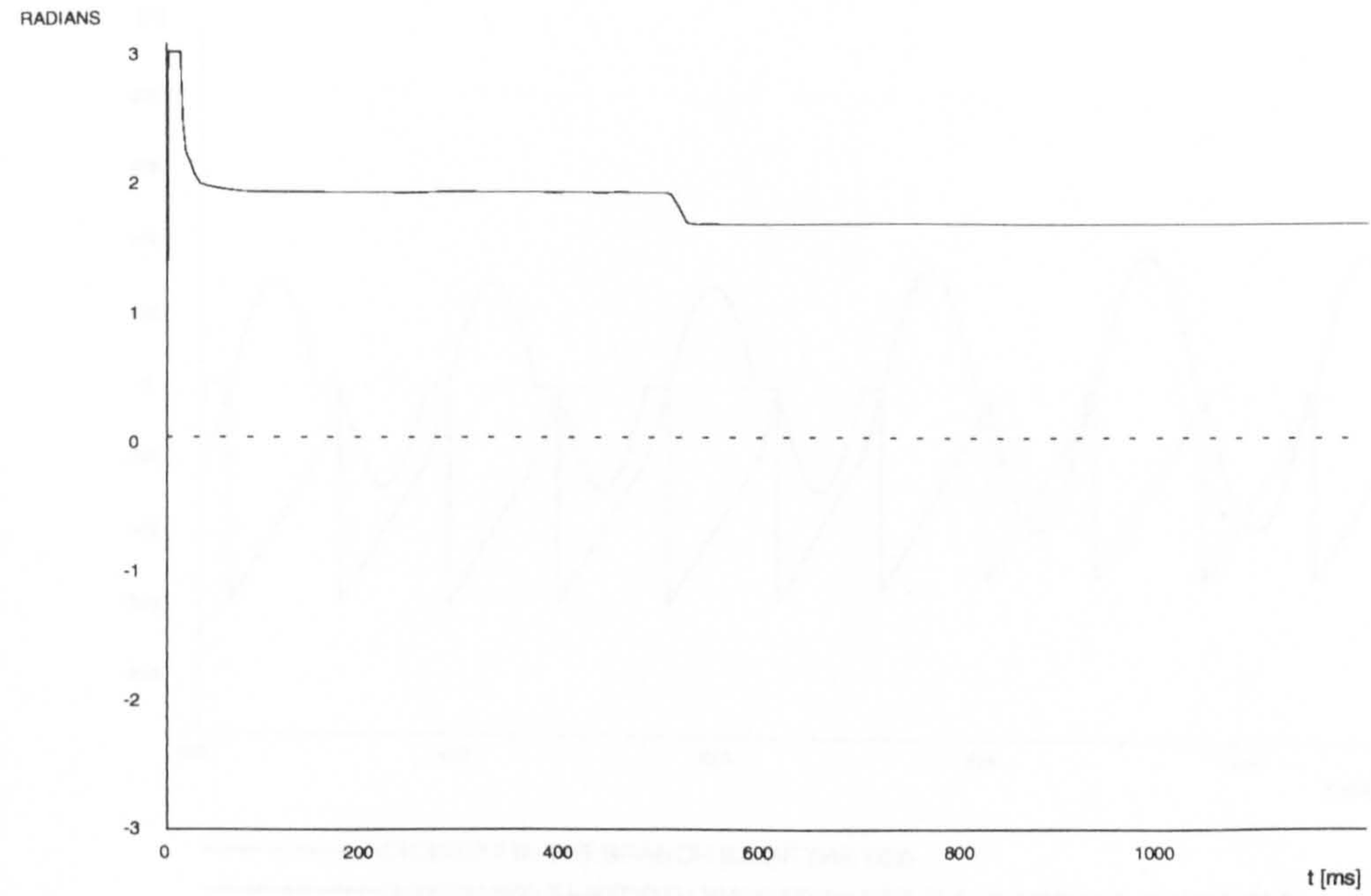

(a) Firing angle α using the SVC model described in figure 7.11

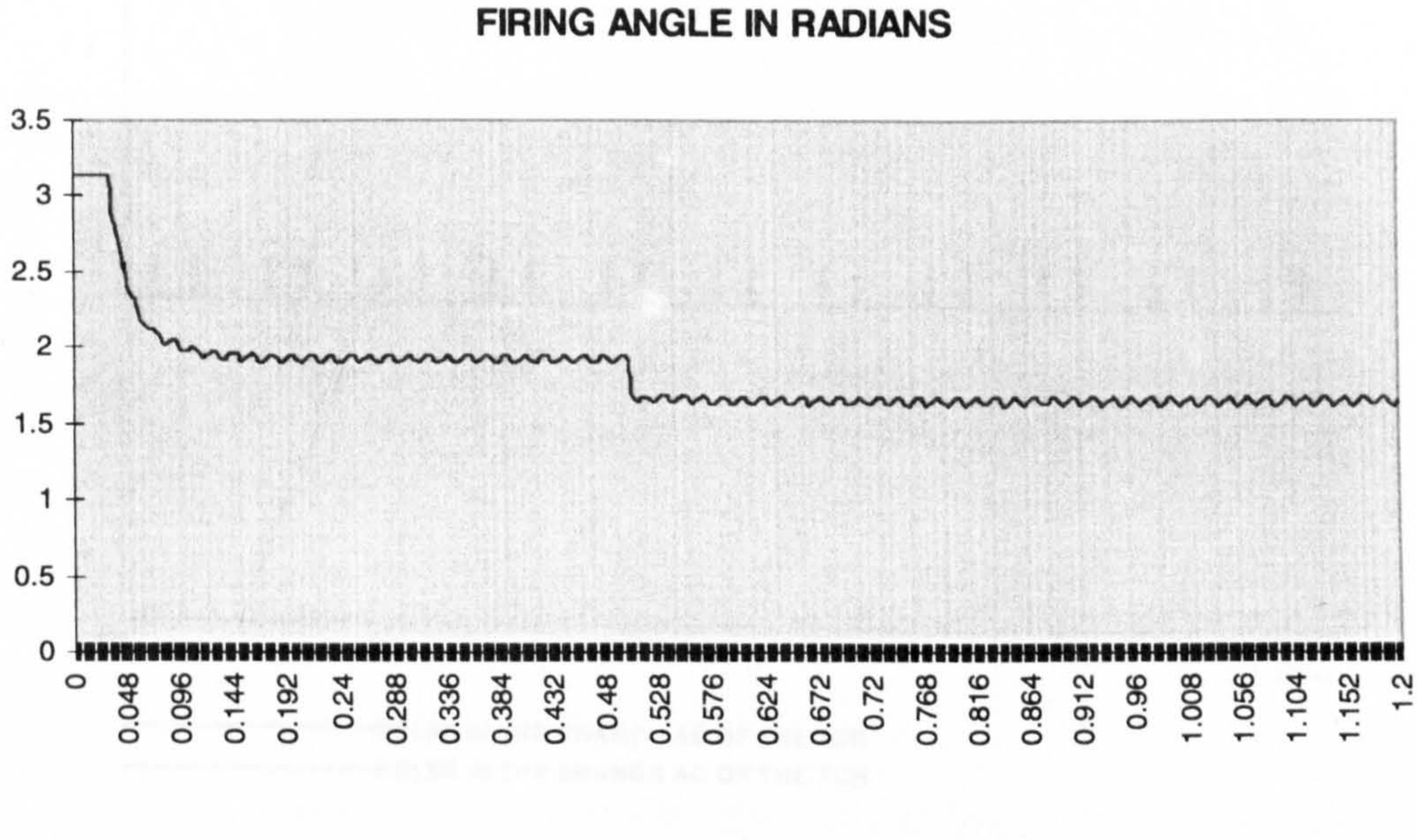

(b) Firing angle α using the SVC model described in figure 7.40

Figure 7.42

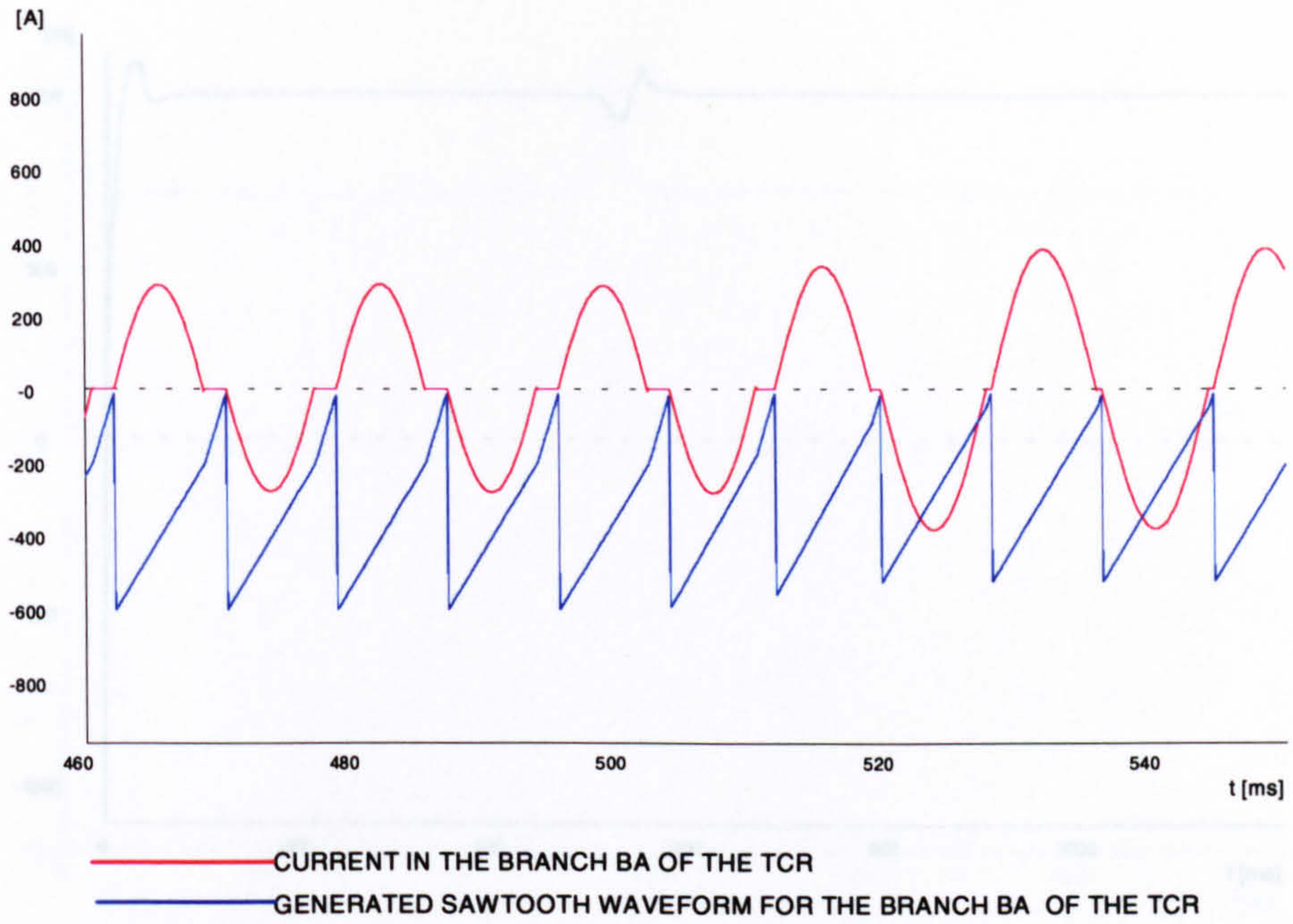

(a) Current and generated sawtooth waveform for the branch BA of the TCR

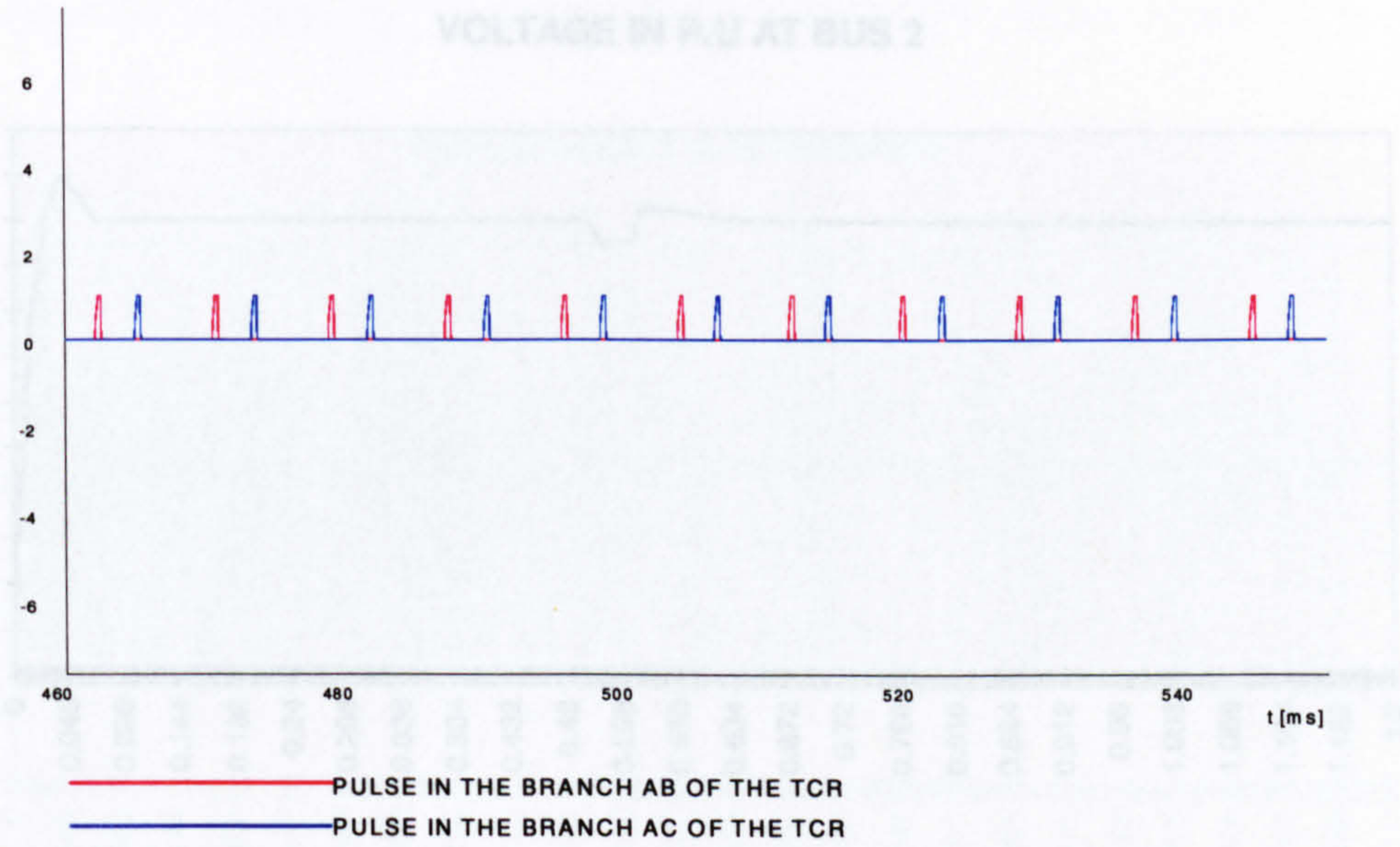

(b) Pulses generated in branches AB and AC of the TCR

Figure 7.43 Response of the firing method under disconnected load conditions

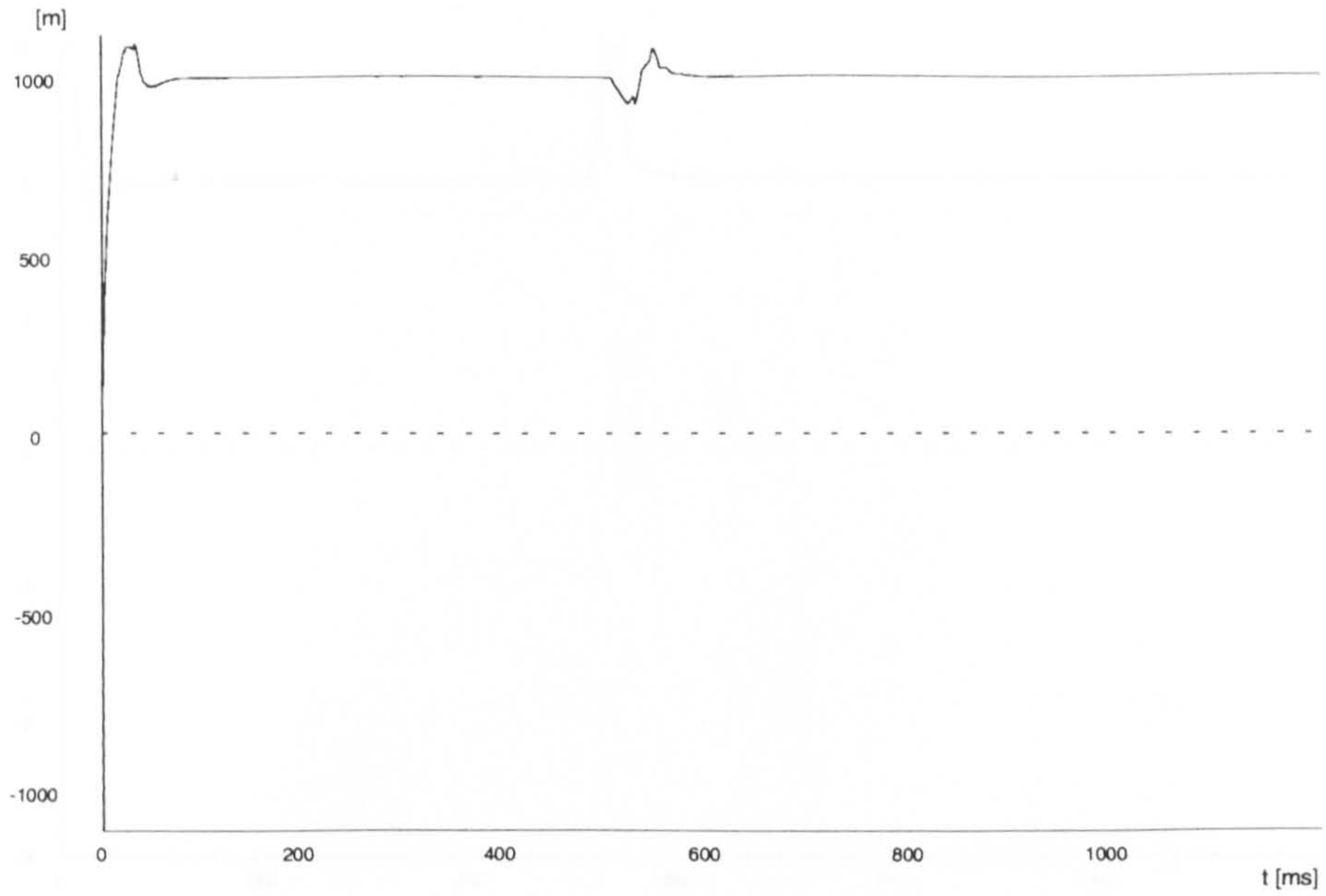

(a) Voltage in p.u at bus 2 using the SVC model described in figure 7.11

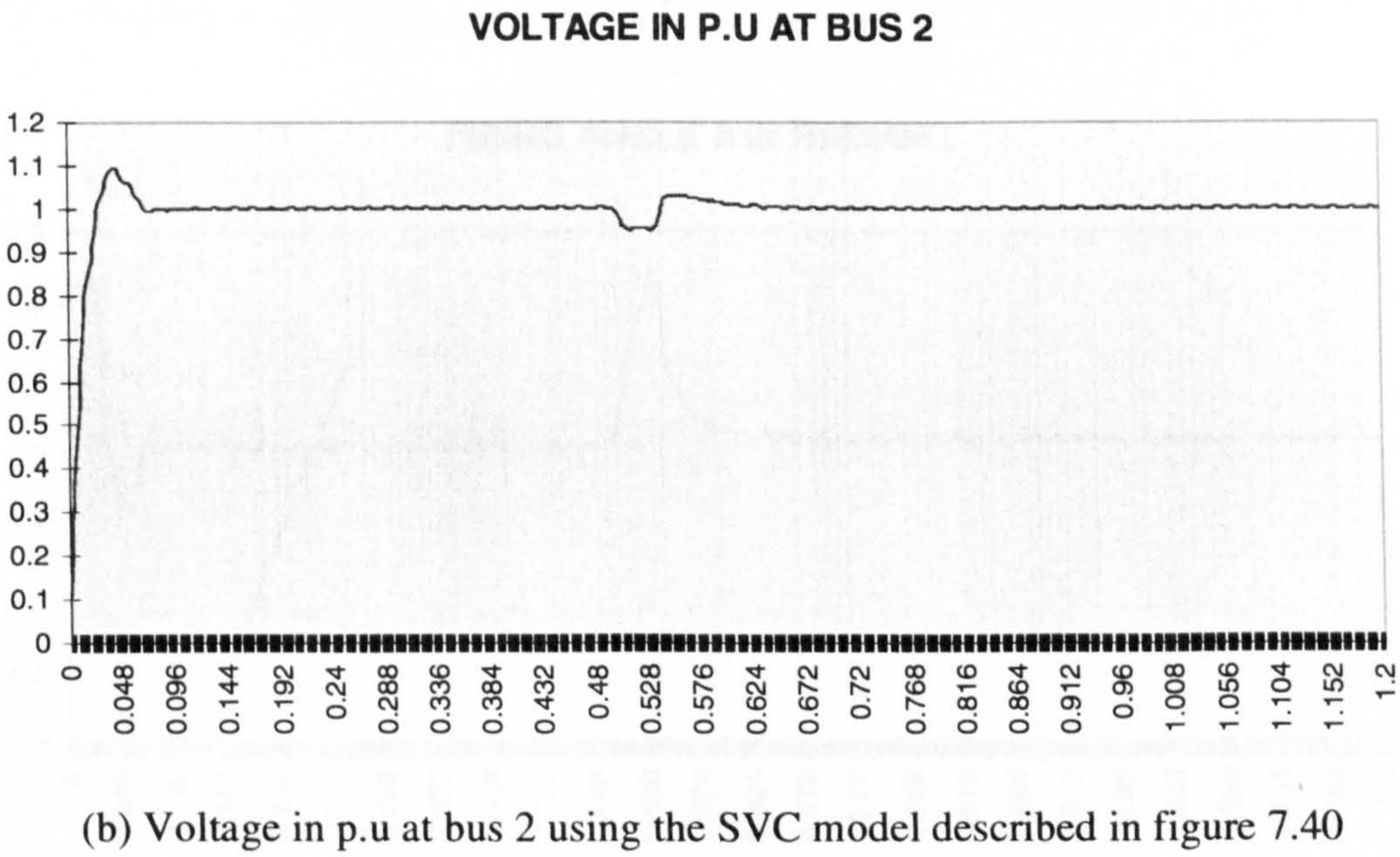

(b) Voltage in p.u at bus 2 using the SVC model described in figure 7.40

Figure 7.44

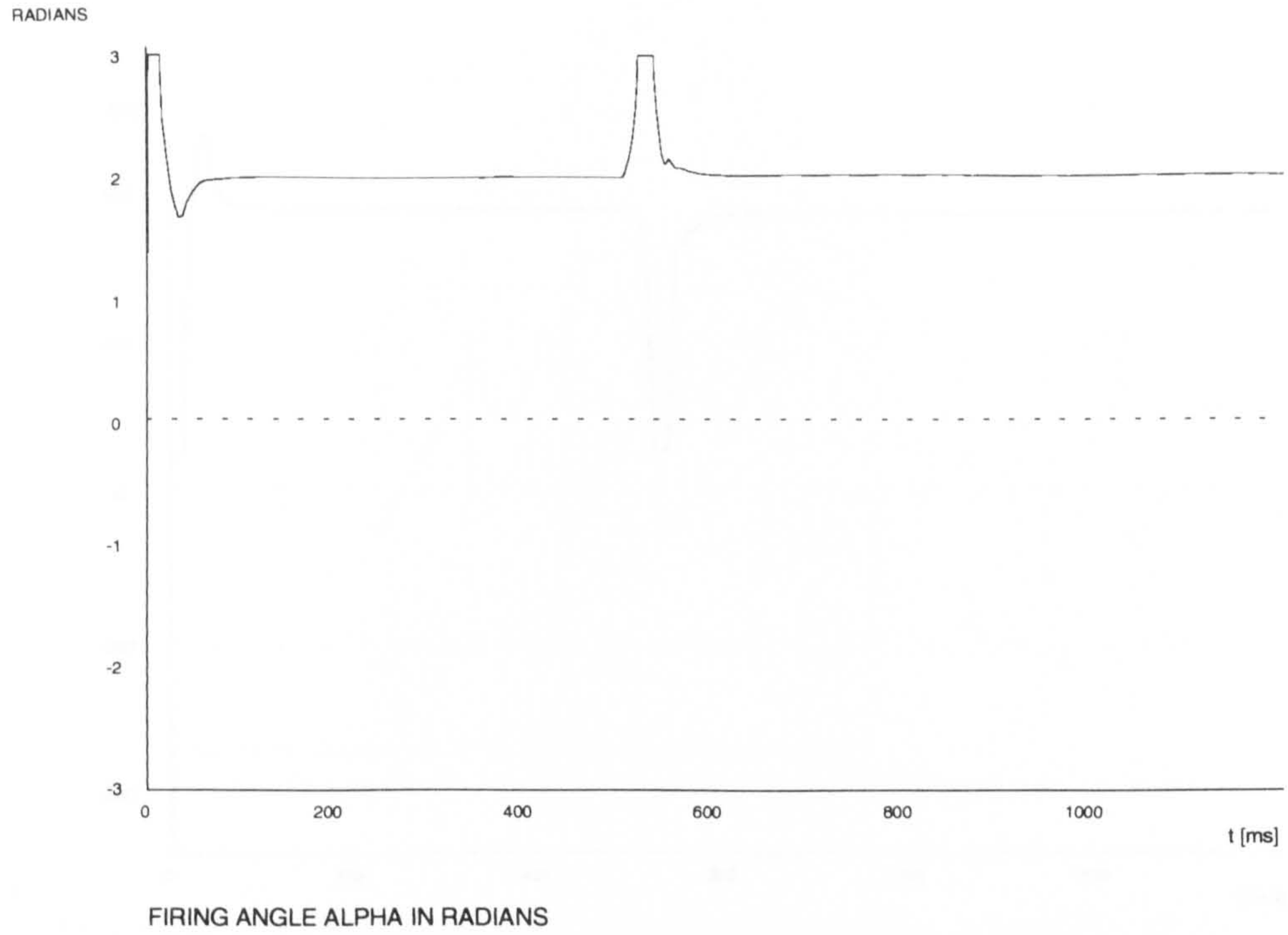

(a) Firing angle α in radians using the SVC model described in figure 7.11

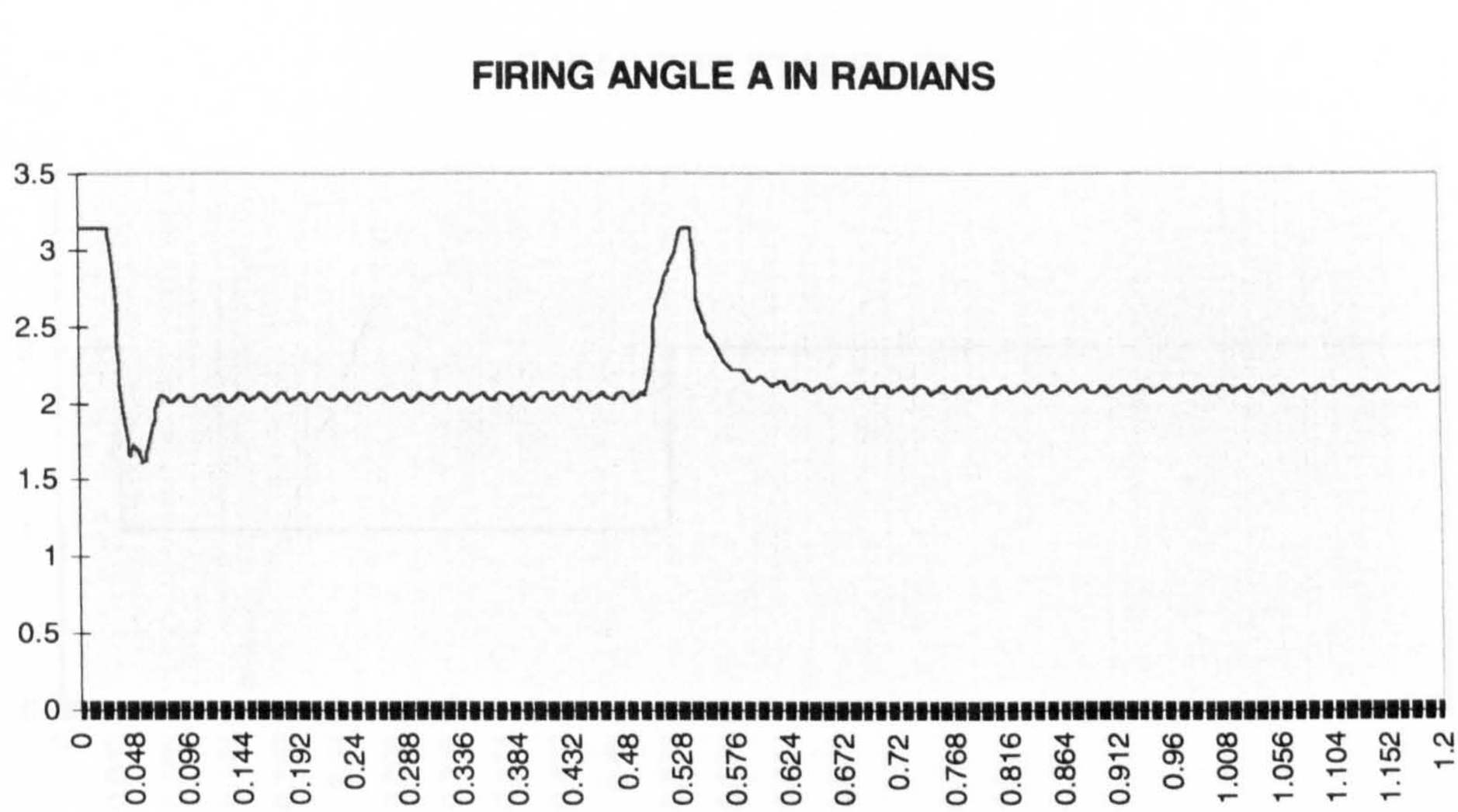

(b) Firing angle α in radians using the SVC model described in figure 7.40

Figure 7.45

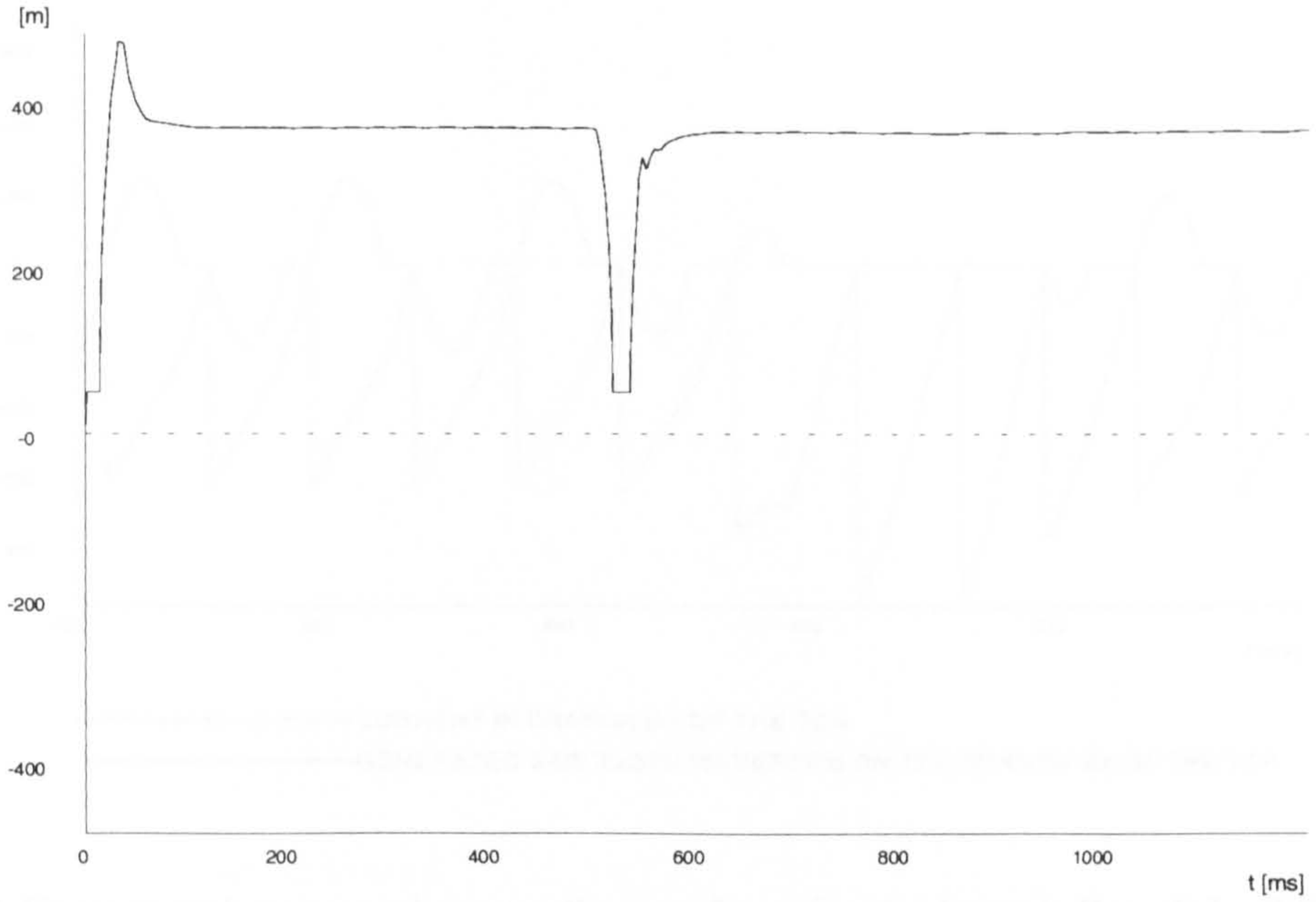

(a) Conduction angle σ ($\sigma_{max} = 0.5$ for 180°) using the SVC model in figure 7.11

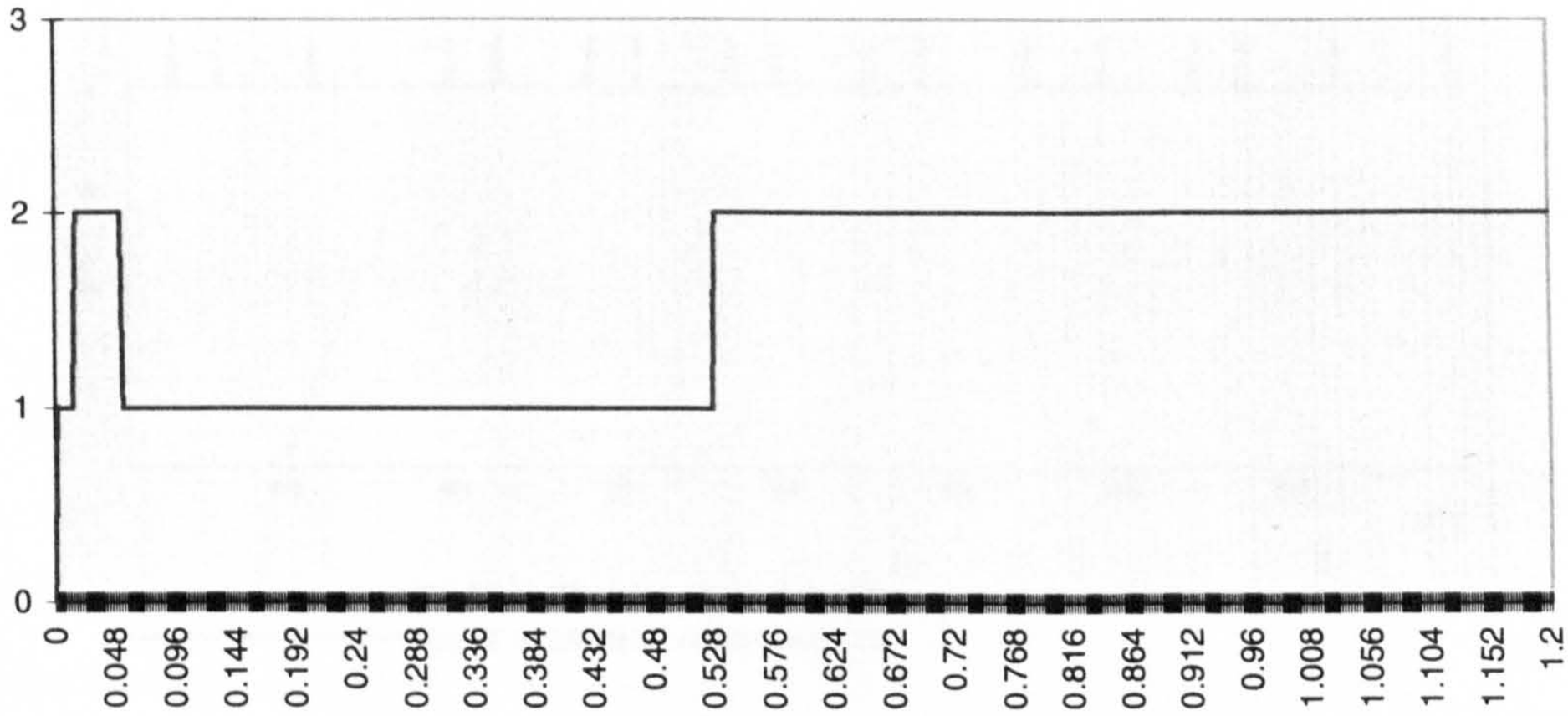

(b) Capacitor stages on using the SVC model in figure 7.40

Figure 7.46

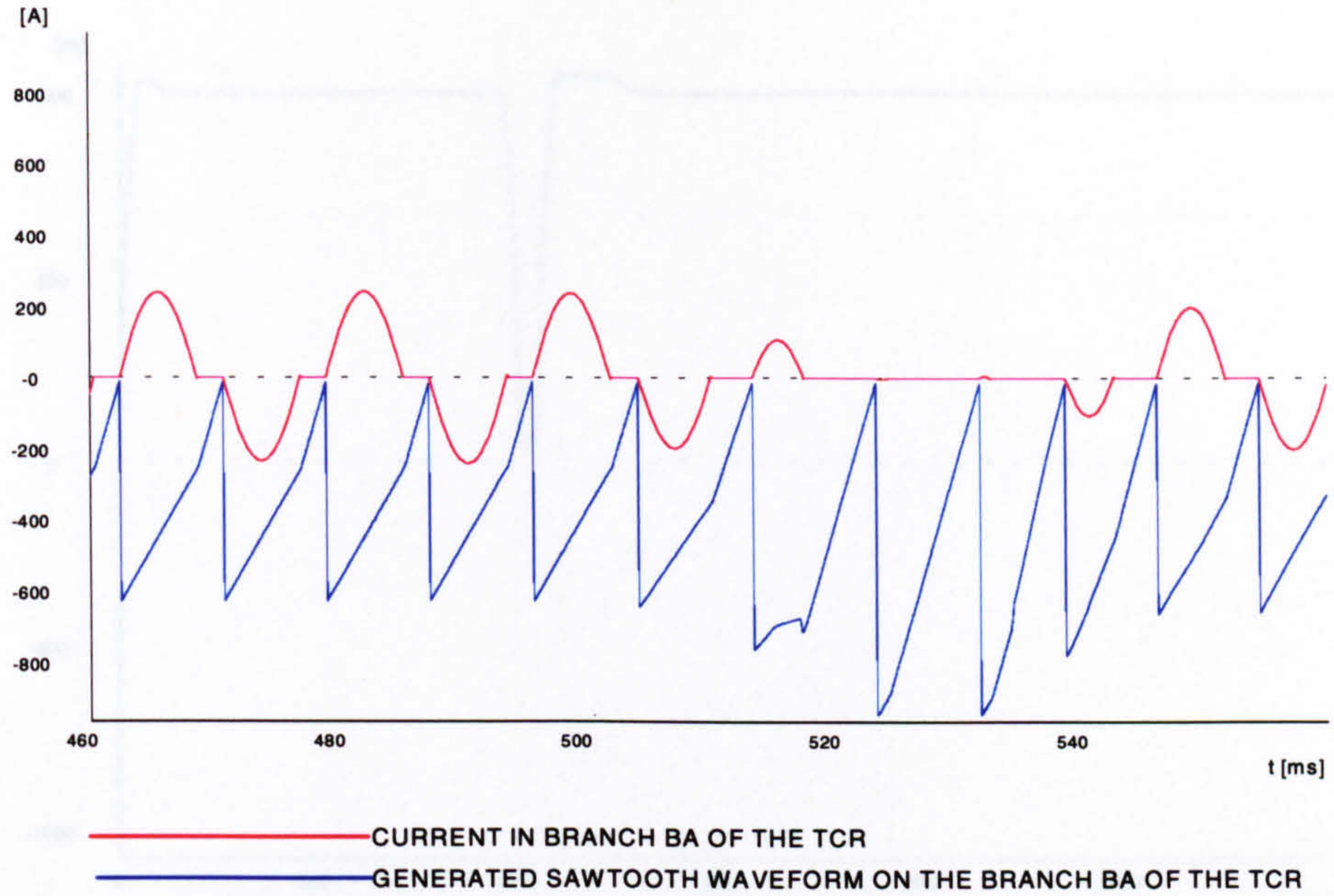

(a) Current and generated sawtooth waveform for the branch BA of the TCR

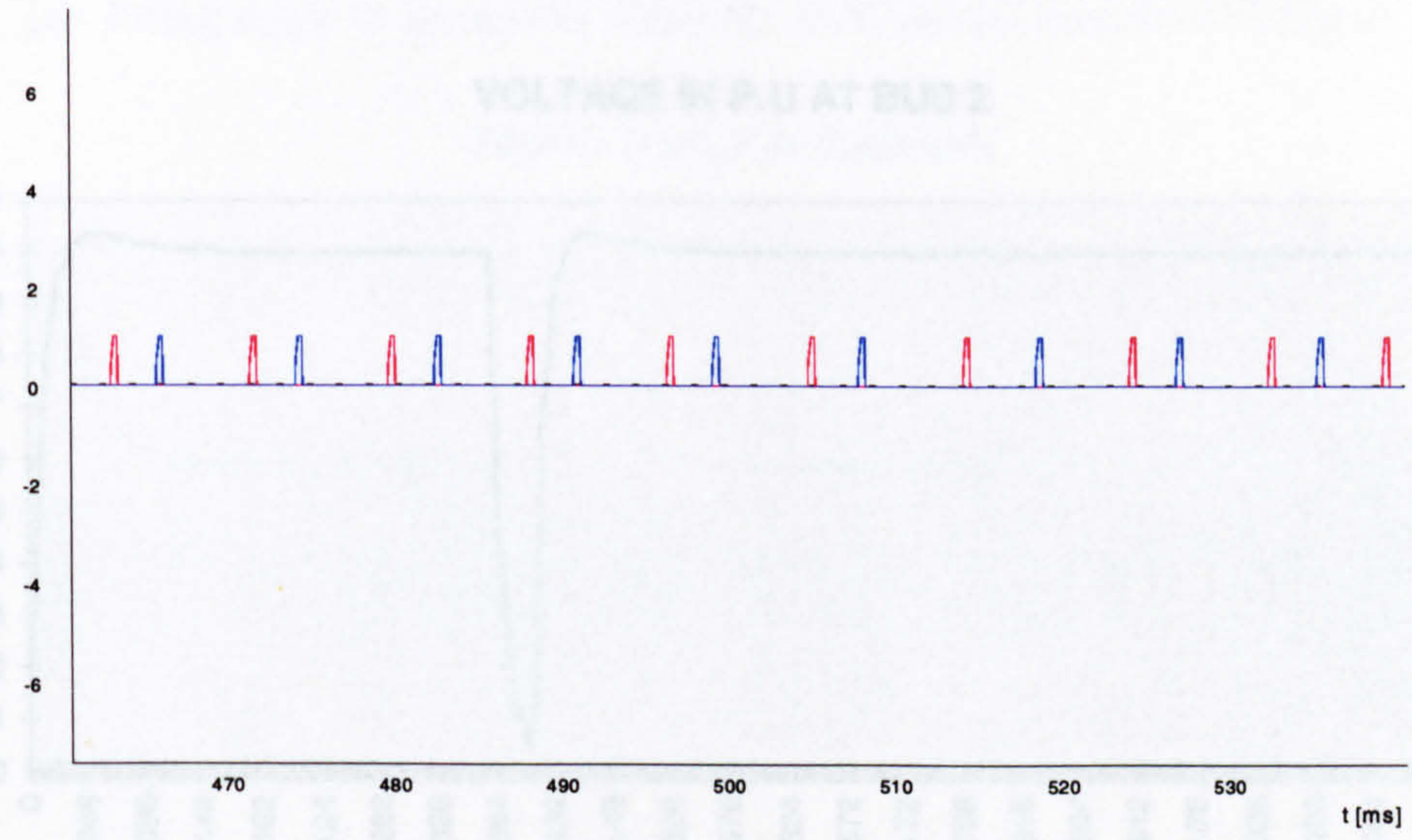

(b) Pulses generated in branches AB and AC of the TCR

Figure 7.47

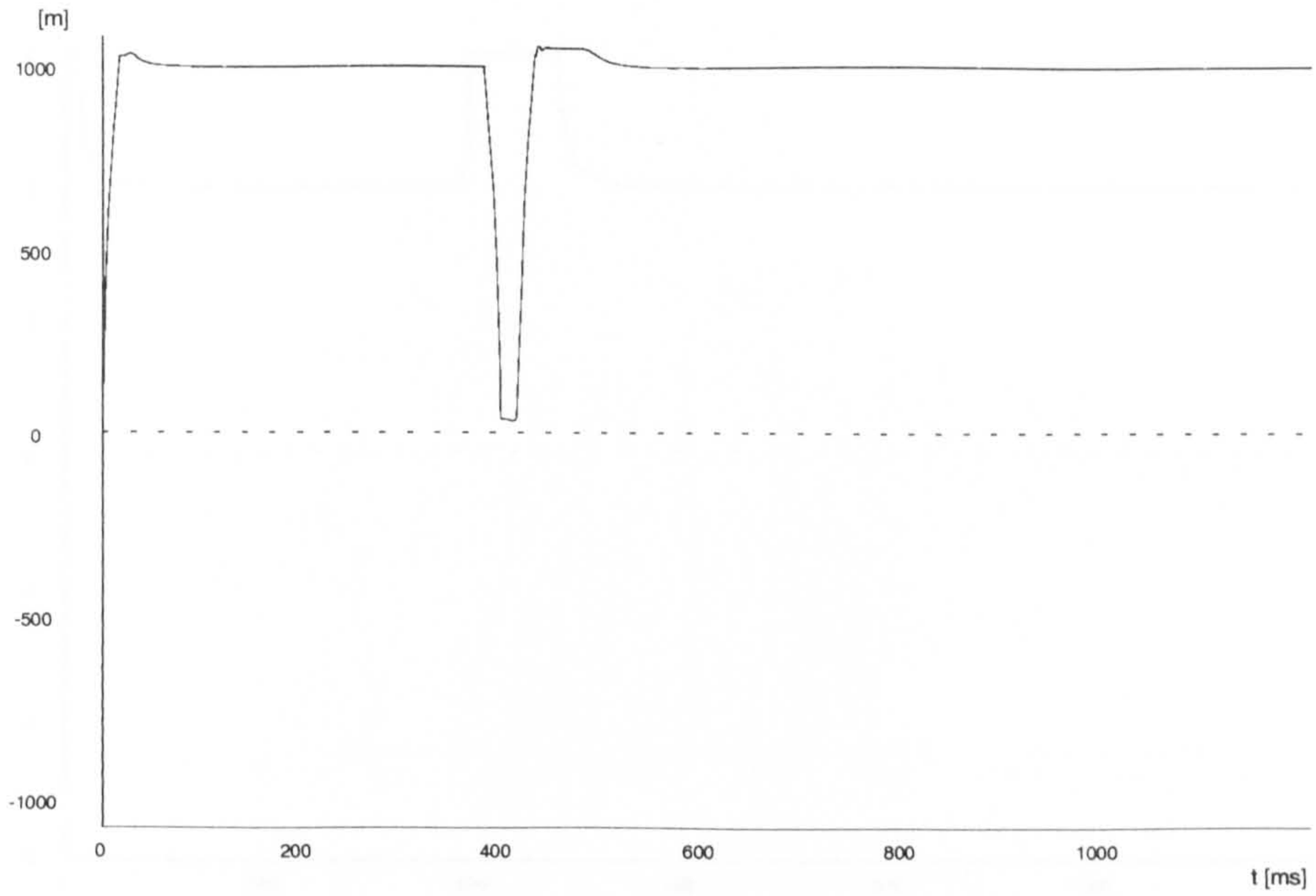

(a) Voltage in p.u at bus 2 using the SVC model described in figure 7.11

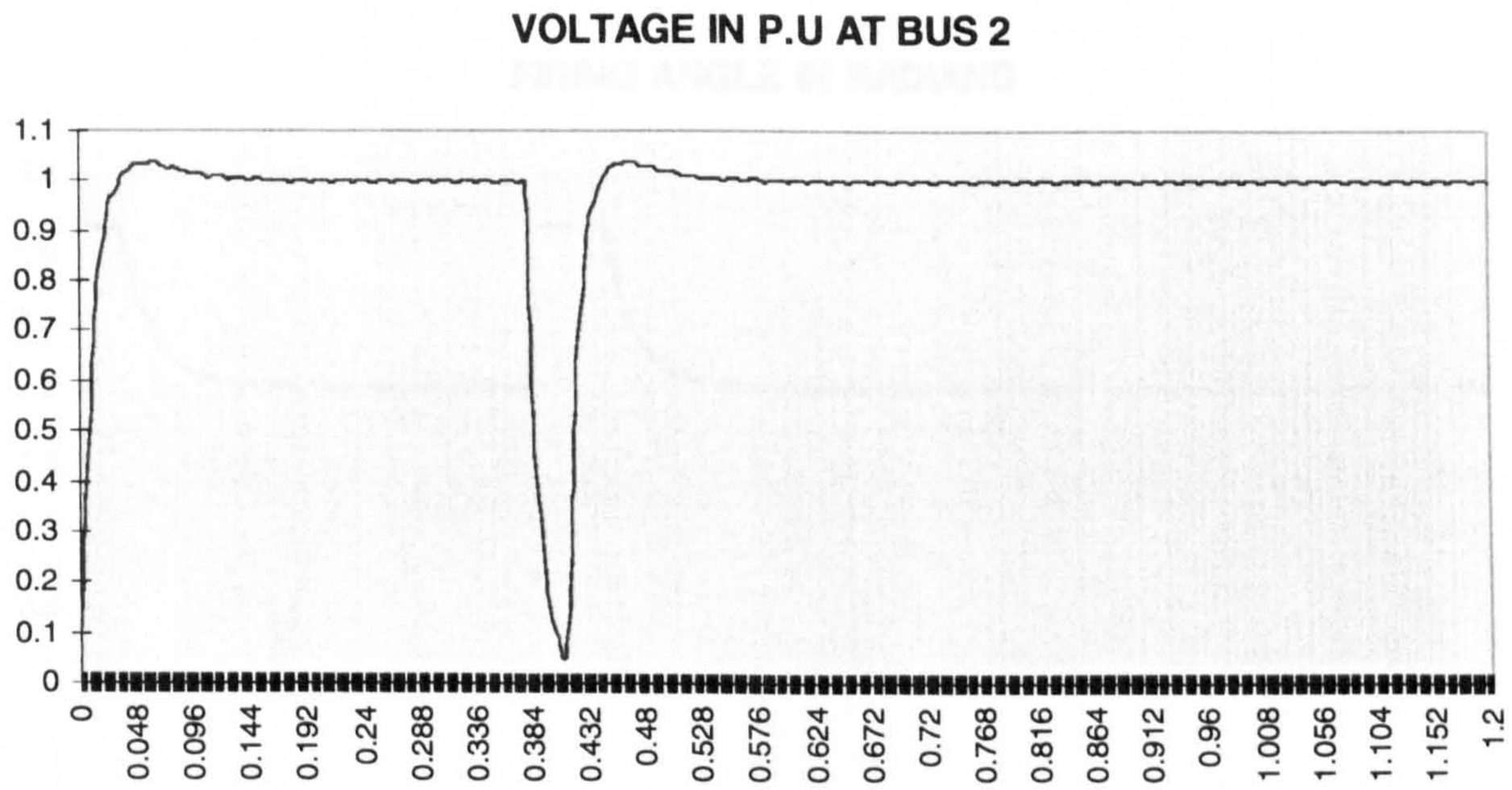

(b) Voltage in p.u at bus 2 using the SVC model described in figure 7.40

Figure 7.48

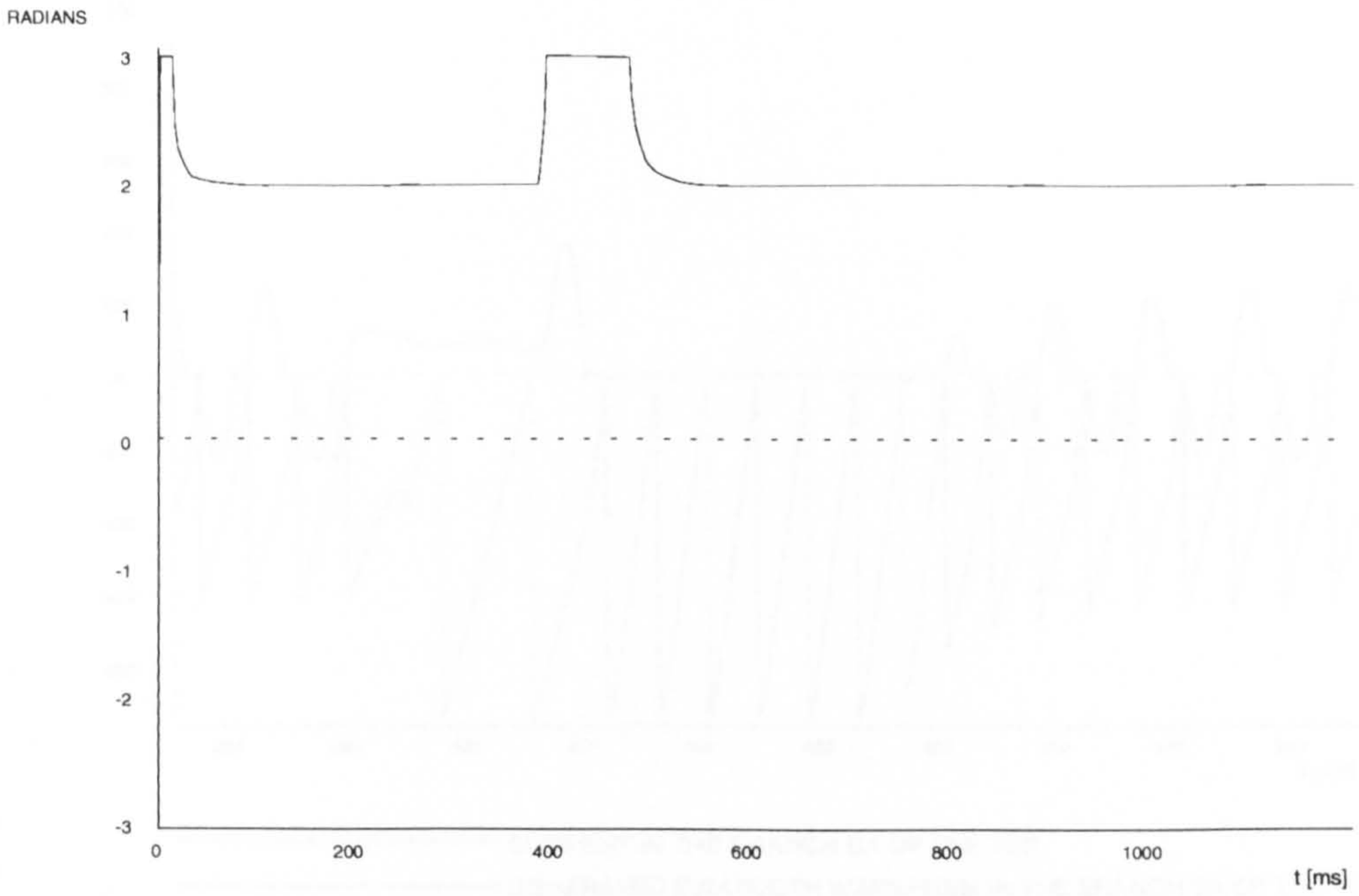

(a) Firing angle α in radians using the SVC model described in figure 7.11

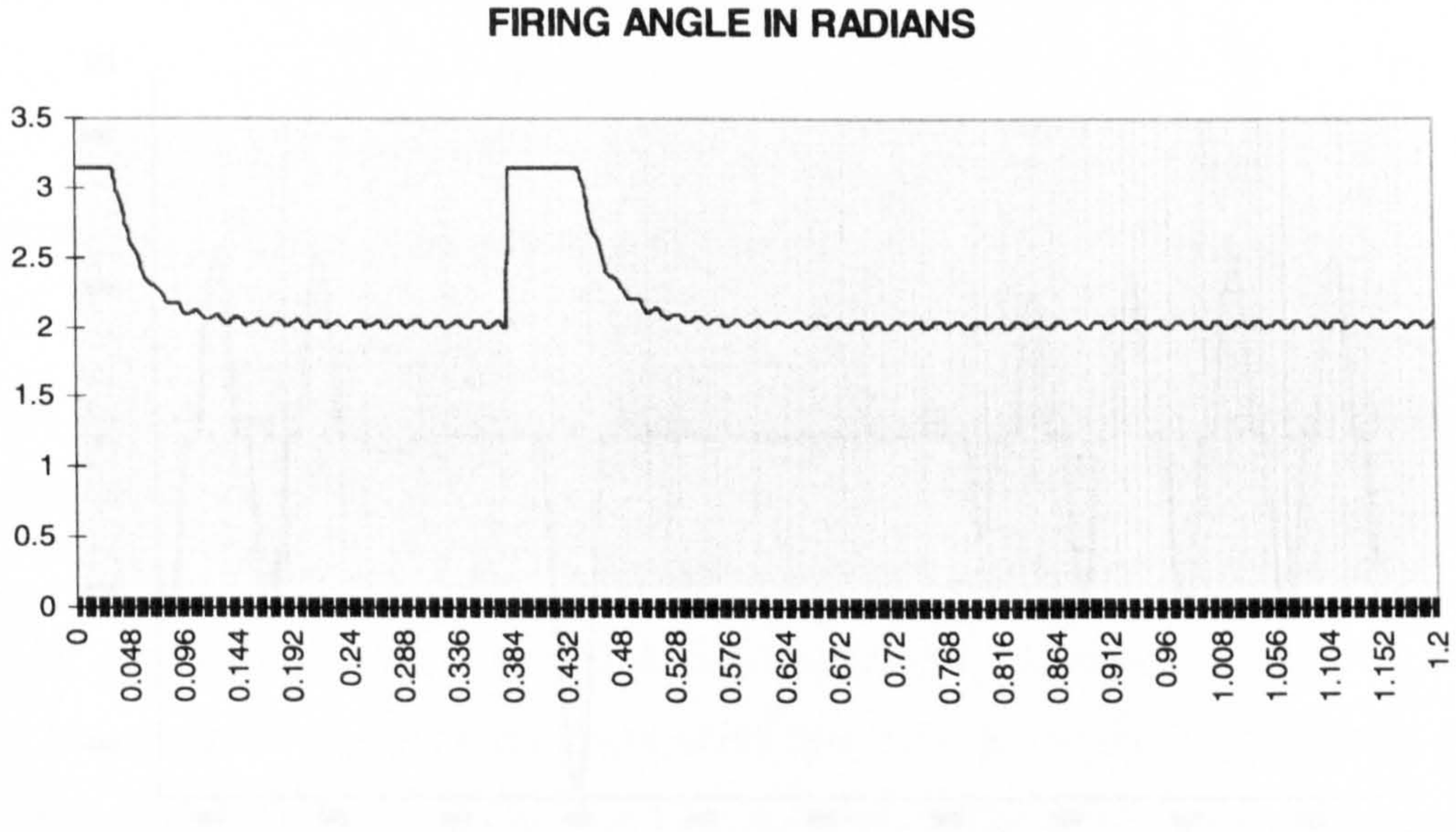

(b) Firing angle α in radians using the SVC model described in figure 7.40

Figure 7.49

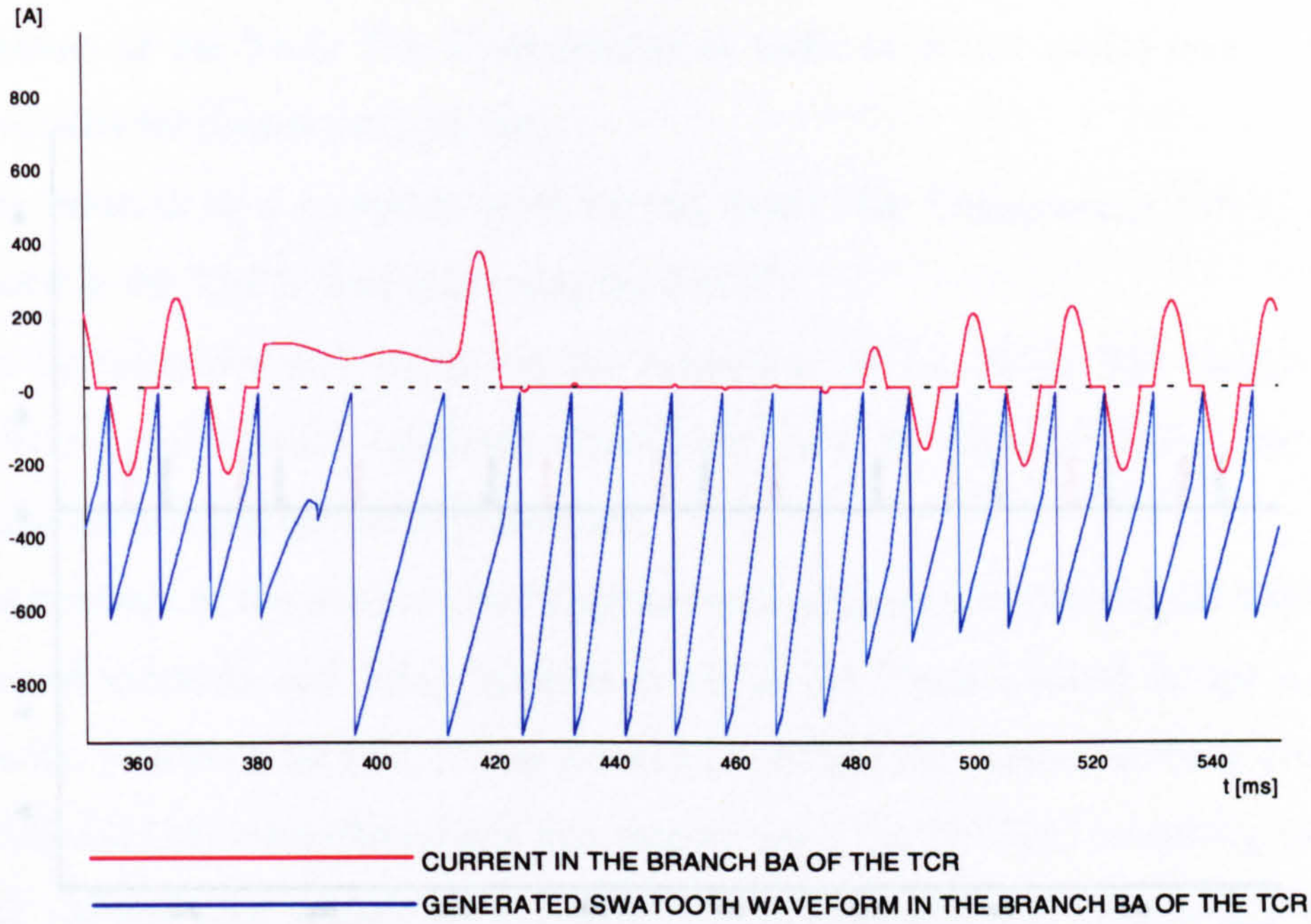

(a) Current and generated sawtooth waveform for the branch BA of the TCR

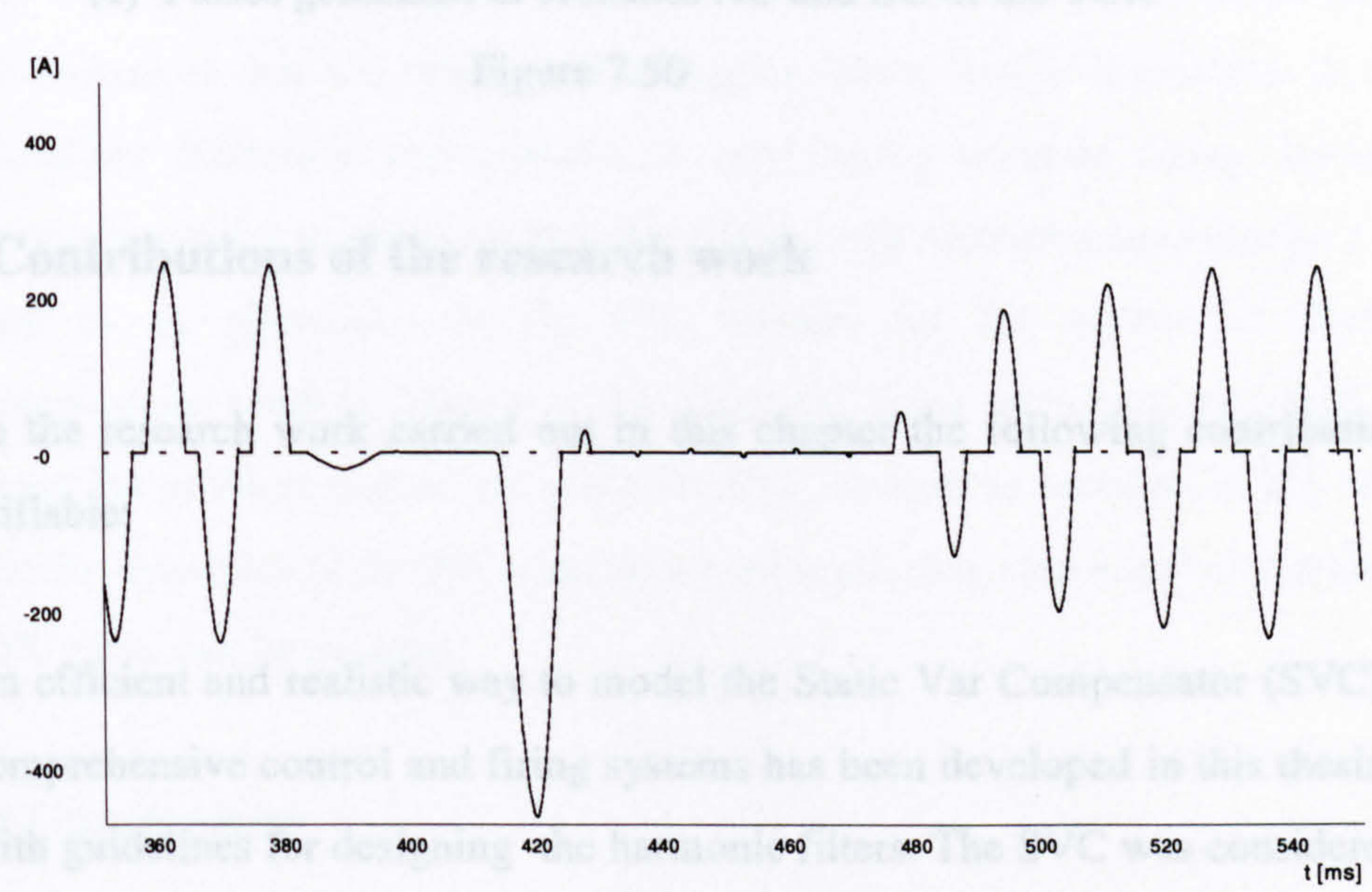

(b) Current in the branch AC of the TCR

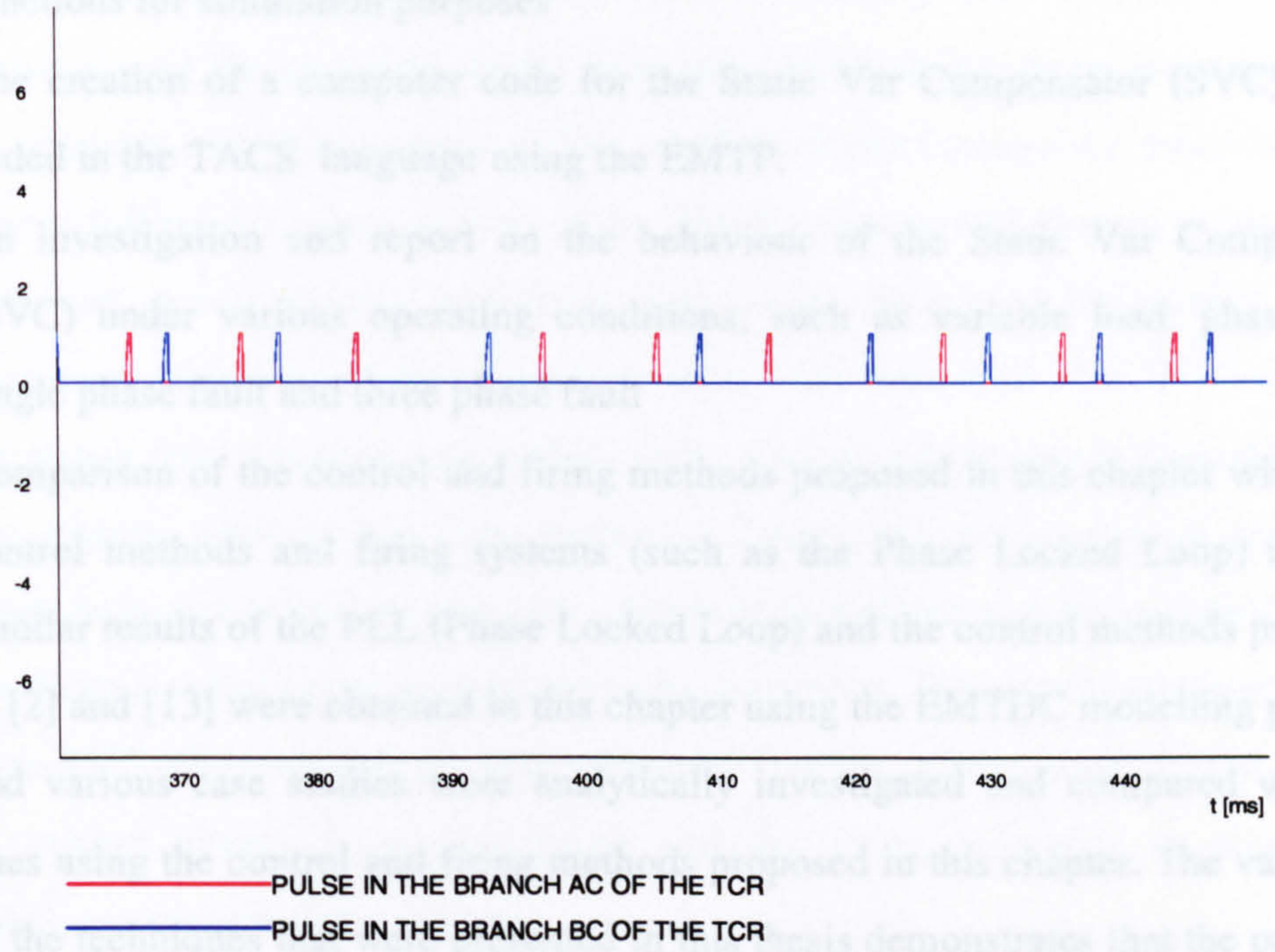

(c) Pulses generated in branches AC and BC of the TCR

Figure 7.50

7.9 Contributions of the research work

From the research work carried out in this chapter the following contributions are identifiable:

- An efficient and realistic way to model the Static Var Compensator (SVC), using comprehensive control and firing systems has been developed in this thesis, along with guidelines for designing the harmonic filters. The SVC was considered to be a continuous variable-shunt susceptance which was adjusted in order to achieve a specified voltage magnitude

- The development of mathematical expressions for the control and the firing systems of the Static Var Compensator in order to derive useful computational functions for simulation purposes
- The creation of a computer code for the Static Var Compensator (SVC) model coded in the TACS language using the EMTP.
- An investigation and report on the behaviour of the Static Var Compensator (SVC) under various operating conditions, such as variable load, phase shift, single phase fault and three phase fault
- Comparison of the control and firing methods proposed in this chapter with other control methods and firing systems (such as the Phase Locked Loop) method. Similar results of the PLL (Phase Locked Loop) and the control methods proposed in [2] and [13] were obtained in this chapter using the EMTDC modelling package and various case studies were analytically investigated and compared with the ones using the control and firing methods proposed in this chapter. The validation of the techniques that were presented in this thesis demonstrates that the proposed SVC controller gives a very good representation of a practical system. The results that were presented using the proposed firing method prove the effectiveness of the technique that was used in this chapter, show that is insensitive to voltage waveform distortion and capable of establishing accurate firing timing in a timescale similar to using the Phase Locked Loop method; consequently it can be used as an alternative to the PLL method for the control of Static Var Compensator models. Moreover, by using the firing technique presented in this thesis the problem caused by using the PLL method as reported in [8], which is that the dynamics of the PLL require a very small time step which demands a high CPU time, can be avoided.

7.10 Conclusions

The work presented in this chapter described a model for digital simulation of Static Var Compensator in power system networks. This work can be used in the preliminary design of Static Var Compensator in power systems.

At the beginning an explanation of the fundamentals of SVC has been presented, followed by the SVC current and voltage equations.

An overview of previous work on SVC modelling was discussed and the effectiveness of the proposed model over other methods has been mentioned. The main concepts and ideas behind a SVC model for electromagnetic transients were presented followed by some aspects of the EMTP program with respect to the control system and power system modelling. The main aspects of the power circuit, measurement, control and firing systems have been described. The SVC response under steady state conditions as well as under various power system disturbances in power system networks has been analysed. Comparison of the control and firing methods proposed in this chapter with other control methods and firing systems (such as the Phase Locked Loop) method were also presented. The simulations have shown that the SVC offers advantages over traditional voltage control methods and that the SVC control system is rapid enough and the firing technique is capable of establishing accurate firing timing .

The SVC model for the EMTP program has provided a tool for studying and assessing the SVC performance in a power system. All simulation results are in accordance with the theory and were validated using similar models and techniques as presented in the reference literature.

7.11 References

1. L.Gyugi, E.Taylor, "Characteristics of Static, Thyristor-Controlled Shunt Compensators for Power Transmission System Applications", IEEE Transactions, Vol.PAS-99,Sept /Oct. 1980, pp 1795-1804.
2. A.M.Gole, V.K.Sood, "A Static Compensator model for use with Electromagnetic Transients Simulation Programs", IEEE Transactions,Vol.5,No.3,July 1990, pp 1398-1407.
3. IEEE Special Stability Controls Working Group, "Static Var Compensator Models for Power Flow and Dynamic Performance Simulation", IEEE Transactions on Power Systems , Vol.9,No.1, Feb 1994,pp 229-239.
4. A.G.Exposito, F.Vazquez ,C.Michell, "Microprocessor-based Control of an SVC for Optimal load Compensation", IEEE Transactions on Power Delivery,Vol.7,April 1992,pp 706-712.
5. J.Ekanayake, "An investigation of an Advanced Static Var Compensator", PhD thesis, UMIST 1995.
6. A.E. Hammad, "Analysis of Power System Stability enhancement by Static Var Compensators", IEEE Transactions on Power Systems ,Vol.1 ,November 1996, pp 222-227.
7. A.N Vasconcelos, A.J.P. Ramos ,J.S Monteiro ,M.Lima, H.Silva ,L.R.Lin, "Detailed Modelling of an actual Static Var Compensator for Electromagnetic Transient Studies", Transactions on Power Systems ,Vol.7,No.1,February 1992, pp 11-17.
8. Tenorio R, "A thyristor controlled series capacitor model for electromagnetic transient studies", MPhil thesis, UMIST 1995.
9. J.A Martinez, "Simulation of a microprocessor controlled SVC",21th European EMTP Meeting, June 5-7 ,1992,Crete(Greece).
10. R.J.Nelson, J.Bian, D.G.Ramey, T.Lemak, T.R.Rietman, J.Hill, "Transient Stability with FACTS Controllers", AC and DC Power Transmission, IEE 1996,pp 269-274.

11. Y.Besanger, J.C.Passelergue, N.Hadjsaid, "Improvement of Power System Performance by inserting FACTS devices", AC and DC Power Transmission, IEE 1996,pp 263-267.

12. Ainsworth J.D, "Phase-locked oscillator control system for thyristor-controlled reactors", IEE Proceedings, Part C, Vol 135, No 2, 1988, pp 146-156.

13. A.M.Gole, V.K.Sood, L.Mootoosamy, "Validation and analysis of a Grid Control System using d-q-z Transformation for Static Compensator Systems", Canadian Conference on Electrical and Computer Engineering, September 1989, pp 745-748

14. R.H.Lasseter, Y.Shern, S.G.Jalali, "Harmonic instabilities in Static Var Compensators", CIGRE Symosium, Tokyo 1995.

15. Y.Lee, S.Bhattachavya, T.Leoberg, A.Hammad, S.Lefebre, "Detailed Modelling of Static Var Compensators using the Electromagnetic Transients Program(EMTP)",IEEE Transactions on Power Delivery ,Vol 7 ,No 2,April 1992,pp 836-847.

16. Lefebvre S, Gerin Lajoie "A Static compensator model for the EMTP", IEEE Transactions on Power Systems, Vol 7, No.2 , May 1992, pp 477-486.

17. Dickmander D, Thorvaldsson B, " Control system design and performance verification for the Chester, Maine Static Var Compensator", IEEE Transactions on Power Delivery, Vol 7, No 3, July 1992, pp 1492-1499.

18. E.W. Kimbark, "Direct Current Transmission", Wiley-Interscience, New-York, NY,1971.

19. W.Scott Meyer, Liu "Alternative Transients Program(ATP),Rule Book", Canadian/American EMTP User Group, 1995.

20. Ainsworth J.D, "The phase-locked oscillator a new control system for controlled static convertors", IEEE Transactions on Power Apparatus and Systems, 1968, pp 859-865.

21. EMTDC - User's Manual, Manitoba HVDC Research Centre, version 2, 1988.

CHAPTER 8

ELECTROMAGNETIC TRANSIENT SIMULATION STUDIES OF THE STATIC COMPENSATOR AND THE UNIFIED POWER FLOW CONTROLLER

8.1 Introduction

This chapter presents modelling and simulation work with respect to power flow controllers and especially to Static Condenser-STATCON (else referred to as Static Compensator-STATCOM) [1-6] and to UPFC (Unified Power Flow Controller) [7-14] devices. The chapter begins by describing the main types and the operating principles of voltage source inverter models for power flow controller studies and follows with a description of techniques for simulating these devices using the Electromagnetic Transient Program-EMTP. The regulation principle of Sinusoidal Pulse Width Modulation-SPWM inverters for realising power flow controllers is also analysed. The simulation results of open-loop STATCON and UPFC models using simple power system networks at the end of this chapter are in accordance with the theory.

8.2 Principles of operation of voltage source inverter models for power flow controller (STATCON-UPFC) studies

A prototype of a three phase six-pulse bridge voltage source inverter, which is the basic model of power flow controllers, is shown in Figure 8.1. The principle of operation is that the Gate Turn Off Thyristors (or transistor) inverter converts a dc voltage into a three-phase ac voltage which is connected to the ac system through a small reactance, usually the leakage reactance of a transformer. Figure 8.2 explains the fundamentals of the STATCON using a simple model[2,6]. The VSI is coupled to the system via a relatively small reactance (X) which is usually the leakage reactance of the step-up transformer used for connecting to the high voltage network. Owing to this reactive coupling, the line current flowing into or out of the VSI is always 90° to the network voltage. When the inverter output voltage is higher than the ac system voltage, the inverter acts as a capacitor so leading reactive current is drawn from the system (vars are generated). When the inverter output voltage is lower than the ac system voltage the inverter acts as an inductor, so lagging reactive current is drawn from the system (vars are absorbed). When the inverter output voltage is equal to the ac system voltage, the reactive power generation is zero. From figure 8.2 the current flowing into the transmission line i_s can be found as :

$$i_s = \pm \frac{V_s - V_I}{jX} \tag{8.1}$$

Therefore the reactive power absorbed or generated by the STATCON (per phase) is:

$$Q = V_s i_s \sin 90^\circ = \mp jV_s \left(\frac{V_s - V_I}{X} \right) \tag{8.2}$$

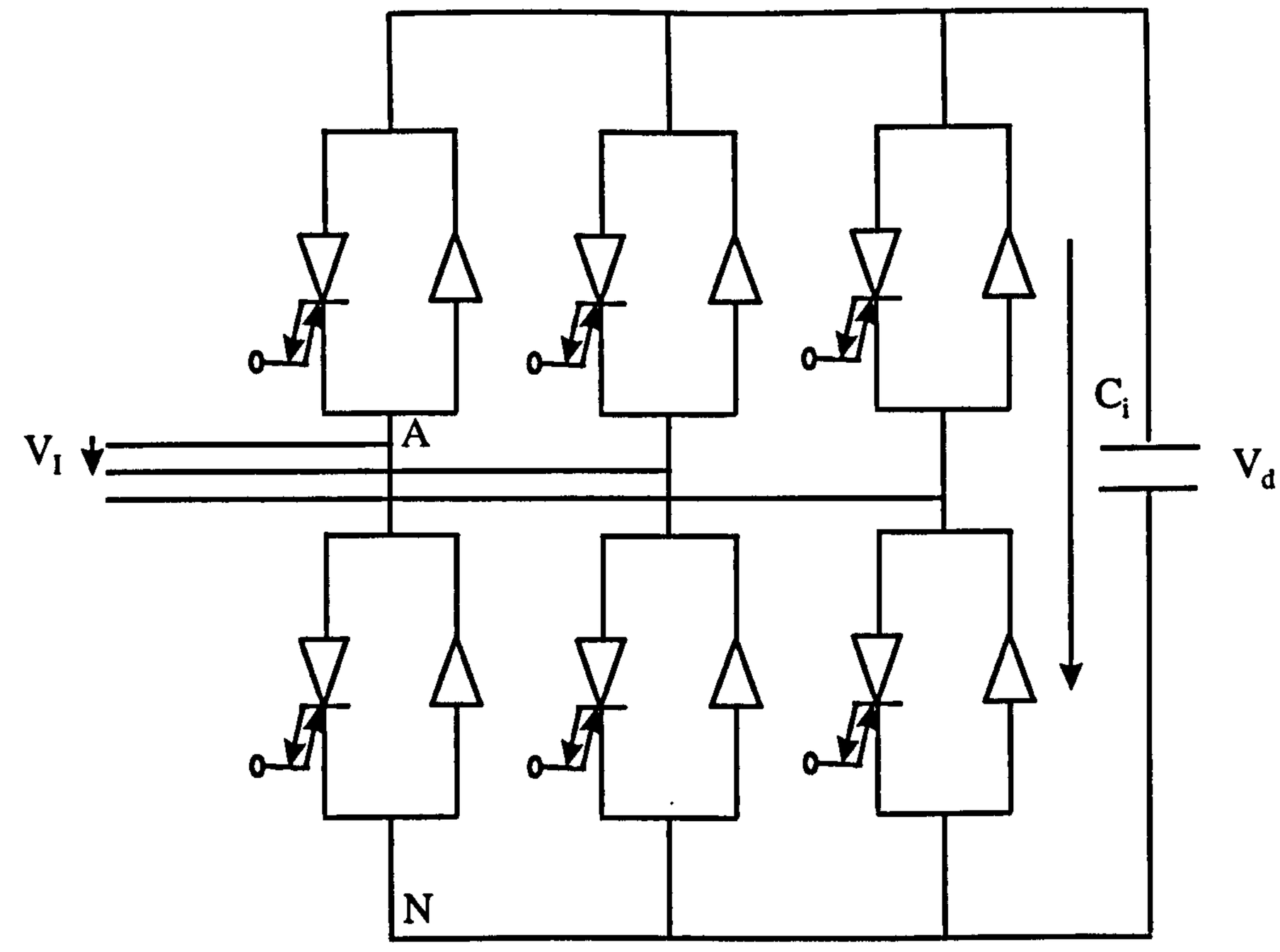

Figure 8.1 Three phase VSI structure

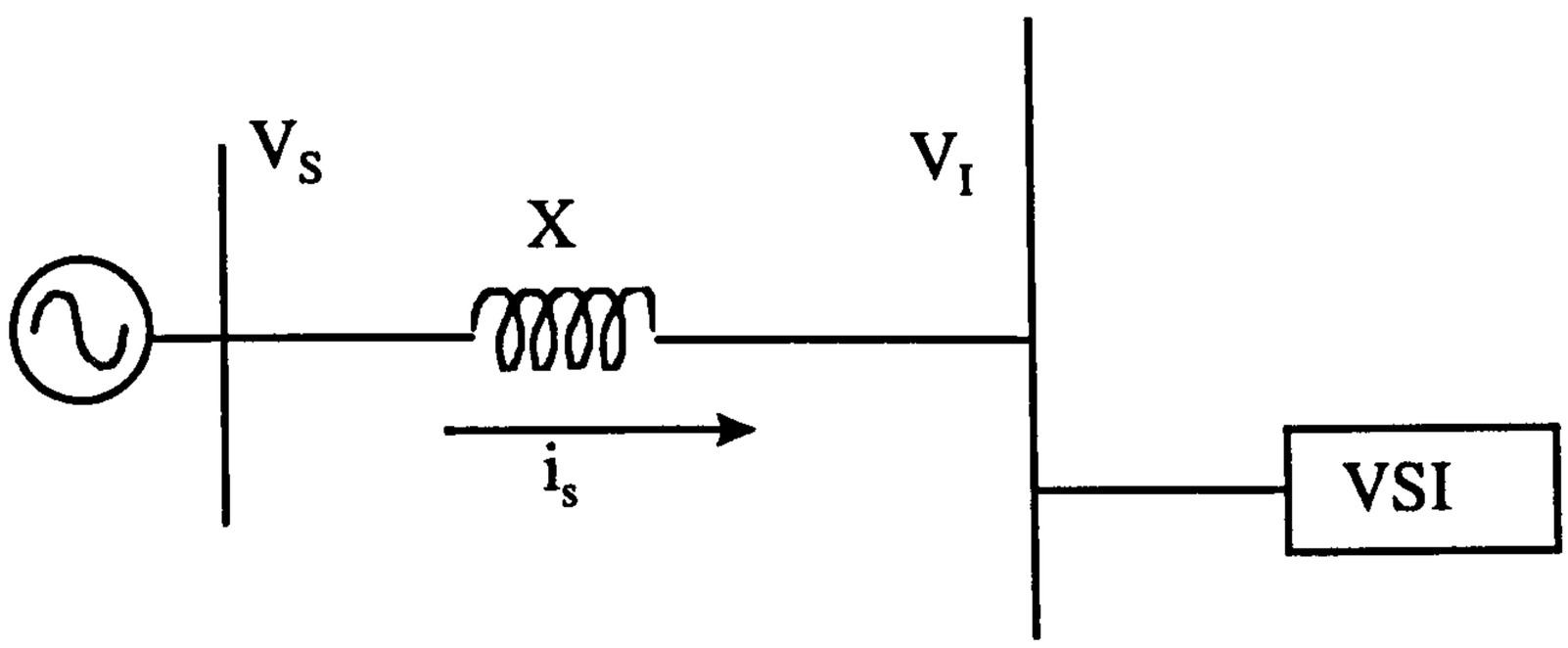

Figure 8.2 Single phase STATCON circuit

The variation in the level of reactive power generated or consumed is achieved through the control action of the bridge and offers fast continuous variation of reactive output power from capacitive to inductive, and a more effective reactive power generation during undervoltages.

Figure 8.3 is used to explain the fundamentals of the UPFC using a simple model. Assume that the voltage source V_{pq} in series with the line can be controlled without restrictions. That is, the phase angle of the phasor V_{pq} can be chosen independently of the line current between 0 and 2π, and its magnitude is variable between zero and a defined maximum value, $V_{pq\,max}$.

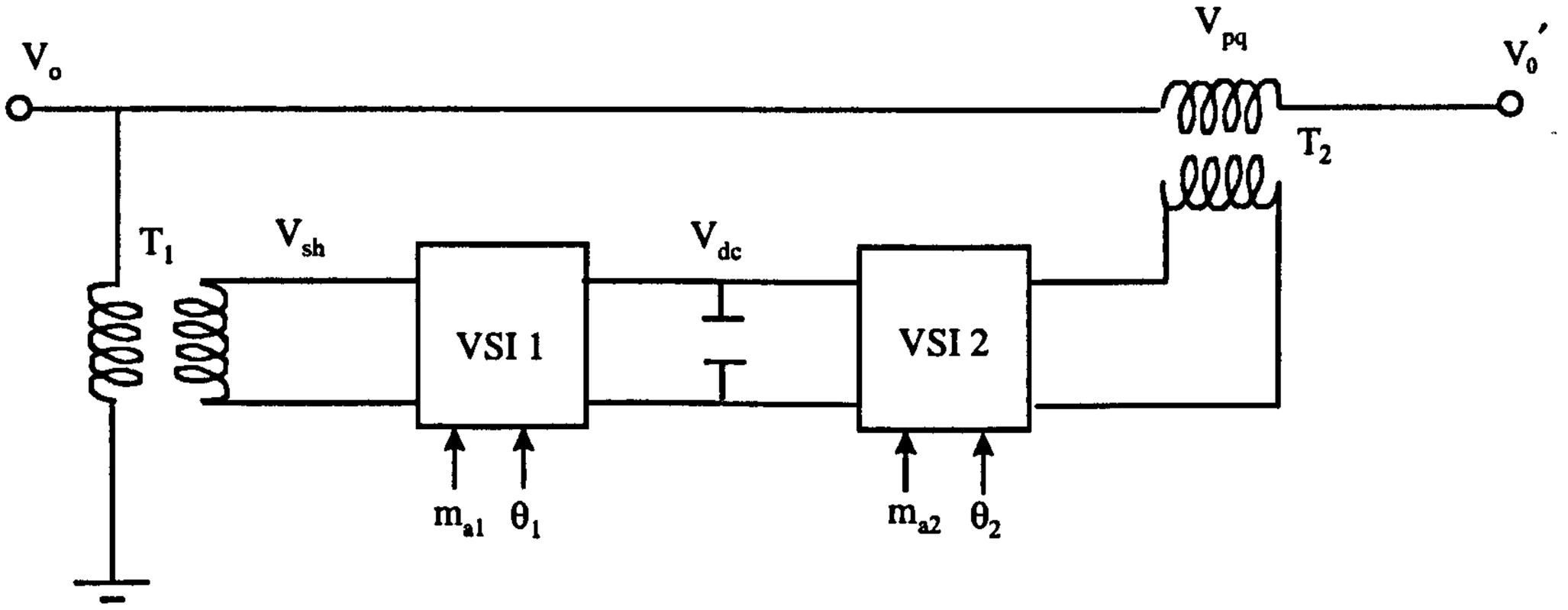

Figure 8.3 Arrangement of the UPFC

Power flow control is achieved by adding voltage source V_{pq} with no angular restrictions, and with magnitude variable between 0 and $V_{pq\,max}$ at the end of the reference phasor V_0 as shown in figure 8.4(a). This means that by appropriate definition (control) of phasor V_{pq}, the generalised power flow controller can be used to accomplish the following objectives[9]:

1. Dedicated terminal voltage regulation or control, which is obtained simply by keeping the angle of V_{pq} zero (i.e. $V_0 \pm \Delta V_0$), and thus changing only the magnitude of V_0' with respect to that of V_0 (or vice versa) as illustrated in figure 8.4 (b).
2. Combined series line compensation and terminal voltage control, which is obtained by defining V_{pq} as a sum of voltage phasors V_c and ΔV_0, that is ,

$V_{pq} = V_c + \Delta V_0$, where phasor V_c is perpendicular to line current I and ΔV_0 is in phase with the terminal voltage phasor V_0 (figure 8.4(c)).

3. Combined phase angle regulation and terminal control, which is obtained by defining V_{pq} as a sum of voltage phasors V_a and ΔV_0, that is, $V_{pq} = V_a + \Delta V_0$, where again ΔV_0 is in phase with the terminal voltage phasor V_0. The selected definition for phasor V_a ensures that the resultant terminal voltage phasor at the end of line segment, $V_0' = V_0 + V_a + \Delta V_0$, has the same magnitude as $V_0 + \Delta V_0$, but its phase angle is different from that of V_0 by α, as illustrated in figure 8.4 (d). In practical terms this means that phase-shifting is achieved without any unintentional magnitude change in the controlled terminal voltage.
4. Combined terminal voltage regulation and series line compensation and phase angle regulation, which can be achieved by synthesising the injected voltage phasor V_{pq} from the three individually controlled phasors, that is $V_{pq} = V_c + V_a + \Delta V_0$, as illustrated in figure 8.5.

For the model illustrated in figure 8.3, the inverter output voltage injected in series with the line acts essentially as an ac voltage source. The current flowing through the injected voltage source is the transmission line current that is a function of the transmitted electric power and impedance of the transmission line. The VA rating of

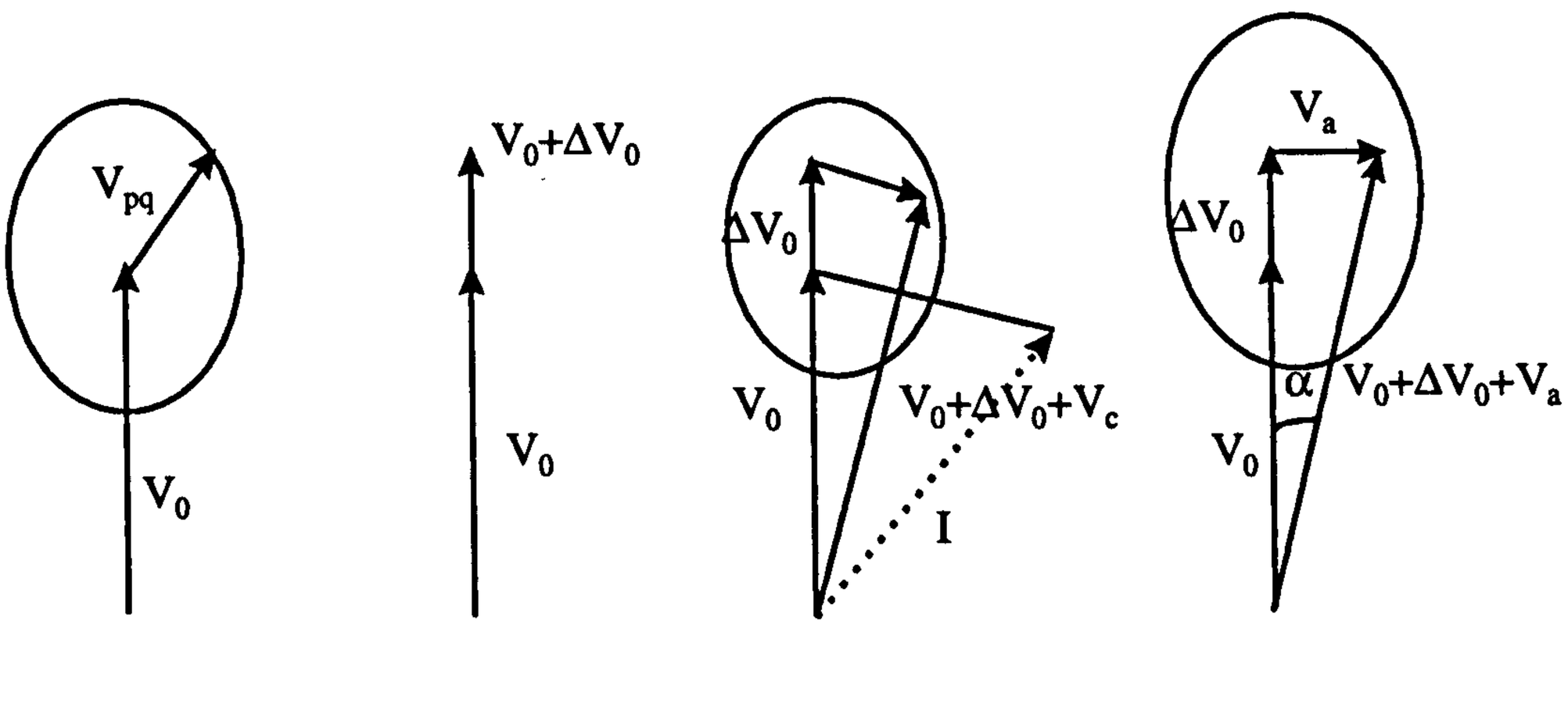

(a) (b) (c) (d)

Figure 8.4 Phasor diagrams illustrating the operation of the UPFC

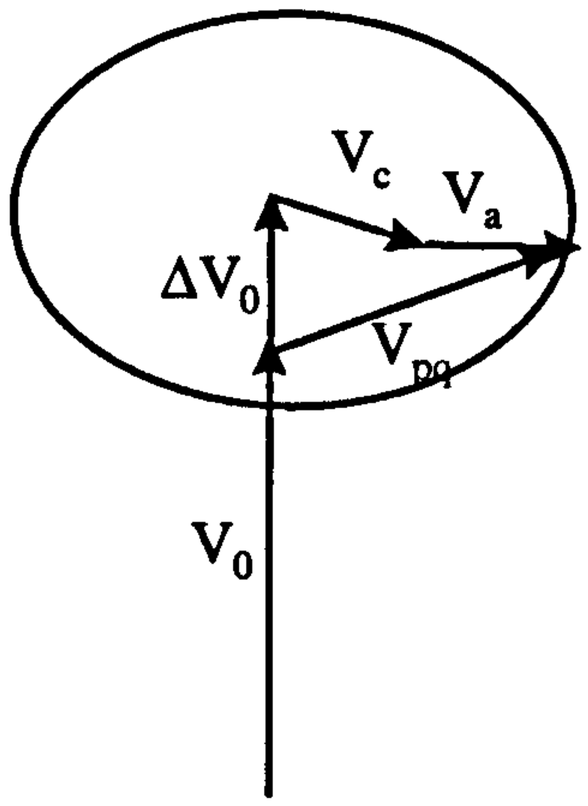

Figure 8.5 Phasor diagram illustrating the operation of the UPFC

the injected voltage source (i.e that of inverter 2) is determined by the product of the maximum injected voltage source and the maximum line current at which power flow control is provided. This total VA is made up of two components: one is the maximum active power determined by the maximum line current and the component of the maximum injected voltage that is in phase with this current, and the other one is the maximum reactive power determined by the maximum line current and the component of the maximum injected voltage that is in quadrature with this current. As known, the voltage sourced inverter used in the implementation, can internally generate or absorb at its ac terminal all the reactive power demanded by the voltage/impedance/phase angle control applied and only the active power demand has to be supplied at its dc input terminal.

Inverter 1 (connected in shunt with the ac power system via a coupling transformer) is used primarily to provide the active power demand of inverter 2 at the common dc link terminal from the ac power system [9-12]. Since inverter 1 can also generate or absorb reactive power at its terminal, independently of the active power it transfers to (or from) the dc terminal, it follows that, with proper controls, it can also fulfil the function of the independent static condenser providing reactive power compensation for the transmission line and thus executing an indirect voltage regulation at the input terminal of the UPFC.

One important issue that should be taken into account when analysing a UPFC (shown schematically in figure 8.3) is that this device is not a lossless FACTS controller (there is active power flow through the shunt and the series connected inverters in practical UPFCs). This active power flow is due to the losses in the transformers and the power semiconductor devices of the UPFC. The losses through the UPFC can reach up to 10-15% depending on the converters configuration and the transformers of the UPFC. The active power losses associated with the shunt and the series connected transformers are a function of the value of their resistance and the current through them. The sources of losses in the power semiconductor devices are:

a) the losses during forward conduction, which are a function of the forward voltage drop and the conduction current
b) the loss occurring in the gate circuit
c) the switching losses, i.e energy dissipated in the device during turn-on and turn-off

The power loss associated with the gate drive can normally be neglected. However in the case of current driven devices like GTOs, this loss may be significant [21].

The switching losses during the turn-on and the turn-off of power semiconductor devices depend on the forward voltage across the device, the current through it and the switching on/off times [21,22]. Losses are also due to the snubber circuits that are used in power converters for the protection of the switching devices. The snubber circuits consist of a series combination of a resistor and a capacitor. In the EMTP simulations carried out later in the chapter use small resistances in series with the semiconductor devices to account for the conduction losses. Simulation results later in this chapter (section 8.8) illustrate the active power flow through the UPFC.

The control of the VSI circuit has been widely used in electrical engineering applications, especially in those with low-voltage small power rating characteristics. The control of the VSI circuit can be divided into the following two general categories:

1) Pulse-width modulated (PWM) inverters[1,4,9,15]: In these inverters, the input dc voltage is essentially constant in magnitude, therefore the inverter must control the magnitude and the frequency of the ac output voltage. This is achieved by PWM of the inverter switches and hence such inverters are called PWM inverters. There are various schemes to pulse-width modulate the inverter switches in order to shape the output ac voltages to be as close to a sinewave as possible. The most popular of these schemes is the sinusoidal PWM (SPWM).

2) Square-wave inverters [2,16,17,18,19]: In these inverters, the input dc voltage is controlled in order to control the magnitude of the output ac voltage, and therefore the inverter has to control only the frequency of the output voltage. The output ac voltage has a waveform similar to a square wave and hence these inverters are called square-wave inverters.

The relationship between the control input and the full-bridge inverter output magnitude can be summarised as shown in Figure 8.6(a), assuming a sinusoidal PWM in the linear range of $m_a \leq 1$ (m_a is the modulating ratio, $m_a = \frac{V_{control}}{V_{tri}}$). From figure 8.1 the peak value of the fundamental frequency component in one of the inverter legs is

$$(\hat{V}_{AN})_1 = m_a \frac{V_d}{2} \tag{8.3}$$

Therefore the line-to line rms voltage at the fundamental frequency, due to 120° phase displacement between voltages, can be written as

$$V_{01} = \frac{\sqrt{3}}{\sqrt{2}}(\hat{V}_{AN})_1 = \frac{\sqrt{3}}{2\sqrt{2}} m_a V_d \cong 0.612 m_a V_d \tag{8.4}$$

For a square-wave switching, the inverter does not control the magnitude of the inverter output, and the relationship between the dc input voltage and the output

magnitude is summarised in Figure 8.6(b). In a similar procedure to the one that was described before

$$V_{01} \cong 0.78 V_d \tag{8.5}$$

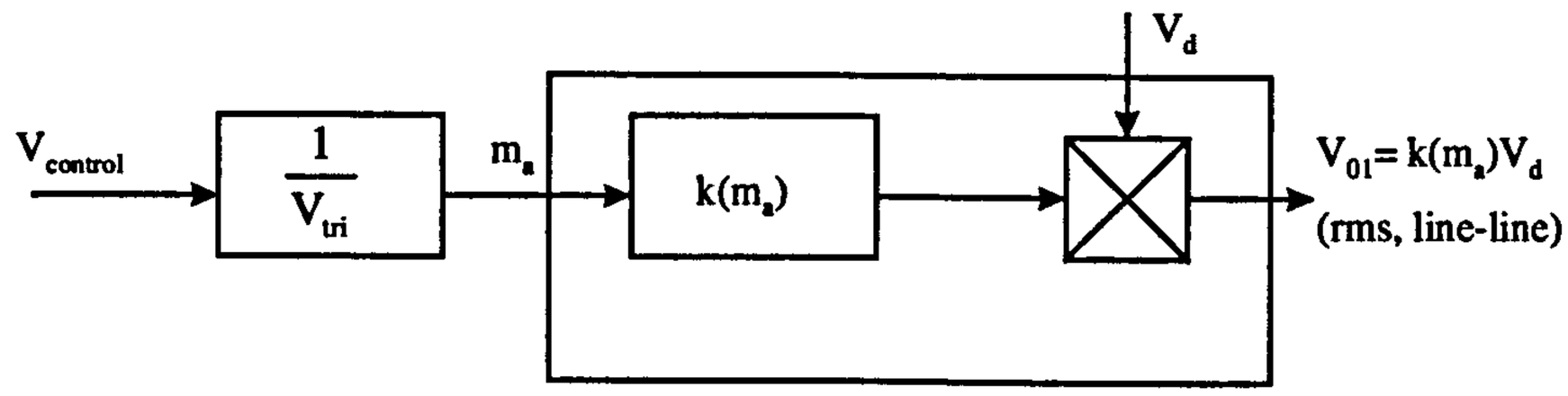

Figure 8.6 Inverter output voltages: (a) SPWM operation, (b) square-wave operation

The square-wave method is widely used in rectifier and inverter applications. Although this method has minimal operating switching losses, it produces harmonics and requires a more complicated magnetic structure. In recent years the PWM method has been used to develop FACTS controllers such as the PWM-STATCON, series type PWM compensator, PWM-UPFC, etc. This is because the PWM inverters have some important characteristics such as[9,10,11,15]:

1) near sinusoidal current waveforms;
2) $0-360^{\circ}$ angle operation;
3) bi-directional power transfer capability through reversal of the direction of flow of the dc link current;
4) direct and continuous control of the source voltage without changing the dc-link voltage.

If the PWM method is used in power flow controllers, they will generate low harmonics, require a simple magnetic structure, and be relatively inexpensive. Thus the PWM design approach was chosen for simulation studies of power flow controllers.

8.3 Electromagnetic Transient Studies of power flow controllers

EMTP - Electromagnetic Transients Program - is a full featured transient analysis program, initially developed for electrical power systems. It is also capable of simulating controls, power electronics, and hybrid situations. The program features an extremely wide variety of modelling capabilities encompassing electromagnetic and electromechanical oscillations ranging in duration from microseconds to seconds.

In EMTP, power systems transients and control systems could be modelled simultaneously to study their dynamic interaction. Sensors pick up signals from the power system for input to the control system (called Transient Analysis in Control Systems-TACS). Commands are forwarded from the control system to the power system as shown in Figure 8.7.

The procedure of setting up models of power flow controllers (such as STATCON and UPFC models) by EMTP/TACS consists of deriving mathematical models from the real-world device configurations. Modelling of the GTO (or transistor) should be simplified in order to match the device provided by EMTP, shown in Figure 8.8. In this case, the GTO becomes an idealised switch, which can be controlled by feedback signals from the network according to the TACS definition. These signals should be carefully chosen and calculated from the control strategy scheme.

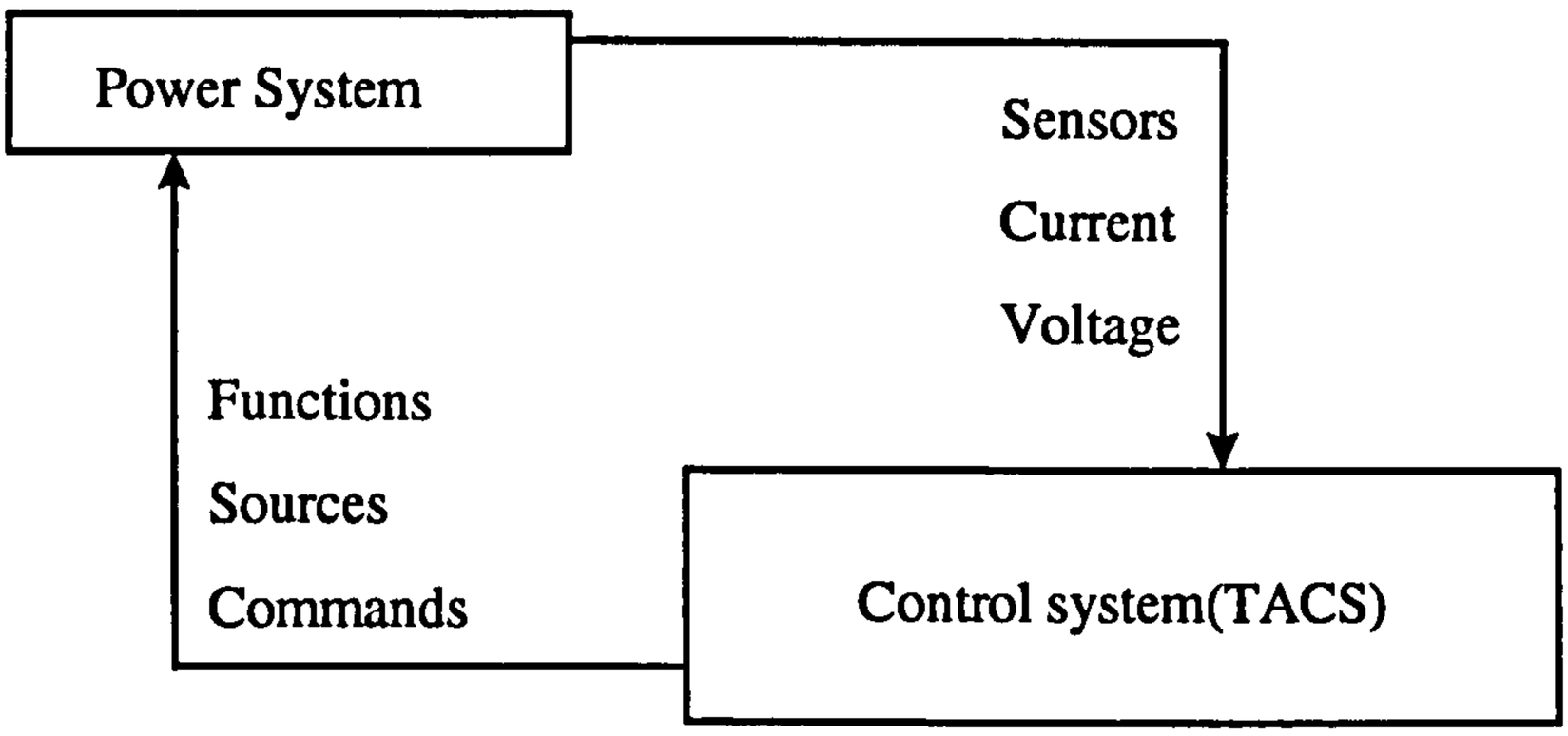

Figure 8.7 Interaction between power system and control system (TACS)

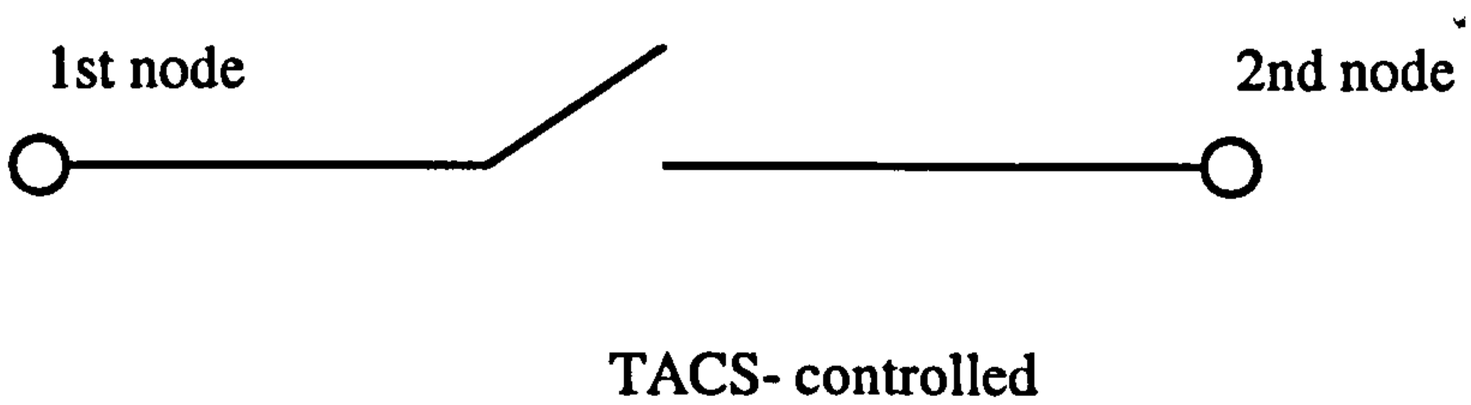

Figure 8.8 Type-13 switch for diode and valve

8.4 SPWM Scheme Generated by EMTP TACS

The SPWM switching module [4,9] is a scheme where a control signal $V_{control}$ (constant sinusoidal wave or varying in time according to control mode) is compared with a repetitive switching frequency triangular waveform, in order to generate the

switching signals. Controlling the switch duty ratios in this way allows the average ac voltage input to be controlled. With reference to Figure 8.9 the frequency of the triangular waveform establishes the inverter switching frequency f_s and is generally kept constant along with its amplitude V_{tri}. The control signal $V_{control}$ is used to modulate the switch duty ratio and has a frequency f_1, which is the desired fundamental frequency of the inverter voltage output, recognising that the inverter output voltage will not be a perfect sine wave and will contain voltage components at harmonic frequencies of f_1.

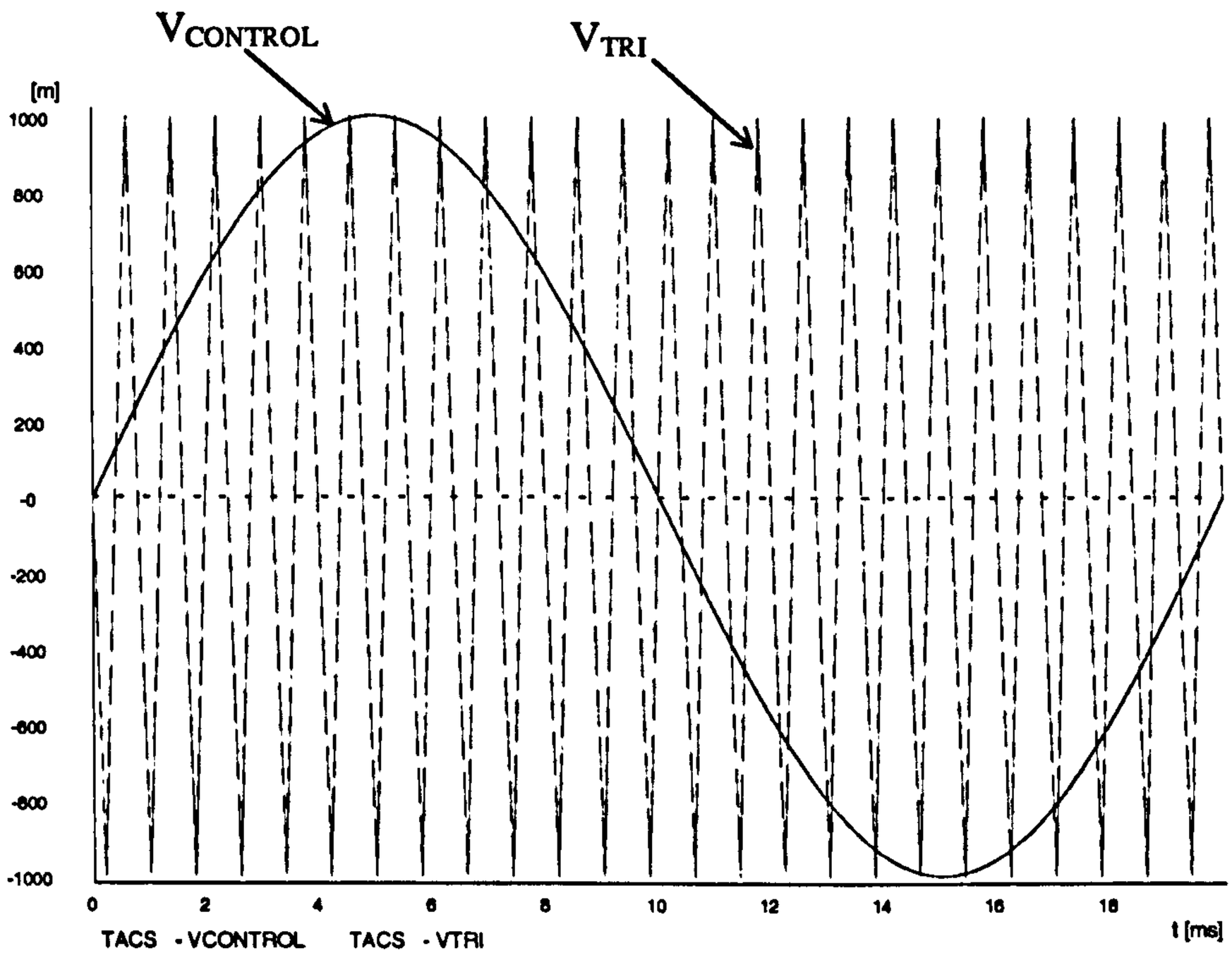

Figure 8.9 Comparison between the control signal and the triangular waveform

Thus, the amplitude modulation ratio m_a is defined as [4]

$$m_a = \frac{V_{control}}{V_{tri}} \tag{8-6}$$

The frequency modulation ratio m_f is defined as

$$m_f = \frac{f_s}{f_1} \tag{8-7}$$

Therefore, three parameters are adjusted to adapt the simulation of power flow controllers and the system interaction:

1) In order to keep the SPWM operating under a linear modulating range, m_a (modulating ratio) should be from 0 to 1. In this case, $V_{control}$ determines the amplitude of the sinusoidal modulating waveform and therefore modifies the positions of its intersections with the constant amplitude triangular carrier waveform. $V_{control}$ is generally derived from the system control objective, whose amplitude and phase depend on their different requirements.

2) Because the power system usually maintains a constant frequency of 50Hz , m_f is chosen as a large number (25 i.e a repetition of 1250Hz for STATCON, 100 i.e a repetition of 5000Hz for the UPFC), which means that the triangular waveform signal and the control signal are synchronised to each other and the amplitudes the harmonics are small. Therefore, the frequencies of both $V_{control}$ and V_{tri} are kept constant during the simulations.

3) The phase displacement θ between $V_{control}$ and V_{tri} could be regulated according to the demands of the magnitude and direction of power flow. Therefore, two regulating parameters m_a and θ can be employed as internal control to manipulate the turn-on and turn-off signals of the VSI in the power flow controllers(one inverter for the STATCON, two back-to-back inverters for the UPFC).

8.5 EMTP Model Development for the STATCON

The simulation system suitable for electromagnetic study is intentionally a simple system whose main objective is to aid understanding of the power flow controllers and their interaction with the system. The system under consideration is illustrated in Figure 8.10 and includes a three-phase 132kV source, a transmission line, an 132/11 kV wye-wye transformer connected to a STATCON and a load connected to the 132 kV network. The whole system contains all of the necessary components which are implemented in the EMTP/TACS data format. In addition to these system circuit components, some factors must be taken into consideration in order to operate the system properly. These factors include initialisation of the converter currents , damping resistance connected in parallel with the transmission line and the use of snubber circuits to avoid numerical instability of the EMTP simulation.

For the modelling of the voltage source, type 14 source model of the normal sinusoidal function as specified in the EMTP manual was used. The transmission line was modelled as a simple resistance and inductance. In parallel with the inductance a resistance was used in order to avoid numerical oscillations. For the transformers, single-phase models were used and the ratio of the primary winding with respect to secondary winding and the leakage reactance of the windings are the input parameters which define the transformer characteristics.

The voltage source inverter is the fundamental component of the STATCON. The three phase, full-wave inversion bridge is built using three identical GTO inverter legs. In the VSI each 6-pulse converter consists of twelve bridge-arms, which are composed of a GTO valve and a diode connected in anti-parallel with the GTO. This is called the switch module. Because of the diode the bridge-arm can conduct current in both directions as long as the GTO has a firing order. Therefore, from a system study point of view it is sufficient to use type-13 switches to model the combination of the GTO valve and the anti-parallel diode. In order to consider the losses in the valves a very small resistor ($0.1\mathrm{m}\Omega$) is connected in series with the controllable switch.

In a real system, a snubber circuit is connected in order to limit the rate of voltage change during turn on/off. In the EMTP model, a snubber circuit is also used in order to avoid numerical oscillations. This circuit consists of a resistor and a capacitor connected in parallel with the GTO valve. Generally, the minimum RC time constant should be greater than 2-3 times the step size.

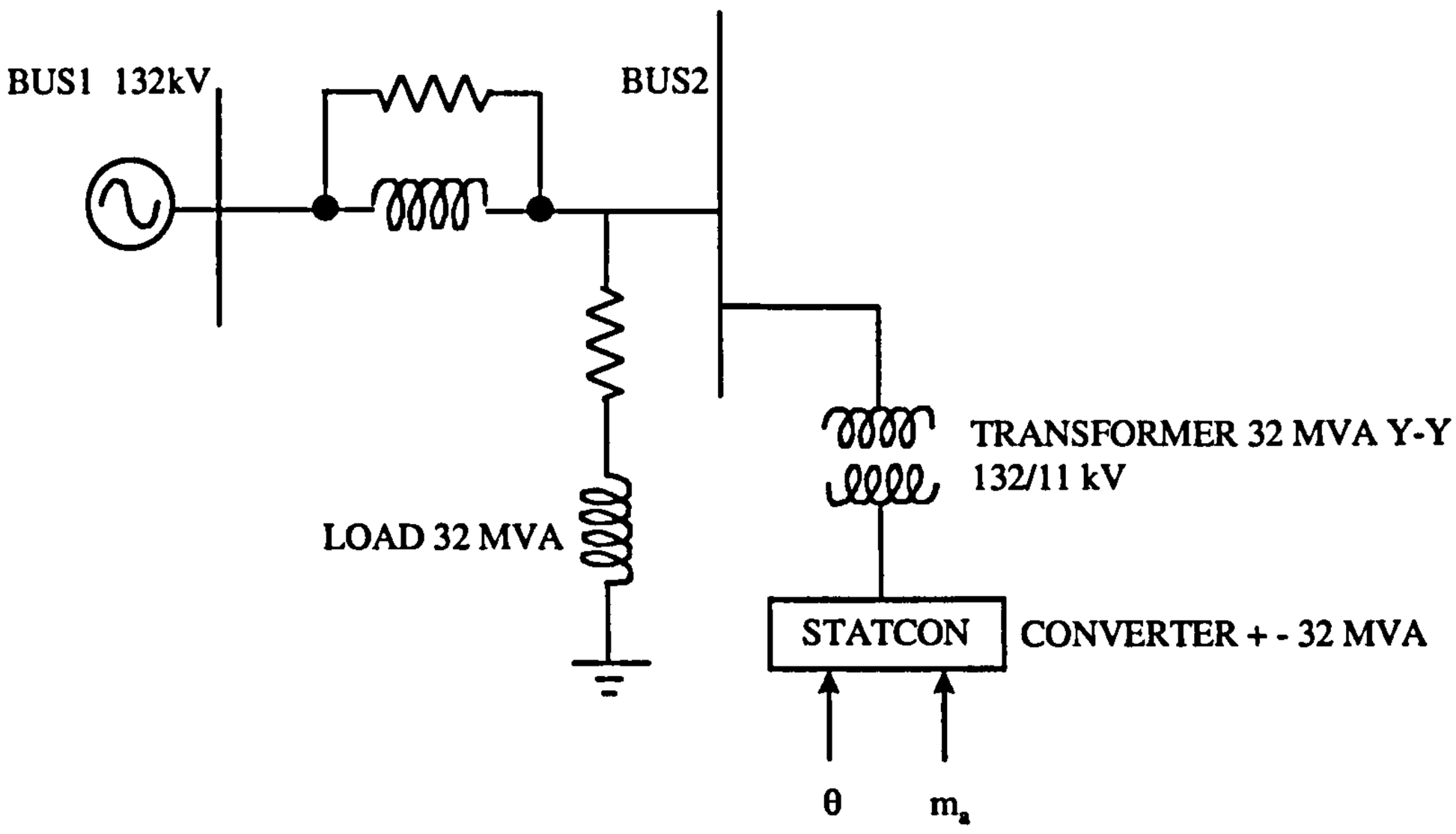

Figure 8.10 STATCON model connected to a power network

To effectively control the STATCON and especially to control the GTO switches, it is necessary to model the generation of SPWM signals which are used to trigger turn on-off the GTOs. In this respect, the Transient Analysis of Control Systems (TACS) of the EMTP provides a method for setting up the SPWM switch scheme for controlling the GTO thyristor valves of the inverter. Using various functions such as the transfer function blocks and FORTRAN-like statements provided by TACS, the SPWM control signal can change. The SPWM control accepts an analogue sinusoidal modulating waveform signal from each of the three phases and an analogue triangular carrier signal, and based on detecting the intersection points it generates gating signals to the GTOs of the bridge. The output of the SPWM signal is $m_a \sin(\omega t + \theta)$ [3,4,9]. From this expression it can be seen that the controlled

variable can have full circular amplitude and phase variation under the control of SPWM.

8.6 Results of simulation of the SPWM STATCON

In this section, simulation results based on SPWM inverters by EMTP are presented. The SPWM switch scheme for controlling the GTO thyristor valves of the inverters has been set up using TACS of the EMTP, in which the SPWM control signal can be generated according to the open-loop simulation studies.

The system under study is shown in Figure 8.10. With a converter rating of ± 32 MVA the dc capacitor voltage corresponding to ± 1 p.u current (where - refers to the lagging and + to the leading current) can be obtained using the equation 8-8

$$V_{LL} = 0.612 m_a V_d \tag{8-8}$$

for $m_a = 1$. This equation assumes that the dc capacitor voltage V_d is constant. However this is not true in practice unless a very large capacitor is used. When a sinusoidal PWM is used for a given STATCON output current, the minimum dc capacitor voltage can be obtained with $m_a = 1$ and only that condition is considered throughout this study.

The following are three sets of typical simulation results:

1) Using $m_a = 1$ the STATCON operates at maximum capacitive current . Figures 8.11-8.17 illustrate results of this study using a constant voltage on the dc link. Figures 8.18-8.20 show results using a finite capacitor(1000μF), C_i. The capacitive STATCON increases the fundamental voltage at bus 2, while the actual voltage waveform at this bus appears with a harmonic component (Figures 8.12,8.19). The effect in the load current is much less due to the associated impedance (Figure 8.15).

The current in the converter in this bus leads the voltage by 90° (Figures 8.14,8.16,8.20).

2) Using $m_a = 0.6$ the STATCON operates at maximum inductive current . Figures 8.21-8.22 illustrate results of this study using a constant voltage on the dc link. The inductive STATCON decreases the fundamental voltage at bus 2 , with the actual voltage waveform illustrated in Figure 8.21 including high order harmonics. Figures 8.23-8.24 show results using a finite capacitor(1000μF), C_i . The current in the converter lags the voltage by 90° (Figure 8.24).

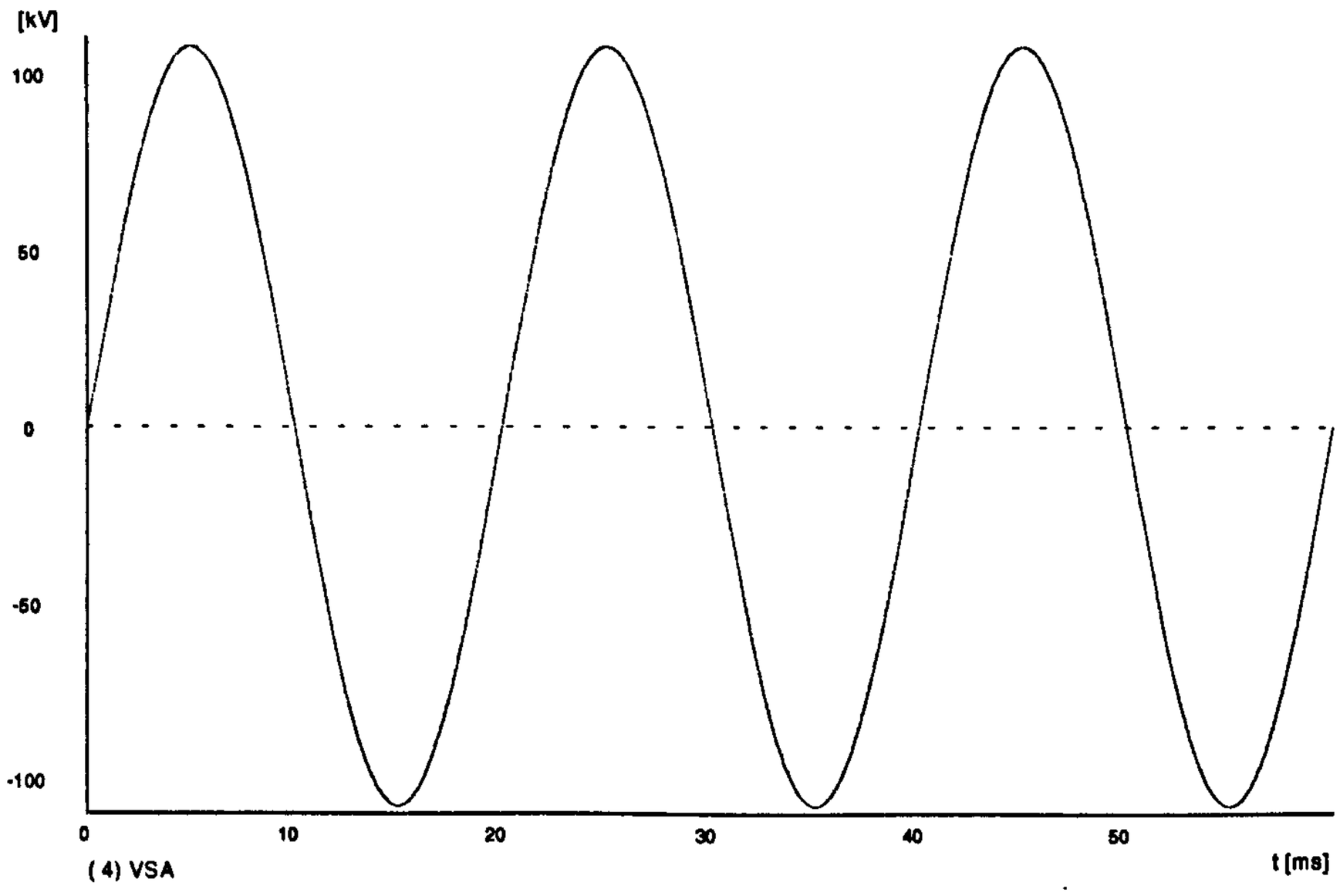

Figure 8.11 Voltage of phase A at bus 1

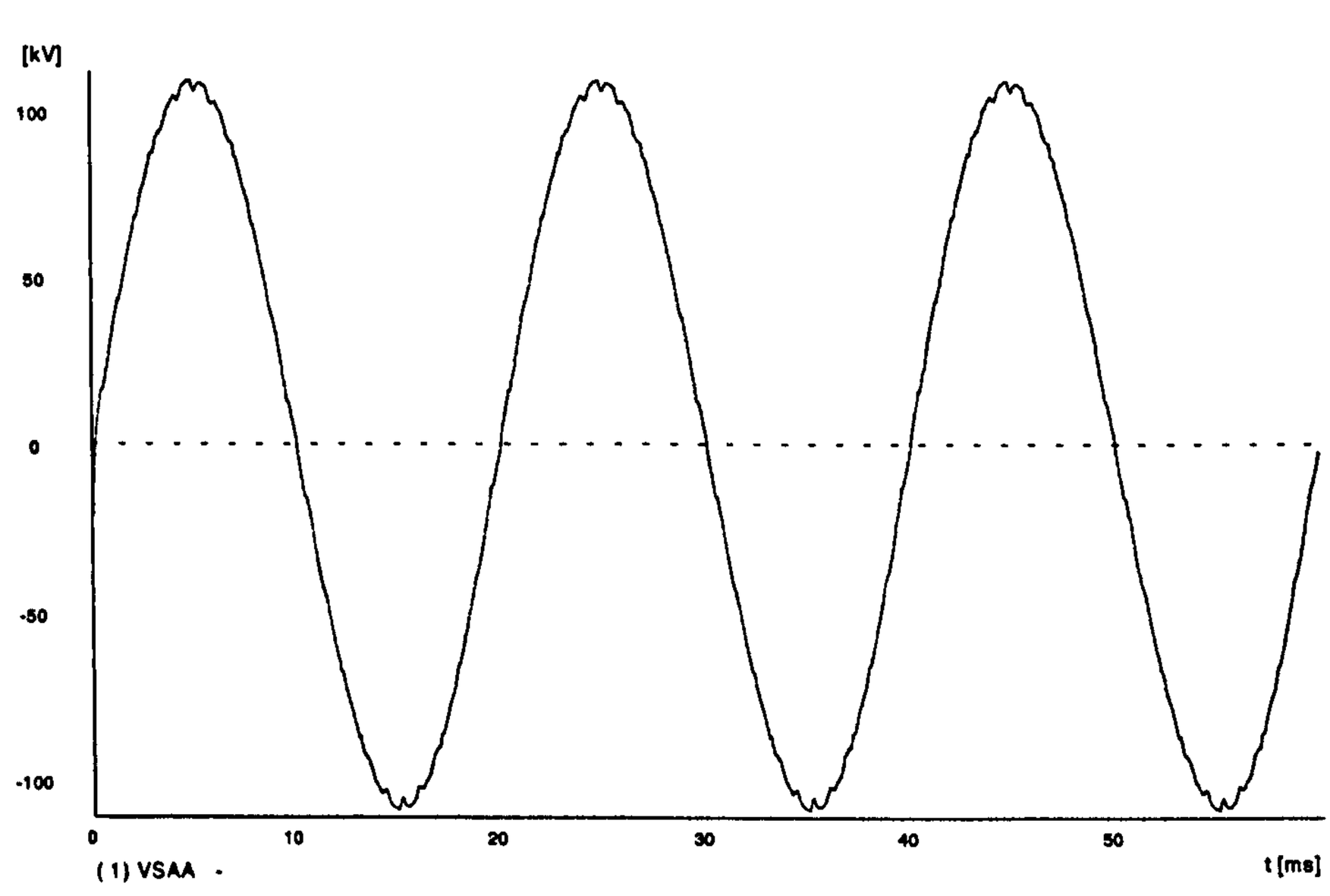

Figure 8.12 Voltage of phase A at bus 2

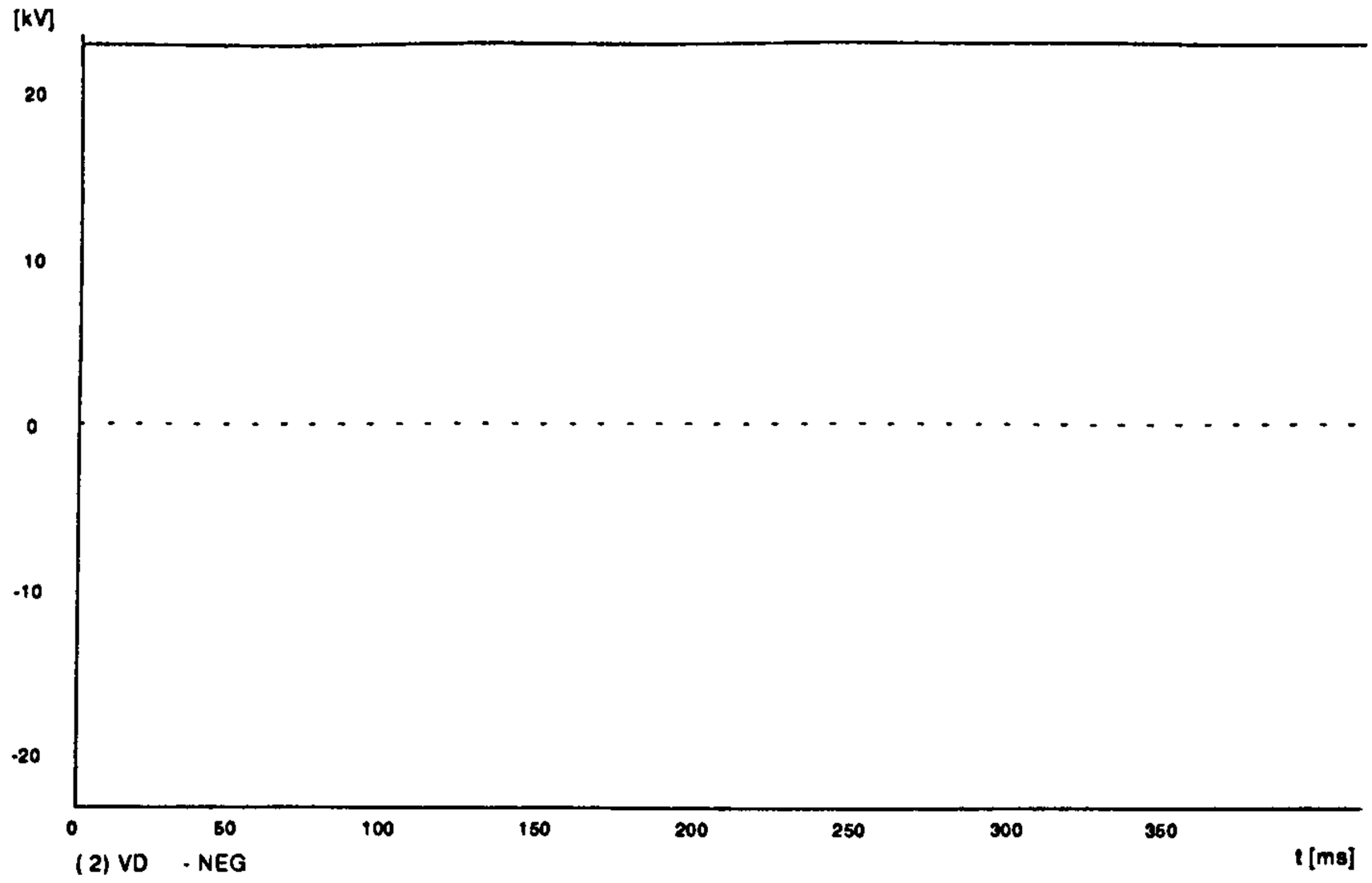

Figure 8.13 DC voltage across the capacitor

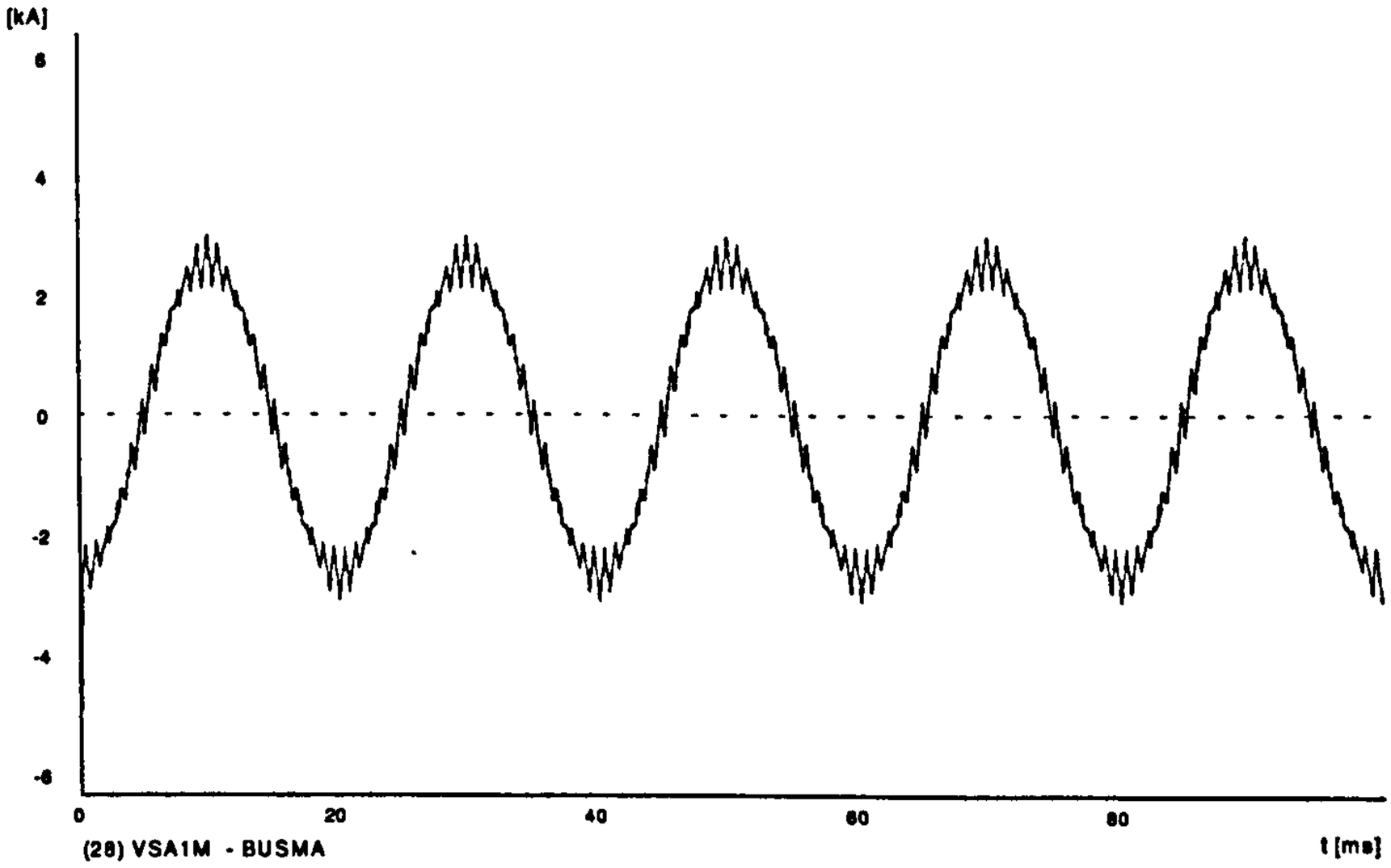

Figure 8.14 Current of phase A flowing from the STATCON to the transformer

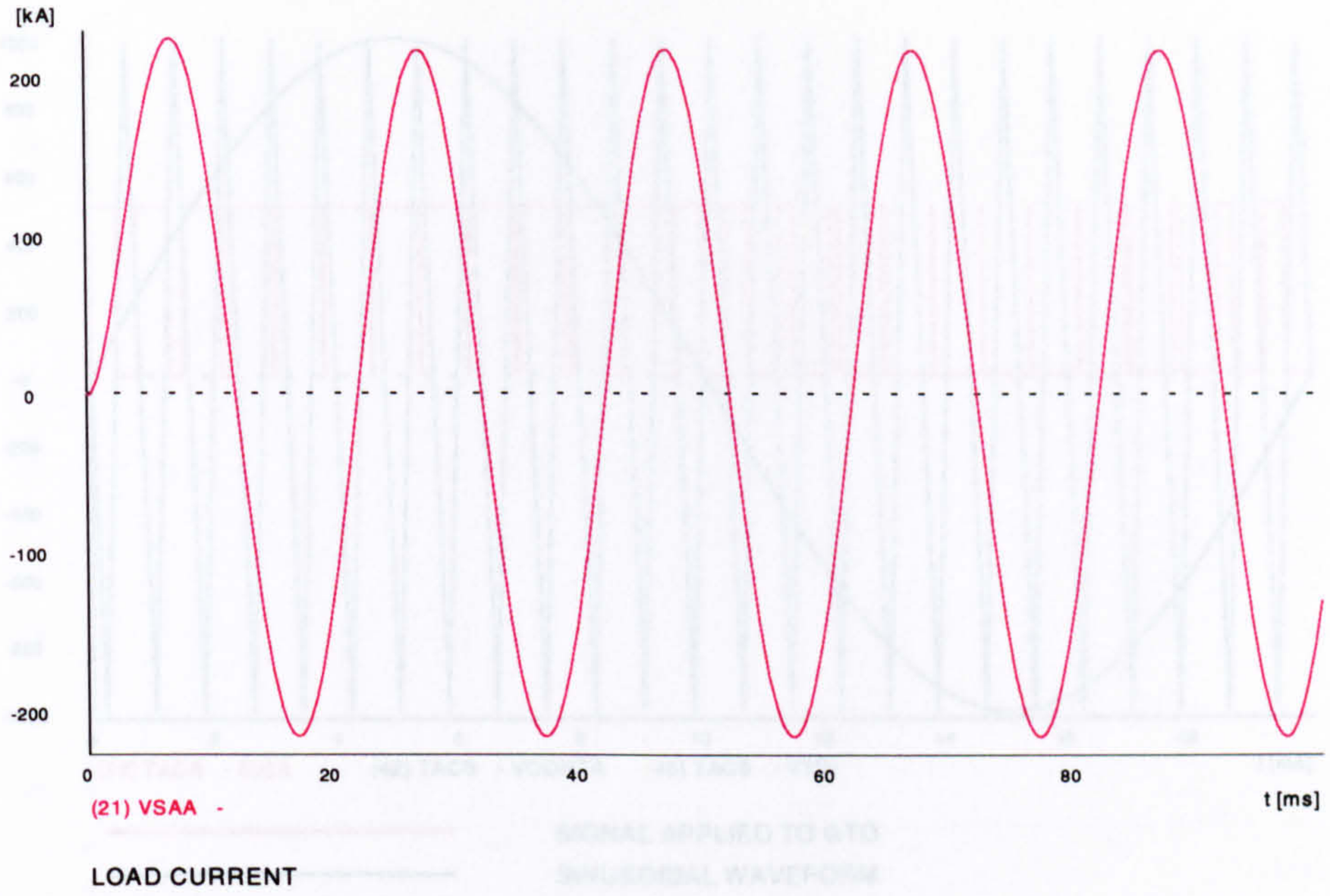

Figure 8.15 Load current

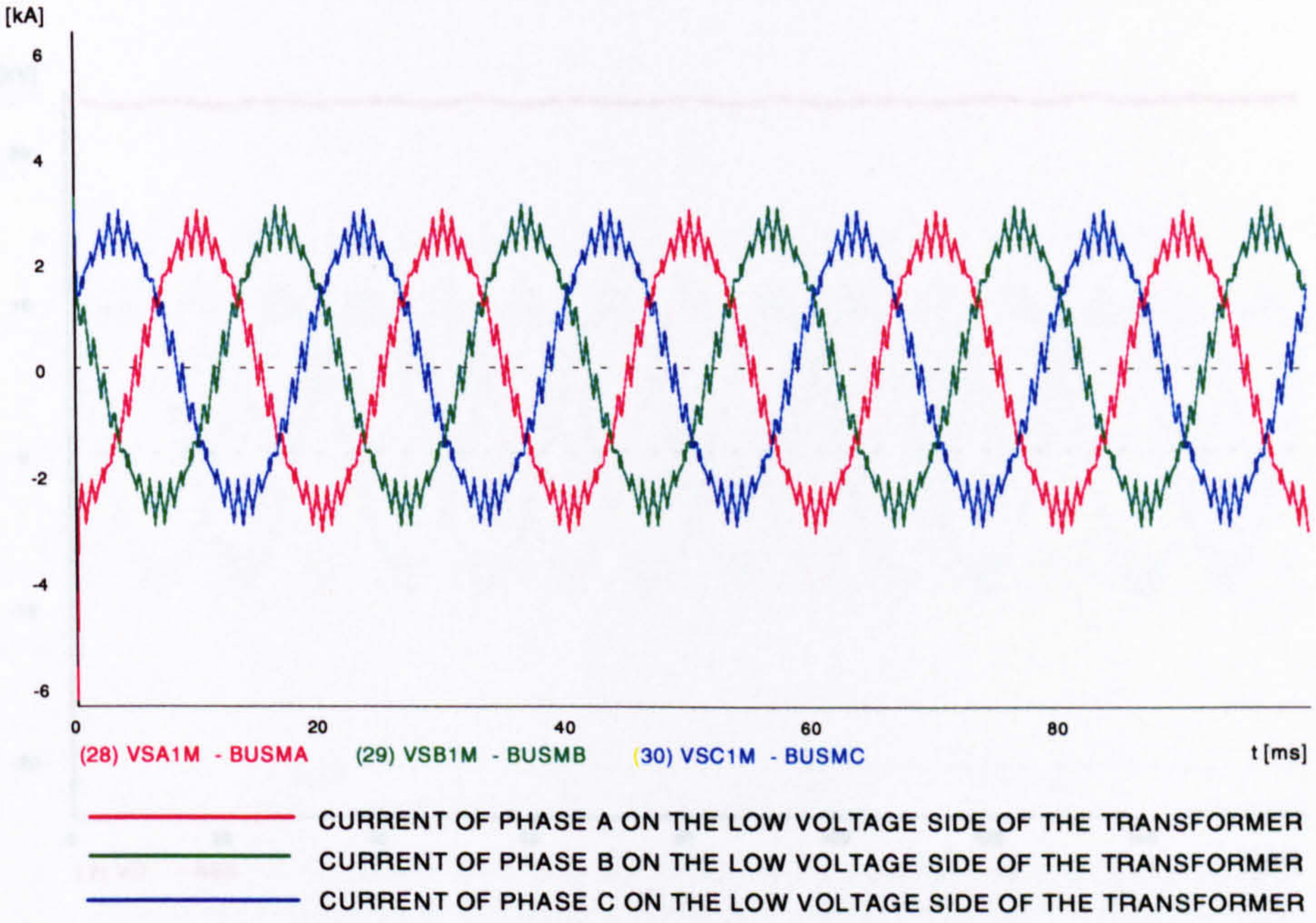

Figure 8.16 Currents flowing from the STATCON to the transformer

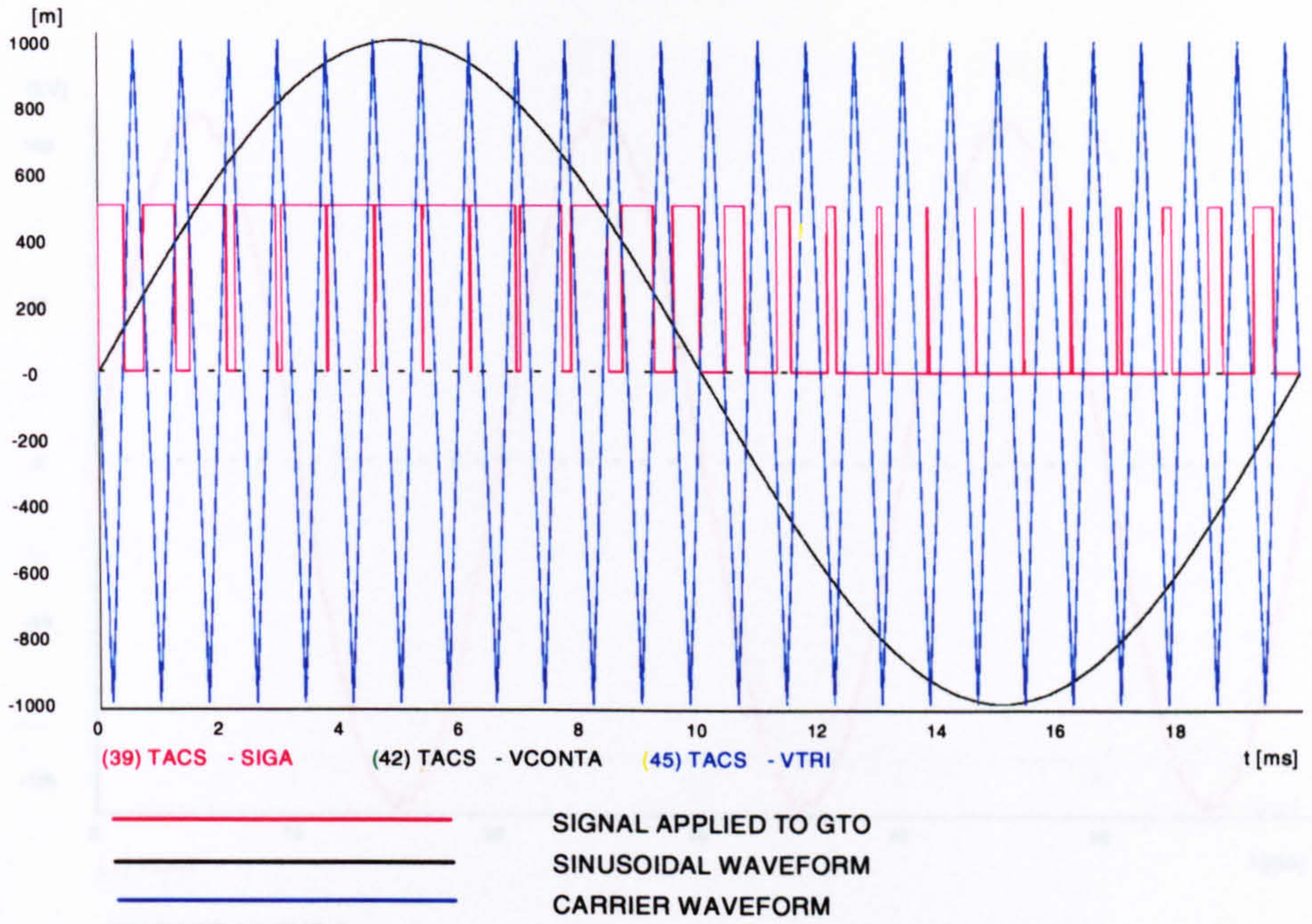

Figure 8.17 PWM generation

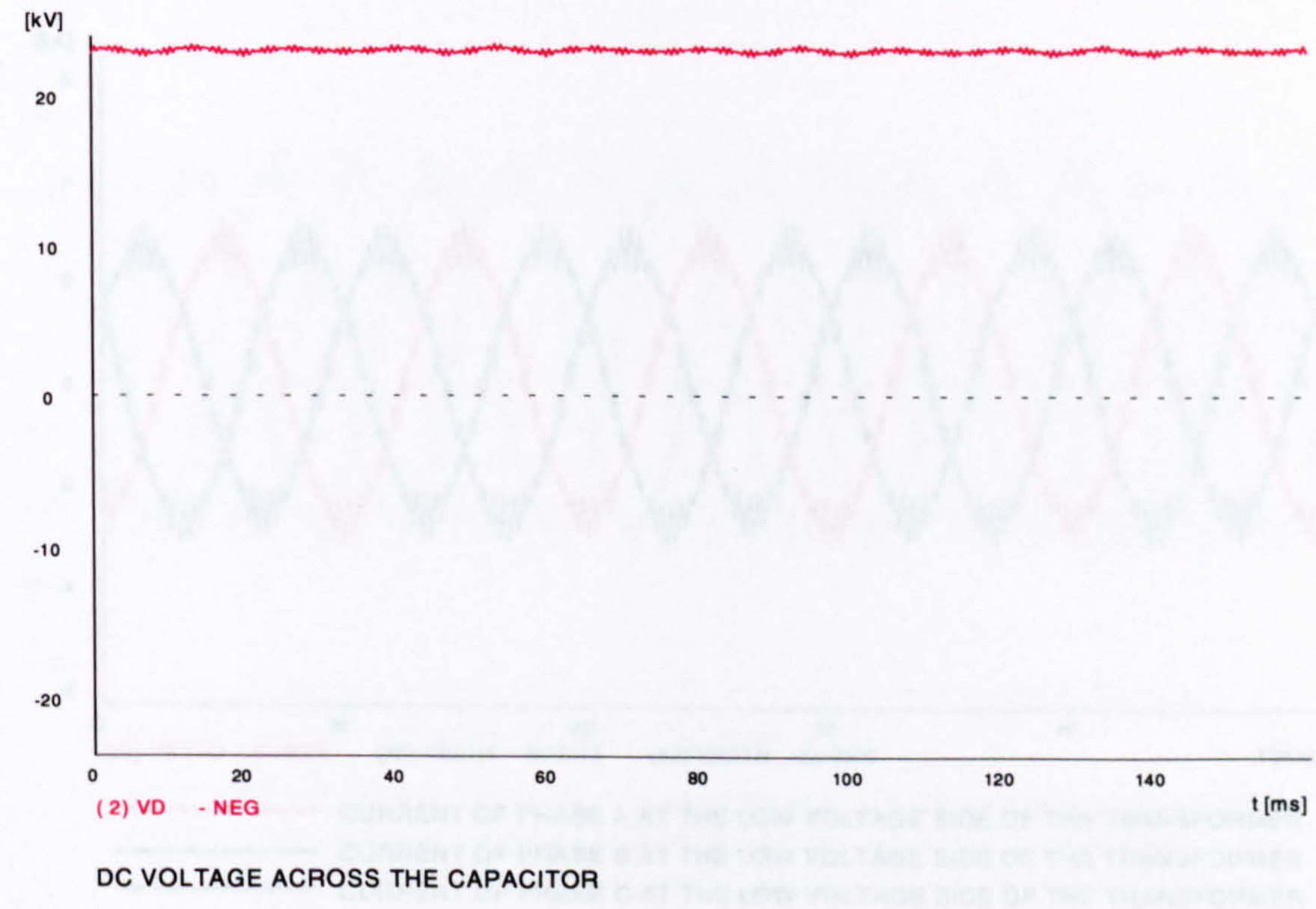

Figure 8.18 DC voltage across the capacitor

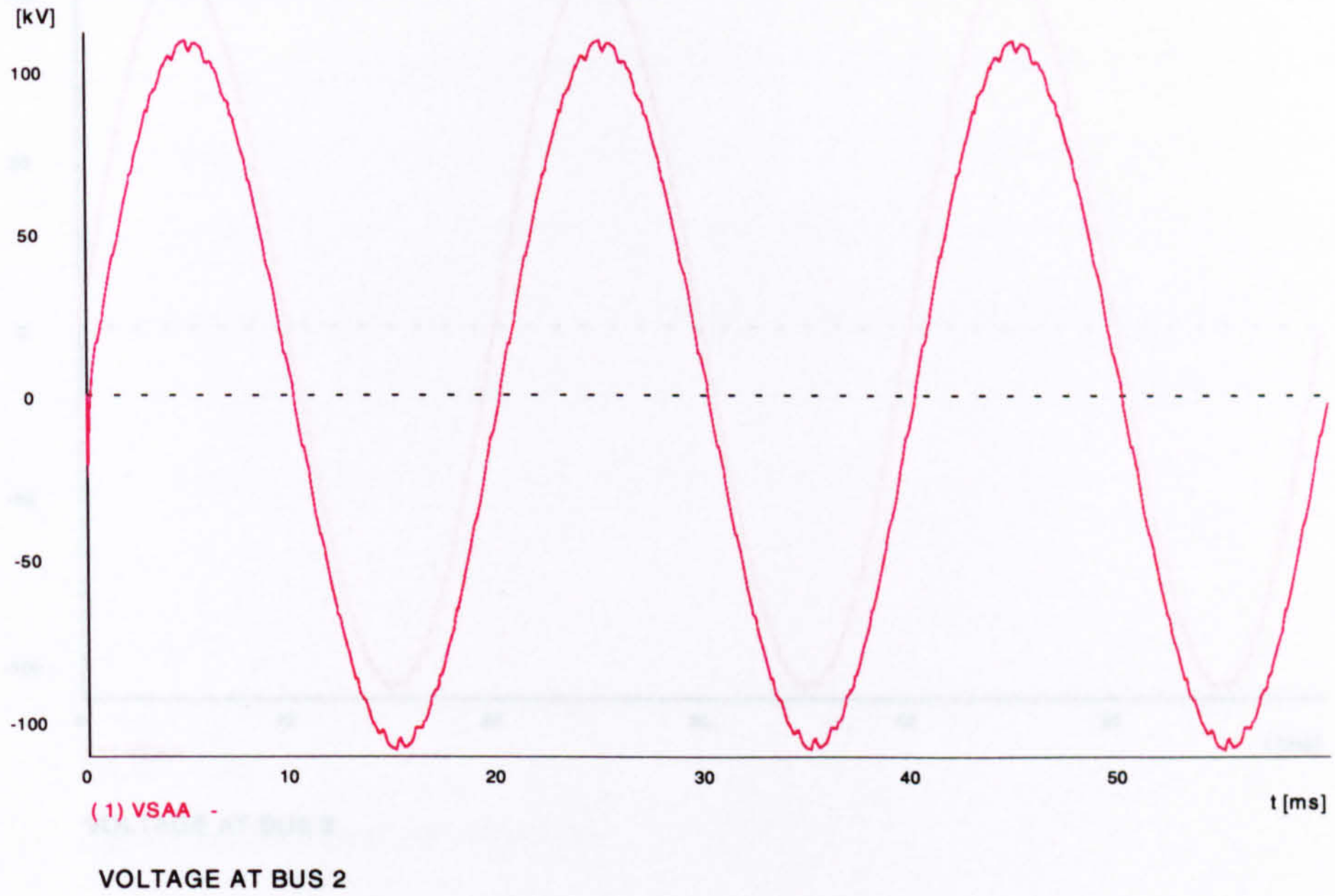

Figure 8.19 Voltage of phase A at bus 2

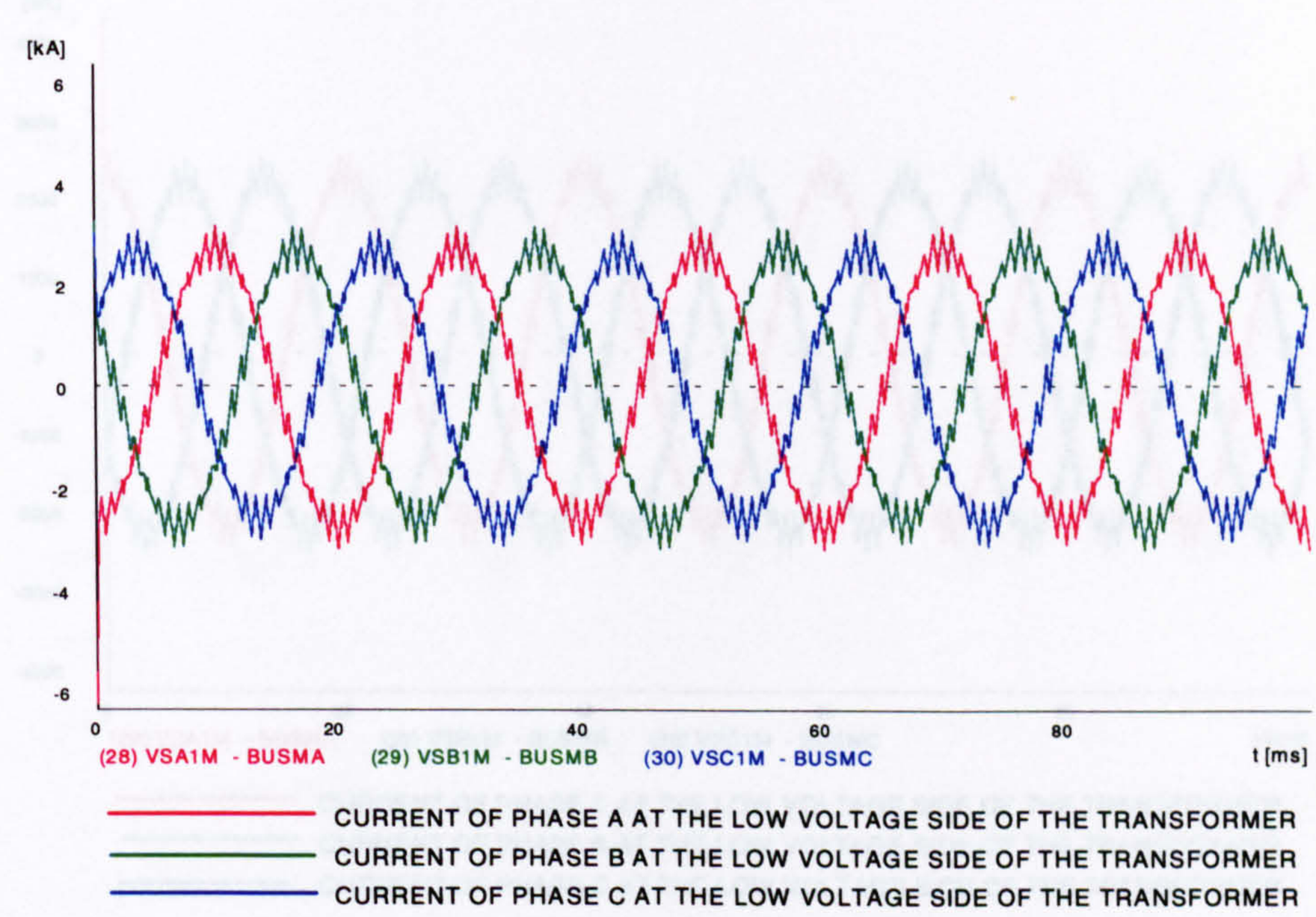

Figure 8.20 Currents flowing from the STATCON to the transformer

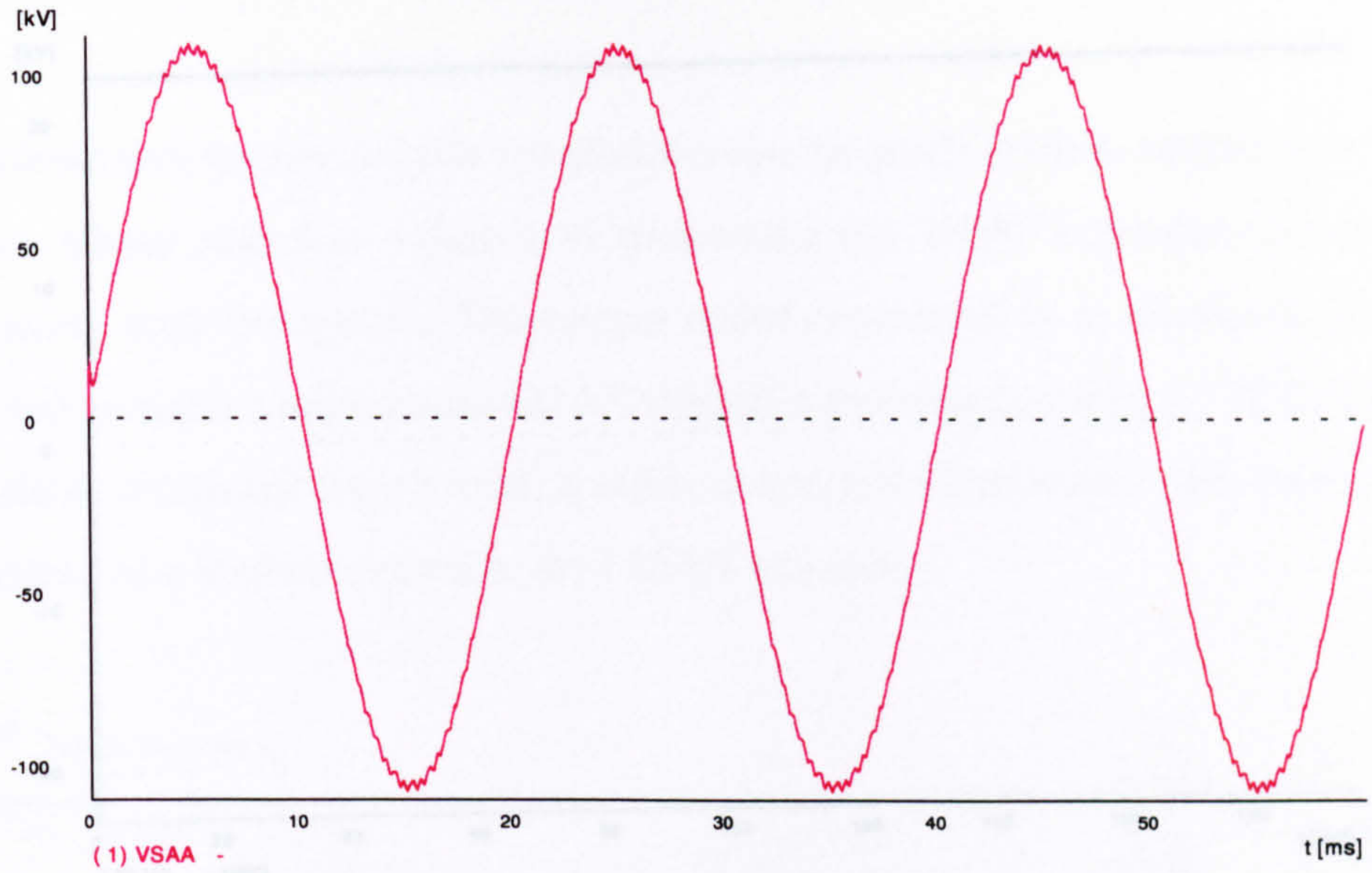

Figure 8.21 Voltage of phase A at bus 2

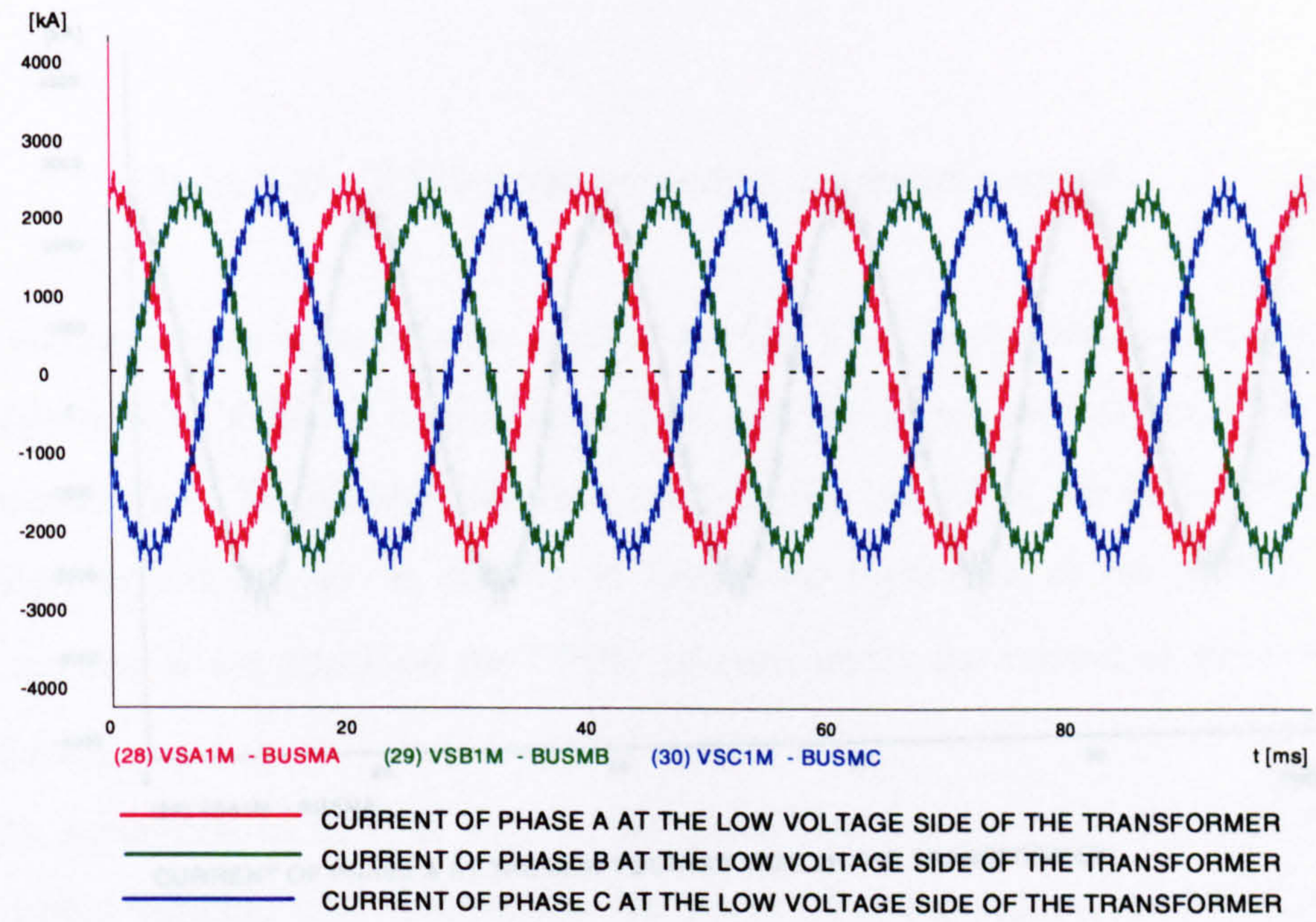

Figure 8.22 Currents flowing from the STATCON to the transformer

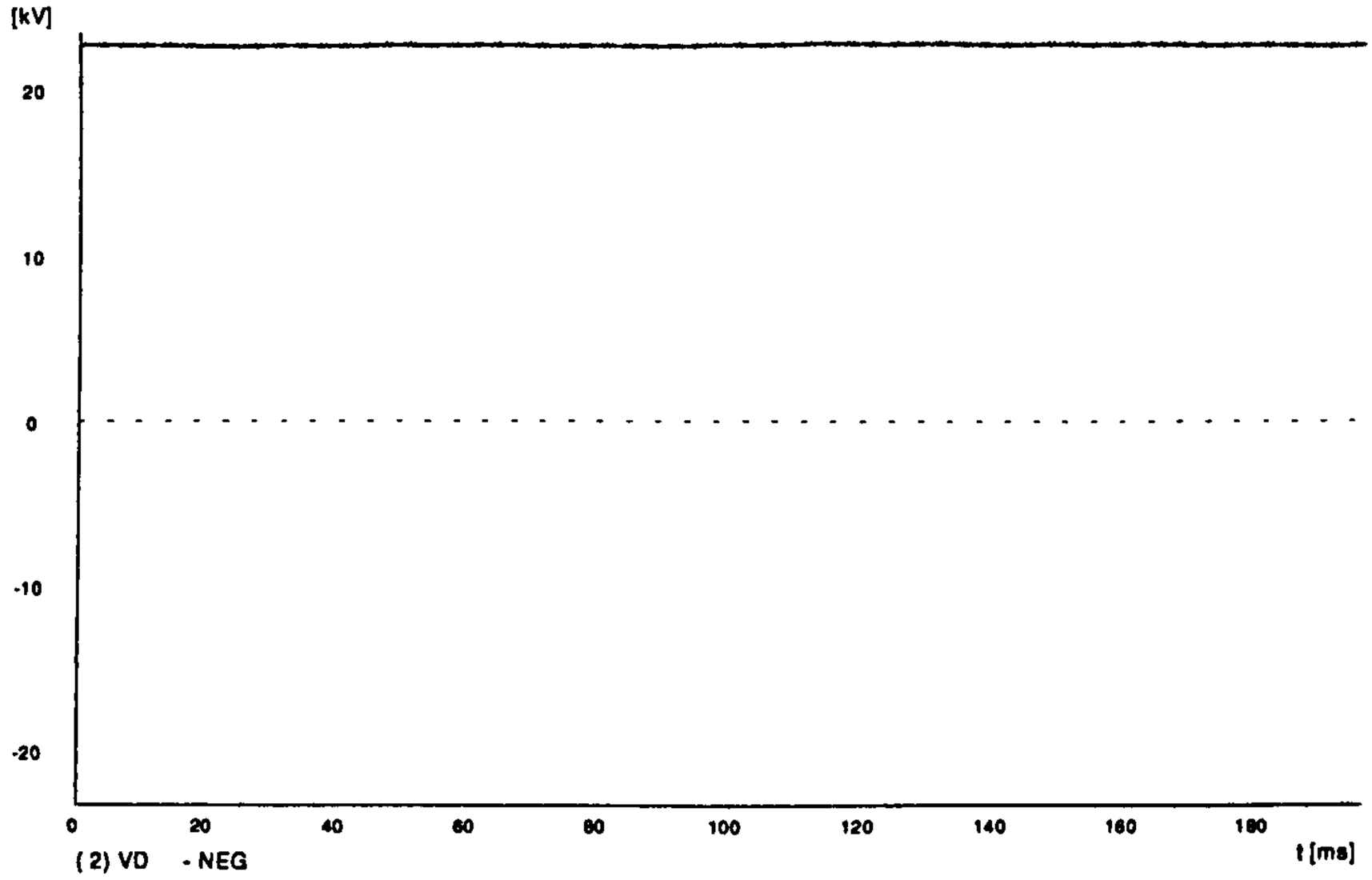

Figure 8.23 DC voltage across the capacitor

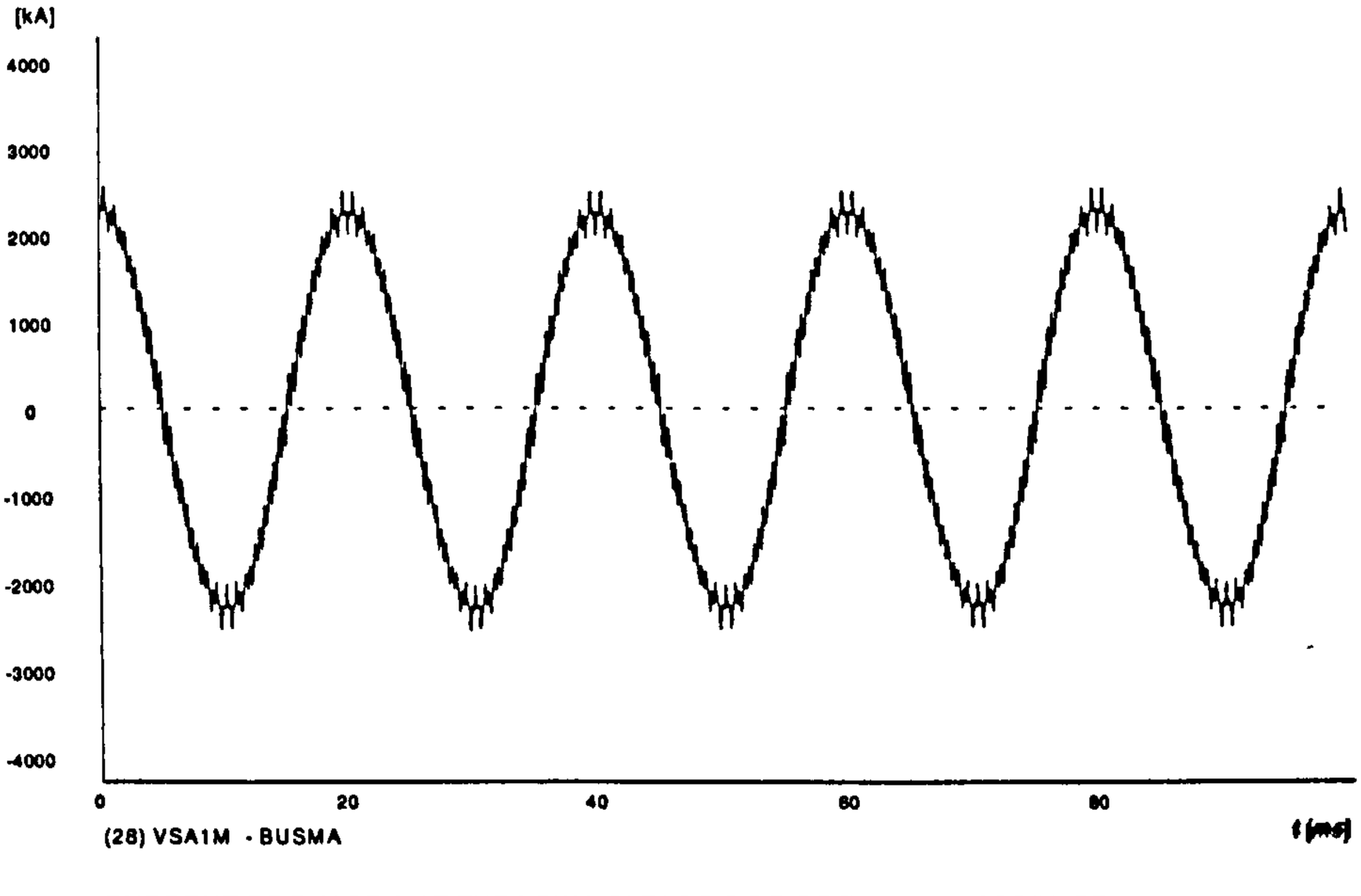

Figure 8.24 Current of phase A flowing from the STATCON to the transformer

8.7 EMTP Model Development for the UPFC

The simulation system suitable for electromagnetic study is often adapted as a simple system whose objective value is to understand the UPFC regulation concept and interaction with the system. The system under consideration is illustrated in Figure 8.25 and includes a three phase 132 kV source, a transmission line, a 132/11 kV wye-wye shunt connected transformer, a series connected transformer , two back to back inverters and a load connected to the 132 kV network.

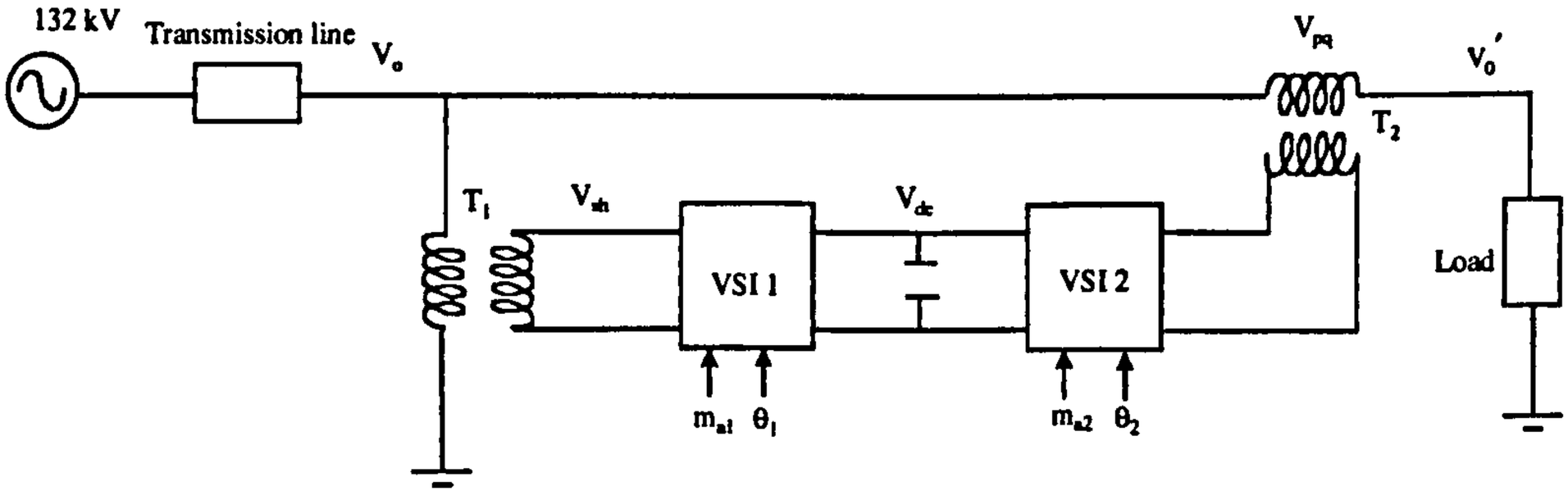

Figure 8.25 UPFC model connected to a power network

The voltage source inverter is the heart of the UPFC. A dc capacitor is the link to the voltage source inverters of the shunt part and the series part of the UPFC. The Sinusoidal Pulse Width Modulation is used for the control of the UPFC. The block labelled $m_a \sin(\omega t + \theta)$ is the key to realise the regulation of the SPWM. When m_a, ω, and θ are specified the UPFC operates under the control of the open-loop controller.

In the generation of SPWM signals, the phase displacement θ is the ideal phase of controlled variable with reference to the phase of connected bus which is assumed zero degrees. This case is the assumption of the existence of a perfect three-phase voltage source (i.e infinite bus) right at the point of common coupling (PCC) between the AC and DC system [20]. In technical terms, it can be said that the

system interface has an infinite strength. However, this is not true in practice because of the voltage distortion at the PCC and the voltage synchronisation problem. The absence of perfect voltage sources at PCC is because as the loading of the system changes, so do the bus voltages. The changes in bus voltages at PCC occur in magnitude as well as in phase angle.

In order to successfully obtain the required information on the phase angle θ of the fundamental voltage on the AC busbar, a voltage synchronisation system is introduced as follows:

Assume AC bus voltage as [20]:

$$V_0 = V_m \cos(\omega t + \theta) \tag{8.9}$$

Through the use of Fourier analysis:

$$C_1 = \frac{2}{T}\int_{t-T}^{t} v(t)\cos\omega t dt = \frac{2}{T}\left\{\int_{0}^{t} v(t)\cos\omega t dt - \int_{t-T}^{0} v(t)\cos\omega t dt\right\} \tag{8.10}$$

$$S_1 = \frac{2}{T}\int_{t-T}^{t} v(t)\sin\omega t dt = \frac{2}{T}\left\{\int_{0}^{t} v(t)\sin\omega t dt - \int_{t-T}^{0} v(t)\sin\omega t dt\right\} \tag{8.11}$$

V_m can be obtained from

$$V_m = \sqrt{C_1^{\,2} + S_1^{\,2}} \tag{8.12}$$

The determination of θ needs more elaboration. The difficulties arise from the lack of structured IF_THEN_ELSE statement in EMTP. To solve this problem the following expression is suggested:

$$\theta = a\tan\left(\frac{-S_1}{C_1}\right) + \{C_1.LT.0\} * \pi \tag{8.13}$$

The above expression will correctly return values of θ ranging from -90° to $+270^{\circ}$, which generally covers the operation range of the phase for any given bus voltages.

In the EMTP, some functions of monitoring variables have been provided, such as voltages and currents and instantaneous powers. However, more practical interest is the average power over a period of time T.

The instantaneous power in any electrical component is given by

$$p(t) = v(t) * i(t) \tag{8.14}$$

The average power over a period time T is formulated by:

$$P = \frac{1}{T}\int_{t-T}^{t} p(t)dt \tag{8.15}$$

The period of time is usually one period of the fundamental frequency. For 50Hz the period is 0.02secs.

The average power P is constant in steady-state. But the average power varies with time during transients. Then the average power P(t) is of interest during the last half cycle on a continuous basis. It can be found by continuously computing p(t) and splitting the integral into two components.

$$P(t) = \frac{1}{T}\left\{\int_{0}^{t} p(t)dt - \int_{0}^{t-T} p(t)dt\right\} = \frac{1}{T}\left[\overline{P}(t) - \overline{P}(t-T)\right] \tag{8.16}$$

The second integral has the value of the first integral delayed by T seconds. This suggests an implementation in TACS as in the figure. The delay of the value of $\overline{P}(t)$ by time T is readily obtained by using TACS device code 53. Its output value is equal to the input value delayed by time T.

A single phase diagram corresponding to a VSI connected to the utility system through a transformer is given in figure 8.26. In this case, the general expression for the apparent power flowing between the AC mains side V_0 and the ac side V_{sh} of the VSI is as follows [11]:

$$S_0 = \frac{V_0 V_{sh}}{X}\sin\theta_1 - j(\frac{V_0 V_{sh}}{X}\cos\theta_1 - \frac{V_0^2}{X}) \qquad (8.17)$$

where θ_1 is the phase displacement between V_0 and V_{sh}.

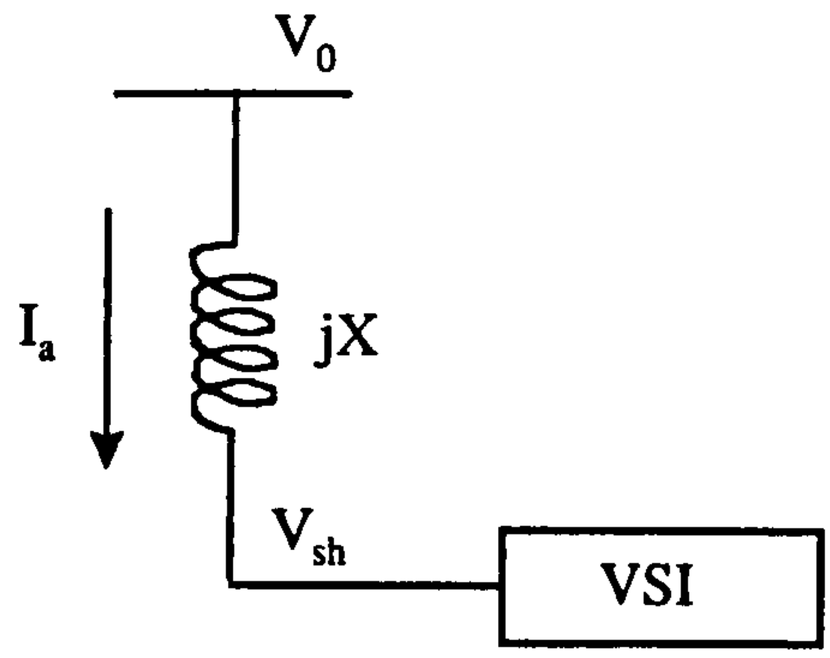

Figure 8.26 A single diagram corresponding to a VSI connected to the utility system through a transformer

When the shunt part and the series part of the UPFC operate under the SPWM, they have different functions. According to the concepts of the UPFC, the functions of the series part are achieved by adding an appropriate voltage phasor V_{pq} to the terminal phasor V_0 as shown in figure 8.27. Because V_{pq} can be regulated by amplitude and angle, it is important to analyse how V_{pq} is regulated by SPWM. It is assumed that the dc link voltage V_{dc} in the UPFC circuit is kept constant by inverter 1, which can be readily realised by changing the phased angle θ_1 between V_0 and V_{sh}. Therefore, the series voltage output of the ac terminal of inverter 2 can be obtained [9]:

$$V_{pq} = T_2 m_{a2} V_{dc}(\cos\theta_2 + j\sin\theta_2)/2 \qquad (8.18)$$

where T_2 is the ratio of the series transformer, m_{a2} is the modulation ratio of inverter 2, and θ_2 is the phase shift angle between V_{pq} and V_0. Thus V_{pq} is defined by m_{a2} and θ_2 and can be proportionally controlled by different m_{a2} and θ_2 according to the concepts of the UPFC which is shown in figure 8.27. In this way, the UPFC can

partially fulfill the functions of voltage regulation, series compensation, phase angle regulation and multi-function power flow control through regulating inverter 2 based on SPWM method.

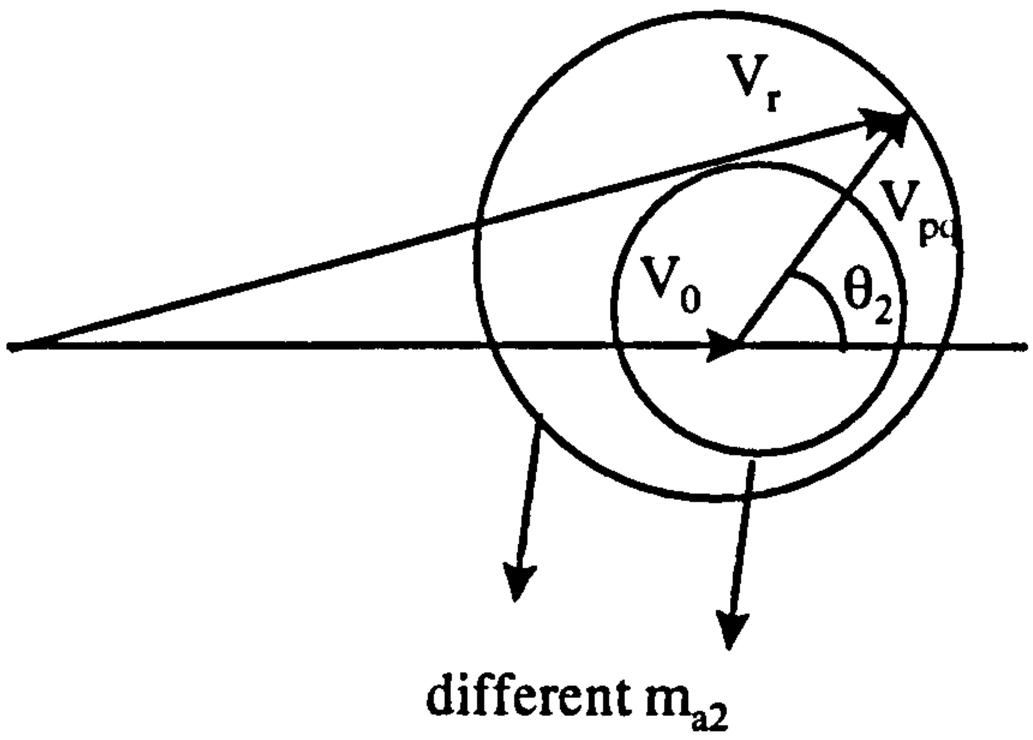

Figure 8.27 Phasor diagram of multiple control scheme

For the shunt part of the UPFC, it not only provides the active power to charge or discharge the dc link capacitor and keep V_{dc} constant, but also can control the voltage V_0 by regulating V_{sh}. It is in principle straightforward to meet the requirements of regulating V_{dc} and V_0 simultaneously with SPWM through control of θ_1 and m_{a1} respectively. However from equation 8.17 the changing of the V_{sh} not only results in the changing of the reactive power flow but also the changing of the active power flow, and can thus lead the changing of V_{dc}. At this time, θ_1 should be regulated in order to keep V_{dc} constant. Under the above assumptions, the inverter 1 has the following operating characteristics [10]:

1. Active power flow is biteral. It goes from V_0 bus to V_{sh} bus for lagging θ_1 and vice versa for leading θ_1;
2. Assuming θ_1 is used to keep V_{dc} constant, the shunt part of the UPFC absorbs reactive power when $V_0 > V_{sh}$, which can be realised through decreasing m_{a1};

3. Assuming θ_1 is used to keep V_{dc} constant, the shunt part of the UPFC supplies reactive power when $V_0 < V_{sh}$, which can be realised through increasing m_{a1}.

The SPWM UPFC can thus control transmission line terminal voltage and power along the line by regulating m_{a1}, θ_1, m_{a2} and θ_2 of inverters 1 and 2.

8.8 Results of simulation of the SPWM UPFC

In this section simulation results through detailed modelling of the UPFC based on SPWM inverters by EMTP are presented. The system under study in figure 8.25 (or in a smaller scale in figure 8.3) is analysed below for various system scenarios and can be used effectively in order to predict the response of the UPFC. In the following seven sets there are some typical simulation results demonstrating voltage and power flow differences for various UPFC operating conditions (sets from 1 to 6) and the active power flow though the UPFC (7^{th} case study):

1. Using $m_{a2} = 1$, $\theta_2 = 0^\circ$, $m_{a1} = 0.6$, with $\theta_1 = -9.60^\circ$ figure 8.28 shows the voltages before the series connected transformer, the voltage across it and the load voltage. The rating of the series connected inverter is ± 17MVA . The load voltage is increased according to equation 8.18. Figure 8.29 illustrates the current at the low voltage side of the shunt connected transformer. This current flows from the VSI to the ac network. In figure 8.30 the load current is presented and in figure 8.31 the active power flow before and after the series part of the UPFC is shown. With $\theta_2 = 0^\circ$ the active power in the load is maximum due to the maximum voltage across it (power as a function of the squared voltage). The active power flow difference in figure 8.31 is also maximum due to the maximum voltage difference between the source (V_0) and the load (V_0') voltage. This power flow difference also includes the losses in the UPFC as were described in section 8.2.
2. For $m_{a2} = 1, \theta_2 = 90^\circ, m_{a1} = 0.6$ with $\theta_1 = -1.60^\circ$ figure 8.32 shows the voltages before the series connected transformer, the voltage across it and the load voltage and figure 8.33 the active power flow before and after the series part of the UPFC.

As expected the load voltage and so the active power at the load terminal is less than in the previous case. The active power flow difference in figure 8.33 is much less than in the previous case and includes the losses in the UPFC as were described in section 8.2.

3. For $m_{a2}=1, \theta_2=180^\circ, m_{a1}=0.6$ with $\theta_1=+6.50^\circ$ figure 8.34 shows the voltages before the series connected transformer, the voltage across it and the load voltage and figure 8.35 the active power flow before and after the series part of the UPFC. According to the equation 8.18 the load voltage is minimal and so does the active power (because the active power is a function of the square voltage). The difference in active powers in figure 8.35 is much higher than in the previous case due to the significant voltage difference between the source (V_0) and the load (V_0') voltages (the active power difference also includes the losses in the UPFC).
4. For $m_{a2}=1, \theta_2=270^\circ, m_{a1}=0.6$ with $\theta_1=-1.85^\circ$ figure 8.36 shows the voltages before the series connected transformer, the voltage across it and the load voltage and figure 8.37 the active power flow before and after the series connected part of the UPFC. As in case (2) the small active power flow difference in figure 8.37 also includes the losses in the UPFC.
5. For $m_{a2}=0.5, \theta_2=180^\circ, m_{a1}=0.6$ with $\theta_1=+4.1^\circ$ figure 8.38 shows the voltages before the series connected transformer, the voltage across it and the load voltage and figure 8.39 the active power flow before and after the series connected transformer. According to the equation 8.18 the load voltage and so the active across the load are now greater than in case 3. The active power flow difference in figure 8.39 is much less than in case (3) due to the decrease in the voltage difference between the source (V_0) and load (V_0') voltages. The power flow difference also includes the losses in the UPFC as were presented in section 8.2.
6. For $m_{a2}=1, \theta_2=180^\circ, m_{a1}=1.0$ with $\theta_1=+2.15^\circ$ figure 8.40 shows the voltages before the series connected transformer, the voltage across it and the load voltage and figure 8.41 the current at the low voltage side of the shunt connected transformer. This current flows from the VSI to the ac network. Compared to the

current in case 1, it has an opposite phase angle, due to the difference at the modulation ratio m_{a1}.

7. Using case 1 as reference (with $m_{a2}=1$, $\theta_2=0^\circ$, $m_{a1}=0.6$, $\theta_1=-9.60^\circ$), an investigation of the active power flow through the UPFC was undertaken using the figure 8.42 by plotting the active power before and after the UPFC. From this figure it can be seen that there is active power flow through the controller that accounts for the losses in the UPFC as described in section 8.2.

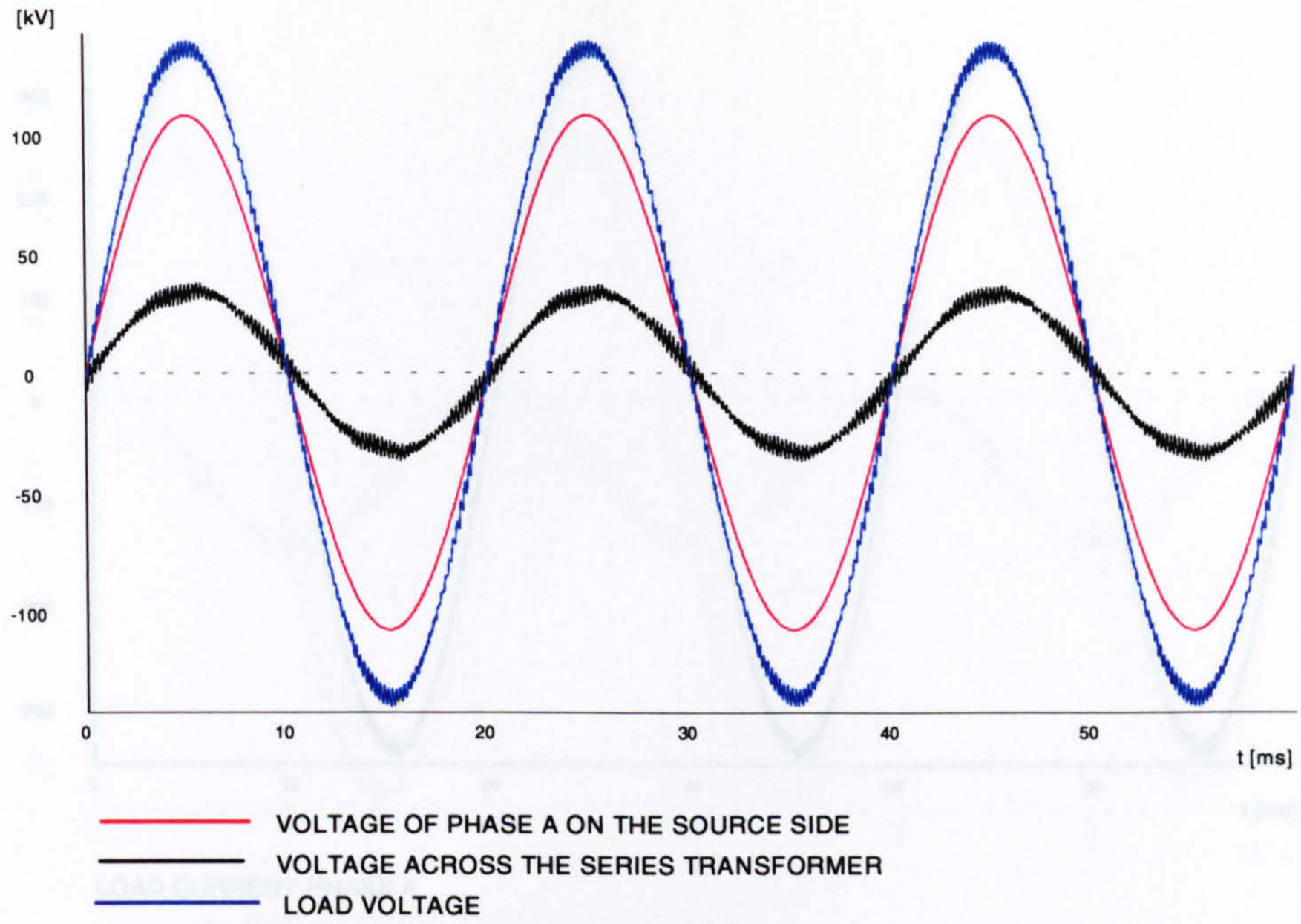

Figure 8.28 Simulation results of V_0, V_{pq}, V_0' with $m_{a2} = 1$, $\theta_2 = 0^\circ$, $m_{a1} = 0.6$

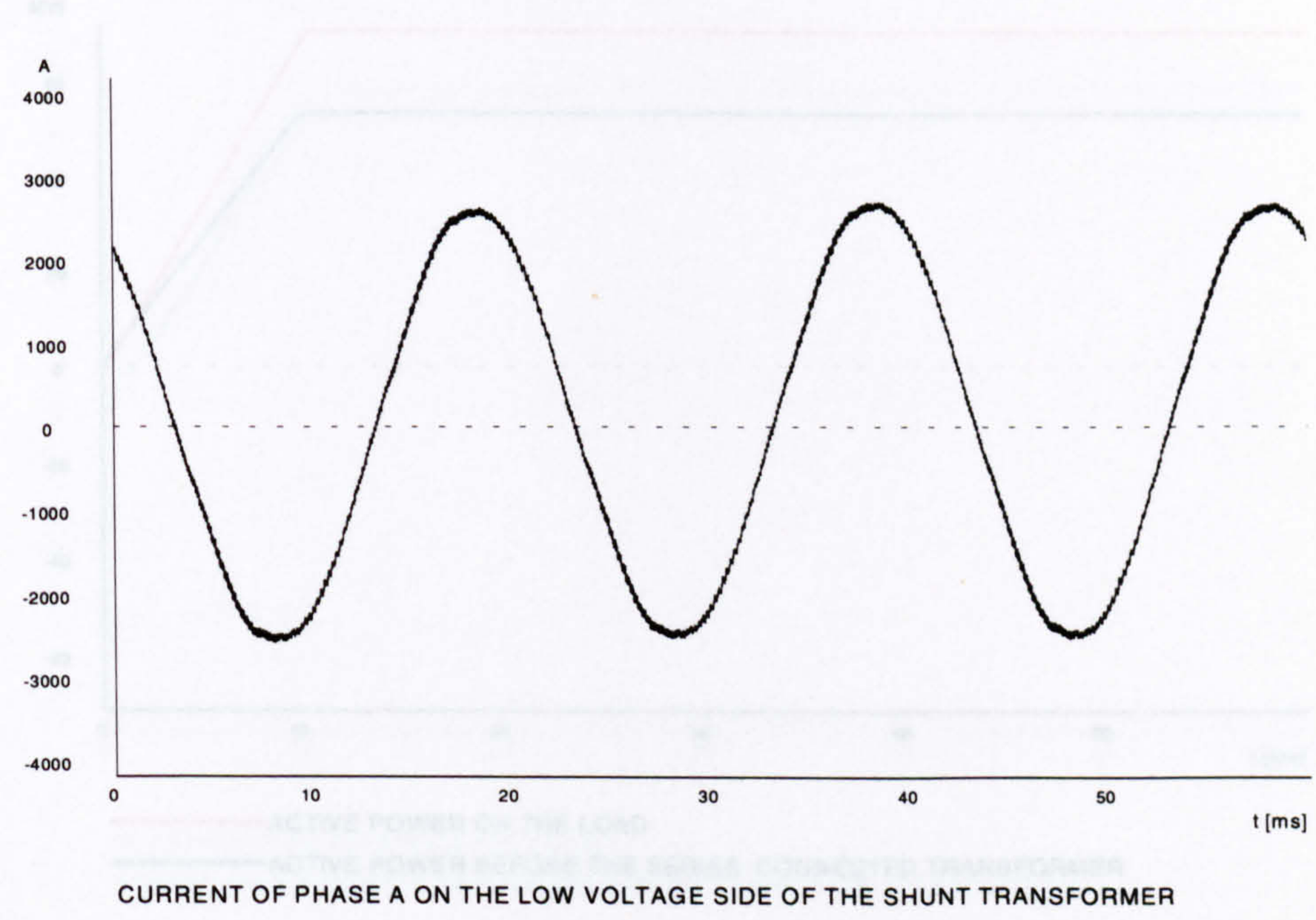

Figure 8.29 Current of phase A on the low voltage side of the shunt transformer

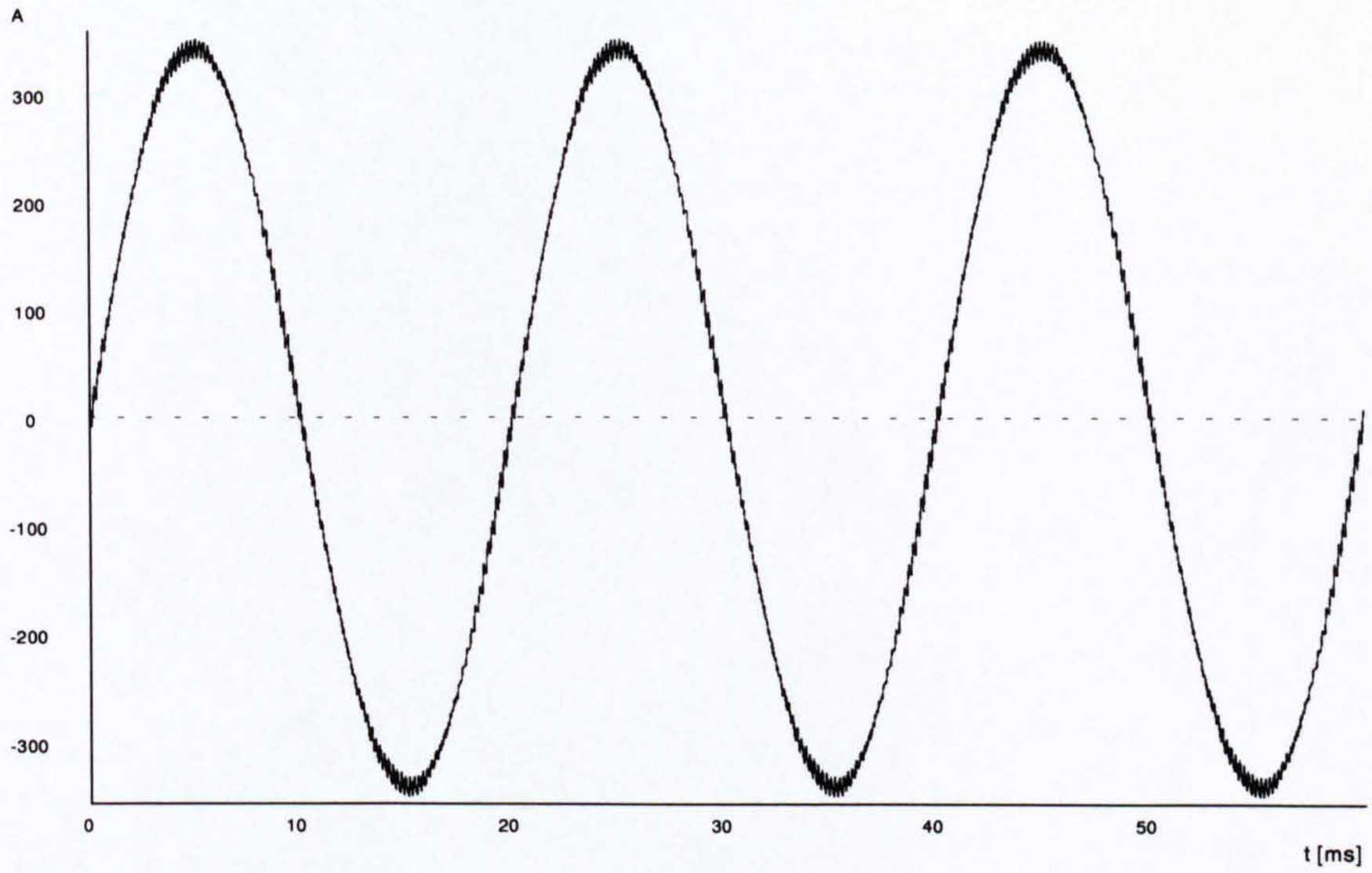

Figure 8.30 Load current-phase A

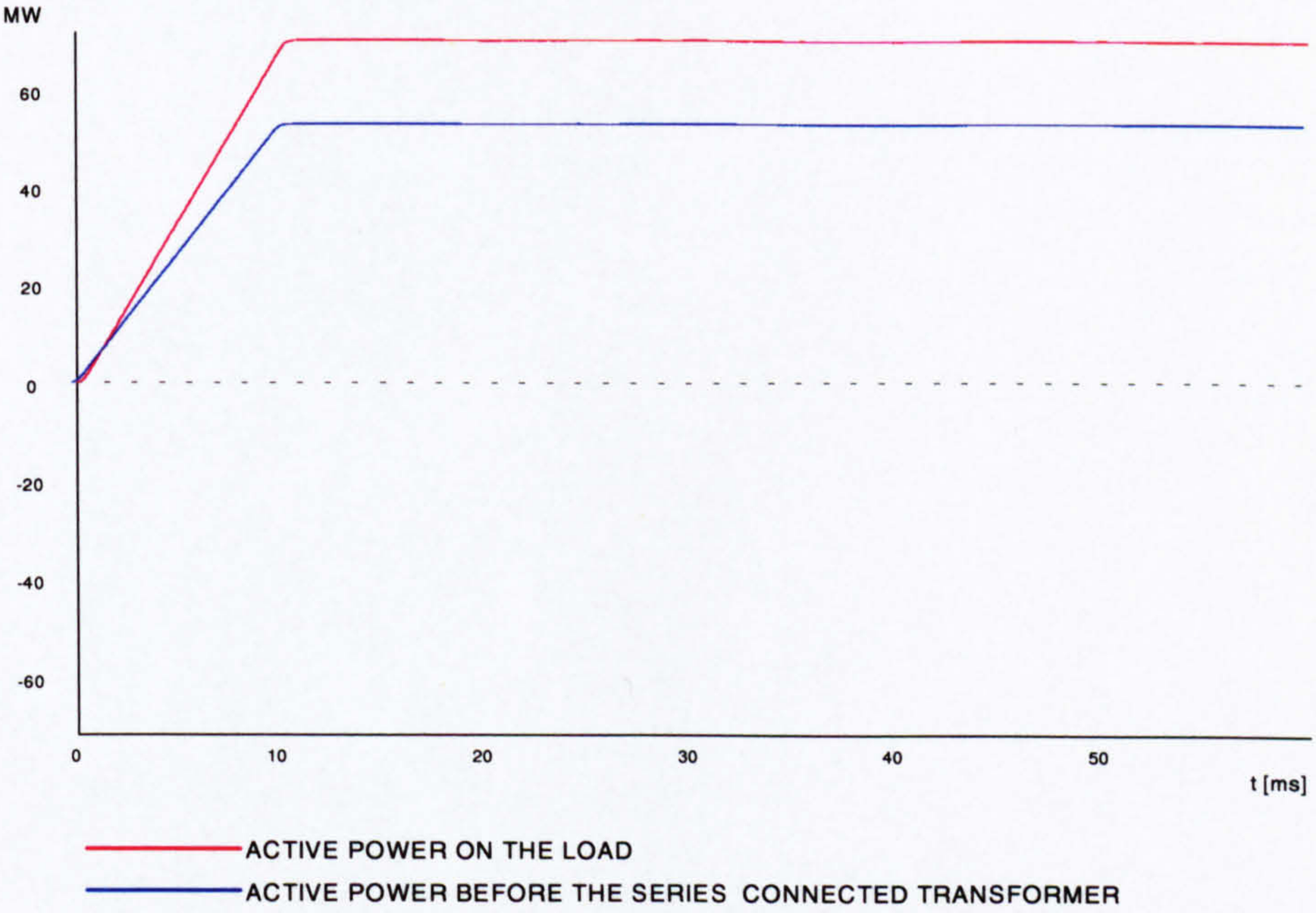

Figure 8.31 Active power flow before and after the series connected transformer

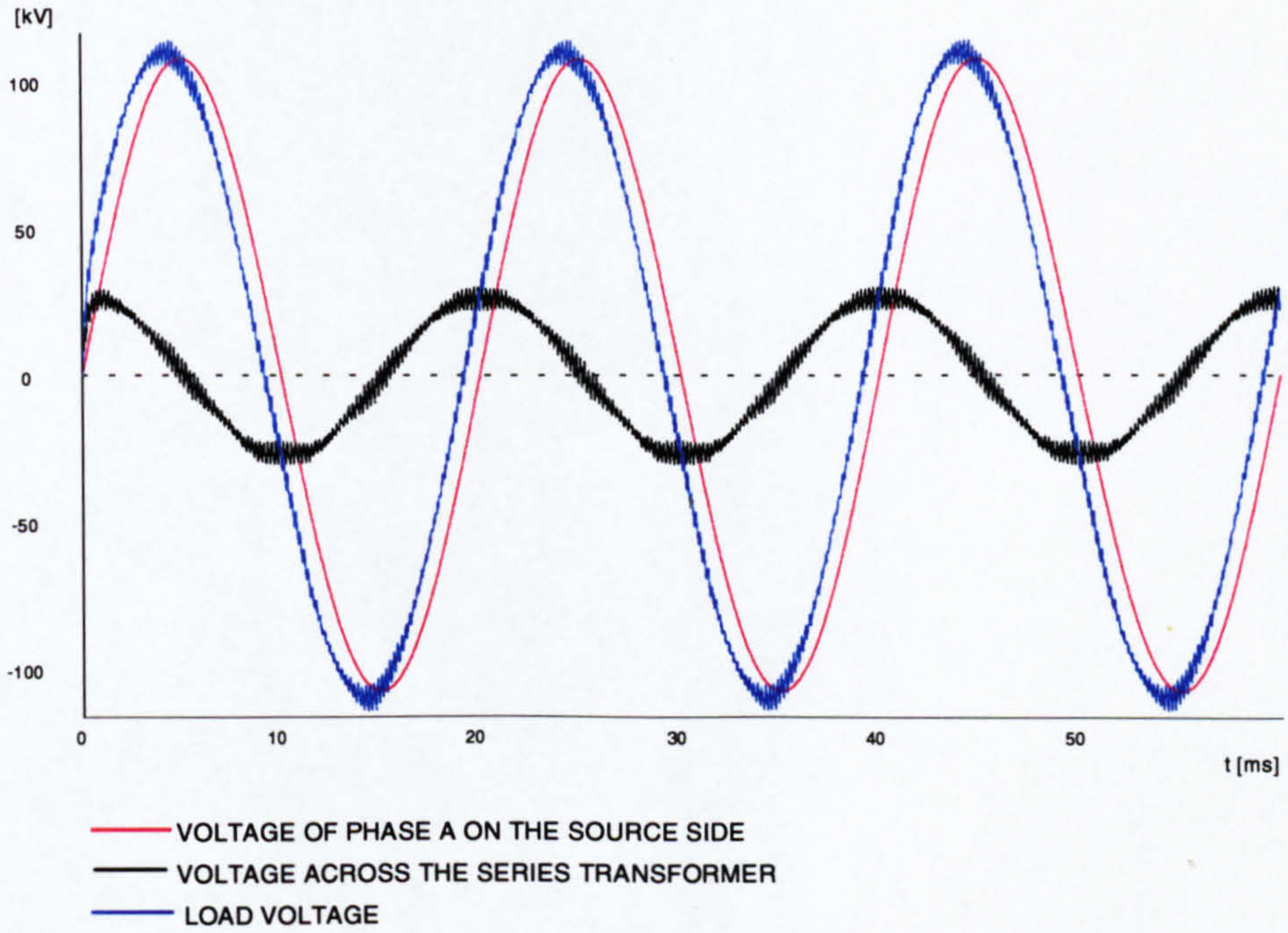

Figure 8.32 Simulation results of V_0, V_{pq}, V_0' with $m_{a2}=1, \theta_2=90^\circ, m_{a1}=0.6$

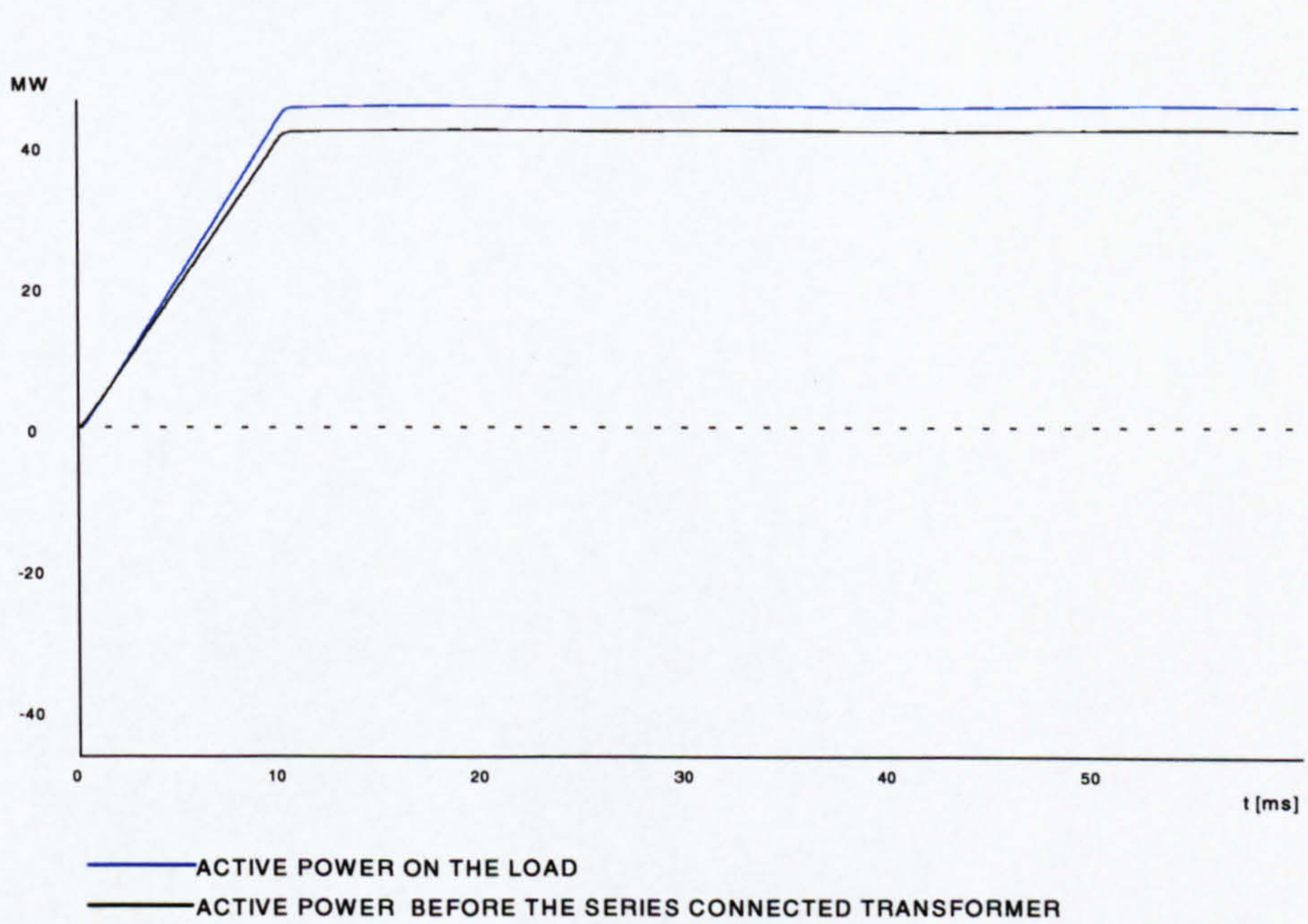

Figure 8.33 Active power flow before and after the series connected transformer

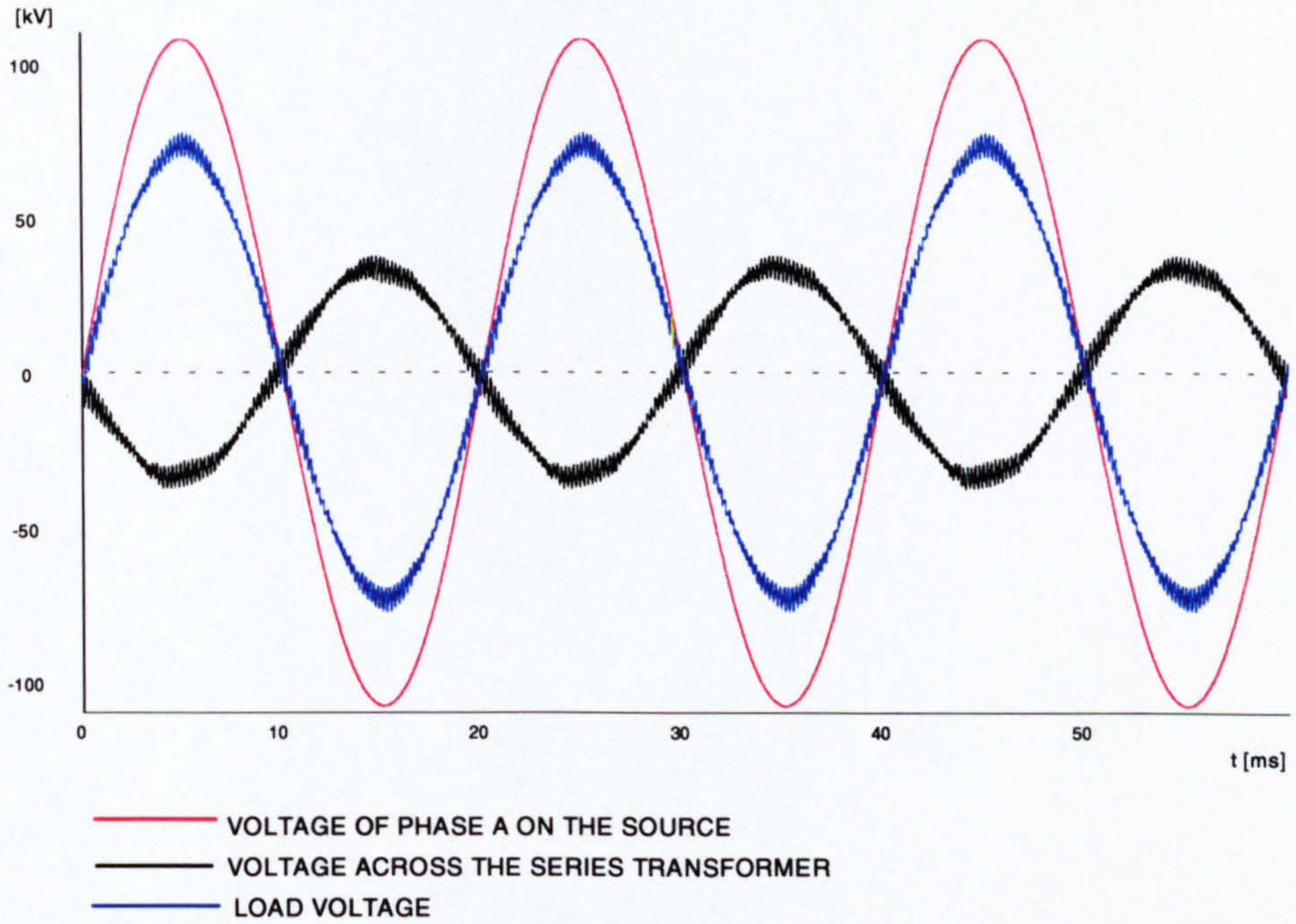

Figure 8.34 Simulation results of V_0, V_{pq}, V_0' with $m_{a2}=1, \theta_2=180^\circ, m_{a1}=0.6$

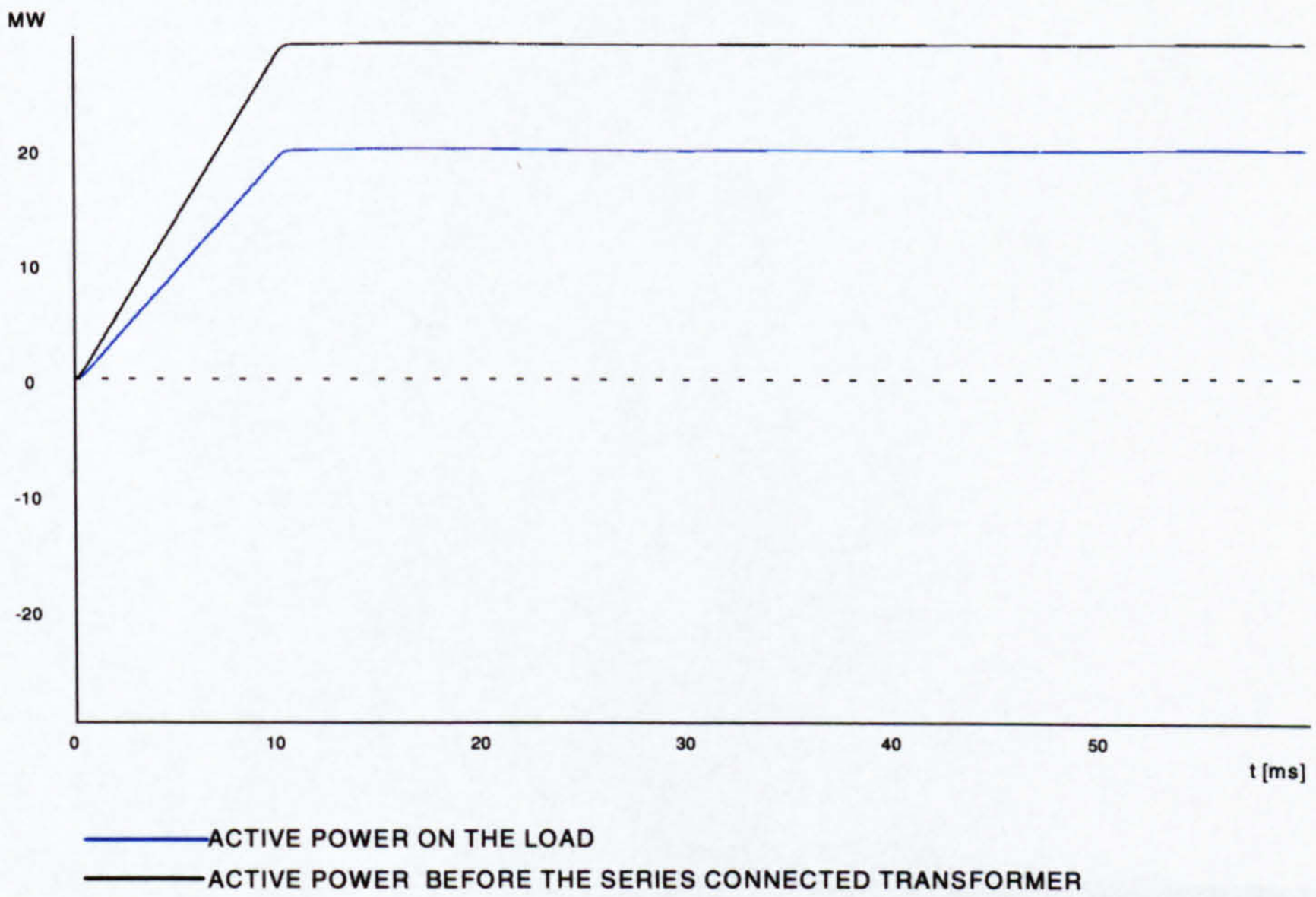

Figure 8.35 Active power flow before and after the series connected transformer

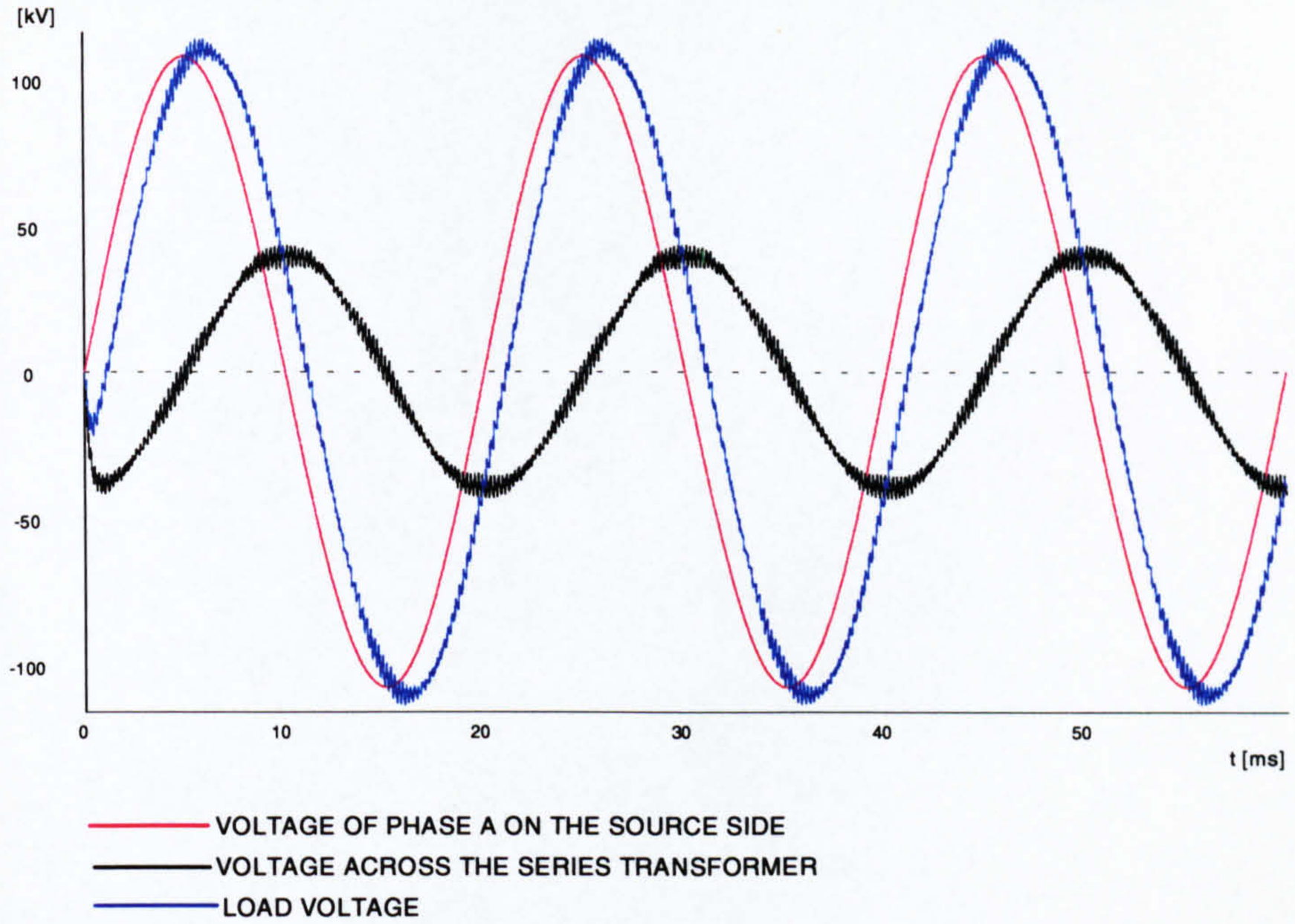

Figure 8.36 Simulation results of V_0, V_{pq}, V_0' with $m_{a2}=1, \theta_2=270^\circ, m_{a1}=0.6$

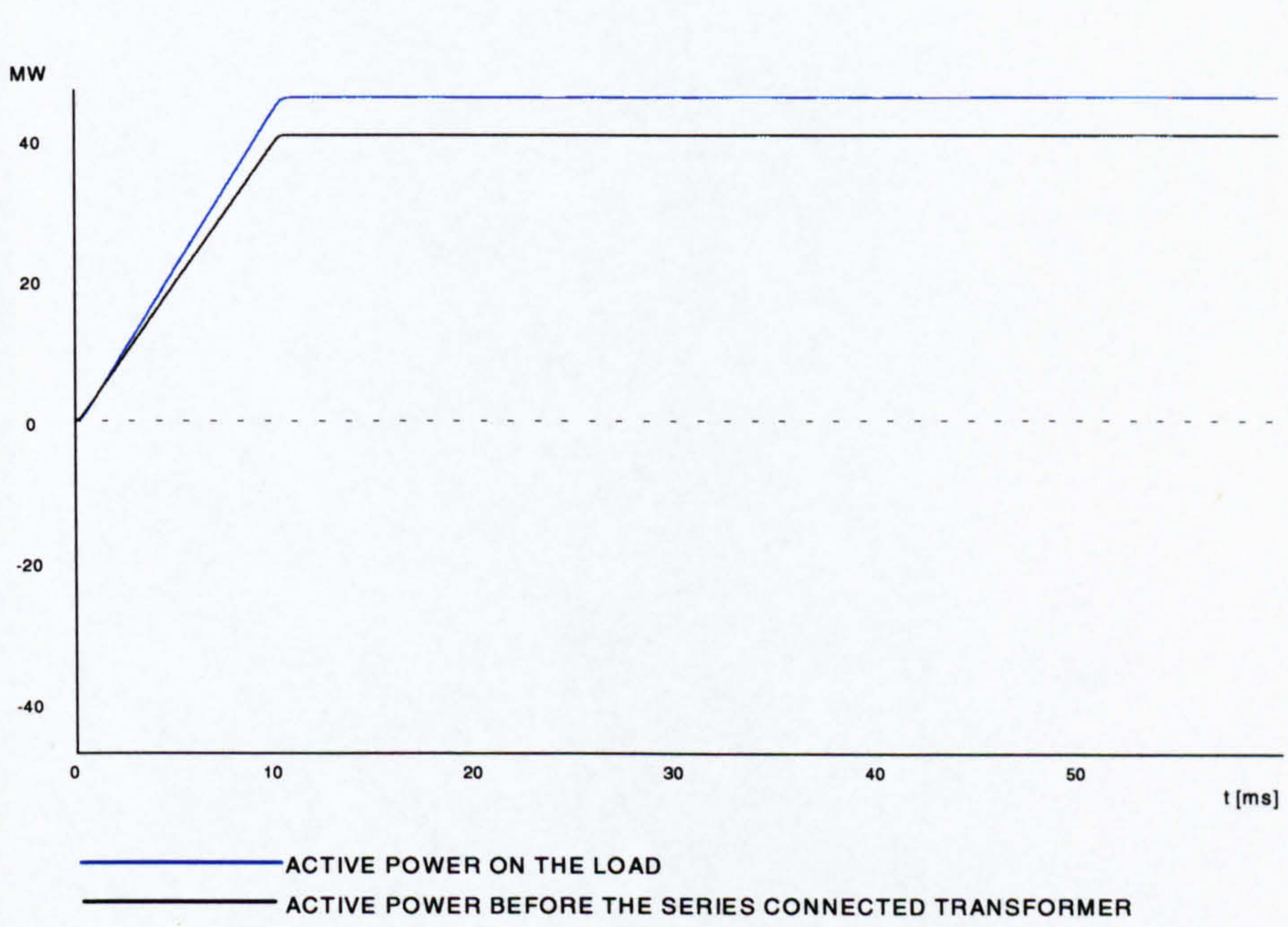

Figure 8.37 Active power flow before and after the series connected transformer

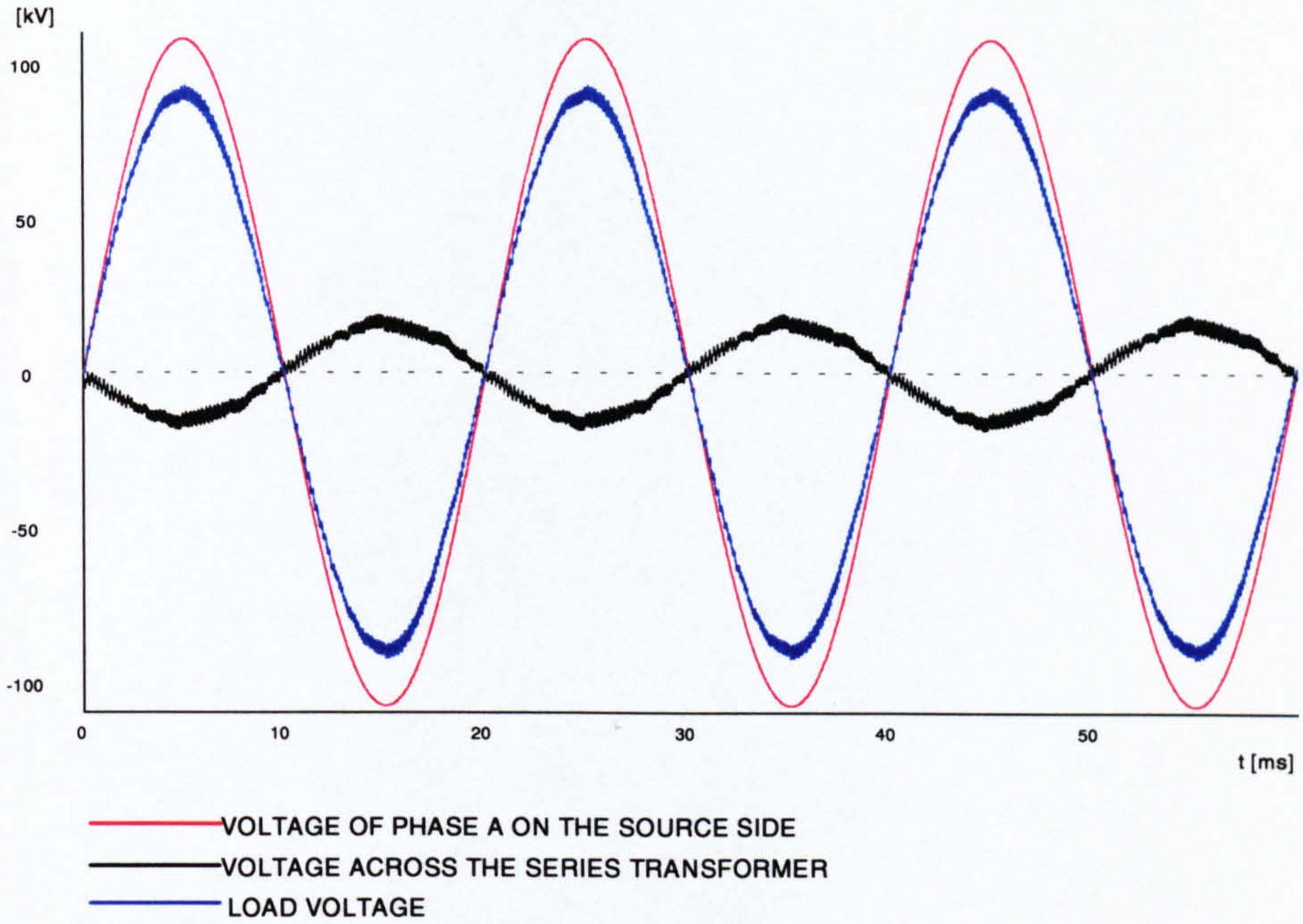

Figure 8.38 Simulation results of V_0, V_{pq}, V_0' with $m_{a2} = 0.5, \theta_2 = 180^\circ, m_{a1} = 0.6$

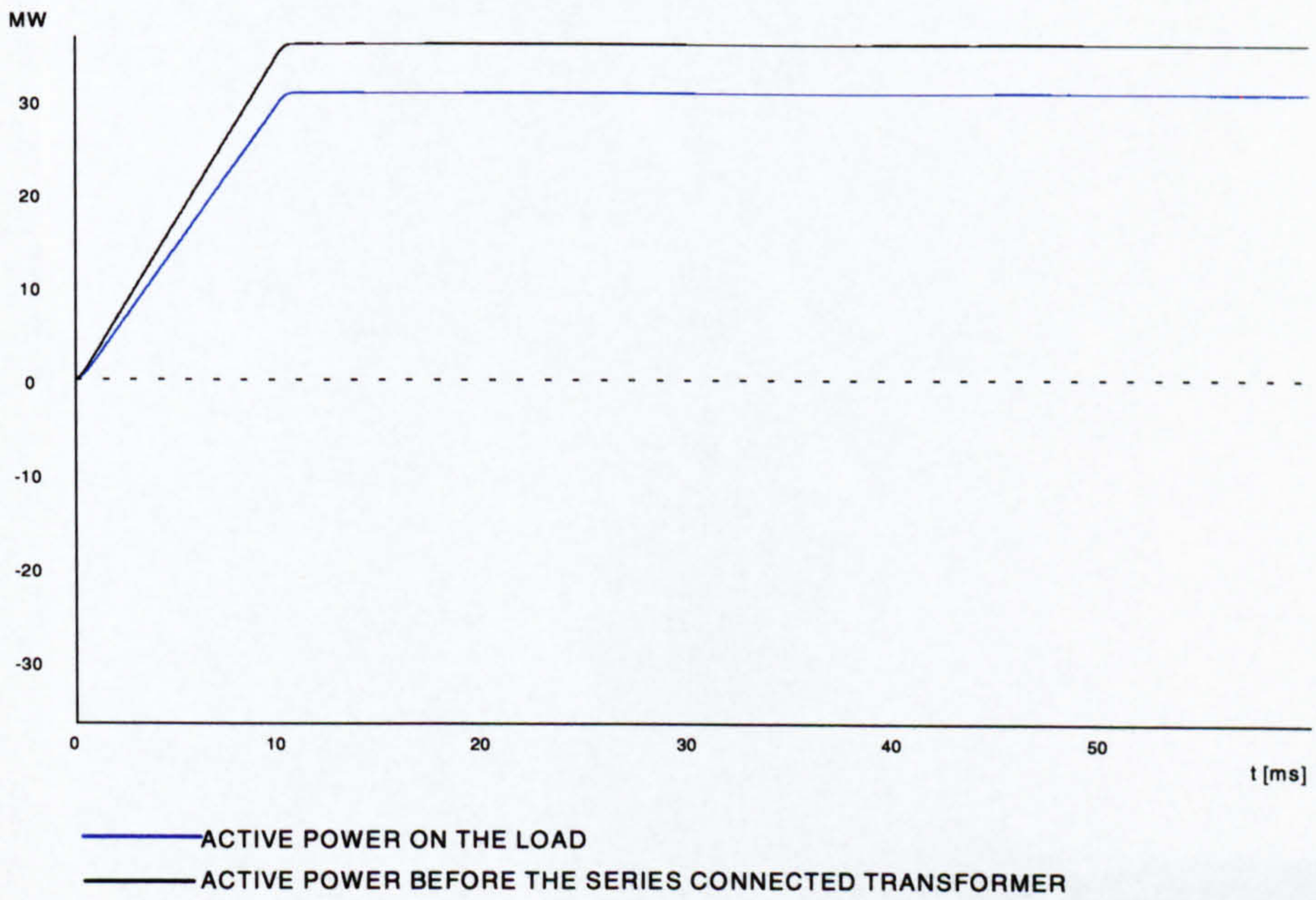

Figure 8.39 Active power flow before and after the series connected transformer

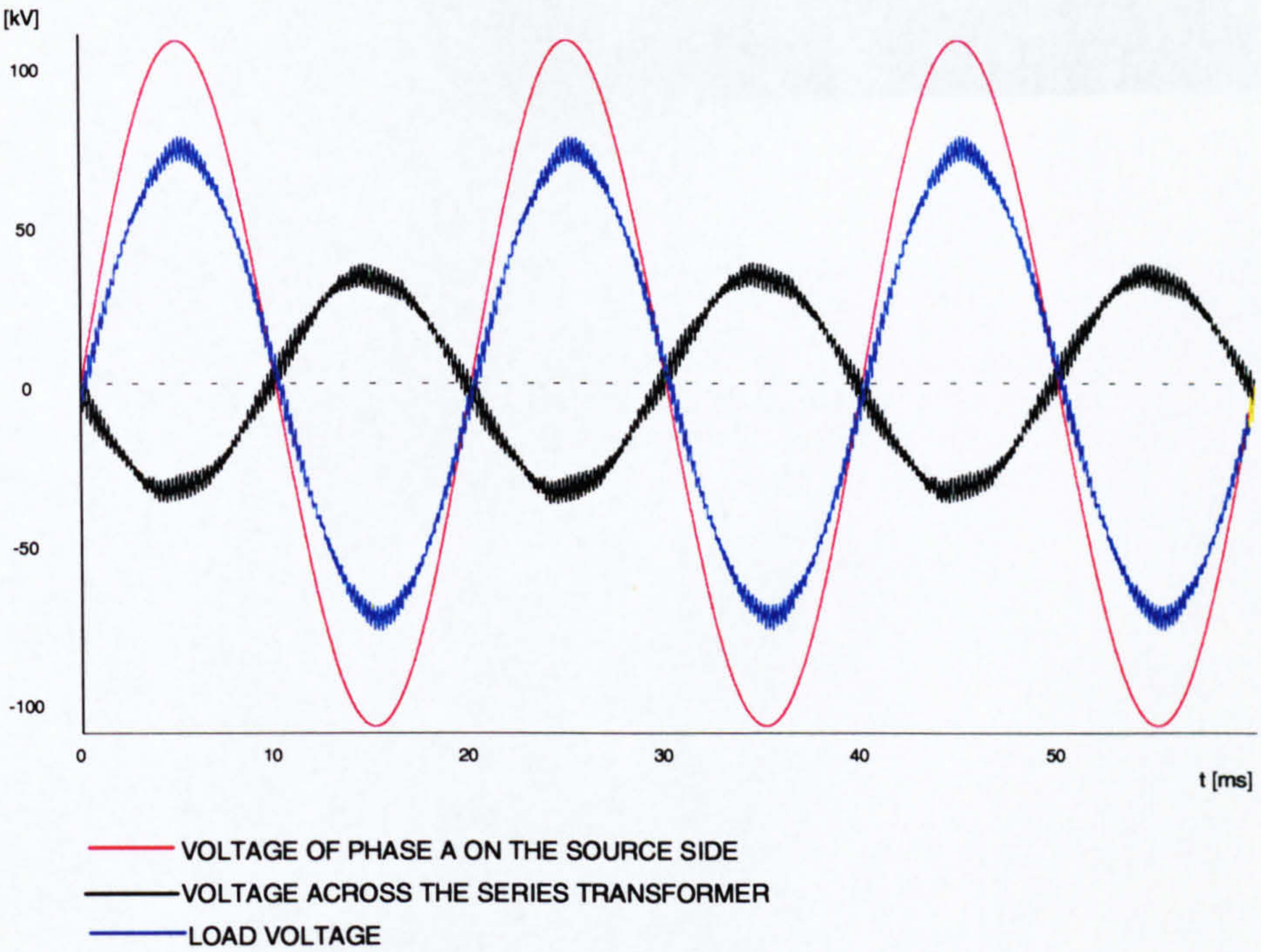

Figure 8.40 Simulation results of V_0, V_{pq}, V_0' with $m_{a2} = 1, \theta_2 = 180^\circ, m_{a1} = 1.0$

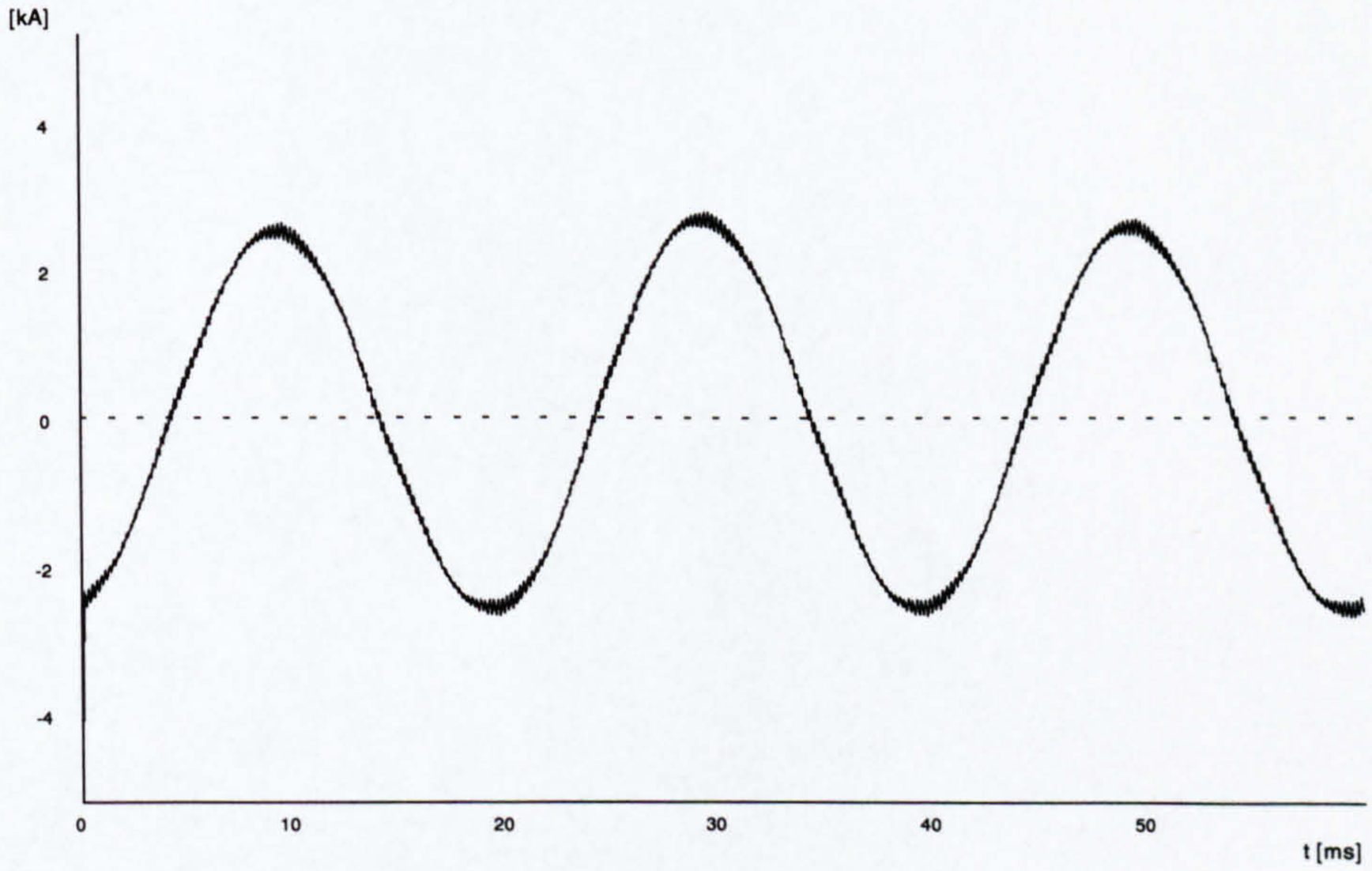

Figure 8.41 Current of phase A on the low voltage side of the shunt transformer

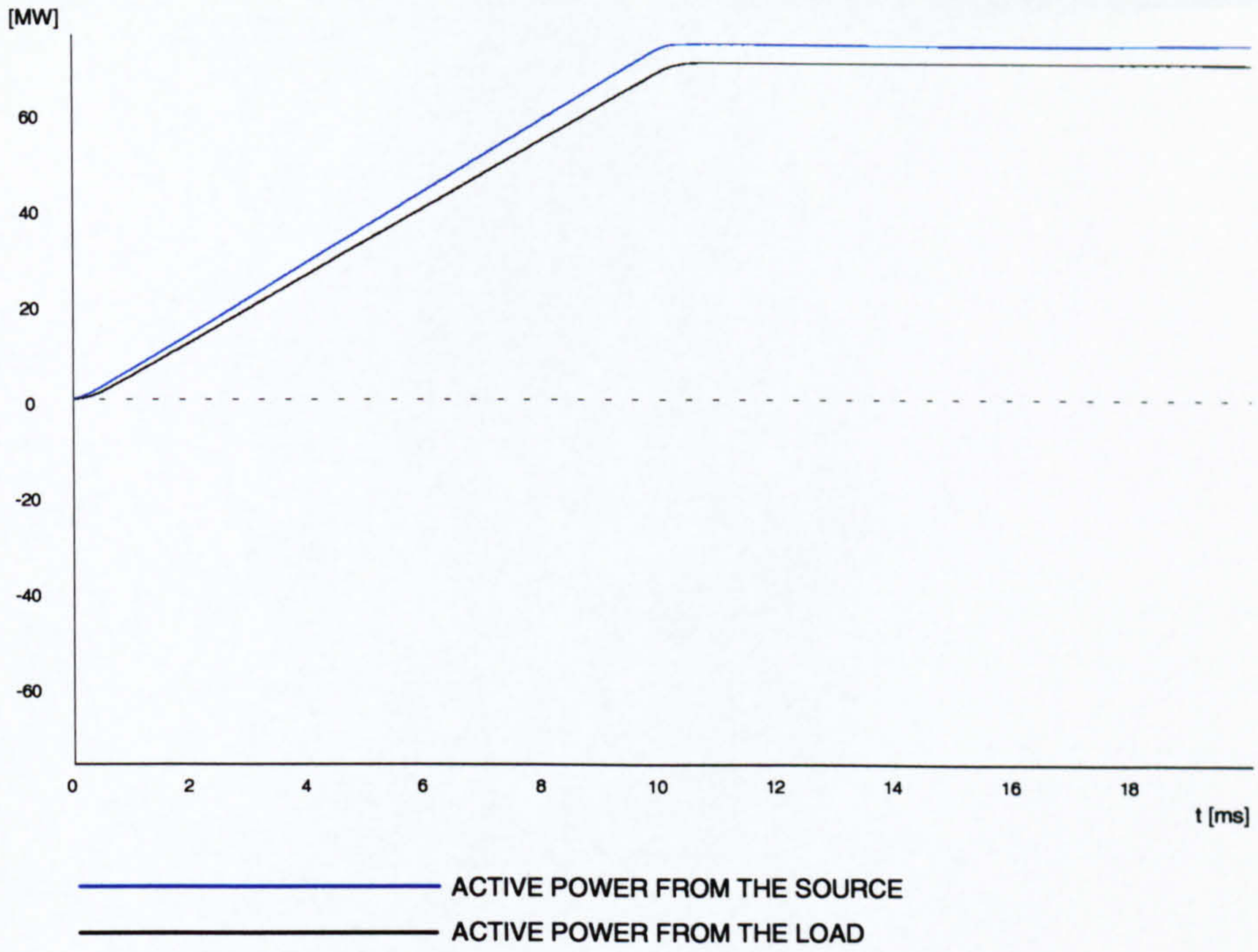

Figure 8.42 Active power flow through the UPFC

8.9 Conclusions

The work presented in this chapter described work on power flow controllers and especially open-loop simulations of the STATCON and the UPFC. Studies have shown that the SPWM is a potentially promising method for effective regulation of power flow controllers.

The effectiveness and the versatility of the above model makes it a useful tool for more advanced power flow analysis in power system networks.

8.10 References

1. G.D. Galanos, C.I. Hatziadoniu, X-J Cheng, D.Maratukulam, "Advanced Static Compensator For Flexible AC Transmission", IEEE Transactions on Power Systems, Vol 8., No 1, February 1993, pp 113-120.
2. C.Schauder, M.Gernhardt, E.Stacey, T.W.Cease, A.Edris, "Development of a ±100MVAR Static Condenser for Voltage Control of Transmission Systems", IEEE Transactions on Power Delivery, Vol 10, No.3, July 1995, pp 1487-1493.
3. L.Hu, R.E.Morrison, "Simulation Study of a transmission system containing two unequally rated parallel lines and a UPFC", AC and DC Power Transmission, No.423,1996, pp 343-350.
4. B.Ooi, S.Z.Dai, F.Galiana, "A Solid-State PWM Phase-Shifter", IEEE Transactions on Power Delivery, Vol 8, No.2, 1993, pp 573-579.
5. Y. Besanger, J.C. Passelergue, N. Hadjsaid, R.Feuillet, "Improvement of power system performance by inserting FACTS devices", AC and DC Power Transmission, No 423, 1996, pp263-267.
6. J.B Ekanayake, N.Jenkins, C.B. Cooper, "Experimental investigation of an advanced static VAr compensator", IEE Proccedings Vol 142, No2, 1995, pp203-209.
7. Gyugyi, L., "Unified Power-flow Control Concept for Flexible AC Transmission Systems", IEE Proceedings, Vol. 139. No. 4, July, 1992, pp 323-331.
8. Gyugyi, L. "Reactive power Generation and Control by Thyristor Circuits", IEEE Trans. Ind. Appl. 1979, pp A1-A15.
9. Liu Y, "Modelling and control of unified power flow controller for reinforcement of transmission systems", PhD thesis, Brunel University, 1997.
10. J Y Liu, Y H Song, A M Foss "Digital studies and simulation of the PWM UPFC using EMTP", Proceedings of the sixth IEE AC/DC International Conference ,IEE, London,1996, pp 351-356.
11. J Y Liu, Y H Song, A M Foss "Analysis and digital simulation of the unified power flow controller", APSCOM, Hong Kong,1995, pp 311-316.

12. Martinez J.A and Capolino G.A "Simulation of power electronics using the EMTP. Part I: Power converters. A survey", UPEC'94, September 14-16, 1994, Galway.

13. Joncquel E, Lombard X, "A unified power flow controller model for the electromagnetic transients program" , EPE 1995, pp 2.173-2.178.

14. Bakhsai A.R, Joos G, Jin H., "EMTP simulation of multi-pulse unified power flow controllers", IEEE Power Apparatus on Systems, 1996, pp 847-852.

15. B.Ooi, X.Wang, "Voltage Angle Lock Loop Control of the Boost Type PWM Converter for HVDC Application", IEEE Transactions on Power Electronics, Vol 5, No2, April 1990, pp 229-235.

16. L.Gyugyi, C.D.Schauder, S.L. Williams, T.R. Rietman, D.R. Torgerson, A. Eldis, "The Unified Power Flow Controller: A New Approach To Power Transmission Control", IEEE Transactions on Power Devivery, Vol 10, No.2 , April 1995, pp 1085-1097.

17. C.Schauder, H.Mehta, "Vector analysis and control of advanced static VAR compensators", IEE Proceedings, Vol.140, No.4 July 1993, pp 299-306.

18. L.Gyugyi, "Dynamic Compensation of AC Transmission Lines by Solid-State Synchronous Voltage Sources", IEEE Transactions on Power Delivery, Vol 9, No.2 April 1994, pp 904-911.

19. L.Gyugyi, "Unified power flow control concept for flexible AC transmission systems", IEE Proceedings Vol.139, No 4, July 1992, pp 323-331.

20. EMTP Rule Book, EPRI/DCG, version 1, 1987.

21. J.Ekanayake, "An investigation of an Advanced Static Var Compensator", PhD thesis, UMIST 1995.

22. Mohan N,Underland T, Robbins W ,"Power electronics: Converters, Applications and Design", John Wiley and Sons 1995.

CHAPTER 9

CUSTOM POWER TECHNOLOGY: CIRCUITRY AND CONTROL FOR MODELLING A SOLID STATE SWITCH WITHIN DISTRIBUTION SYSTEMS

9.1 Introduction

Power disturbances, which can cause electrical "pollution" over a large section, increase the cost in critical customer equipment. However, a new generation of power electronic devices is becoming available for use on distribution systems, which will enable utilities to provide premium-quality electricity to customers with sensitive loads. This technology is commonly referred to as Custom power [1-6] .

This chapter begins with a general description of this new family of devices for distribution systems. The three main Custom power devices, the Dynamic Voltage Restorer(DVR), the Distribution Static Condenser(D-STATCON) and the solid state switch are presented. Three devices based on the solid state switch are also reported, followed by their design specifications and the individual rating and application requirements. A control strategy is presented in order to assist power system engineers in the applications of devices based on the solid state switch in distribution systems.

9.2 Custom power technologies optimise distribution services

The term Custom Power describes the value-added power that electric utilities and other service providers will offer their customers in the future. The improved level of reliability of this power, in terms of reduced interruptions and less variations, will lead to a solution of which the prominent feature will be the application of power electronic controllers to utility distribution systems.

Flexible AC Transmission systems and Custom Power have been developed to serve the transmission and the distribution systems respectively. Despite having a common technology base in power electronics, they serve different purposes and have different economical justifications[1,2].

Industrial and commercial customers are adding computer controlled and microprocessor-based equipment for automated control. Although these devices enhance the productivity of the customers, they are not without their own set of unique requirements. One of these requirements is the need for high quality power containing minimum voltage variations. The performance of such customer equipment can be adversely affected by

1) Line voltage sags and swells
2) momentary interruptions
3) transients and harmonic distortion.

Transients, harmonics and momentary interruptions have grown in recent years and electric utilities are faced with resolving these complaints and correcting the problems.

About 90% of outages affecting customers originate on the utility distribution system and are due to causes such as lightning and line faults[1].

In today's globally competitive markets, businesses are less willing to tolerate production loss and defects caused by power supply problems. The incidence of brief outages will play a pivotal role in relations between a utility and its customers.

Up until now, many customers with sensitive loads have installed their own uninterruptible power supply (UPS) to provide "ride through" capability[4]. Commercial users of computer equipment have installed UPS to keep computer systems operating for short interruptions or allow for an orderly shut-down in the case of blackout. But these battery dependent devices bring problems of their own. They are often expensive and energy inefficient, and they require maintenance that may exceed the owner's resources. Installing a UPS may also be difficult on some customer premises because of severe space constraints or changing facility requirements. From the above discussion it is clear that customer-side solutions are not always the best or the most economical method to remedy failures in power supply reliability. Uninterruptible power supply units and mechanically switched feeder transfers installed and operated by customers are costly and inefficient. In capital costs alone they result in energy losses as high as 20 percent in some instances.

One solution lies with the development of a new family of power electronic devices, called Custom power, capable of high voltage and current applications, suitable for operation in distribution and industrial environments, typically at the 11kV voltage level. This technology has become available due to the recent developments in the semiconductor industry, particularly the introduction of the Gate Turn Off (GTO) Thyristor, the Insulated gate Bipolar Transistor (IGBT) and the MOS controlled Thyristor (MCT). These devices have suitable characteristics for switching applications, namely high voltage and current capacity up to 5kV at 4kA and high frequency switching capability up to 10kHz. The important point, is the rapid advancements in device development, which suggests that, in the near future, present ratings will be improved significantly.

9.3 Main Custom Power devices

a) Dynamic Voltage Restorer (DVR)

A Custom Power device now entering utility service is the Dynamic Voltage Restorer (DVR), a solid-state controller that protects a critical load from power line disturbances. Connected in series with the primary distribution feeder providing power to a sensitive load, it compensates for momentary voltage sags, swells, transients, and harmonics by exchanging real and reactive power with the line.

A DVR consists of a dc-ac power inverter based on insulated gate bipolar transistor (IGBT) technology, which is connected in series to a distribution line through a set of three single-phase injection transformers. When a voltage disturbance occurs on the incoming distribution feeder, the DVR restores the quality of the voltage waveform to the load by injecting a voltage into the feeder that compensates for the problem.

The dc side of the inverter is connected to a dc link that provides a regulated dc voltage source, which the IGBT switches convert into a synchronous ac voltage of controllable amplitude, phase angle, and frequency.

A complete DVR model with its associated controls will be presented in chapter 10.

b) Distribution Static Condenser (D-STATCON)

A technology that provides a function complementary to that of the DVR is the distribution static condenser (D-STATCON), which protects the distribution system from power "pollution" caused by the disturbing effects of certain customer loads. In a typical application, it would be placed between the feeder and a heavy, fluctuating load, whose operation would otherwise produce voltage sages, swells, and harmonics that could adversely affect other customers power quality. The D-STATCON can also be used with a solid-state breaker and an energy storage subsystem to support the downstream load during the operation of a feeder breaker or another upstream power interruption.

Like the DVR, the D-STATCON consists of an IGBT-based dc-ac power inverter. In contranst to the DVR, however, the D-STATCON is connected in shunt (rather than in series) to a distribution feeder through a coupling transformer that matches the inverter ac output voltage to the distribution system voltage. In this configuration, the D-STATCON exchanges only reactive power with the line and provides voltage regulation and power factor correction to the load by injecting current that is in quadrature with the distribution feeder voltage. If any energy storage subsystem is added, the D-STATCON can also supply real power to the load once the solid-state breaker has disconnected the load from the feeder during an upstream power disturbance. Harmonic currents required by nonlinear loads can also be provided by the D-STATCON.

c) Solid state switch

Circuit breaking is a relatively new application for solid state technology although thyristors have been employed for many years in HVDC transmission and motor drive applications.

A major device in the Custom Power Product family is the Solid State Switch[3,7,8]. Advanced current interruption technology utilising high power solid state switches offers a viable solution to most of the distribution problems that result in voltage sags, swells and power outages. Solid state fast acting (sub-cycle) breakers can instantaneously interrupt the current flow when a fault takes place in a feeder. They can also transfer sensitive loads from a normal supply that experiences a disturbance to an alternative supply that is unaffected by the disturbance. In this application the solid state switch acts as an extremely fast conventional transfer switch that allows restoration of power of specific quality to the load in ¼ cycle.

Sometimes the solid-state switch is combined with a current limiting reactor. In this case the solid state switch can rapidly insert the current limiting device into the distribution line to prevent excessive fault current from developing from sources of high short circuit capacity.

Optional configurations for the solid-state switch include current limiting, transfer switch and fault conducting capabilities.

The remainder of this chapter concentrates on the development of a solid-state switching device.

9.4 Applications of the solid state switching devices

Typical substation configurations will be used to illustrate the potential applications of the solid-state switch. Figure 9.1 shows the possible locations for a solid state switch for application within in distribution systems. A solid-state circuit breaker will interrupt a fault very quickly in less than ½ cycle and also provide a controlled path for the fault current. A solid-state transfer switch will select between two sources and provide the best available power downstream. A Current limiting interrupting switch would not only limit but would completely interrupt the current flowing through the tie, and would not have to coordinate directly with downstream or upstream circuit breakers. A solid state breaker must coordinate with the upstream or downstream protection devices. The capability of the solid state switch in terms of protection performance depends on the current and voltage ratings of its semiconductor devices. Commercially available GTOs (Gate Turn Off Thyristors)and SCRs (Silicon Controlled Rectifiers) can be used for this purpose.

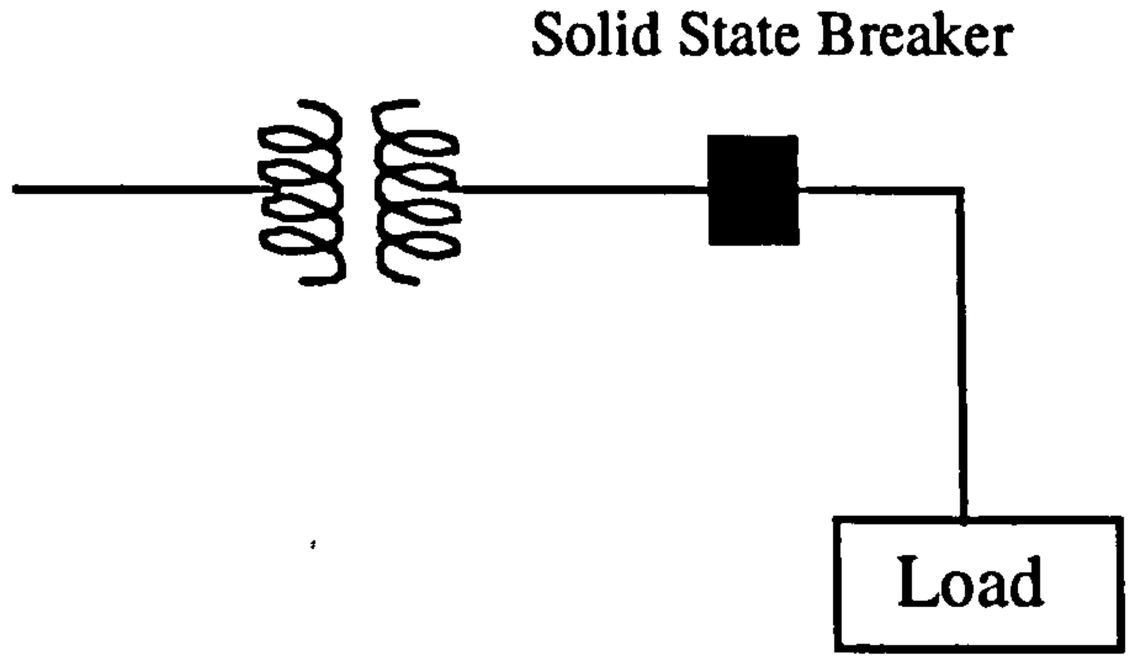

(a)

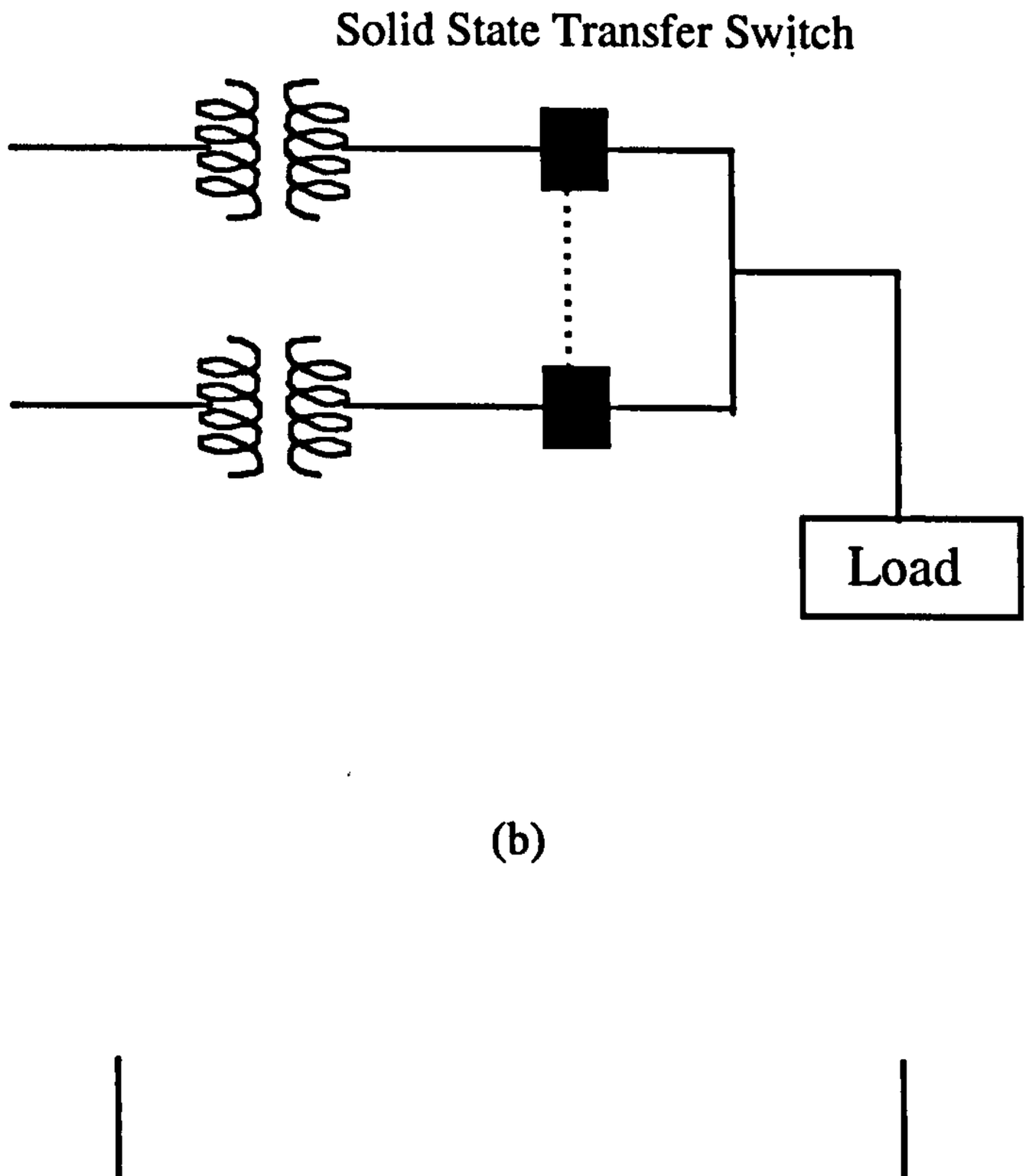

Figure 9.1 Solid State Switching devices

9.5 Design of solid state switches

The main characteristic of GTO devices is that they can interrupt current immediately by the application of an appropriate gate control signal. The maximum current that can be interrupted by a GTO is 3kA . The voltage rating for the GTO is 4.5kV. However due to the more complex internal structure of the GTOs (compared to the SCRs) they cannot handle very high surge currents that occur during system faults. Therefore the only operating mode allowed for the GTO breaker is the instantaneous interruption of a detected overcurrent.

The advantage of SCR devices compared to GTOs of the same size is that they can handle considerably higher surge currents[7]. They are also available commercially with higher nominal current rating and lower conduction losses. These losses are almost half of the GTO's at 600A. It is possible to maintain 15 kA fault current for 15 cycles using SCRs breakers. Paralleling SCR switches is possible with minimum increase of circuit complexity if higher fault current capabilities are required.

The disadvantage of SCR breakers is their inability to interrupt current on demand. SCR breakers open when the current amplitude drops to a near zero level[7].

A simplified arrangement for the solid state breaker is shown in Figure 9.2. It consists of 3 parallel connected branches: a branch composed of GTO thyristors, a branch composed of SCRs in series with a current limiting reactor and a zinc oxide arrester.

Under normal load conditions, the GTOs are gated continuously and maintain full conduction. The GTOs are rated for maximum normal line current, but not rated for fault currents. When a fault occurs on the load side of the SSB (Solid State Breaker), a control circuit is activated by the instantaneous magnitude and/or rate-of-rise of current which results in a turn-off of the GTOs. The GTOs respond within a few microseconds of the control signal being applied and are capable of turning off current considerably higher in magnitude than the maximum continuous current. In this way the fault current is quickly limited before it reaches a destructive level. In

order to achieve the voltage required for application to the utility systems, a number of GTO modules are required connected in series within the SSB. After the turning off of the GTOs , the SCRs thyristors are activated. The SCR switch is normally open and has no continuous current rating. Its function is to conduct fault current to facilitate the operation of conventional protective devices on the load side of the SSB. For this purpose it is rated for short duration fault surge currents[8]. The current limiting reactor will ensure that the fault current in the system is kept as low as practically possible in order to limit the required surge current rating of the thyristor based switch and also to minimise stresses on the distribution system. The zinc oxide arrester is used in order to provide a limit for the voltage across the semiconductor devices. If the fault current in the SCR switches remains for too long, then a control signal de-activates these switches and thus no more current flows in the SSB. In this case the switch connected in series with the 3 parallel connected branches transits to the open state .

Figure 9.3 shows a simplified scheme for the solid state transfer switch. The solid state transfer switch (SSTS) selects between two or more sources of power and provides the best available power to the electrical load downstream. The SSTS is a solid state switch based on the SCR device. The SCR operates in two modes:

1. ON-state: forward conduction, low impedance; or
2. OFF-state: open circuit; almost infinite impedance.

The basic ON-state and OFF-state properties of the SCR are used to form an intelligent switch which can choose between two upstream power sources and provide the best available power to the electrical load downstream. The basic configuration is that of back-to-back SCRs on the preferred and alternate sides of the switch. An SCR allows conduction only in the forward direction.
During normal operation, all SCRs associated with the preferred source are in the ON-state, while those associated with the alternate source are in the OFF-state.

Current sensing circuits constantly monitor the states of the preferred and alternate sources and feed the information to a supervisory microprocessor controller. Upon sensing the loss of the preferred source, the microprocessor controller forces the gate-driven SCRs on the alternate side to turn ON. The transfer from the preferred to the alternate source is very fast (less than ¼ electrical cycle).

Figure 9.4 illustrates a simplified scheme for the Current limiting interrupting switch(CLIS). When a fault occurs on the load side of the CLIS, a control signal initiates the turn-off, the GTOs current is diverted into the snubber capacitor, which limits the rate of rise of voltage across the valve until it reaches the clamping level established by the zinc oxide arrester. Then the CLIS completely interrupts the current flow. When the fault is cleared the GTOs can be turned back on at an instant when the voltage across them is close to zero. An isolating switch is included as part of the CLIS to provide the necessary isolation when the CLIS is open. This switch is operated automatically by the CLIS controller.

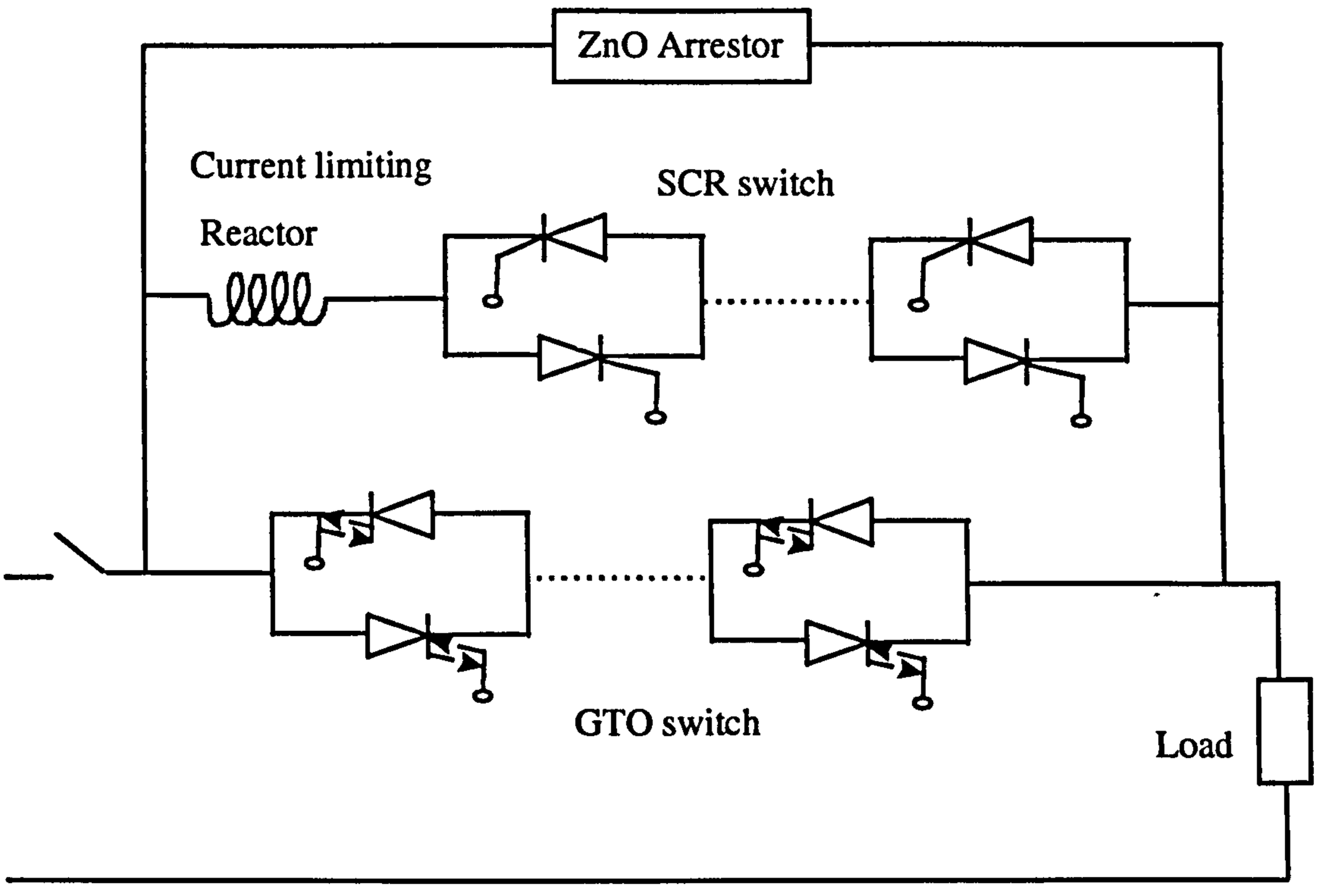

Figure 9.2. SSB circuit configuration

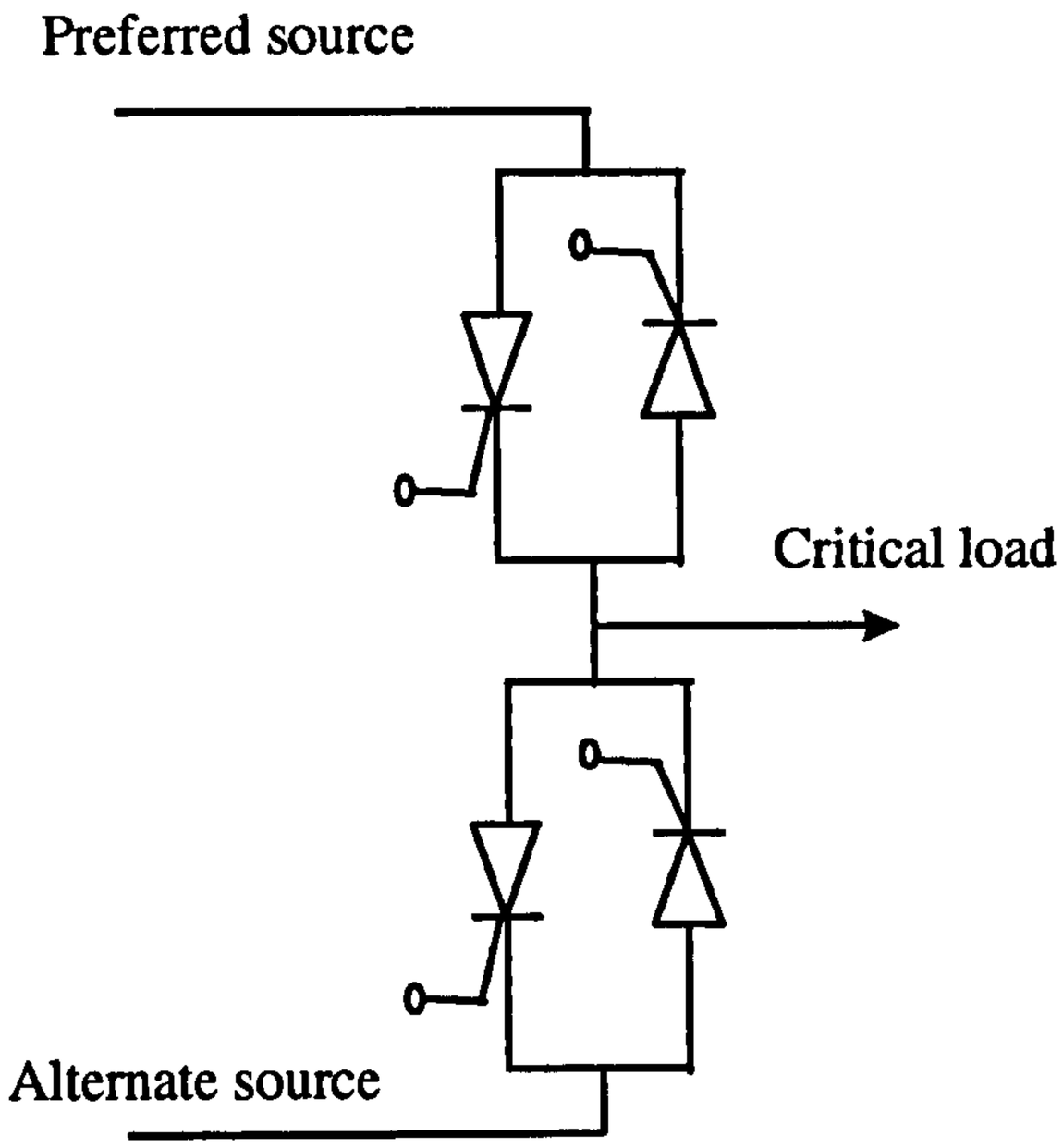

Figure 9.3. SSTS circuit configuration

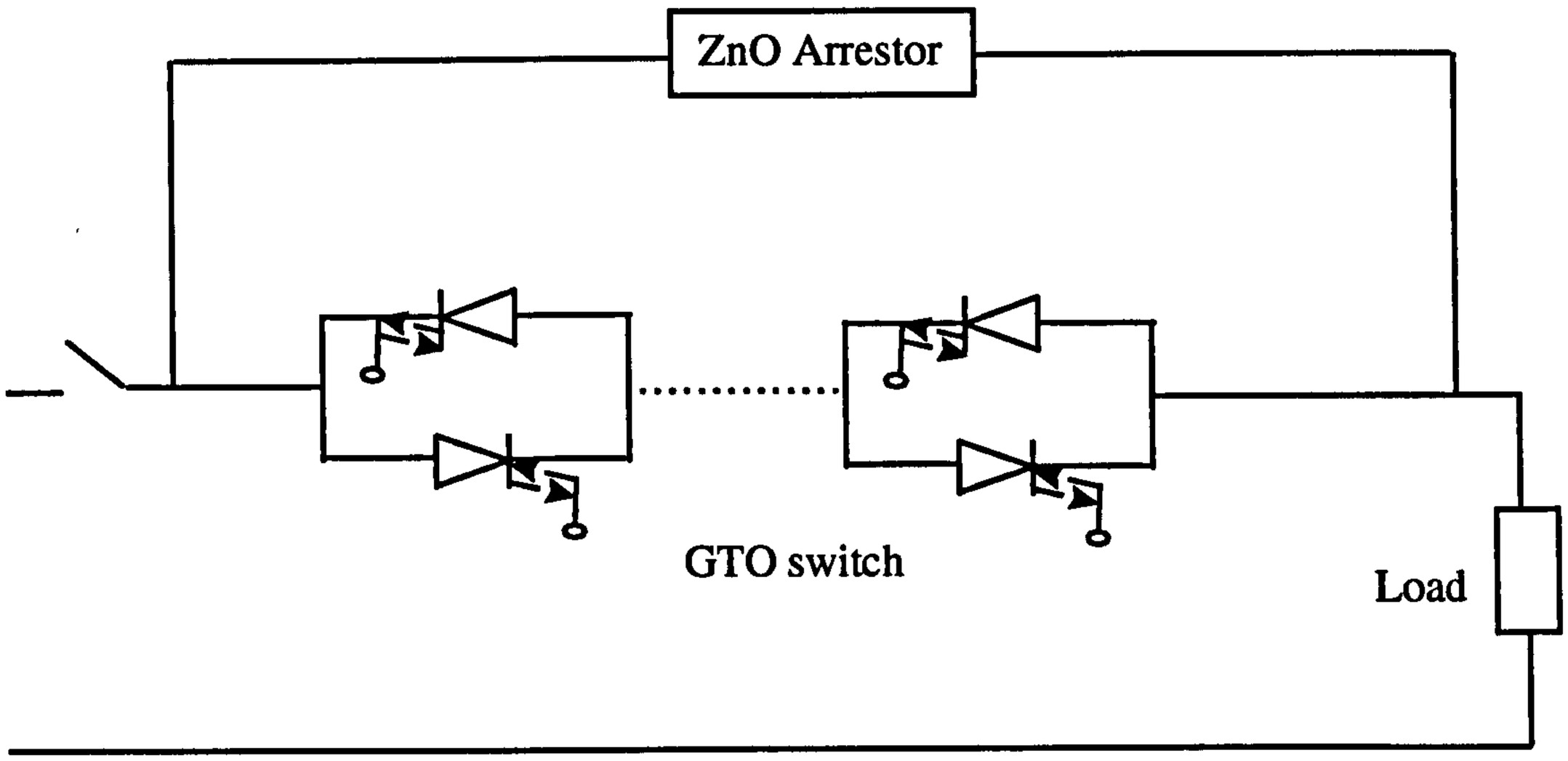

Figure 9.4. CLIS circuit configuration

9.6 Solid state switch rating requirements

Any SSB, SSTS or CLIS has to be designed safely to carry the highest continuous current that will flow under normal circumstances. In order for the switches to carry the current, GTOs and SCRs with an appropriate rms rating have to be used.

The GTO cannot be placed in a situation where it would be subjected to a fault current for a duration more than one cycle. The GTOs would have to switch off any overload or fault current before it reaches their maximum turn-off limits. For most of the cases the SCRs are able to conduct fault currents (full or limited) for a period of time (10 to 15 cycles), repeatedly (3 to 4 times, consistent with the fault clearing sequences of existing distribution reclosers), in order to maintain coordination with conventional protection equipment in the system.

9.7 Applications of solid state switching devices

For the SSB, the current interrupting device must limit the fault current in order to maintain co-ordination with the downstream protection devices. For the solid state transfer switch, because of the very small time delay in the current transfer (almost ¼ cycle) there is usually no need for co-ordination with other protection devices. For the CLIS, interruption of the bus-tie fault current takes place in less than one half of a cycle, therefore it can not be co-ordinated with any downstream device[7,8].

9.8 Design specifications for solid state switches

A SSB must meet the following requirements:

a) Limit the system short circuit current so that it does not exceed the momentary or interrupting rating of the downstream protection controlled devices, such as circuit breakers and automatic reclosers.
b) Maintain the limited fault current for an acceptable number of operations without interruption, until the fault is cleared by a downstream device.

c) Reset automatically after the fault is cleared by a downstream device.

d) Limit transient voltages to the same level as permitted by other protective system components, such as circuit breakers or reclosers

A SSTS must meet the following requirements:

a) Transfer the current in less than ½ cycle;

b) Reset only when the faulted bus goes healthy;

c) Be able to choose between two unhealthy sources in less than ½ cycle

A CLIS must meet the following requirements

a) Interrupt the current in less than ½ cycle;

b) Reset only when both buses are healthy;

c) Include isolate switch to open when the CLIS is tripped to open.

9.9 Control functions of the solid state switches[7,8,9]

A generic control system for the three different types of solid state switches is illustrated in figure 9.5. In order to control any of the solid state switches , instantaneous parameters, obtained from the distribution system are compared with external commands (which are reference signals for either normal or abnormal conditions). The output signal goes to either the GTOs or the SCRs thyristors which subsequently interrupt or restore the current flow in the distribution line.

For the SSB the control strategy includes the following steps:

1. Detect the rms phase current, and the rate-of-rise of the current ($^{di}/_{dt}$), under normal circumstances (steady state conditions).
2. If there is any change from the steady state conditions, then the GTOs are turned off, and the SCRs are turned on.

3. If the fault is cleared in less than 15 cycles, then the SCRs are turned off and the GTOs are turned on.
4. If the fault remains then the SCRs are switched to open.
5. After the fault is cleared by the downstream protection devices then the GTOs are turned on.

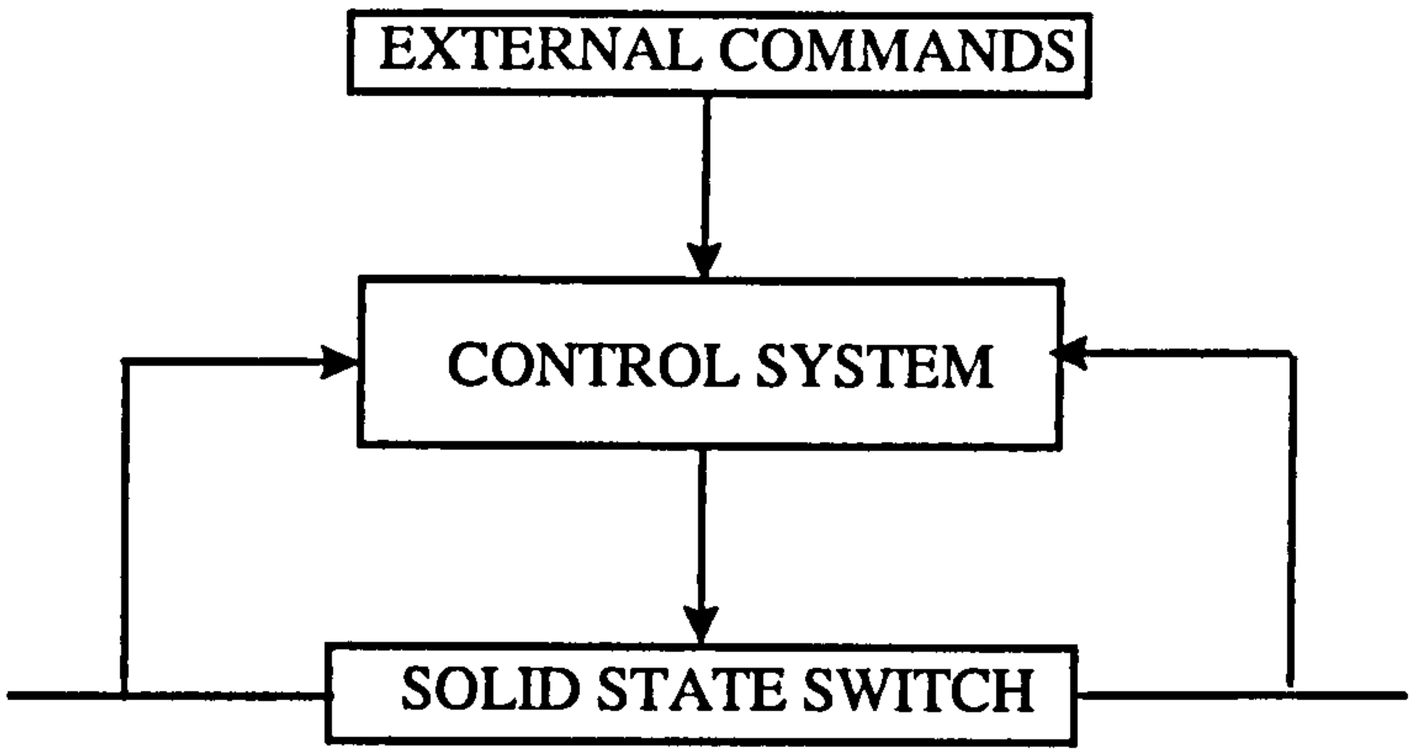

Figure 9.5

For the SSTS the control strategy includes the following steps:

1. Detect the rms phase current, the rate-of-rise in the current $^{di}/_{dt}$, the rms voltage magnitude and the rate of rise in the voltage $^{dv}/_{dt}$,under normal events (steady state conditions), from the preferred source.
2. If both feeders are "unhealthy" then use as preferred source the feeder that has its parameters closest to those described by 1.
3. If there is any change from the events described by 1, then the SCRs from the preferred source are turned off, and the SCRs from the alternative source are turned on.

4. After a period of time if the detected signals in the preferred source are the same with these in step 1 the SCRs at the preferred source are turned on and the SCRs at the alternate source are turned off.

For the CLIS the control strategy includes the following steps:

1. Detect the rms phase current, and the rate-of-rise in the current $^{di}/_{dt}$, under normal circumstances (steady state conditions).
2. If there is any change from the steady state conditions, then the GTOs are turned off.
3. After the fault is cleared by the downstream protection devices then the GTOs are turned on.

The control strategy for each of the solid-state switching devices may also include other parameters such as limitation of transient voltages, overload current ratings, minimum and maximum interrupting current, zinc oxide clamping voltage and other functions.

9.10 Conclusions

As more sensitive equipment is employed in industrial, commercial and domestic situations, greater attention is being paid to the topic of power quality. New technology, such as the DVR, the D-STATCON and the solid state switch, will provide many new possibilities for both plant protection and improved operation of existing systems. In this chapter a study of the three main types of solid state switches has been performed, including rating requirements and potential applications. A control strategy has been described for the applications of these solid state switching devices to distribution systems.

9.11 References

1. Hingorani N, "Introducing custom power", IEEE Spectrum, June 1995, pp 41-48.
2. Douglas J, "Custom power :Optimising distribution services", EPRI Journal, June 1996, pp 1-6.
3. Reason J. "Speed alone won't solve power-quality problems", Electrical World, August 1996, pp 19-25.
4. Taylor G "Power quality hardware solutions for distribution systems: Custom power", American power conference, pp 11/1-11/7.
5. Osborne MM, Kitchin RH, Ryan HM, "Emergence of custom power technology in distribution systems", Proceedings of the Universities Power Engineering Conference, 1995, Vol 2, pp 777-780.
6. Mohapatra GR, Zayegh A, Kalam A, Coulter RJ, "Energy sources, energy storage and power electronic devices", Proceedings of the Universities Power Engineering Conference 1996, Vol 1 ,pp 155-158.
7. Smith R.K., Slade P.G., Sarkozi M., Stacey E.J., Bonk J.J., Mehta H., "Solid state distribution current limiter and circuit breaker: application requirements and control strategies", IEEE Transactions on Power Delivery, Vol 8, No.3, July 1993, pp 1155-1164.
8. Woodley N, Sarkozi M, Lopez F, Tahiliani V, Malkin P, "Solid-state 13-Kv distribution class circuit breaker: planning, development and demonstration", IEE Conference Publication 1994, pp 163-167.
9. Hughes K, "High-power solid-state switch test facility: Applications and capabilities", IEEE Proceedings 1993, pp1305-1311.

CHAPTER 10

MODELLING, SIMULATION AND DESIGN OF A DYNAMIC VOLTAGE RESTORER MODEL (DVR) FOR DISTRIBUTION SYSTEM ARCHITECTURES

10.1 Introduction

Economic pressures on industry to automate processes and improve efficiencies have resulted in a steady increase in the number and size of loads that are not tolerant of voltage sags. Since sags are the most common form of disruption (6 to 10 times more common than interruptions[1]), this problem demands a solution. One initiative to address this issue is the development of the Dynamic Voltage Restorer (DVR)[2-8].

The DVR uses a power electronic inverter to inject voltage in series with the source to supplement the source voltage during voltage sags. Power can be transferred from high-voltage phases to low-voltage phases during unbalanced faults. Short time energy storage can be used to provide the supplemental energy needed to keep load voltage at acceptable levels.

Sags can originate from faults at the local distribution system or in the transmission system. Studies [5-8] have shown that transmission faults, while relatively rare can cause widespread sags that may constitute a major source of process interruptions for very long distances from the faulted point. Distribution faults are considerably more

common but the resulting sags are more limited in geographic extent. The DVR can correct sags resulting from faults in either the transmission or the distribution system. Analysis [8] indicates that deep voltage sags, even of relatively short duration, can have significant costs because of the proliferation of voltage-sensitive computer-based and variable speed drive loads. The fraction of load that is sensitive to low voltage is expected to grow rapidly in the coming decades.

This chapter presents modelling and simulation work with respect to the Dynamic Voltage Restorer for use within distribution systems. It begins with a general description and the operating principles of the DVR, followed by an economic consideration and a cost estimation of this custom power device. Previous literature work related to the DVR is also reported, and an innovative control system useful for the design of a Dynamic Voltage Restorer model for distribution system architectures is presented. This design method can assist power system planners and engineers for applications of these devices in power systems. The simulation results at the end of the chapter of open and closed loop control using a real distribution system network for different system disturbances, are in accordance with the theory. Validation of the proposed controller was also taken by comparing simulation results of the modelling method described in this chapter and results from previous performance tests presented in [11] for actual system scenarios.

10.2 Operating principles of a DVR

Figure 10.1 shows a block diagram of the DVR power circuit. When examining the DVR it can divided into 4 component blocks, these being:

1) Energy storage device
2) DC to DC Power controller
3) A three phase voltage converter
4) Three single phase series injection transformers

The design of the DVR allows real and reactive power to be either supplied or absorbed when operating. If a small fault occurs on the protected system then the DVR can correct it using only reactive power generated internally[5].

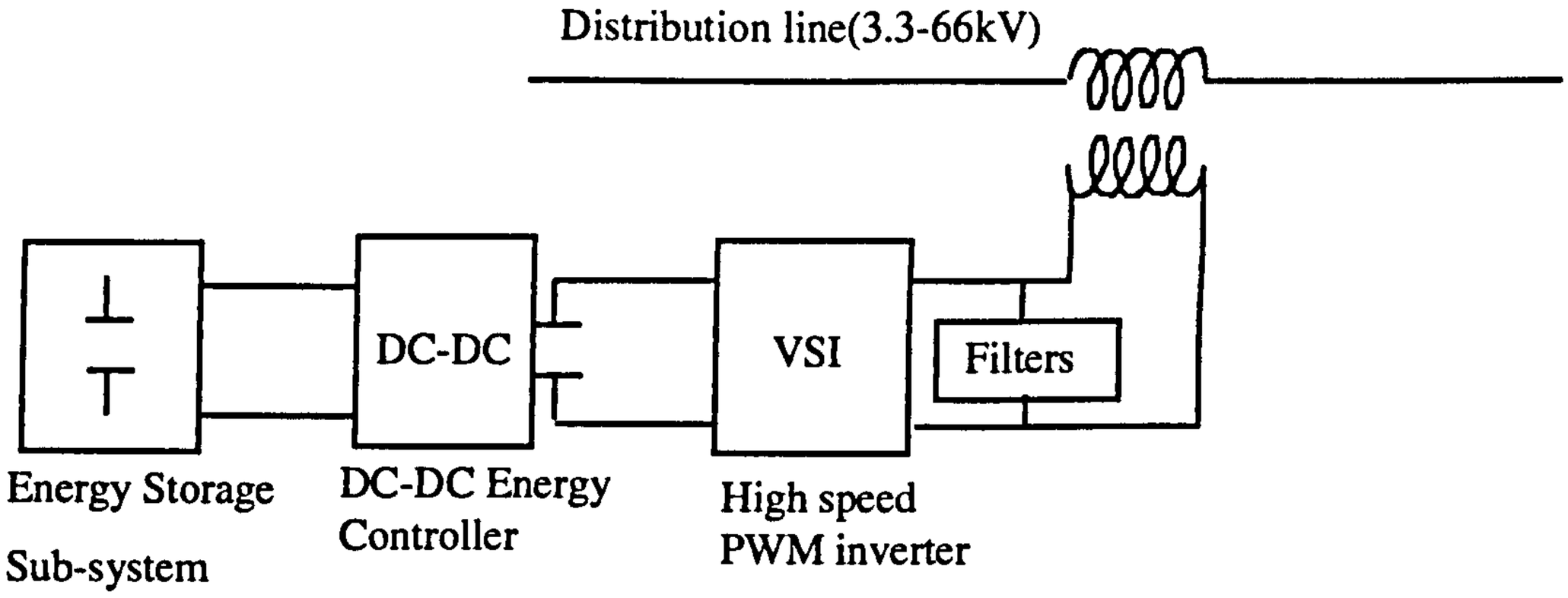

Figure 10.1

For correction of larger faults the DVR may be required to develop real power. To enable the development of real power an energy storage device must be used, presently the DVR design uses a capacitor bank. Once the fault has been corrected and the supply is operating under normal conditions the DVR replenishes the energy expended from the healthy system. The rating (in terms of energy storage capabilities) of the capacitor bank is dependent upon system factors such as the rating of the load and the duration and depth of anticipated sags. When correcting a large sag (using real power), the power electronics are fed from the capacitor bank via a DC-DC voltage conversion circuit.

The core element in the DVR design is the three phase voltage converter. This inverter utilises solid-state power electronics (Insulated Gate Bipolar Transistors, IGBTs) to convert DC to AC and back again during operation. The DVR connects in series with the distribution line through an injection transformer, actually three single-phase transformers. The primary side (connected into the line) must be sized to carry the full line current. The primary voltage rating is the maximum voltage the DVR can inject into the line for a given application. The DVR rating (per phase), is the maximum injection voltage times the primary current. The bridge outputs on the

secondary are filtered before being applied to the injection transformer. The bridges are independently controllable to allow each phase to be compensated separately. The output voltage wave shapes are generated by pulse-width modulated switching.

For the system in figure 10.1 the power supplied by the DVR, P_{DVR} is the difference between the total power supplied to the load and the power supplied by the source.

It is not necessary for the load voltage to be exactly in phase with the source voltage, the load voltage vector can be at any point on its locus of amplitude. This is shown below in figure 10.2

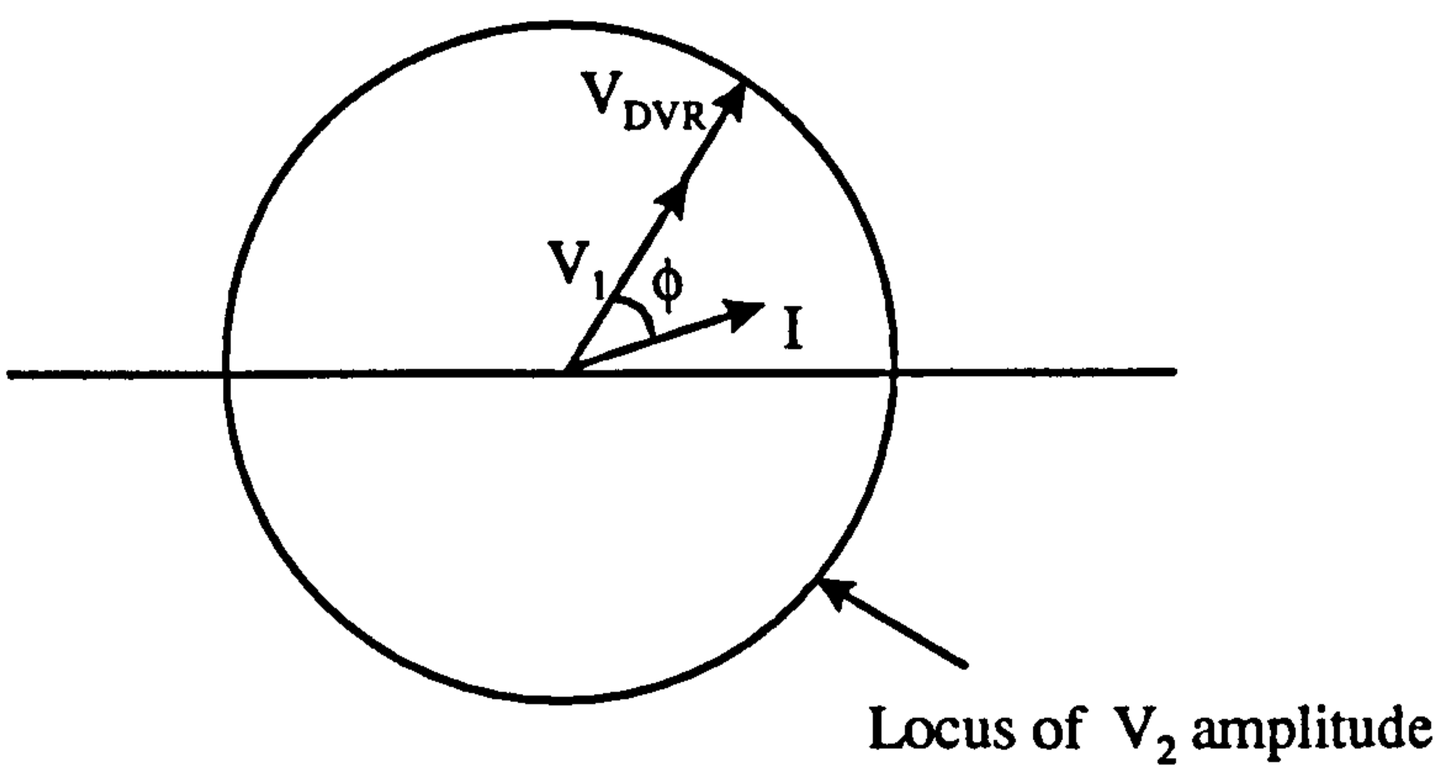

Figure 10.2 Vector diagram for real power compensation

The three phase power from the source entering the DVR, P_{in} and the power leaving the DVR to the load, P_{out} are derived from the following. V_1 is the source voltage (V_S), V_2 is the load voltage (V_L) and α the angle between them, phase currents are assumed equal (Figure 10.4).

$$P_{in} = V_{1A}I\cos(\varphi-\alpha) + V_{1B}I\cos(\varphi-\alpha) + V_{1C}I\cos(\varphi-\alpha) \qquad (10.1)$$

$$P_{out} = V_{2A}I\cos\varphi + V_{2B}I\cos\varphi + V_{2C}I\cos\varphi \qquad (10.2)$$

The difference between output and input power ΔP, is supplied by the energy storage system. To compensate the sag using zero energy requires $\Delta P = 0$. Since the three output voltages will be equal, the subscripts for V_2 can be dropped.

$$\Delta P = P_{OUT} - P_{IN} = 3V_2 I\cos\varphi - (V_{1A} + V_{1B} + V_{1C})I\cos(\varphi - \alpha) = 0 \quad (10.3)$$

$$\alpha = \varphi - \arccos\frac{3V_2\cos\varphi}{V_{1A} + V_{1B} + V_{1C}} \quad (10.4)$$

With the above equations it can be shown for a balanced three phase sag where $V_{1A} = V_{1B} = V_{1C} = V_1$ the minimum voltage which can be corrected using zero energy is given by:

$$V_1 = V_2\cos\varphi \quad (10.5)$$

And where a sag occurs on only one phase (A), $V_{1B} = V_{1C} = V_1$ the limit is given by

$$V_{1A} = 3V_2\cos\varphi - 2V_1 \quad (10.6)$$

Typically there is a phase difference between the source and load voltages, therefore the injected voltage from the DVR must increase over the point where the source and load voltages are in phase.

Below the vector diagram illustrates the DVR correcting a balanced three phase sag using zero energy. The amplitude of the V_{DVR} has increased over that shown in figure 10.2, and the DVR acts as a linear capacitor in series with the load.

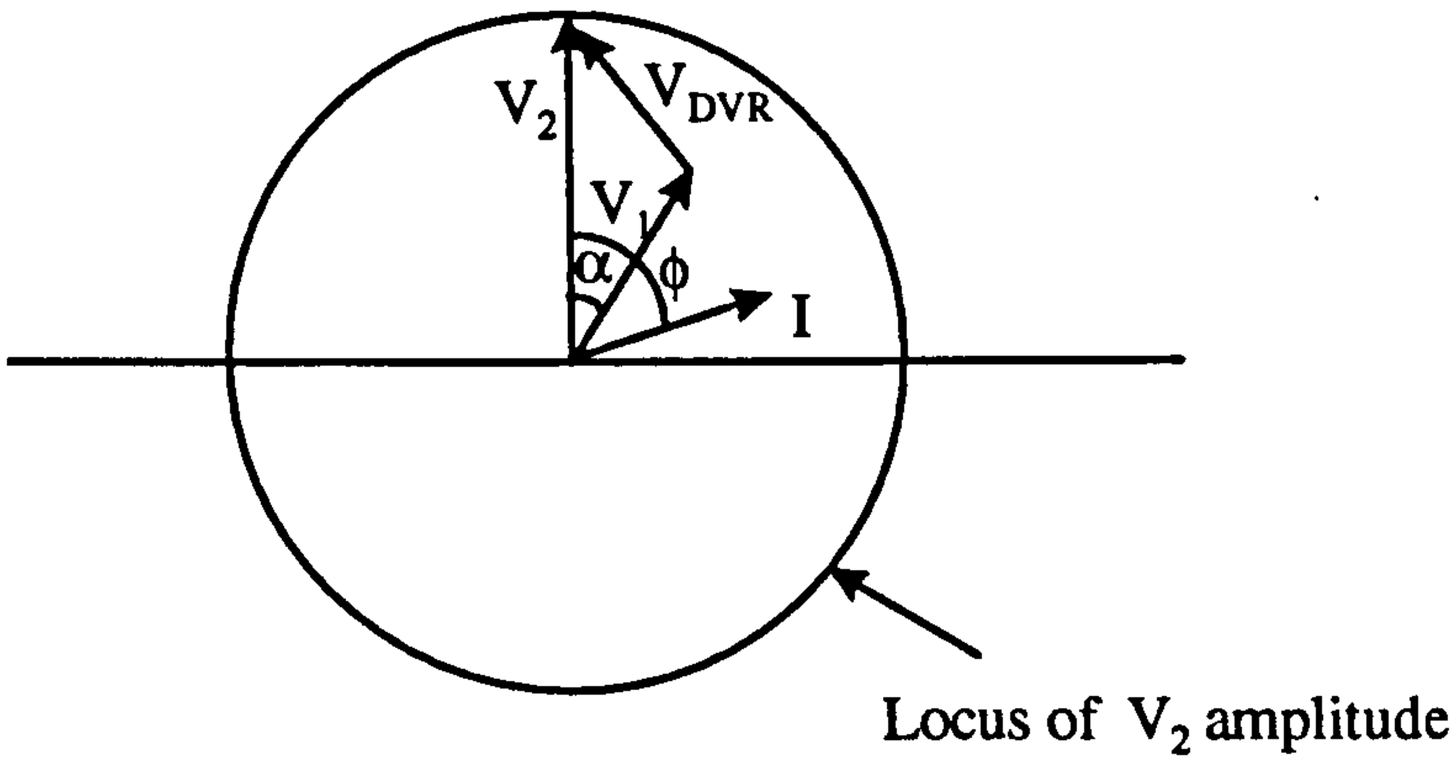

Figure 10.3 Vector Diagram for reactive power compensation

When a voltage sag reaches a value below the limit for correction using zero energy, the energy storage system within the DVR has to be used to aid voltage correction.

The analysis below uses the following nomenclature:

- Source voltages are given by subscript S.
- Load voltages are given by subscript L.
- DVR injected voltages are given by subscript D.
- The red, yellow and blue phases are given by the subscripts R, Y and B.

The phase voltage definition is derived from the load voltage:

$$V_{LR} = \sqrt{2}\left|V_{LR} \sin \omega t\right| \tag{10.7}$$

Load current in the red phase $I_R = \sqrt{2}\frac{\left|V_{LR}\right|}{Z}\sin(\omega t - \varphi)$ (10.8)

where $\cos\varphi$ is the power factor of the load.

The active power P, is the average of the instantaneous power over one cycle, the active power to the load in the red phase is:

$$P_{LR} = \frac{\left|V_{LR}\right|^2}{Z}\cos\varphi \tag{10.9}$$

The source voltage is defined as :

$$V_{SR} = \sqrt{2}\left|V_{SR}\right|\sin(\omega t - \alpha) \tag{10.10}$$

where α is the phase difference between source and load voltages.

The active power drawn from the source is :

$$P_{SR} = \frac{\left|V_{SR}\right|\left|V_{LR}\right|}{Z}\cos(\varphi - \alpha) \tag{10.11}$$

The active power out of the DVR is the difference between the active power drawn from the load and the active power supplied by the source.

$$P_D = \frac{1}{Z}(|V_{LR}|^2 + |V_{LY}|^2 + |V_{LB}|^2)\cos\varphi - (|V_{SR}||V_{LR}| + |V_{SY}||V_{LY}| + |V_{SB}||V_{LB}|)\cos(\varphi - \alpha) \quad (10.12)$$

If it is possible to compensate the voltage sag using zero energy then $P_D = 0$, hence:

$$\alpha = \varphi - \cos^{-1}\frac{(|V_{LR}|^2 + |V_{LY}|^2 + |V_{LB}|^2)\cos\varphi}{(|V_{SR}||V_{LR}| + |V_{SY}||V_{LY}| + |V_{SB}||V_{LB}|)} \quad (10.13)$$

When it becomes necessary to draw energy from the storage system (the term to the right is greater than unity), from equation 10.11, $\alpha = \varphi$ to give maximum possible active power.

The injection voltage of the DVR is the difference between the source and the load voltages, thus for the red phase

$$V_{DR} = V_{LR} - V_{SR} \quad (10.14)$$

giving $V_{DR} = \sqrt{2}|V_{LR}|\sin\omega t - \sqrt{2}|V_{SR}|\sin(\omega t - \alpha)$ using

$\sin(A \pm B) = \sin A\cos B \pm \cos A\sin B$ we can arrive at:

$$V_{DR} = \sqrt{2}(|V_{LR}| - |V_{SR}|\cos\alpha)\sin\omega t + \sqrt{2}|V_{SR}|\sin\alpha\cos\omega t \quad (10.15)$$

Similar equations can be derived for yellow and blue phases.

Equation 10.15 can be further defined as:

$$V_{DR} = |V_{DR}|\sin(\omega t - \beta) \quad (10.16)$$

Assuming β to be the phase angle of the modulus of the injected voltage. Comparing 10.15 and 10.16 the following are derived :

$|V_{DR}|\sin(\omega t-\beta)=\sqrt{2}|V_{LR}|\sin\omega t-\sqrt{2}|V_{SR}|\sin(\omega t-\alpha)$, giving:

$|V_{DR}|^2=(|V_{LR}|-|V_{SR}|\cos\alpha)^2+(|V_{SR}|\sin\alpha)^2$ or

$|V_{DR}|^2=|V_{LR}|^2+|V_{SR}|^2-2|V_{LR}||V_{SR}|\cos\alpha+(|V_{SR}|\sin\alpha)^2$ (10.17) and also:

$$\beta=\tan^{-1}\frac{|V_{SR}|\sin\alpha}{|V_{LR}|-|V_{SR}|\cos\alpha} \qquad (10.18)$$

Figure 10.5 is used to explain the fundamentals of the DVR using a simple model[9,10]. The series connected voltage source V_{pq} is controlled in order to keep the voltage at the bus V_o' at a constant in both phase angle and magnitude in case of a voltage disturbance at the source terminals V_o. The main functions of power flow controllers were analysed in detail in section 8.2

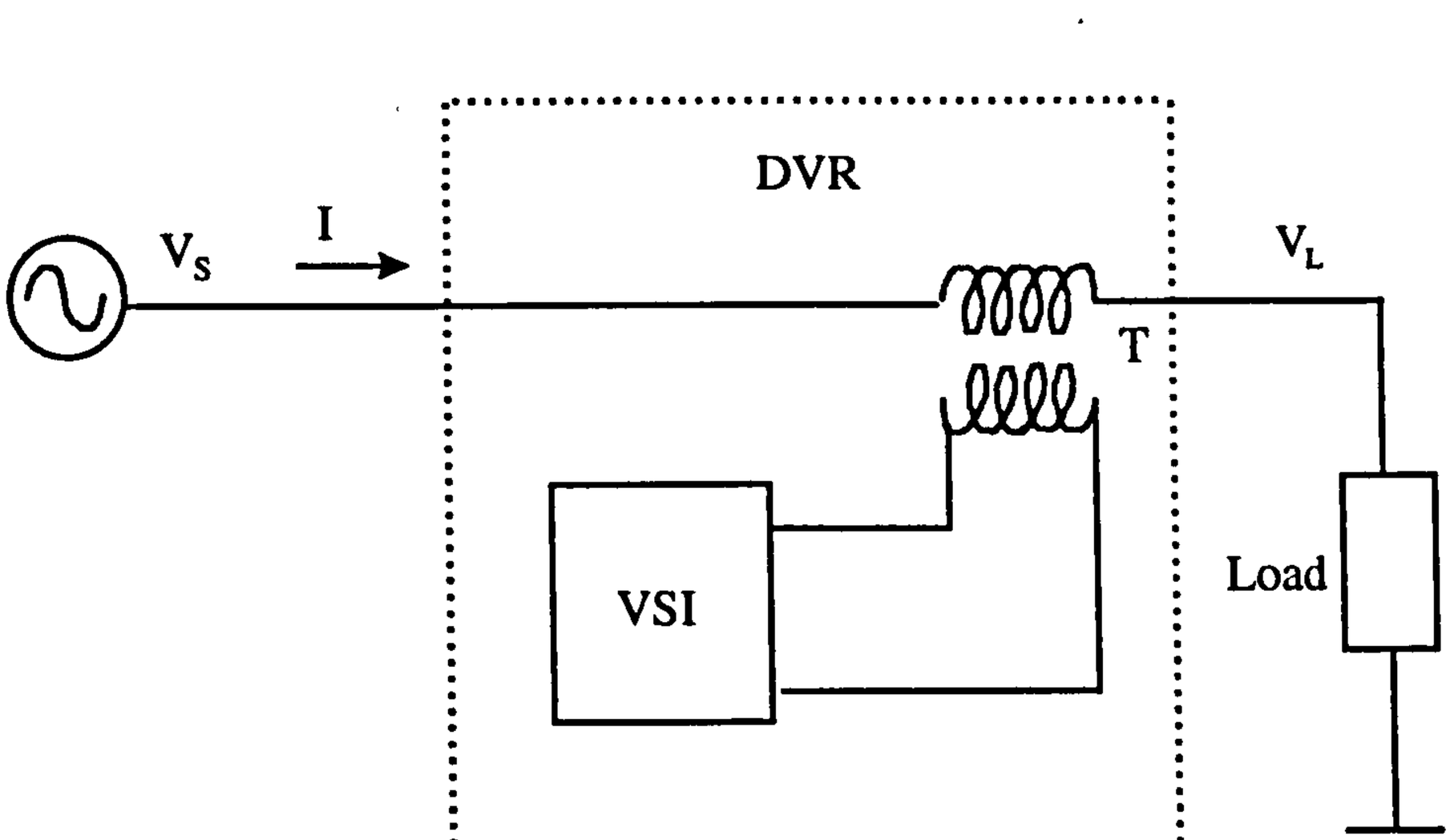

Figure 10.4

There are three main factors when establishing the rating of a DVR unit: the magnitude of the injected voltage which describes the maximum depth of the sag for which a DVR can restore voltage; the load current and the amount of energy storage, which in turn determines the maximum duration for which a three phase sag can be corrected at the maximum injected voltage. The MVA rating is derived from the injected voltage and the rated load current. The DVR MVA rating is effected by the series injection transformers. The MVA rating is not normally dependent upon the amount of energy storage available.

The DVR has a typical rating from 2-8 MVA. The DVR rating is related to the load rating and injection voltage capability as follows:

$$MVA_{DVR} = RatedMVA \times InjectedVoltage_{max}(p.u) \tag{10.19}$$

In the event of a voltage surge or overvoltage, the DVR is required to compensate by acting as a virtual inductor in series with the line.

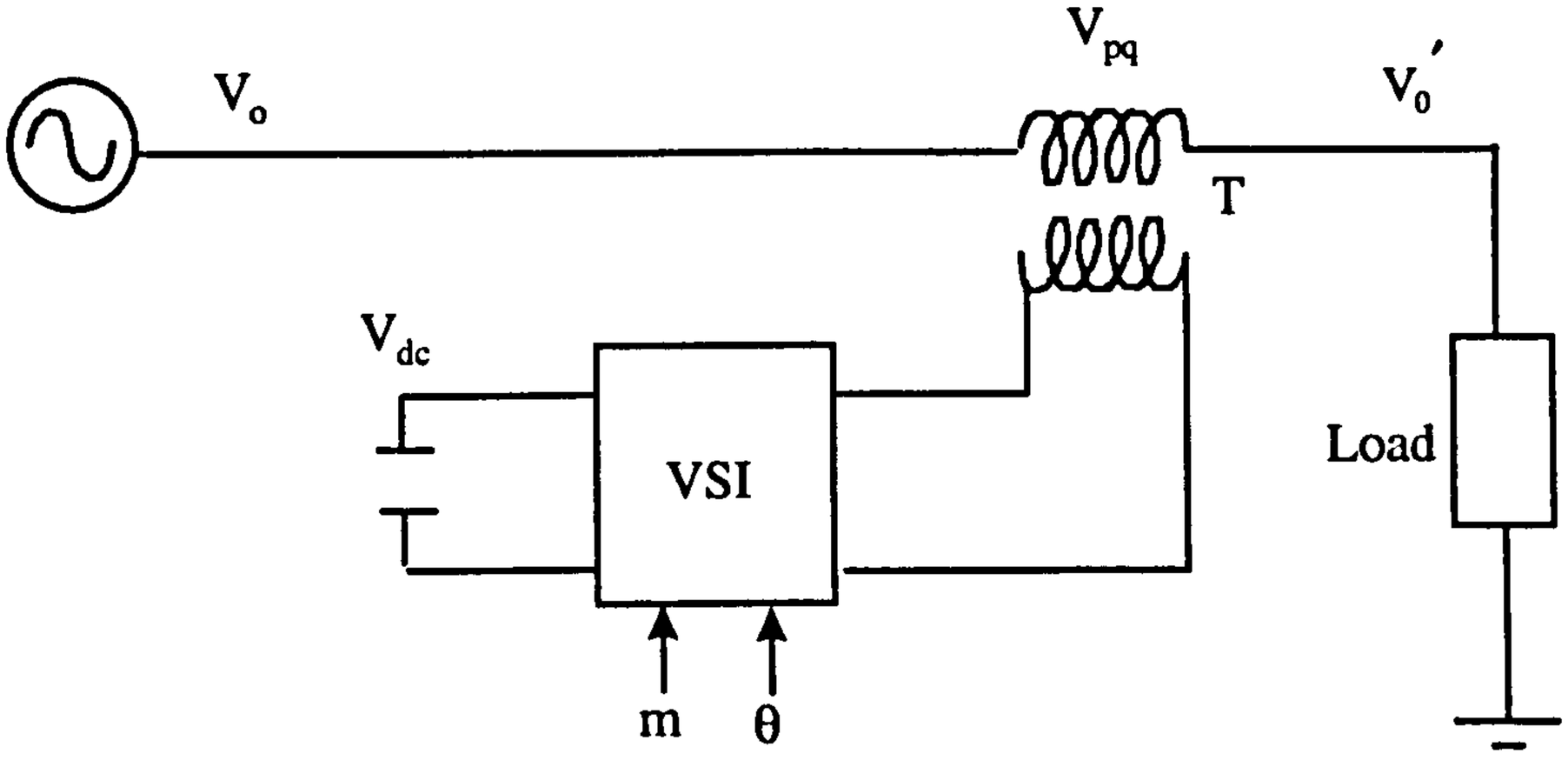

Figure 10.5

10.3 DVR Ride-through time and economic considerations

Installing a DVR on a transmission system can give many advantages in addition to stopping the load from observing the effects of fault conditions, the DVR has the

capability to support the load for a time period in excess of the sag/surge duration. This ability is referred to as "ride-though" and is defined as; the time that a DVR can correct the output voltage to its fully rated value or its maximum capability[6-7]. The ride though time t (secs) can be derived from the active power injected P, and the amount of energy storage available from the capacitor bank, E. Hence for a large three-phase sag, using $E = P \times t$, $t = E/P$ (10.20)

In an adjacent feeder where a fault has occurred and the feeder is protected by a recloser, there will be repeated sags during a brief time interval. The stored energy will decrease (if necessary) during each sag. The DVR will attempt to replenish the lost energy between sags. Thus, ride-though time will be longer than an equivalent sag of duration equal to the total duration of all the sags.

The cost for loss production at Caledonian Paper in Scotland was about £100,000 per day [5] and was the result of a single voltage dip on the supply. Usually a utility will estimate the cost of an outage per kWh of lost revenue, this method however does not reflect the true cost to a voltage sensitive consumer with a continuous process, such as Caledonian Paper. When a manufacturer is forced to stop production through fault conditions such costs as; clean up time, wastage of partially complete materials and maintenance requirements also need to be considered. The above costs equally apply for a one second sag which shuts down a plant or a twenty minute outage, hence to a sensitive consumer there is no distinction between the two events. It is the frequency and severity of such electrical disturbances and their associated costs which should be measured against the capital cost and payback period of a DVR.

Present estimates of the cost of dynamic voltage restoration equipment range from £150K to £250K per MVA. The savings associated with avoidance of voltage sags can quickly offset the cost of a DVR. Using representative sag data, payback periods of two years or less will be common.

10.4 Overview of previous work

The use of the Dynamic Voltage Restorer to keep the voltage constant at the load terminals during disturbances in the transmission or the distribution system, has been reported in the literature the last 3-4 years.

G.Taylor described the operating principles of the Dynamic Voltage Restorer together with other custom power solutions[1].

R.Buxton and G.Taylor reported the benefits of the Custom Power technology, described some basic Custom Power controllers and presented test results from DVR installations [11].

M.Osborne, R.Kitchin and H.Ryan reported the benefits of the use of DVRs compared to other custom power solutions[2,6].

G. Mohaparta, A.Zayegh, A.Kalam and R.Coulter analysed the use of the DVR in a system with other energy storage devices[3].

Fenwick in cooperation with Reyrolle Projects Limited developed a report [12] with the basic operating principles, a cost estimation and presented results illustrating the DVR performance.

R. Nelson and N.Woodley presented a simple methodology to estimate the size of a DVR necessary to minimise total customer costs[7,8].

Finally, Abi-Samra, N.Neft and A.Sundaram presented the operating principles ,the rating and measurements of an actual DVR established at the Caledonian Paper Mill[5].

It appears from the above that there are some papers relevant to the DVR based either on practical measurements or describe the operating principles and the main use (such as voltage support) of the DVR in a distribution system. However there are no papers describing the internal control system of the DVR. In this chapter an innovative closed loop control system is presented, analysed in detail tested under various system disturbances and validated using results from DVR installations. This system can be included in the design process and can be used as a promising method for applications of DVRs in distribution system architectures.

10.5 EMTP Model Development for the DVR

The electromagnetic transient model of the DVR depends on its power device configuration and the modulation method adopted. In general, through electromagnetic transient studies of the DVR, people can evaluate impacts of the DVR to the power system. These achievements can include:

(i) Understanding DVR operation theory

(ii) Setting up DVR internal control scheme

(iii) Designing filters

(iv) Computing maximum regulating capabilities by the DVR.

These studies can provide foundations for designing DVRs for use within distribution systems.

For simulating the DVR, the DVR model should be set up according to its implementation by use of power electronics devices.

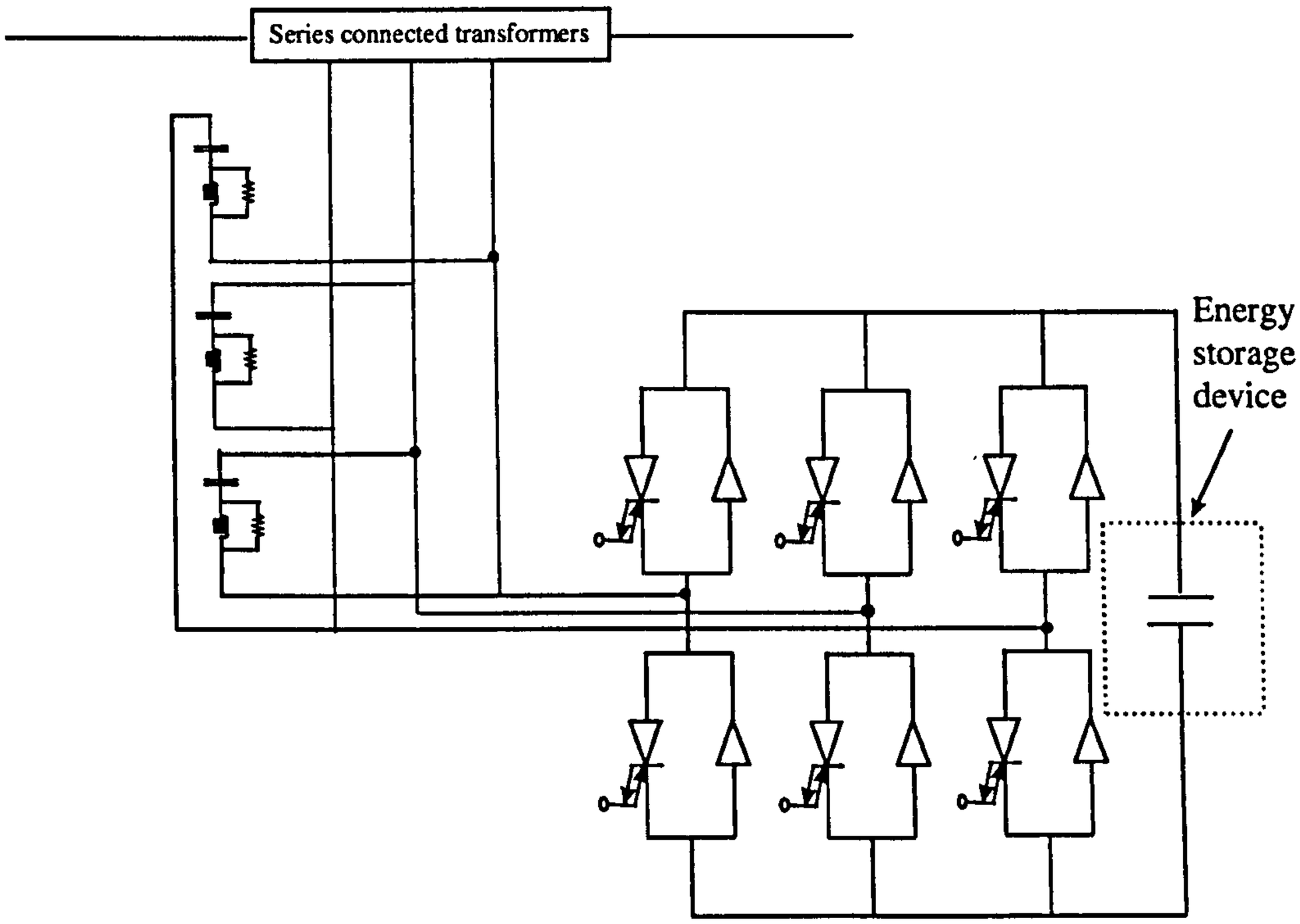

Figure 10.6 DVR power circuit model for electromagnetic purposes

The three phase voltage converter is the fundamental component of the DVR. This model is built using three identical IGBTs inverter legs.

Although not yet available in ratings comparable to GTOs and thyristors, the IGBT has much lower switching losses than the GTO and is therefore much better suited to applications involving switching frequencies in excess of about 1 kHz. IGBTs have minimal gate drive and snubbing requirements; moreover, voltage and current ratings of IGBTs have recently been increasingly rapidly, driven by pressure from traction markets.

Each IGBT valve has an antiparallel diode across it. This diode permits bidirectional power flow. A snubber circuit is also used in order to avoid numerical oscillations. This circuit consists of a resistor and a capacitor connected in parallel with the IGBT valve.

For the modelling of the energy storage device a constant dc voltage is assumed. This provides real power flow in the case of large voltage sags.

Damped filters are connected at the output of the inverter bridges in order to absorb the harmonics that the inverter generates. The filters consist of a capacitor connected in series with parallel R-L models, and are tuned at the switching frequency of the converter in order to smooth the DVR output. The filtered output goes to single phase transformers connected in series with the distribution line.

The simulation system suitable for electromagnetic study is intentionally a simple real power system whose main objective is to aid understanding of the DVR and its interaction with the system. The system under consideration is illustrated in figure 10.7 and it includes a three phase 11kV source, a 4 MVA Dynamic Voltage Restorer model and a power load with a rating of 8.3 MVA. The parameters of the system and the system itself were the same as those at the Caledonian Paper mill.

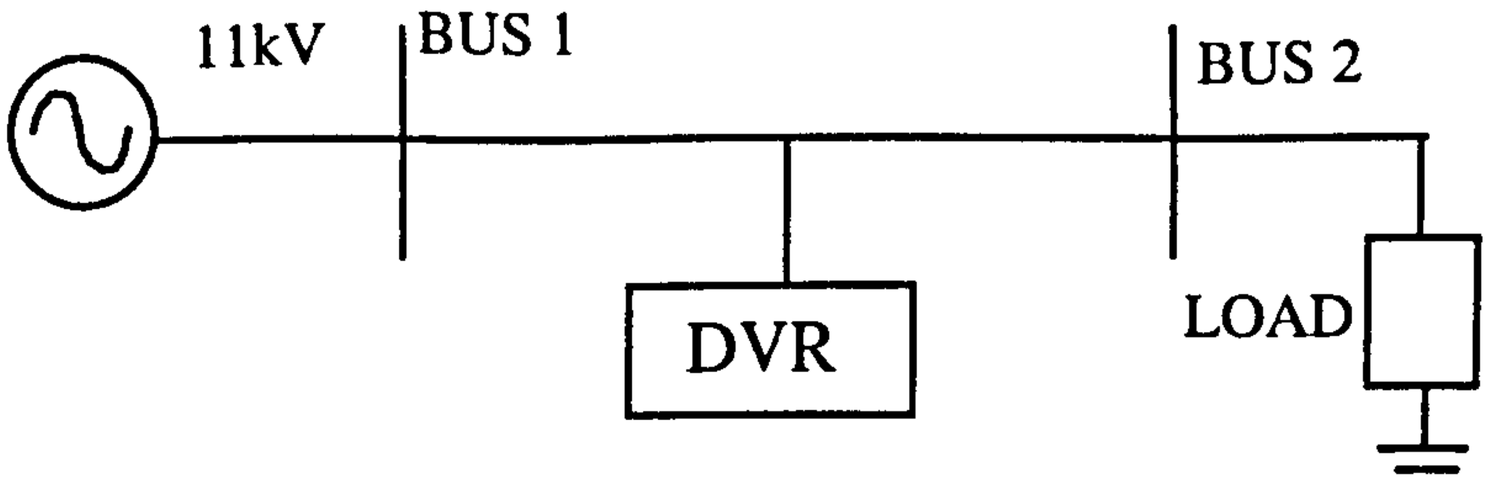

Figure 10.7 DVR model connected to the distribution system

For this model, the switching frequency of the DVR is 5kHz, and the filters were tuned to this frequency in order to absorb the harmonic component that the converter generates. The voltage at the dc source (capacitor bank) is 8kV. The transformer current ratio T, is 1.1 for all the three single phase transformers.

10.6 Design of the closed-loop control system of the DVR

The closed-loop control system proposed for regulating the Dynamic Voltage Restorer is illustrated in figure 10.8. Using IGBTs the DVR converts DC to AC and back again during operation. The sinusoidal voltage waveform injected into the transmission system is synthesised by high speed switching of the DC source. For the control of the inverter the PWM technique was used. The main principles of this method and its applications to power flow controllers were extensively analysed in 8.2. According to figure 10.5, V_{pq} can be regulated by amplitude and angle and so it is important to analyse how V_{pq} is regulated by Sinusoidal Pulse Width Modulation. By keeping the voltage V_{dc} constant, the series voltage output of the ac side terminal of the inverter can be obtained by:

$$V_{pq} = TmV_{dc}(\cos\theta + j\sin\theta)/2 \qquad (10.21)$$

where T is the ratio of the series transformer, m the modulation ratio and θ is the phase shift angle between V_{pq} and V_o. Open loop control can be achieved by randomly changing m and θ. For closed loop control the system in figure 10.8 is used. For the control of m, in the case of a disturbance the actual voltage for each

phase is compared with a reference value obtained from measurements at the steady state and the resulting signal is amplified by a proportional gain which value depends on the voltage injection capability of the DVR. For the control of θ the control of the active power flow at the load terminals is used. The real power flow is compared with a reference value for each phase, obtained again from measurements at steady state conditions, and the output goes to a PI controller for each phase. In this way individual control for each of the DVR outputs can be achieved. The resultant modulating signal is compared with a carrier in order to generate the switching instants for the IGBTs.

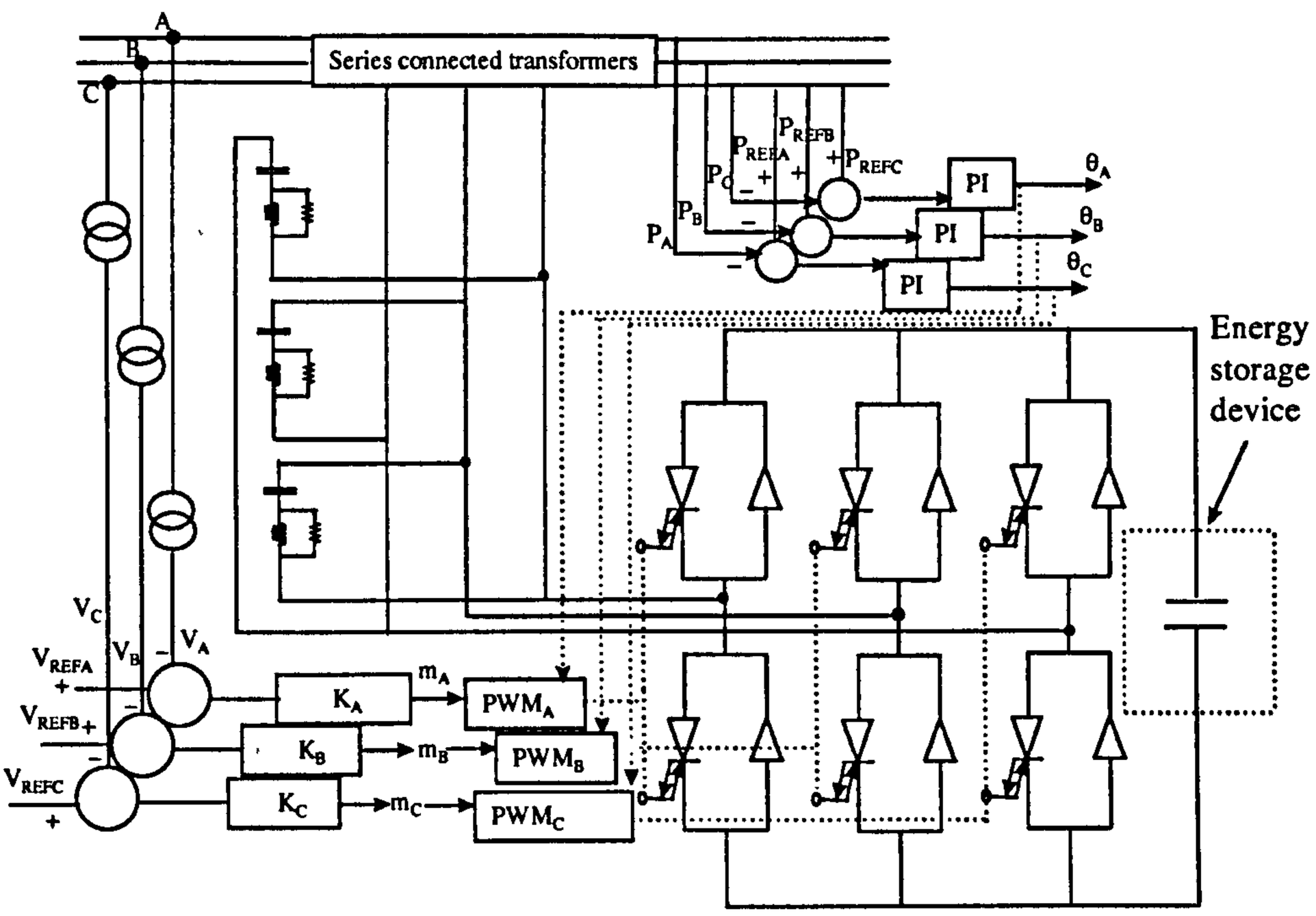

Figure 10.8 Design of the closed loop control system for the DVR

10.7 Open-loop simulation results of the DVR

In this section, simulation results using open loop control based on the PWM technique are presented. The system under study is shown in figure 10.7. For this system the following are two sets of some typical open-loop simulation results:

1) A voltage drop of 27% has been assumed at the source terminals for phase A, at 50msecs with a duration of 100msecs. For the PWM control method m is chosen at 0.55 and $\theta = 0^{\circ}$. Using these parameters the voltage at the load terminals remains almost the same before the sag, as illustrated in the figure 10.9. Figure 10.10 shows the voltage across the series connected transformer of phase A. In figure 10.11 the current through the load is presented.

2) A voltage swell of 27% has been applied at 50msecs and removed at 150msecs. For the control of the converter using the PWM method m is chosen at 0.55 and $\theta = 180^{\circ}$. The voltage at the load terminals remains almost constant as in the previous case and represented in the figure 10.12. In this study the voltage at the series connected transformer has an opposite polarity with the one in case 1), due to the different phase angle θ (figure 10.13). When the overvoltage occurs, this voltage is subtracted from the source voltage in order to keep the voltage constant at the load terminals. The current though the load is illustrated in the graph 10.14.

10.8 Closed-loop simulation results of the DVR

Detailed modelling of the DVR can be achieved by applying the closed loop control system illustrated in figure 10.8. In order to test the effectiveness of this controller a typical voltage sag is applied at 50msecs and removed at 150msecs for the three phases A,B and C. It is shown in the figures 10.15-10.17 that the voltages in the three phases reach the pre-disturbance conditions in less than 10msecs. This can be achieved by injecting the correct amount of voltage during the voltage sag. The voltage at the series connected transformer is illustrated in the figure 10.18. In figure 10.19(b) the current of phase A of the load is plotted. The control of the DVR using the PWM method is dependent through regulation of m and θ for each phase. The modulation ratios for the three phases are plotted in figure 10.20 (a)-(c) and the different phase angles used for the modulation signals are represented in 10.21(a)-(c). (In these cases the positive of the series connected voltages meets the positive of the voltage source). As can be observed, these angles reach 180° in less than 10msecs.

In order to validate the simulation results carried out in this chapter using the proposed modelling technique a comparison was made with results obtained from field tests of the DVR performance presented in [11] for a DVR installation. These tests include the response of the DVR under a severe single phase voltage sag. For these operating conditions and using the control system presented in this thesis from figure 10.8 simulation results were carried out and illustrated in figure 10.22. From the results in figure 10.22 (a) it is clear that for a severe single phase sag (the source voltage drops significantly to 25% almost of the rated) the response of the DVR is rapid enough (around 10msec) and brings the voltage back to acceptable levels. The results of this graph show very good similarity with the ones presented in [11] for the same system conditions. It should be addressed that the DVR in this example is fully utilised (in terms of the injected voltage). This is clear from figure 10.22 (b) where the modulation ratio reaches 1.0 at steady state conditions. Figure 10.22 (c) shows the response of the phase angle.

It is obvious from the above analysis, that the internal control system responds immediately and acts effectively during various system disturbances and can be used as a promising design method for effective regulation of the DVR in distribution system architectures.

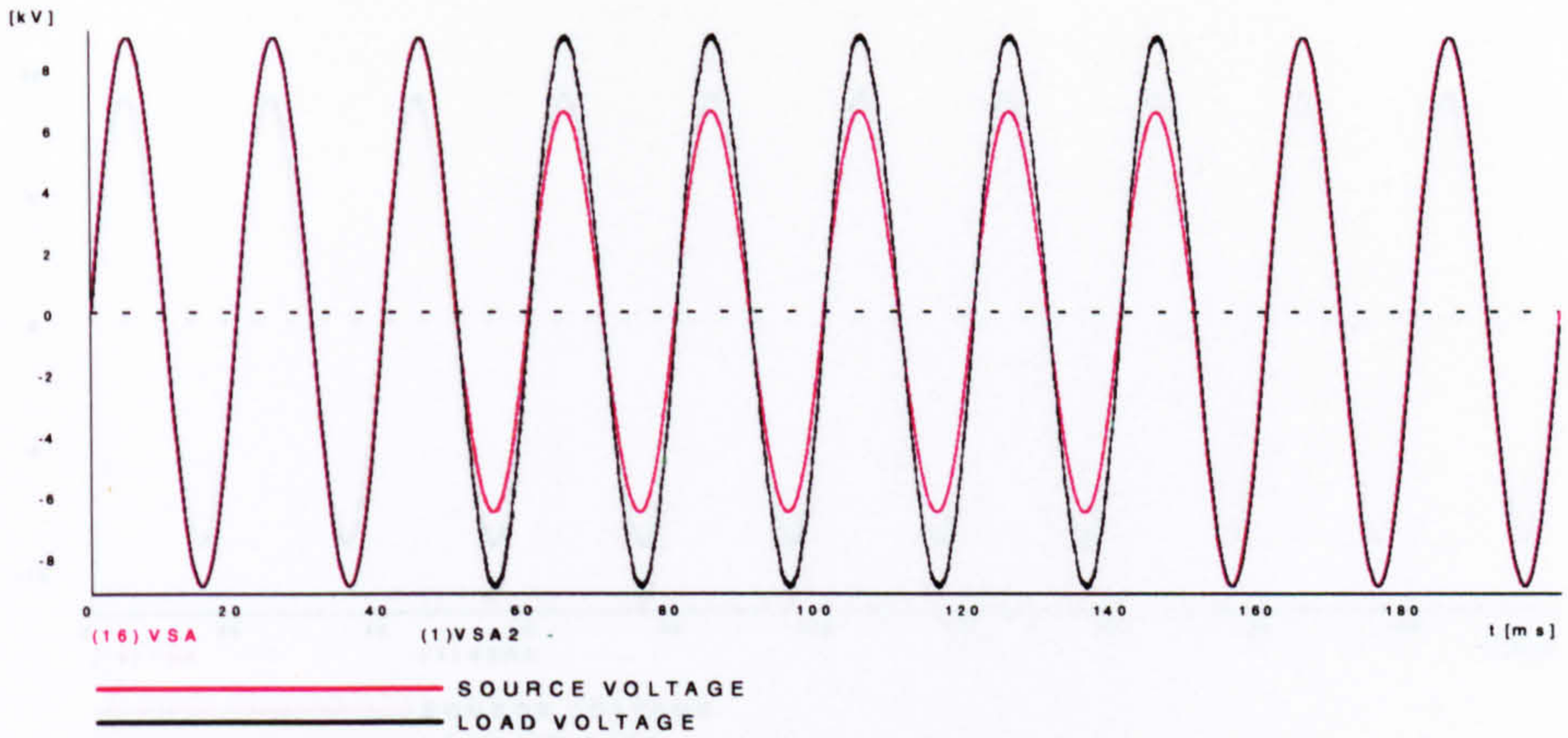

Figure 10.9 Source and load voltages of phase A

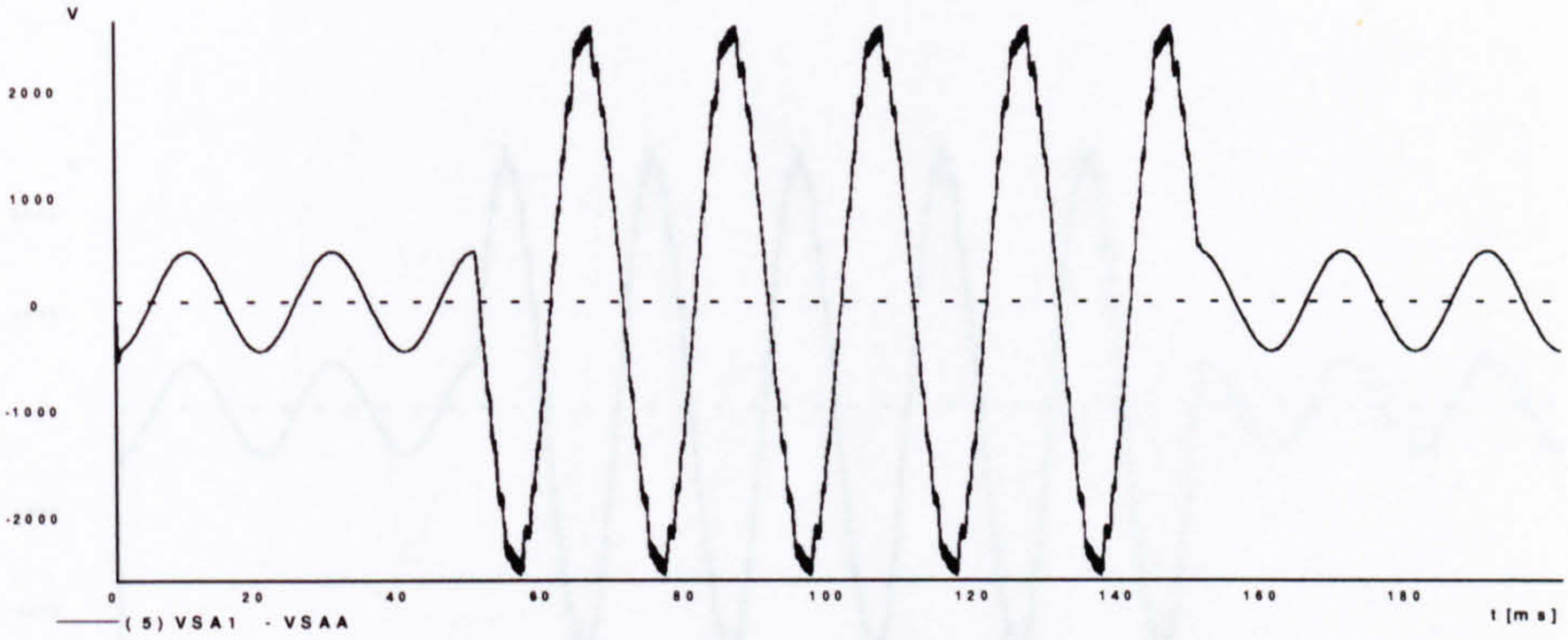

Figure 10.10 Voltage across the series connected transformer(phase A)

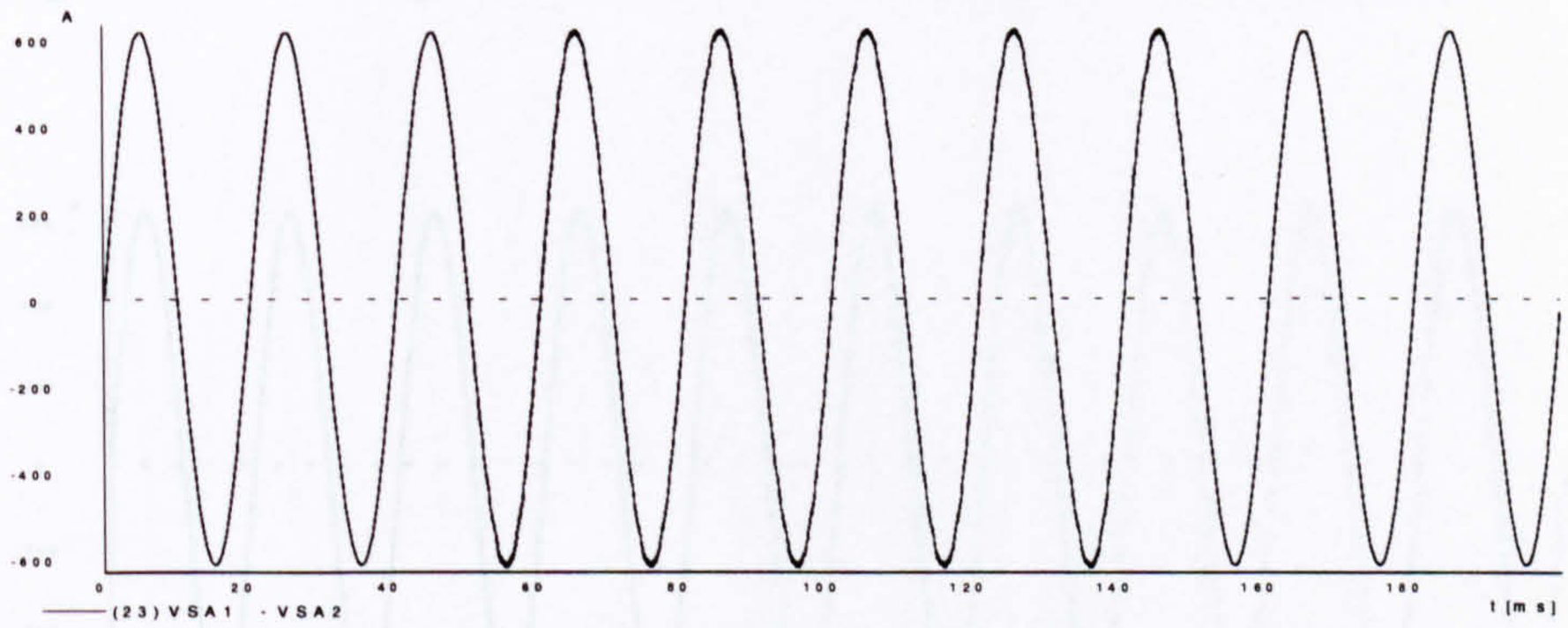

Figure 10.11 Load current phase A

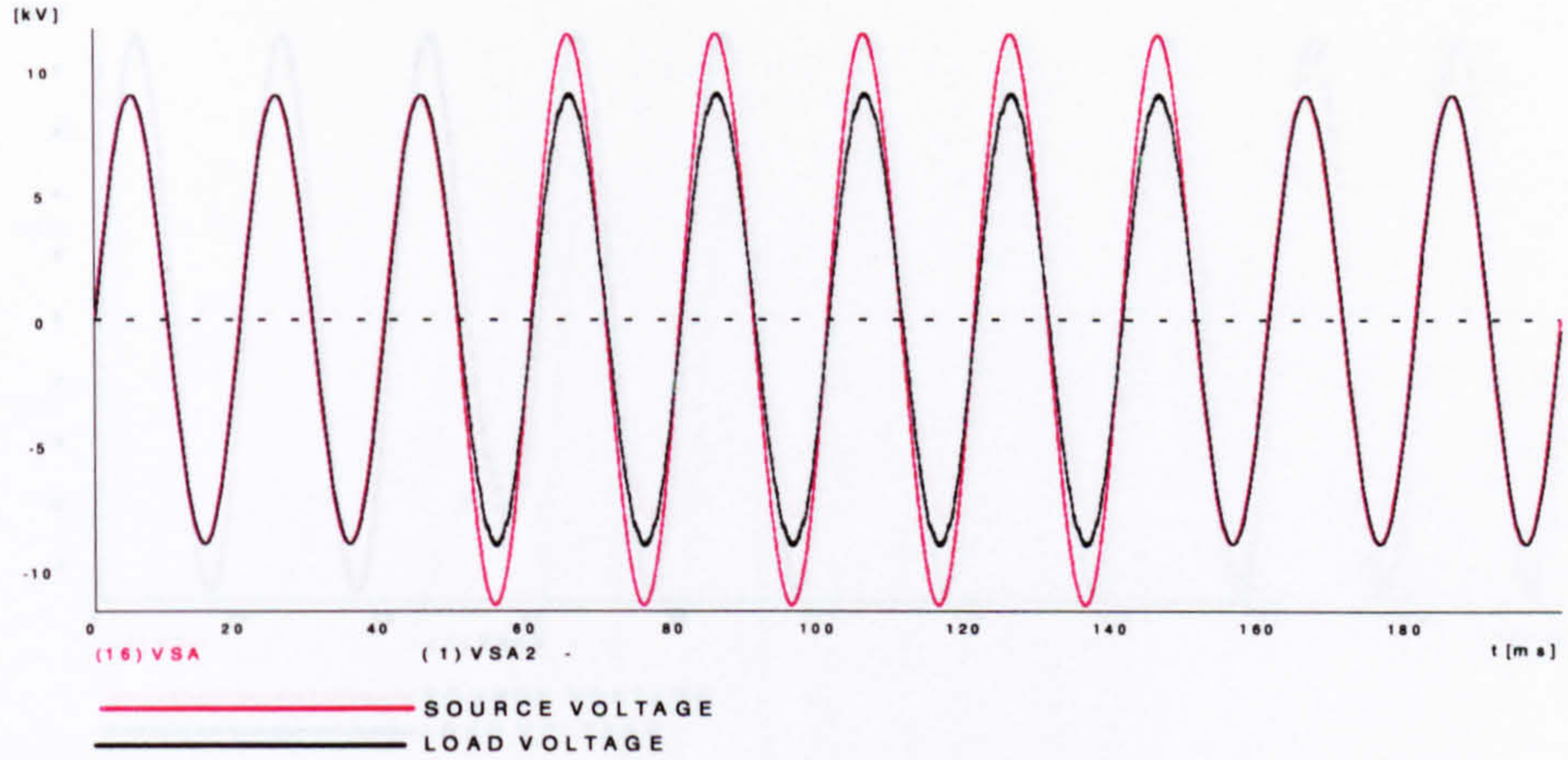

Figure 10.12 Source and load voltages of phase A

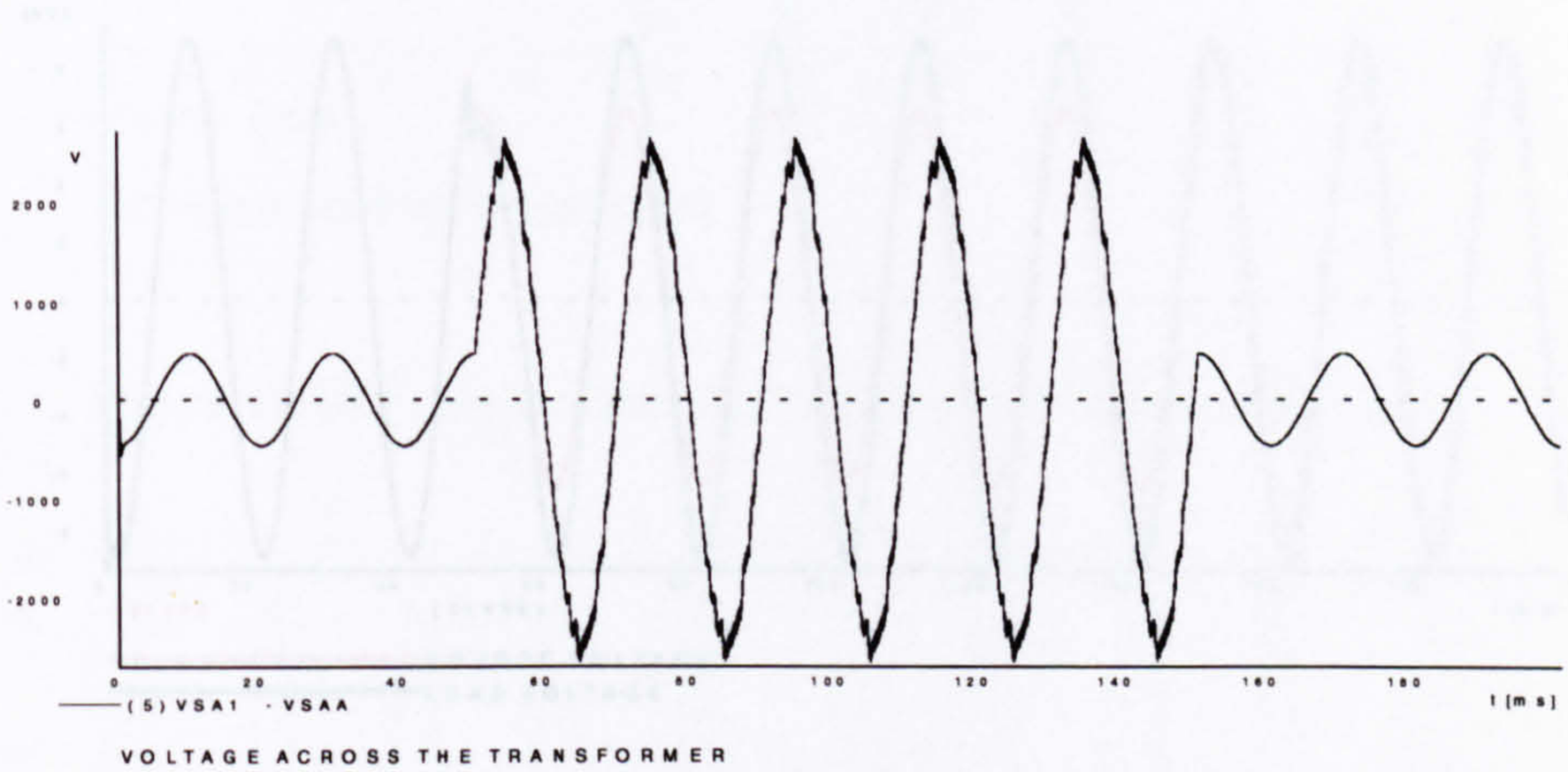

Figure 10.13 Voltage across the series connected transformer(phase A)

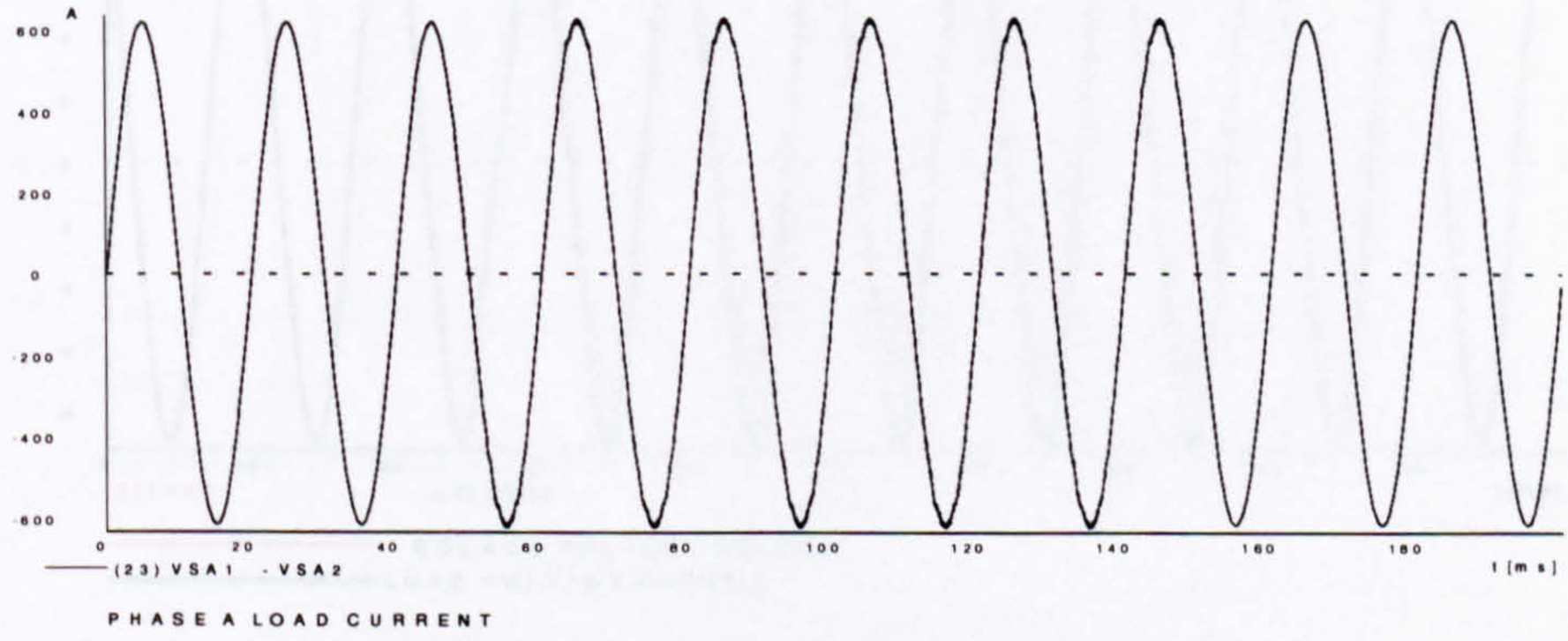

Figure 10.14 Load current phase A

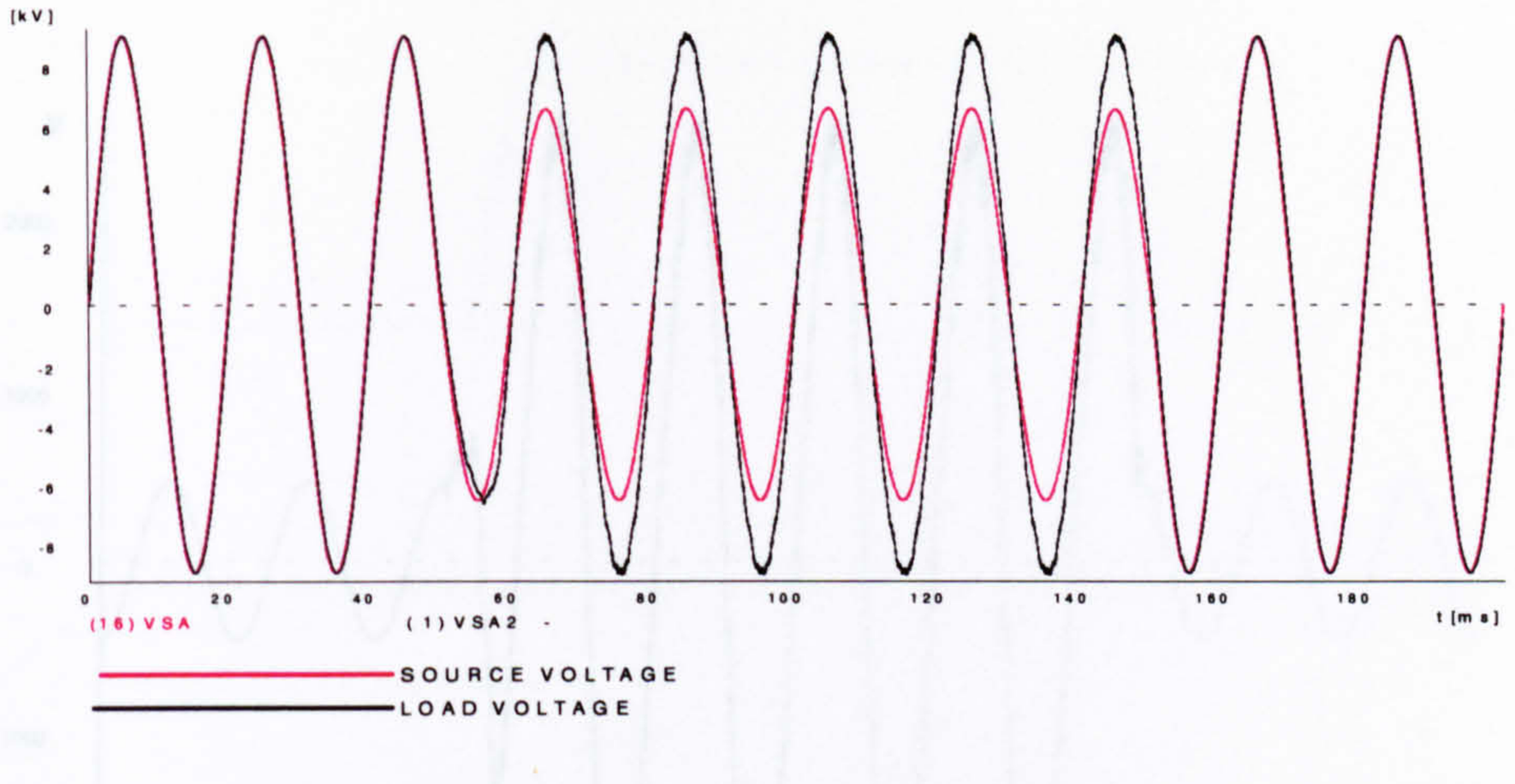

Figure 10.15 Source and load voltages of phase A

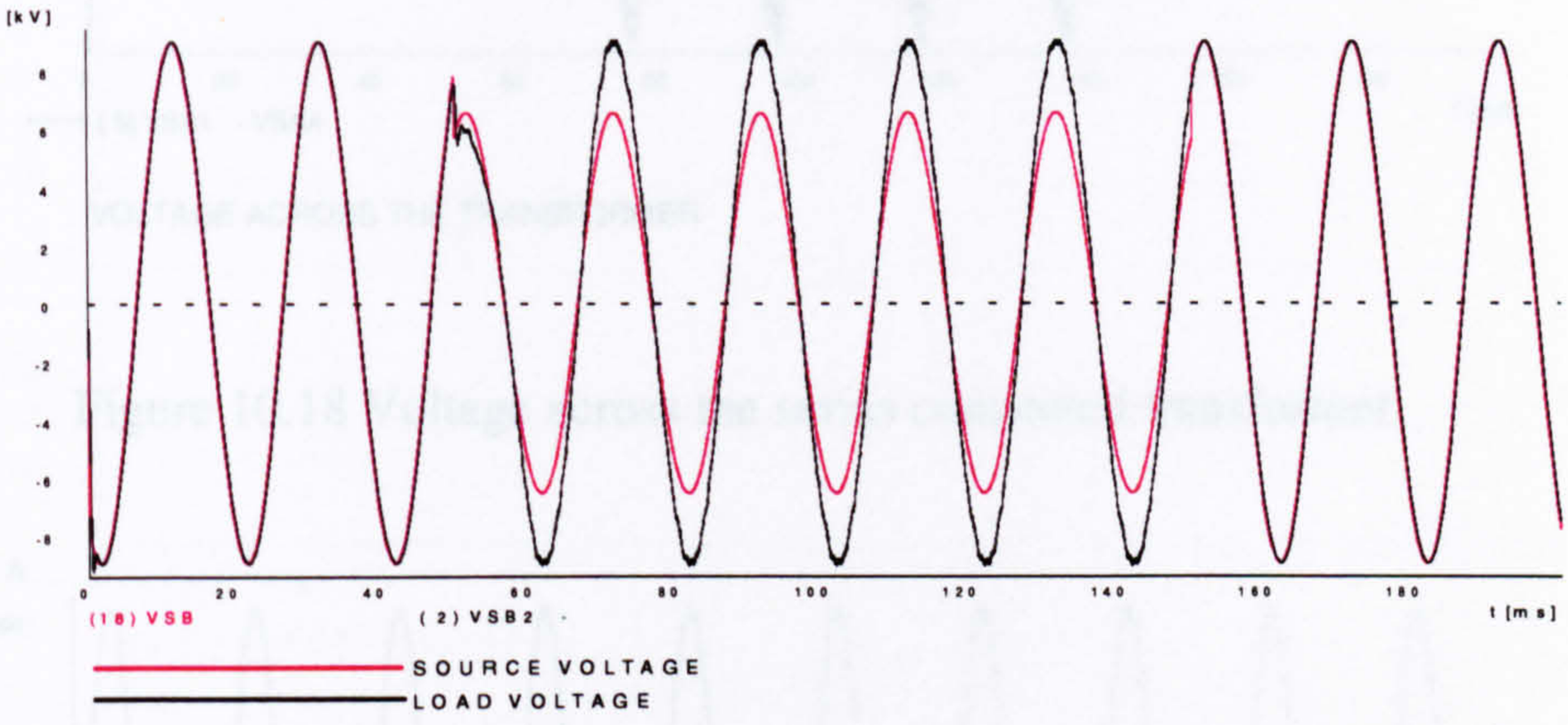

Figure 10.16 Source and load voltages of phase B

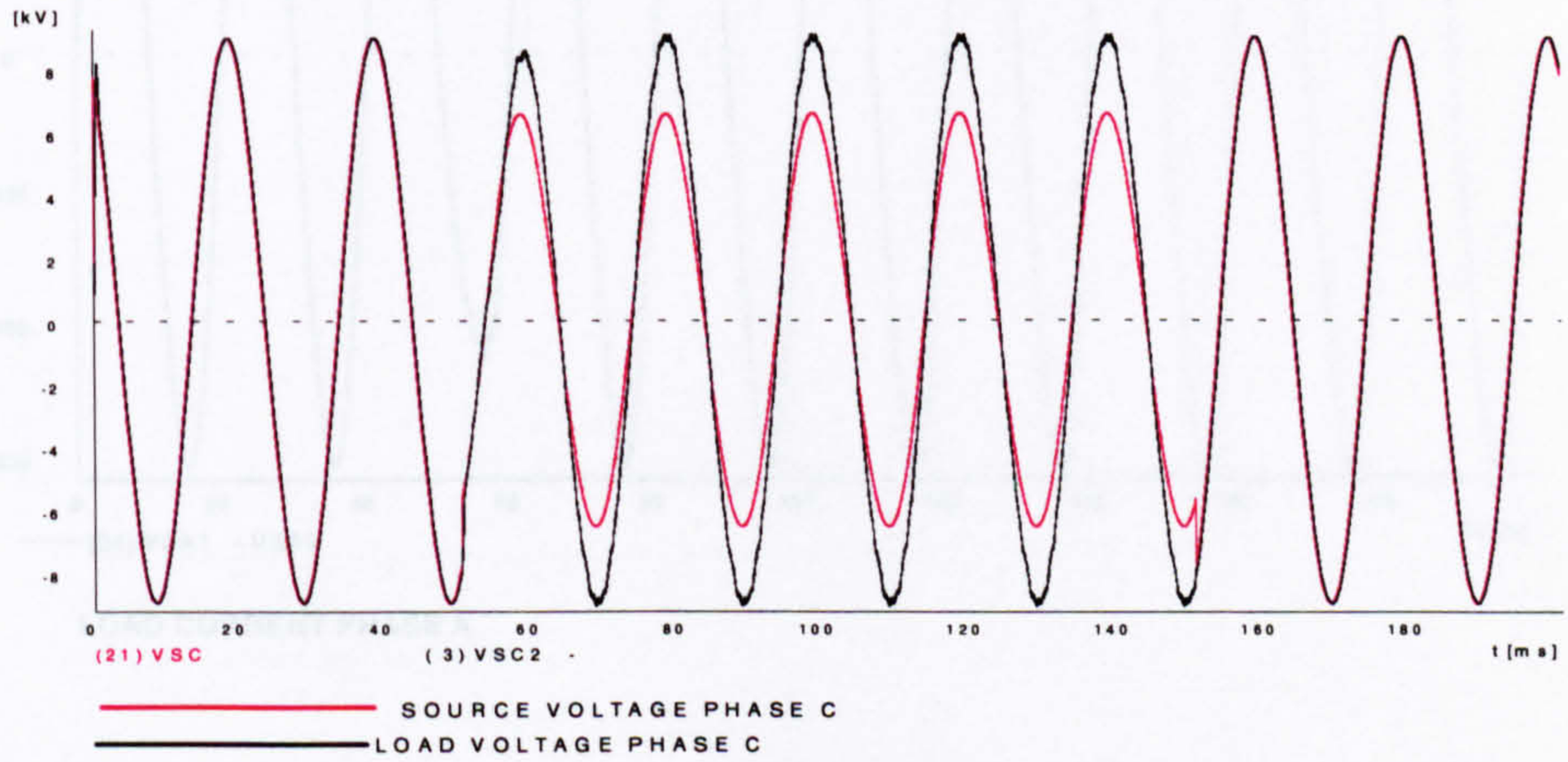

Figure 10.17 Source and load voltages of phase C

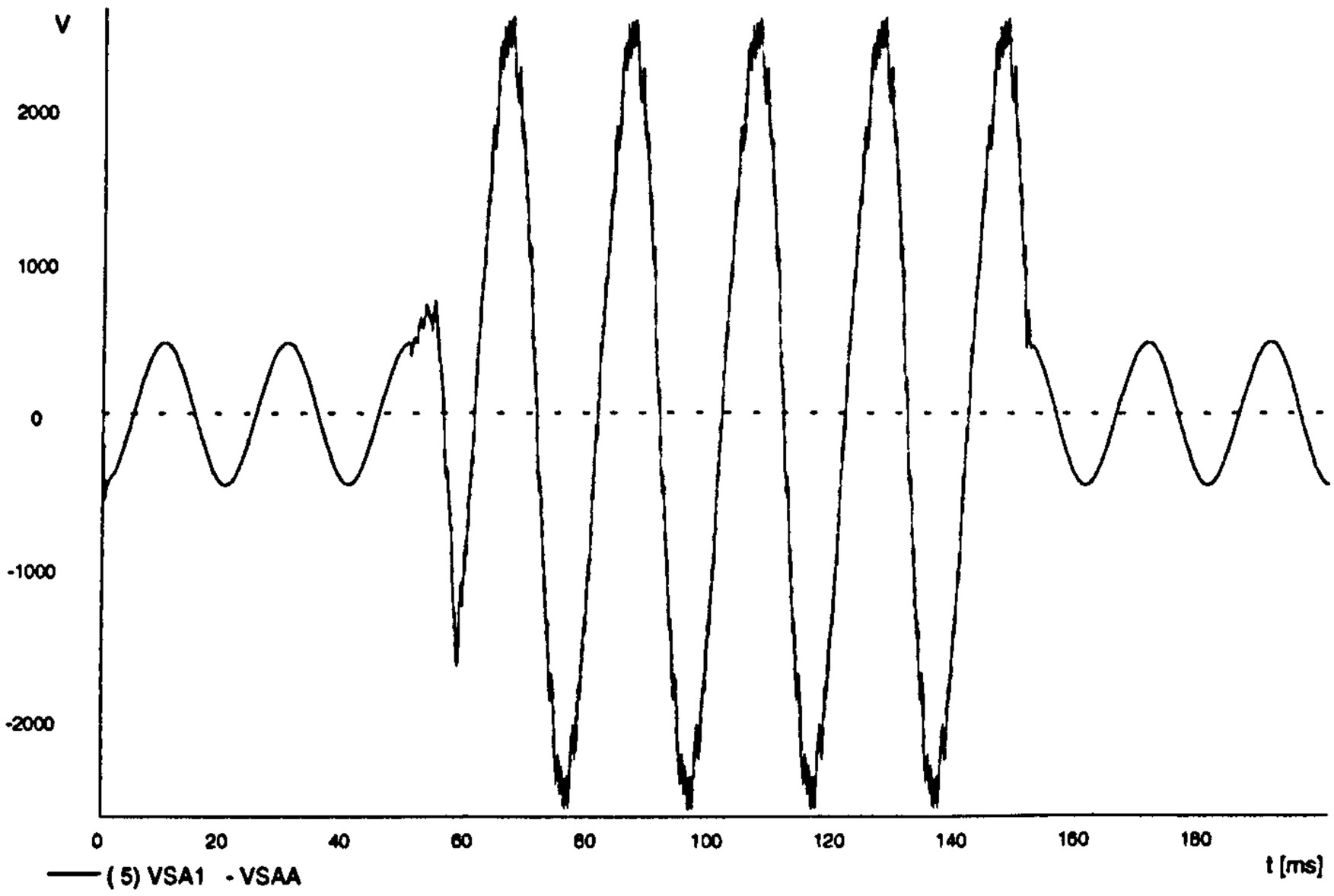

VOLTAGE ACROSS THE TRANSFORMER

Figure 10.18 Voltage across the series connected transformer

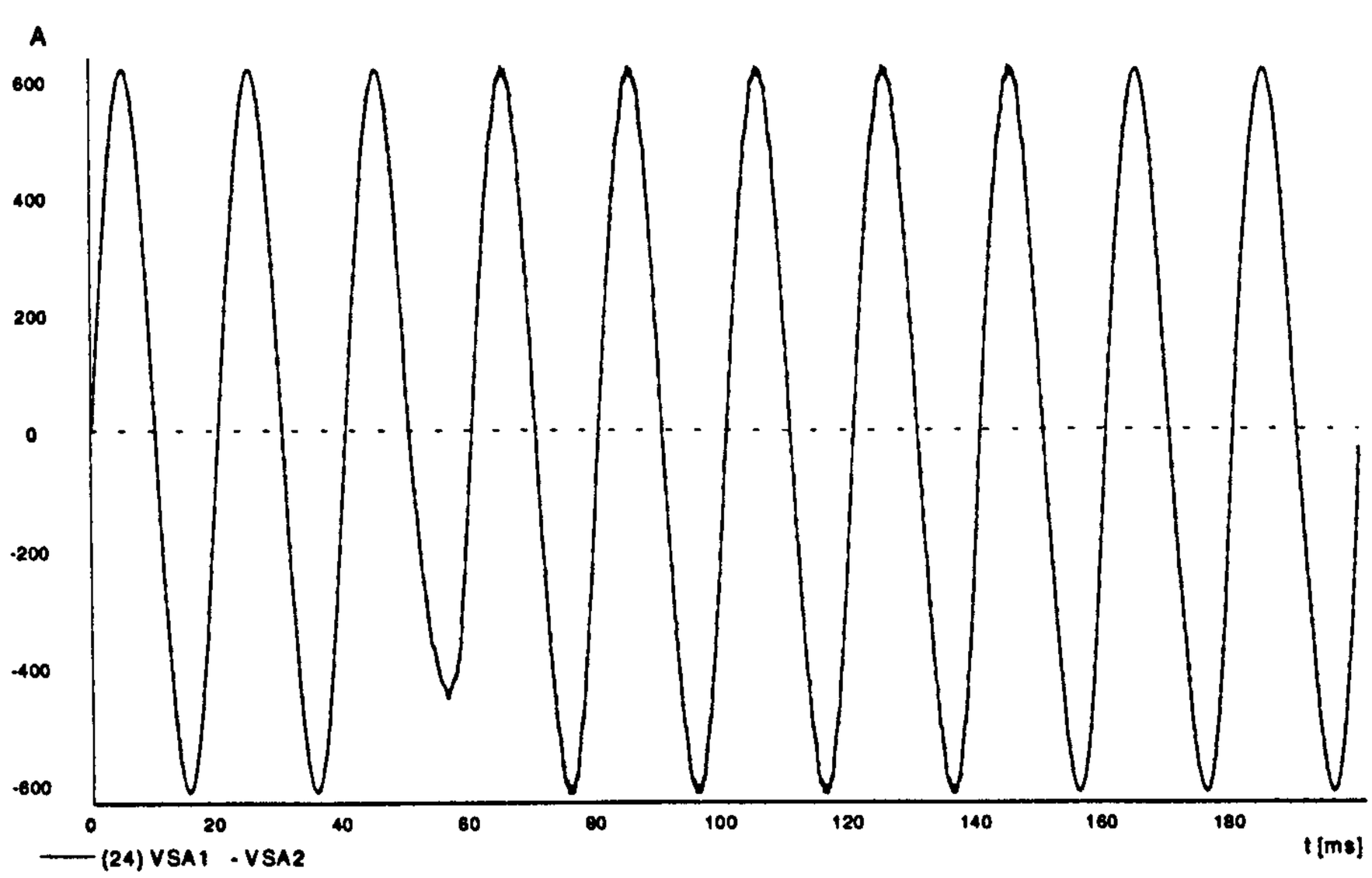

LOAD CURRENT PHASE A

Figure 10.19 Load current phase A

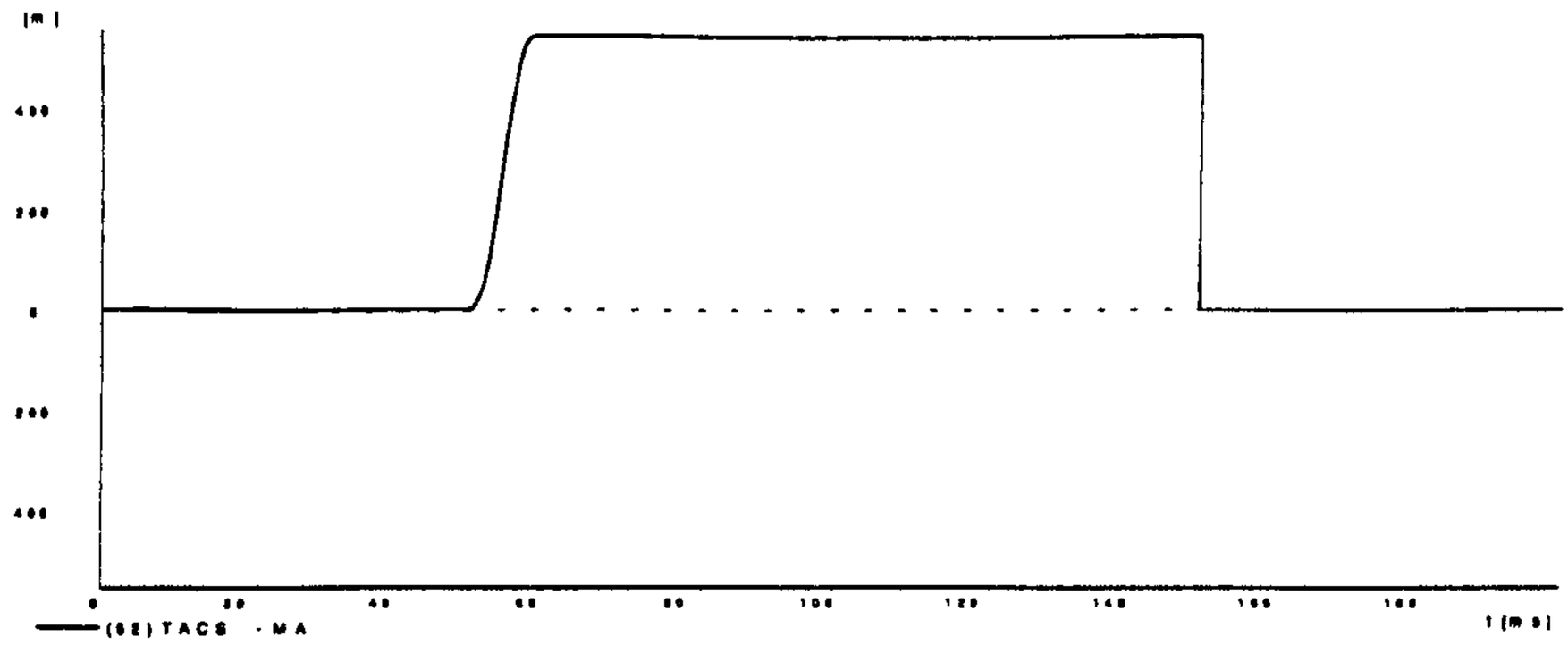

(a) Modulation ratio phase A

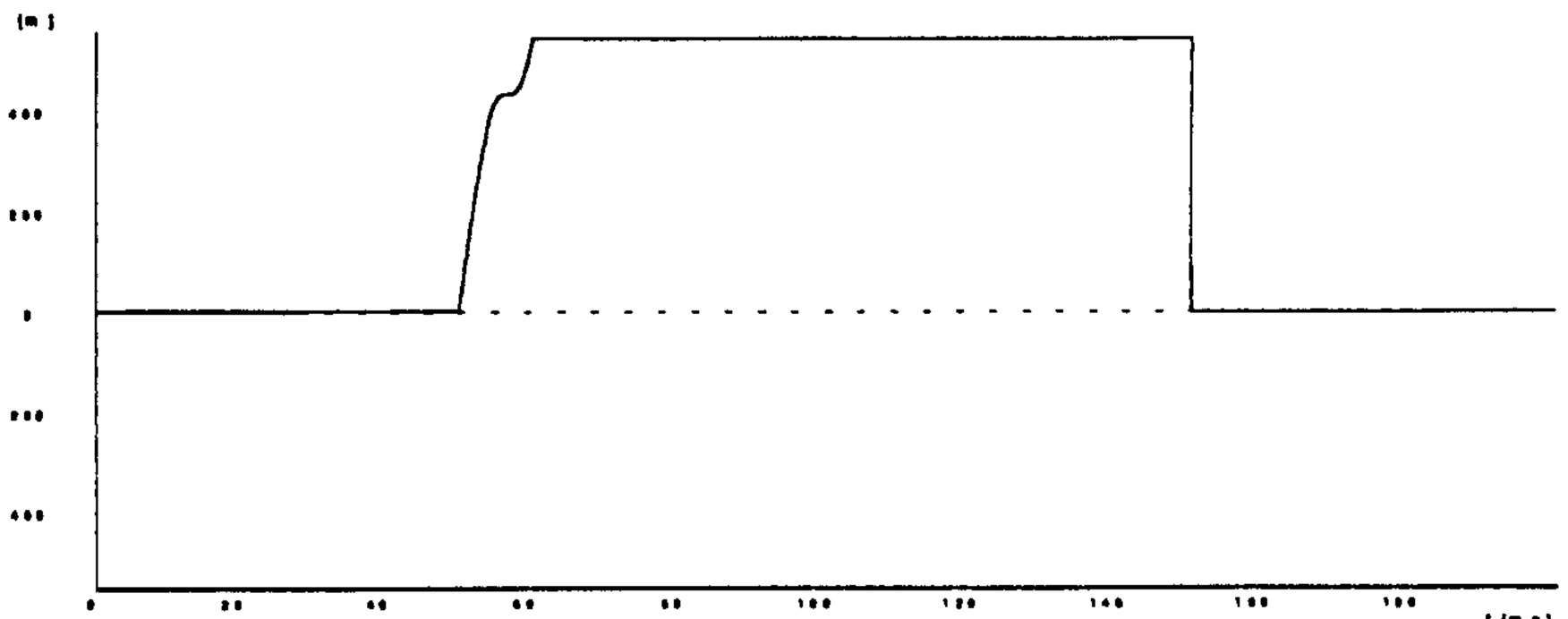

(b) Modulation ratio phase B

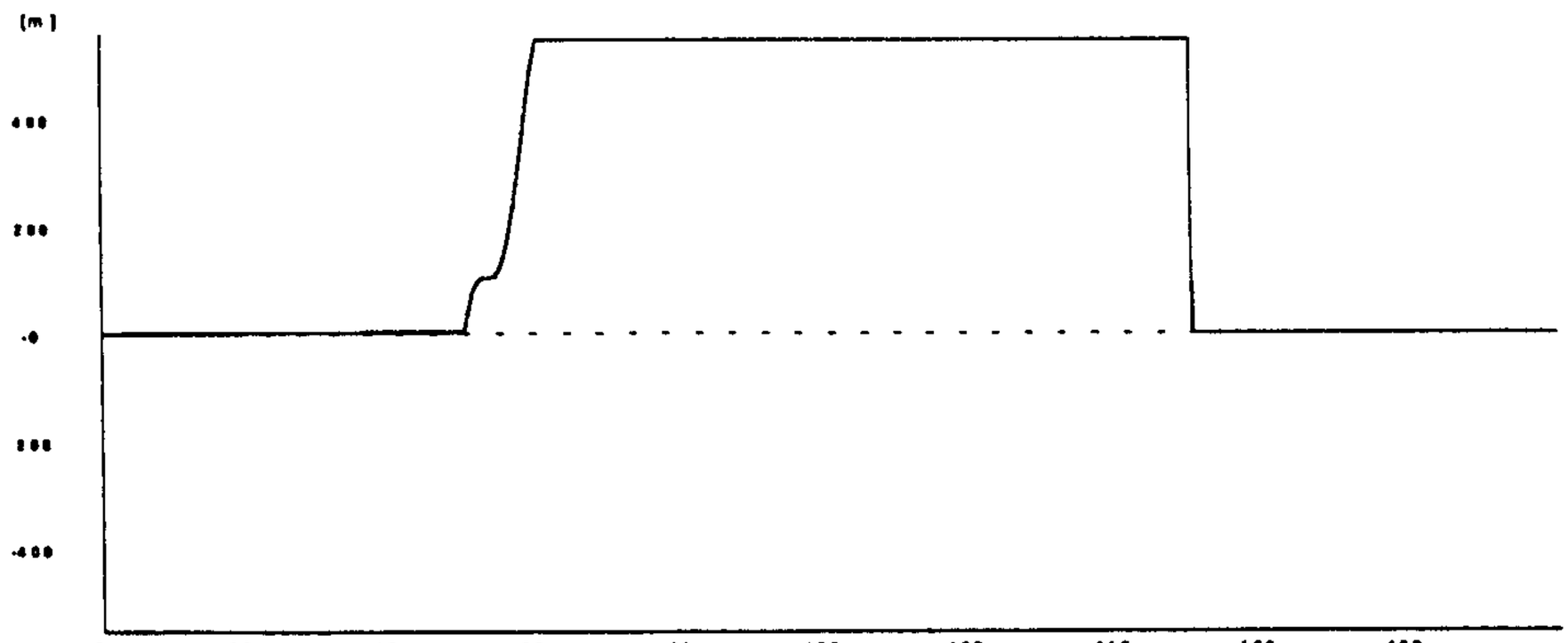

(c) Modulation ratio phas7e C

Figure 10.20

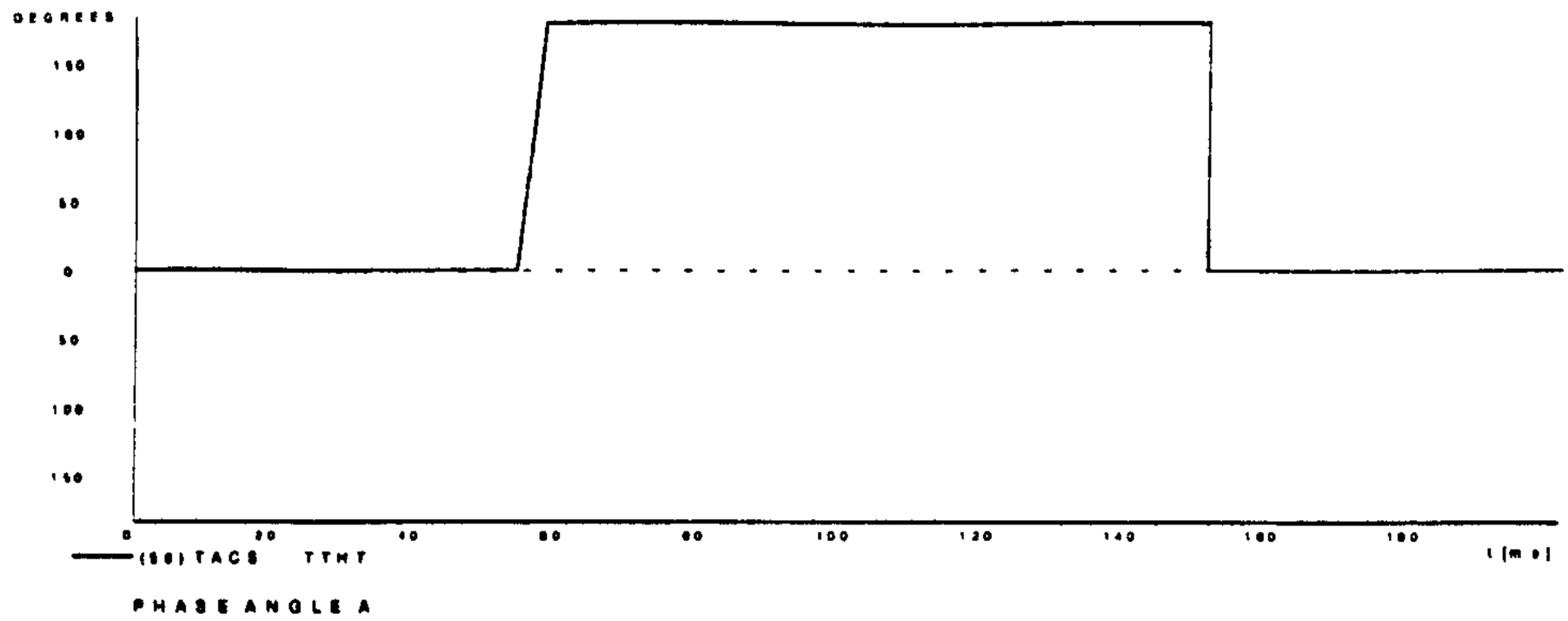

(a) Phase angle A

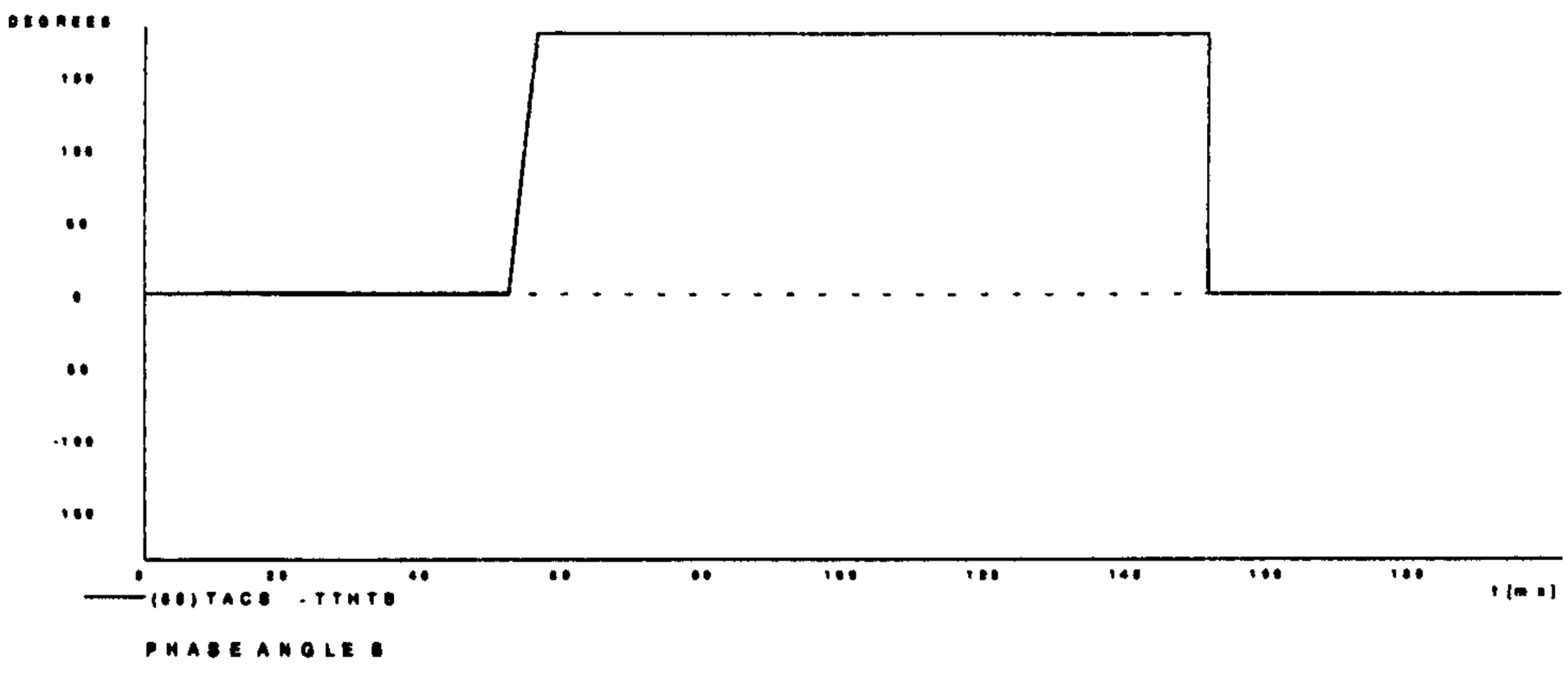

(b) Phase angle B

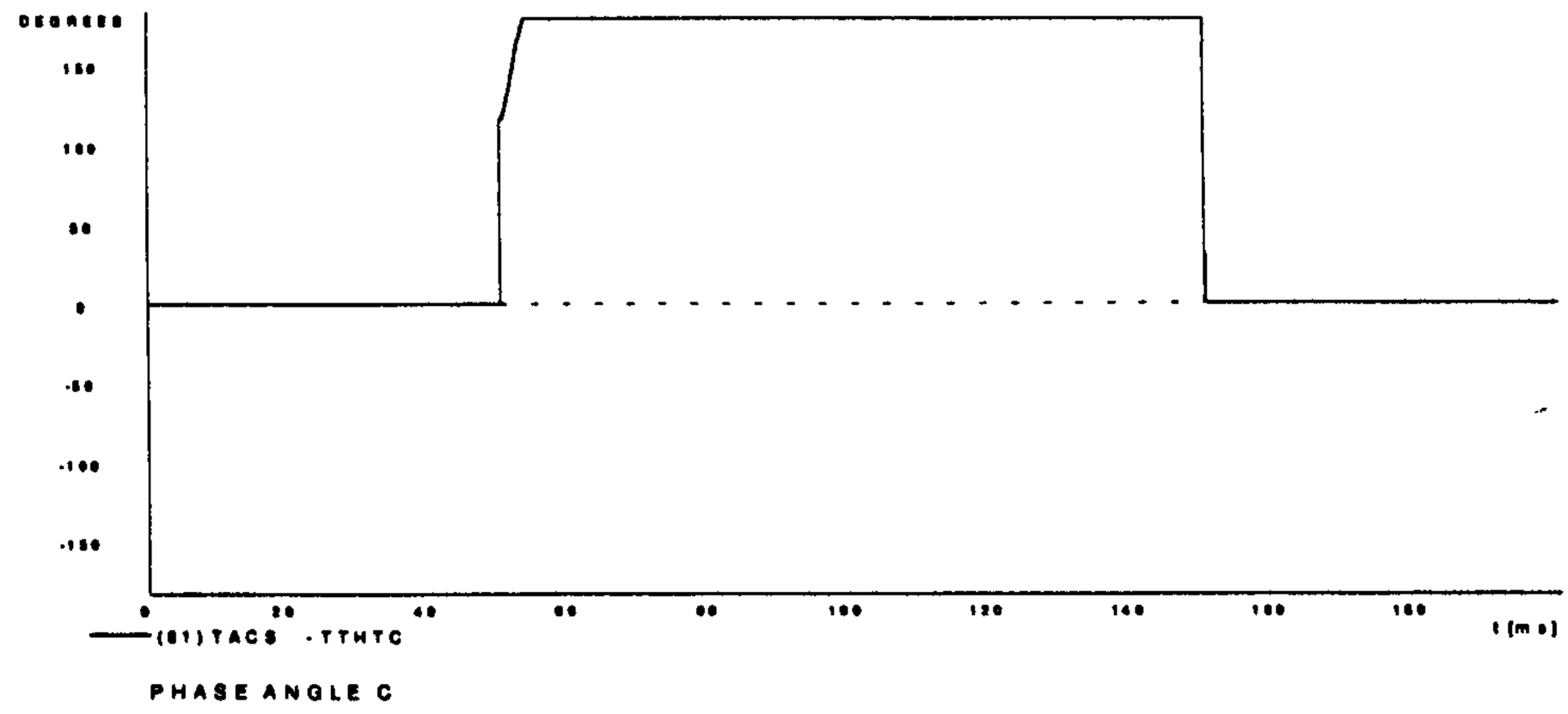

(c) Phase angle C

Figure 10.21

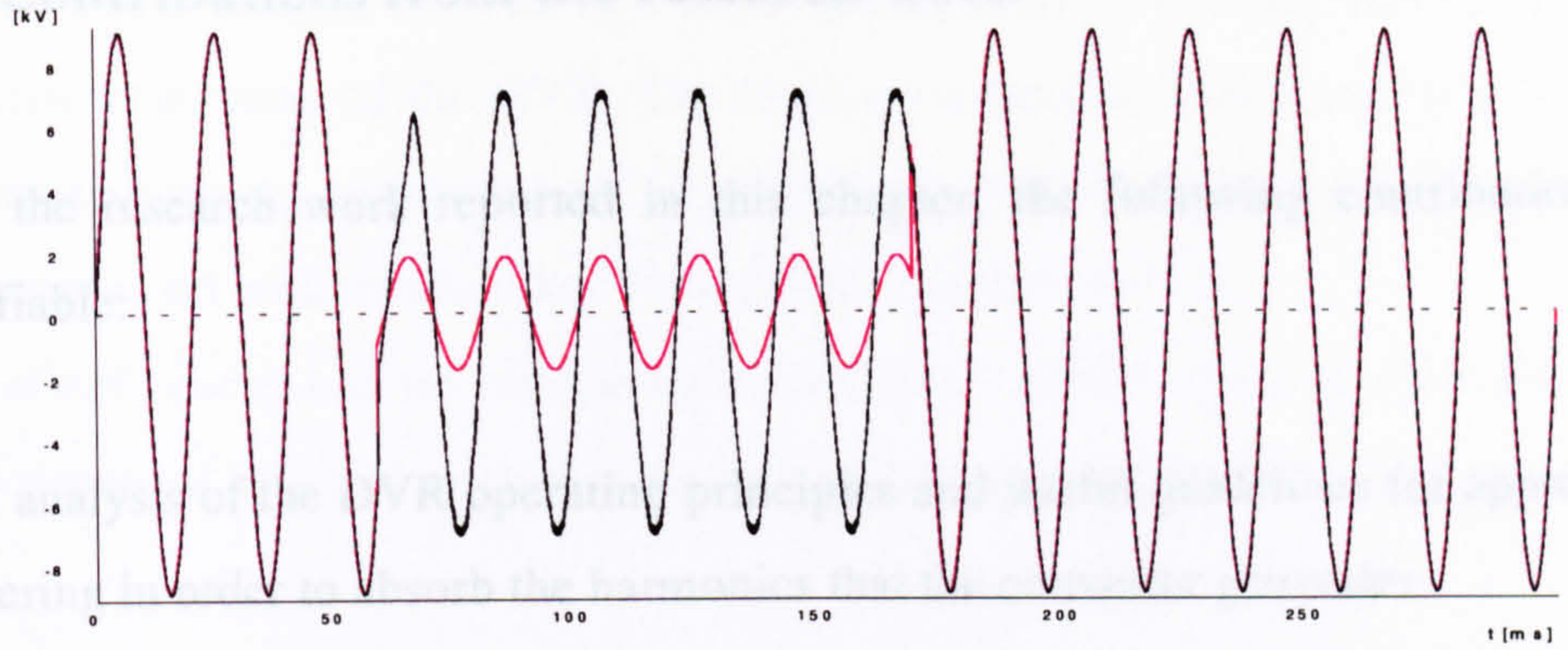

(a) Source and load voltages

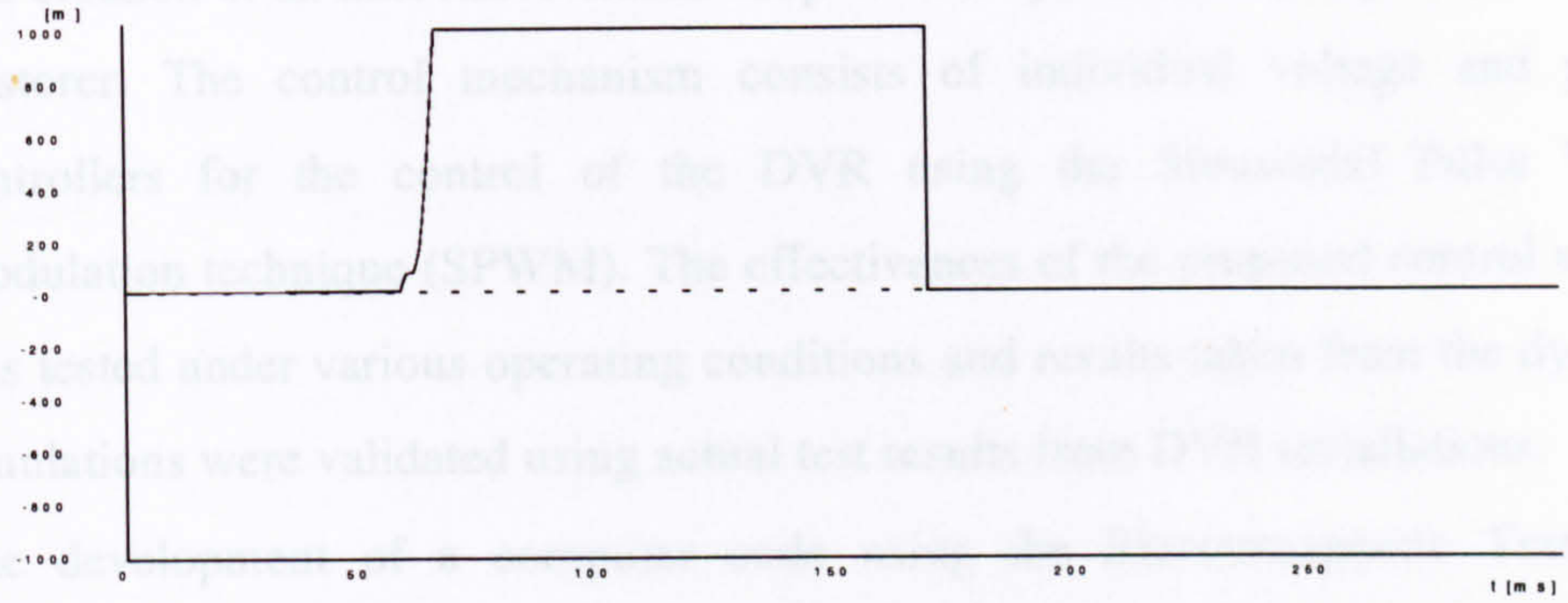

(b) Modulation ratio

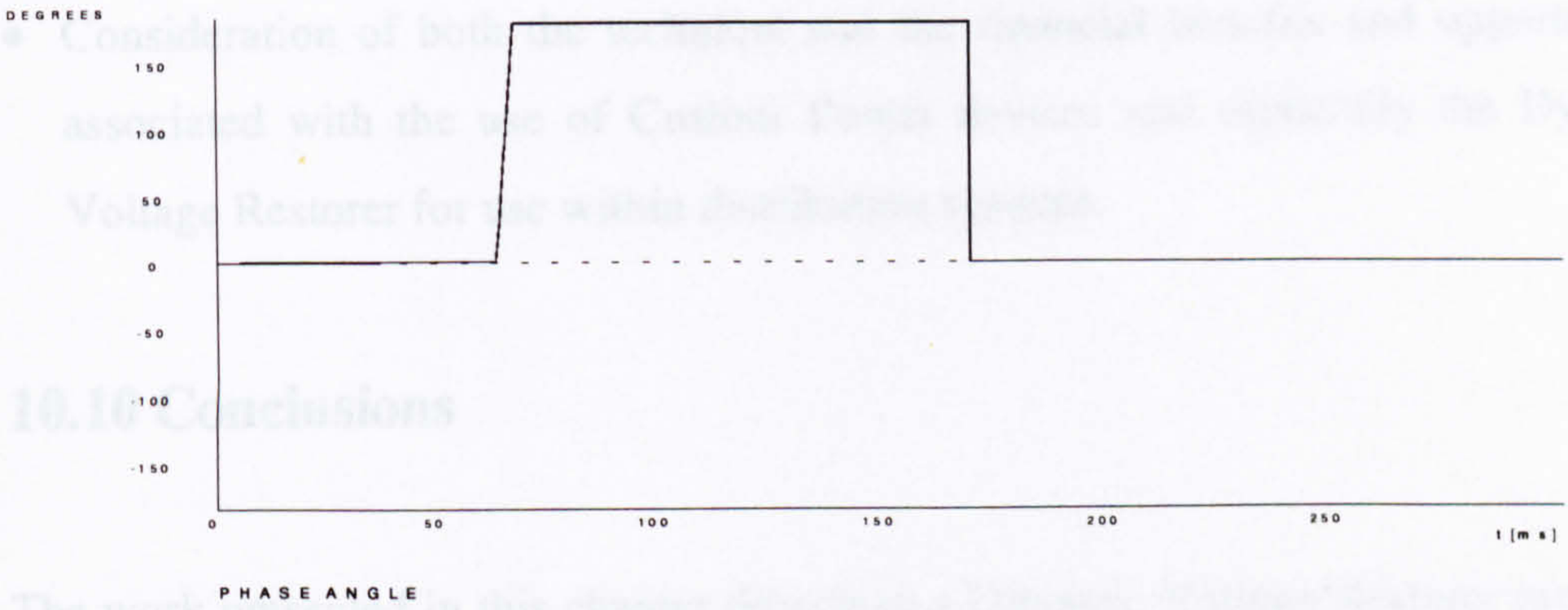

(c) Phase angle

Figure 10.22 DVR performance under a severe single phase voltage sag

10.9 Contributions from the research work

From the research work reported in this chapter, the following contributions are identifiable:

- An analysis of the DVR operating principles and useful guidelines for appropriate filtering in order to absorb the harmonics that the converter generates .
- The development of an open-loop control system for a DVR model. Results obtained from the dynamic simulations carried out in this chapter for various system disturbances (voltage sags and swells) were used in order to illustrate the described theory .
- The creation of an innovative closed-loop control system for the Dynamic Voltage Restorer. The control mechanism consists of individual voltage and power controllers for the control of the DVR using the Sinusoidal Pulse Width Modulation technique (SPWM). The effectiveness of the proposed control system was tested under various operating conditions and results taken from the dynamic simulations were validated using actual test results from DVR installations.
- The development of a computer code using the Electromagnetic Transients Simulation Program (EMTP) based on the control system described in this chapter can be used for the effective design of the DVR and its associated controls and filters.
- Consideration of both the technical and the financial benefits and opportunities associated with the use of Custom Power devices and especially the Dynamic Voltage Restorer for use within distribution systems.

10.10 Conclusions

The work presented in this chapter described a Dynamic Voltage Restorer model for use within distribution systems. The operating principles and previous related work with respect to this custom power device were reported. An innovative control

system was presented and can be used as a potentially promising design method for effective regulation of the DVR. The simulation results, illustrated for a number of different operating conditions are in accordance with the theory and were validated by comparison with results taken from DVR installations [11].

The effectiveness and the versatility of the above model makes it a useful tool for applications of this custom power device in distribution networks.

10.11 References

1. Osborne MM, Kitchin RH, Ryan HM, "Emergence of custom power technology in distribution systems", Proceedings of the Universities Power Engineering Conference, 1995, Vol 2, pp 777-780.
2. Taylor G "Power quality hardware solutions for distribution systems: Custom power", IEE Colloquium (Digest), 1995, No. 069, pp 11/1-11/9.
3. Mohapatra GR, Zayegh A, Kalam A, Coulter RJ, "Energy sources, energy storage and power electronic devices", Proceedings of the Universities Power Engineering Conference 1996, Vol 1 ,pp 155-158.
4. Taylor G.A, Burden A.B. "Wide area power quality-decision processes and options for sensitive users", CIRED, 1997, pp 2.30.1-2.30.5.
5. Abi-Samra, N., Neft C, Sundaram A., Malcolm W., " The distribution system voltage restorer applications at industrial facilities with sensitive loads", 1995 PCIM Power Systems World Conference.
6. Osborne M, Kitchin R, Ryan H, "Custom power technology in distribution systems: an overview", IEE Symposium, pp 10/1-10/10.
7. Nelson R J, Woodley N H, Ramey D G, "Requirements for dynamic voltage restoration to relieve distribution system voltage sags", Proceedings of the American power conference, 1995, pp 1530-1534.
8. Nelson R J, Woodley N H, Gurlaskie G, "Voltage sag relief : Guidelines to estimate DVR equipment ratings", Proceedings of the American power conference, 1996, pp 1338-1343.
9. Taylor G "Power quality hardware solutions for distribution systems: Custom power", IEE Colloquium (Digest), 1995, No. 069, pp 11/1-11/9.
10. Osborne MM, Kitchin RH, Ryan HM, "Emergence of custom power technology in distribution systems", Proceedings of the Universities Power Engineering Conference, 1995, Vol 2, pp 777-780.
11. Buxton R, Taylor G "Improving power quality with custom power solutions and decision processes", DISTRIBUTECH/Power Quality Conference, Amsterdam, Jan 1998, pp 1-10.

12. Fenwick A, "Power quality Management: Dynamic Voltage Restorer", final year project, University of Sunderland , 1998.

13. Dugan R, McGranaghan M, Wayne H, 'Electrical Power Systems Quality', McGraw-Hill, 1995.

14. Hingorani N, "Introducing custom power", IEEE Spectrum, June 1995, pp 41-48.

15. Douglas J, " Custom power : Optimising distribution services", EPRI Journal, June 1996, pp 1-6.

CHAPTER 11

CONCLUSIONS AND RECOMMENDATIONS FOR FURTHER WORK

11.1 Review and conclusions

This thesis has concentrated on the subject of modelling, control and design of various power electronic based devices, such as variable speed drives, Flexible AC Transmission Systems (FACTS) and Custom Power devices for applications in power systems. When a new technology is researched with the objective of being employed to assist power systems in different ways, the availability of simulation and modelling techniques is a decisive factor in quantifying benefits and encouraging the introduction of this technology. A number of main conclusions, drawn from throughout the thesis, are summarised below:

- Six-step, various PWM (such as natural sampling, regular symmetric sampling, regular asymmetric sampling) and vector control methods can be used for the control of adjustable speed drives (Chapters 2 and 3). PWM software implemented techniques, such as the regular symmetric and the regular asymmetric sampling were used as alternative to the analogue based technique natural sampling, and their use is expected to increase in the future due to the

advances the microprocessor technology. Using indirect vector control methods (Chapter 3), accurate speed control can be achieved even at zero speed [1].

- Interactions between AC and DC power systems have always provided a challenge for power system planners and engineers [2-12]. Disturbances to supply systems caused by converter loads can only be tolerated within prescribed limits. Taking account of the three-phase machine load, converter operation creates harmonic currents that cause additional losses in lines, transformers and machines. A modelling technique for a complete generic multi-machine AC/DC power system was developed (Chapters 4 and 5), comprising various generation units and their associated controls. The developed computer program was used to simulate multi-machine AC/DC power systems with variable speed drive models and associated filters to absorb the unwanted harmonics.
- FACTS technology has been developed in order to provide both greater operating flexibility and better utilisation of transmission systems. This strong trend towards optimised power systems is due to the need for competitiveness and efficiency in the new deregulated environment among electric utilities [13]. In addition, problems associated with environmental impact, rights-of-way, regulatory pressures, and high costs have postponed the construction of new transmission lines, while the demand for electric power has continued to grow (Chapter 6).
- One of the major products of FACTS devices is the Static Var Compensator (Chapter 7). A modelling method for digital simulation of the Static Var Compensator (SVC) in power system networks was described. The SVC response under steady state conditions as well as under various power system disturbances has been analysed using results from dynamic simulations. The proposed approach have shown that the SVC offers advantages over traditional methods and the SVC control system is rapid enough and acts effectively.
- Advances in semiconductor technology have allowed the use of power flow controllers within transmission systems. Modelling and simulation work with respect to power flow controllers and especially to STATCON and the UPFC have been presented (Chapter 8). Simulation results of open-loop STATCON and

UPFC models using simple power system networks were illustrated for a number of case studies.

- Custom Power technology includes a new generation of power electronic devices available for use on distribution systems, which will enable utilities to provide premium-quality electricity to customers with sensitive loads [14]. An analytical investigation of three main types of solid state switches was performed including rating requirements and potential applications. A generic control strategy was adopted in order to apply these devices in distribution systems (Chapter 9).
- An innovative control system technique was used in order to apply and design a Dynamic Voltage Restorer (DVR) model with its associated filtering in distribution systems. Different case studies were investigated using open and closed loop control simulation results (Chapter 10).

In conclusion, this thesis has achieved its objective of developing new modelling methods and techniques for various power electronic based models for use in power systems such as variable speed drives, flexible ac transmission systems (FACTS) and Custom Power devices and integrating them using different simulation paradigms. The open modelling architecture for the three different categories (variable speed drives, FACTS, Custom Power) enables future power systems developments to be included. The modelling procedures are useful for validating the performance of power system networks with power electronic devices and identifying and explaining events and/or problems, for provision of training and education of engineers in the field of power electronics and designing new power electronics implementations.

11.2 Objectives of the research work

In order to explore the wide area of applications, the objectives of this thesis were:

a) To develop various models of variable speed drives suitable for power system studies:

- Six step, open and closed loop voltage fed inverter drive
- Natural sampling, open and closed loop voltage fed inverter drive
- Regular symmetric sampling, open and closed loop voltage fed inverter drive
- Regular asymmetric sampling, open and closed loop voltage fed inverter drive
- Indirect vector controlled voltage fed inverter drive

b) To verify the ability of the variable speed drives to carry out their intended functions in electric power networks:

- To develop digital computer programs based on the latest control techniques suitable for the analysis of the dynamic performance of variable speed drives
- To develop equations and guidelines to model power system components in electric networks
- To develop a general algorithm for modelling and simulation of multi-machine power systems with interconnected AC/DC converter stations/variable speed drives
- To investigate the effect of harmonic penetration caused by the AC/DC converter stations/variable speed drives in electric power systems
- To provide filter circuit configurations for absorption of the unwanted harmonics caused by the AC/DC converter stations/variable speed drives

c) To create a library of dynamic models of FACTS devices for use within transmission systems based on the :

- Static Var Compensator (SVC)
- Static Condenser (STATCON)
- Unified Power Flow Controller (UPFC)

d) To verify the ability of the FACTS devices to carry out their intended functions in electric power networks:

- To develop a control system for modelling and simulation of a Static Var Compensator (SVC)
- To investigate the effect of the SVC on the dynamic and transient stability of a power system
- To provide filter circuit configurations for absorption of the unwanted harmonics that the SVC generates in power systems
- To develop open loop control systems for modelling and simulation of a Static Condenser (STATCON) and a Unified Power Flow Controller (UPFC)
- To investigate the effect of the STATCON and the UPFC in real and reactive power flow in transmission systems

e) To create dynamic models of Custom Power devices for use within distribution systems such as the :

- Solid State Switch
- Dynamic Voltage Restorer (DVR)

f) To develop computer simulation programs and control strategies for application of Custom Power devices in distribution systems:

- To propose a control strategy for modelling and design of a solid state switch
- To develop a novel simulation program for modelling of a Dynamic Voltage Restorer (DVR)
- To design a DVR and its associated filters, using results taken from the dynamic simulations

11.3 Statement of contributions resulting from the research work

In terms of the novelty of the research reported in this thesis, the following contributions are identifiable:

- The development of computer simulation programs based on the control systems presented in this thesis for the six step and the PWM techniques (such as the natural sampling and the symmetric/asymmetric sampling) along with an investigation on the dynamic behaviour of the six step and the PWM inverters under various operating conditions.
- The development of a computer program for the closed-loop vector control method coded in the Fortran language and a report on the behaviour of indirect vector control machines under various operating conditions, such as free acceleration to rated speed, step load applied on the shaft of the motor, fast speed reversal and operation in the field weakening region.
- The development of a new generalised approach to power system modelling, which incorporates modelling of AC systems with DC converter stations/variable speed drives.
- The creation of a computer code for the interconnected AC/DC power system and variable speed drives coded in the Fortran language and an investigation on the influence of harmonic pollution to power systems using DC converter stations. Results from the dynamic simulations carried out in this thesis are presented for a number of operating conditions. Where appropriate, analytical equations and explanations are given which will ensure acceptable system conditions.
- An efficient and realistic method to model the Static Var Compensator (SVC), using comprehensive control and firing systems has been developed, along with guidelines for designing the harmonic filters. The SVC was considered to be a continuously variable-shunt susceptance which was adjusted in order to achieve a specified voltage magnitude.
- Comparison of the control and firing methods proposed in this chapter with other control methods and firing systems (such as the Phase Locked Loop) method. The validation of the techniques that were presented in this thesis demonstrates that the proposed SVC controller gives a very good representation of a practical system. The results that were presented using the proposed firing method prove the effectiveness of the technique that was used in this thesis, show that is insensitive to voltage waveform distortion and capable of establishing accurate firing timing

in a timescale similar to using the Phase Locked Loop method; consequently it can be used as an alternative to the PLL method for the control of Static Var Compensator models. Moreover, by using the firing technique presented in this thesis the problem caused by using the PLL method which is that the dynamics of the PLL require a very small time step which demands a high CPU time, can be avoided.

- The problems encountered in the process of building power flow controllers such as the Static Condenser (STATCON) and the Unified Power Flow Controller (UPFC) and the way of handling them using the Electromagnetic Transients Program (EMTP) were discussed and useful guidelines were given for applications of such power electronic based devices by power system engineers using the EMTP.
- The development of a generic control strategy for control and design for a number of devices based on the solid state switch.
- The creation of an innovative closed-loop control system for the Dynamic Voltage Restorer. The control mechanism consists of individual voltage and power controllers for the control of the DVR using the Sinusoidal Pulse Width Modulation technique (SPWM). The effectiveness of the proposed control system was tested under various operating conditions and results taken from the dynamic simulations were validated using actual test results from DVR installations.
- The development of a computer code using the Electromagnetic Transients Simulation Program (EMTP) based on the control system described in this chapter can be used for the effective design of the DVR and its associated controls and filters.

The contributions of this research work are mainly concerned with benefits to both the academic community as well as to power system planners and engineers :

From an academic point of view, is it believed that the modelling methods and techniques presented and demonstrated in this thesis, will help researchers in the field of power electronics to:

- gain a better understanding of new modelling tools and methodologies for a wide range of power electronic based devices (variable speed drives, FACTS, Custom Power devices)
- gain a better knowledge for the control of these devices in power systems, since there is insufficient research related in this area, due to the fact that this technology is based on the semiconductor technology that has been introduced relatively recently
- use some of the modelling techniques as the basis for the simulation and control of other power electronic devices (e.g. use the method for the DVR as the basis for modelling the Distribution STATCON)
- propose and evaluate various power system configurations from the results of the dynamic simulations carried out in this research project

From an industrial perspective, is it believed that the proposed computer simulation programs will help power system engineers and planners to obtain a better understanding of :

- a complete system solution incorporating power system and power electronics components
- how the power electronic devices (variable speed drives, FACTS, Custom Power devices) :

⇒work

⇒can be controlled

⇒can be incorporated in power system architectures

⇒can be designed with significant economic impact

⇒can be tested in a more optimal fashion though the availability of well-defined and validated mechanisms.

11.4 Future work

In the near future it is expected that power systems will undergo significant changes in their architecture. With the introduction of new distributed sources of electrical energy (embedded generation), the overall character of the power system and its dynamic behaviour will gradually change. Moreover, the advances of semiconductor and microprocessor technology will reduce the cost of the power electronic devices even more. This produces a whole range of new issues to be addressed in the power electronics systems design.

The process of integration of different simulation programs and modelling methods in this thesis offers new opportunities for evaluation of the performance of power electronic based devices in power systems under continuously changing circumstances. The following activities appear to be a natural continuation of the work described in this thesis:

- depending on the future demands of the utility companies, the existing library of variable speed drives can be extended to include other control techniques such as the harmonic elimination method
- the control methods described and demonstrated in this thesis for the variable speed drives, can be applied to other motor drives, such as synchronous motor drives
- an investigation of the dynamic response of an AC/DC interconnected power system with variable speed drives under fault conditions or other system disturbances
- future work in the FACTS area should perhaps include an analytical study of a power system with various FACTS controllers described in this thesis, such as SVCs, STATCONs and UPFCs in order to increase the power transfer and improve the transient stability of power networks. It would be useful to investigate if the individual controllers will operate effectively in this integrated modelling power system

- simulations of faults on the system or within the internals of inverter bridges of the STATCON/UPFC. Both are important to evaluating the performance of the STATCON/UPFC because faults within or outside the STATCON/UPFC may lead to distortions of their waveform outputs and thus worsening the system operational quality
- evaluation of losses in the STATCON/UPFC. As the GTO-based voltage source inverter adopts the high frequency PWM method and thus increases the switching losses of the circuits, it is important to develop methods to accurately estimate these losses
- future work in the Custom Power area may include modelling, control and design of a Distribution Static Condenser (D-STATCON) model using a similar approach to that of the DVR
- modelling, simulation and analysis of a distribution system with solid state switches, Dynamic Voltage Restorers and other Custom Power devices in order to evaluate the distribution system performance in this integrated environment
- investigate the effect of FACTS or Custom Power controllers on the protection devices within the system
- incorporate the Dynamic Voltage Restorer or other Custom Power devices in a system with embedded generators and other energy storage devices, in order to evaluate the response of the integrated system, under the requirements of new distribution network designs.

11.5 References

1. Peter, V.A.S. "Vector control of a.c machines," Oxford University Press, New York, 1990.
2. Taleb M, Ortmeyer T.H., "Examination of the current injection technique", IEEE Transactions on Power Delivery, Vol 7, January 1992, pp 442-448.
3. Emanuel A, Yang M, "On the harmonic compensation in nonsinusoidal systems", IEEE Transactions on Power Delivery, Vol 8, January 1993, pp 393-399.
4. Mohan N, Rastogi M, Naik R, "Analysis of a new power electronics interface with approximately sinusoidal 3-phase utility currents and a regulated dc output", IEEE Transactions on Power Delivery, April 1993, pp 540-546.
5. Grotzbach M, Frankkenberg W, "Injected currents of controlled AC/DC converters for harmonic analysis in industrial power plants", IEEE Transaction on Power Delivery, Vol 8, April 1993, pp 511-517.
6. Woodford D, "Secondary arc effects in AC/DC hybrid transmission", IEEE Transactions on Power Delivery, 1992, pp 704-711.
7. Carpinelli G., Gagliardi F., Russo M., Sturchio A., "Steady state mathematical models of battery storage plants with line-commutated converters", IEEE Transactions on Power Delivery, Vol. 8, No.2, April 1993, pp 494-501.
8. Hingorani N.G., Hay J.L, Crosbie R.E., "Dynamic simulation of h.v.d.c transmission systems on digital computers", Proceedings of IEE, May 1966, pp 793-805.
9. Htsui J.S.C., Shepherd W., "Method of digital computation of thyristor switching circuits", Proceedings of IEE, August 1971.
10. Rumph E., Ranade S., "Comparison of suitable control systems for HVDC stations connected to weak ac systems. Part II. Operational behaviour of the HVDC transmission", IEEE Transactions on Power Delivery, May 1971, pp 555-564.

11. Hingorani N, Burbery F., "Simulation of AC system impedances in HVDC system studies", IEEE Transactions on Power Apparatus and Systems, May 1970, pp 819-826.

12. Rumph E., Ranade S., "Comparison of suitable control systems for HVDC stations connected to weak ac systems. Part I. New control systems" Transactions on Power Delivery, May 1971, pp 549-555.

13. Lavsey, E., Weaver, T. IEEE-CIGRE Working Groups Joint Document: "FACTS Overview", IEEE Publication , April, 1995, pp 95-108.

14. Hingorani N, "Introducing custom power", IEEE Spectrum, June 1995, pp 41-48.

APPENDIX 1

PRINCIPAL DATA FOR THE STUDY OF THE SIX-STEP AND PWM INVERTER CONTROL OF THE INDUCTION MOTOR

INDUCTION MOTOR DATA

Rating (KVA)	2797.5
Terminal voltage (kV)	6.6
No. of poles	4
Power factor	0.8
Rated line current (A)	244.72
Stator resistance	0.012
Stator leakage reactance	0.1
Magnetising reactance	4.93
Rotor resistance	0.012
Rotor leakage reactance	0.12
Inertia constant	0.502

FILTER DATA

Filter resistance	0.05
Filter reactance	0.5
Filter capacitance	0.002

APPENDIX 2

PRINCIPAL DATA FOR THE STUDY OF THE FIELD-ORIENTED CONTROL OF THE INDUCTION MOTOR

INDUCTION MOTOR DATA

Rating (KVA)	6.9
Terminal voltage (kV)	0.415
No. of poles	6
Power factor	0.8
Rated line current (A)	9.6
Stator resistance	0.025
Stator leakage reactance	0.075
Magnetising reactance	2.0
Rotor resistance	0.02
Rotor leakage reactance	0.075
Inertia constant	0.2

DC FILTER DATA

Filter resistance	0.05
Filter reactance	0.5
Filter capacitance	0.002

APPENDIX 3

PRINCIPAL DATA FOR THE SIMPLE AC/DC POWER SYSTEM

Generator type : gas

Generator data:

Rating (MVA)	10.0
Terminal voltage (kV)	6.6
D-axis Mutual reactance X_{ad}	1.070pu
Q-axis Mutual reactance X_{aq}	0.784pu
Stator leakage reactance X_{al}	0.12pu
Field leakage reactance X_{fl}	0.086pu
Daxis Damper Leak. reac. X_{lkd}	0.0231pu
Qaxis Damper Leak. reac. X_{lkd}	0.0231pu
Stator resistace R_S	0.0073pu
Field resistance R_F	0.0012pu
D-axis Damper resistance R_{kd}	0.0457pu
Q-axis Damper resistance R_{kq}	0.015pu
Inertia constant H (sec)	1.89

Automatic regulator data (IEEE type 2):

Amplifier gain(K_A)	550.0
Exciter gain(K_E)	1.0
Regulator feedback gain(K_F)	0.05
Rectifier time constant(T_R)	0.02
Amplifier time constant (T_A)	0.1
Exciter time constant $(T_E)_l$	0.137
Feedback time constant T_{F1}	0.6
Feedback time constant T_{F2}	0.137
Amplifier output limiter:max	10.1
Amplifier output limiter:min	0.0
Exciter saturation factors:max	1.9
Exciter saturation factors:min	1.82

Single shaft gas turbine and governor data:

Speed governor gain(K_1)	25.0
Valve positioner gain(K_2)	1.0
Fuel system gain(K_3)	1.0
Fuel Flow Feedback gain(K_4)	0.0
Speed gov. leadconstant (T_{D1})	0.0
Speed gov. lag constant (T_{G1})	0.01
Valve position time const.T_{G2}	0.01
Fuel system time constant T_{G3}	0.2
Power limit:max	1.5
Power limit:min	-0.1

Transformer data:

Rating (MVA)	5.0
Primary resistance(pu)	0.00235
Primary leakage reactance pu	0.0306
Secondary resistance(pu)	0.00235
Secondary leakage reactance	0.0306
Magnetising reactance (pu)	37.23
Connection type	delta-star

Static load 1 and 2 data:

Rating (MVA)	10.0
Resistance(pu)	10.0E5
Reactance pu	10.0E5

Induction motors 1 and 2 data:

Rating (MVA)	2.1
Stator resistance (pu)	0.0092
Stator leakage reactance (pu)	0.0717
Rotor resistance (pu)	0.0070
Rotor leakage reactance(pu)	0.0717
Magnetising reactance(pu)	4.1340
Inertia constant (sec)	0.67
Load torque coefficient: a_0	0.0
Load torque coefficient: a_1	0.0
Load torque coefficient: a_2	0.8
Load torque coefficient: a_3	0.0

5^{th} order harmonic filter:

Rating(MVA)	4.0
Resistance(pu)	0.015
Reactance pu	0.3064
Capacitance pu	7.66

7^{th} order harmonic filter:

Rating(MVA)	4.0
Resistance(pu)	0.021
Reactance pu	0.3064
Capacitance pu	15.01

11^{th} order harmonic filter:

Rating(MVA)	4.0
Resistance(pu)	0.009
Reactance pu	0.0826
Capacitance pu	10.00

13^{th} order harmonic filter:

Rating(MVA)	4.0
Resistance(pu)	0.0107
Reactance pu	0.0826
Capacitance pu	13.95

Variable speed drive data:

Rating (MVA)	2.8
Stator resistance (pu)	0.012
Stator leakage reactance (pu)	0.1
Rotor resistance (pu)	0.012
Rotor leakage reactance(pu)	0.12
Magnetising reactance(pu)	4.93
Inertia constant (sec)	0.502
Load torque coefficient: a_0	0.0
Load torque coefficient: a_1	0.0
Load torque coefficient: a_2	0.8
Load torque coefficient: a_3	0.0
Resistance on the dc filter	0.05
Reactance on the dc filter	0.5
Capacitance on the dc filter	0.002
Set speed	1.0
Resistanceon conv.transformer	0.0
Reactance on conv.transformer	0.138

APPENDIX 4

PRINCIPAL DATA FOR THE MULTI-MACHINE AC/DC POWER SYSTEM WITH VARIABLE SPEED DRIVES

Generators 1 and 2 type : gas

Generators data:

Rating (MVA)	10.0
Terminal voltage (kV)	6.6
D-axis Mutual reactance X_{ad}	1.070pu
Q-axis Mutual reactance X_{aq}	0.784pu
Stator leakage reactance X_{al}	0.12pu
Field leakage reactance X_{fl}	0.086pu
Daxis Damper Leak. reac. X_{lkd}	0.0231pu
Qaxis Damper Leak. reac. X_{lkq}	0.0231pu
Stator resistace R_S	0.0073pu
Field resistance R_F	0.0012pu
D-axis Damper resistance R_{kd}	0.0457pu
Q-axis Damper resistance R_{kq}	0.015pu
Inertia constant H (sec)	1.89

Automatic regulators data (IEEE type 2):

Amplifier gain(K_A)	550.0
Exciter gain(K_E)	1.0
Regulator feedback gain(K_F)	0.05
Rectifier time constant(T_R)	0.02
Amplifier time constant (T_A)	0.1
Exciter time constant $(T_E)_1$	0.137
Feedback time constant T_{F1}	0.6
Feedback time constant T_{F2}	0.137
Amplifier output limiter:max	10.1
Amplifier output limiter:min	0.0
Exciter saturation factors:max	1.9
Exciter saturation factors:min	1.82

Single shaft gas turbines and governors data:

Speed governor gain(K_1)	25.0
Valve positioner gain(K_2)	1.0
Fuel system gain(K_3)	1.0
Fuel Flow Feedback gain(K_4)	0.0
Speed gov. leadconstant (T_{D1})	0.0
Speed gov. lag constant (T_{G1})	0.01
Valve position time const.T_{G2}	0.01
Fuel system time constant T_{G3}	0.2
Power limit:max	1.5
Power limit:min	-0.1

Transformer data:

Rating (MVA)	7.5
Primary resistance(pu)	0.00235
Primary leakage reactance pu	0.0306
Secondary resistance(pu)	0.00235
Secondary leakage reactance	0.0306
Magnetising reactance (pu)	37.23
Connection type	delta-star

Data for static loads 1 and 2:

Rating (MVA)	10.0
Resistance(pu)	10.0E5
Reactance pu	10.0E5

Induction motors 1 and 2 data:

Rating (MVA)	2.8
Stator resistance (pu)	0.012
Stator leakage reactance (pu)	0.1
Rotor resistance (pu)	0.012
Rotor leakage reactance(pu)	0.12
Magnetising reactance(pu)	4.93
Inertia constant (sec)	0.502
Load torque coefficient: a_0	0.0
Load torque coefficient: a_1	0.0
Load torque coefficient: a_2	0.8
Load torque coefficient: a_3	0.0

Induction motors 3 and 4 data:

Rating (MVA)	2.1
Stator resistance (pu)	0.0092
Stator leakage reactance (pu)	0.0717
Rotor resistance (pu)	0.0070
Rotor leakage reactance(pu)	0.0717
Magnetising reactance(pu)	4.1340
Inertia constant (sec)	0.67
Load torque coefficient: a_0	0.0
Load torque coefficient: a_1	0.0
Load torque coefficient: a_2	0.8
Load torque coefficient: a_3	0.0

5^{th} order harmonic filter at node 1:

Rating(MVA)	4.0
Resistance(pu)	0.015
Reactance pu	0.3064
Capacitance pu	7.66

7^{th} order harmonic filter at node 1 :

Rating(MVA)	4.0
Resistance(pu)	0.021
Reactance pu	0.3064
Capacitance pu	15.01

11^{th} order harmonic filter at node 1:

Rating(MVA)	4.0
Resistance(pu)	0.009
Reactance pu	0.0826
Capacitance pu	10.00

13^{th} order harmonic filter at node 1:

Rating(MVA)	4.0
Resistance(pu)	0.0107
Reactance pu	0.0826
Capacitance pu	13.95

5^{th} order harmonic filter at node 2:

Rating(MVA)	3.0
Resistance(pu)	0.015
Reactance pu	0.3064
Capacitance pu	7.66

7^{th} order harmonic filter at node 2:

Rating(MVA)	3.0
Resistance(pu)	0.021
Reactance pu	0.3064
Capacitance pu	15.01

11^{th} order harmonic filter at node 2:

Rating(MVA)	3.0
Resistance(pu)	0.009
Reactance pu	0.0826
Capacitance pu	10.00

13^{th} order harmonic filter at node 2:

Rating(MVA)	3.0
Resistance(pu)	0.0107
Reactance pu	0.0826
Capacitance pu	13.95

Variable speed drive 1 data:

Rating (MVA)	2.8
Stator resistance (pu)	0.012
Stator leakage reactance (pu)	0.1
Rotor resistance (pu)	0.012
Rotor leakage reactance(pu)	0.12
Magnetising reactance(pu)	4.93
Inertia constant (sec)	0.502
Load torque coefficient: a_0	0.0
Load torque coefficient: a_1	0.0
Load torque coefficient: a_2	0.8
Load torque coefficient: a_3	0.0
Resistance on the dc filter	0.05
Reactance on the dc filter	0.5
Capacitance on the dc filter	0.002
Set speed	1.0
Resistanceon conv.transformer	0.0
Reactance on conv.transformer	0.138

Variable speed drive 2 data:

Rating (MVA)	2.1
Stator resistance (pu)	0.092
Stator leakage reactance (pu)	0.0717
Rotor resistance (pu)	0.0070
Rotor leakage reactance(pu)	0.0717
Magnetising reactance(pu)	4.134
Inertia constant (sec)	0.67
Load torque coefficient: a_0	0.0
Load torque coefficient: a_1	0.0
Load torque coefficient: a_2	0.8
Load torque coefficient: a_3	0.0
Resistance on the dc filter	0.05
Reactance on the dc filter	0.5
Capacitance on the dc filter	0.002
Set speed	1.0
Resistanceon conv.transformer	0.0
Reactance on conv.transformer	0.138